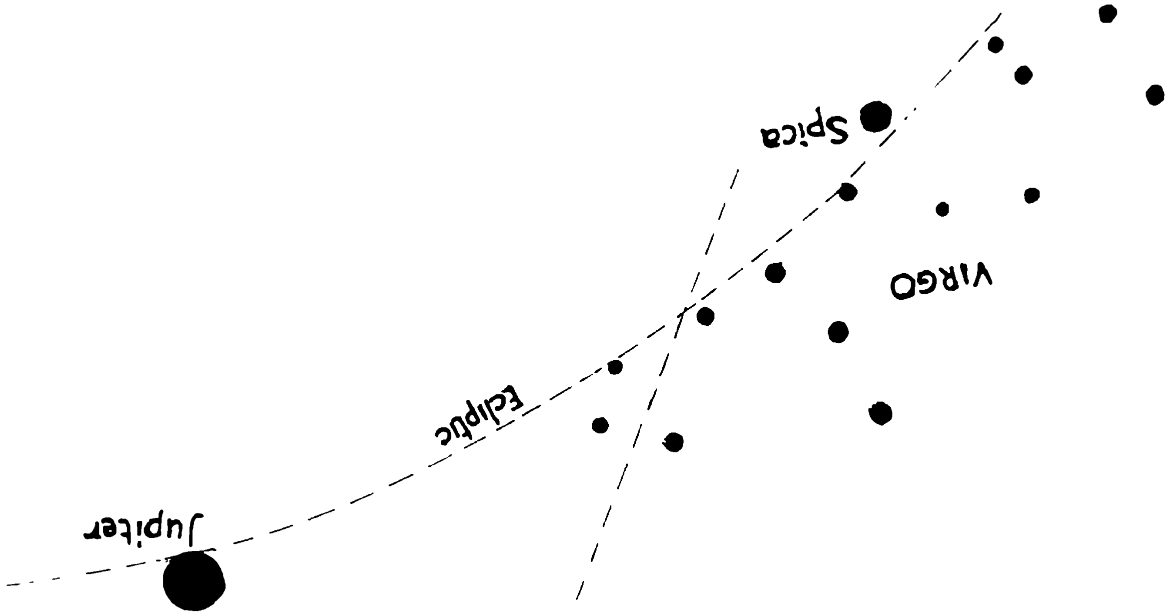

THE VIRGO PROJECT

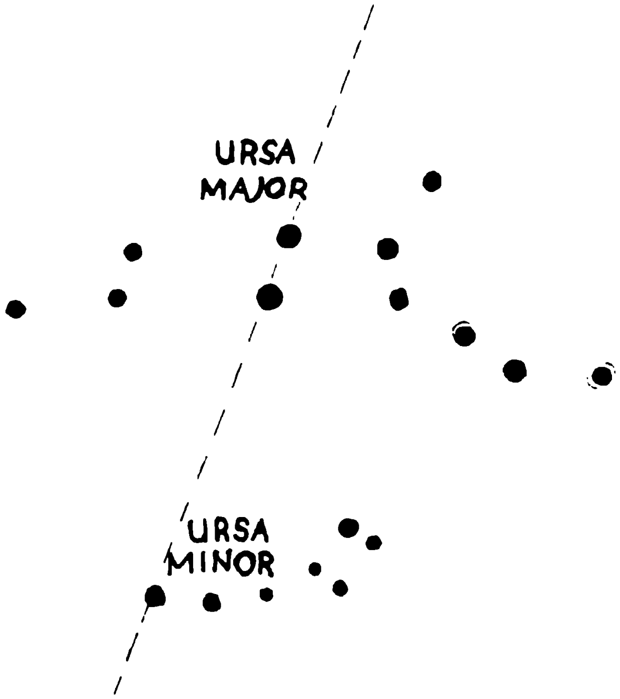

THE VIRGO PROJECT

THE VIRGO PROJECT

INFN Sez. di Pisa
Dipartimento di Fisica
dell'Università di Pisa

C. BRADASCHIA
R. DEL FABBRO
A. DI VIRGILIO
A. GIAZOTTO
H. KAUTZKY
V. MONTELATICI
D. PASSUELLO

CNRS-Lab. de Gravitation
et de Cosmologie Relativiste
Orsay - Paris

A. BRILLET
O. CREGUT
P. HELLO
C.N. MAN
P.T. MANH
A. MARRAUD
D. SHOEMAKER
J-Y. VINET

INFN Sez. di Napoli
Dipartimento di Scienze Fisiche
dell'Università di Napoli

F. BARONE
L. DI FIORE
L. MILANO
G. RUSSO
S. SOLIMENO

CNRS-Universitè Paris 6

J.M. AGUIRREGABIRIA
H. BEL
J-P. DURUISSEAU
G. LE DENMAT
Ph. TOURRENC

Dipartimento di Elettronica
delle Università
di Salerno e di Napoli

M. CAPOZZI
M. LONGO
M. LOPS
I. PINTO
G. ROTOLI

Groupe d'Astrophysique
Relativiste
Observatoire de Meudon

T. DAMOUR
S. BONAZZOLA
J.A. MARCK
Y. GOURGHOULON

CNR Frascati

F. FULIGNI
V. IAFOLLA
G. NATALE

University of Illinois
at Urbana, USA

L.E. HOLLOWAY

Instituto de Fisica [1] - USP, Instituto Astronomico e Geofisico[2] - USP, Centro Basileiro de Pesquisas Fisicas[3] - CNPQ, Observatorio Nacional- CNPQ[4], Instituto de Fisica GW- UniCAMP.[5]

M. S. D. CATTANI[1]
J. A. F. DE FREITAS PACHECO[2]
C. O. ESCOBAR[1]
C.A. GÃLVAO[3]
N.O. SANTOS[4]
A. TURTELLI JR[5]
W. VELLOSO[2,*]

* Present address: INFN laboratory, via vecchia livornese 582/a, Pisa, Italy

" First results on the electronic cooling for the Pisa seismic noise super-attenuator for Gravitational Wave detection "

A. GIAZOTTO; " Interferometric detection of gravitational waves", Phys. rep. 1989

A. GIAZOTTO; " Estimate of the cosmic ray background in an interferometric antenna for gravitational wave detection"

PRICES

SOCOMIN IMPIANTI: Virgo Antenna constructions costs

LEYBOLD: Vacuum pumps costs

THERMOSYSTEM SPA: Clean rooms class 10000 costs

COPY OF:" Comune di Cascina: Deliberazione del Consiglio Comunale n. 100 dell' 8 maggio 1989

OGGETTO: *Antenna interferometrica a grande base per la ricerca di onde gravitazionali"*

Altimetria del sito lungo l' alloggiamto dell'interferometro

Foreword

This document describes the proposal made by the members of the VIRGO collaboration for the construction of a large interferometer to detect Gravitational Waves.

The VIRGO interferometer is a two waves interferometer having two perpendicular symmetrical arms of physical length L= 3 km. The use of a Fabry-Perot cavity in each arm brings the optical armlength to 120 km.The optical components of the interferometer are located inside evacuated instrumentation chambers connected by a 1m diameter evacuated pipe. Each critical optical component is isolated from the seismic noise by a multistage, multidimensional, seismic noise attenuator. The optical noise is brought to a very low level by the use of an ultrastable high power Nd:YAG laser and of an optimized detection technique involving the "recycling" of the light.

The existence of gravitational waves is predicted by most theories of gravitation, including General Relativity. It has been indirectly demonstrated by the study of the period of pulsar PSR 1913+16, which allowed the verification of the predictions of General Relativity with a precision of a few %, but all the attempts to detect them directly have remained unsuccessful yet.

The first goal of the VIRGO project is to succeed in detecting gravitational radiation from fast, massive objects in our galaxy or in nearby ones. It is designed for broadband detection (10 Hz to 3 kHz), in order to get the best chance of detecting different kinds of known sources, from pulsars to supernovae, alone or in coincidence with other detectors. The sensitivity goal has been chosen so that it reaches the range where one *expects* to observe at least a few events per year, while the instrument still relies on available technologies. Different possibilities of improving further on the sensitivity are already being studied both theoretically and experimentally. The vacuum system and the instrumentation chambers are designed to allow for these improvements.

The discovery of Gravitational Radiation will be a major event in the history of physics, and will open a new era in the observation and understanding of the Universe: it will provide the first tests of the dynamical side of General Relativity, the first measurements of the properties of the graviton and will ultimately generate a new kind of astrophysics. *Therefore, VIRGO obviously concerns different fields of physics from gravitation to particle physics and astrophysics.*

Gravitational waves of astrophysical origin are produced in a wide frequency range. Ground based experiments, such as VIRGO, have access to the high frequency domain (10 Hz to 10^4 Hz) where frequent events from a variety of sources are expected, while Doppler tracking of satellites and space-based interferometers can explore the region of very low frequencies (10^{-5} Hz to 1 Hz) which is forbidden to ground-based experiments, because of the seismic noise. These possibilities are complementary.

The ground based search for gravitational waves has been going on for more than 20 years, which have seen the development of a few generations of mechanical detectors based on the original idea of J.Weber. The sensitivity of these instruments has improved by more than three orders of magnitude since the first Weber's bar, and the best ones are now reaching the point where *it could be possible to detect* the explosion of a supernova in our galaxy, an event which may happen a few times per century. Obtaining a higher event rate requires the capability of detecting as far as the Virgo cluster, which contains about 300 large galaxies. This represents a new step of three orders of magnitude in sensitivity, and we believe that this calls for a different technology: very large interferometers, such as VIRGO, do have the potential sensitivity, plus the advantage of a wideband response, which allows not only for the *detection*, but also for the *observation* of a variety of sources.

VIRGO must be considered both as an experiment and as a step towards a future observatory,: *the immediate goal of the VIRGO experiment is to realize, or to participate in, the first detection of gravitational radiation., but it also has tlong term goal of being one component of the gravitational wave detectors network which will involve other detectors in other countries*, and provide data of astrophysical interest. These goals imply a *collaboration* with the other groups having similar projects, without excluding some *competition*.

The group leaders from Italy, France, Germany, Scotland, and the USA have agreed to exchange all information and to collaborate on all the aspects of the construction of large interferometers in order to generate the international effort required by the birth of gravitational astronomy. In particular, it has been decided to standardize the data acquisition and data analysis, to exchange technologies, and to design all the projects to be compatible with a common sensitivity goal. *This insures the credibility and the long term success of all the projects*, but it is not intended to unify the construction time schedules.

VIRGO is in a very good position today as far as succesfully realizing the first detection because of its unique capability of operating at low frequency, which should give it a chance to detect *alone* either pulsars or coalescing binaries.

All the other projects are presently restricted to the detection of high frequency signals, whose validation requires, for pulses, the observation of a coincidence between two or more detectors: here again, if it's realized rapidly, VIRGO has a good chance of participating to the first detection, together with the first other interferometric detectors, or with a state-of-the-art bar detector, such as the Italian ones, or even with a neutrino detector and with conventional astronomy.

The timescale for the construction of VIRGO is therefore an important subject to consider in relation with the other projects in the world. With reasonable funding and a quick staff increase, the construction of VIRGO could start at the beginning of 1991 and would be completed about five years later. The American LIGO, the MIT-Caltech project of 2 interferometric antennas, has a good chance to be approved by NSF this summer and to start in 1991. If it were approved, it would be advisable to adjust the VIRGO timetable in order to ensure the simultaneous completion of the 3 antennas. The British and German groups are going to present a common proposal before the end of 1989; they could also start in 1991-1992. The Japanese and Australian proposals will probably be presented a bit later.

The design of Virgo involves many new scientific and technical developments in interferometry, optics, lasers, seismic isolation, and even vacuum technology. Nobody ever built such a large and sensitive interferometer, but solutions to the scientific problems have been found and/or tested in the laboratories, and solutions to many technical problems have been found in cooperation with European companies. *The feasibility of VIRGO is now demonstrated on most critical points.* A few important studies still remain to be completed before the final design. They are either industrial studies which are too expensive to be funded before the project is approved, or scientific studies which require some supplementary staff, or collaboration related studies, such as data acquisition and analysis.

The construction of VIRGO is a sum of technological investments : it will require and help a number of high technology companies (French and Italian) to improve on their present products and it will give them a higher competence.

The Franco-Italian collaboration in this project is necessary and sufficient. There is a quasi perfect complementarity between the experimental groups, a minimum redundancy as concerns the theoretical part and all the aspects of the problem are covered. It is clearly the scientific interest of France and Italy to approve and to formalize rapidly this collaboration. A wider global collaboration, for instance, would delay the construction, would probably not be less expensive, would profit less to French and Italian firms, and would not guarantee us such a strong scientific position. On the other hand, the proposed collaboration could trigger a profitable challenge to high technology French and Italian firms.

This does not mean that the VIRGO collaboration is isolated or closed; we were actually instrumental in generating cooperation inside Europe and with the USA and we are presently discussing collaborations with Brasilian and Indian institutes. The VIRGO collaboration remains open to collaborations with other countries and institutions.

All the members of the VIRGO collaboration have participated to the preparation of this document, which was elaborated with the editorial assistance of N. Galeotti and C. Trecul. This is the result of about 5 years of research by all the members of the group.

Many ideas in this proposal are the results of conversations and collaborations with our colleagues at the Max-Planck Institut in Garching, at the Universities of Glasgow and Cardiff, at M.I.T. and at Caltech.

A. Giazotto
(INFN and Universita di Pisa)

A. Brillet
(CNRS and Universités Paris VI and XI)

Chapter 1

Scientific motivations

1) SCIENTIFIC MOTIVATIONS

The building of an interferometric gravitational wave detector constitutes a wide-scope experiment which can be expected to bring important progress in several fields of science: gravitational physics, nuclear physics, astrophysics, applied physics.

In addition this project constitutes a motivation for researches in various scientific domains (e.g. quantum optics). In this chapter, after having recalled the basic properties of gravitational waves, we shall discuss the main astrophysical sources of gravitational waves, and the expected characteristics of the signals they emit. Then we shall list the various scientific benefits that could result from the direct detection of gravitational waves.

Our conclusions will be that the Virgo experiment, thanks in particular to its ability to look for signals at low frequencies (a few tens of Hertz), has a good chance, even when operating alone, of detecting gravitational wave signals emitted by inspiralling neutron-star binaries and of probing in a physically interesting way, the rotational asymmetry of pulsars. With less certainty (because of our ignorance about the strength and number of emitted signals), it could also detect the gravitational wave bursts emitted by supernovae.

1.1) PROPERTIES OF GRAVITATIONAL WAVES

Gravitational waves, as predicted by Einstein's theory of gravitation, are "waves of deformation of space" which propagate with the velocity of light and whose effect on an assembly of (freely falling) particles is to modify their relative positions.

Specifically, let L^i, $i=1,2,3$, be the position vector of a particle with respect to some (arbitrary) central particle (the distance $L = [(L^1)^2 + (L^2)^2 + (L^3)^2]^{1/2}$ having the operational meaning of the "radar distance", i.e. the light travel time between the two particles). Then, a gravitational wave is described by a 3 x 3 matrix, $h_{ij}(t, \vec{x})$, whose elements are dimensionless. The effect of the dimensionless "gravitational wave amplitude" is to modify the relative position vector, $L^i \rightarrow L^i + \Delta L^i$, with

$$\Delta L^i = \sum_{j=1}^{3} \frac{1}{2} h_{ij} L^j \qquad (1.1)$$

In General Relativity the wave amplitude h_{ij} propagates with the velocity of light and causes purely anisotropic displacements in the plane transverse to the direction of propagation. Mathematically, these properties are encoded in the equations :

$$\left(\nabla^2 - \frac{1}{c^2}\frac{\partial^2}{\partial t^2}\right) h_{ij} = 0 \qquad (1.2a)$$

$$\sum_{j=1}^{3} h_{jj} = 0 \qquad (1.2b)$$

$$\sum_{j=1}^{3} \frac{\partial h_{ij}}{\partial x^j} = 0 \qquad (1.2c)$$

The general "progressive plane wave" solution of eqs (1.2) can be written as

$$h_{ij}(t, \bar{x}) = h_+(t - \bar{n}.\bar{x}/c)\left[p^i p^j - q^i q^j\right] + h_\times(t - \bar{n}.\bar{x}/c)\left[p^i q^j + p^j q^i\right] \qquad (1.3)$$

where n is the unit vector pointing in the direction of propagation of the wave and where p and q are any two unit vectors making with n an orthonormal euclidean triad (n, p, q). We see that a general plane wave is described by two angles (direction of n) and two functions of time (the two independent "linear polarizations" $h_+(t)$ and $h_\times(t)$ lying in the plane transverse to the direction of propagation). If such a wave is Fourier-analyzed, it is described at each frequency, f, by six numbers: two direction angles, two amplitudes and two phases (the relative phase measuring the degree of "elliptical polarisation" of the wave). Figure 1.1.1 represents the observable effect, according to eq. (1.1), of each of the linear polarizations h_+ and $h_\times$ (considered separately) on a ring of particles located in the plane transverse to the direction of propagation (using p and q as coordinate axes).

A very important feature of gravitational waves is that they are so weakly coupled to matter that their absorption, scattering and dispersion in completely negligible in all astrophysical situations (see e.g. section 2.4.3 of Thorne [1983]). This is in marked contrast with electromagnetic waves and even with neutrinos for which, for example, the dense inner shells of a supernova are opaque (while they are completely transparent to gravitational waves). The only exception would be the super-dense Planck era of very early

cosmology (section 7.2 of Zel'dovich and Novikov [1983]). Although big mass concentrations have no direct scattering or absorption effect on gravitational waves, they have an indirect effect on their propagation via the curvature of space-time that they generate. This can cause, e.g., some deflection and focusing of gravitational radiation, in the same manner as electromagnetic radiation can be deflected and focused by the curvature associated with lumps of matter ("gravitational lenses"). See section 9.3.5 of Thorne [1987] for a catalogue of wave-propagation effects.
Finally, let us note that a clear indirect evidence of the existence of gravitational waves has already been obtained through the comparison between the extremely precise timing data of the binary pulsar PSR1913+16 (Taylor [1987] ; Taylor and Weisberg [1989]) and the theoretical predictions concerning general relativistic effects (and particularly gravitational radiation damping effects) in the timing of binary pulsars (Damour and Deruelle [1986] ; Damour [1987]). An additional astrophysical evidence for the reality of gravitational radiation damping effects comes from the satisfactory agreement between the observations and the theory of the period distribution of cataclysmic variables (see e.g. King [1988]). This indirect evidence is important to the projects of direct detection of gravitational radiation in that it confirms the soundness of the predictions of Einstein's theory concerning the generation of gravitational waves by material sources used below.

1.2) SOURCES OF GRAVITATIONAL WAVES

Gravitational radiation is coherently generated by the non-spherically symmetric motion of mass distributions. In order of magnitude the dimensionless amplitude h emitted by a localized material source is given by

$$h \approx \frac{4G\,\varepsilon_{ns}\,E_{kin}}{c^4\,r} \qquad (1.4)$$

where G is Newton's constant, c the velocity of light, r the distance away from the source, E_{kin} the total kinetic energy of the source and ε_{ns}, with $0 \le \varepsilon_{ns} \le 1$, the fraction of the kinetic energy which is non-spherically symmetric and thereby effective in generating gravitational waves.
For a given noise level in the detector, as described by the square root of the spectral density of the squared relative displacement noise, say h_n (f) measured in $H_z^{-1/2}$, the detectability of a certain type of astrophysical source depends on three factors: the amplitude level of the gravitational waves at the

Earth, their temporal characteristics (burst-like, periodic or stochastic) and the number of such sources. Let us examine in turn the three main categories of sources, when classified by their temporal behaviour.

1.2.1) BURST SOURCES

The term "burst" will refer to gravitational wave signals which last only for times short compared to a typical observing run. They can be further classified according to their "Q-factor", i.e. the number of (typical) cycles during the burst. The Q factor is important in that it determines the bandwidth, $\Delta f \approx f_c/Q$, around some characteristic frequency f_c, of the signal within which one can look for the signal. In coarse order of magnitude (see chapter 3 for a more precise analysis), this leads to a signal over noise ratio

$$\frac{S}{N} \approx \frac{|h_s(t)|}{\tilde{h}_n(f_c)(\Delta f)^{1/2}} \approx \frac{Q^{1/2}|h_s(t)|}{\tilde{h}_n(f_c)\, f_c^{1/2}} \qquad (1.5)$$

where $|h_S(t)|$ is the characteristic level of the dimensionless amplitude of the gravitational wave signal, and where $h_n(f)$ (with dimensions $Hz^{-1/2}$) is the noise level of the detector. The noise level aimed at by the Virgo experiment will be discussed in detail below, for the present order-of-magnitude purposes we shall take

$$\tilde{h}_n(f) \approx 10^{-23}\,Hz^{-1/2}, \text{ for } f \geq 200\,Hz, \qquad (1.6)$$

with a progressive worsening of $\sim h_n(f)$ as the frequency decreases down to a few tens of Hertz.

A prominent type of source of low-Q bursts of gravitational radiation are the stellar collapses. These should be at least as numerous as the type II supernovae (but there could be also plenty of "optically silent" collapses). The collapses can lead to the formation either of a neutron star or a black hole. At present, there are no reliable estimates of the generation of gravitational waves by realistic collapses to the neutron star stage. Moreover, the number of such events per galaxy and per year is poorly known ($\approx$ one every 30 years) and might be underestimated (Blair [1983]). It is however clear that in order to reach the level of several events per year one must consider a volume of space of radius $\approx$ 10 Mpc which includes the Virgo cluster of galaxies (which gives its name to the project). Using then the order of magnitude formula (1.4) with $E_{kin} \approx 3 \times 10^{53}$ erg and $r \approx 10$ Mpc one gets

$$h \approx 3\left(\frac{\varepsilon_{ns}}{0.1}\right) \times 10^{-22} \qquad (1.7)$$

The estimate (1.7) indicates that a reasonably asymmetric ($\varepsilon_{ns} \approx 0.1$) supernova collapse in the Virgo cluster, generating a low-Q burst around the kHz (i.e. $\Delta f \approx f_c \approx 10^3$ Hz) would reach the noise level *(1.6)*. At present, *it is* impossible to make firmer statements about the detectability of gravitational radiation from supernovae. One will probably have to wait for the development of fully relativistic numerical simulations of realistic 3D stellar collapses. See e.g. Thorne [1987] for a review of the presently existing attempts at improving the rough estimate (1.7). Figure 1.2.1 shows the result of a fully relativistic but 2D (axisymmetric) numerical simulation of a collapse leading directly to the formation of a black hole (Stark and Piran [1986]). (That type of collapse does not seem to be a very efficient generator of gravitational waves, but the Fig. 1.2.2 illustrates the possibility that the emitted waves carry a lot of physical and astrophysical information).

Very interesting sources of high-Q bursts of gravitational waves are the late stages of coalescence of binary systems of neutron stars or black holes. The binary pulsar PSR1913+16 gives the example of an orbital system of two neutron stars which is slowly spiralling in under the influence of gravitational radiation damping: indeed, the timing data shows that the semi-major-axis of the orbit is decreasing by about 2 meters per year. In about 3.5 10^8 years this system will be reduced to a very close system of two neutron stars which will emit a long train of gravitational waves of increasing frequency, up to the point where the tidal forces will disrupt the stars and make them merge into a single object. The gravitationally interesting swan-song of such a system consists of about the last minute before the final coalescence, during which it emits a quasi periodic gravitational wave train whose frequency continuously increases from about 30 Hz up to about 1 kHz. The Q-factor of the part of this wave train around the frequency f is (Schutz [1986] ; Thorne [1987])

$$Q \approx f^2/(df/dt) = 5.8 \times 10^3 \left(\frac{M}{M_O}\right)^{-5/3} \left(\frac{f}{30\,\mathrm{Hz}}\right)^{-5/3} \qquad (1.8)$$

where the "mass parameter" M is equal to $m_1^{3/5}\, m_2^{3/5} / (m_1 + m_2)^{1/5}$. The corresponding gravitational wave amplitude is:

$$h \approx 4.5\ 10^{-24} \left(\frac{M}{M_O}\right)^{5/3} \left(\frac{f}{30\,\mathrm{Hz}}\right)^{2/3} \left(\frac{100\,\mathrm{Mpc}}{r}\right) \qquad (1.9)$$

Contrary to the case of supernovae where the wave amplitude, eq.(1.7), was highly uncertain, the amplitude emitted by coalescing binaries is well under control (especially for low frequencies $f \leq 100$ Hz). However, there is considerable uncertainty in the number of coalescences. Estimates based on the knowledge that PSR1913+16 will become such a system in a rather short time (astrophysically speaking) suggest that there would be several events per year within a distance $\approx$ 100 Mpc (Clark et al. [1979] ; Schutz [1989a]). At such large distances the gravitational wave amplitude (1.9) seems a priori very small compared to the estimated supernova signal (1.7). However, its detectability in the low frequency domain $f \approx 30$ Hz is greatly enhanced, with respect to the detectability of a $\approx$ 1 kHz burst, by the fact that the bandwidth, $\Delta f \approx f/Q$, with Q given by eq. (1.8), is quite small : $\Delta f \approx 5 \times 10^{-3}$ Hz. It is therefore an important aspect of the Virgo experiment that it aims at getting a good sensitivity at the low frequencies $\approx$ 30 Hz. Even if the noise level expected for higher frequencies, eq. (1.6), is worsened by a factor 3 around 30 Hz, it can be seen from eqs (1.5) and (1.9) that several wave trains emitted by inspiralling compact binaries should be observable each year with S/N > 2. The important conclusion that coalescences as far away as 100 or 150 Mpc can be detected with a noise level $\approx 3 \times 10^{-23}$ $Hz^{-1/2}$ at 30 Hz, obtained here from a crude order-of-magnitude analysis, seems confirmed by a finer study of the data analysis of signals having the known time behaviour of inspiralling binaries (see e.g. Schutz [1989b]).

These wave trains can be detected with only one detector and, once seen in the low-frequency domain, the precise analysis of their theoretically well determined higher-frequency parts will become possible and will lead to a solid confirmation (or infirmation) that they were indeed gravitational waves emitted by an inspiralling binary.

There are other potentially interesting gravitational wave bursts, notably the more speculative, but visible at very large distances, signals emitted by coalescing binary systems of black holes, see Thorne [1987].

1.2.2) PERIODIC SOURCES

The term "periodic" refers to extremely high-Q gravitational signals which are coherent over long periods. Eq.(1.5) shows then that very small amplitudes become detectable.

A prominent type of periodic gravitational source is a slightly asymmetric rotating neutron star in our Galaxy. This can be a radio pulsar or an accreting neutron star. For pulsars, the possibility offered by the Virgo experiment of looking at low frequencies is again quite important as most known pulsars are rather slow. Very little is known about the realistic values of the degree of asymmetry (relative deviation from axisymmetry) of pulsars. Let us only say that a one-year integration at the known (gravitational wave) frequency of a pulsar like the Crab ($f \approx$ 60 Hz) or Vela ($f \approx$ 22 Hz), with the expected noise level, would allow one to detect gravitational wave amplitudes much smaller than the presently known theoretical upper limits. This would entitle us to get very valuable information about the structure of rotating neutron stars. Let us also point out the possible existence of periodic gravitational wave emission by fast spinning accreting neutron stars undergoing the "Chandrasekhar-Friedman-Schutz" instability (Wagoner [1984]). Their detection, especially if realized in conjunction with a corresponding X-ray detection, could give a wealth of new information about neutron stars.

1.2.3) STOCHASTIC SOURCES

The term "stochastic" refers to a random superposition of overlapping burst, or periodic, waves emitted by many different sources. In particular, one expects that part of this random background has a cosmological origin : e.g. phase transitions in the early universe, or gravitational decay of cosmic strings.
The analysis of the detectability of such a stochastic background (e.g. Thorne [1987] ; Schutz [1989b]), shows that it can be done at only one site by correlating, for instance, the data from a full size interferometer with the data from a half size one, and that it could put firm constraints on several cosmological scenarios.

1.3) EXPECTED SCIENTIFIC BENEFITS

The expected scientific benefits of the detection of gravitational wave signals concern: 1. fundamental physics, 2. astrophysics, 3. applied physics. Moreover, 4., the Virgo experiment serves the useful role of "driver" in several fields of physics.

1.3.1) FUNDAMENTAL PHYSICS

In view of the key role of the gravitational force for the unification of all fundamental interactions, the direct detection of gravitational waves, i.e., in quantum language, the detection of the "graviton", is of comparable importance to the detection of the intermediate bosons W and Z. The direct measurement of the mass and spin of the graviton (i.e. the velocity and

polarization properties of a gravitational wave) can be obtained from the data of a network of detectors (see chapter 3).
Moreover, the observation of gravitational waves gives access to the study of several extreme situations of physics. Namely :
- the strong gravitational field regime, accessible through the observation of gravitational collapse especially down to the black hole state. Gravitational wave observations are our best hope of proving the existence of black holes and measuring their properties.
- the very condensed matter regime, accessible through the observation of neutron stars : in principle gravitational wave observations can see the vibrating modes and the deformation of neutron stars, and measure their masses. These informations will be of great relevance for nuclear physics by giving us a handle on the equation of state at nuclear and supranuclear densities.
- the very early universe, and the physics of unification of interactions, accessible through the possible observation of stochastic gravitational waves generated during early phase transitions, or by the gravitational decay of cosmic strings. It is important to stress that, because of their extremely weak coupling to matter, gravitational radiation is our only hope of looking back to the Planck era (temperature $\approx 10^{32}$ K).

1.3.2) ASTROPHYSICS

Because the absorption of gravitational waves is negligible (even much more than for neutrinos), their detection would open a new and very transparent "window" on the universe. Certainly the opening of this completely new information channel will increase considerably, or even revolutionize, our comprehension of the universe.
Gravitational waves carry information about the coherent bulk motion of mass distributions. That information is orthogonal, and complementary, to the one carried by electromagnetic waves, or neutrinos. Examples of information carried by gravitational waves are :
- dynamics of gravitational collapse,
- rotation and asymmetry of progenitors,
- existence and properties of black holes,
- measurement of the mass of neutron stars,
- possibility to measure directly the absolute distance to a galaxy $\approx$ 100 Mpc away (without using a ladder of intermediate measures) (Schutz [1986]),
- linear mass density of cosmic strings.

Generally speaking, gravitational waves can allow us to see deeply into electromagnetically or neutrinically opaque regions, and this applies in particular to the very early universe.

1.3.3) APPLIED PHYSICS AND ENGINEERING

The obtention of the aimed at sensibility necessitates to push to extreme limits existent technologies. The results obtained so far by the members of the Virgo project are already considerable. One can mention for instance :

- coherent addition of lasers,
- "recycling" of light,
- external modulation,
- ultrastabilization of a YAG laser (10^{-3} Hz),
- construction of a low-frequency seismic super-attenuator.

Let us note in passing that the Virgo experiment, through its need of very advanced technologies, can provide a stimulus for the industries of the countries involved in it.

1.3.4) THE VIRGO EXPERIMENT AS A "DRIVER" OF OTHER FIELDS OF PHYSICS

It is important to mention that besides the direct scientific benefits that are likely to come out of the Virgo experiment, this experiment has the useful effect of providing a motivation and/or a stimulus for several scientific researches. Let us quote :

- the theoretical and experimental studies of "squeezed states" (quantum optics),
- the development of new numerical methods (numerical relativity),
- the theoretical and experimental study of the nonlinear dynamics of a pendular Fabry-Perot (retarded differential equations).

Let us finally mention that, once constructed, the Virgo interferometer could also be used for various researches in atomic physics and in the quantum mechanics of macroscopic objects.

Figure captions, chapter 1

Fig.1.1.1 (a) A circle of free particles before a wave travelling in the z direction reaches them. (b) Distortions of the circle produced by a wave with the '+' polarization. The two pictures represent the same wave at phases separated by 180°. Particles are positioned according to their proper distances from one another. (c) As (b) for the 'x' polarization.

Fig. 1.2.1 (from Thorne [1987] : The gravitational wave form produced by the gravitational collapse of an axisymmetric rotating star to produce a Kerr black hole, as computed by Piran and Stark (1986) using numerical relativity techniques. The star and the black hole it forms both have $J/M^2 = a/M = 0.63$ (where J is angular momentum and M is mass). The dashed curve is a fit, to the wave form, of a superposition of the waves from the two most slowly damped quadrupolar normal modes of a non-rotating hole with mass M, $h_+ \propto \mathrm{Real}\{A_1 e^{-i\omega_1 t} + A_2 e^{-i\omega_2 \tau}\}$ with $\omega_1 = (0.374-0.089i)/M$, $\omega_2 = (0.348-0.274i)/M$. The fitting amplitudes are $A_1 = -0.9-1.1i$, $A_2 = 0.9+1.4i$. Thus, these two modes are roughly equally excited by the collapse.

Fig.1.2.2 (from Schutz, 1986) : The expected signal from a pair of 1 M_O stars near coalescence. For ease of viewing, the frequency of the waves has been reduced by a factor of 20, but the relative rate at which the frequency and amplitude increase are realistic. The horizontal scale is in seconds, the vertical scale arbitrary. The zero of time is taken to be the point at which the frequency is 100 Hz (5 Hz as drawn here).

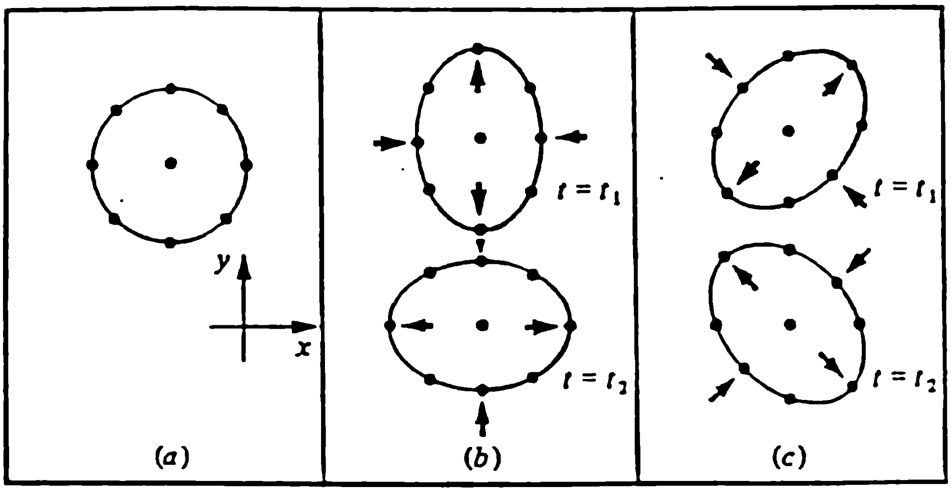

Fig. 1.1.1

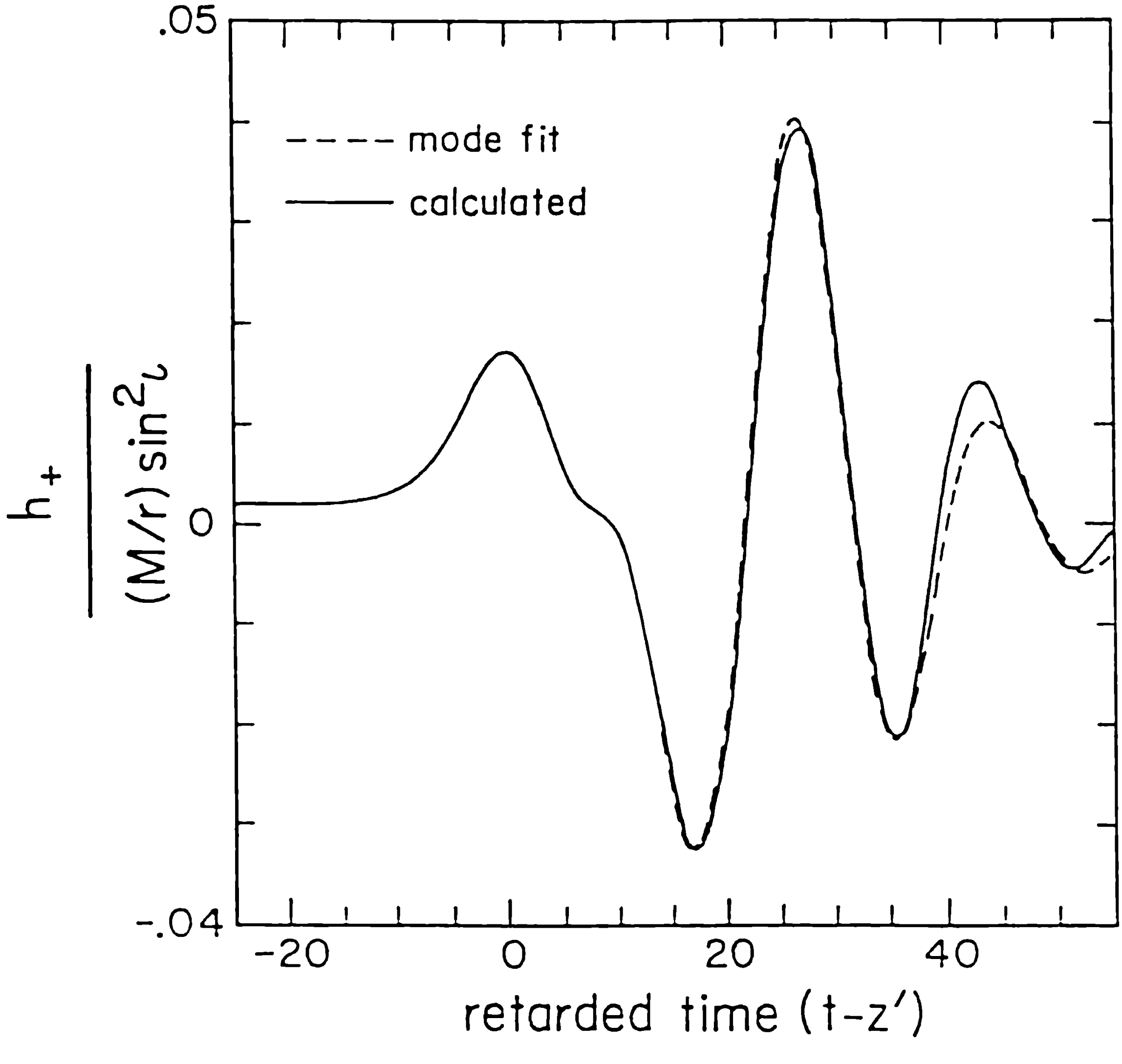

.05
0
-.04
---- mode fit
calculated
$\frac{h_+}{(M/r)\sin^2\iota}$
-20
0
20
40
retarded time (t-z′)

Fig. 1.2.1

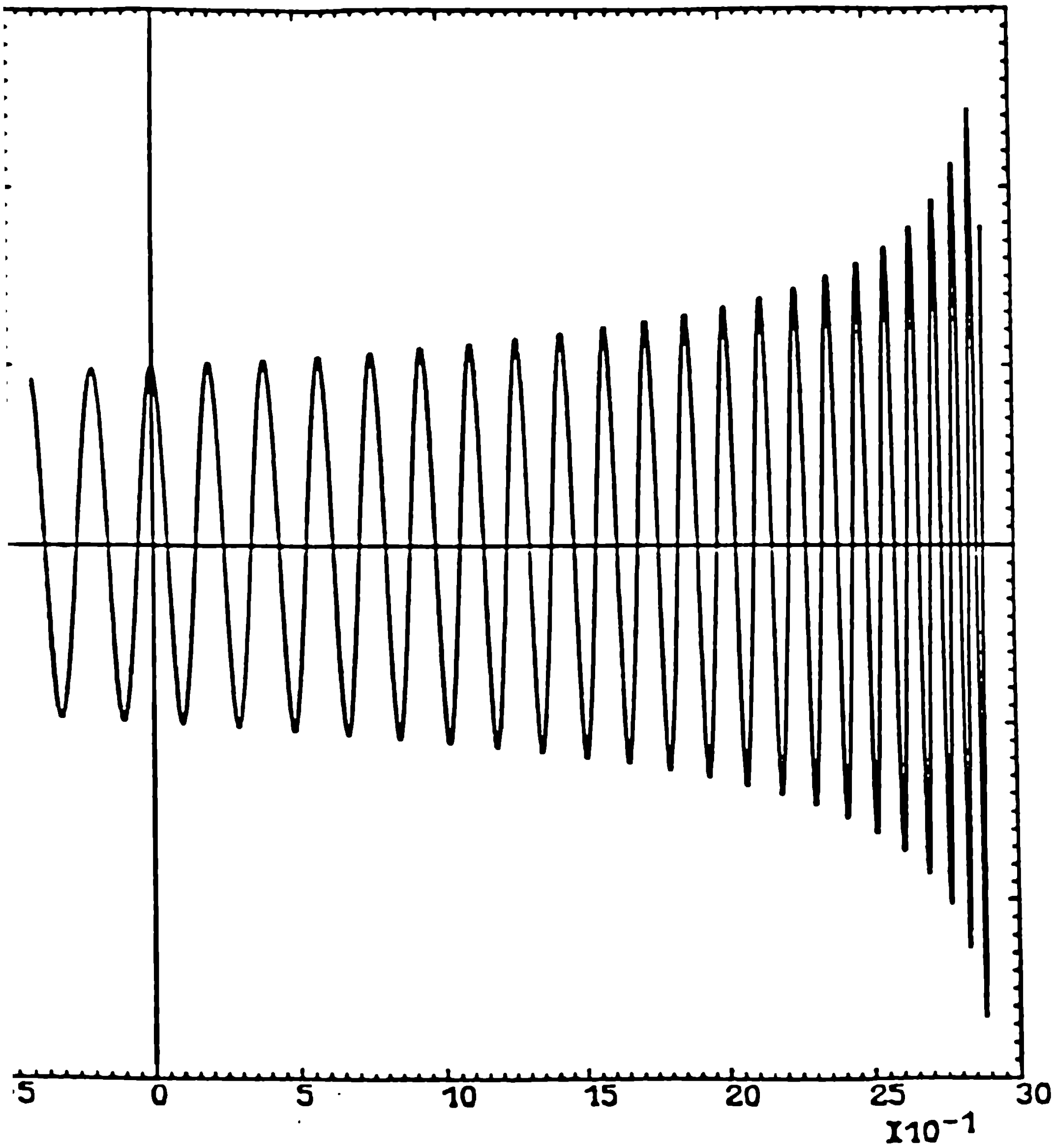

Fig. 1.2.2

Chapter 2

INTERFEROMETRIC DETECTION OF GRAVITATIONAL WAVES

INTRODUCTION

The basic and first idea of the interferometric detection of GW resides, clearly stated, in a paper of Gertsenshtein and Pustovoit [1963], their idea is "...it should be possible to detect gravitational waves by the shift of the bands in an optical interferometer". The first complete work on the noises competing with the GW signal in an interferometric antenna is due to Weiss [1972]; it is also his merit the idea of using a "stable" cavity such as the Herriot [1964] delay line, and fast light phase modulation for getting rid of the laser's amplitude fluctuations. But the very first experimental attempt, giving high sensitivity in the test masses displacement measurement, is due to Forward [1978]. Forward used retroflectors to reflect the beam back to a beam splitter and used active controls for locking the interferometer to a fringe; he obtained a spectral strain sensitivity of $\tilde{h} > 2.10^{-16}(Hz)^{-1/2}$ for $\nu > 2$ KHz.

The Munich Max Plank's group (Billing et al.[1979]) following Weiss' delay lines idea carried out the construction of a 30 m interferometer having a sensitivity $\tilde{h} \simeq 8.10^{-20}\ (Hz)^{-1/2}$.

The alternative method to delay lines is that of using Fabry-Perot cavities; this scheme, which was pursued by Drever (Drever et al.[1980] and [1981]), is very elegant even if it requires more sophisticated optical and feed back design than in the delay line case.

Two Fabry-Perot interferometers are now working in Glasgow and Caltech with a sensitivity $\tilde{h} \simeq 1.2\ 10^{-19}\ Hz^{-1/2}$ (Ward et al.[1987]) and $\tilde{h} \simeq 5.10^{-19}\ Hz^{-1/2}$ (Spero [1986]) respectively.

Several optical schemes have been invented for increasing the interferometer's sensitivity: light power recycling (Drever [1982]) allows the reuse of the unused interferometer's light, the synchronous recycling scheme (Ruggiero [1979], Drever [1981]) allows an increase in the interferometer's sensitivity to periodic signals as do the methods of Detuned recycling (Vinet et al.[1988]) and Dual recycling (Meers [1988]) .

Of all these schemes only that of power recycling has been tested experimentally (Rüdiger et al.[1987], Man et al.[1987]) with success. All the signal recycling schemes will be tested, perhaps painfully, in the future kilometric interferometers.

Another approach to an increase in sensitivity has been given by Caves [1980] who was the first to realize that photon number fluctuations in the interferometer's arms could be produced by vacuum fluctuations of the light field at the unused port of the beam splitter; the idea was to inject into this port a squeezed photon state i.e. a state having phase fluctuation smaller than the poissonian one but with larger amplitude fluctuation. The existence of these states has been demonstrated experimentally and this has led the Munich group (Gea-Banacloche and Leuchs [1987]) to experimentally explore the sqeezing route.

2.1) THE GENERATION OF GRAVITATIONAL WAVES (GW) AND THE TRANSVERSE TRACELESS GAUGE

In Einstein's Theory of General Relativity (TGR) (Einstein [1916]) Gravitational Waves (GW) are shown to be ripples in the space time curvature propagating with the speed of light. Under the hypothesis of weak fields a perturbation $h_{\mu\nu}$ to the flat metric tensor

$$\eta_{\mu\nu} = \begin{pmatrix} 1 & 0 & 0 & 0 \\ 0 & -1 & 0 & 0 \\ 0 & 0 & -1 & 0 \\ 0 & 0 & 0 & -1 \end{pmatrix} \qquad (2.1.1)$$

is created by the energy momentum tensor τ_{ik} according to the equation (see MTW)

$$\Box \Psi_{ik} = \frac{8\pi G}{c^4} \tau_{ik} \qquad (2.1.2)$$

where $\Psi_{ik} = h_{ik} - \frac{1}{2} \delta_{ik} h^{\mu}_{\mu}$. G is the Newton constant and c the speed of light.

From a momentum energy conservation

$$\partial_\mu \tau_{\mu\nu} = 0 \qquad (2.1.3)$$

and considering that $\tau_{00} = \rho c^2$, where ρ is the matter density, it follows (Landau and Lifshitz [1951])

$$\Psi_{\alpha\beta} = -\frac{2G}{c^4 R_0} \left[\frac{\partial^2}{\partial t^2} \int \rho \, x^\alpha x^\beta \, dv \right]_{t - \frac{R_0}{c}} \qquad (2.1.4)$$

where R_0 is the distance from the source; eq. (2.1.4) is valid when the matter speed is << c and when the GW wavelength is much larger than the source dimensions.

From eq. (2.1.4) it follows that the GW field is produced by the second moment of the mass distribution.
Since ψ_μ is a symmetric tensor it has 10 independent elements which are reduced to 6 since eq. (2.1.3) gives

$$\partial_\mu \psi_{\mu\nu} = 0 \qquad (2.1.5)$$

The number of independent elements of $\psi_{\mu\nu}$ can be further reduced by applying the coordinate transformation

$$x'_\mu = x_\mu + \varepsilon_\mu \qquad (2.1.6)$$

where ε_μ are infinitesimal functions which must leave unchanged the line element

$$ds^2 = g_{\mu\nu} dx^\mu dx^\nu \qquad (2.1.7)$$

Eq. (2.1.7) imposes

$$\Box \varepsilon_\mu = 0 \qquad (2.1.8)$$

and

$$h'_{\mu\nu} = h_{\mu\nu} - \frac{\partial \varepsilon_\mu}{\partial x_\nu} - \frac{\partial \varepsilon_\nu}{\partial x_\mu} \qquad (2.1.9)$$

Hence writing ψ_{ik} as a plane wave propagating in the $\vec{k}$ direction at speed c

$$\begin{cases} \psi_{ik} = A_{ik} e^{ik_r x^r} \\ k^r k_r = 0 \end{cases} \qquad (2.1.10)$$

and putting (see eq. (2.1.9))

$$\varepsilon_\mu = C_\mu \, e^{ik_r x^r} \qquad (2.1.11)$$

we can define a 4 velocity V^k and choose C_μ such as to give

$$A_{ik} V^k = 0 \qquad (2.1.12)$$

But these four equations are not independent since $k^i A_{ik} V^k = 0$ for any given k hence a further condition can be applied and we impose

$$A^{\mu}_{\mu}=0 \tag{2.1.13}$$

This condition gives $h^{\mu}_{\mu} = 0$ and

$$\psi_{\mu\nu} = h_{\mu\nu} \tag{2.1.14}$$

Eq.s (2.1.5), (2.1.12), (2.1.13) define the Transverse Traceless (TT) gauge (see MTW); by choosing $V^0 = 1$, $\vec{V} = 0$ we obtain

$$
\begin{aligned}
&h^{TT}_{\mu 0}=0 && \text{i.e only spatial components} \neq 0 \\
&h^{TT}_{KJ,J}=0 && \text{i.e. divergence free spatial components} \\
&h^{TT}_{KK}=0 && \text{traceless}
\end{aligned}
\tag{2.1.15}
$$

Let us assume the wave propagates along the x_3 axis, then

$$k = (k,00,k) \tag{2.1.16}$$

and from eq. (2.1.15) it follows

$$h^{TT}_{3K}=0 \qquad h^{TT}_{11}=-h^{TT}_{22}=0 \qquad h^{TT}_{12}=h^{TT}_{21} \tag{2.1.17}$$

In matrix form

$$h^{TT}_{ik} = \begin{pmatrix} 0 & 0 & 0 & 0 \\ 0 & h^{TT}_{11} & h^{TT}_{12} & 0 \\ 0 & h^{TT}_{12} & -h^{TT}_{11} & 0 \\ 0 & 0 & 0 & 0 \end{pmatrix} = h^{TT}_{11} \begin{pmatrix} 0 & 0 & 0 & 0 \\ 0 & 1 & 0 & 0 \\ 0 & 0 & -1 & 0 \\ 0 & 0 & 0 & 0 \end{pmatrix} +$$

$$+ h^{TT}_{12} \begin{pmatrix} 0 & 0 & 0 & 0 \\ 0 & 0 & 1 & 0 \\ 0 & 1 & 0 & 0 \\ 0 & 0 & 0 & 0 \end{pmatrix} = A_{+}\, e^{+}_{ik} + A_{x}\, e^{x}_{ik} \tag{2.1.18}$$

The two polarizations e^{+}_{ik} and e^{x}_{ik} are exchanged by a rotation R of $\frac{\pi}{4}$ around the x_3 axis i.e.:

$$R\left(\frac{\pi}{4}\right) = \frac{1}{\sqrt{2}} \begin{pmatrix} 0 & 0 & 0 & 0 \\ 0 & 1 & 1 & 0 \\ 0 & -1 & 1 & 0 \\ 0 & 0 & 0 & 0 \end{pmatrix}$$

$$R\left(\frac{\pi}{4}\right) e^{+} \; R^{-1}\left(\frac{\pi}{4}\right) = -e^{\times} \qquad (2.1.19)$$

$$R\left(\frac{\pi}{4}\right) e^{\times} \; R^{-1}\left(\frac{\pi}{4}\right) = e^{+}$$

This behaviour under rotation is proper to a spin 2 field.
The Riemann tensor

$$R_{iklm} = \frac{1}{2}\left(\frac{\partial^2 h_{im}}{\partial x^k \, \partial x^l} + \frac{\partial^2 h_{kl}}{\partial x^i \, \partial x^m} - \frac{\partial^2 h_{km}}{\partial x^i \, \partial x^l} - \frac{\partial h^2_{il}}{\partial x^k \, \partial x^m}\right) \qquad (2.1.20)$$

with the conditions of eq. (2.1.11) becomes simply

$$R_{iklm} \Rightarrow R_{0\alpha 0\beta} = -\frac{1}{2} \ddot{h}^{TT}_{a\beta} \qquad (2.1.21)$$

The TT part of the eq. (2.1.4) can be evaluated by applying to $\psi_{\alpha\beta}$ the TT projection operator (see MTW)

$$P_{jk} = \delta_{jk} - n_j \, n_k \qquad (2.1.22)$$

where $\bar{n}$ is the unit vector in the direction in which we want to evaluate the TT part of the GW amplitude; hence

$$\psi^{TT}_{\alpha\beta} = P_{\alpha j} \, \psi_{jl} \, P_{l\beta} - \frac{1}{2} P_{\alpha\beta} \, \psi_{lm} \, P_{lm} \qquad (2.1.23)$$

It is easy to verify that from eq.s (2.1.23), (2.1.4), (2.1.15) it follows $\psi^{TT}_{\alpha\beta} \, n_\beta = 0$, $\psi^{TT}_{\alpha\alpha} = 0$ and

$$h^{TT}_{\alpha\beta} = -\frac{2G}{c^4 R_0}\left[\frac{\partial^2}{\partial t^2}\int \rho \left(P_{\alpha j} \, x^j \, x^l P_{l\beta} - \frac{1}{2} P_{\alpha\beta} \, x^l \, x^m P_{lm}\right) dv\right] =$$

$$= -\frac{2G}{c^4 R_0} \ddot{D}^{TT}_{\alpha\beta} \qquad (2.1.24)$$

where $D_{\alpha\beta}$ is the reduced quadrupole momentum of the GW emitting mass system.

2.2) THE DETECTION OF GW

A particle moving freely under the action of a gravitational force has its coordinates x^{μ} satisfying the geodesic equation

$$\frac{d^2x^{\mu}}{d\tau^2}+\Gamma^{\mu}_{\nu\lambda}\frac{d\,k^{\nu}}{d\,\tau}\frac{d\,x^{\lambda}}{d\,\tau}=0 \tag{2.2.1}$$

where τ is proportional to the particle's proper time and

$$\Gamma^{\mu}_{\nu\lambda}=\frac{1}{2}g^{\mu m}\left\{\frac{\partial\, g_{m\nu}}{\partial\, x^{\lambda}}+\frac{\partial\, g_{m\lambda}}{\partial\, x^{\nu}}-\frac{\partial\, g_{\nu\lambda}}{\partial\, x^{m}}\right\} \tag{2.2.2}$$

are the Christoffel symbols

It is always possible to find a space time trajectory in which $\Gamma^{\mu}_{\nu\lambda}=0$ at any time; along this trajectory the particle is freely falling.

It's easy to show that the separation ξ^{α} between two particles A and B satisfy the geodesic deviation equation

$$\frac{D^2\,\xi^{\alpha}}{d\,\tau^2}+R^{\alpha}_{\beta\gamma\delta}\,\xi^{\gamma}\,\frac{d\,x^{\beta}}{d\tau}\,\frac{d\,x^{\delta}}{d\tau}=0 \tag{2.2.3}$$

where D^2 is the second covariant derivative

$$\frac{D^2\,\xi^{\alpha}}{d\,\tau^2}=\frac{d^2\,\xi^{\alpha}}{d\,\tau^2}+\frac{d\,\Gamma^{\alpha}_{\beta\mu}}{d\,\tau}\,\xi^{\beta}\,\frac{dx^{\mu}}{d\,\tau}+\Gamma^{\alpha}_{\beta\mu}\,\frac{d}{d\,\tau}\left(\xi^{\beta}\,\frac{dx^{\mu}}{d\,\tau}\right)+$$

$$\Gamma^{\alpha}_{\beta\mu}\left[\frac{d\,\xi^{\beta}}{d\,\tau}+\Gamma^{\alpha}_{\beta\mu}\,\xi^{\beta}\,\frac{dx^{\mu}}{d\,\tau}\right]\frac{dx^{\mu}}{d\,\tau} \tag{2.2.4}$$

With the purpose of evaluating ξ^{α} let's put $\bar{x}=0$ in the center of mass system (CMS) of particle A, (see MTW), the time x_0 equal to the proper time τ and the coordinate axis connected to gyroscopes carried by A. At $\bar{x}=0$, since A is freely falling along the geodesic line we obtain:

$$\left(\Gamma^{\alpha}_{\beta\gamma}\right)_{\bar{x}=0} = \left(\frac{d\,\Gamma^{\alpha}_{\beta\gamma}}{d\,\tau}\right)_{\bar{x}=0} = 0 \tag{2.2.5}$$

and eq. (2.2.2) becomes

$$\frac{D^2\,\xi^{\alpha}}{d\,\tau^2} = \frac{d^2\,\xi^{\alpha}}{d\,\tau^2} \tag{2.2.6}$$

Introducing eq.s (2.1.21) and (2.2.6) in eq (2.2.3) and considering that to first order in $h^{TT}_{\mu\nu}$ $t \equiv \tau$, where t is the observation time; we obtain

$$\frac{d^2\,\xi^{\alpha}}{d\,t} = -R_{\alpha\,0\,\beta\,0}\;\xi^{\beta} = \frac{1}{2}\,\frac{d^2}{d\,t^2}\,h^{TT}_{\alpha\beta}\;\xi^{\beta} \tag{2.2.7}$$

From eq. (2.2.7) we can see the effects of the GW polarization on the detector; if the GW is propagating along the z axis and the masses A and B are located as in Fig. 2.2.1, then

$$\xi^{\alpha} = (x_A - x_B)^{\alpha} \tag{2.2.8}$$

Putting

$$F_{\alpha} = M\,\frac{d^2\,\xi^{\alpha}}{d\,t^2} = \frac{1}{2}\,M\,\frac{d^2}{d\,t^2}\,h^{TT}_{\alpha\beta}\;\xi^{\beta} \tag{2.2.9}$$

and considering that the only independent components of $h^{TT}_{\alpha\beta}$ are h^{TT}_{11} and h^{TT}_{12} we can write the projection F of F_{α} along the line connecting A to B:

$$F(\theta,\phi) = \frac{F_{\alpha}\,\xi^{\alpha}}{|\xi|} = \frac{|\xi|}{2}\,M\,\left\{\ddot{h}^{TT}_{11}\;\sin^2\theta\cos 2\varphi + \ddot{h}^{TT}_{12}\;\sin^2\theta\sin 2\varphi\right\} \tag{2.2.10}$$

In eq. (2.2.10) the tidal character of the force produced by a GW is clearly shown by the term $|\xi|$. It is also evident from eq. (2.2.10) that $F = 0$ if the mass separation ξ^{α} is in the GW propagation direction.

In the interferometric antenna the mirrors are attached to masses suspended with wires like pendula. With reference to Fig. 2.2.2, the beam splitter in the axis origin has mass m_1 and the other two mirrors have mass m_2 and m_3 respectively and are placed at a distance L from the axis origin; $\vec{\xi}_i$ are the distances of the mass m_i from the CMS.

The CMS coordinates are

$$x_{cms} = \frac{L\, m_3}{m_1 + m_2 + m_3} \qquad y_{cms} = \frac{L\, m_2}{m_1 + m_2 + m_3} \tag{2.2.11}$$

For the sake of simplicity we assume that the GW is propagating along the z axis; under this condition, using eq. (2.2.7), the mirror's acceleration produced by the GW interaction becomes

$$\begin{aligned}
(\ddot{x}_1)_{GW} &= -\frac{1}{2}\left(\ddot{h}^{TT}_{11}\, x_{cms} + \ddot{h}^{TT}_{12}\, y_{cms}\right)\\
(\ddot{x}_3)_{GW} &= -\frac{1}{2}\left(\ddot{h}^{TT}_{11}(L - x_{cms}) - \ddot{h}^{TT}_{12}\, y_{cms}\right)\\
(\ddot{y}_1)_{GW} &= -\frac{1}{2}\left(\ddot{h}^{TT}_{21}\, x_{cms} + \ddot{h}^{TT}_{22}\, y_{cms}\right)\\
(\ddot{y}_2)_{GW} &= \frac{1}{2}\left(-h_{21}\, x_{cms} + h^{TT}_{22}(L - y_{cms})\right)
\end{aligned} \tag{2.2.12}$$

The mirror motion equations read

$$\begin{aligned}
\ddot{x}_1 + \frac{1}{\tau_1}(\dot{x}_1 - \dot{\bar{x}}_1) + \frac{g}{l_1}(x_1 - \bar{x}_1) &= (\ddot{x}_1)_{GW}\\
\ddot{x}_3 + \frac{1}{\tau_3}(\dot{x}_3 - \dot{\bar{x}}_3) + \frac{g}{l_3}(x_3 - \bar{x}_3) &= (\ddot{x}_3)_{GW}\\
\ddot{y}_1 + \frac{1}{\tau_1}(\dot{y}_1 - \dot{\bar{y}}_1) + \frac{g}{l_1}(y_1 - \bar{y}_1) &= (\ddot{y}_3)_{GW}\\
\ddot{y}_2 + \frac{1}{\tau_2}(\dot{y}_2 - \dot{\bar{y}}_2) + \frac{g}{l_2}(y_2 - \bar{y}_2) &= (\ddot{y}_2)_{GW}
\end{aligned} \tag{2.2.13}$$

where τ_i and l_i are, respectively, the relaxation time and the length of the i-th pendulum and $\bar{x}_i$, $\bar{y}_i$ are the pendula suspension point displacements due to seismic noise.

Eq. (2.2.13) can be solved exactly, but for sake of simplicity we assume $\tau_i = \tau_j$ and $l_i = l_j$, then we can subtract the first equation from the second and the third from the fourth, obtaining

$$\begin{aligned}
\Delta\ddot{x} + \frac{1}{\tau}(\Delta\dot{x} - \Delta\dot{\bar{x}}) + (\Delta x - \Delta\bar{x})\,\omega_0^2 &= -\frac{1}{2}\,\ddot{h}^{TT}_{11}\, L\\
\Delta\ddot{y} + \frac{1}{\tau}(\Delta\dot{y} - \Delta\dot{\bar{y}}) + (\Delta y - \Delta\bar{y})\,\omega_0^2 &= -\frac{1}{2}\,\ddot{h}^{TT}_{22}\, L
\end{aligned} \tag{2.2.14}$$

where $\Delta x = x_1 - x_3$, $\Delta y = y_1 - y_2$, $\Delta\bar{x} = \bar{x}_1 - \bar{x}_3$ and $\Delta\bar{y} = \bar{y}_1 - \bar{y}_2$, $\omega_0^2 = g/l$ and $\tau = \tau_i$.

In a single pass interferometer the phase change is

$$\Delta\varphi = 4\pi \frac{(\Delta x - \Delta y)}{\lambda} \tag{2.2.15}$$

where λ is the light wave length; hence considering that when the GW is propagating along the z axis $h_{11}^{TT} = -h_{22}^{TT}$ and putting $\Delta\bar{\varphi} = 4\pi(\Delta\bar{x} - \Delta\bar{y})/\lambda$ we obtain

$$\Delta\ddot{\varphi} + \frac{1}{\tau}\left(\Delta\dot{\varphi} - \Delta\dot{\bar{\varphi}}\right) + \omega_0^2\left(\Delta\varphi - \Delta\bar{\varphi}\right) = \frac{4\pi}{\lambda}\ddot{h}_{11} L \tag{2.2.16}$$

This equation can be easily integrated giving (Pizzella [1975])

$$\Delta\varphi(t) = \frac{4\pi L}{\lambda\,\tilde{\omega}_0}\int_0^t \sin\tilde{\omega}_0(t-\eta)\, e^{-\frac{t-\eta}{2\tau}}\left[\ddot{h}_{11}^{TT}(\eta) + \frac{1}{\tau}\Delta\dot{\bar{\varphi}}(\eta) + \omega_0^2\Delta\bar{\varphi}(\eta)\right] d\eta$$

$$\tilde{\omega}_0 = \sqrt{\omega_0^2 - \frac{1}{4\tau^2}} \tag{2.2.17}$$

For understanding the effect of the GW on $\Delta\varphi$ we can neglect the seismic noise contribution and study the behaviour of eq. (2.2.17) assuming two simple functional characters for $h(t) = h_{11}^{TT}(t)$. In the first case we assume $h(t)$ to be a pulse having a duration $\Delta t << 1/\omega_0$ and amplitude h_0:

$$h(\eta) = h_0\left[\theta(\eta) - \theta(\eta - \Delta t)\right] \tag{2.2.18}$$

Inserting eq. (2.2.18) in eq. (2.2.17) and assuming the pendula mechanical quality factor $Q = \omega_0 \cdot \tau >> 1$ we obtain

$$\Delta\varphi(t) = \frac{4\pi L}{\lambda} h(t) + \frac{4\pi L}{\lambda} h_0 \left\{\omega_0 \Delta t \sin(\omega_0 t)\, e^{-\frac{t}{\tau}} + O\left((\omega_0 \Delta t)^2\right) + O\left(\frac{1}{Q^2}\right)\right\} \tag{2.2.19}$$

Eq. (2.2.19) shows that in the interferometric detector the measurement of $\Delta\varphi$ gives a precise measure of $h(t)$; the term in h_0, which represents the "memory" that the pendula have of the GW for $t>\Delta t$, being multiplied by $\omega_0 \Delta t<<1$, can be neglected.

In the second case we consider a periodic GW having amplitude

$$h(t) = h_0 e^{-i\Omega_g t} \tag{2.2.20}$$

Inserting h(t) in eq. (2.2.16) we obtain for $t >> \tau$

$$\Delta\varphi = \frac{4\pi L}{\lambda} \frac{\Omega_g^2 e^{i\Omega_g t} h_0}{\omega_0^2 - \Omega_g^2 + \frac{i\Omega_g}{\tau}} \tag{2.2.21}$$

For $\Omega_g > \omega_0$ and Q>>1, eq. (2.2.20) becomes

$$\Delta\varphi = \frac{4\pi L}{\lambda} h_0 e^{i\Omega_g t} \tag{2.2.22}$$

Eq. (2.2.22) shows that with an interferometric detector it is possible to measure distortionless h(t) even for a periodic GW; hence the very peculiarity of this detector is due to the low value of the pendula resonance frequency ν_0, which can be made as low as few Hz, giving the possibility, in principle, to detect low frequency GW. Furthermore the possibility of making L very large (some Km), in virtue of eq. (2.2.9), would allow the operation of the antenna at room temperature while maintaining high sensitivity even in presence of noises, such as the thermal one, which are dominant at low frequency.

For the evaluation of the phase shift due to the GW interaction of photon beam bouncing between two mirrors, it is opportune to choose a coordinate system in which the mirrors are at rest; in this system the only GW interaction with the photon beam is due to the metric coefficients change.

In fact if the mirrors are freely falling (i.e.: with suspensions having no rigidity), then in the TT system they are at rest; this is easily shown considering that to first order in $h_{\alpha\beta}^{TT}$ from eq.s (2.2.2) and (2.2.4) it follows

$$\Gamma^{\alpha}_{\beta\mu} \Rightarrow \Gamma^{\alpha}_{\beta o} = -\frac{1}{2} \dot{h}^{TT}_{\alpha\beta}$$

$$\frac{D^2\xi^{\alpha}}{d\tau^2} = \frac{d^2\xi^{\alpha}}{dt^2} - \frac{1}{2}\ddot{h}^{TT}_{\alpha\beta}\xi^{\beta} = -R^{\alpha}_{0\gamma 0}\xi^{\gamma} = -\frac{1}{2}\ddot{h}^{TT}_{\alpha\beta}\xi^{\beta} \tag{2.2.23}$$

and hence $\left(\ddot{\xi}^{\alpha}\right)_{TT} = 0$.

A matrix approach method, used extensively for the evaluation of the phase shift due to GW interaction with a photon bouncing between freely falling mirrors is due to Vinet [1986]. The method is based on the consideration that due to eq. (2.2.23) the only effect of the GW on a photon is contained in the perturbed ds^2

$$ds^2 = c^2\,dt^2 - (1+h(t))\,dx^2 - (1-h(t))\,dy^2 \qquad (2.2.24)$$

where $h(t) = h\cos\phi$, with $\phi = \Omega_g t + \varphi$ and the photon is supposed to travel along the x or y axis.

If the photon is scattered back by a mirror at distance $x=L$, then from eq. (2.2.24) it follows that the round trip retarded time is

$$t_r = t - \frac{2L}{c} - \varepsilon h \frac{L}{c} \frac{\sin\eta}{\eta} \cos(\phi-\eta) \qquad (2.2.25)$$

where $\eta = \Omega_g L/c$ and $\varepsilon = \pm 1$ if the photon is travelling along x or y respectively.

If the time dependent part of the EM fields along the trajectory is taken to be

$$A(t) = \left(A_0 + \frac{1}{2} h\, e^{i\phi} A_1 + \frac{1}{2} h\, e^{-i\phi} A_2\right) e^{-i\omega t} \qquad (2.2.26)$$

where $\omega = 2\pi\nu_0$ (ν_0 = Laser frequency) then substituting eq. (2.2.25) in eq. (2.2.26) gives (to first order in h)

$$A(t) = e^{i\omega\left(\frac{2L}{c} - t\right)} \left[A_0 + \frac{h}{2} e^{i\phi} \left(A_1\, e^{-i2\Omega_g \frac{L}{c}} + i\omega\varepsilon \frac{L}{c} \frac{\sin\eta}{\eta} e^{-i\eta} A_0\right) + \frac{h}{2} e^{-i\phi} \left(A_2 e^{i2\Omega_g \frac{L}{c}} + i\omega\varepsilon \frac{L}{c} \frac{\sin\eta}{\eta} e^{i\eta} A_0\right.\right.$$

$$(2.2.27)$$

This can be put in matrix form

$$\begin{pmatrix} A_0 \\ A_1 \\ A_2 \end{pmatrix}' = D \begin{pmatrix} A_0 \\ A_1 \\ A_2 \end{pmatrix} \qquad (2.2.28)$$

where

$$D = x \begin{pmatrix} 1 & 0 & 0 \\ i\varepsilon\xi \frac{\sin\eta}{\eta} e^{-i\eta} & \bar{y} & 0 \\ i\varepsilon\xi \frac{\sin\eta}{\eta} e^{i\eta} & 0 & y \end{pmatrix} \qquad (2.2.29)$$

and $\xi = \omega L/c$, $x = e^{2i\xi}$, $y = e^{2i\eta}$.

This approach can be applied to interferometric GW detectors because in these kind of antenna the observation frequency is always above the mirror suspension mode frequencies, hence the mirrors can be considered as being freely falling.

2.3) DELAY LINES (DL) INTERFEROMETERS

The necessity of increasing the interferometer phase shift due to a GW signal, is dictated by the existence of noises which are affecting purely the phase of the optical rays without creating real displacements of the mirrors.
To overcome the effects due to these noises, that will be named "phase noises" in contrast to "displacement noises" , it is very important to find an optical scheme allowing the beams to bounce back and forth in the optical cavities.
Actually the ultimate phase noise is the photon counting noise $\Delta\phi_{PC}(t)$ due to the anticorrelated fluctuations Δn of the photon number n in the interferometers arms according to the uncertainty relation

$$\left\langle \Delta\phi_{PC}(t)^2 \right\rangle^{1/2} = \Delta\phi_{PC} \geq \frac{1}{\Delta n} \qquad (2.3.1)$$

For a photon coherent state $\Delta n = \sqrt{n}$, hence

$$\Delta\phi_{PC} \geq \frac{1}{\sqrt{n}} = \sqrt{\frac{h\,\nu_0}{W_{eff}\,t}} \qquad (2.3.2)$$

where h is Planck's constant; ν_0 the laser frequency, W_{eff} the light power in the interferometer arms and t the measurement time.
If the light makes 2N reflections (see Fig. 2.3.1) the phase shift due to the mirror displacement $\Delta x_{1,2} = \pm \frac{h(t)}{2} L$ is

$$\varphi_{1,2} = \frac{4N\pi}{\lambda}\Delta x + \bar{\varphi}_{1,2} = \varphi_{s/2} + \bar{\varphi}_{1,2} \qquad (2.3.3)$$

where $\bar{\varphi}_{1,2}$ are given fixed phase shifts in the two arms and Δx has been evaluated in the limit $\Omega_g \frac{L}{c} \ll 1$.
With reference to Fig. 2.3.1 the recombined beams carry the powers

$$W_\pm = R^{4N}\frac{W}{2}\left(1 \pm \cos\left(\varphi_s + \varphi_0 + \Delta\phi_{PC}\right)\right) \qquad (2.3.4)$$

where R^2 is the intensity reflectivity of the mirrors, $\varphi_0 = \bar{\varphi}_1 - \bar{\varphi}_2$ and $\Delta\phi_{PC}$ has been evaluated for $W_{eff} = WR^{4N}$.

Putting $\varphi_0 = \frac{\pi}{2}$, measuring W± with photodiodes PD having efficiency η and forming the current difference, we obtain

$$\Delta I^2 \cong I_0^2\left[\left(\frac{4N\pi}{\lambda}h(t)L\right)^2 + \Delta\phi_{PC}^2\right] + \Delta I_{SN}^2 \qquad (2.3.5)$$

where $I_0 = \frac{W_e}{h\nu_0}\eta R^{4N}$ and $\Delta I_{SN} = e\sqrt{\frac{WR^{4N}}{t\,h\,\nu_0}\eta(1-\eta)}$ are the photodiode mean current and current fluctuation respectively; e is the electric charge.
The GW detection condition, introducing eq. (2.3.2) in eq. (2.3.5) and using eq. (2.3.3), reads

$$h(t) > \frac{\lambda}{4N\pi L}\sqrt{\frac{h\nu_0}{Wt\eta R^{4N}}} \qquad (2.3.6)$$

where the assumption $2\Omega_g\frac{NL}{c} \ll 1$ has been made. Eq. (2.3.6) shows that 2N reflections increase accordingly the S/N ratio for the photon counting noise.
The DL scheme was first studied by Herriot et al. [1964]; the laser beam is entering into the cavity through a hole in the near mirror with coordinate (x_0,y_0) and slopes (x'_0, y'_0) (see Fig. 2.3.2) and is reflected back and forth between the mirrors having distance L and focal length f respectively.
Defining

$$\cos\theta = 1 - \frac{L}{2f} \qquad (2.3.7)$$

where θ is the rotation angle of the beam spot on the mirrors (see Fig. 2.3.3), the coordinates of the n-th spot are

$$\begin{aligned} x_n &= x_0\cos n\theta + \sqrt{\frac{L}{4f-L}}\left(x_0+2f\,x'_0\right)\sin n\theta \\ y_n &= y_0\cos n\theta + \sqrt{\frac{L}{4f-L}}\left(y_0+2f\,y'_0\right)\sin n\theta \end{aligned} \qquad (2.3.8)$$

$$4f-L > 0$$

which can be put in the form

$$\begin{aligned} x_n &= A\sin(n\theta+\alpha) \\ y_n &= B\sin(n\theta+\beta) \end{aligned} \qquad (2.3.9)$$

where

$$A^2 = \frac{4f}{4f-L}\left(x_0^2 + Lx_0\left(x_0'\right) + Lf\left(x_0'\right)\right)^2$$

$$tg\alpha = \sqrt{\frac{4f}{L}-1}\ \frac{1}{1+2f\frac{x_0'}{x_0}} \qquad (2.3.10)$$

and similarly for B and β.

If A=B the spots lies on a circle; the beam reentrance condition is fulfilled when

$$2k\theta = 2J\pi \qquad J, k \text{ integers } J \neq k \qquad (2.3.11)$$

k being the number of spot on a single mirror.

The DL is a very flexible method to cope with the misalignments due to the mirror movements (Goorvitch [1975], Billing et al.[1979]). Fattaccioli et al.[1986] have shown that the total optical phase shift is independent upon tiltings ($\Delta\vartheta$) and transversal mutual mirror translations (Δx) up to second order in $\frac{\Delta x}{R}$, and $\Delta\vartheta$ respectively, R being the radius of the spot circle on the mirrors, if the DL is perfectly reentrant and aligned.

With the purpose of reducing the light scattering from the entrance hole in the mirrors close to the beam splitter (Schilling et al.[1981]), the size of the input beam should be sufficiently reduced increasing the beam angular spreads $\Delta x'_c$ and $\Delta y'_c$.

The spot diameters due to these spreads

$$\Delta x_n = \sqrt{\frac{L}{4f-L}}\ 2f \sin n\theta \quad \Delta x'_0$$
$$\Delta y_n = \sqrt{\frac{L}{4f-L}}\ 2f \sin n\theta \quad \Delta y'_0 \qquad (2.3.12)$$

do not increase indefinitely with N but vary cyclically with n; this focusing characteristic is very relevant for avoiding the beam size divergence when N is large, and careful evaluation of the beam entrance parameters is needed to avoid geometrical overlapping of the spots.

Actually two contiguous spots on a mirror are associated with different delays; if they do overlap the light diffused by the mirror coatings is sent in the wrong beam then causing noise due to the finite size of the laser line width.

The calculation of the light phase shift due to a GW interaction in a DL without the constraint $2\Omega_g \frac{NL}{c} << 1$ has been done by Vinet [1986] and Vinet et al.[1988].

Let's consider a D.L. of length L in which the beam is making 2N reflections and having iR_1 and iR_2 amplitude reflectivity mirrors. By repeated application of the operator D (see eq. (2.2.29)) we obtain the 2N reflection operator.

$$iM = (iR_1)^{N-1}(iR_2)^N D^N =$$

$$= (-)^{N-1}(R_1)^{N-1} R_2^N x^N \begin{pmatrix} 1 & 0 & 0 \\ i\varepsilon\xi\frac{\sin\eta N}{\eta} e^{-i\eta} & y^{-N} & 0 \\ i\varepsilon\xi\frac{\sin\eta N}{\eta} e^{i\eta} & 0 & y^N \end{pmatrix} \tag{2.3.13}$$

where the signal is contained in the two matrix elements M_{12} and M_{13} ; by putting

$$\tau_s = 2\frac{NL}{c} \tag{2.3.14}$$

we see that the M_{12} and M_{13} maximum happens when

$$\eta N = \frac{\Omega_g \tau_s}{2} = \frac{\pi}{2} \tag{2.3.15}$$

while the signal is zero when

$$\frac{\tau_s \Omega_g}{2} = n\pi \quad (n= 1,2...)$$

From eq.s (2.2.27) and (2.3.7) it follows that the maximum phase shift $\Delta\phi_{DL}$ of the light wave due to the GW interaction in two DL (see Fig. 2.3.1) is

$$\Delta\phi_{DL} = 2h\omega\frac{L}{c}\frac{\sin \Omega_g \frac{L}{c} N}{\Omega_g \frac{L}{c}} \tag{2.3.16}$$

2.4) FABRY PEROT (FP) INTERFEROMETERS

The FP theory is largely described in many books (see for example Born and Wolf [1964], Hernandez [1986]); with reference to Fig. 4.1, M_1 and M_2 are two mirrors located at positions x_1 and x_2 respectively $[x_2 - x_1 = L]$; the amplitude reflectance iR_i , the transmittance T_i and the loss B_i of the mirrors satisfy the relation

$$T_i^2 + R_i^2 + B_i^2 = 1 \qquad i=1,2$$

A light beam of frequency $\nu_0 = \frac{\omega_0}{2\pi}$ entering the cavity with amplitude A_0 is partially transmitted with amplitude A_t and partially reflected with amplitude A_r.

If A_2 and A_3 are the transmitted and reflected waves amplitude inside the cavity, then

$$A_r = iR_1 A_0 + T_1 A_3$$

$$A_2 = T_1 A_0 + iR_1 A_3 \qquad (2.4.1)$$

$$A_3 = iR_2 D A_2$$

where D is defined in eq. (2.29).

The solution is

$$A_r = i\left(R_1 + \left(R_1^2+T_1^2\right) R_2 D\right)\left(1 + R_1 R_2 D\right)^{-1} A_0 = iF A_0 \qquad (2.4.2)$$

An evaluation of F gives the relevant matrix elements (Vinet [1986])

$$F_{11} = i\,\frac{R_1 + \left(R_1^2+T_1^2\right) R_2 x}{1 - R_1 R_2 x}$$

$$F_{21} = \frac{\varepsilon T_1^2 R_2 \xi \frac{\sin\eta}{\eta}}{\left(1 - R_1 R_2 x\right)} \frac{e^{-i\eta} x}{\left(1 - R_1 R_2 x \bar{y}\right)} \qquad (2.4.3)$$

$$F_{31} = \frac{\varepsilon T_1^2 R_2 \xi \frac{\sin\eta}{\eta}}{\left(1 - R_1 R_2 x\right)} \frac{e^{i\eta} x}{\left(1 - R_1 R_2 x y\right)}$$

where x and y have been defined in eq. (2.29).

From eq.s (2.27) and (2.4.3) it is possible to evaluate the maximum phase shift $\Delta\phi_{FP}$ for a cavity configuration similar to the one shown in Fig. 2.3.1 under the condition x=+1 (optical resonance condition):

$$\left(\Delta\phi_{FP}\right) = 2\,\frac{\left(T_1^2 R_2\right) h\,\omega \frac{L}{c}}{\left(1-R_1 R_2\right)^2} \frac{1}{\sqrt{1+F' \sin^2 \frac{\Omega_g L}{c}}} \qquad (2.4.5)$$

where $F' = \frac{4R_1R_2}{(1-R_1R_2)^2}$, $T_2 << T_1$ and the realistic condition $\Omega_g \frac{L}{c} << 1$ has been assumed. In analogy to eq. (2.3.8), defining the cavity storage time

$$\tau_s = 2\frac{L}{c}\frac{\sqrt{R_1 R_2}}{1-R_1 R_2} \qquad (2.4.6)$$

making the approximation $R_i \cong 1 - \frac{T_i^2 + B_i^2}{2}$ and putting $B_i << T_i$ we finally obtain

$$\left|\Delta\phi_{FP}\right| \cong \omega h \tau_s \frac{2\,T_1^{\,2}}{T_1^{\,2}+T_2^{\,2}}\sqrt{\frac{R_2}{R_1}}\;\frac{1}{\sqrt{1+\Omega_g^2\tau_s^2}} \qquad (2.4.7)$$

The comparison between $\left|\Delta\phi_{DL}\right|$ and $\left|\Delta\phi_{FP}\right|$ is shown in Fig. 2.4.2; $\left|\Delta\phi_{FP}\right|$ is plotted for $T_2 << T_1$; this experimental condition is particularly useful in the interferometers using light recycling because very little power is flowing out of the far mirror.

2.5) THE NOISE DUE TO PHOTON COUNTING ERROR AND POWER RECYCLING

In paragraph 2.3) we have shown how the phase fluctuations in the two interferometer's arms are producing noise; in particular the fluctuation of the photodiodes currents (see eq. (2.3.5)) ΔI_{SN} , have been considered as a source of photon counting error. But also in the case $\Delta I_{SN}=0$, ($\eta=1$) the interferometer's output current is still fluctuating. To explain this fact it was necessary to make an accurate analysis of the photon beam - beam splitter interaction. Two approaches lead to the same result: in the first (Edelstein et al. [1978]) the beam splitter is shown to create two anticorrelated photon beams having n_1 and n_2 photons each, in such a way that the difference of the photon number fluctuation Δn_1 and Δn_2 in the two beam does not cancel even when $\bar{n}_1 = \bar{n}_2$.

In the second approach (Caves [1980]) the zero point vacuum fluctuations of the photon field entering from the open beam splitter port (see Fig. 2.5.1) produce anticorrelated photon number fluctuations in the interferometer's arms.

The r.m.s. fluctuations $\sqrt{\overline{\Delta n_i^2}} = n_i$ are producing both a phase noise $\Delta\phi_{PC} \simeq 1/\sqrt{n}$ where $n=n_1+n_2$, and a fluctuation in the differential radiation pressure on the interferometer's mirrors which produces the differential momentum $\Delta P = \sqrt{n}\,\frac{h\nu_0}{c}\,2N$.

The equivalent displacement noise producing the phase shift $\Delta\phi_{PC}$ is $\Delta x_{PC}=\frac{\Delta\phi_{PC}}{2N}\frac{\lambda}{4\pi}$; hence in the measurement time t the total displacement $\sqrt{\Delta x_{PC}^2+\left(\frac{\Delta P\, t}{2M}\right)^2}$ is minimum when

$$W=\frac{1}{4N^2}\frac{Mc^2}{\omega t^2} \tag{2.5.1}$$

The existence of this optimal laser power relies on the fact that the photon number fluctuations are anticorrelated in the two interferometer's arms.
The minimum displacement is

$$\Delta x_{QL}=\sqrt{\frac{h\,4\pi\, t}{M}} \tag{2.5.2}$$

which is very close to the standard quantum limit for the accuracy with which the displacement of a mass M can be measured in the time t.
As we have seen in paragraph 2.3) in a multireflection interferometer the h sensitivity, with respect to the photon counting error, is increasing with the number of reflections, with the arm length and with the effective detected power.
Using eq.s (2.3.2) and (2.3.16) we see that the best sensitivity in h for a DL system is obtained when $\tau_s=\frac{T_g}{2}$:

$$h_{DL}>\frac{1}{2\nu_0 T_g}\sqrt{\frac{h\,\nu_0}{\eta\, W\, T_g\, R^{4N}}} \tag{2.5.3}$$

where T_g is the GW pulse length.
If the GW is periodic the sensitivity is increased by the square root of the numbers of cycles observed.
If $\frac{\Omega_g\tau_s}{2}<<1$, eq. (2.5.3) becomes

$$h_{DL}>\frac{1}{\omega\tau_s}\sqrt{\frac{h\,\nu_0}{\eta\, W\, t\, R^{4N}}} \tag{2.5.4}$$

Analogously for a FP system, from eq.s (2.3.2) and (2.4.7) we obtain:

$$h_{FP}>\frac{1}{\omega}\frac{T_1^2+T_2^2}{2T_1^2}\sqrt{\frac{R_1}{R_2}}\frac{\sqrt{1+\Omega_g^2\tau_s^2}}{\tau_s}\sqrt{\frac{h\,\nu_0}{\eta\, W\, t}} \tag{2.5.5}$$

For $T_2 << T_1$, $\left(R_1/R_2\right)^{\frac{1}{2}} \cong 1$, and $\Omega_g \tau_s > 1$, eq. (2.5.5) becomes:

$$h_{FP} > \frac{1}{2 \nu_0 T_g} \sqrt{\frac{h \nu_0}{\eta W T_g}} \cong h_{DL} \tag{2.5.6}$$

The difference between eq.s (2.5.3) and (2.5.6) lies in the fact that for the FP case, unlike in the DL case, the maximum sensitivity is obtained for any $\tau_s > \frac{1}{\Omega_g}$.

If $\Omega_g \tau_s < 1$, eq. (2.5.5) becomes

$$h_{FP} > \frac{1}{2 \omega \tau_s} \sqrt{\frac{h \nu_0}{\eta W T}} \cong \frac{1}{2} h_{DL} \tag{2.5.7}$$

It has also been shown (Edelstein et al.[1978]) that the maximum sensitivity occurs when the signal is taken from one of the photodiodes having the illuminating beam brought to the extinction; the argument runs as follows: Eq. (2.3.4) gives the current

$$I_- = \frac{I_0}{2} \left(1 - \cos(\varphi_0 + \varphi_s)\right) \tag{2.5.8}$$

the current ΔI_s due to the signal being

$$\Delta I_s \cong \frac{I_0}{2} (\sin \varphi_0) \varphi_s$$

The current fluctuations are the sum of the Poissonian beam fluctuations plus the statistical fluctuations due to the diode detection inefficiency $1-\eta$ (see eq. (2.3.5)) i.e.:

$$\Delta I^2 = e\left[\eta \frac{I_0(1-\cos\phi_0)}{2t} + (1-\eta) \frac{I_0(1-\cos\phi_0)}{2t}\right] = e \frac{I_0(1-\cos\varphi_0)}{2t} \tag{2.5.9}$$

where t is the measurement time.

The measurability condition for φ_s reads $\Delta I_s^2 \geq \Delta I^2$, hence

$$h > \frac{\lambda}{4N\pi L} \sqrt{\frac{h \nu_0}{\cos^2\frac{\varphi_0}{2} W R^{4N} \eta t}} \tag{2.5.10}$$

which is minimum for $\varphi_0=0$ (see eq. (2.3.6)), i.e.: in the beam extinction condition.

From this condition using eq. (2.3.4), putting $\bar{\varphi}_1 - \bar{\varphi}_2 = \varphi_o << 1$ and with $\varphi_s = \frac{4N\pi}{\lambda} h(t)L<<1$, it follows that the two light beams have the intensities:

$$W_\pm \cong R^{4N}\frac{W}{2}\left[1 \pm \left(\cos\varphi_0 - \varphi_s \sin\varphi_0\right)\right] \tag{2.5.11}$$

where we have chosen the relative fixed phase in such a way to have $W_+=R^{4N}W$ going toward the Laser. This light, can be recycled (Drever [1982]) according to the scheme of Fig. 2.5.2.

In this arrangement the beam W_+ is recycled by means of the mirrors BSR and MR. The position of the latter, and hence the phase shift, is changed by the transducer PZT driven by the PD2 signal.

For evaluating the power increase due to recycling in a DL, let us consider that the typical energy loss is, per cycle

$$\Delta W = \left(1-R^{4N}\right) W \tag{2.5.12}$$

The maximum sensitivity in a DL system happens for $\tau_s = \frac{1}{2\nu_g}$ and since

$$R^{4N} \cong 1 - 2\frac{\pi c}{L\Omega_g}\frac{1-R^2}{2} \tag{2.5.13}$$

It follows

$$W_R = W\frac{L\Omega_g}{\pi c\left(1-R^2\right)} \tag{2.5.14}$$

Hence, from eq. (2.5.13) it follows that the overall power gain is a function of Ω_g and the sensitivity in h (see eq. (2.5.3)) becomes

$$(h_{DL})_R = \sqrt{\left(\frac{\left(1-R^2\right)\pi c}{L\Omega_g}\right)}\ h_{DL} = \frac{1}{2}\sqrt{\frac{h\lambda\,\pi\left(1-R^2\right)\nu_g}{R^{4N}\eta W L 4\pi T_g}} \tag{2.5.15}$$

Let's now evaluate the analogous formula eq. (2.5.14) in case of a FP system.

The schematic diagram of Fig. 2.5.3 shows that in the FP recycling scheme the recycling mirror MR is positioned directly on the laser beam. The correct phase, obtained by driving PZT with the signal of the photodiode PD2, gives minimum signal in PD2.

In analogy with the DL system we evaluate the light power lost in the mirror collision; let's suppose that $T_2<<T_1$, in this case the reflected amplitude is, at optical resonance, :

$$A_r \cong \frac{-R_1+R_1^2+T_1^2}{1-R_1} A_0 i \tag{2.5.16}$$

Using the equation $R_1^2 + T_1^2 + B_1^2 = 1$, it follows

$$A_r = A_0 \left(1 - \frac{B_1^2}{1-R_1}\right) i \tag{2.5.17}$$

In a single mirror hit the power loss is

$$\Delta W \cong -W \frac{2\, B_1^2}{1-R_1} \tag{2.5.18}$$

Hence, if we attribute the whole loss to the close mirror, the power enhancement due to recycling should be

$$W_R \cong W \frac{1-R_1}{2\, B_1^2} \tag{2.5.19}$$

Since the storage time in the cavities should be comparable to the recycling one and because it is convenient to have $\Omega_g \tau_s = 1$, it follows

$$\tau_s = \frac{2L}{c} \frac{\sqrt{R_2 R_1}}{1-R_1 R_2} = \frac{1}{\Omega_g} \tag{2.5.20}$$

Since, for the sake of simplicity, we have put $R_2=1$, then

$$1-R_1 \cong \frac{2L\, \Omega_g}{c} \tag{2.5.21}$$

This gives

$$W_R = W \frac{L\, \Omega_g}{c\, B_1^2}$$

$$(h_{FP})_R \cong h_{FP} \left(\frac{B_1^2 c}{L\, \Omega_g}\right)^{\frac{1}{2}} \tag{2.5.22}$$

Experimental results on power recycling have been obtained by Rüdiger et al.[1987] using a simple 0,3 m arm DL interferometer having 2N=2. A recycling factor up to 15 was obtained with a total power of 2w.

Similar results where obtained in Orsay (Man et al.[1987]). It was shown that the recycling factor was limited by the loss of the Pockels cells situated in the arms of the interferometer. Better results were obtained later using the external modulation technique (see below).

2.6) LASER INTENSITY NOISE

The Laser power can be represented as

$$W(t) = W_o + \delta W(t) \tag{2.6.1}$$

where W_0 is the mean power and $\delta W(t)$ is the instantaneous power fluctuation. The current I_- of eq. (2.5.8) refers to an ideal case where the optical elements have no losses; in the real case we have

$$\begin{aligned} I_- &= e\frac{W(t)}{h\nu}\left[A - B\cos(\varphi_o + \varphi_s)\right] \\ I_+ &= e\frac{W(t)}{h\nu}\left[C + D\cos(\varphi_o + \varphi_s)\right] \end{aligned} \tag{2.6.2}$$

where $A \geq B \geq 0$ and $C \geq D \geq 0$ are coefficients close to the detection efficiency η and in general unequal, $\varphi_s = \dfrac{4N\pi hL}{\lambda}$ and φ_0 a given phase.

It is then evident that since $A \neq B$, then $I_- \neq 0$ when $\varphi_0 = 0$ and this produces the noise:

$$\Delta I_- = \delta W(t)(A - B)\frac{e}{h\nu}$$

The power spectral noise $\dfrac{\delta W(\omega)}{W_0}$ typically reaches the shot noise limit $\sqrt{\dfrac{h\nu}{W}}$ for frequencies larger than $\sim 10^7$ and $\sim 10^5$ Hz for A_r (Winkler [1977], Rüdiger et al.[1981]) and Nd-YAG Lasers respectively.

Hence it is possible to modulate at high frequency the relative phase of the interferometer's arms (Weiss [1972]) by means of Pockels cells and then synchronously detect the signal.

This phase can be represented as:

$$\varphi_M = \varepsilon_M \sin\omega_M t + \bar{\varphi}_0(t) \tag{2.6.3}$$

where ε_M and ω_M are the amplitude and frequency of the modulation and $\bar{\varphi}_0(t)$ is a slowly varying phase, with respect to ω_M, determined by the feedback (FB) loop in such a way to minimize I_-.

Introducing eq. (2.6.3) in eq. (2.6.2) and retaining terms up to $\sin(\omega_M t)$ we obtain

$$I_- = \frac{c\,W(t)}{h\nu}\Big[A - B\cos(\varphi_s + \varphi_0 + \bar{\varphi}_0)\,J_0(\varepsilon_M)$$

$$-2B\sin(\varphi_s + \varphi_0 + \bar{\varphi}_0)\,J_1(\varepsilon_M)\sin(\omega_M t)\Big] \qquad (2.6.4)$$

where J_0 and J_1 are Bessel functions.

The synchronous detection gives:

$$U = \frac{1}{T}\int_t^{t+T} I_-(t)\sin\omega_M\,dt = \frac{c\,W_0}{h\nu}\Big[\big(A - B\cos(\varphi_s + \varphi_0 + \bar{\varphi}_0)\,J_0(\varepsilon_M)\big)$$

$$\frac{\delta W(\omega_M)}{W_0} - B\sin(\varphi_s + \varphi_0 + \bar{\varphi}_0)\,J_1(\varepsilon_M)\Big] \qquad (2.6.5)$$

where $\delta W(\omega_M)$ is the laser power noise spectral density evaluated at the frequency $\omega_M / 2\pi$ and the integration time satisfies the inequality \f(2π,ω$_M$) <<T<<$\frac{1}{v_g}$.

It is possible to drive the Pockels cells with the low pass filtered signal U with the purpose of keeping I_- close to extinction hence minimizing the photon counting noise: in the limit of very large loop gain this gives $\bar{\varphi}_0 = -\varphi_0$.

From this condition and from eq.s (2.6.4) and (2.6.5) it follows that the currents due to the signal (U_S) and to the noise (U_N) are:

$$U_S \equiv -\frac{c\,W_0}{h\nu} B\,\varphi_s\,J_1(\varepsilon_M)$$

$$U_N = \Big\{\Big[\frac{c\,W_0}{h\nu}(A - B\,J_0(\varepsilon_M))\,\frac{\delta W(\omega_M)}{W_0}\Big]^2 + \qquad (2.6.6)$$

$$\frac{c^2\,W_0}{h\nu}\,(A - B\,J_0(\varepsilon_M))\Big\}^{1/2}$$

The last term in the RHS of U_N is due to the photon counting noise.

The best value of ε_M maximizes the S/N ratio, or equivalently the quantity $J_1(\varepsilon_M)/U_N$ (Shoemaker et al.[1987a]).

In a large kilometric interferometer the beam size will be of the order $= 10^{-1}$ m with the purpose of minimizing the size on the far mirror; this implies the use of Pockels cells having large aperture; unpractical for being carried by the test masses. This requirement can be circumvented using an external modulation scheme, shown in Fig. 2.6.1, in which a small fraction of the incident light is sent, through a Pockels cell, to interfere with the beam containing the GW signal. The Pockels cell is modulated at a frequency where the laser amplitude noise has reached the shot noise; the signal is obtained by making synchronous detection with the modulation signal. In this scheme the noise is $\simeq \sqrt{2}$ higher (Man [1988], The Virgo project [1988]) than in the internal modulation one, but the external modulation has the advantage to bring a net sensitivity improvement because enhances the recycling factor.

2.7) THE NOISE DUE TO THE LASER LINEWIDTH

Laser frequency fluctuations produce phase noise in an interfero-meter with arms having unequal length.
If ν_0 and $\Delta\nu$ are the laser mean frequency and the r.m.s. frequency fluctuation respectively, then the r.m.s. phase fluctuation due to the arm difference ΔL is:

$$\Delta\varphi \cong 2\pi\,\Delta\nu\,\Delta L/c \qquad (2.7.1)$$

It is then very important to avoid that rays having large ΔL interfere.
In a multipass DL interferometer the light hitting the mirrors is scattered by the reflecting coating and enters into the optical path of one of the other DL beams. This phenomenon, even if the scattered beam intensity is of the order of $\varepsilon \cong 10^{-4} - 10^{-5}$ of the incident one, may create a large background because the interference of the scattered beam with the main one has an amplitude proportional to $\sqrt{\varepsilon}$.
Different methods have been adopted to get rid of this phenomenon (Schilling et al.[1981] ; Schnupp et al.[1985]); a method (Rüdiger et al.[1981]) consists in "whitening" the laser light spectrum in such a way that rays having a different path length create phase shift having null r.m.s. value.
A more precise evaluation of this noise can be done supposing that the laser frequency fluctuations can be taken into account by means of a random phase $\phi_R(t)$ introduced into the wave function representing a monochromatic wave, i.e.:

$$\psi = A_0\, e^{i\omega t + i\phi_R(t)} \qquad (2.7.2)$$

where ϕ_R satisfy the correlation relation

$$\dot{\phi}_R(t)\,\dot{\phi}_R(t') = (2\pi)^2\,\Delta\nu^2\;g(t-t') \qquad (2.7.3)$$

and $g(0) = 1$.

If the wave Ψ is split by the beam splitter and then brought to interference after reflection on the far mirrors (distant L and $L+\Delta L$ respectively), the intensity of the interference will be

$$I \propto \sin^2\left[\phi_R\left(t-\frac{L}{c}\right)-\phi_R\left(t-\frac{L+\Delta L}{c}\right)+2\,\phi_g(t)\right] \tag{2.7.4}$$

$$\phi_g(t)=h\,\omega\frac{L}{c}\;\frac{\sin\Omega_g\frac{L}{c}N}{\Omega_g\frac{L}{c}}\;e^{i\Omega_g t}$$

where ϕ_g (see eq. (2.3.10)) is the phase shift produced in the DL interferometer by the GW assumed to be periodical.Since $\frac{\Delta L}{c}<<\frac{1}{\Delta v}$ it follows that we can expand ϕ_R in a Taylor series obtaining:

$$I \propto \sin^2\left[\dot{\phi}_R(t)\frac{\Delta L}{c}+2\;\phi_g(t)\right] \tag{2.7.5}$$

we can now evaluate the noise Fourier spectrum

$$|\phi_N(\Omega)|^2=\left|\frac{\Delta L}{C}\int_0^T\dot{\phi}_R(t)\,e^{i\Omega t}\,dt\right|^2 \tag{2.7.6}$$

and comparing it with the signal:

$$|\phi_s(\Omega)|^2=\left|\int_0^T\phi_g(t)\,e^{i\Omega t}\,dt\right|^2 \tag{2.7.7}$$

where T is the measurement time

From eq. (2.7.3) and (2.7.6) it follows

$$|\phi_N(\Omega)|^2=\left(\frac{\Delta L}{c}\right)^2(2\,\pi)^2\,\Delta v^2\int_0^T\int_0^T g(t-t')\,e^{i\Omega(t-t')}\,dt\,dt' \tag{2.7.8}$$

where the measurement time $T>>1/\Omega$.

Putting $g(z)=\int_{-\infty}^{\infty}Q(\omega)\,e^{-i\omega z}\,d\omega$, eq. (2.7.8) becomes:

$$|\phi_N(\Omega)|^2=\left(\frac{\Delta L}{c}\right)^2(2\,\pi)^2\,\Delta v^2\int_{-\infty}^{\infty}Q(\omega)\,\frac{4\sin^2\left[(\Omega-\omega)\frac{T}{2}\right]}{(\Omega-\omega)^2}\,d\omega \tag{2.7.9}$$

Since the function $\frac{\sin^2 x \frac{T}{2}}{x^2}$ can be approximated with $\frac{T\pi}{2}\delta(x)$ we obtain

$$|\phi_N(\Omega)|^2 \cong \left(\frac{\Delta L}{c}\right)^2 (2\pi)^2 \Delta v^2 \frac{\pi T}{2} Q(\Omega) \tag{2.7.10}$$

The quantity $S = 2\pi\sqrt{\frac{\pi}{2}}\,\Delta v\, Q^{1/2}$ is measured in $Hz/\sqrt{Hz}$ and gives the linear spectral density of the laser frequency fluctuations.
Comparing eq.s (2.7.10) with (2.7.7) we obtain the measurability condition for h when the DL storage time is optimal (see eq. (2.3.9))

$$h(\Omega_g) > \frac{\Delta L\, \Delta v}{\omega C}\,\Omega_g \sqrt{\frac{\pi^3}{2}\frac{Q(\Omega_g)}{T}} \tag{2.7.11}$$

Eq. (2.7.10) shows that $S(\Omega)$ can be measured by means of an arm length unbalance ΔL. The line width can be reduced by means of active systems; one method consists in operating a reference FP cavity (Drever et al.[1983] , Hough et al.[1987] , Shoemaker et al.[1987a]) fed with a small fraction of the laser light phase modulated at the frequency v_M by means of a Pockels cell. If the laser frequency is tuned to one of the FP resonances the reflected light has the two sidebands at frequency $\pm v_M$ having opposite sign amplitudes, giving zero output in a photodiode. If the laser frequency fluctuates the two sidebands amplitudes will not cancel anymore and gives a signal in the photodiode, which can be synchronously detected. The signal is proportional to the laser frequency displacement Δv with respect to the FP resonance frequency. It can be fed to a laser intracavity Pockels cell (for high frequency FB) and to a PZT (for low frequency FB) which moves one of the laser mirrors for stabilizing the frequency. The limiting noise is the shot noise; taking it into account for a cavity having no losses, the line width becomes

$$\Delta v \geq \frac{1}{2\pi\,\tau_S}\sqrt{\frac{hv}{w_S t}} \tag{2.7.12}$$

where τ_S is the reference cavity storage time, w_S is the power used in the stabilization circuit and t the observation time.
With the purpose of further reducing the laser linewidth, the Munich group (Billing et al.[1983] ; Shoemaker et al.[1985]) interfered the beam W_+ (see Fig. 2.3.1) with a small fraction of the laser beam obtaining an output from the photodiode PD2 proportional to $\Delta v L$, where L is the total optical path-length in the DL. This signal and that from the reference FP where added for improving

the stabilization; in Fig.2.7.1 (Shoemaker et al.[1985]) the upper curve represents the unstabilized laser line spectral density, the mid curve shows when it where it is reduced by means of the reference FP cavity while the lower curve is the line spectral density when both reference cavity and the whole interferometer are used. The final integrated line width was $\simeq$3Hz with a reduction of $\simeq 10^6$ with respect to the unstabilized one.
A frequency noise of 12,5 $\mathrm{mHz}/\sqrt{\mathrm{Hz}}$ was obtained with a diode pumped Nd : YAG laser, actively frequency stabilized with respect to a reference FP cavity (Shoemaker et al.[1989]).
The effects due to the laser linewidth in FP interferometers involve a more complex mechanism than in a DL interferometer; from eq.s (2.7.2) and (2.4.1) we can evaluate the reflected amplitude

$$A_r(t) = iR_1\,\psi(t) + iR_1\,T_1^2 \sum_{n=0}^{\infty} (-R_1 R_2)^n\, \psi\!\left(t - 2(n+1)\frac{L}{c}\right) \qquad (2.7.13)$$

putting

$$\psi(t) = \int_{-\infty}^{\infty} \psi(\omega)\, e^{i\omega t}\, d\omega$$

we obtain

$$A_r(t) = i \int_{-\infty}^{\infty} d\omega\, \psi(\omega) \left[R_1\, e^{i\omega t} + R_2 T_1^2\, \frac{e^{i\omega\left(t - 2\frac{L}{c}\right)}}{1 + R_1 R_2\, e^{-2i\omega\frac{L}{c}}} \right] \qquad (2.7.14)$$

In an analogous way to eq. (2.7.4) combining the A_r's from the two arms onto the beam splitter, the intensity on the photodiode is

$$I \propto \left| \int_{-\infty}^{\infty} \left\{ \left(R_1 e^{i\omega t} + R_2 T_1^2 \frac{e^{i\omega\left(t - \frac{2L}{c}\right)}}{1 + R_1 R_2 e^{-2i\omega\frac{L}{c}}} \right)_{\text{Arm 1}} + \right.\right.$$

$$\left.\left. + e^{i\varphi} \left(R_1 e^{i\omega t} + R_2 T_1^2 \frac{e^{i\omega\left(t - \frac{2L}{c}\right)}}{1 + R_1 R_2 e^{-2i\omega\frac{L}{c}}} \right)_{\text{Arm 2}} \right\} \psi(\omega)\, d\omega \right|^2 \qquad (2.7.15)$$

where φ is a given phase shift. It is evident from eq. (2.7.15) that unlike in the DL case, even when $(L)_{\text{Arm 1}} = (L)_{\text{Arm 2}}$, there is incomplete cancellation of the laser line width noise unless the mirror transmittance and losses in the two arms are equal.

2.8) THE NOISE PRODUCED BY THE LATERAL BEAM JITTER

If the beam splitter is not symmetrical between the two interferometers' arms, but deviates by an angle $\delta\alpha$, then a lateral beam jitter δx will produce the phase shift (Billing et al.[1979])

$$\Delta\phi \cong 2\, \delta\alpha\, \delta x \frac{4\pi}{\lambda} \qquad (2.8.1)$$

Two methods have been adopted for reducing this noise:
the first uses a mode cleaner (Rüdiger et al.[1981] , Meers [1983]), while the second, a simpler one even if 30-50% of the laser power gets lost, is the use of a monomode optical fiber coupler as suggested by R.Weiss of MIT. The experimental set up, shown in Fig. 2.8.1, consists of a monomode fiber lit by a microscope objective; a $\lambda/2$ plate placed before the fiber and a linear polarizer placed after hold the right polarization. In Fig. 2.8.2 (Shoemaker et al.[1985]) the residual lateral beam jitter is shown as measured by a position sensitive diode: the top curve represents the laser beam jitter, the middle one the beam jitter after a mode cleaner and the lower one the beam after the monomode fiber; a displacement $\simeq 10^{-11} \frac{m}{\sqrt{Hz}}$ for $\nu > 100$ Hz was obtained.
A recycling cavity would filter out the fast laser frequency and amplitude fluctuations, as well as most of the beam geometry jitter.

2.9) THE NOISE DUE TO THE GAS PRESSURE FLUCTUATIONS

This phase noise originates from the fluctuations of the refractive index in the interferometer's vacuum pipes.

The laser light is bouncing between the mirrors of either the FP or the DL system; the number of gas molecules contained in the light pipe is then fluctuating almost in a Poissonian (there may be convective motion also) way hence varying the refraction index (Brillet [1984,1985], Hough et al.[1986]).

This can be shown as follows: if V is the average light pipe volume (not the vacuum pipe diameter) the total number of gas atoms in this volume is

$$n(t) = V \sum \frac{\rho_i(t)}{m_i} = V \sum n_i(t) \tag{2.9.1}$$

where ρ_i and m_i are the density and the mass of the i-th gas component and $n_i(t)$ the istantaneous molecule number of the i-th gas component.

The number fluctuations $\delta n_i(t)$ of the i-th component satisfy the correlation relation

$$\overline{\delta n_i(t)\, \delta n_i(t')} = \overline{n_i}\, g_i(t-t') \tag{2.9.2}$$

where $\overline{n_i}$ and g_i are the average number and the correlation function of the i-th gas component respectively with the condition $g_i(0) = 1$.

The function g_i is a complex function of the light beam geometry; let's, for the sake of simplicity, approximate the light pipe volume to a cylinder having length L and diameter D. Under this condition the correlation time is $\cong \frac{D}{V_i}$, where V_i is the speed of the i-th gas component molecule. The light phase shift due to the gas refraction index ε_i is (we are considering a DL)

$$\phi_G(t) = \frac{4\pi N L}{\lambda} \sum \left(\varepsilon_i(t) - 1\right) \tag{2.9.3}$$

The phase fluctuation $\delta\phi_G$, is

$$\delta\phi_G(t) = \frac{4\pi N L}{\lambda} \sum \frac{\delta n_i(t)}{\overline{n_i}} \left(\overline{\varepsilon}_i - 1\right) \tag{2.9.4}$$

In Ω space, using eq. (2.9.2), the noise is:

$$\left|\delta\phi_G(\Omega)\right|^2_{DL} = \left(\frac{4\pi N L}{\lambda}\right)^2 \Sigma_i \int_0^T e^{i\Omega(t-t')} \int_0^T \frac{\left(\varepsilon_i - 1\right)^2 g_i(t-t')}{\bar{n}_i} \, dt\, dt' \qquad (2.9.5)$$

where T is the measurement time.

Assuming the simple correlation function $g(t-t') = 1 - \theta\left(|t-t'| - \frac{D}{Vi}\right)$, $\bar{\varepsilon}_i - 1 = \alpha_i \frac{P_i}{P_{0i}}$, where P_i and P_{0i} are the pipe and atmospheric partial pressure respectively, $\bar{n}_i = P_i \frac{\pi}{4} D^2 L / K \tilde{T}$ ($\tilde{T}$ is the temperature), eq. (2.9.5) becomes

$$\left|\delta\phi_G(\Omega)\right|^2_{DL} = \left(\frac{4\pi N L}{\lambda}\right)^2 \Sigma_i \frac{2 \sin\left(\Omega \frac{D}{Vi}\right)}{\Omega} T \left(\alpha_i \frac{P_i}{P_{0i}}\right)^2 \frac{K \tilde{T}}{2N P_i \frac{\pi}{4} D^2 L} \qquad (2.9.6)$$

The h measurability condition for a DL interferometer is (see eq. (2.7.6)):

$$\tilde{h}_{DL}(\Omega) > \sqrt{16 \Sigma_i \frac{\sin\Omega \frac{D}{Vi}}{\Omega} \left(\frac{\alpha_i}{P_{0i}}\right)^2 \frac{K \tilde{T} P_i}{N \pi D^2 L}} \cdot \frac{NL\Omega}{c \sin \frac{\Omega NL}{c}} \qquad (2.9.7)$$

For a FP interferometer working at optical resonance we obtain the following result (for the definitions see eq.s (2.4.1) and (2.4.5))

$$\left|\delta\phi_G(\Omega)\right|^2_{FP} = \sum_i \left(\sqrt{8}\, T_1^2 R_2 \omega \frac{L}{c} \left(\bar{\varepsilon}_i - 1\right)\right)^2 \frac{T}{\bar{n}_i} \frac{\sin\left(\Omega \frac{D}{Vi}\right)}{\Omega} \cdot \frac{1}{\left(1 - R_1 R_2\right)^4} \cdot \frac{1}{\left(1 + F' \sin^2 \Omega \frac{L}{c}\right)}$$

(2.9.8)

comparing eq. (2.9.8) with the Fourier transform (see eq. (2.7.7)) of eq. (2.4.5) we obtain the measurability condition

$$\tilde{h}_{FP} \leq \sqrt{\sum_i 2 \frac{\left(\bar{\varepsilon}_i - 1\right)^2}{\bar{n}_i} \frac{\sin\left(\Omega \frac{D}{Vi}\right)}{\Omega}} \qquad (2.9.9)$$

$\tilde{h}_{FP}$ is larger than $\tilde{h}_{DL}$ because the light pipe volume in the FP case is 2N smaller than that of the DL.

In Fig. 2.9.1, $\tilde{h}_{FP}$ is plotted as a function of the pressure for H_2 (full line) and N_2 (dotted line) in the frequency interval $0<\nu<10^3$ Hz, for the pressure values 10^{-6} mbar (a), 10^{-7} mbar (b) and 10^{-8} mbar (c).

A calculation taking into account a better approximation of the correlation function has been performed by Rüdiger [1988].

2.10) THE THERMAL NOISE

The mass of the mirror is driven by the stochastic forces produced by the thermal noise; we are considering here both the forces acting on the mirror suspensions and those producing an excitation of the mirror normal modes. For the former case, if τ is the mirror suspension relaxation time, the r.m.s stochastic spectral force is (Uhlenbeck and Ornstein [1930])

$$F = \sqrt{\frac{2 K \tilde{T} M}{\tau}} \; \frac{N}{\sqrt{Hz}} \tag{2.10.1}$$

where M is the mirror mass, $\tilde{T}$ the temperature and K the Boltzmann constant. The thermal stochastic force f(t) satisfies the correlation relation

$$\overline{f(t)\, f(t')} = F^2 \delta(t - t') \tag{2.10.2}$$

The mirror displacement $x(\Omega)$ in Ω space is evaluated using eq.s (2.17) and (2.10.2); in analogy with eq. (2.7.7) we obtain:

$$|x_i(\Omega)|^2 \cong T \frac{2 K \tilde{T}}{M \tau} \frac{1}{\left(\Omega^2 - \omega_p^2\right)^2 + \frac{\Omega^2}{\tau^2}} \tag{2.10.3}$$

where T is the measurement's time and $\nu_p = \omega_p/2\pi$ the pendulum frequency. The pendula thermal noise gives the following limit on the measurability for $\tilde{h}$.

$$\tilde{h} > \frac{1}{\Omega^2 L} \sqrt{\frac{2 K \tilde{T}}{M} \Sigma \frac{1}{\tau}} \tag{2.10.4}$$

where the sum is extended to the mirror number.

With the purpose of evaluating the thermal noise produced by the mirror normal modes we can approximate the mirror with many harmonic oscillators each having frequency ν_i relaxation time τ_i and equivalent mass M_i. In proximity of the i-th frequency the displacement in the Ω space is sufficiently well described by eq. (2.10.3) replacing ω_p with $\omega_i = 2\pi\nu_i$.

Since we consider the frequency region $\nu_p << \nu << \nu_i$ we can approximate eq. (2.10.3) in the following way

$$|x_i(\Omega)|^2 \cong T \frac{2K\tilde{T}}{M_i \tau_i} \frac{1}{\omega_i^4} \tag{2.10.5}$$

being $\omega_i \tau_i = Q_i$, the $\tilde{h}$ measurability condition is

$$\tilde{h} > \frac{1}{L} \sqrt{2K\tilde{T} \Sigma \frac{1}{M_i Q_i \omega_i^3}} \tag{2.10.6}$$

Where the sum is extended to both the mirror number and to the longitudinal modes.

Assuming Q_i to be independent upon a scale transformation changing the mirror dimensions, it follows that eq. (2.10.6) is independent too. This is not true anymore for eq. (2.10.4) which shows that an increase in the mass M reduces the thermal noise.

2.11) THE SEISMIC NOISE.

The seismic noise is the dominant source of displacement of the mirrors suspension points. The r.m.s. spectral displacement can be sufficiently well approximated by the formula

$$x_T = \frac{a}{\nu^2} \frac{m}{\sqrt{Hz}} \tag{2.11.1}$$

where $a \cong 10^{-9}$ at a depth of $\cong 10^3$ m up to $a \cong 10^{-6}$ at the earth surface in a relatively quiet place. The use of active seismic isolation schemes is strongly limited by the difficulty of making multiple three-dimensional (3D) systems, this necessity is dictated by the fact that a non isolated degree of freedom reintroduces the seismic noise even if the others degrees of freedom are isolated.

For this reason passive schemes have been adopted, able to isolate in vertical direction as well (Giazotto [1987] , Shoemaker et al.[1987a]).

The basic idea is to use a multiple stage pendulum with the masses supported by springs. It can be shown that the frictionless transfer functions for both the vertical and horizontal directions can be brought to the following canonical form

$$F = \pi_{n=1}^{N} \frac{\omega_n^2}{\left(-\Omega^2 + \omega_n^2\right)} \tag{2.11.2}$$

where F is the transfer function, $\nu_n = \omega_n/2\pi$ is the n-th mode frequency and N is the number of masses.Above the resonances $F \propto \Omega^{-2N}$, but the presence of friction and nonlinearities can give a slower decrease with frequency as well as coordinate mixing.
In the interferometric antennas aiming to reach very low frequency ($\nu \geq 10$ Hz) the seismic isolation requires a very careful design with the purpose of avoiding mechanical resonances falling into the interval $10 \leq \nu \leq 100$ Hz; these are produced mainly by the springs' rocking and normal modes.
The general problem of cool damping (Forward [1978] , Kuroda et al.[1982]) of the pendula normal modes has been solved by means of both electromagnetic or electrostatic force actuators.
The seismic noise affects the interferometer phase also by means of the interaction of the mirror scattered light with the vacuum pipe walls (Billing et al.[1983]): the scattered light is reflected by the pipe walls and then reenters the main beam by means of a second scattering process. Since the pipe walls are vibrating, due to the seismic noise, they change the phase of the scattered beam; the interference of the scattered beam with the main one then reintroduces the seismic noise despite the seismic isolation of the mirrors.
The use of diaphragms in the vacuum pipe can prevent the scattered light which hits the pipe walls to reenter into the main optical path (Thorne [1989]).

2.12) EFFECTS DUE TO THE RADIATION PRESSURE ON THE MIRRORS

As it has been shown in paragraph 2.5, radiation pressure creates a differential motion of the interferometer's mirrors and this effect can be easily evaluated:
since $\sqrt{n} = \sqrt{\frac{w\,t}{h\nu}}$ is the fluctuation of the number of photons impinging on the mirrors in the time t, the momentum fluctuation is $\Delta P = \frac{h\nu}{c}\sqrt{\frac{w\,t}{h\nu}}$, from which it follows the rms differential spectral force $\Delta\tilde{F} = \frac{h\nu}{c}\sqrt{\frac{w}{h\nu}}$.
In a DL system having 2N beams, these force fluctuations are coherently added and the measurability condition for $\tilde{h}$ is (see eq. (2.9))

$$\tilde{h}_{DL} > \frac{1}{M\Omega^2 L}\,\frac{2\,N}{c}\,\sqrt{W\,h\,\nu} \qquad (2.12.1)$$

where W is the incident power.
In a FP cavity having the input mirror with amplitude transmittance T_0 and the far one with T_1 the intracavity power, at optical resonance is:

$$W_{in} = W\ T_0^2\ \frac{F^2}{\pi^2} \tag{2.12.2}$$

where $F \equiv \frac{\pi\sqrt{R_0 R_1}}{1-R_0 R_1}$ is the cavity "finesse".
If $T_0 \gg T_1$ eq (2.12.2) becomes

$$W_{in} \simeq W\ \frac{2}{\pi}\ F \tag{2.12.3}$$

The fluctuations of the incident power will be coherently transmitted to the mirror for frequencies smaller than $1/\tau_s$; in this case the measurability condition for $\tilde{h}$ is

$$\tilde{h}_{F \cdot P} > \frac{1}{M\Omega^2 L}\ \frac{2\ F}{\pi c}\ \sqrt{W h \nu} \tag{2.12.4}$$

Assuming $\Omega=60$, $M=4.10^2$, $L=3\ 10^3$ m, $h\nu \simeq 10^{-19}$ J , $\frac{2}{\pi}F \simeq 2N \simeq 30$ from eq.s (2.12.1) and (2.12.4) it follows

$$\tilde{h}_{DL} = \tilde{h}_{FP} \simeq 2 \cdot 10^{-26}\sqrt{W}\quad Hz^{-1/2} \tag{2.12.5}$$

Eq. (2.12.5) shows that Kilowatts of power can be used before reaching the photon counting limit of eq. (2.3.2).
In a FP interferometer the radiation pressure can create multistability (Deruelle and Tourrenc [1984], Tourrenc and Deruelle [1985]). Following the approach of Aguirregabiria and Bel [1987] we consider a pendular cavity as shown in Fig. 2.12.1. The reflection and transmittance coefficients of the mirror M_1 , are $R = \cos\theta\ e^{-i\mu}$ and $T= i\ \sin\theta\ e^{-i\mu}$ respectively. P is the incident light power, $D_s + x(t)$ the mirror separation and $\phi_A = \sqrt{P}\ \exp\left[-i\left(\frac{2\pi}{\lambda}\right)(ct + \alpha)\right]$ the incident light field. The light field $\phi(t)$ on the M_2 mirror is

$$\phi(t) = T\ \phi_A\left(t - \frac{D_s + x(t)}{c}\right) - R\ \phi(\hat{t}) \tag{2.12.6}$$

where the retarded time $\hat{t}$ is defined

$$c\ (t - \hat{t}) = D_s + x(t) + x(\hat{t}) \tag{2.12.7}$$

Neglecting the effects of the delay, the M_2 mirror motion equation is

$$\ddot{x} + \frac{\Omega}{Q}\dot{x} = -\Omega^2 x + \frac{2|\phi|^2}{Mc} =$$

$$-\Omega^2 x + \frac{2P}{Mc} \frac{\sin^2\theta}{1 + \cos^2\theta + 2\cos\theta \left[\frac{4\pi}{\lambda}(D_s + x) - \mu\right]} \tag{2.12.8}$$

where M is the M_2 mirror mass, Ω the pendulum circular frequency and Q the mechanical quality factor.

The relative maxima of the RHS of eq. (2.12.8) with good approximation, occurs when $x = \frac{\lambda}{4\pi}\left[(2n + 1)\pi + \mu\right] - D_s = x_n$ ($n = 0, \pm 1, \pm 2 ...$) as shown in Fig. 2.12.2.

The peak heights $J = \frac{4P}{Mc\Omega^2}\frac{F}{\pi}$, where F is the finesse, can be increased more and more in such a way to have a new peak crossing the $y = 0$ axis and consequently a new stability point $\left(\frac{\partial y}{\partial x} < 0\right)$

The delay can be taken into account writing eq. (2.12.6) in the following way (Aguirregabiria and Bel [1987])

$$f(t) = 1 + \cos\theta \, e^{ix_s} e^{i(x(t - r_1) - x_s)} f(t - r_1) \tag{2.12.9}$$

where r_1 is the time needed by the light to make a round trip in the cavity ending at time t, x_s is the equilibrium point and

$$f(t) = -\frac{i\phi(t)}{\sqrt{P}\sin\theta} e^{i\left[\,2\pi/\lambda\,(ct - D_s - x + \alpha) + \sigma\right]} \tag{2.12.10}$$

Iteration of eq. (2.12.9) gives

$$f = 1 + \sum_{n=1}^{\infty}\left(\cos\theta\, e^{i x_s}\right)^n \exp\left[i\left(\sum_{J=1}^{n}\left(x_{(J)} - x_s\right)\right)\right] \tag{2.12.11}$$

where $x_{(J)} \simeq x(t - Jr)$ and $r = \frac{2D_s}{c}$.

The pendulum motion equation becomes

$$\ddot{x} + \frac{\Omega}{Q}\dot{x} = -\Omega^2 x + \frac{2P}{Mc}\sin^2\theta\, |f|^2 \tag{2.12.12}$$

The dominant reduction of the hereditary equation of motion, evaluated up to second order in the displacement $x(t) - x_s$ can be put in the form (Bell et al.[1988])

$$\ddot{Y} + K\dot{Y} + \bar{\Omega}^2 x = 0 \tag{2.12.13}$$

$$K = \left(\left\{ \frac{1}{Q} - \frac{8\, r\, y_s}{\beta\theta^2 \left(1 + y_s^2\right)^3} \right\} - \frac{8\, r \left(1 - 5\, y_s^2\right)}{\beta\theta^2 \left(1 + y_s^2\right)^4} y \right) \Omega$$

$$\bar{\Omega}^2 = \left(\left\{ 1 + \frac{2\, y_s}{\beta \left(1 + y_s^2\right)^2} \right\} + \frac{1 - 3\, y_s^2}{\beta \left(1 + y_s^2\right)^3} y \right) \Omega^2$$

where $y_s = \frac{2\, x_s}{\theta^2}$ and $\beta = \frac{\theta^4\, MC}{16\, P}$ and $Y = \frac{2(x(t) - x_s)}{\theta^2}$.

The effect of the delay is then to add a new "friction" term (Deruelle and Tourrenc [1984]).

To demonstrate the presence of the chaos we write eq. (2.12.12) putting $z = x(t) - x_s$

$$\ddot{z} + \frac{\Omega}{Q} \dot{z} + z = \left(|g|^2 + 2\mathrm{Re}\, g\right) S \tag{2.12.14}$$

where $\varepsilon = \frac{4\pi}{\lambda} (D_s + x_s) - \mu - (2\, n+1)\, \pi$,

$$S = \frac{2P}{Mc} \frac{\sin^2\theta}{1 + \cos^2\theta - 2 \cos\theta \cos\varepsilon}$$ and

$$g = \frac{f}{f_0} - 1 = \cos\theta\; e^{i\varepsilon} \left[e^{i\, [\, 4\pi/\lambda\;\, z(\hat{t})]} \left(g(\hat{t}) + 1\right) - 1 \right] \tag{2.12.15}$$

where $c\, (t - \hat{t}) = 2\, (D_s + x_s) + z + z(\hat{t})$.

Linearizing and then iterating eq. (2.12.15), eq. (2.12.14) becomes (Aguirregabiria and Bel [1987])

$$\ddot{z} + \frac{\Omega}{Q} \dot{z} + r^2 z = - \frac{8\pi}{\lambda} S \sum_{K=1}^{\infty} \mathrm{Im} \left(\cos\theta\, e^{i\varepsilon} z\, (\hat{t}_k)\right) \tag{2.12.16}$$

where $(\hat{t}_k)$ is the retarded time iterated k times. Putting

$$z = e^{\lambda t} \tag{2.12.17}$$

we obtain the characteristic equation

$$\lambda^2 + \frac{\Omega}{Q}\lambda + r^2 = -\frac{8\pi}{\lambda} \; S \cos\theta \sin\varepsilon \; \frac{1}{R} \cdot \frac{1}{1 + R^{-1} \left[(e^{\lambda r} - 1) + (e^{-\lambda r} - 1) \cos^2\theta \right.} \tag{2.12.18}$$

where $R = 1 + \cos^2\theta - 2\cos\theta\cos\varepsilon$ and $r = \frac{2\left(D_s + x_s\right)}{c}$. Due to eq. (2.12.17) instability occurs when $Re\ \lambda > 0$ hence the point $Re\ \lambda = 0$ is the bifurcation point.

The power p for any r, giving rise to instability, has also been evaluated.

In the VIRGO Project (1987, 1988) having arm length 3 Km, λ = 1μm, power 500 W, mirror mass 400 Kg, finesse F=30 and pendular mechanical quality factor $Q \simeq 10^6$ the retarded effects (Tourrenc, private communication) give the unstable mirror motion equation

$$Y = A \exp(2.10^{-3}\, t) \sin(6t + \phi) \tag{2.12.19}$$

This instability seems to be easily corrected for by means of the mirror damping active feedback.

2.13) COSMIC RAYS BACKGROUND

The interaction of particle with matter excite oscillation modes which can be experimentally detected.

In an experiment (Beron and Hofstadfer [1969]) the modes of a piezoelectric disc have been excited by an electron beam containing 10^4 - 10^6 particle per pulse of 1 μs duration.

In a subsequent experiment (Grassi Strini et al.[1980]) the interaction of 30 MeV protons with an Al rod .2m long and 3 10^{-2}m diameter was studied.

The effect was the excitation of the rod's fundamental longitudinal mode with an amplitude

$$\xi = \frac{\alpha}{C_v} \frac{W}{M} \frac{L}{\pi} \frac{2}{} \cos\frac{\pi x}{L} \tag{2.13.1}$$

where L is the rod length, W the energy lost by the hitting particles, α the rod thermal linear expansion coefficient, c_v the specific heat at constant volume, M the mass of the rod and x the distance from the center at which the particles cross the rod.

Theoretical calculations (Allega and Cabibbo [1984] , Bernard et al.[1984]) have been performed giving good agreement with eq. (2.13.1).

The interferometer mirrors when hit by a cosmic ray undergoes both the excitation of the internal degree of freedom and of the suspension pendulum modes.

The mirror internal degrees of freedom are excited both by the heat produced with an amplitude given by eq. (2.13.1), and by the differential momentum released by the cosmic ray.

An evaluation of the mirror pendulum mode excitation by cosmic muons has been done by Weiss [1972] considering only ionization losses.

In a subsequent work of Amaldi and Pizzella [1986] the effect of production of knock-on electrons, bremstrahlung, direct pair production and photo-nuclear interactions by muons was shown to be crucial for the evaluation of the cosmic muons noise in a bar antenna. A montecarlo simulation of the background due to high cosmic muons in a bar antenna has been done by Ricci [1987].

A calculation taking into account both the ionization losses and the four mentioned processes for an antenna having 3 km arm length and 400 kg quartz mirror mass, has been done by Giazotto [1988].

The results show that muons of 10^2 GeV give 1 m_s pulses having $h \simeq 10^{-23}$ with a frequency of 10^2 year^{-1} and 10^4 GeV muons give $h \simeq 10^{-21}$ with a frequency of 10^{-6} year^{-1}.

For periodic GW the calculation gives the following measurability condition for $\tilde{h}$

$$\tilde{h} > \frac{10^{-25}}{\nu^2} \qquad \mathrm{Hz}^{-1/2} \tag{2.13.2}$$

where the GW frequency ν has been assumed to be larger than the pendulum frequency and smaller than the mirror lowest frequency mode.

2.14) TABLE OF NOISES

We evaluate the dominant noises assuming the following values of the experimental parameters:

Interferometer arm length	$L = 3$ Km
Interferometer Finesse	$F = 40$
Light wavelength	$\lambda = 1\ \mu m$
Laser power	$W_L = 25$ W
Recirculated power	$W = 1$ KW
Mirror weight	$M = 300$ Kg
Mirror lowest pendulum frequency	0.24 Hz
Mirror lowest normal mode	1.9 KHz
Reference spectral strain	$\tilde{h} = 3.10^{-23}\ Hz^{-1/2}$

Photon counting noise

$$\tilde{h} \sim \frac{\lambda}{2\pi\, L \cdot F}\sqrt{\frac{h\nu}{W}} \cong 1.5\ 10^{-23}\frac{1}{\sqrt{Hz}} \tag{2.14.1}$$

Laser linewidth

$$\frac{\widetilde{\Delta\nu}}{\nu} < \left(\frac{\Delta F}{F} + \frac{\Delta L}{L}\right)^{-1} 2\pi\, \tilde{h} \tag{2.14.2}$$

Assuming $\tilde{h} \cong 3.10^{-23}\frac{1}{\sqrt{Hz}}$ and $\left(\frac{\Delta F}{F} + \frac{\Delta L}{L}\right)^{-1} \cong 10^{3}$ it follows that the laser linear spectral density of the frequency fluctuations must be:

$$\frac{\widetilde{\Delta\nu}}{\nu} \cong 6\ 10^{-20}\frac{1}{\sqrt{Hz}} \tag{2.14.3}$$

Laser amplitude fluctuations

The modulation is supposed to be at frequency where the laser amplitude fluctuations are at shot noise level; it is important, anyway, to have a very efficient laser amplitude fluctuation reduction system because, due to the high power stored in the cavities (40 KW) and to the interferometer's asymmetries, the fluctuation in radiation pressure can create a noise. The mirror displacement is then

$$\Delta x = \frac{W_F \cdot l}{C\ M\ g} \cong 1.6\ 10^{-7} \tag{2.14.4}$$

where l is the pendulum length.

If β is the interferometer's asymmetry assumed to be $\sim 10^{-2}$, then the limit on $\tilde{h}$ is

$$\tilde{h} = \frac{\Delta x}{L}\ \beta \cdot \frac{\widetilde{\Delta W_l}}{W_L} \tag{2.14.5}$$

which implies $\frac{\widetilde{\Delta W_l}}{W_L} < 10^{-10}$, where ΔW_L are the laser power fluctuations.

Gas pressure fluctuations

Assuming H_2 to be the remnant gas in the vacuum pipe from eq.(2.9.9) it follows for H_2

$$\tilde{h} \lesssim \sqrt{2\ \frac{\left(\bar{\varepsilon}_i - 1\right)^2}{\bar{n}_i}\ \frac{\sin \Omega \frac{D}{V}}{\Omega}\ \frac{P}{P_0}} \cong 7.10^{-25} \left(\frac{P}{10^{-7}\,\mathrm{mb}}\right)^{1/2} \frac{1}{\sqrt{\mathrm{Hz}}} \tag{2.14.6}$$

Thermal noise

From eq. (2.10.4) it follows that the mirror pendular thermal noise at room temperature is:

$$\tilde{h} \cong 2.10^{-21} \left(\frac{10\ \mathrm{Hz}}{\nu}\right)^2 \left(\frac{3\ 10^3\ \mathrm{m}}{L}\right)\left(\frac{10^6}{Q}\right)^{1/2} \left(\frac{300\ \mathrm{Kg}}{M}\right)^{1/2}\ \mathrm{Hz}^{-1/2} \tag{2.14.7}$$

The mirror normal modes contribute to the thermal noise according to eq. (2.10.6). Assuming the first longitudinal normal mode at ν_M = 2500 Hz, equivalent mass ≅150 Kg and Q ≅ 10^5, we obtain for ν < 2500 Hz

$$\tilde{h} \cong 7.5 \quad 10^{-24} \left(\frac{3\ 10^3\ m}{L}\right)\left(\frac{150\ Kg}{M}\right)^{1/2} \left(\frac{10^5}{Q}\right)^{1/2} \left(\frac{\nu_M}{2500}\right)^{3/2} \quad Hz^{-1/2} \qquad (2.14.8)$$

Seismic noise

It is supposed the seismic noise to be negligible for ν > 10 Hz since a 3 Dimensional (3D) 7-fold filter is used. According to eq. (2.11.9), for frequencies higher than the normal modes frequencies, the seismic noise transfer function F is behaving like:

$$F \propto \left(\frac{\pi_{n=1}^{7}\ \omega_n^2}{\Omega^{14}}\right)_{vertical} + \alpha \left(\frac{\pi_{n=1}^{7}\ \omega_n^2}{\Omega^{14}}\right)_{horizontal} \qquad (2.14.10)$$

where α is the vertical to horizontal coupling coefficient.
As it will be shown in §3 a 3D 7-fold pendulum has been built in Pisa having the following values of the parameters:

$$\left(\pi_{n=1}^{7}\ \omega_n^2\right)_{vertical} = 7\cdot 10^{16}$$

$$\left(\pi_{n=1}^{7}\ \omega_n^2\right)_{horizontal} = 1.6\cdot 10^{13} \qquad (2.14.11)$$

$$\alpha = .01$$

2.15) Estimation of foreseen sensitivity

The Virgo antenna sensitivity in h is computed by evaluating the noise level. It is shown from the previous paragraphs that the thermal, the seism ans photon counting are the limiting noise sources in different region of the spectrum. In Fig.2.15.1 the dotted curves show the h power spectra of this four noise sources while the continuous line shows the Virgo resultant noise as incoherent sum of the different sources; all the parameters used in the computation are the same of paragraph 2.14 "Table of noises". Fig. 2.15.2 shows the expected sensitivity for periodic signal integrated in one year and

Fig. 2.15.3 the sensitivity for inpulsive signal, where the integration time depends on the frequency ν and is $^1/_\nu$..

Figure captions, chapter 2

Fig.2.2.1 In an inertial system having the origin in the mass A CMS the effect of a GW traveling along the z axis is to displace the mass B from the equilibrium position by an amount $\Delta\xi_\alpha = h^{TT}_{\alpha\beta}\frac{\xi_\alpha}{2}$ (see eq. (2.7)).

Fig.2.2.2 The interferometer's mirrors having mass m_1 , m_2 and m_3 are located at (x,y) positions (0,0) , (0,L) and (L,0) respectively. The mirror's acceleration produced by a GW traveling along the z axis is calculated introducing the mirror's coordinates with respect to the CMS, ξ_i, in eq. (2.9). The inertial reference system has the origin in the mirror's CMS system.

Fig.2.3.1 In the Delay Line scheme, the Laser beam is entering the two optical cavities and bounces 2N times between the mirrors with the purpose to increase the S/N ratio of the GW signal to the photon counting noise.

Fig.2.3.2 The laser beam is entering the DL at the position (x_0, y_0) and angle $(x'_0 y'_0)$ then is bounced 2N times and leaves the cavity from the entrance hole.

Fig.2.3.3 The beam is entering the DL at position n=0, is reflected from the far mirror at positions n=1,3,5 and from the close one at positions n=2,4. $2N\theta$ can be larger than 2π.

Fig.2.4.1 Schematic diagram of the light field amplitudes inside a cavity; composed by the mirrors M_2 and M_2 having reflectivity iR_1 and iR_2 and transmittance T_1 and T_2 respectively. The amplitude A_3 is connected to A_2 through the operator defined in eq. (2.2.29) containing the effect due to the GW interaction.

Fig.2.4.2 Comparison between the phase shift due to the GW amplitude h of a FP ($T_2 << T_1$) and a DL interferometer having the same storage time τ_s. When $\Omega_g \tau_s >> 1$ the phase shifts are comparable, as it is shown by the eq.s (2.4.7) and (2.3.16).

Fig.2.5.1 The light field vacuum fluctuations entering the unused port of the beam splitter BS produces the anticorrelated intensity fluctuations in the interferometer's arms.

Fig.2.5.2 The beam w_- can be brought to extinction by means of the Pockels cells PC; in this condition w_+ is maximum and can be reused when M_R gives the right phase shift. This is obtained displacing M_R by means of the piezoelectric transducer PZT driven by the PD2 signal.

Fig.2.5.3 The power recycling scheme for a FP interferometer.

In analogy to the scheme of Fig. 2.5.2 the photodiode PD2 signal is used to displace the mirror M_R in such a way to have minimum illumination of PD2.

Fig.2.6.1 The external modulation scheme: a small fraction of the incident power is sent through the Pockels cell PC to interfere with the outgoing amplitude A containing the GW signal. The PC is modulated at a frequency where the laser amplitude noise reaches the shot noise. Synchronous detection gives the signal S.

Fig.2.7.1 The laser spectral line density before stabilization (from Shoemaker et al.[1985]) is shown in the upper curve; in the mid one the spectral line density after stabilization with a reference FP cavity is shown while in the lower one it is shown the spectral line density after the combined stabilization with the reference FP cavity and the total DL optical path.

Fig.2.8.1 The laser beam jitter is strongly reduced by injecting the beam in the monomode optical fiber OF. The injection is performed by means of the microscope objective M; the $\lambda/2$ plate and the polarizer P restore the plane polarization.

Fig.2.8.2 The lateral beam jitter (from Shoemaker et al.[1985]) as measured with a position sensitive diode; the upper curve is the unfiltered laser beam, the middle one represents the beam jitter after a mode cleaner and the lower represents the jitter after a monomode optical fiber.

Fig.2.9.1 The limits on the spectral strain amplitude for a FP interferometer having arm length L = 3 Km, as given by the pipe vacuum fluctuations in the frequency interval $0<\nu<10^3$ Hz and for three pressures:

a) $p = 10^{-6}$ mbar, b) $p = 10^{-7}$ mbar, c) $p = 10^{-8}$ mbar.

The dot line is N_2 and the continuous one is H_2.

Fig.2.12.1 Radiation pressure displaces the mirror M_2 from its equilibrium position. x(t) is then a multistable function of the radiation pressure.

Fig.2.12.2 Plot of the RHS of eq.(2.12.8); if the laser power P increases the peak at x_{n+2} may cross the y=0 axis thus creating a new stability point $\left(\frac{\partial y}{\partial x} < 0\right)$

Fig.2.15.1 Sensitivity in h power spectrum expressed as $1/\sqrt{Hz}$ of the proposed antenna, determined as a limit of different noises in the frequency interval between 1 and 10.000 Hz. The dotted curves are different noise sources while the continuous line refers to the incoherent sum, the parameters used in the computation are the same of paragraph 2.14.

Fig.2.15.2 Sensitivity in h of the antenna, determined as a limit of different noises in the frequency interval between 1 and 10.000 Hz. The curves refer to periodic signal and the integration time is one year; the dotted curves are different noise sources while the continuous line refers to the incoherent sum, the parameters used in the computation are the same of paragraph 2.14.

Fig.2.15.3 Sensitivity in h of the antenna, determined as a limit of different noises in the frequency interval between 1 and 10.000 Hz. The curves refer to pulse signals and the integration time is $1/\nu$, where ν is the frequency; the dotted curves are different noise sources while the continuous line refers to the incoherent sum, the parameters used in the computation are the same of paragraph 2.15.

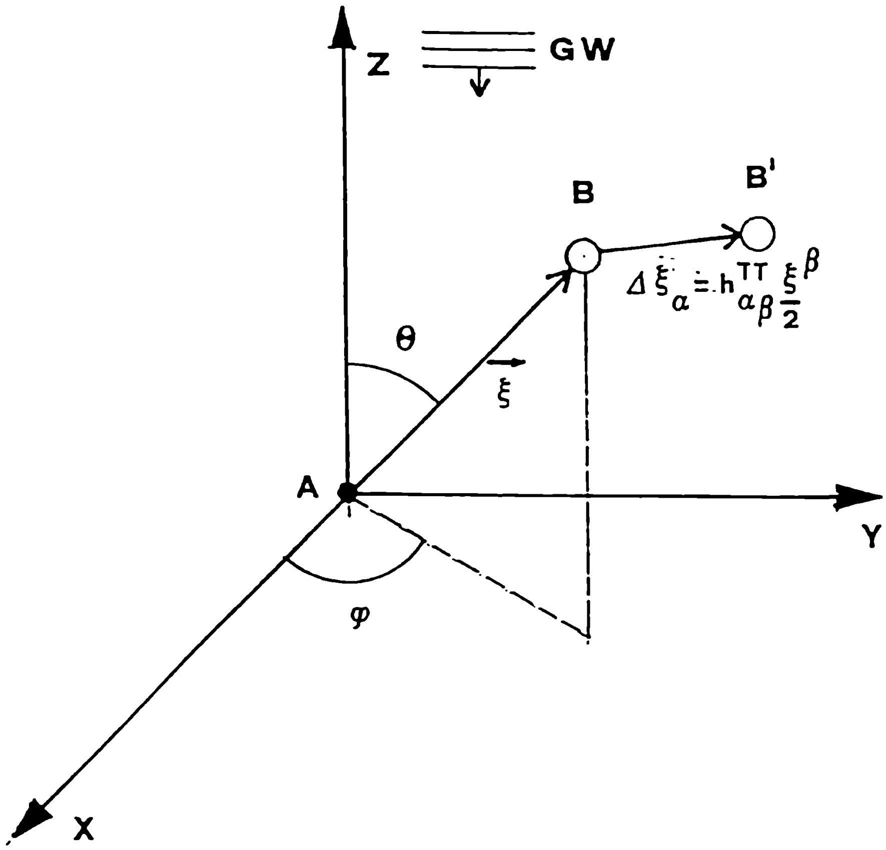
Z
GW
B
B'
$\Delta\ddot{\xi}_\alpha \doteq \ddot{h}^{TT}_{\alpha\beta}\frac{\xi^\beta}{2}$
θ
$\vec{\xi}$
A
Y
φ
X

Fig. 2.2.1

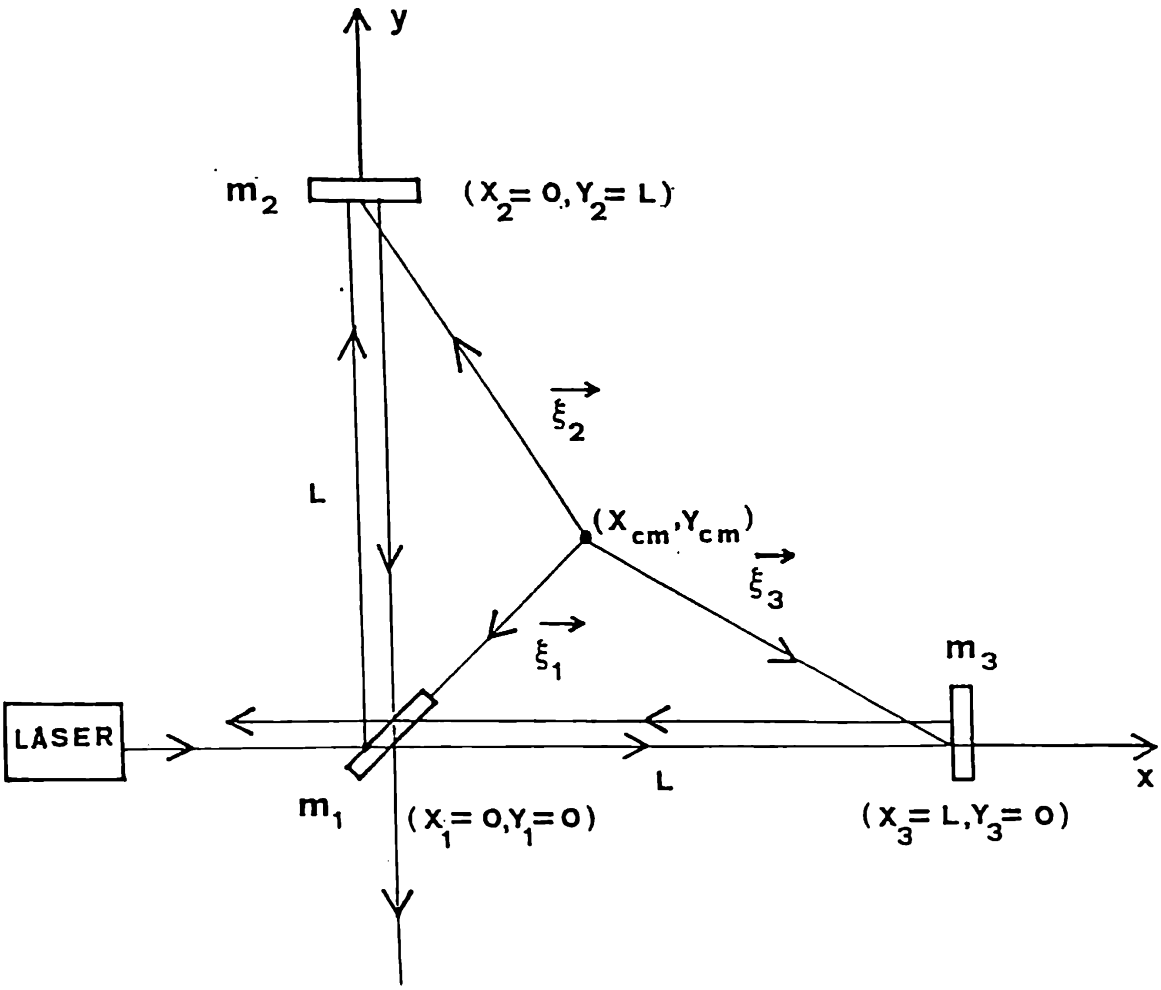

Fig. 2.2.2

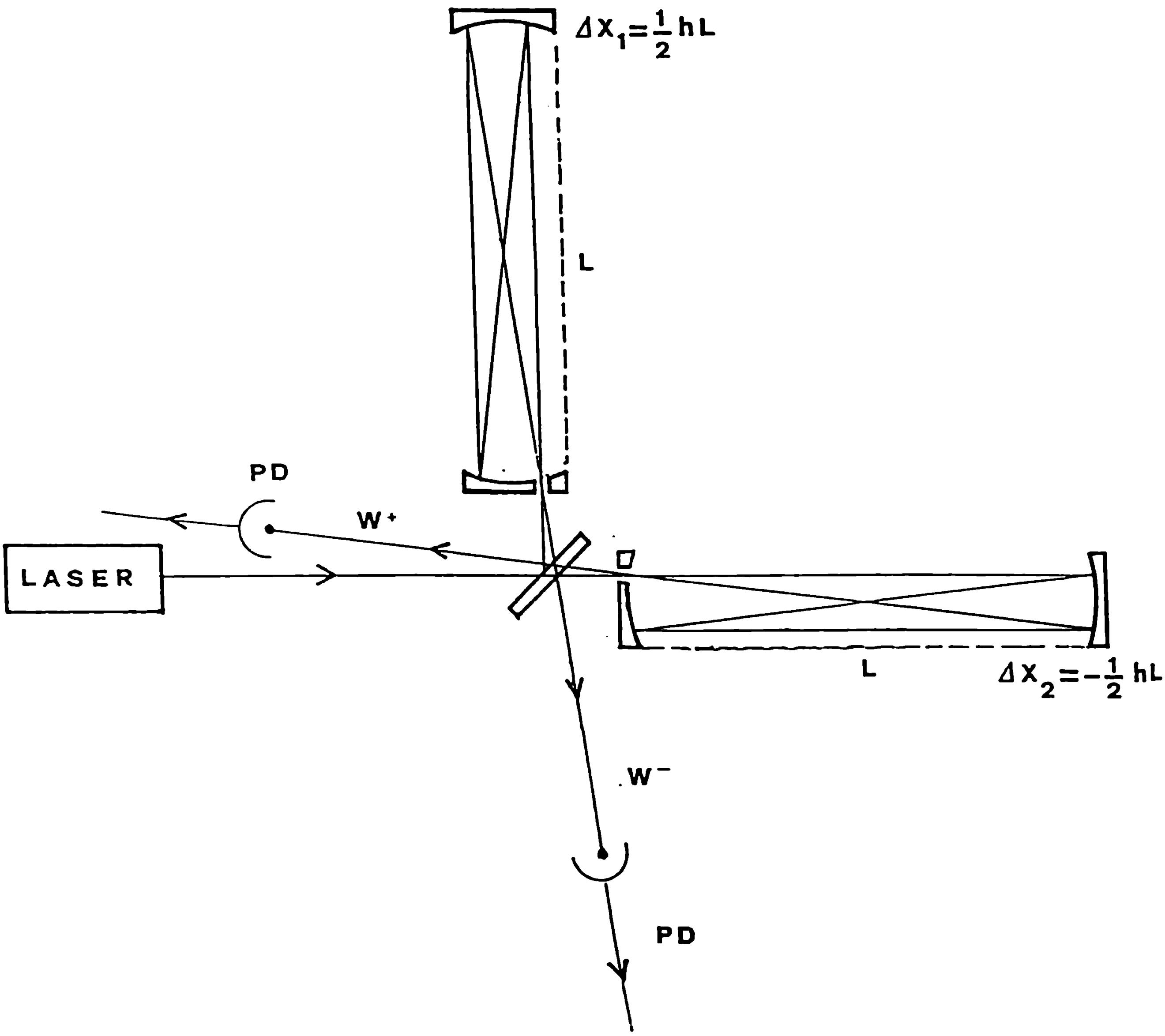

Fig. 2.3.1

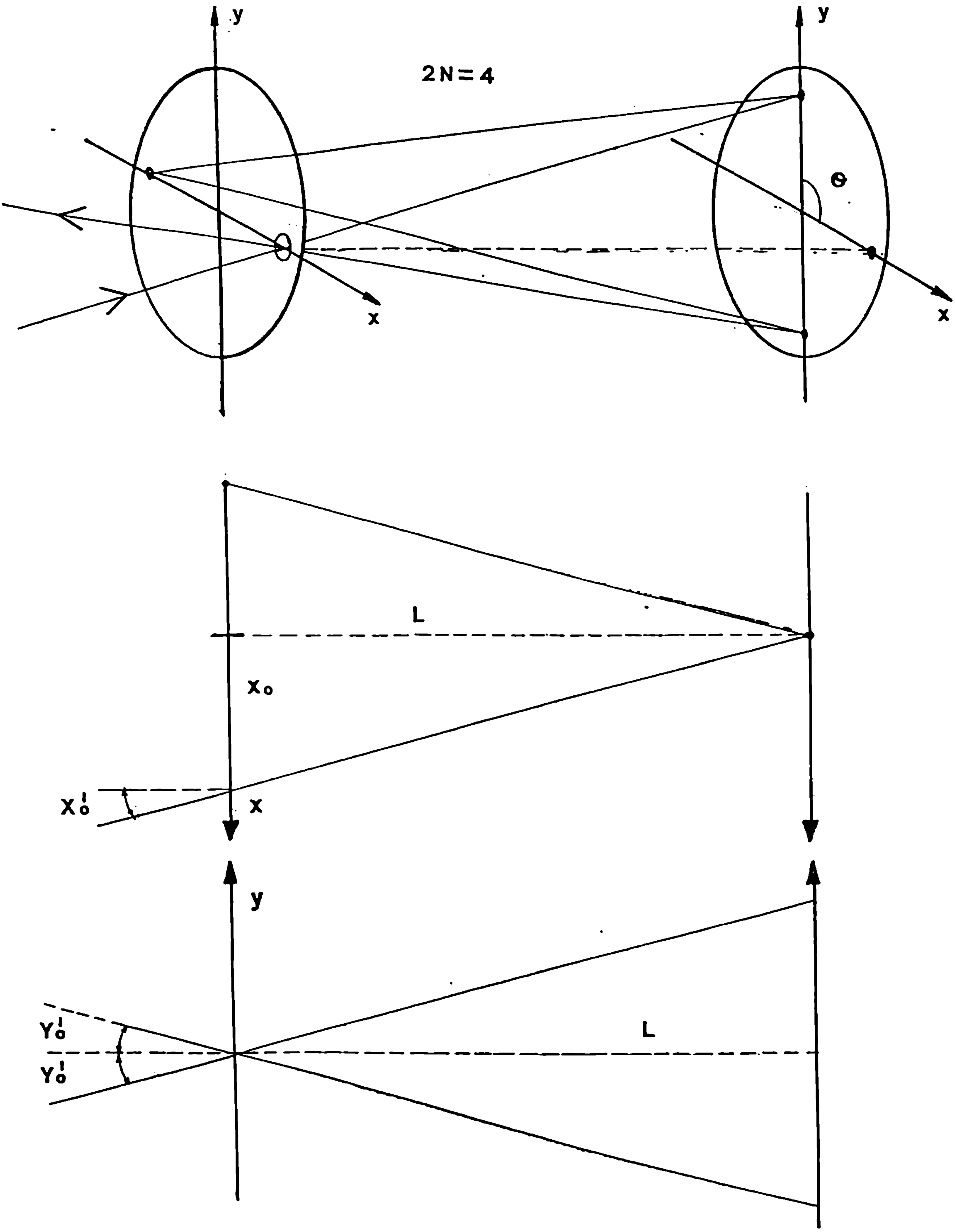

Fig. 2.3.2

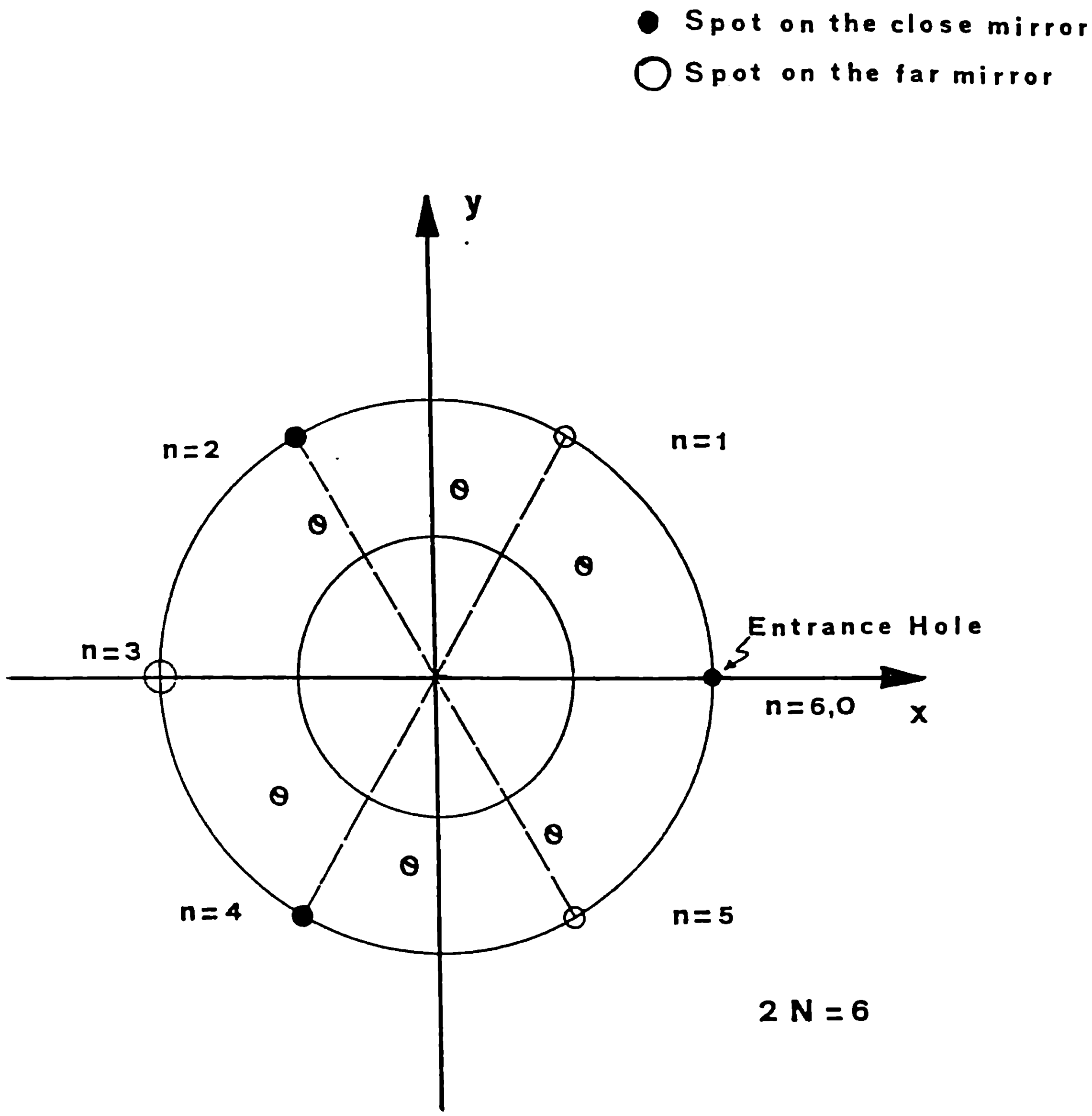
Spot on the close mirror
Spot on the far mirror
y
n=1
n=2
n=3
n=4
n=5
n=6,0
x
Entrance Hole
θ
2 N = 6

Fig. 2.3.3

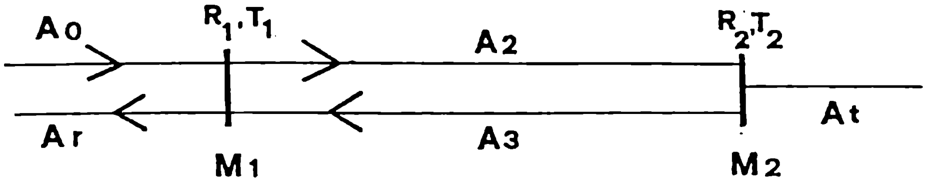

Fig. 2.4.1

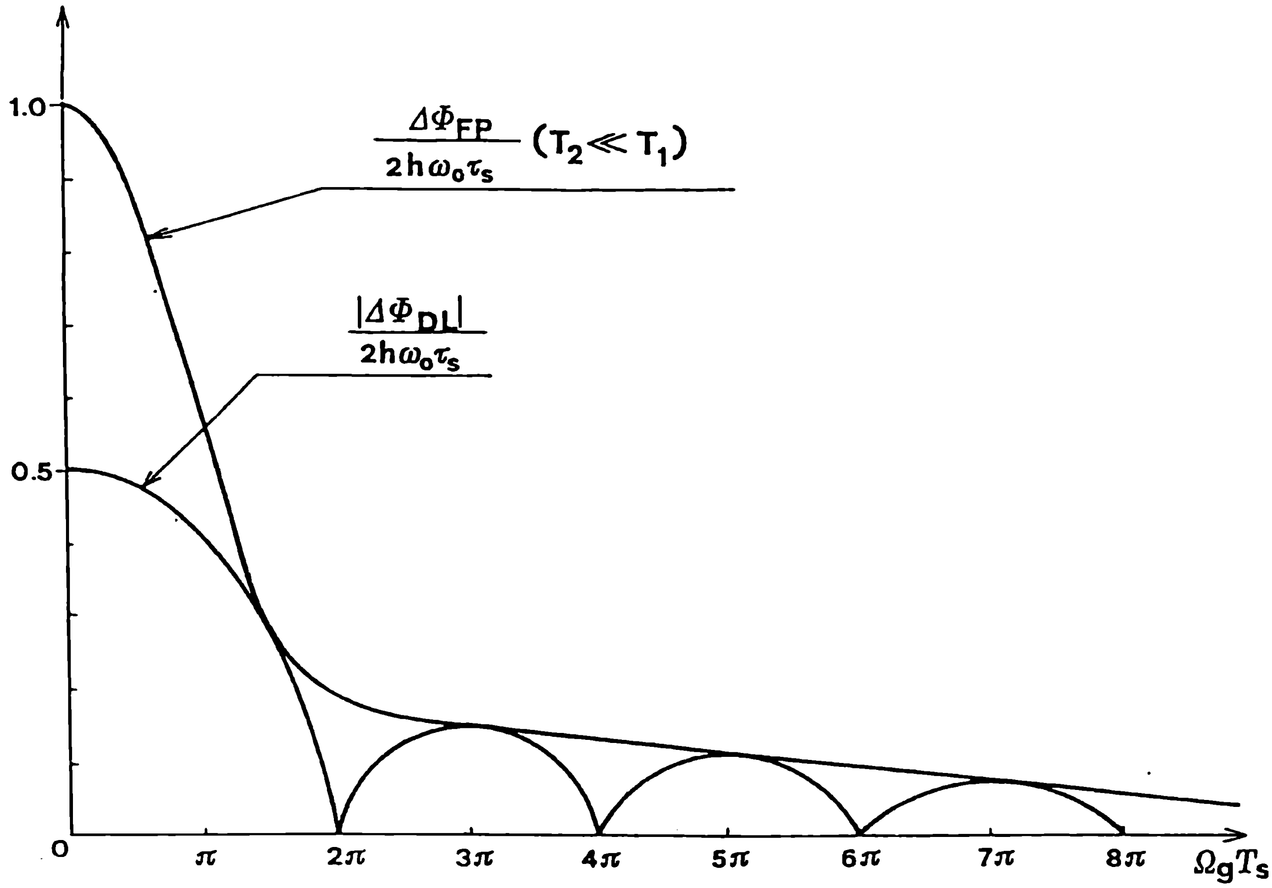

1.0
0.5
0
$\frac{\Delta\Phi_{FP}}{2h\omega_0\tau_s}$ $(T_2 \ll T_1)$
$\frac{|\Delta\Phi_{DL}|}{2h\omega_0\tau_s}$
π
2π
3π
4π
5π
6π
7π
8π
$\Omega_g T_s$

Fig. 2.4.2

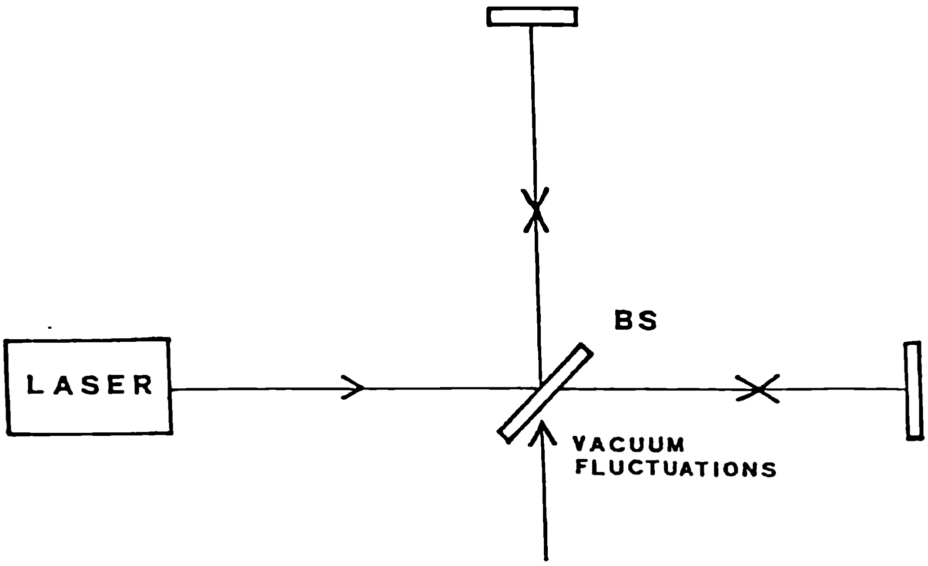

Fig. 2.5.1

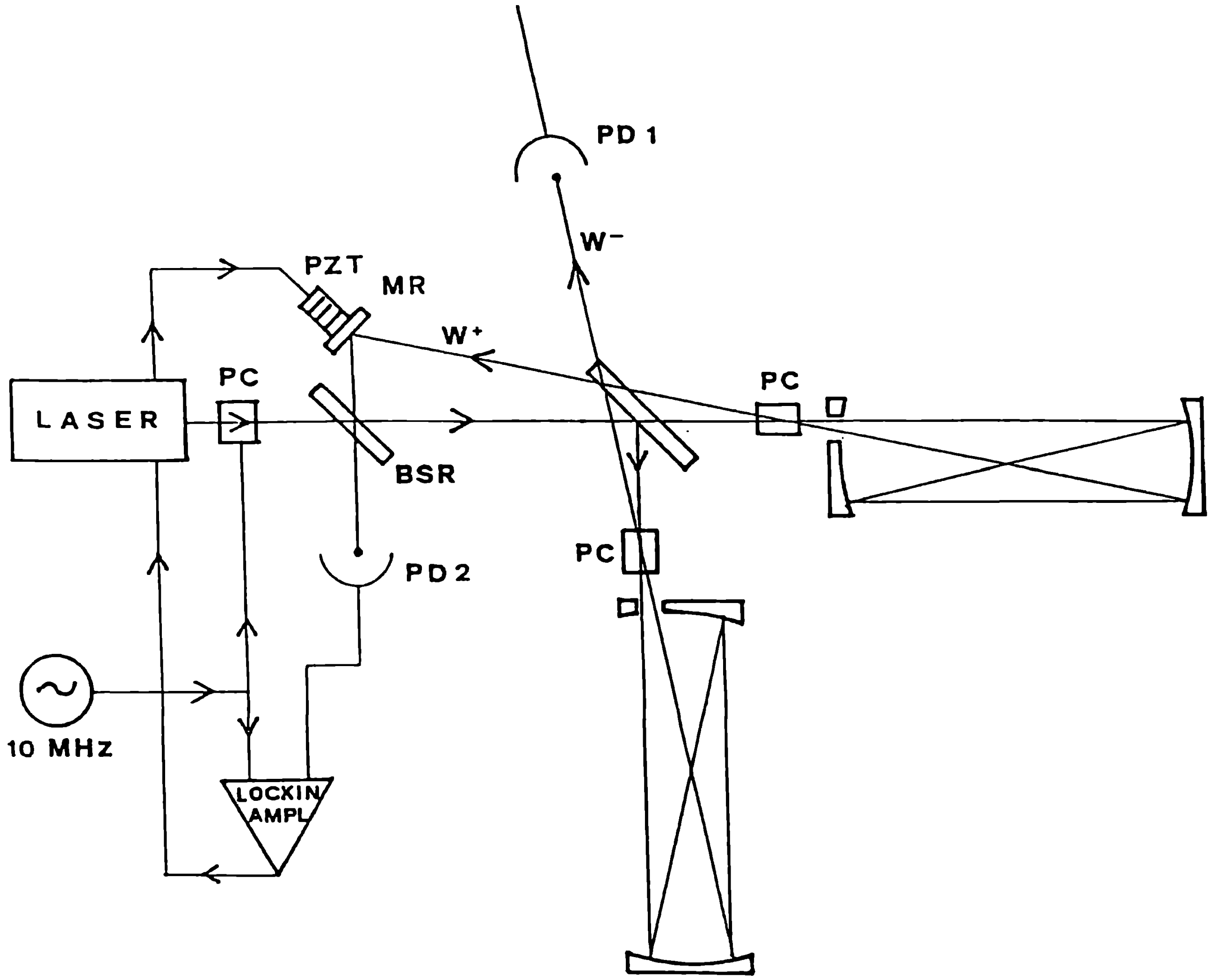

Fig. 2.5.2

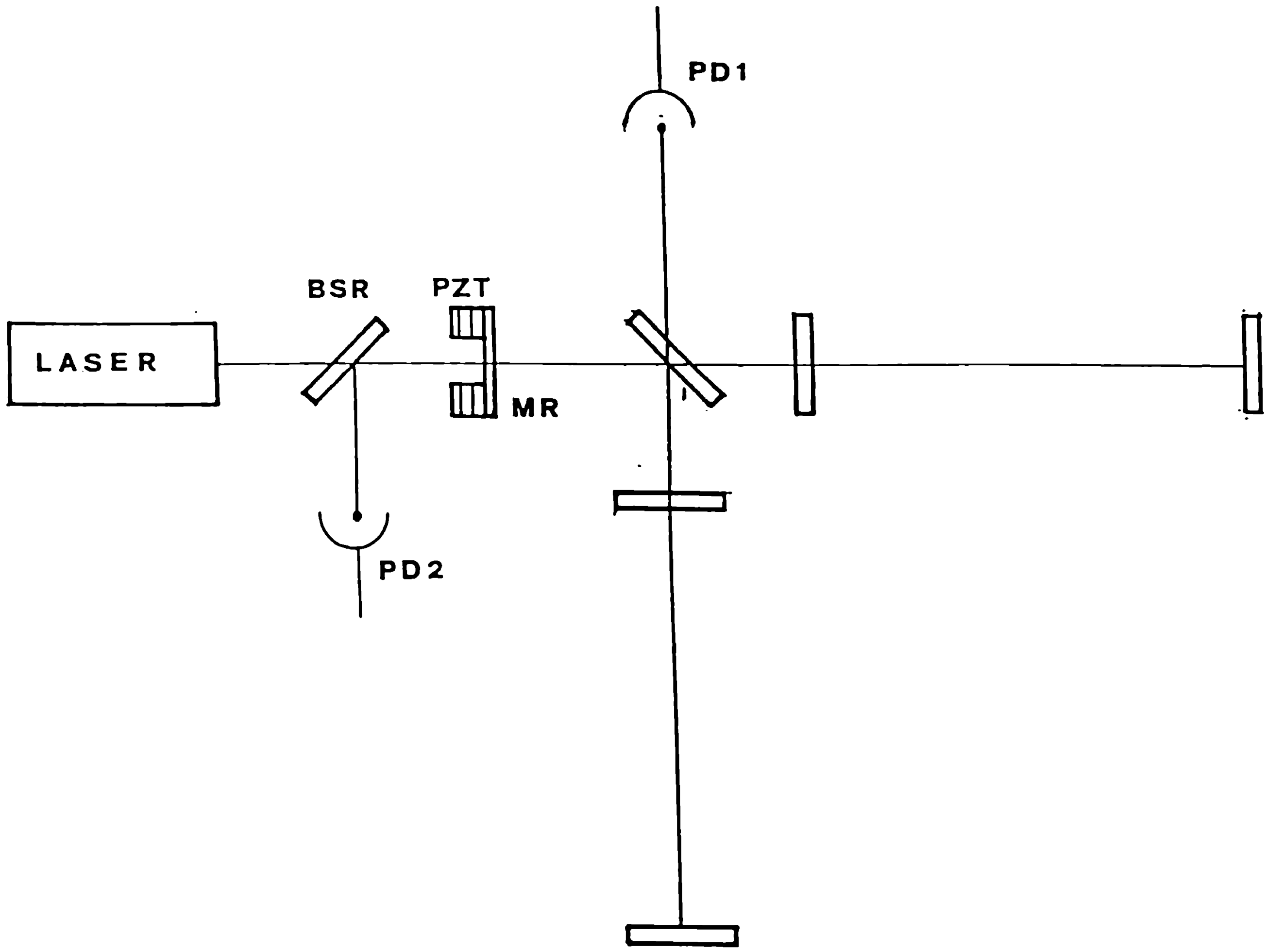

Fig. 2.5.3

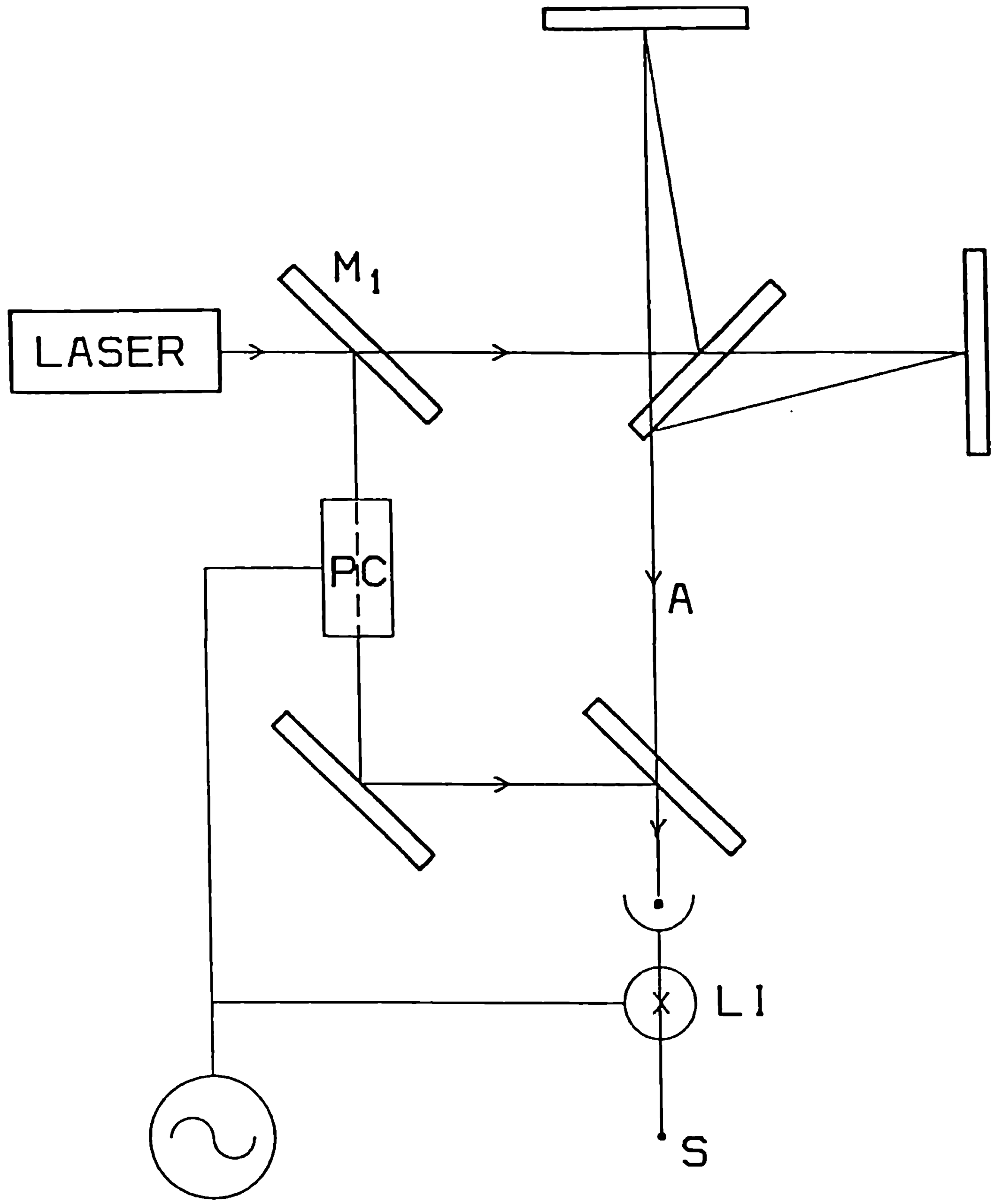

Fig. 2.6.1

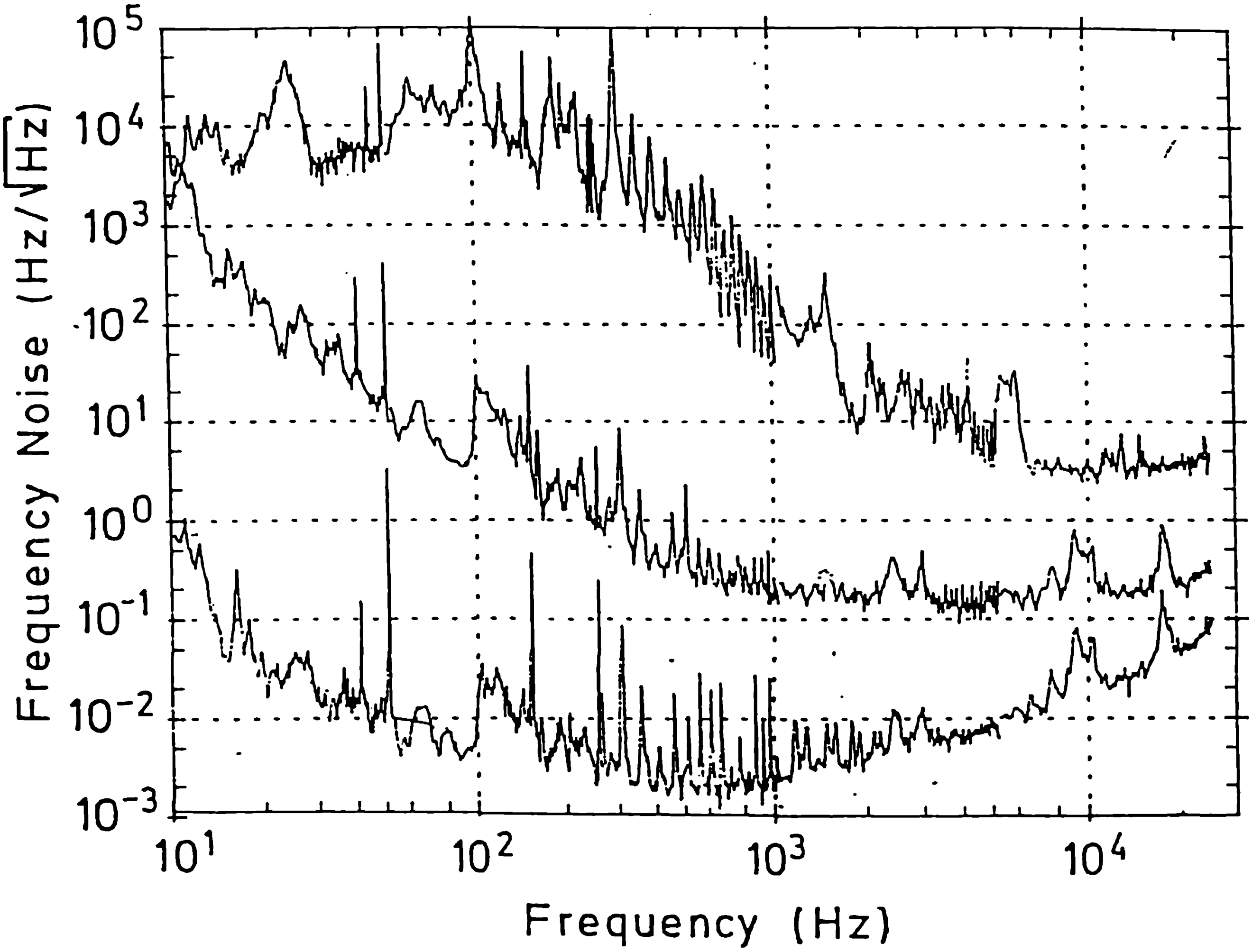

Frequency Noise (Hz/√Hz)
Frequency (Hz)
10^5
10^4
10^3
10^2
10^1
10^0
10^{-1}
10^{-2}
10^{-3}
10^1
10^2
10^3
10^4

Fig. 2.7.1

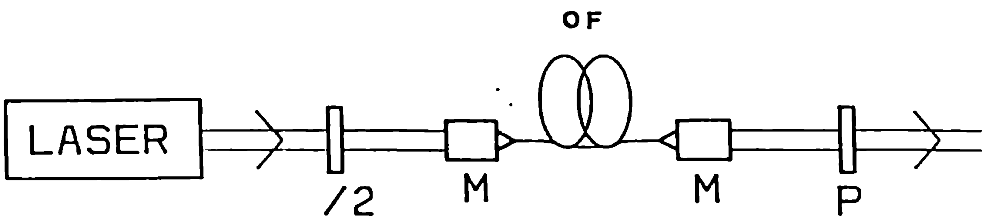

Fig. 2.8.1

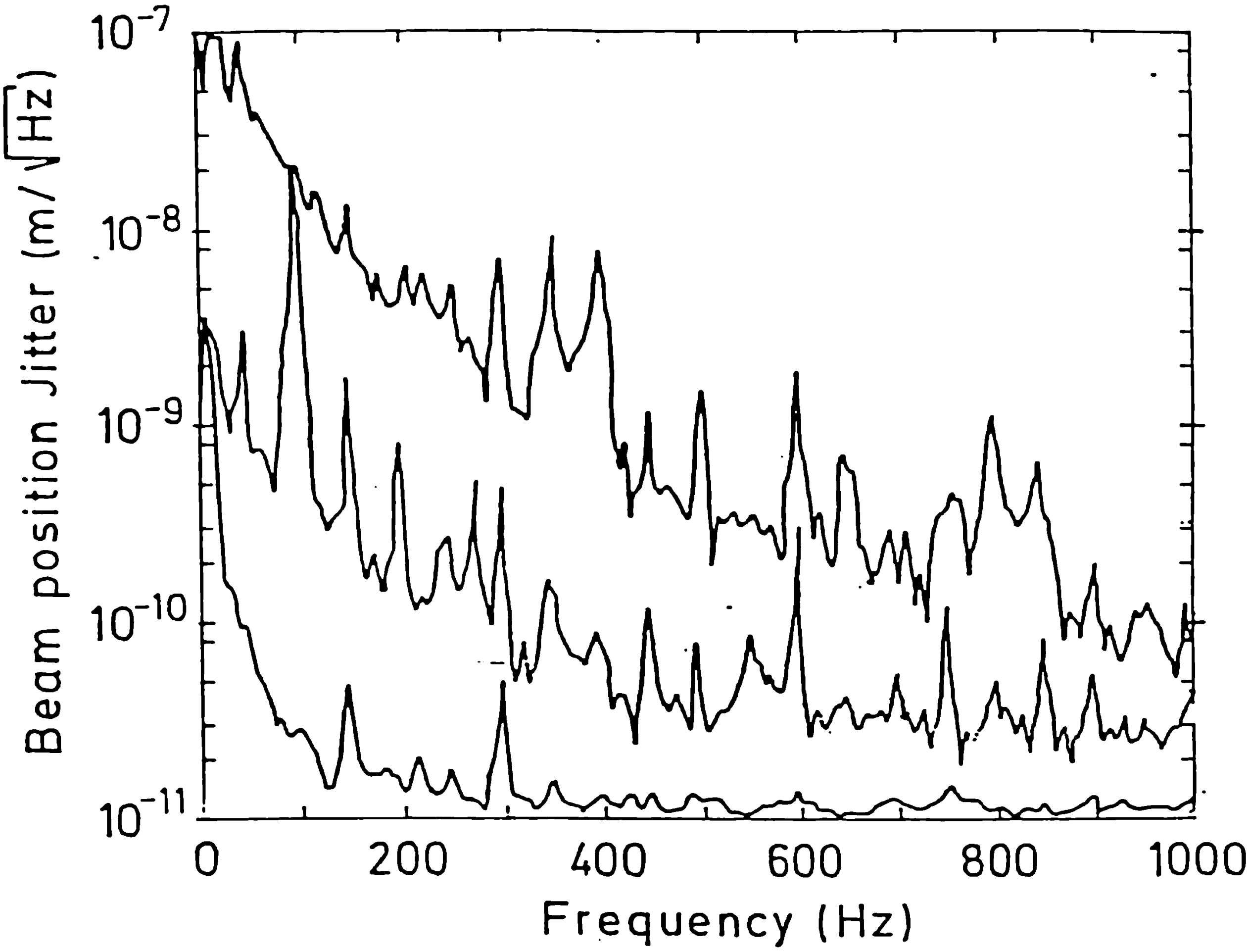

10^{-7}
10^{-8}
10^{-9}
10^{-10}
10^{-11}
Beam position Jitter (m/$\sqrt{Hz}$)
0
200
400
600
800
1000
Frequency (Hz)

Fig. 2.8.2

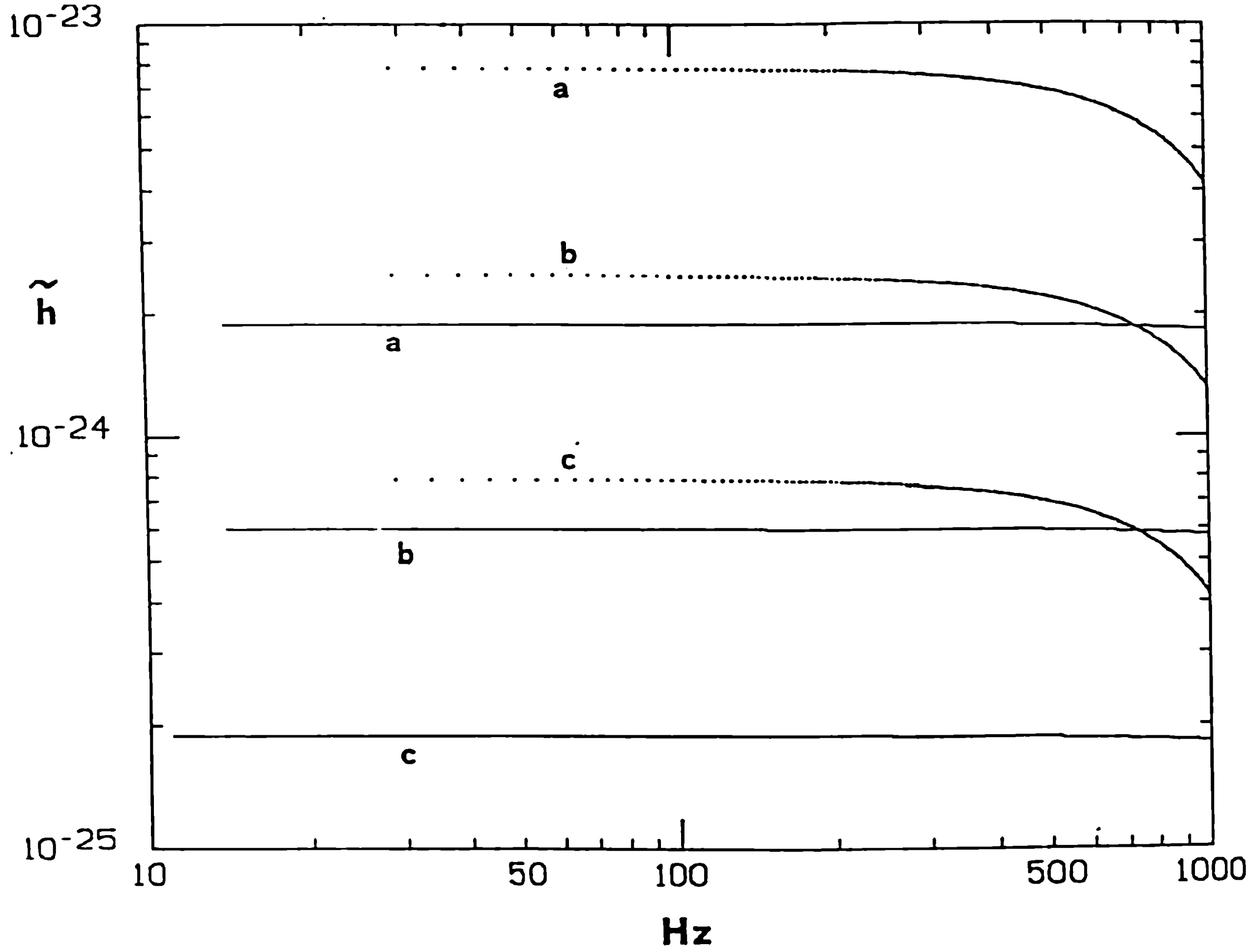

Fig. 2.9.1

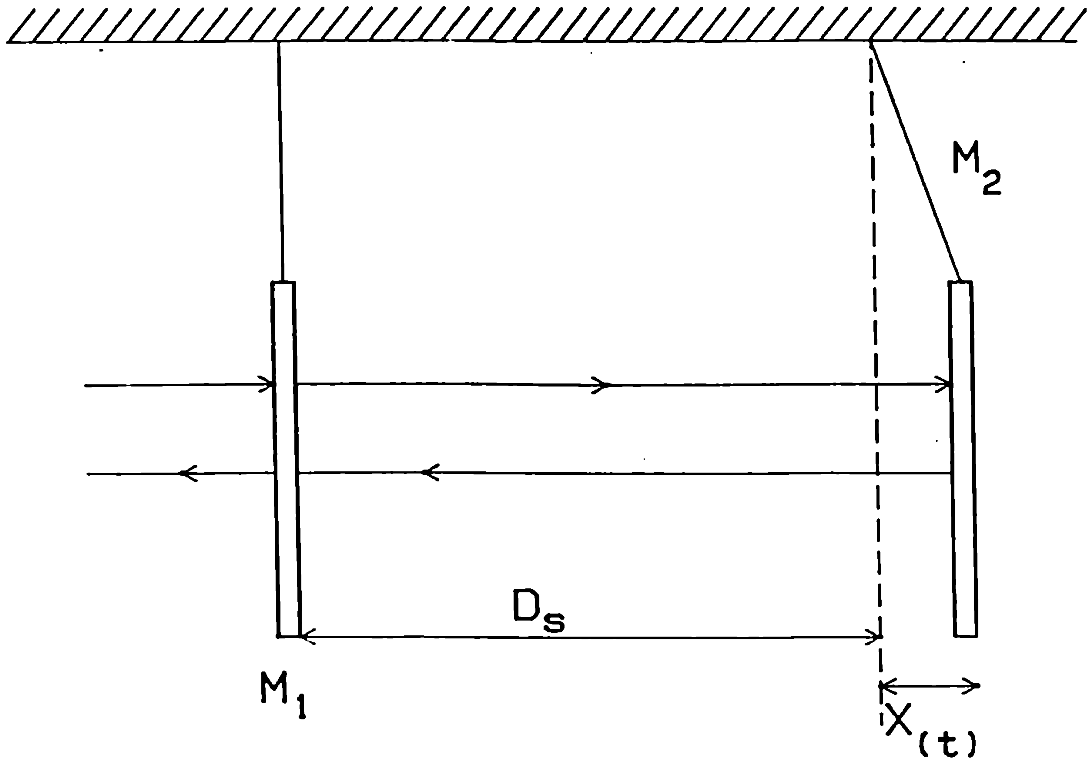

Fig. 2.12.1

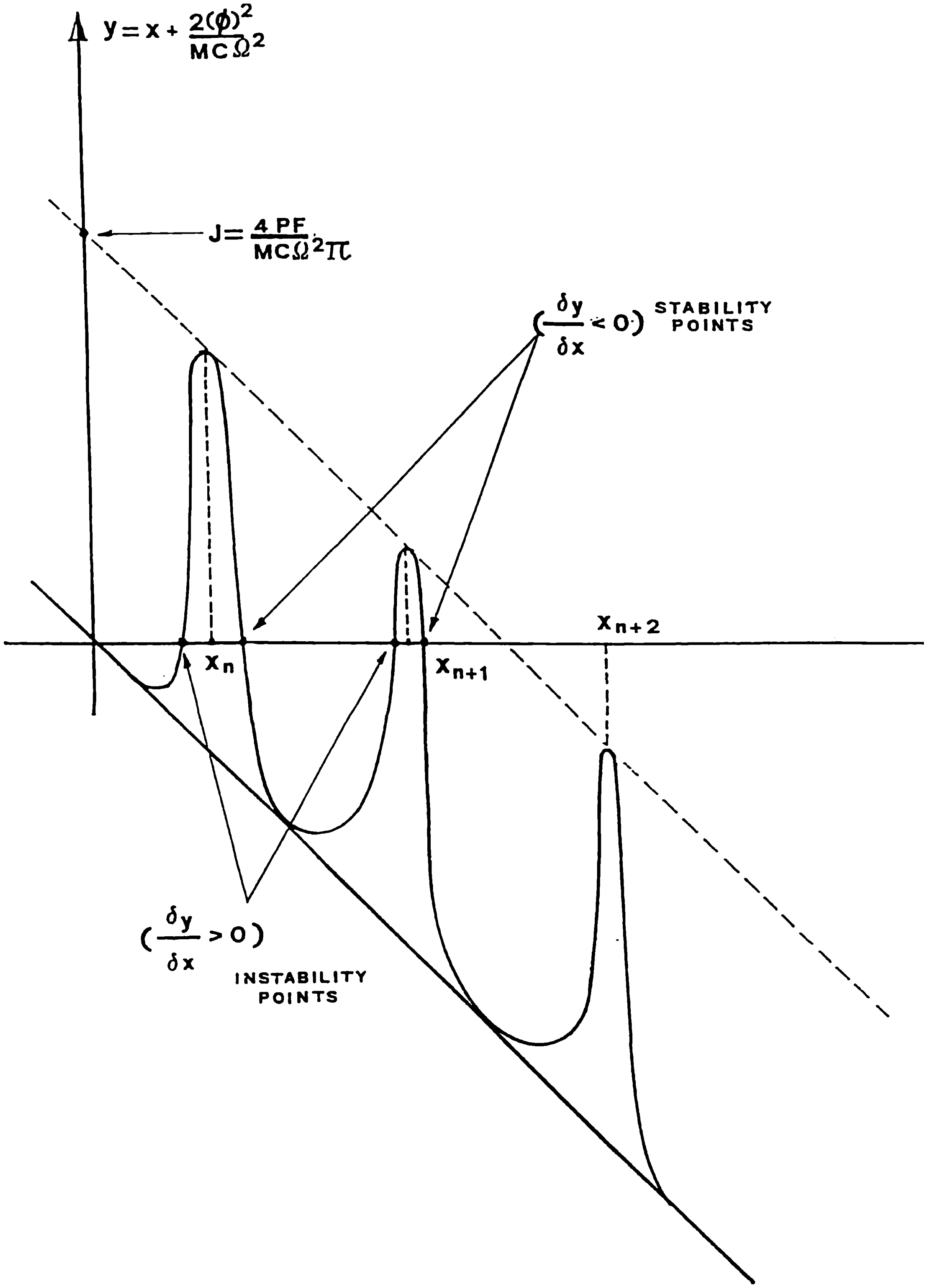

$y = x + \frac{2(\phi)^2}{MC\Omega^2}$
$J = \frac{4\,PF}{MC\Omega^2\pi}$
$(\frac{\delta y}{\delta x} < 0)$ STABILITY POINTS
x_n
x_{n+1}
x_{n+2}
$(\frac{\delta y}{\delta x} > 0)$
INSTABILITY POINTS

Fig. 2.12.2

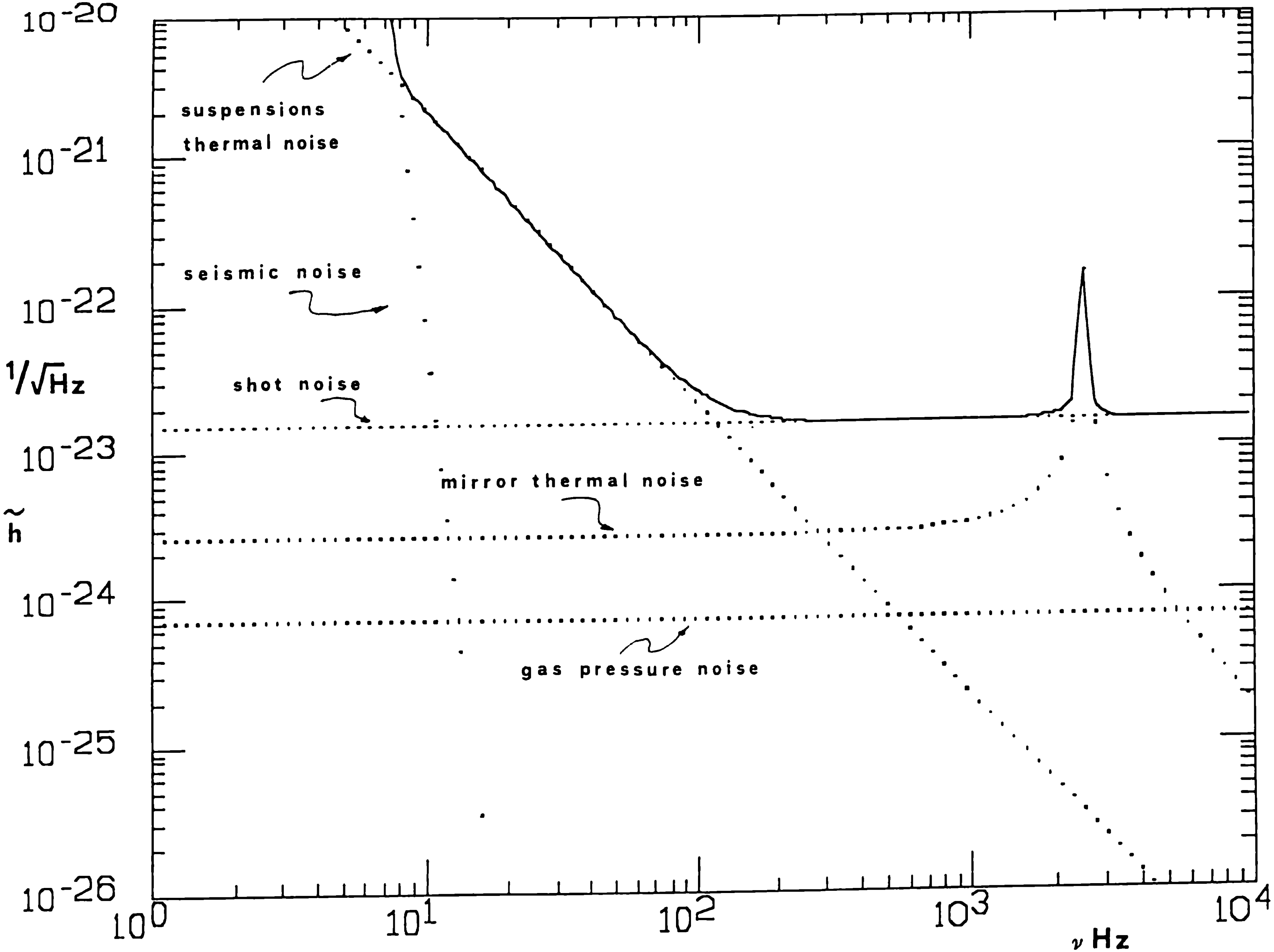

suspensions thermal noise
seismic noise
shot noise
mirror thermal noise
gas pressure noise
$^1/\sqrt{Hz}$
$\tilde{h}$
10^{-20}
10^{-21}
10^{-22}
10^{-23}
10^{-24}
10^{-25}
10^{-26}
10^0
10^1
10^2
10^3
10^4
ν Hz

Fig. 2.15.1

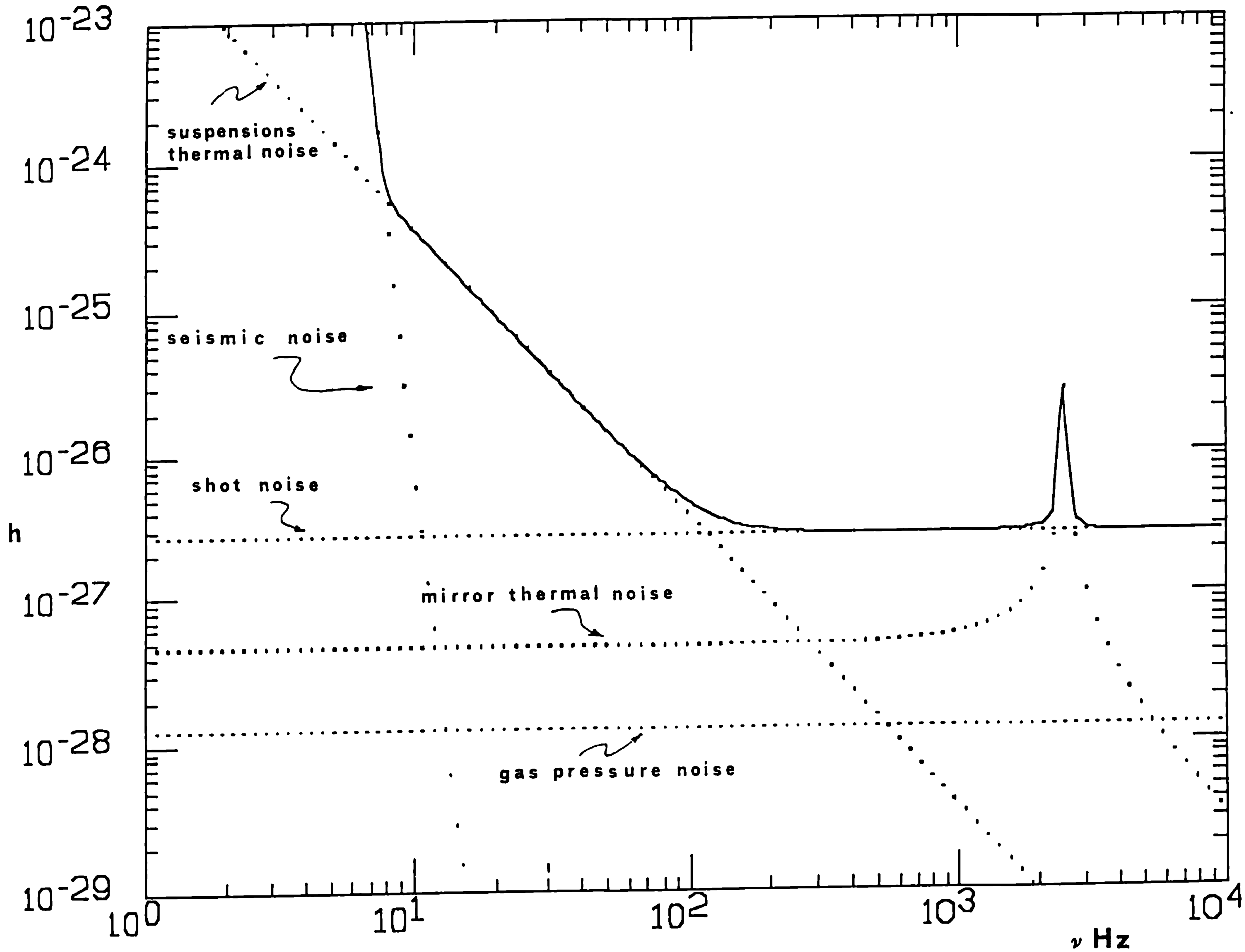

suspensions
thermal noise
seismic noise
shot noise
mirror thermal noise
gas pressure noise
h
ν Hz

Fig. 2.15.2

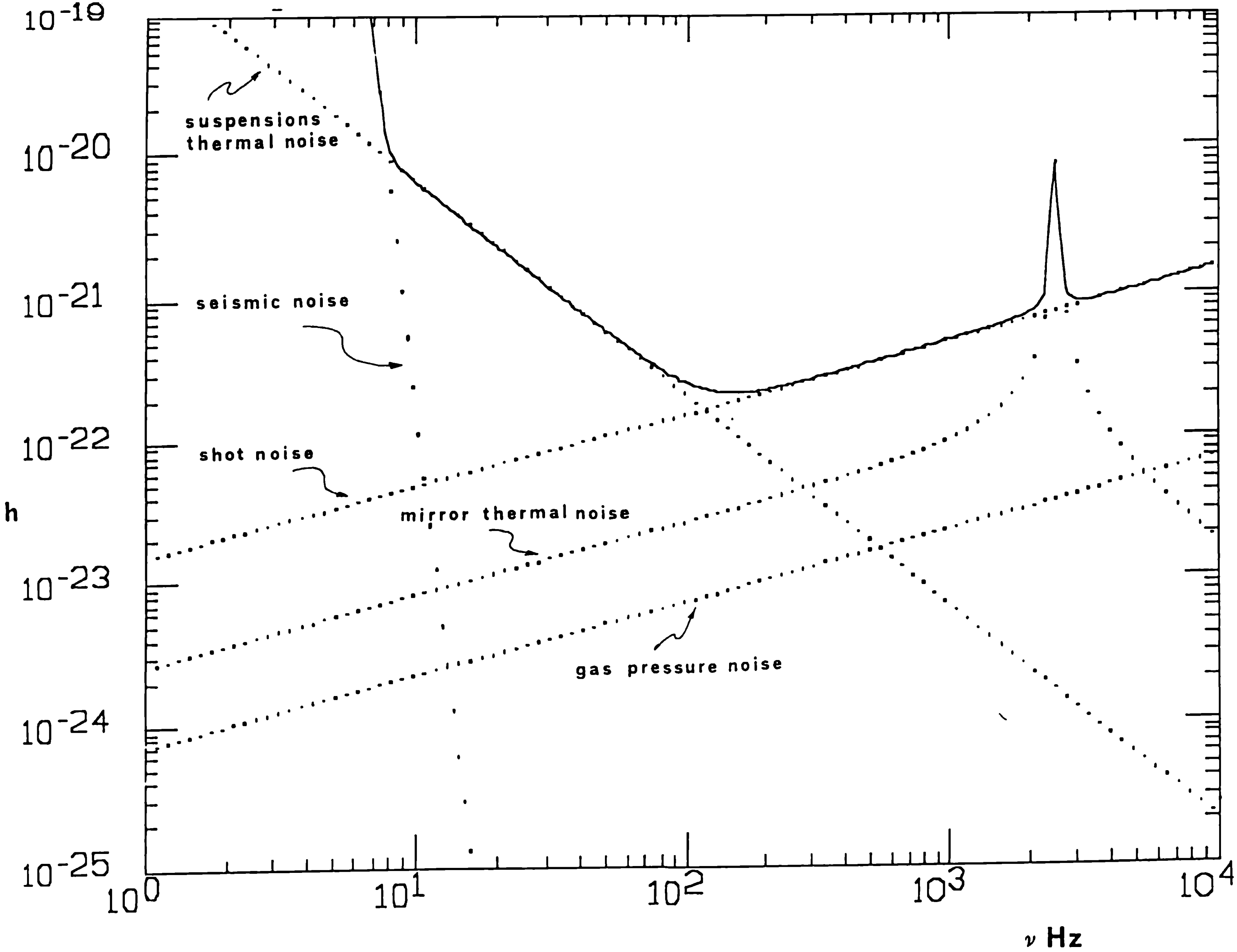

10^{-19}
10^{-20}
10^{-21}
10^{-22}
10^{-23}
10^{-24}
10^{-25}
h
suspensions thermal noise
seismic noise
shot noise
mirror thermal noise
gas pressure noise
10^{0}
10^{1}
10^{2}
10^{3}
10^{4}
ν Hz

Fig. 2.15.3

Chapter 3

Description of VIRGO

3.0 Outline

3.0.1) SENSITIVITY GOALS

The general concept of the VIRGO interferometer is the logical consequence of the scientific arguments developed in the previous chapters.

The sensitivity goals must be ambitious enough to reach the range where the astrophysicists predict at least a few events per year, and modest enough to ensure the feasibility of the experiment.

We aim for a shot-noise limited sensitivity at high frequency of :

$$\tilde{h} = 3.10^{-23}\ \mathrm{Hz}^{-1/2} \text{ above 200 Hz.}$$

Around 10 Hz, the sensitivity should be approximately equally limited by the seismic noise and by the thermal noise of the suspension around $\tilde{h} = 1.10^{-21}$ $1/\sqrt{\mathrm{Hz}}$ or $h = 2.10^{-25}$ for an integration time of one year.

The achievement of these performances would give us a *very good chance* to detect the signals from supernovae up to the VIRGO cluster. It would *ensure* enough sensitivity to detect coalescing binaries as far as 100 MPsec. It would allow us to *expect* the observation of pulsar signals from our galaxy.

3.0.2) GENERAL CONCEPT

The VIRGO interferometer is basically a Michelson interferometer (MITF), with two 3 km long, perpendicular arms. The large length of 3 km is chosen mainly to decrease the influence of displacement noises, like seismic noise and thermal noises (see 3.4).

Each arm contains a "gravito-optic transducer", constituted by a 3 km long Fabry-Perot cavity having a finesse of the order of 40 (see 3.1). This optimizes the sensitivity to gravitational waves in the frequency domain around 1 kHz and prevents any difficulty with the effects of radiation pressure .

The use of a "light recycling" technique reduces the required laser power from 500 W to 10W (see 3.2).

The laser source is frequency and amplitude stabilized using very fast, ultrahigh gain, shot-noise limited servo-loops (see 3.3).

The critical components of the interferometer, i.e. two mirrors in each arm, the beamsplitter and the recycling mirror, are seismically isolated by multidimensional "Superattenuators" (see 3.4).
The position and the alignment of the optical components are maintained by local servo-loops under global computer control (see 3.5).
The whole system operates under a high vacuum, in order to avoid acoustic noise and fluctuations in the index refraction (see 3.6).
A suitable site for the construction of VIRGO has been found in Cascina, near Pisa (see 3.7).
Data acquisition consists in running the apparatus and recording the fluctuations of the phase difference between the beams reflected by the two transducers, with a bandpass of 10 Hz to 3 kHz, while monitoring the environment and the apparatus parameters (see 3.8).

3.0.3) EXPLOITATION

Once the interferometer functions with a high enough sensitivity, it requires little human intervention, except for maintenance. There will be some filtering of the data, inside the VIRGO group, to characterize the noise statistics of the VIRGO interferometer, to look for periodic or quasi periodic sources and to preselect possible gravitational bursts. Agreements with all the other groups will result in an exchange of recorded data, to allow the astrophysicists to extract more complete information and to confirm the pulses by an analysis of the coincidences (see 3.8).

3.1 Optics

3.1.1) OPTICAL COMPONENTS

3.1.1.1) SPECIFICATIONS AND GENERALITIES

The main constraints on the optical system come from the shot-noise limitation and from the demand of wideband operation : in order to reach the required sensitivity of $h = 3\ 10^{-23}\ Hz^{-1/2}$ in a device optimized for the detection of signals around 1 kHz, it is necessary that the effective light power incident on the beamsplitter of the Michelson interferometer be larger than 500 W. This calls for a high power laser, and a special optical design involving a "recycling" technique, which itself requires very high quality optical components and optical coatings.:
The purpose of this section is to describe and to justify the optical scheme we have designed for the VIRGO project, including the laser source. The design is based on experimental data obtained by the GROG in Orsay, on computer simulations (GROG, Palaiseau), and on many interactions with manufacturers of optical components. The laser part is also based on experimental results obtained in Orsay and on some reasonable extrapolations on the evolution of commercial lasers.

3.1.1.2) BEAM GEOMETRY

3.1.1.2.1) OPTICAL DESIGN

The basic principles of the interferometric detection of gravitational waves have been recalled above. Among the two possibilities for the gravito-optic transducers, we have chosen the Fabry-Perot solution, because of its higher flexibility and because it requires smaller mirrors (the very large diameter mirrors which are required for a delay-line system may be very difficult to manufacture, and are presently nearly impossible to coat with the best coating technologies). In order to reach the 500 W power, the first generation of antenna will use recycling, in its most simple version, standard recycling, and a 10 to 50 Watts Nd:YAG laser operating at 1.06 μm. Fig.3.1.1 shows a schematic representation of the VIRGO interferometer:

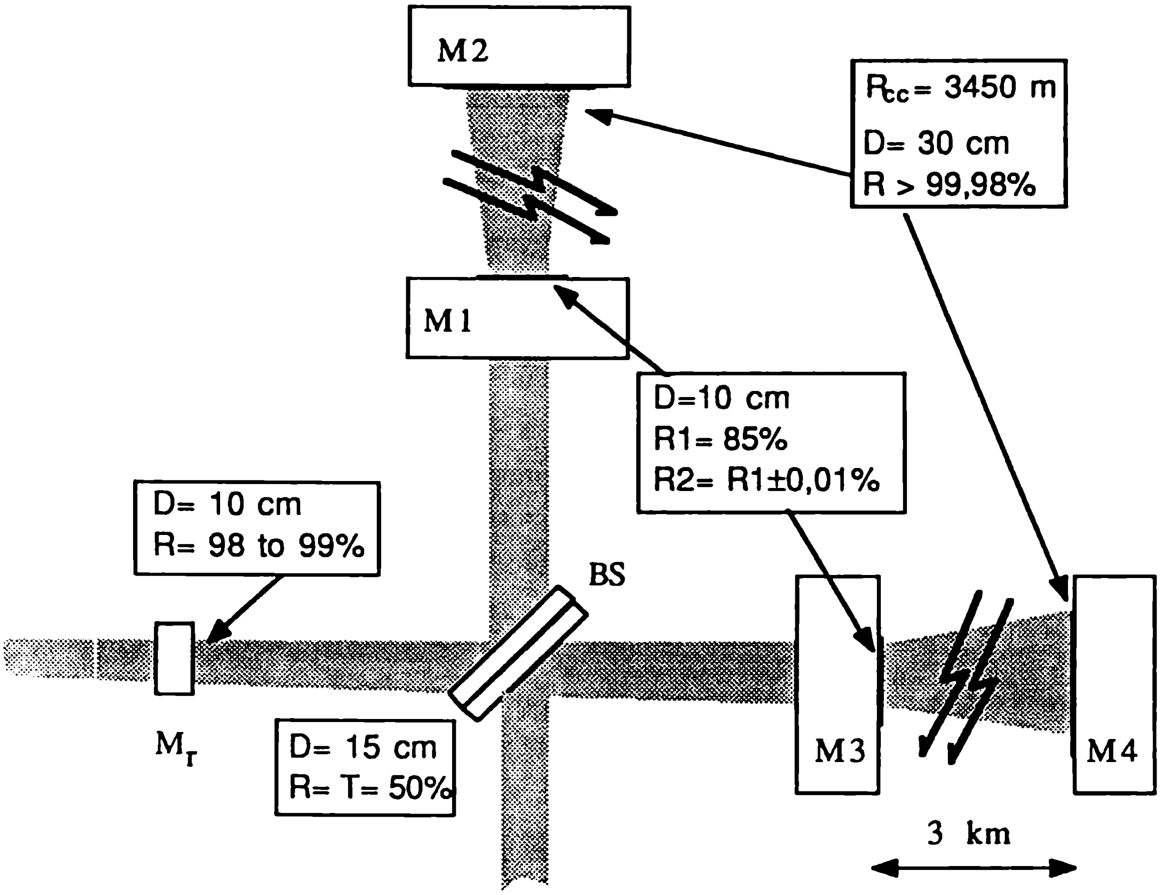

Figure 3.1.1 : Schematic representation of a recycling MITF with Fabry-Perot gravito-optic transducers

In order to minimize the contribution of shot-noise, the MITF is tuned to a transmission minimum, so that most of the incident light is reflected and can be "recycled" by the mirror M_R (Drever,[1981]), provided the resonant cavity formed by M_R and by the MITF as a whole is kept on resonance with the laser frequency (this idea has been checked experimentally in Orsay). In the following, we will be mainly concerned with the efficiency of the recycling, i.e. the ratio S of the light power circulating in the interferometer at resonance to the light power delivered by the laser (the theoretical sensitivity improves as $\sqrt{S}$). The contrast of the MITF is also a very important parameter, but less stringent (if the contrast is not very high, then S cannot be large).

The value of S is determined by the "equivalent reflectivity " R_{eff} of the interferometer, and equal to $S = \frac{1}{1 - R_{eff}} = \frac{1}{T_{eff}}$ when the transmission of the recycling mirror M_R is properly chosen.

The factors which contribute to decrease R_{eff} may have various origins:

a- pure energy losses in the arms of the MITF: absorption or scattering of the mirrors b- non perfect recombination of the two beams on the beamsplitter due to misalignments, wavefront distortions (mirror surfaces, coatings inhomogeneity, diffraction by finite apertures, beamsplitter and mirror substrate wavefront), depolarization.

The effective losses l_{eff} are the sum of both contributions. For the first case, we will simplify the problem and assume that the missing photons are just lost, and do not interfere at any level, while in the second case the losses result from incomplete interference of the distorted reflected beam with the incident laser beam (supposedly Gaussian, TEM_{00}). We expect to reach the sensitivity goal with a laser power of a few tens of watts and a recycling factor of the order of $S \approx 100$, which requires that the effective losses l_{eff} be smaller than 1%.

3.1.1.2.2) BEAM GEOMETRY

Inside the Michelson interferometer (MITF), the geometry of the beams is determined by the eigenmodes of the resonant cavities in the two arms. Assuming everything is perfect, these beams will be Gaussian. They should be matched with the incident laser beam and with the eigenmode of the recycling cavity. In practice, the confocal parameter of this eigenmode is very large, compared with the metric distances which separate M_R, BS, M1 and M3, so that we can assume the beam geometry to be constant in the central area. (this is justified by numerical tests).

The main optical design constraints, which determine the curvature radius of the mirrors of the Fabry-Perot cavities are the following :

a- the transverse extension of the beams should be kept small on all mirrors, for many reasons: diffraction losses, cost of the vacuum tank, homogeneity and even feasibility of the coatings. A few tens of centimeters is the maximum reasonable mirror diameter, and this diameter should exceed by a factor 2.5 the beam diameter at $1/e^2$ intensity points, in order to reduce diffraction losses to a tolerable level.

b- this same beam diameter should be particularly small in the central area, to allow for the use of the most homogeneous optical materials for the beamsplitter and the substrate of the input mirrors M1 and M3, minimizing wavefront distortions.

c- it is preferable to use non degenerate cavities, so as to avoid exciting high order modes when the interferometer is locked on the TEM_{00} mode, but slightly misaligned or mismatched. To characterize a cavity, for given values of the cavity length and of the curvature radius, we have defined a merit factor M in the following way:

$$\frac{1}{M^2} = \sum_{k=1}^{\infty} \frac{1}{\left(\nu_k - \nu_0\right)^2 k!}$$

where ν_k and ν_0 are the resonant frequencies of the TEM_{00} and of the $TEM_{m\,n}$ modes (k=m+n), as calculated from the theory of the Fabry-Perot resonator with spherical mirrors (Abderrazik [1967]) that is:

$$(\nu_k - \nu_0) = \frac{k}{\pi} \cos^{-1}[1-(\frac{L}{Rcc})]$$

where R_{cc} is the curvature radius of the end mirrors of the cavities. The weighting factor $1/k!$ represents the probability of excitation of the $TEM_{m\,n}$ mode, for a small misalignment (Bayer-Helmes [1983]). It decreases when the mode order m+n increases, so that we can reasonably stop the expansion at k=10.

The merit factor has the dimension of a frequency separation, expressed in units of the cavity free spectral range. Its value is zero in the case of a degenerate cavity.

d- both arms should be very symmetrical, to reduce the influence of the laser frequency and amplitude jitter.

The obvious way to realize condition b is to choose flat mirrors for M1 and M3 : this localizes the beam waist on these mirrors. Fig.3.1.2 represents M as a function of R_{cc} for a cavity length of 3 km.

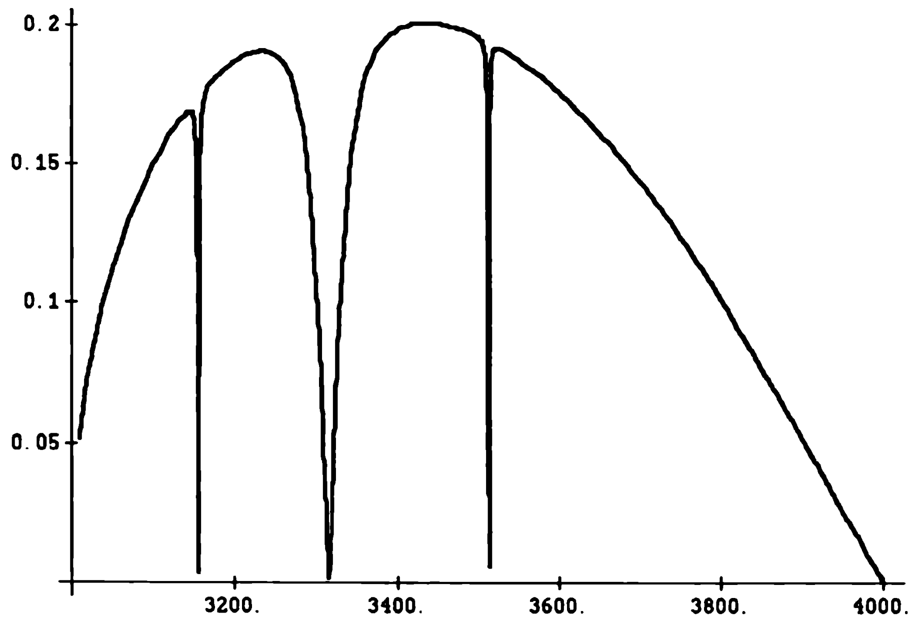

Fig.3.1.2 : The degeneracy merit factor β as a function of the curvature radius

The curvature radius R_{cc} of M2 and M4 can be selected from Fig.3.1.3 which represents the beam diameter on M1 (M3) and on M2 (M4), as a function of R_{cc} for L = 3 km.

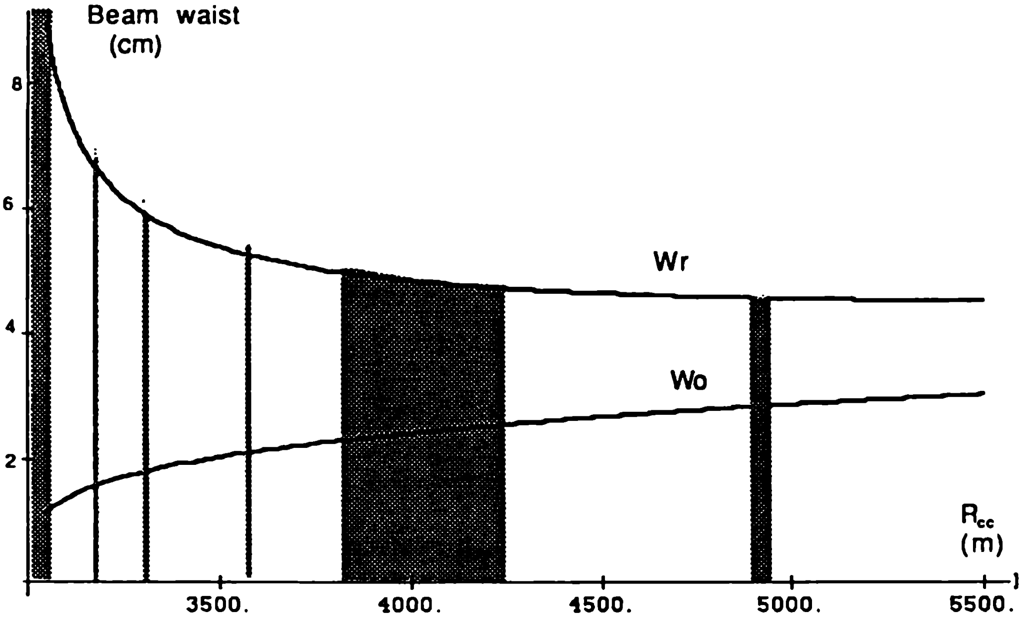

Fig 3.1.3 : Beam waist size on input (w_o) and output (w_r) mirrors

The shaded areas correspond to the zones where the merit factor M is less than 0.10. The choice of R_{cc} = *3450m* is reasonable: it leads to a $1/e^2$ beam diameter of the order of 14 cm on M2 and M4, and of 4 cm on M1 and M3, and is not too close from degeneracy for any mode with m+n<11. The region around 4500m is also interesting from the viewpoint on degeneracy, but it leads to a too wide waist size on the input mirror.

It is clear from Fig.3.1.3 that this already puts some constraint on the precision of the radius of curvature: a relative precision $\Delta R / R_{cc} = 3\,\%$ is required.

3.1.1.3) MIRROR COATINGS

3.1.1.3.1) LOSSES

Let's call l_m the average energy loss per mirror in the Fabry-Perot cavities, Ri and T_i the reflexivity and transmission of the input mirrors (M1 and M3), R_e the reflexivity of the end mirrors (M2 and M4), which are not supposed to transmit. This gives the relations: $l_m = 1 - Ri - T_i = 1 - R_e$ When both T_i and l_m are much smaller than one and $l_m << T_i$, which is the interesting case, Ti is related to the finesse by $T_i = \backslash/(2\pi F)$ and it is easy to show that, on resonance, the effective energy loss l_{eff} due to the mirror's losses amounts to: $l_{eff} \approx 4/\pi . l_m F$. It results that the mirrors losses should be $l_m << \pi . l_{eff} / 4.F = 2.10^{-4}$, a performance

that can be guaranteed only by the use of the best coating technologies, such as Ion beam Assisted Deposition (I.A.D) or Ion Beam Sputtering (I.B.S.), which have been developed in the last decade for gyrolaser's mirrors.
The two causes for losses in mirror coatings are absorption and scattering. In classical thermally evaporated multidielectric coatings, the absorption can be made small, as shown by the high power handling capacity of some laser mirrors, but scattering remains high because the dielectric layers show some vacancies. This is attributed to the low energy of the molecules. In Ion Assisted techniques, the accelerated ions can communicate kinetic energy to the molecules. This results in a better "filling factor" of the layers; they become more resistant to chemical and mechanical aggressions, and scatter less. Since the layers follow the irregularities of the substrate, this improvement is achieved only at the condition that the substrate has a very low roughness, what is called "superpolish" and means a RMS roughness of the order of 1 A° on a very small transverse scale, and of 0.1 A° on a millimeter scale.
A few firms in Europe have developed or will have soon have developed the IAD or IBS techniques for coating mirrors. The need for very low scattering coatings came from the development of gyrolasers, at the beginning of the 80's, and these technologies are still partially classified, but are becoming commercial.
We have developed our own technique for measuring the losses of very high reflectivity mirrors, and we have tested in the last 5 years different "supercoatings" from different manufacturers (Ojai (USA), British Aerospace, Balzers). All these coatings were operating at 515 nm, not a favorable wavelength because of absorption problems and because the scattering is higher for short wavelengths (it varies as $1/\lambda^2$) The measured losses varied between $5\ 10^{-5}$ and $3\ 10^{-4}$, depending on the producer and even on the precise position of the measurement point on one single mirror. The cleanliness of the mirror is critical, and, in an non filtered room, the best results could not be maintained for a long period without cleaning the mirror. This is quite encouraging anyway, because it suggests that even better results can be expected at 1.06 µm .
In the very near future, we are going to test supermirrors at 1.06 µm, from a US producer and from SAGEM.
We have also tested high quality mirrors developed by Matra for very high power lasers at 1.06 µm. They use standard technology, and their losses are of the order of 10^{-3}, although they certainly have a very low absorption.

We can reasonably expect that the total losses will be of the order of 10^{-4}, or even much lower.
Both Matra and Sagem are interested in producing the mirrors for VIRGO. Matra has a coating plant for large mirrors, but is only starting to study IAD. Sagem has the technology, but is not yet able to produce large mirrors.

3.1.1.3.2) HOMOGENEITY AND REPRODUCIBILITY

The homogeneity of the coatings is important for the preservation of the wavefront. There is no guaranteed figure on the homogeneity of a large area supercoating, but the specialists seem to think that it will be good enough for our needs.
The precise value of the reflectivity of each mirror is important too. Our main concern is that the two arms of the MITF should be as much symmetrical as possible, this symmetry being the condition for the rejection of all the laser noises (frequency, amplitude and beam geometry, see Chap.2). There is no difficulty with the high reflectivity end mirrors, but it is much more difficult to obtain a good precision on the reflectivity of a partially transmitting mirror : for the input mirrors, which should transmit around 15% in intensity, the equality of their reflectivities could presently be guaranteed to 0.5%. A much better figure could be obtained if the mirrors where smaller, because they could be coated simultaneously.
The beamsplitter may be the largest cause of asymmetry : it is difficult to guarantee its transmission (or reflection) to better than 1% without new studies.

3.1.1.4) OPTICAL SIMULATION

The losses of the MITF will also originate in the wavefront distortions due to the imperfections of the optical surfaces and materials, to their misalignments, and to their finite transverse size, which produces diffraction. Since the instrument is complicated and we want to evaluate the combined effect of different perturbations, these imperfections can be better studied with a numerical program, which we have specially developed.

3.1.1.4.1)- THE PARAXIAL PROPAGATION METHOD

A simulation program must be able to represent short and long range free propagation, reflection and refraction of the light beams. We shall see that for all these purposes, a paraxial approximation can be employed.
Consider the case of long range free propagation (along the arms) : if the spots on the cavity mirrors have roughly equal diameters, which is the case in a confocal cavity, an elementary Gaussian calculation tells us that this typical diameter is

$$2w = 2\sqrt{L\,\lambda/\pi}$$

for L= 3 km, λ= 1.06 µm, this gives 2w = 6.4 cm. If the mirror diameter D is about 5w, then D= 16 cm. The angular deviation of a light ray bouncing in between the mirrors is thus less than 5.10^{-5} Rd, and a paraxial theory of light propagation seems to be relevant.

If now we consider short range free propagation (interferometric area), we see that the parameter $L\lambda/w^2$ where L represent the propagation length is about 10^{-3} which justifies again trying a paraxial approximation.

We are going to develop this idea.

a) Theoretical framework

The optical elements of the interferometer are a succession of nearly plane surfaces in between which the light propagates freely in the vacuum. The first step of the modelization method is to represent the transfer of a monochromatic wave function

$$\Psi(t, x, y, z) = e^{-i\omega t} A(x, y, z)$$

from one end of the interferometer arm to the other, i.e from a surface (S) to the plane z=L. The Kirchhoff integral giving the optical field A at z=L knowing it on the surface (S) reads :

$$A(x, y, L) = \frac{k}{2i\pi}\int_{(S)} \frac{e^{ikR}}{R}\left(1+\frac{i}{kR}\right)\frac{\mathbf{n'.R}}{R}\,A(x', y', z')\,ds' \qquad (1)$$

where $\mathbf{n'}$ is the inward normal to the surface (S) , and

$$R = \sqrt{(x-x')^2 + (y-y')^2 + (L-z')^2}$$

In order to evaluate the relative weights of the elements entering formula (1), let us introduce the length L = 3 km of the interferometer arms, the effective half width of the arm H = 0.2m (which exceeds the mirrors radii and a fortiori the beam waists) , and the wavelength λ = 1.06 mm. We see for instance that

$$1/kR \sim \lambda / 2\pi L = 5.6\ 10^{-11} \quad \text{and}$$
$$1 - \mathbf{n'R} / R \sim (H/L)^2 = 4\ 10^{-9}$$

It is easily seen that a rms roughness of 0.2 Å, corresponding to a very good optical surface, gives, via the phase of the exponential factor, perturbation terms of about 10^{-4} of the main term (geometrical noise). The preceding terms are therefore strongly dominated by the surfaces geometrical noise, and eq. (1) may be written :

$$A(x\,,\,y\,,\,L) = \frac{k}{2i\pi}\int_{(S)} \frac{e^{ikR}}{R}\; A(x'\,,\,y'\,,\,z')\,ds' \qquad (\,2\,)$$

Suppose now the optical surface (S) to obey the equation $z = f(x\,,\,y)$; the curvature radii being always of the same order as L, it is easily seen that $|\,f(x\,,\,y)\,| < f_0\,\lambda$ where f_0 is a dimensionless factor of at most several units. Then we may write :

$$R = \sqrt{(x-x')^2 + (y-y')^2 + [L - f(x',y')]^2} = \sqrt{\rho^2 - 2L\,f + f^2}$$

with

$$\rho = \sqrt{L^2 + \delta^2} \qquad \text{and} \quad \delta^2 = (x-x')^2 + (y-y')^2$$

We have $\delta/L \sim 2\sqrt{2}\,H / L = 1.9\;10^{-4} \Rightarrow \delta^2/2\,L^2 \sim 1.8\;10^{-8}$

The first terms to be considered in the development of R are thus :

$$R = \rho - f + f\left(1 - \frac{L}{\rho}\right) \sim \rho - f + f\,\frac{\delta^2}{2L^2} \Rightarrow kR \sim k\rho - kf + kf\,\frac{\delta^2}{2L^2}$$

but $\left|\,kf\,\dfrac{\delta^2}{2\,L^2}\,\right| \leq 2\,\pi\,f_0\;1.8\;10^{-8} \sim 10^{-7}\,f_0$ Rd. It turns out that this term is to be discarded as being far below the geometrical noise level.

For the same reason, we have

$$\frac{1}{R} = \frac{1}{\rho}\left(1 + \frac{f}{\rho}\right) \sim \frac{1}{\rho}\left(1 + \frac{f}{L}\right)$$

but $f/L \sim \lambda/L \sim$ 10-9 so that we shall take $1/R = 1/r$. We have further

$$A(x'\,,\,y'\,,\,f(x'\,,\,y')\,) = A(x'\,,\,y'\,,\,0) + \frac{\partial A}{\partial z}(x'\,,\,y'\,,\,0)\;\;f(x'\,,\,y') + \;....$$

For a nearly Gaussian wave, we can write :

$$\left|\frac{\partial A}{\partial z}\right| \sim \left|\frac{1}{2ik}\Delta A\right| < k\frac{H^2}{L^2}$$

and consequently

$$\left|f\frac{\partial A}{\partial z}\right| < kf\,H^2L^{-2} = f_0 \,.\, 3\;10^{-8}$$

Owing to the preceding considerations, the Kirchhoff integral reduces to

$$A(x\,,\,y\,,\,L) = \frac{k}{2i\pi}\int \frac{e^{ik\rho}}{\rho}\, e^{-ikf(x'\,,\,y')}\, A(x'\,,\,y'\,,\,0)\,dx'dy' \qquad (3)$$

Now

$$\rho = \sqrt{L^2+\delta^2} = L\left(1+\frac{\delta^2}{2L^2} - \frac{\delta^4}{8L^4} + \ldots\right)$$

so that

$$k\rho \cong kL + \frac{k\delta^2}{2L} - \frac{k\delta^4}{8L^3}$$

for the last term, we have :

$$\frac{k\delta^4}{8L^3} < \frac{16\,\pi\,H^4}{\lambda\,L^3} = 2.8\;10^{-6}$$

For the denominator of the integrand of (3) we get :

$$\frac{1}{\rho} = \frac{1}{L}\left(1 - \frac{\delta^2}{2L^2} + \frac{3\,\delta^4}{8L^4} + \ldots\right) < \frac{1}{L}\left(1 - \frac{4H^2}{L^2}\right) = \frac{1}{L}\,(1\; - \;1.6\;10^{-8}\,)$$

so that $r^{-1} = L^{-1}$.

Finally, the wave at z=L may be computed by the following sequence :

- compute the wave at z=0

- multiply it by the phase lens factor $\Phi = \exp(-ikf(x', y'))$
- compute the convolution product with the paraxial Green function

This can be summarized by

$$A_L = G * [\Phi A_0] \qquad (4)$$

For the paraxial Green function, we may take either

$$G_1(x, y) = -\frac{ik}{2\pi}\frac{e^{ik\sqrt{L^2 + x^2 + y^2}}}{\sqrt{L^2 + x^2 + y^2}}$$

with an accuracy equivalent to 10^{-8} Rd in the phase of the wave, or

$$G_2(x, y) = -\frac{ik}{2\pi}\frac{e^{ikL}}{L}\, e^{ik\frac{x^2 + y^2}{2L}}$$

with an accuracy of about 10^{-6}.

The convolution product that appears in (4) reduces to a pair of Fourier transforms :

$$A_L = F^{-1}[\, F(G) \,.\, F(\Phi A_0)\,]$$

which shows that we only need to know the Green function in the Fourier space, namely :

$$\tilde{G}_1(p, q) = \frac{e^{iL\sqrt{k^2 - p^2 - q^2}}}{\sqrt{1 - (p^2 + q^2)/k^2}} \qquad \text{for} \quad p^2 + q^2 < k^2$$

or simply

$$\tilde{G}_2(p, q) = e^{ikL}\, e^{-i\frac{L}{2k}(p^2 + q^2)}$$

The results presented below were obtained using the latter expression. A similar approach has been developed by (Sziklas and Siegman,[1975]). In the interferometric area, the paraxial approximation is now justified by the weak diffraction rate due to the particular features of the beams in this region : the waists of the two beams are located on the front mirrors and are of large size. However, in this first step in the evolution of the simulator, we shall neglect the diffraction in this area so far as recycling is not included in the scheme. More attention will be paid to this subject in next papers.

b) The PPM Algebra

The elementary transformations undergone by the light ray in the arms of the interferometer are

- refraction in transmitting mirrors or splitters
- long range free propagation (arms)
- short range free propagation (interferometric area)
- reflection on mirror coatings

Owing to the preceding analysis, to each of these we may associate a linear operator acting on the wave complex amplitude. Refraction and reflection are represented by operators of the form

$$T = t\, e^{i\, f(x,y)} . d(x,y) \quad , \quad R = i\, r\, e^{i\, g(x,y)}\, d(x,y)$$

where t and r are the ordinary scalar amplitude transmission and reflection coefficients and f, g two real functions representing the local phase change due to either the reflecting surface shape (for a mirror) or the variable optical thickness (for a lens). d(x,y) represents the diaphragm function of the optical element : d is zero outside , and unity inside.

f and g may be the sum of a large class of terms including the ideal geometrical form and various perturbation terms such as :

- aberrations : a sum of Zernike polynomials in x/ρ and y/ρ (ρ being the circular diaphragm radius) with given RMS amplitudes
- misalignment : a linear gradient in the phase and no displacement of the diaphragm contour (rotation of the element's axis) or a global translation
- roughness : random deviations from the ideal surface with calibrated self-correlation and standard deviation.

The long range free propagation is represented by the propagator

$$P = F^{-1}\, \tilde{G}\, F \qquad (4)$$

In order to illustrate working with the PPM algebra , consider for instance a Fabry Perot cavity having a front mirror M1 and a rear mirror M2 (see fig.3.1.4 for notation) with the corresponding operators T_1, R_1 , R_2 :

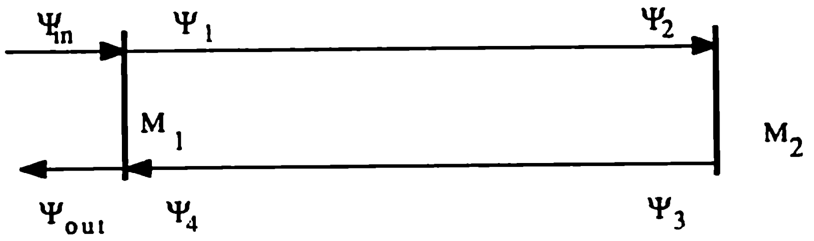

Fig.3.1.4 : Notations for the simulation of a Fabry-Perot cavity

that lead to the implicit equation Ψ_1 obeys :

$$\Psi_1 = T_1 \Psi_{in} + R_1 P R_2 P \Psi_1 \qquad (5)$$

Resolution of (5) is the central task of the algorithm we describe below.

3.1.1.4.2)- DESCRIPTION OF THE ALGORITHM

a) Discretization of waves and operators

The waves amplitudes , and consequently the operators acting upon them are sampled on a square grid at equal intervals (which is required when a discrete Fourier Transform (DFT) is to be employed). This gives a collection of square arrays of complex numbers. Actions of reflection and refraction operators result in ordinary product of arrays , while propagation, according to (4) is performed by means of a two-dimensional DFT, then an ordinary array product and finally a reciprocal DFT. This representation of diffraction is especially interesting, because a number of efficient FFT routines are available for performing DFT's.

b) Simulation of a cavity

For a given input amplitude Ψ_{in} , we have to compute the amplitude Ψ_{out} reflected back by the cavity. The method suggested by (5) requires first the iterative calculation of Ψ_1 from an approximate solution until the required precision is reached. As an approximate solution, we can take the exact eigenmode of the unperturbed cavity times the resonance coefficient , so that in the ideal interferometer, the equation (5) is satisfied, and consequently the solution is reached within 1 iteration.

Let us point out that we can tune the cavity at resonance by adding a uniform phase φ to the propagator's : This is equivalent to adjusting the cavity length. In order to find the value φ_0 for which resonance occurs, we could perform the iterative calculation of Ψ_1 with different values of φ and try to maximize $\| \Psi_1 \|$ by some procedure, but such a method would be very expensive in terms of computation time. Fortunately, it is possible to get information about the resonance conditions without running many times the cavity procedure, by a very simple perturbation calculus : If we restrict our attention to small perturbations of an ideal system, we can give an explicit first order estimation of φ_0. In practice, the finesse of the cavities to be considered is not so high, and the accuracy of the first order estimation is almost always sufficient.

Let us develop this idea. Call

$$C = R_1 P R_2 P$$

the cavity operator. Thus (5) reads :

$$\Psi_1 = \Psi_s + C e^{i\varphi} \Psi_1 \qquad (\Psi_s = T_1 \Psi_{in}) \qquad (6)$$

The uniform adjustable phase φ allows the tuning of the cavity. We shall consider that the situation described by the preceding equation is a perturbation of a reference system where mirrors have ideal shapes, indefinite extension and ideal positions. Denote by C_0 the corresponding (unperturbed) operator ; its eigenvalues and associated eigenvectors are

$$\{ \Phi_n^{(0)} , \lambda_n^{(0)} \}$$

Within the paraxial approximation, the $\Phi_n^{(0)}$ are also modes of free propagation, and therefore, the input wave may be chosen proportional to $\Phi_0^{(0)}$ so that :

$$\Psi_s^{(0)} = S \, \Phi_0^{(0)}$$

the zero order solution of (6) is thus :

$$\Psi_1^{(0)} = \frac{S}{1-\lambda_0^{(0)} e^{i\varphi_0}} \Phi_0^{(0)}$$

which is made resonant by choosing $\varphi_0 = -\operatorname{Arg}(\lambda_0^{(0)})$. Return now to the perturbed system : At first order, we can develop the solution Ψ_1 of eq.(6) in a series of the $\Phi_n^{(0)}$:

$$\Psi_1 = A\left[\Phi_0^{(0)} + \sum_p \alpha_p \Phi_p^{(0)} \right]$$

and we can always write

$$C \Psi_1 = \lambda \Psi_1 + \Psi'_1$$

where λ and Ψ'_1 are completely determined by the condition

$$(\Psi'_1 , \Phi_0^{(0)}) = 0$$

(,) denoting the Hermitian scalar product.

Eq. (6) thus becomes :

$$A\left[\Phi_0^{(0)} + \sum_p \alpha_p \Phi_p^{(0)} \right] = \Psi_s + \lambda e^{i\varphi} A\left[\Phi_0^{(0)} + \sum_p \alpha_p \Phi_p^{(0)} \right] + e^{i\varphi} \Psi'_1$$

which by projection onto $\Phi_0^{(0)}$ gives

$$A = \frac{(\Psi_s , \Phi_0^{(0)})}{1 - \lambda e^{i\varphi}} \frac{1}{1+\alpha_0}$$

It becomes now clear that the value of φ which maximizes $\| \Psi_1 \|$ is

$$\varphi'_0 = -\mathrm{Arg}(\lambda) \qquad (7)$$

Finally, it is easy to show that, at first order we have :

$$\lambda = \left(C\Phi_0^{(0)} , \Phi_0^{(0)} \right) \qquad (8)$$

which is a well known result of the perturbations theory. Implications of eq. (7) and (8) are interesting : we can estimate the resonant phase by only one round trip in the cavity.

c) Simulation of a Michelson Interferometer

3.1.1.4.3) RESULTS

With two resonant cavities we can now construct a simple Michelson interferometer by splitting an input amplitude Ψ_{in} into two waves Ψ_a and Ψ_b which are used as input amplitudes for the two cavity routines, then recombining them on the splitter with a variable phase lag α. Variations of α result in variations of the integrated power on the two gates of the interferometer; by searching for a maximum and for a minimum of the output power, it is possible to obtain both the contrast of the interferometer and the reflected power. We also compute the projection of the reflected amplitude on the laser's , so as to estimate the recycling efficiency. When the phase is tuned to give the dark fringe, the chart of the intensity distribution in the dark field is output (see Fig. 3.1.10) in order to build a typology of the different perturbations.

a)- Finite mirror size

The transverse extension of the Gaussian beams is theoretically infinite. It is possible to determine analytically the fraction of energy lost through a single aperture, but this picture is not complete when the aperture is part of a resonant cavity, because it evaluates the energy of the transmitted beam, but not its geometry. The simulation code allowed us to evaluate the effective losses as a function of the diameter of the mirrors. The results show a very fast variation of the losses with the ratio K of mirror diameter to beam diameter: the losses are very high when K<2, and totally negligible when K>2.5. This steep variation of the losses with the mirror diameter allows us to choose arbitrarily the minimum mirror diameters: 10 cm at the center and 30 cm for the end mirrors. These values will be fixed now on and used in all the further runs of the simulation.program.

b)- Mirror's displacements and misalignments

Fig.3.1.5 shows the variation of the losses when the end mirror of one arm (M2 or M4) is rotated, the other mirrors staying perfectly aligned. The losses are defined as the complement to unity of the maximum fraction of the light which is reflected by the MITF and couples back into the incoming TEM_{00} mode.

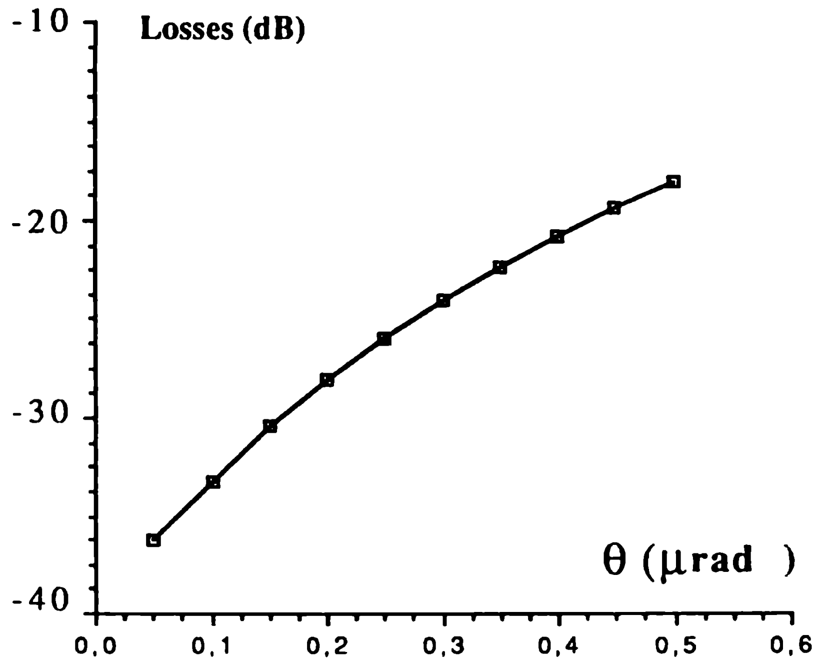

Fig.3.1.5 : Reflection losses of the MITF for a misalignment θ of the end mirror.

The alignment precision should be close to 0.3 μrd. The system is much less sensitive to a rotation of the front mirrors, for which the tolerance is of the order of 1 μrd.

The pointing stability of the incident laser beam should also be of the same order of magnitude (< 0.5 μrd).

Fig.3.1.6 shows the effect of translating one of the end mirrors (M2 or M4).

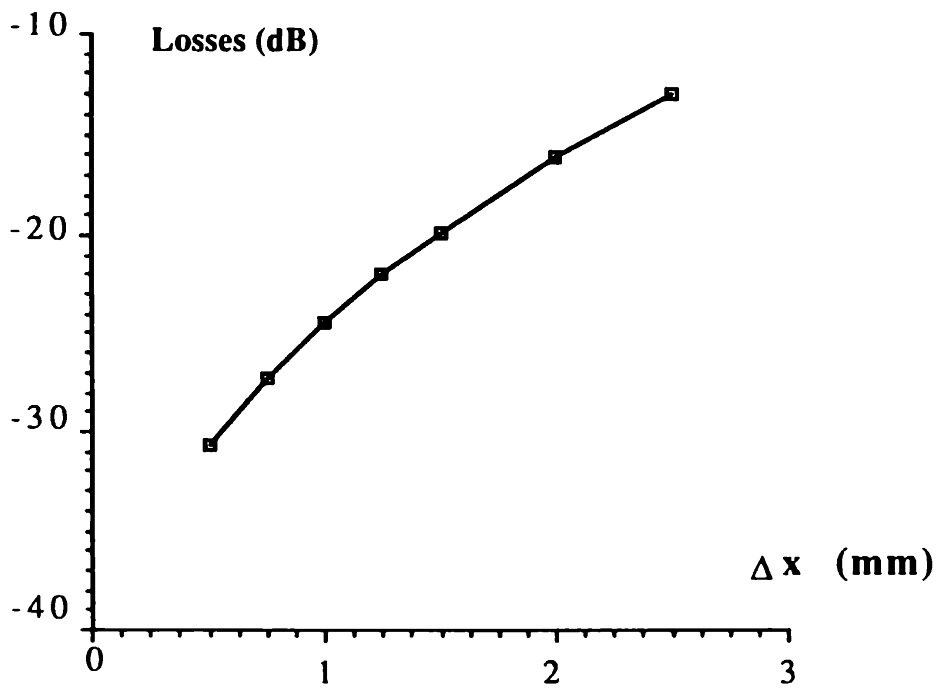

Fig.3.1.6 : Reflection losses of the MITF for a translation of an end mirror

The loss it induces is a combination of aperture effect and misalignment. The positioning precision of the mirrors should better than 1 mm. The (flat) front mirrors are, of course less sensitive to translations: there is only an aperture effect, which becomes significant when the displacement is larger than 1 cm.

c)- Variations of the radius of curvature

The radius of curvature of the end mirrors, R_{cc}= 3.45 km, is very large, so that its concavity is small: $h=\frac{D_e^2}{4\ R_{cc}}$ = 1 µm, where D_c is the diameter of the part of the mirror on which most of the beam energy is concentrated (i.e. the beam gaussian diameter, W= 12 cm) A precision of $\lambda/10$ in the manufacture of the mirror leaves a relative incertitude of 10 % on R_{cc}. The result of the simulation is given Fig.3.1.7, where the two curves are for positive and negative relative deviations of the radius of curvature.

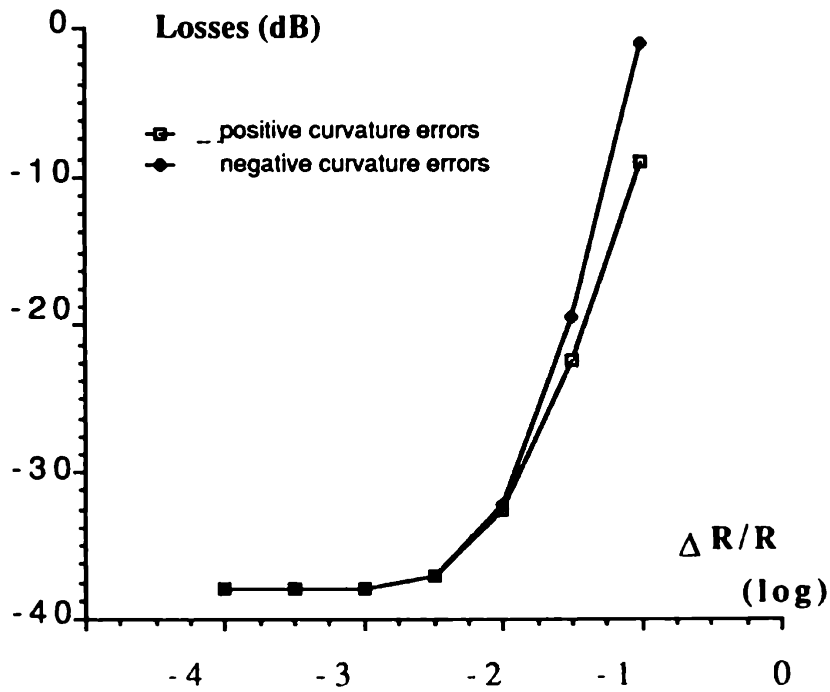

Fig.3.1.7 : Reflection losses of the MITF for a relative error $\Delta R/R$ in the radius of curvature of one of the end mirrors

We see that a precision ΔR/R <3% is required.

d)- Large scale wavefront deformations

We also simulated the existence of random large scale deformations of the mirrors generated by different combinations of Zernike polynomials. The results depend on the particular combination of polynomials, because the wavefront distortion is more sensitive to the defects which occur near the beam center than on its periphery. This can be represented by Fig.3.1.8, where the shaded area represents the dispersion of the results between two rather different combinations of Zernike polynomials giving the same RMS deformation.

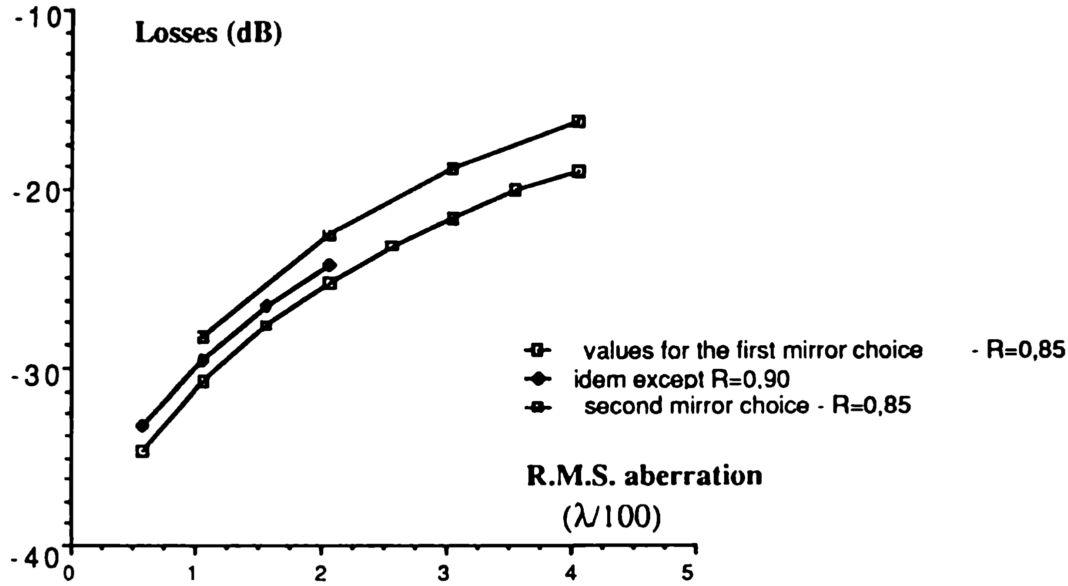

Fig.3.1.8 : Reflection losses of the MITF for a given RMS surface error
(the three curves show the variation of the sensitivity to surface defects with the finesse and with the shape of the defect)

This puts a limit of the order of λ/40 for the quality of the mirror surfaces. The constraint on the wavefront distortion due to the inhomogeneity of the input mirrors material is of the same order of magnitude. If the mirror is 10 cm thick, this implies an index homogeneity better than 2.5 10^{-7}, quite a difficult value to obtain, even with the best kinds of fused silica.

c)- Short correlation range random deformations

Random deformations with a short correlation range can be simulated by attributing to each of the cells of the Fourier transform grid representing an optical element a random phase shift, the R.M.S. amplitude of which is fixed. This can simulate, for instance, the index inhomogeneities of the material of mirrors M1 and M3, or the roughness of the mirror surfaces, for spatial frequencies lower than the inverse of the cells dimensions. The results concerning the roughness of an end mirror are given on Fig.3.1.9.

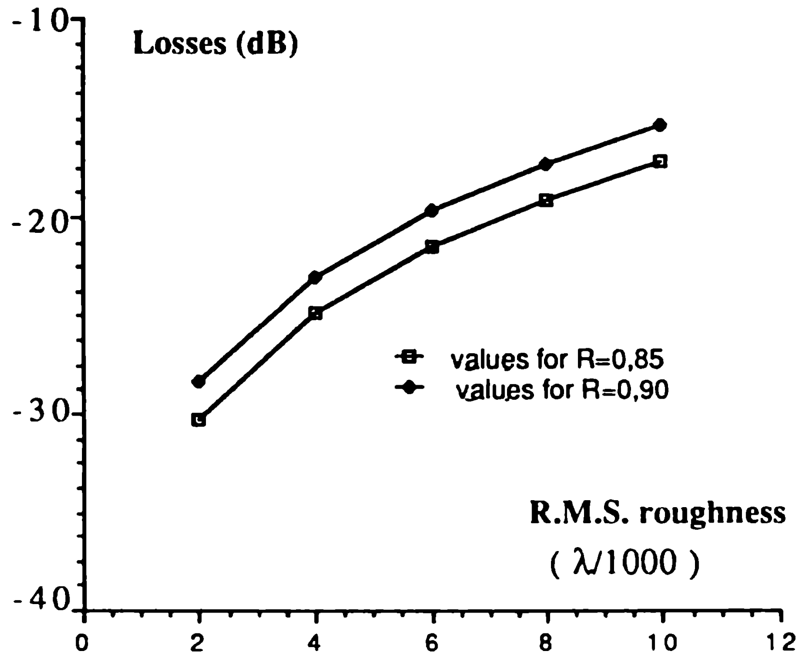

Fig.3.1.9.:
Reflection losses of the MITF for a given RMS roughness of one of the end mirrors

The requirement is that this roughness be smaller than λ/200. This is not a difficulty : the roughness of "superpolished" mirrors on the same scale (a few mm), is typically better than λ/1000. The same constraint applies to the index inhomogeneities inside the material of the input mirrors; we will have to check that.

3.1.1.4.4) PRELIMINARY SPECIFICATIONS OF THE OPTICAL COMPONENTS

It is clear that the most critical points will be the short and large scale deformations of the mirrors, the precision of the curvature radii, and the homogeneity of the input mirrors material. The specifications on the alignment of the mirrors and their positioning may seem severe, but these parameters can be adjusted efficiently by high precision servo-systems, and will not limit the performance in practice. Therefore, we have run the program with combinations of the perturbations c), d), and e) on each mirror and in the input mirrors material, in order to define the real mirror requirements. Table3.1 gives a set of specifications, which corresponds to feasible components and provides satisfactory results : the corresponding recycling factor is of the order of 60, so that the sensitivity goal would be reached with a laser power of the order of 10 Watts. The contrast of the interferometer in these conditions will be about 99% (without mode cleaner). Fig.3.1.10 shows the intensity profile of the corresponding "dark fringe".

BEAMSPLITTER	
Surfaces	
Surface quality	$\lambda/50$ RMS
Substrate	
Integrated inhomogeneity	$< \lambda/30$ RMS
Coatings	
A.R	$< 1\ 10^{-3}$
Reflective	R=T= 0.5± 0.005
END MIRRORS	
Minimum usable diameter	30 cm
Front surface :	
surface curvature	R_{cc} = 3450±100 m
surface quality	$\lambda/50$ RMS
roughness	$\lambda/1000$ RMS
Coating	
reflectivity	> 0.9998
total losses	< 200 ppm
INPUT MIRRORS	
Minimum usable diameter	10 cm
Front surface :	
Curvature	∞
Surface quality	$\lambda/50$ RMS
Roughness	$\lambda/1000$ RMS
Coatings	
a) Reflective	0.85± 0.01
Total losses	< 200 ppm
b) A.R.	< 0.1 %
Substrate	
Integrated inhomogeneity	$< \lambda/30$ RMS
Integrated birefringence	< 100 nm

Table 3.1 Specifications of the optical components

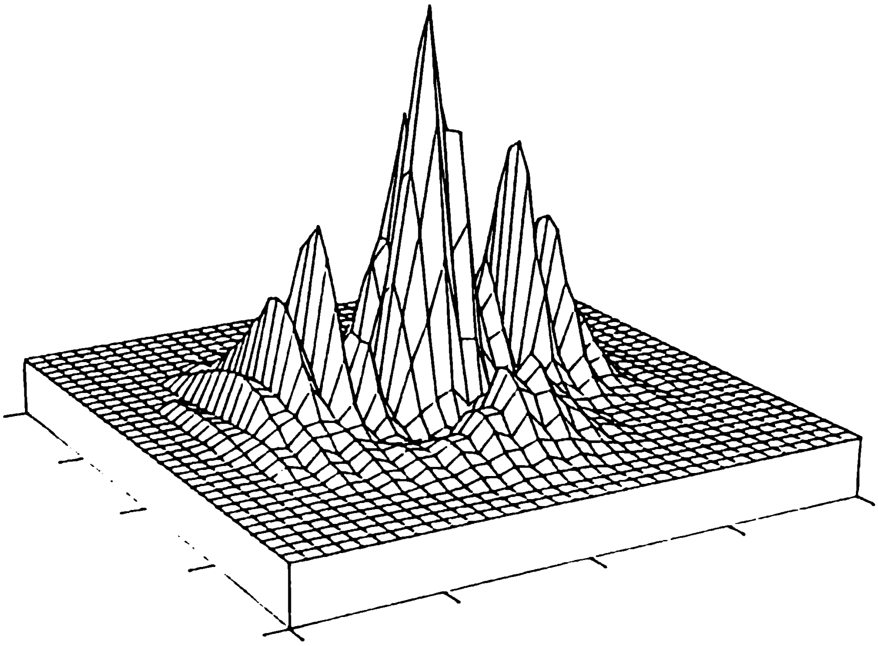

Fig.3.1.10 : Residual light intensity on the dark fringe (simulation)

Since wavefront distortions are here the main cause of losses, the power transmitted on the "dark fringe" in the case of a recycling system is a large fraction of the laser power. (30 % in this case). The difference between the mirrors produce a relative difference in the light powers stored in the two arms This gives an asymmetry of the order of 3% which is of the same order of magnitude as the asymmetry expected from the inaccuracy of the coatings; a kind of compensation may be achievable in some cases.

As we said earlier, the dispersion of the results for a given RMS value of the deformations is about a factor 10 depending on the relative weight of the Zernike polynomials. This demonstrates that the classical way of specifying the quality of optical components is not adequate for use with typical Gaussian laser beams.

This also means that the realization of the VIRGO mirrors will ask for a close collaboration between the manufacturer and us. It suggests that, for a set of mirrors of a given quality, it will be possible, using the simulation code after having measured their Zernike polynomials, to determine the best combination of mirrors, and their best relative orientation in order to reduce the total losses. This optimization will also take into account the measured characteristics of all the coatings, in order to improve simultaneously the symmetry of the MITF.

3.1.1.5) MECHANICAL AND THERMAL SIMULATION

It is important to evaluate the deformations of the mirrors and of the optical wavefront which will result from the weight of the mirrors, as a function of their shape and of the way they are suspended. Similarly, absorption of light in the coatings or in the bulk material will generate heating, expansion, and index variations.
Preliminary studies of these two kinds of effects have been done using finite elements programs, applied to a simple cylindrical mirror. They show that the mechanical deformation will not be very critical, but that thermal deformations can become a serious problem, even with good coatings having an absorption coefficient of 10^{-4}. The poor thermal conductivity of silica, which will be the mirror material, does not help in this respect.
The thermal lensing effect due to index variations related to absorption in the material has not been studied yet. We have ideas on how to compensate for these effects, but to develop them requires the thermal modelization of the mirror. This is one of the priorities for the near future.

3.1.2) INTERFEROMETRY

3.1.2.1) RECYCLING

The theory of recycling interferometers has been done mainly by the GROG, in collaboration with B.Meers from Glasgow. This work resulted in the publication of a few papers, the most significant one being enclosed here as Appendix 3.1. The important conclusions are that :

- recycling is the appropriate solution to the lack of power of existing CW single frequency lasers; with very good (but feasible) optics, the effective power can be increased by a factor $S \cong 100$ in a wideband device using standard recycling, and by $S > 1000$ in a narrow band interferometer using synchronous recycling.
- the recently proposed techniques of detuned recycling and of dual recycling offer the possibility of realizing some "intermediate" configurations, where both the bandwidth and the sensitivity are tunable and lie between those of the wideband and narrow band devices. Their sensitivity to the optical losses of the components of the interferometer is also different, so that they may allow the optimization of the device performance; in particular, the possibility of using detuned recycling, which is a specific

property of the Fabry-Perot devices, looks very promising, because it allows one to modify the response of an interferometer without requiring any other change than an offset in two servo-loops. In the following, we will consider only the standard recycling technique, which we are going to use in the first generation of VIRGO.

3.1.2.2) DETECTION TECHNIQUES

3.1.2.2.1) THE MICHELSON INTERFEROMETER

From the viewpoint of the interferometric technique, the important figure to remember is that we have to measure a relative phase shift of the beams reflected by the two arms of the Michelson interferometer (MITF) :

$\delta\Phi = 1.5\ 10^{-11}$ rd.Hz$^{-1/2}$, in the frequency range from 10 Hz to a few kHz.

To be able to measure such a small phase shift, the detection should be shot-noise limited, with a laser power of at least 500 Watts, at 1.06µm.

In this section,we first recall the simple theory of a Michelson interferometer (MITF) with a D.C. detection, and we establish its ultimate shot-noise limited sensitivity. In the following paragraphs, we describe the different high frequency detection techniques and we compare their limit sensitivities to that of the MITF in DC detection. In the case of imperfect contrast, we show that mode filtering of the beam is necessary to recover the ultimate detection sensitivity.

3.1.2.2.2) DC MICHELSON:

Let us recall first the basic formulas for the standard MITF shown on Fig 3.1.11 a. The DC detection of the transmitted port gives the following signal:

$$P = \frac{P_0}{2}\left(1 + C\cos\Phi\right)$$

where P_0 is the power incident on the MITF and C is the contrast of the fringes defined as

$$C = \frac{P_{max} - P_{min}}{P_{max} + P_{min}}$$

Φ is the phase difference between the two arms, carrying the effect of the gravitational wave. The sensitivity of this kind of detection to a phase shift $d\Phi$ is the derivative of the signal P relative to Φ:

$$\frac{dP}{d\Phi} = -\frac{P_0}{2}C\sin\Phi$$

If the system is shot-noise limited, the spectral density of the noise, measured in terms of current on the photodiode is :

$$I_{shot} = e\sqrt{\frac{\eta P_0}{h\nu}}\sqrt{1 + C\cos\Phi}\ \mathrm{Hz}^{-1/2}$$

where e is the electron charge, η is the detector quantum efficiency and ν the laser frequency. This noise current is equivalent to a phase shift $\delta\Phi$ measured in the system, related to the above sensitivity by the expression:

$$\delta\Phi = \frac{I_{shot}}{\frac{e\eta}{h\nu}\left|\frac{dP}{d\Phi}\right|} = \sqrt{\frac{2h\nu}{\eta P_0}}\ \frac{\sqrt{1 + C\cos\Phi}}{C\sin\Phi}\ \mathrm{Hz}^{-1/2}$$

this is the minimum detectable phase shift of the system. In the case of a perfect contrast (C= 1), the best sensitivity is obtained for the system sitting on the dark fringe, ($\Phi = \pi$), and :

$$\delta\Phi_o = \sqrt{\frac{2h\nu}{\eta P_0}}\ \mathrm{Hz}^{-1/2}$$

We will take this value as the reference value for the sensitivity in the following discussions

In practice, the contrast is always smaller than unity, and the system should be detuned slightly from the dark fringe in order to optimize the sensitivity. This new position is a function of the contrast defect $1-C$, assumed small:

$$\cos\Phi = -1 + \sqrt{2(1 - C)}$$

and the remaining power on that new position is :

$$P_{rem} = \frac{P_0}{2}\sqrt{2(1 - C)}$$

As the MITF is not exactly on the dark fringe, we must investigate the effects of the amplitude fluctuations of the laser on the detection: let $\Delta P/P$ be this relative amplitude fluctuation. Its effect on the output current ΔI_{rem} should be smaller than the shot noise limit at this level, $\sqrt{2eI_{rem}}$. Then the relative amplitude fluctuations should follow the condition :

$$\frac{\Delta P}{P} < \sqrt{\frac{2h\nu}{\eta P_{rem}}}$$

For a contrast of 1.10^{-4} and P_0= 500 W, then P_{rem}= 3.5 W, and we find the condition:

$$\Delta P/P < 3.10^{-10}\ \mathrm{Hz}^{-1/2}.$$

This is a very difficult condition to fulfill in the low frequency range, because the measurement can be spoiled by laser amplitude noise and 1/f noise in the photodetectors and the electronics. The solution to this type of problem is to use a high frequency modulation technique, which performs a frequency transposition allowing one to get rid of the low frequency fluctuations.

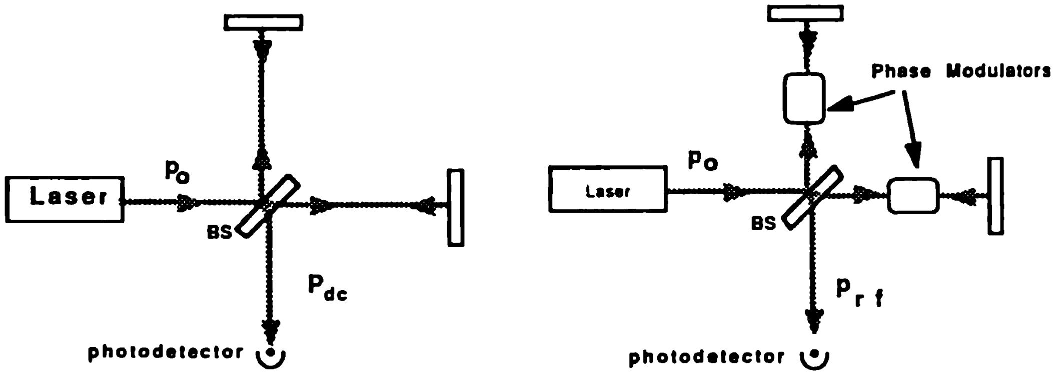

Fig.3.1.11 : Michelson interferometer
a) : D.C.detection
b) : Internal phase modulation

3.1.2.2.3) INTERNAL MODULATION

The "classical" way to operate a MITF in high frequency range, with a shot-noise limited sensitivity, is described in Fig 3.1.11.b: the armlength is modulated at high frequency (10 MHz), with opposite phases in the two arms. The modulation frequency is chosen to be higher than the frequency at which excess noise in the laser power disappears below the shot-noise for the power to be detected. The phase difference Φ is modulated in the form: $\Phi = \Phi_0 + m \cos \Omega t$. The output power of the transmission port is then written as :

$$P_{RF} = \frac{P_0}{2}(1 + C\ J_0 \cos \Phi_0 - 2\,C\,J_1 \sin\Phi_0 \sin \Omega t)$$

where J_0 and J_1 are the Bessel functions of zero and first orders of the modulation m. This power is minimized by maintaining the MITF tuned to a dark fringe ($\Phi_0 = \pi$), and by trying to keep its contrast as high as possible. The signal is then detected at the modulation frequency Ω and the sensitivity of the system to a phase shift $d\Phi$ is the derivative of the signal P_{RF} relative to Φ_0:

$$\frac{d P_{RF}}{d\,\Phi_o} = P_0\,C\,J_1 \cos \Phi_o$$

In the same way, we can define a minimum detectable phase shift which is then :

$$\delta\Phi = \sqrt{\frac{2h\nu}{\eta P_0}}\ \frac{\sqrt{1 + C\,J_0 \cos \Phi_o}}{C\,J_1 \cos\Phi_o}$$

Depending on the contrast, one can find an optimum modulation depth which maximizes the phase sensitivity of the measurement :

$$J_1 = (2(1-C))^{1/4}$$

and the expression of the sensitivity is:

$$\delta\Phi = \sqrt{\frac{2h\nu}{\eta P_0}}\left[1+\left(\frac{((1-C))}{2}\right)^{\frac{1}{2}}\right] Hz^{-\frac{1}{2}}$$

We can see that the power on the dark fringe, with the internal modulation technique, is the same as in DC detection:

$$P_{rem} = \frac{P_0}{2}\sqrt{2(1-C)}.$$

The sensitivity limit of this technique is the same also as in the case of DC detection; then the demand on the amplitude stability is the same, but here the advantage is that the power stability requirement is in the high frequency range.

3.1.2.2.4) EXTERNAL MODULATION

Besides the fact that the phase modulator might not be able to stand the light power in the MITF arms, the loss that it introduces inside the recycling cavity limits the recycling factor. In order to use recycling techniques and to minimize the losses due to the phase modulators inside the MITF, one can put them out of the MITF in an external arm, to perform a kind of heterodyne detection of the beam transmitted by the MITF. The figure 3.1.12 gives an experimental set-up.

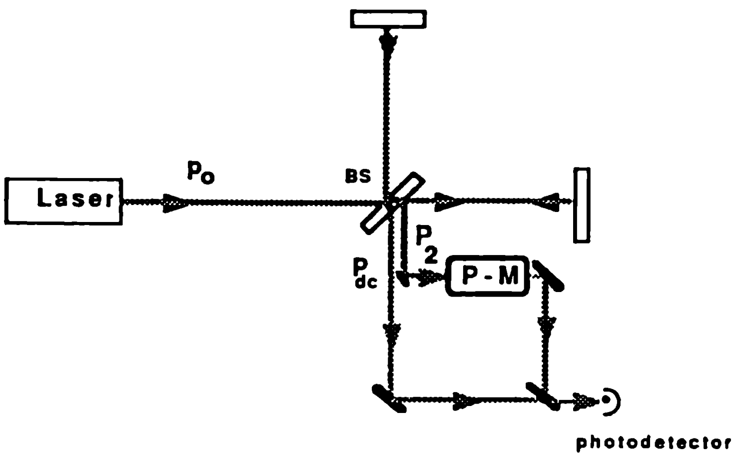

Fig.3.1.12 : External modulation

There is now a second interferometer, which is a Mach-Zehnder (MZ) .Considering the MZ, one has the same kind of configuration as previously, that is an interferometer with internal modulation, and in which one arm is the MITF, whose output is variable in amplitude and in phase.
It is important to realize that the observed contrast defect is always due mainly to the distortions of the wavefronts in the interferometer arms, rather than to an inequality in their reflectivities. The output beam from the MITF can be expressed as the sum of two components : the interference between the undistorted beams, supposed to have a TEM_{00} geometry, and some higher order components (TEM_{mn}), that we suppose not to interfere. Then we express the output of the MZ as :

$$P_{ext} = P_{00}\frac{(1-C_r)}{2} + P_2 + P_{mn} - 2\sqrt{P_{00}P_2\frac{(1-C_r)}{2}})\cos\Theta$$

where Θ is the phase difference between the beams having travelled in the external arm and in the MITF (Θ contains the gravitational wave signal), and C_r is the contrast due to the difference in reflectivities. P_2 is the power diverted to the external arm. The relation between the different powers is:

$$P_0 = P_1 + P_2 = P_{00} + 2\,P_{mn} + P_2$$

The phase modulation is in the external arm and Θ gets the form :

$$\Theta = \Theta_0 + m\cos\Omega t$$

So we can separate this expression in two terms: the DC signal, contributing to the shot noise, and the modulated term, containing the signal. After some algebra, we obtain the expression of the minimum detectable phase shift :

$$\delta\Phi = \frac{\sqrt{P_{00}\frac{(1-C_r)}{2} + P_2 + P_{mn} - 2J_0\sqrt{P_{00}P_2\frac{(1-C_r)}{2}}}}{J_1\sqrt{P_{00}P_2(1-C_r)}}$$

In the same way as with internal modulation, the phase of the external arm has to be adjusted to a dark fringe, in order to make the system sensitive to the gravitational wave. The optimum values of P_2 and m are functions of C_r and of P_{mn}/P_{00}
In the limit of good contrast ($C_r \approx 1$), and no beam defect ($P_{mn} = 0$), the S/N is the same as in the case of internal modulation.
When the beam distortion undergone inside the MITF is not negligible i.e. if $P_{mn} \geq 10^{-4}$, the DC term which contributes to the shot noise increases, while the sensitivity of the detection remains roughly constant, and to recover an optimum of the sensitivity, one has to modulate quite strongly. In that case, the sensitivity is $\sqrt{2}$ times worse than in the ideal case of internal modulation. One might think of using two photodiodes to monitor the fringes signal from the MZ; the shot noise in the detection is then the square root of the sum of

each photodiode shot noise, and the signal is twice that of each photodiode. The best sensitivity is reached by maximizing J_1 which corresponds to a high modulation level (m=1.8, giving $J_1 = 0.58$), and the sensitivity limit is $1/(\sqrt{2}\, J_1) = 1.2$ times worse than in the case of the internal modulation. This is still slightly better than the detection with one photodiode, but the best thing to do in presence of beam distortion coming from the MITF is to reduce the total power reaching the detector by spatially filtering the beam. Then, the sensitivity is again very close to the optimum, as long as $P_{mn} << 1$.

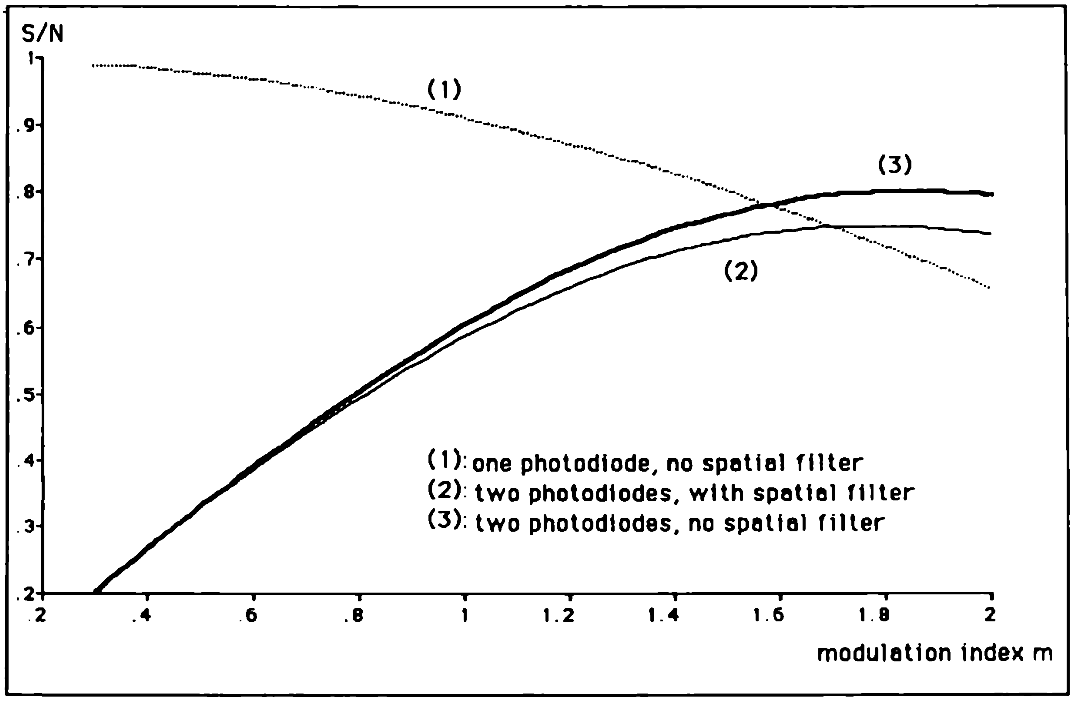

Fig.3.1.13 : Compared sensitivities of external modulation techniques

The figure 3.1.13 shows the compared signal to noise ratio in the three kinds of detection described, versus the modulation index. The beamsplitters of the MZ have been adjusted to the optimum value in each case, the contrast defect is 10^{-4} and the beam distortion (P_{mn}) is 10^{-3}. One can see that, without spatial filtering, it is better using two photodiodes instead of one and to modulate strongly.

Table 3.2 gives the sensitivity limits for all the cases. It also includes the external modulation with an Acousto-Optic shifter, which will be mentioned in the paragraph f) of this section.

External modulation techniques will reintroduce a high sensitivity to laser frequency fluctuations if the arms of the MZ have different lengths. This

	Internal Modulation	External Modulation with Phase Modulator		External A-O shifter	Frontal Modulation
Limit phase sensitivity	$\left(\frac{2\eta P_0}{h\nu}\right)^{1/2}$	id*	id. $\frac{\sqrt{3}}{\sqrt{2}}$	id.$\sqrt{2}$	id*
remarks		use of one photodiode	use of two photodiodes		modulation frequency matches pathlength of MITF
observations	advantage: easy to implement drawback: losses of phase modulation inside the MITF	advantage: extra losses inside the MITF-allows high recycling gain drawback: decrease in sensitivity if no mode cleaner used			

(* with mode cleaner)

TABLE 3.2

difficulty is overcome by using as the reference beam a reflection from the second face of the MITF beamsplitter (see fig 3.1.12). In this way, the light has travelled the same length in the two arms, and this scheme does not introduce more sensitivity to the frequency fluctuations of the laser.

3.1.2.2.5) RECYCLING WITH EXTERNAL MODULATION

To recycle the reflected light R_M from the MITF, we insert a front mirror which has a transmittance T_r. The recycling factor, which is the enhancement factor of the incident light is then :

$$S = \frac{T_r}{\left[1 - \sqrt{1-T_r}\sqrt{R_M} \right]^2}$$

For a given overall loss of the MITF, the transmissivity of the front mirror should be equal to the sum of the MITF transmission and of its loss, in order to optimize the recycling gain. The incident laser power P_0 is multiplied by a factor S and the highest S/N is now $\sqrt{S}$. So the minimum detectable phase shift in external modulation is then :

$$\delta\Phi = \frac{\sqrt{S\,P_{00}\frac{(1-C)}{2} + P_2 + S\,P_{mn} - 2J_0\sqrt{S\,P_{00}P_2\frac{(1-C)}{2}}}}{J_1\sqrt{S\,P_{00}P_2(1+C)}} \quad \mathrm{Hz}^{-1/2}$$

The same discussions as above concerning how to overcome the presence of beam defects is still valid, except that the recycling cavity enhances the effect of beam defects by the factor $\sqrt{S}$. The limit sensitivity can be obtained with the same detection configuration as in the case of no recycling.

3.1.2.2.6) EXTERNAL ACOUSTO-OPTIC SHIFTER

In the external arm of the MZ, one can also use an Acousto-Optic (A-O) frequency shifter, and then make an heterodyne detection of the signal from the MITF. In that case, even with a maximum efficiency of the A-O, the sensitivity is $\sqrt{2}$ times worse than with the phase modulation.

3.1.2.2.7) FRONTAL MODULATION

Another modulation scheme has been proposed (Schnupp [1988]), where the phase modulator is placed in the incident beam, in front of the recycling mirror. The interferometer phase shift induced by the gravitational wave is detected on the transmitted port, as usual, in the signal demodulated at the modulation frequency. The modulation frequency Ω has to fulfill some conditions because:

- the sidebands must be resonant in the recycling cavity, otherwise the effective modulation index will be very small :

$$\frac{\Omega L_m}{2c} = n\ 2\pi$$

where n is an integer number, and L_m is the equivalent length of the recycling.cavity If the gravito-optic transducer in each arm is a Fabry-Perot cavity of length L, the condition $\frac{\Omega L}{2c} = n\ 2\pi$ must also be verified (for another value of n), in order not to reintroduce laser frequency noise.

• the signal must have a maximum sensitivity to the phase difference (Φ) of the MITF; if R_r and R_M are respectively the intensity reflectivities of the recycling mirror and of the MITF, we get a relation between these reflectivities, the modulation frequency Ω and the residual path-length δ of the MITF:

$$cos(\frac{\Omega\,\delta}{2\,c}) = \sqrt{R_r R_M}$$

This condition also ensures the optimum enhancement of the modulation index inside the recycling cavity. When R_r is optimized, this reduces to:

$$\frac{\Omega\,\delta}{2\,c} = \sqrt{\frac{2}{S}} \quad (\pm 2\,n\,\pi)$$

With this frontal modulation, one also expects an induced amplitude modulation on the detected phase difference of the MITF. If m is the modulation index of the incident beam, the phase difference is modulated with an amplitude $\Delta\phi = m\ \sqrt{1 - R_r R_M}$. The optimum modulation index depends on the kind of loss encountered in the MITF; with a dominant absorption loss, the modulation can be small to reduce the amplitude modulation effects. With a dominant loss due to beam distortion, one should filter spatially the outgoing beam of the MITF to recover the optimum sensitivity.

This technique seems to be very promising for the kilometric antenna; unfortunately, due to the relation between the path-length and the modulation frequency, it is not easy to test it in a small system, because the modulation frequency will be too high, in the gigaHertz range.

3.1.2.3) EXPERIMENTAL RESULTS

A rigid prototype has been implemented in Orsay, in order to test the different kinds of modulation techniques.

With the internal modulation technique the shot noise limited sensitivity has been reached for powers ranging from 10 to 200 mW, both in Orsay and in Garching. This corresponds to a phase sensitivity :

$$\delta\Phi = \sqrt{\frac{2h\nu}{\eta P_0}} = 1.4\ 10^{-9}\ \mathrm{rd.Hz}^{-1/2}\text{, or to } \tilde{h} = 2\ 10^{-21}\ \mathrm{Hz}^{-1/2}$$

in a full size antenna.

Another important experiment was to verify that this phase sensitivity can be maintained when the interferometer is no more a simple MITF but contains a Fabry-Perot in each arm: the sensitivity is then amplified by the equivalent number of bounces in each arm, which is equivalent to the finesse of the Fabry-Perot . This experiment has been realized for the first time in Orsay with Fabry-Perot of finesse 150 in each arm and by recombining the reflected light from each arm.

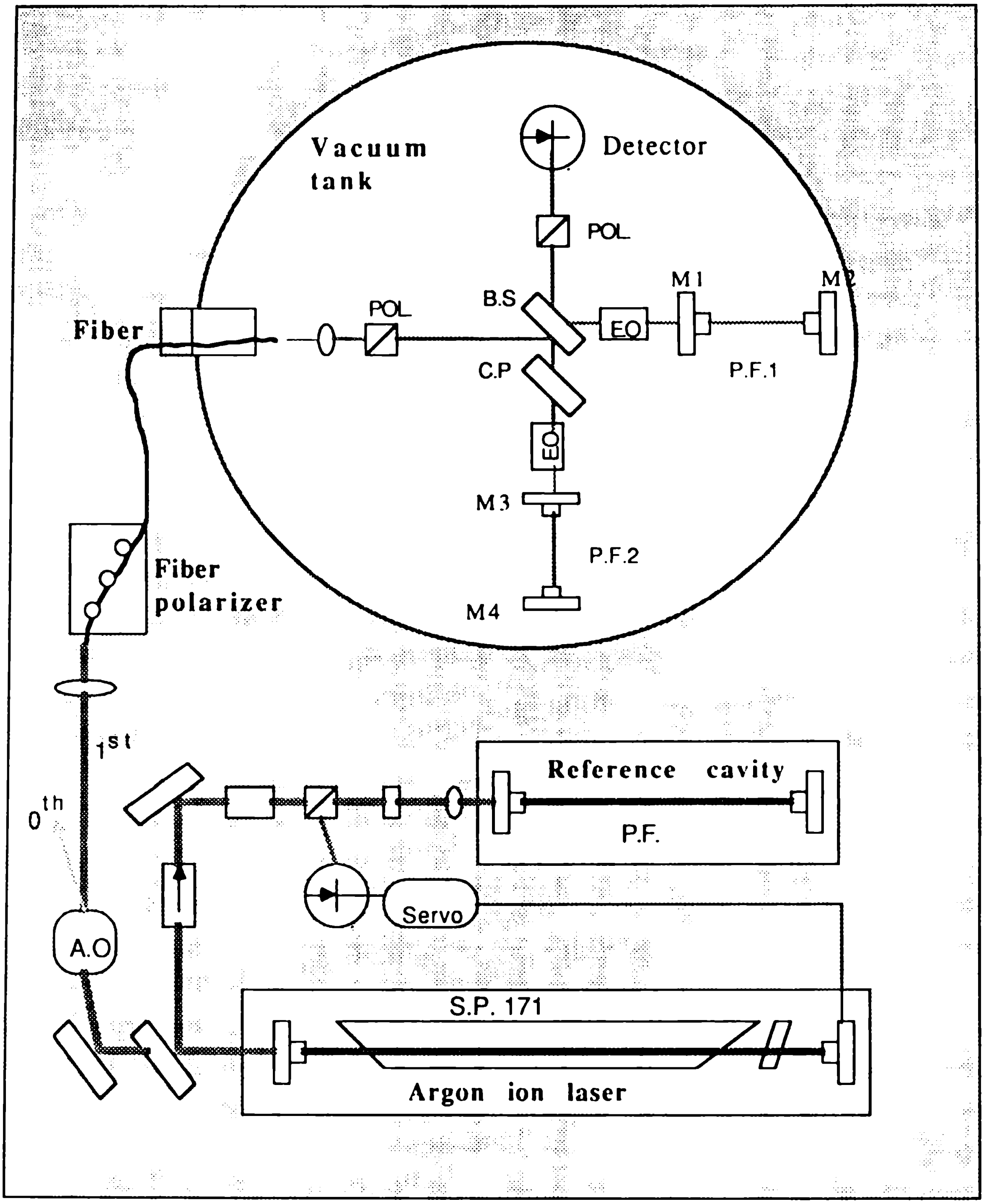

Fig.3.1.14: Experimental set-up
Michelson-Fabry-Perot interferometer

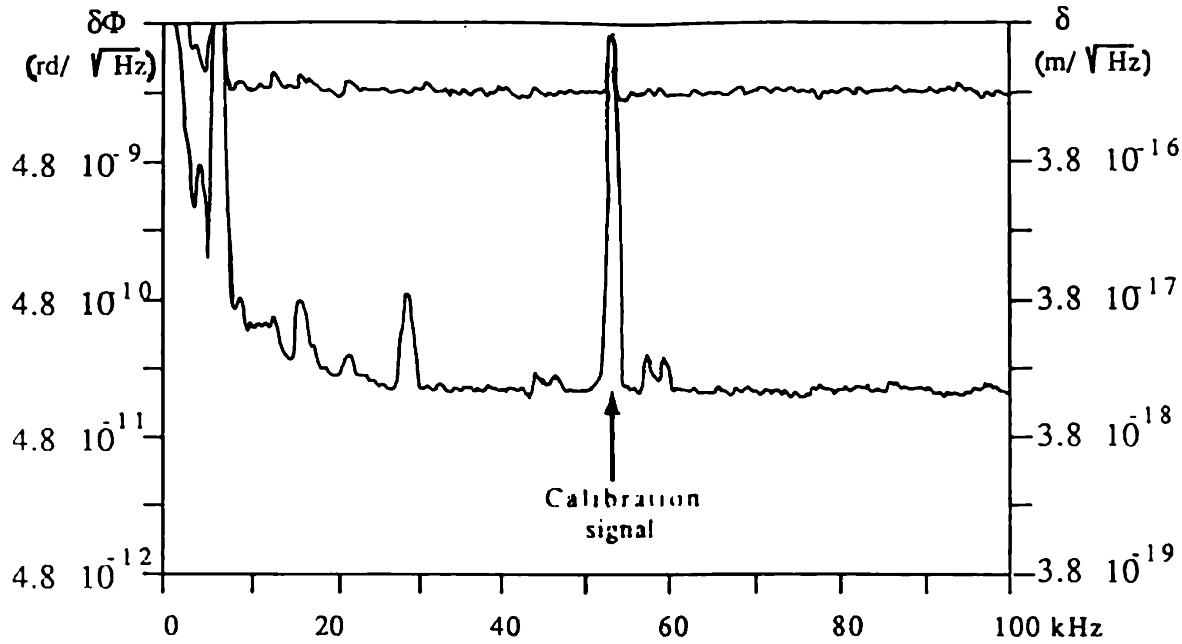

Fig.3.1.15 : Spectral density of length fluctuations of a Michelson interferometer

top curve : simple MITF

bottom curve : with Fabry-Perot cavity in both arms

(the left scale is valid only for the top curve)

Fig 3.1.14 shows the block diagram of this experiment, and Fig 3.1.15 shows the spectral density of the path-length difference of the MITF, in the frequency range 0 to 100 kHz, both for the simple MITF and for the MITF with the Fabry-Perot cavities in each arm. The improvement by two orders of magnitude of the mirror displacement sensitivity is exactly the expected result

Recycling experiments have been done in Orsay, (Man et al.[1987]) and in Garching (Schnupp et al [1987]); with a typical overall loss of 1% and a recycling mirror $T_r = 2\%$, we have achieved a recycling factor of 40 .

External modulations using one and two photodiodes have been tested in Orsay in a recycling MITF. The optical configuration used in those experiments corresponds to the scheme of Fig.3.1.12 : the external light is derived from an extra reflection of the beamsplitter, so it has travelled the same way as that of the MITF arms. We effectively checked out that there were no extra sensitivity to the laser frequency fluctuations (Man et al.[1988]).

In this experiment, we encountered a power limitation above which we observed optical damage on the beamsplitter This limitation appeared for an incident power of 0.3W, corresponding to a stored power of 12W. This is quite encouraging, because, although we did not use "supercoatings", this corresponds to an intensity of 6kW/cm^2 which is about the same as what we expect to reach in VIRGO. The sensitivity was shot-noise limited for low modulation index, but remained a few dB worse than the optimum value because we did not have a mode cleaner at that time. The best sensitivity we measured corresponds to an effective power of 2 W ($\delta\Phi = 3\ 10^{-10}$ rd.Hz$^{-1/2}$)

3.1.2.4) SCATTERED LIGHT

The problem of the effect of scattered light on the interferometer performance is quite complex. The effect is that light which is scattered by any optical component can find its way back to the signal detector, where it will interfere with the signal beam. It will produce a phase shift of the detected light, which scales with its amplitude (as opposed to intensity). Then even a very weak scattered light intensity (10^{-10}) may produce a noticeable phase shift ($2\pi\ 10^{-5}$ rd). This may become dangerous either if the scattered light optical path is very different from the main beam path, because it will increase the system sensitivity to laser frequency fluctuations, or if the scattered beam is reflected from a moving surface, such as the pipe walls, for instance. The first effect will be unimportant because of the very high stability of the laser. The second one can be made negligible only by decreasing as much as possible the amount of scattered light, and by preventing it from reaching the detector after having bounced on the pipe walls.

We will use "supermirrors" made with the best coating technologies on a superpolished substrate to reduce the total scattering coefficient of each surface below 10^{-4}.

The effect of light baffles placed inside the pipe to trap the scattered light has been studied by K.Thorne recently (Thorne,[to be published]). His results show that the effect of scattered light can be made negligible by inserting a large number of these traps (>100) in each arm of the MITF, and he proposes that they be placed inside the tube once forever. This solution is possible, but unpleasant, because it leaves no possibility of error. If the edges of the traps, for instance, are not sharp enough, their efficiency will decrease very much and it will be suitable to change them.

We have not yet chosen a final solution to this problem. Numerical simulations using a Monte-Carlo method or using an adapted beam propagation program are being made in Pisa and Palaiseau. They will check Thorne's calculations, and test some new ideas.

The important idea here is that Thorne's work gives a solution to the problem. We may improve it, but the question of feasibility is already answered.

3.1.3) IMPLEMENTATION

3.1.3.1) THE LIGHT INJECTION AND DETECTION SYSTEM

Up to now, we have only considered a simplified interferometer reduced to its 6 fundamental optical components. It is time to consider the complete optical device, which involves many more components, whose functions are:

a)- to bring the laser beam inside the vacuum tank: the beam can be transported by a set of mirrors through a window, or by a monomode fiber. This second solution, already implemented on the prototype interferometers in Orsay and Pisa, will be the preferred one if its efficiency can be brought up to about 80%. (we presently obtain about 60% with green Argon laser light, but it is reasonable to expect some improvements in the near future). The main advantage of the fiber is that it delivers a very stable output beam, of constant geometry.

b)- to eliminate as much as possible all the beam fluctuations, by filtering it and by providing ways to servo-stabilize it. Active stabilization with fast, high gain, servo-loops acts as a high pass filter for the fluctuations, and can reduce dramatically the frequency and amplitude noise of the lasers in the low frequency range of interest (10 Hz-10 kHz). The other frequency range of interest is the 10 MHz range, around the modulation frequency, which lies outside of the bandwidth of the servo-loops. The best way we have found to suppress fluctuations in this frequency range is to use a Fabry-Perot cavity in transmission : this acts as low pass filter, with a bandwidth : $\Delta\nu = \frac{c}{2LF}$. If one chooses a length (L) of 10 m and a finesse (F) of 100, then $\Delta\nu = 150\ kHz$, and the fluctuations around 10 MHz are suppressed by a factor of the order of 100. The nice thing about this device is that it suppresses all kinds of fluctuations. It was first introduced as a mode-cleaner (spatial filter) by the Garching group, which did not realize at that time that it could also be a low pass filter for frequency and amplitude fluctuations. The characteristics of mode cleaners are described in section 3.3. We intend to include such a cavity inside the central part of the vacuum tank.

c)- to transform the beam geometry, in order to match it to the interferometer eigenmode. This is realized by a beam expander placed between the mode-cleaner cavity and the input of the interferometer.

d)- to provide the modulations necessary to the control of the interferometer and to the extraction of the signal This is the most complex part of the system. It must serve the following functions :

- locking of the Fabry-Perot cavities in both arms
- locking of the recycling cavity
- locking of the Michelson interferometer to a dark fringe
- locking of the mode cleaners
- optimized detection of the signal

e)- to reject the unwanted geometrical and frequency components of the output beam. This will be realized by a second mode-cleaner. This device is important, because it prevents useless light to reach the photodetectors. This improves the apparent contrast of the interferometer and reduces the amount of energy which has to be transferred to the modulation sidebands : it results that the sensitivity is improved, and that the demand on the detectors average output current is lowered.
Fig. 3.1.16 shows a simplified block diagram of the ensemble.

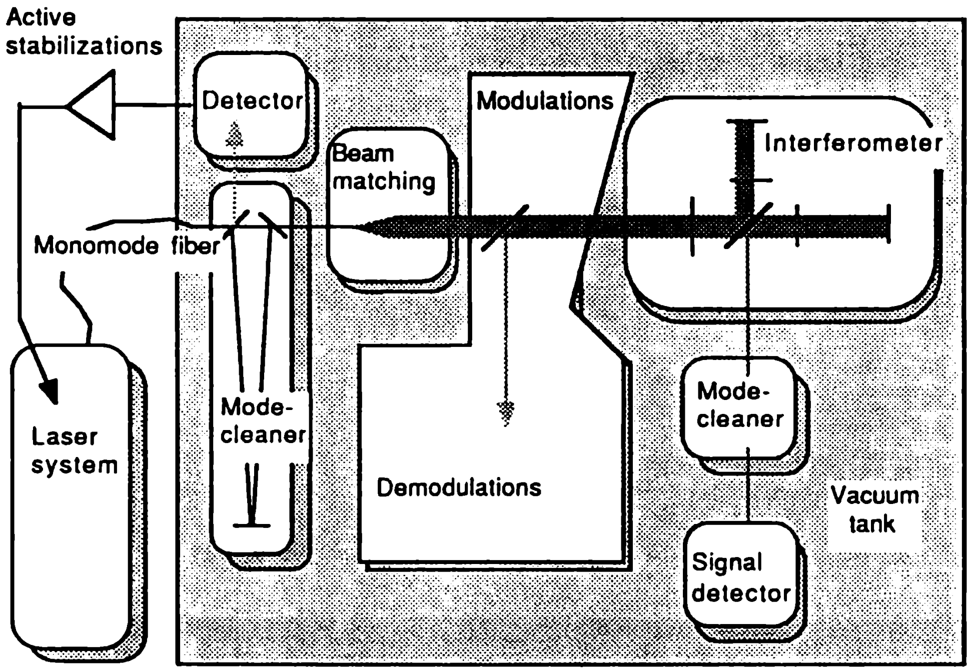

Fig.3.1.16 Functional block-diagram of the VIRGO interferometer

Fig. 3.1.17 gives a more detailed view of the modulations and of the stabilization loops involved in the global control of the interferometer, in the case of a frontal external modulation.

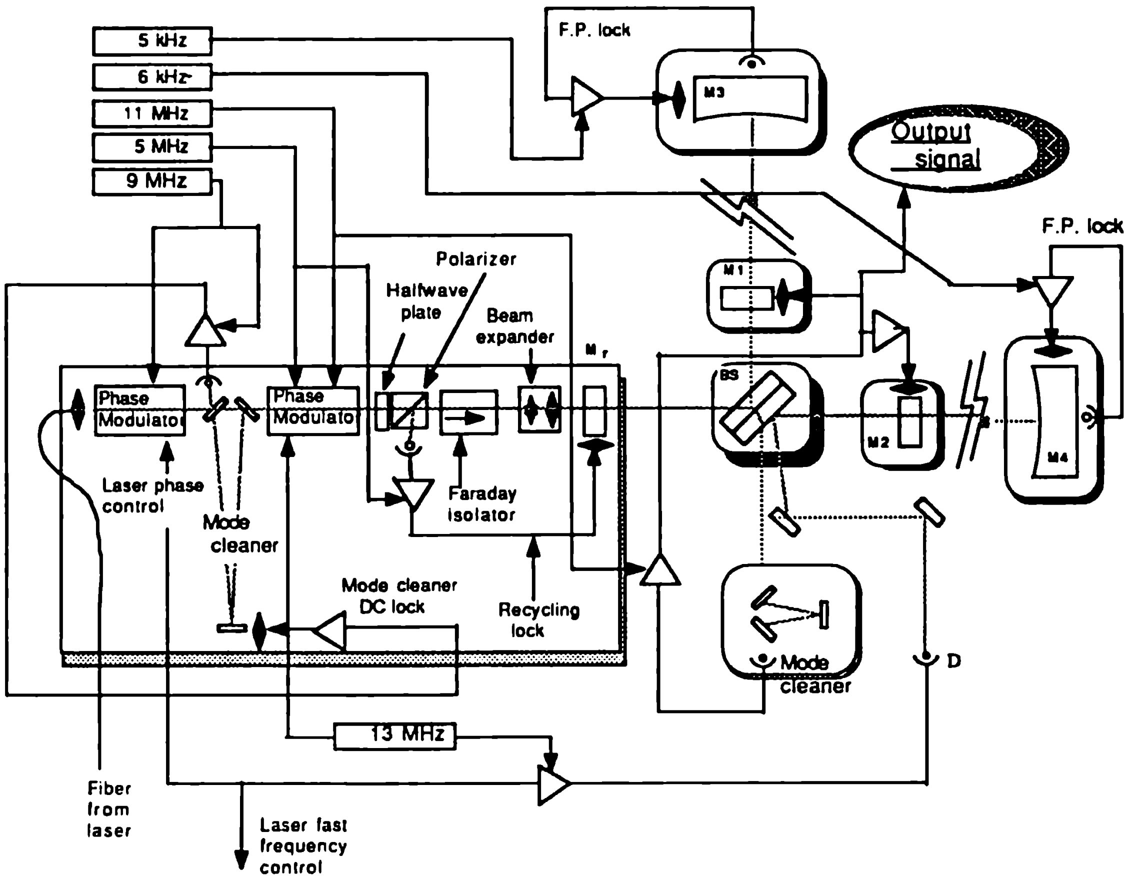

Fig.3.1.17: Global control of the interferometer

In the scheme proposed here, the laser frequency is prestabilized before the fiber, and the final frequency control is realized with one of the long cavities as a reference (13 MHz modulation). The mode-cleaner itself is stabilized on the laser frequency, and the other Fabry-Perot gravito-optic transducer is locked to the laser (with the low frequency modulation-demodulation at 5 kHz, and the feedback loops acting on M3). The 5 MHz phase modulation serves to lock the recycling cavity to the laser. The MITF is locked on the dark fringe by monitoring and demodulating the signal at 11 MHz after the output mode-cleaner and by feeding back the error signal differentially on the mirrors M1 and M3. If the unity gain frequency of this loop is higher than the observational frequency range, the gravitational signal is contained in the control voltage applied to the transducers on M1 and M3.

The exact modulation frequencies are determined by the exact dimensions of the apparatus: the 5 MHz must be chosen so that the sidebands at $\nu_l \pm 5$ MHz are reflected by the recycling cavity, while the sidebands generated by the 11

MHz modulation must be resonant with the recycling cavity <u>and</u> with both Fabry-Perot cavities.

For this global frequency control to function, it is necessary that each suspended mass be aligned and prestabilized with a local control loop (see 3.5). The important point at this time is that we do have a solution for ensuring the control of the system; there are other possibilities and refinements, some of which may appear to be useful. Changing from this solution to a better one is a minor piece of work once the transducers and the electronic loops have been understood and developed.

Fig. 3.1.18 describes a possible setup for the optical system we will use to inject light in the interferometer.

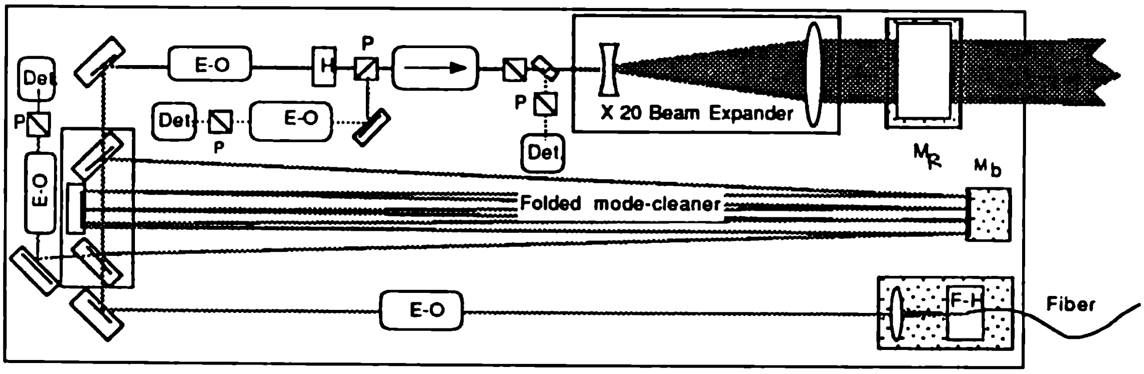

Fig. 3.1.18 : Schematic of the light injection bench

Light coming from a monomode fiber is phase modulated (at 9 MHz) and sent through a folded ring-cavity mode-cleaner. The light reflected by the mode-cleaner is sent to a detector and demodulator system, to generate the error signal for locking the mode-cleaner to the laser frequency. Folding the ring cavity decreases the intensity on the mirrors for a given selectivity. When the system is locked, the amount of reflected light should be small, but it reaches 100% of the laser power when out of lock, so the detector will need to be protected : one possibility is to precede it by a fast electro-optic (E-O) shutter which can attenuate the beam in less than a microsecond as soon as it becomes too intense. The other obvious possibility is to attenuate the beam permanently, if no shot-noise constraint is present..

The light transmitted by the mode-cleaner is modulated again (at 5 and 11 MHz), passed through a Faraday isolator to prevent optical feedback, and expanded to match the interferometer beam geometry, before reaching the recycling mirror M_R. The detector which measures the light reflected by the recycling cavity has the same problems and the same protection as the first one.

For the purpose of power stabilization, a small fraction of the beam is diverted towards another detector, just before the beam expander.

Both the fiber and the final beam expanders must have a very good dimensional stability, or better, a remote fine adjustment capability, in order to maintain the perfect alignment and matching of the beam (an automatic fiber alignment and a remotely controlled beam expander have been built and tested in Orsay).

All these components will be integrated on a single suspended mass.

3.1.3.2) MIRRORS MECHANICAL DESIGN

3.1.3.2.3) LARGE MIRRORS

The large mirrors of the interferometer (M_1 through M_4) are interesting pieces of high technology. They should not only have a very high optical quality and state of the art coatings, but also they should obey some mechanical constraints :

-they should be heavy to decrease the thermal noise of the suspension (see 2.10.4). As described in Chapter 2, this formula is valid above the pendulum highest resonance frequency, i.e. above a few Hz in our case, and the corresponding noise varies as $1/\omega^2$, so it becomes negligible at high frequency.

- they should also be made of one single piece and have a simple shape, so that their mechanical resonances are of high Q and at high frequency, in order to decrease their own internal thermal noise (see 2.10.6). This formula is valid below the lowest resonance frequency of the mass. Since ω_0 is roughly inversely proportional to $M^{1/3}$, the noise is roughly independent of the mirror's mass, as long as the mirror is not so large as to present resonant frequencies within the detection range.

- the product of the inhomogeneity of the material by the thickness of the input mirror should be small enough to keep the wavefront distortion below the specifications. For an inhomogeneity $\delta n = 2\ 10^{-7}$, the maximum thickness is of the order of 10 cm.

Then, one has to look for a good compromise between the constraints of high sensitivity at low frequency and at high frequency and the thickness limitation.

The choice of the material is quite restricted : it has to be highly transparent and homogeneous, to have a low damping coefficient, and to be manufacturable in large dimensions. Only fused silica responds to these conditions.

We first tried to design very heavy mirrors, for low noise at low frequency. After some iterations between a material producer (Heraeus) and a coating specialist (SAGEM), we ended up with a mirror shape such as described on Fig.3.1.19 a. The conical shape is made necessary by the requirements of the coating technology (the back of the mirror is A.R.coated). It would be possible in that way to reach a mass of 200 kg. This mirror would be realized by "fusing" a disk of very high quality and thickness 7 cm to a massive conical piece of lower optical quality. The whole object is made of silica. The drawbacks of this design are that it is difficult to polish and to coat, and that its lowest resonance frequency is a bit too low (1.3 kHz)

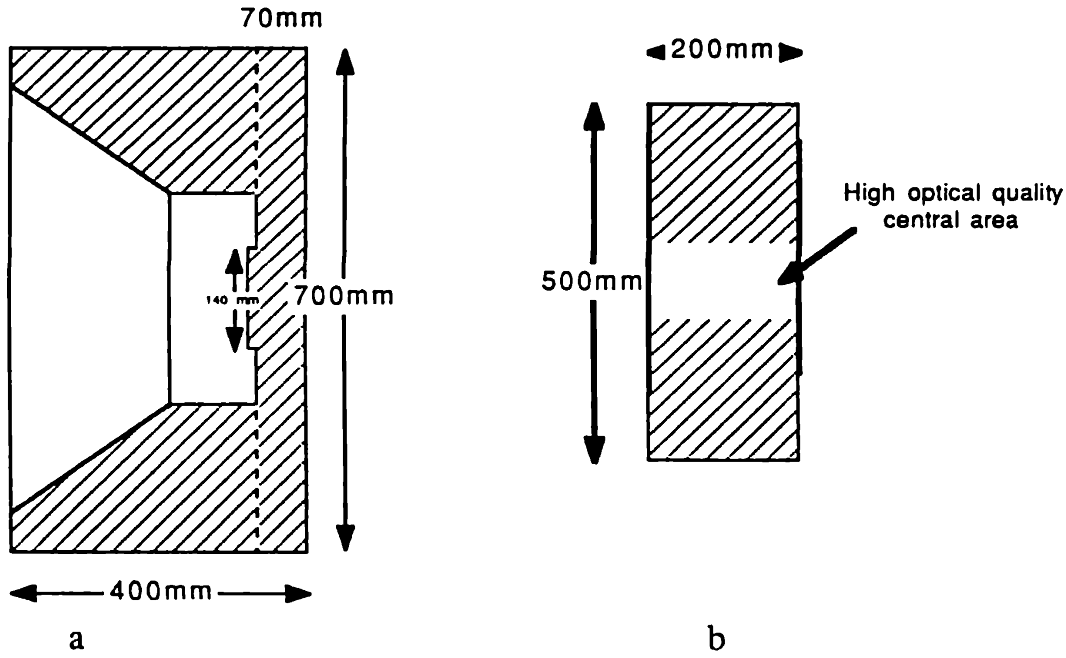

Fig.3.1.19 Possible mirrors designs

a) a high mass conical mirror, obtained by "fusing" a high optical quality disk on a massive cone.

b) a high resonance frequency, single piece, disk shaped mirror

It seems now that it will be possible to get very high optical quality silica disks of thickness 20 cm and diameter 50 cm (Fig."3.1.19 b), with index inhomogeneities smaller than 2 10^{-7} RMS in the central area. This could represent a good compromise, although the wavefront distortion may be a bit too high. But the RMS specification is not well adapted here, and we will have to make the measurement in terms of Zernike polynomials. The mirror mass is 90 kg, the polishing and coating will be much easier, and the first resonance frequency is higher (about 3 kHz).

These two designs should give satisfactory results. The final choice will depend on further iterations with the silica producers and the coating firms, on cost evaluations, on the results of modelizations of the mirrors resonances, and of some more theoretical and investigations on the thermal noise.

3.2 Laser and detectors

3.2.1) SPECIFICATIONS AND PROPOSED DESIGN

Let us remind the requirements for the laser :
It should be a monomode single frequency laser, with an output power of more than ten watts initially, scalable to 100 Watts in the future.
Its frequency and output power must be extremely well controlled. This is realized by active servo loops.
Its wavelength is not a critical parameter : it must be chosen as the result of a compromise between many different considerations:

- the sensitivity for a given laser power improves as $\frac{1}{\sqrt{\lambda}}$
- the beam diameter increases as $\sqrt{\lambda}$, asking for bigger optics as λ increases
- the apparent quality of the optical components improves proportionally to λ as concerns the polishing, and to λ^2 as concerns light scattering
- the laser power is to be weighed by the efficiency η of available photodetectors at its specific wavelength. Silicon detectors provide $\eta \approx 1$ from $\lambda = .5$ to $.85\ \mu m$, while InGaAs detectors provide $\eta \approx 1$ from $\lambda = 1$ to $1.6\ \mu m$.

Within the range of .5 to 1.5 µm, the main element of the choice is finally the existence of an appropriate laser. All the prototypes around the world have been using Argon ion lasers at the wavelength of 515 nm, because it was the only reasonable and commercial laser for low and intermediate powers.
As we have demonstrated a few years ago, it is possible indeed to use an array of 4 to 5 phase locked Argon ion lasers to obtain a single frequency output power of 20 Watts, by injection-locking these lasers together. That seemed to be the only possibility for a while, in spite of the many inconvenients of Argon ion lasers:

- their low efficiency (typically 10^{-4} in single frequency operation) makes them very costly in the case of a continuous operation, both because of the power and the water consumption. For 1 year of operation at an output power of 20 W, the required power is about 2 10^6 kWh, and the cooling water consumption of 20 000 m^3.

- the lifetime of a laser amplifier tube at full power is of the order of 1000 h, so that more than 30 tubes per year would be needed, for a total cost of nearly 6 MF, or 1.2 GIL, and at least 30 days of operation in non optimal conditions.

This is still the direction pursued by the other groups at the present time (although there is an evolution towards Nd:YAG lasers), but we do not think it is the best way to go anymore, since the development of high power laser diodes in the mid 80's has opened a new era where very reliable, powerful and efficient solid-state lasers are becoming available.

In 1986, we decided to start studying the possibility of using Nd:YAG lasers for illuminating the interferometer. At that time, it was possible to buy multimode YAG lasers with output powers in excess of 100 Watts. These lasers were pumped by Krypton lamps and were not optimized for monomode operation, but they appeared to be able to deliver more than 10W, for an electrical consumption of 10 kW; this is an efficiency of .1 %, already 100 times better than in the case of an Argon laser. The krypton lamps have a lifetime of the order of 500 h, but they are 100 times cheaper than an Argon tube

Furthermore, the promise is that it will become possible in the future to replace krypton lamps by laser diodes, providing an efficiency higher than 10 %, and lifetimes of the order of 50000 h. The wavelength of the YAG laser (λ=1.06 μm) is still in a convenient range, now that very efficient InGaAs photodetectors have been developed (for communications applications). We even think that this wavelength is preferable to the 515 nm wavelength because it reduces the problems of scattered light and of mirror surfacing. Let us add that it is also possible to frequency double a low power ND:YAG laser with a very high efficiency, so that it will be soon possible.to use the YAG laser at the wavelength of 532 nm, if this appears to be advantageous. At the present time very high doubling efficiencies have been obtained at low power, but the lifetime of the nonlinear crystals used to get this result is quite short.

The cost of the very high power laser diodes which are necessary for pumping a 20 W YAG laser is still dissuasive, so we are presently working at an intermediate solution which consists in a high power krypton lamp pumped laser, which is used to amplify the low power, but ultrastable beam delivered by a diode pumped YAG laser.

Therefore, we decided that the best solution would be to use a Nd:YAG laser at 1.06 µm. In a first step the high power oscillator would be a lamp-pumped YAG rod. Its frequency stability would be obtained by injection locking from a diode-pumped stabilized low power oscillator. This solution could be satisfying for the first generation of VIRGO. It would be easy to replace the lamp-pumped device by a diode-pumped high power device once the cost of diodes becomes reasonable.

3.2.2) THE LOW POWER DIODE PUMPED LASER

The diode pumped laser has been studied and developed in Orsay during the last two years. Fig.3.2.1 represents its cavity.

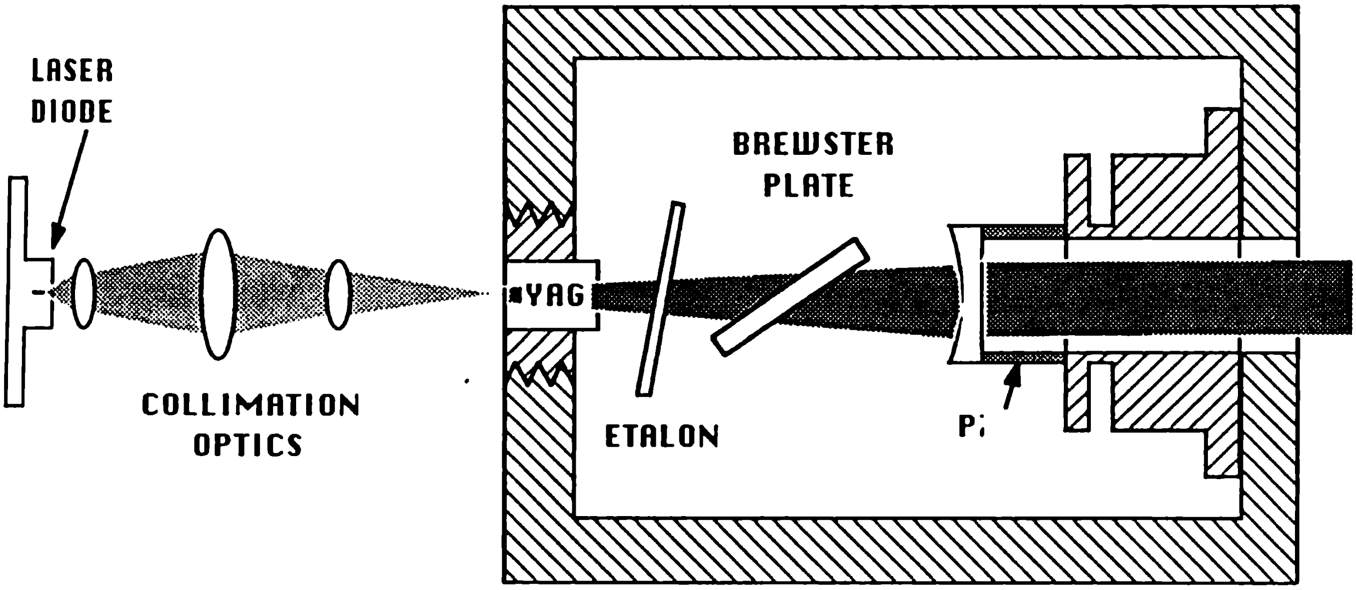

Figure 3.2.1 : Optical scheme of the diode-pumped Nd:YAG laser

It is a standard end pumped laser, with a cavity length of 5 cm. The pump laser is a 500 mW diode. It delivers now a maximum power of 40 mW, and can be actively stabilized to generate a beam of ultra-high spectral purity (a linewidth of the order of 1 mHz). This device is described in an Appendix. It is very likely one of the two or three most stable lasers in the world presently, and the most stable Nd:YAG laser ever realized. Its

spectral density of frequency fluctuations is of 0.01 $Hz^{-1/2}$. It is limited by the shot noise of the frequency discriminant and by the finesse of the reference Fabry-Perot cavity, and can be improved by about three orders of magnitude, if required.
The output power of 40 mW is still low, but this can be improved: we are starting a collaboration with the German company MBB, who has already realized similar (but unstabilized) devices having an output power of the order of 500 mW.

3.2.3) THE HIGH POWER LASER

3.2.3.1) DESIGN

The design of the high power device is conditioned by some particular characteristics of the YAG crystal.

a) thermal lensing effect

The low efficiency of lamp-pumping a Nd:YAG crystal produces a strong heating of the laser head, which must by avoided by water cooling. The combined effect of heating and cooling creates radial temperature gradients in the YAG rod, with a cylindrical symmetry. Since the optical index depends on the temperature, this produces a power dependent positive lens effect in the crystal.

b) thermal birefringence

The thermal gradient produces stresses in the material, which create birefringence; in each point of the crystal, the main axes of the ellipsoid are radial and tangential. This has two detrimental effects : the geometry of the birefringence does not allow for the propagation of a linearly polarized beam, and it also creates bifocusing, the focal length of the thermal lens varying by as much as 20% depending on the polarization.

c) spatial hole-burning

The presence of a standing wave inside the crystal generates a spatial modulation of the gain saturation. So, even in an homogeneously broadened medium, all the Nd^{3+} ions do not collaborate equally to the laser effect, and it becomes difficult to obtain a single frequency operation.

d) description of the present laser

We have chosen to use a ring cavity to avoid the spatial hole-burning problem. The birefringence is compensated by using a pair of similar amplifiers, with a 90° polarization rotation between them. The initial polarization is defined by a polarizing beamsplitter, and re-established after the second amplifier by a half wave plate. Tunable output coupling is obtained by a small rotation of the plate. It generates a component on the orthogonal polarization, which is reflected by the beamsplitter and used as the output beam.

Faraday rotation is used to ensure unidirectionnal operation.

The cavity geometry is calculated for being dynamically stable and for optimum beam size inside the amplifiers. The beam is symmetrical relative to the median plan between the amplifiers.Fig.3.2.2 shows the optical scheme of this cavity.

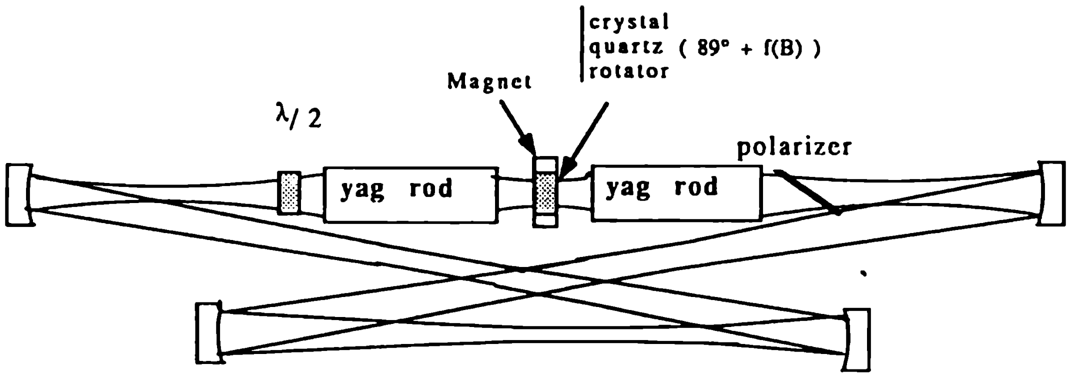

Figure 3.2.2 : Optical scheme of the High power Nd:YAG laser

The mechanical design is intended for some versatility, allowing different trials, and for stability. It uses a frame of three Invar rods, to which each optical component is connected rigidly with an individual Aluminium structure. The amplifier heads, which show vibrations induced by the water cooling, are not connected to the frame. We had developed and used this technique previously for the design of stable Argon lasers. Fig.3.2.3 shows the mechanical setup.

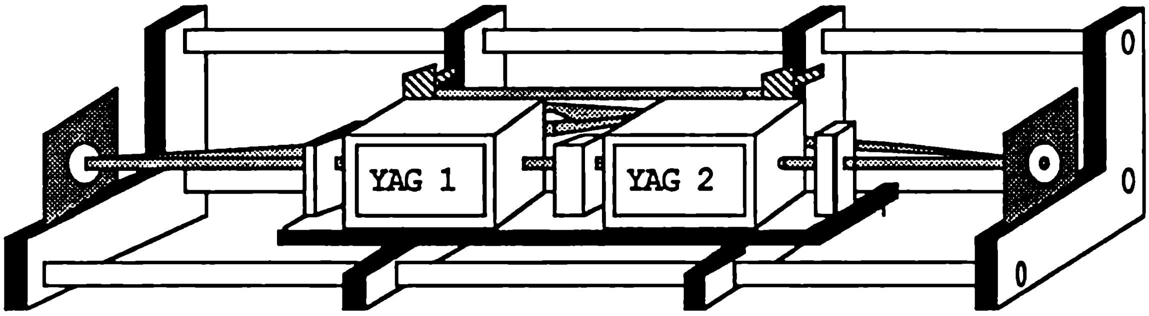

Figure 3.2.3 Mechanical setup for the high power Nd:YAG laser

3.2.3.2) PRESENT RESULTS

The high power device has been constructed and operates roughly as expected.It presently generates 18W TEM_{00} in unidirectionnal operation. The output beam is not single frequency yet, as this was expected, because the gain is not completely homogeneously broadened. It becomes single frequency just by adding an uncoated etalon in the cavity, with an output power of 15 W. The free running stability is not very good, but seems sufficient to allow for standard stabilization techniques to function.
The injection locking system is set-up, but has not been operated successfully yet, by lack of power from the master oscillator. Preliminary experiments show that the high power stage can operate as a regenerative amplifier : we have measured a gain of 100 and obtained a power of about 2 W in these conditions. This could be an alternative solution in case we find unexpected difficulties with the injection locking technique

3.2.3.3) FUTURE WORK

The development of a high power diode pumped device is one of the parts of the VIRGO project which has important technological fallouts :

this should produce multiwatt single frequency lasers with an efficiency higher than 10% and a nearly infinite lifetime. If the YAG is pumped by a number of fiber coupled diodes, for instance, it will be possible to change a failing diode without disturbing the laser. (note that the lifetime of a diode can reach 50 000 hours, anyway)

The cost of high power laser diodes is still a bit too high (10 kFF, or 2 MIL per Watt at best), but this cost still represents more the research investment than the production cost. It must decrease very rapidly, since there are now a few firms in the world which are able to produce multiwatt diodes. We are starting to study possible high power diode pumped lasers. Quantel in France, and MBB in Germany, have expressed the will to collaborate with us in this direction. We would start very soon the construction of such a laser, if we get the manpower to do it.

3.2.4) DETECTORS

The main requirements for the important photodetectors (those who control frequency stabilization loops as well as the signal detector or detectors) are their quantum efficiency which must be close to unity, their frequency response which should allow for the detection of signals at 10 MHz, their ability to deliver high average currents (100 mA) without saturation, and their ability to stand high levels of illumination for short periods of time (>10W for 1μs).

The candidate materials at 1.06 μm are silicon (Si) and Indium Gallium Arsenide (InGaAs)

3.2.4.1) SILICON DETECTORS

Silicon has all the qualities except the quantum efficiency, because the wavelength is a bit too long and Si becomes slightly transparent. One can enhance its sensitivity by using a highly resistive material: the photodiode spectral sensitivity is directly related to the depletion depth, which depends on the operating bias voltage and on the resistivity. The quantum efficiency is given by the relation :

$\eta = (1 - e^{-\delta t})$ where δ is the absorption coefficient at the wavelength λ, and t is the depletion depth. At 1.06 μm, the absorption coefficient is 35 cm^{-1} so the depletion depth must reach about 660 μm for a quantum efficiency of 90%. This can be achieved starting from a highly resistive material, with a polarization of a few hundred volts.We have not verified the properties of such a slightly exotic detector. It may be that its high resistance will make it unsuitable for high frequency operation.

It is useful to put an antireflective coating on the detector, because of its high refractive index. We have also tried successfully to orient it at Brewster's angle in order to facilitate the penetration of the (polarized) light.

3.2.4.2) INGAAS DETECTORS

InGaAs is a recently developed material, which was studied for the needs in fiber communications at 1.3-1.55 μm. It has a much larger absorption coefficient than Si at 1.06 μm, and its quantum efficiency can be made higher than 95%, which is excellent.

Its power handling properties are supposed to be as good as for Silicon.

Its frequency response is very good too, but this material is not yet available with the wide area that is required to fulfill the high power conditions.

This is not a problem in principle, it just happens that there are not many needs for large surface InGaAs detectors outside of the VIRGO project. It will be necessary to ask for a special fabrication and to test their performance. This study remains to be done.

The two possibilities have to be explored more deeply before we arrive to the final design for the detectors.

3.3 Laser stabilization

3.3.1) LASER FREQUENCY STABILIZATION

3.3.1.1) REQUIREMENTS AND LASER NOISE

The effect of laser frequency fluctuations on the interferometer noise has been discussed in detail in Chapter.2. The simplified relation to remember is the one which links the spectral density of the relative laser frequency fluctuations to its equivalent noise in terms of a gravitational signal:

$$\tilde{h} \approx \frac{\widetilde{\delta\nu}}{\nu}\left(\frac{\Delta L}{L}+\frac{\Delta F}{F}\right)$$

where F is the average finesse of the cavities, and Δ denotes an asymmetry between the two arms. If we assume an asymmetry of 1%, for instance, we find that the laser frequency fluctuations should be very low :

$$\frac{\widetilde{\delta\nu}}{\nu} \leq \frac{\tilde{h}}{\alpha} \approx 3.10^{-21}\ \mathrm{Hz}^{-1/2}, \text{ or } \widetilde{\delta\nu} \leq 10^{-6}\ \mathrm{Hz.Hz}^{-1/2}$$

This requirement is very stringent and requires that the laser be very well stabilized : in the frequency range of interest, all the lasers have an important excess frequency noise, of mechanical and acoustical origin. High power lasers have the supplementary problem that they need water or gas cooling, which generates vibrations, and long term thermal fluctuations. The typical spectral density of frequency fluctuations of a (stable) high power laser is of the order of 10 $\mathrm{kHz.Hz}^{-1/2}$ around 1 kHz, 10^{11} times more than the requirement.

Therefore, the difficulties are to find an appropriate reference, to which the laser frequency will be locked, and to realize servo-loops with a high enough gain, a high enough dynamic range, and a low enough intrinsic noise. We will see below that there are solutions to these problems, which consist in using the large Fabry-Perot gravito-optic transducers as frequency references, and in cascading servo-loops to get the gain and the dynamic range.

3.3.1.2) REFERENCE CAVITY AND DETECTION TECHNIQUE

3.3.1.2.1) PRINCIPLE

As mentioned in the previous section, the length of an optical cavity will be used as the reference for the laser frequency stabilization. The sensitivity of the cavity as a frequency discriminator is greatest near or on a longitudinal resonance, because it is there that the change in intensity or phase of the light in the cavity is the most rapid for a given change in the frequency of the incident light. One simple scheme uses the light transmitted through the cavity. If the cavity is held on the side of a resonance, small changes in the incoming light frequency (small in comparison with the cavity linewidth) are converted linearly into changes in the transmitted light intensity. The are several problems associated with this arrangement: a small usable dynamic range, sensitivity to power fluctuations, and a need for a transmitted beam among them.

An alternative detection scheme, using methods first developed by Pound for use in microwave systems and applied first by Drever, Hall, et al (Drever et al., [1981]) to laser stabilization uses the light reflected by the cavity in the vicinity of resonance. This light is composed of two components: that light which was simply reflected from the entrance mirror, and that light which entered the cavity, contributed to the resonance phenomenon, and then left via the entrance mirror. The 'stored' light undergoes a very steep change of phase with respect to the second contribution from the directly reflected light as the frequency of the incoming light passes through the resonance frequency of the cavity. The optical interference between these two contributions allows the detection of the phase difference, and thus of the frequency of the incoming light compared to the resonance frequency of the cavity.

The optical arrangement used to separate the incident and reflected light is shown in Fig. 3.3.1. The e.g. vertically linearly polarized incoming beam passes through the 'easy' axis of the polarizing beamsplitter **BS**, and is converted into right hand circularly polarized light by the $\lambda/4$ plate **L4**. After reflection from the cavity **FP**, the direction of the circular polarization is reversed, and upon falling on the $\lambda/4$ plate is converted into horizontal linearly polarized light. This is the 'hard' axis of the polarizing beamsplitter, and thus the light is reflected onto the photodiode **PD**.

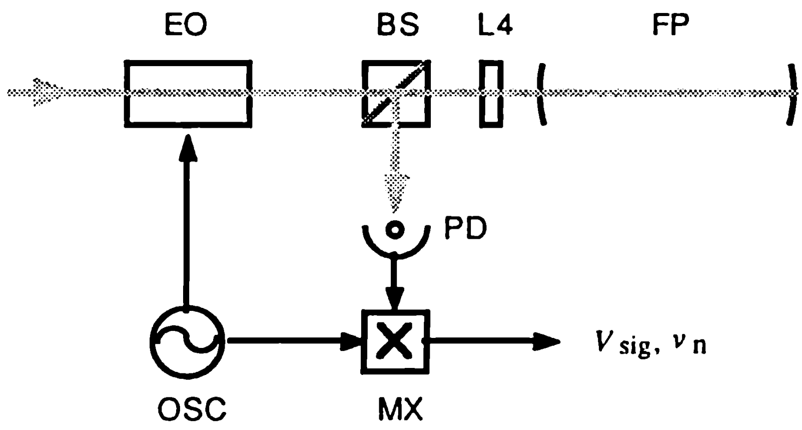

Fig. 3.3.1: The Pound-Drever technique

3.3.1 2.2) SENSITIVITY OF POUND-DREVER TECHNIQUE

In practice, a phase modulation of depth δ and frequency Ω is impressed by the electro-optic modulator **EO** on the incoming light to aid in the detection. The frequency of this phase modulation is chosen to be greater than the cavity linewidth $\Delta v = c/2lF$; to a good approximation, the light power in the phase modulation sidebands does not enter the cavity, but is reflected by the input mirror. The photocurrent from the photodiode is amplified and converted into a voltage, demodulated at the modulation frequency Ω by the mixer **MX**, and low pass-filtered to recover the low frequency component. The variation of this signal with the frequency detuning of the laser relative to the cavity is shown in the Appendix 3.3. In the immediate vicinity of the resonance of the cavity, the voltage at the output of the low pass filter is :

$$V_{sig} = \Delta v \frac{16l}{\pi c} F^2 T_1 \beta J_0(\delta) J_1(\delta) G_1 I_{max} \left[1 + \left(\frac{2 v_F}{\Delta v_c} \right)^2 \right]^{-\frac{1}{2}}$$

where Δv is the difference between the cavity resonant frequency and the incident light frequency. The cavity is of length l and of finesse $F = \pi \sqrt{r_1 r_2}/(1 - r_1 r_2)$; the two mirrors have amplitude reflectivities r_1 and r_2; the entrance mirror has a power transmission T_1. A fraction β of the incident light is matched to the TEM_{00} mode of the cavity. The Bessel functions J_0 and J_1 have as their argument the phase modulation strength δ impressed by the phase modulator. The photocurrent off resonance is I_{max}. and G_1 is the net gain, in V/A, of the photodiode amplifier and the mixer. The Fourier frequency of the laser frequency fluctuations is v_F. Here we have assumed that the frequency of the phase modulation is much greater than the cavity linewidth Δv_c, that the deviation from resonance Δv is much smaller than Δv_c, and that higher order terms in the Bessel function expansion of the phase modulation sidebands are negligible. The Fourier frequency v_F must be much less than the inverse round trip time $v_F \ll c/2l$. Fundamental is the assumption that the mirrors of the cavity are well isolated from mechanical disturbances; any motion of the mirrors Δx will appear as frequency fluctuations : $\Delta x/l = \Delta v/v$.

To calculate the sensitivity of this frequency detection method, an expression for the noise in the measurement is needed. In the ideal case, the limiting noise comes from the shot noise of the photocurrent. In addition, there will be (at least) a noise term from the photodiode amplifier, which will add incoherently with the shot noise. Thus one can write for the voltage noise spectral density after the low-pass filter

$$\tilde{v}_n = G_1 \sqrt{2} \sqrt{2e(I_{mod} + I_{amp})}$$

where I_{amp} is the amplifier noise expressed as an equivalent photocurrent, and I_{mod} is the photocurrent on the cavity resonance and with the phase modulation. The additional factor of $\sqrt{2}$ comes from the fact that the noise in the upper and lower sidebands are both mixed down to the same (positive) frequency, and add incoherently.

Several remarks are useful. In the limit where the amplifier noise I_{amp} is much smaller than I_{mod}, which is the normal operating regime, the signal grows linearly with the incident intensity and the noise as the square root; thus, the overall signal-to-noise S/N grows with the square root of the incident intensity.
The effect of changes in the mirror characteristics is somewhat more complicated: the finesse, for r_1 and r_2 close to 1, is effectively determined by the term in the denominator: $F \approx \pi /(1-r1r2)$. The mirrors have a reflectivity r, a transmission t, and losses p in amplitude; their sum of their squares is, by definition: $r^2+t^2+p^2=1$. For the reflection detection scheme, the second mirror M_2 in the cavity is chosen to have the highest reflectivity possible, as the light lost in transmission (or to losses) is not used. The entrance mirror M_1, on the other hand, must be carefully chosen. In the regime where the losses are much smaller than the transmission, the finesse F is roughly proportional to the inverse of T_1, and the signal v_{sig} grows linearly with the finesse. If, however, the transmission is made much smaller than the loss, the net signal will become smaller, and although the resonance will be very narrow, the resulting S/N will be degraded. There is an optimum in this continuum; it is for the case where the transmission of the input mirror is equal to the total loss in the cavity (due to p_1, p_2 and t_2). For this case, on the cavity resonance and for perfect matching (β=1), the intensity of the light directly reflected from M_1 is equal to the intensity of the light leaving the cavity through M_1, but the two are opposite in phase and destructively interfere; the light on the photodiode would fall to zero if there were no modulation. Thus this is the best case not only for the signal term, because it results in the greatest change in the signal voltage V_{sig} for a given change in the incident frequency, but also for the noise term where the reduction in the light intensity on resonance results in a reduced shot noise. The S/N degrades much more slowly for the case of total loss smaller than the transmission of the input mirror, so this is the preferred case.
Similarly, it is seen that the matching β affects not only the signal V_{sig} linearly (by influencing the amount of light in the TEM_{00} mode), but also the noise term (by influencing the contrast of the interference between the directly reflected and the stored light).

The modulation depth δ affects the signal term through the product of $J_0 J_1$, which has a maximum for $\delta \approx 1.1$; but because the current I_{mod} is a function of the modulation depth,

$$I_{mod} = I_{max}\left[1 - J_0^2 \beta \frac{I_{max} - I_{min}}{I_{max}}\right]$$

(where I_{min} is the photocurrent on the cavity resonance but without the phase modulation), the noise term is also influenced by the choice of the modulation depth, and the optimum S/N will be found for $\delta < 1.1$ in general.

The last term in the equation for V_{sig} has the characteristic of a low-pass filter with a corner frequency of $\Delta\nu_c = c/2lF$. The signal is still usable for higher frequencies, but the dependence of the amplitude and phase on the frequency and must be taken into account in the design of the feedback transfer function and the shot noise limited S/N falls with with increasing frequency. However, once the Fourier frequency is comparable with or higher than the inverse round trip time of $2l/c$, the amplitude and phase of the signal goes through violent changes; it is not practical to use the cavity as a frequency discriminator in this regime.

A two-stage frequency stabilization system is envisaged for the VIRGO project. An initial reference cavity will receive a small fraction of the laser power; the error signal from this detection system will be used to prestabilize the laser light before coupling into the principal interferometer. A second cavity, consisting of the VIRGO interferometer itself, will be used to generate the final error signal which will be used to further stabilize the light to the length of the VIRGO interferometer.

The first cavity will be of the order of l=50 cm in length, and will consist of two mirrors rigidly fixed to a reference spacer. This cavity will be seismically isolated to avoid mechanical excitation and placed in a vacuum system to avoid problems due to statistical or thermally induced index fluctuations. Mirrors with losses of the order of p^2=100 parts per million (ppm) are currently available, with minimum transmissions of the same order; this indicates that the input mirror should have a transmission of roughly T_1=300 ppm for the optimum S/N ratio, resulting in a finesse of roughly 10000. The optimum modulation δ can be chosen, and the mode matching factor β can be quite close to the ideal value of 1. The photocurrent off resonance I_{max} will be determined by the laser power that we choose to direct into the prestabilization system, and the photodiode quantum efficiency. If 250 mW are taken from the laser power to realize this lock, the shot noise limited signal to noise ratio will be roughly 1.10^{-5} Hz/$\sqrt{\text{Hz}}$.

The second cavity could be formed by one of the two arms of the main interferometer. The mirror losses will be of the same order as for the small cavity, p^2=100 ppm, and the transmission of the input mirror will be $T_1 = 0.15$, giving a finesse of 40. Only a small part of the total power in the cavity will be used for this second step of frequency stabilization, but due to the great length of the cavity a very high sensitivity will be reached : for one-half watt of light diverted to the measurement system (about 10^{-4} of the total power), the shot noise limited signal to noise ratio will be roughly $2\ 10^{-7}$ Hz/$\sqrt{\text{Hz}}$. The cavity linewidth will be only $\Delta\nu_C = c/2lF = 1.25$ kHz. This means that the shot noise limited frequency stability rolls off at 6 dB/oct above this frequency, but remains low enough for all frequencies of astrophysical interest The other limiting factor in this second servo-loop is given by the maximum usable frequency of the cavity, given by the inverse round trip time of $c/2l$= 50 kHz. For frequencies approaching this value, the phase of the recuperated signal changes rapidly, and so the maximum unity gain frequency for a servo-loop incorporating this cavity cannot exceed $\approx$2 5 kHz. The next section will describe methods to exploit the available bandwidths to the maximum.

3.3.1.3) SERVO-LOOP DESIGN AND PERFORMANCE

The goal in the design of the servo-loops for the frequency stabilization is to achieve shot-noise limited performance over the frequency range of interest, given the constraints imposed by the cavity and transducer characteristics. The power allocated to the frequency stabilization system can be adjusted to ensure that the detection sensitivity for the GW's will be limited by the shot noise in the main interferometer. The cavity characteristics are determined either by the state of the technology of mirrors or the demands of the optical design for the detection of the gravitational radiation. No single transducer has all of the characteristics necessary to achieve the stated goal; thus a combination is used.

3.3.1.3.1) TRANSDUCERS

The fundamental tradeoff is between dynamic range and speed. Fortunately, the laser frequency noise spectrum is a strongly falling function of the measurement frequency: a large dynamic range is only needed at low frequencies (several hundred MHz at frequencies less than 10 Hz, corresponding to changes in a laser cavity length of several μm), and high frequency correction signals are typically very small (several hundred Hz RMS for frequencies >10 kHz, corresponding to changes in a laser cavity length of $\approx 10^{-5}\lambda$). A combination of transducers can be used to take care of this range of parameters.The available transducers will be discussed in order of decreasing dynamic range and increasing speed.

For suspended test masses (see section 3.5), the only transducers which are sufficiently non-invasive (from the point of view of thermal noise) are electrostatic or magnetic motors. The electrostatic system usually consists of a grounded test mass and a stationary polarized pusher-plate (mounted on the position reference) which form together a parallel plate capacitor; the attraction is always positive, but the force can be varied by varying the voltage on the pusher-plate. In this case, the actuator is simply a conductive coating on the test-mass, and the system is easily shielded from outside influences. The force is a non-linear function of the applied voltage, but the excursions are small in comparison with the capacitor plate spacing. The magnetic system takes the form of small permanent magnets mounted on the test masses, with stationary electromagnets mounted on the position reference (see 3.5). Attractive and repulsive forces are possible. These two transducers have a dynamic range of the order of 1mm, or $\approx$ 1000 wavelengths, which is more than enough to correct for any slow changes in laser frequency. The frequency response is determined by the suspended mass pendulum transfer function; for frequencies much higher than the resonant frequency, f>1 Hz, the transducer transfer function (TF) falls as f^{-2}. The power handling capability is of course determined by the mirrors themselves.

Piezoelectric transducers (PZT) work by exerting a force between a mirror and a reference mass (e.g., a mirror mount). The force is proportional to the applied voltage; the hysteresis typical of PZT's is not a problem if the transducer is in a servo-loop. PZT's are unsuitable for use on test masses due to their low intrinsic resonance quality factor (Q) but are well suited for use on laser cavity mirrors. The usable frequency range is limited by the first resonance of the mirror-PZT-reference mass system, where the PZT acts as a spring; thus, by reducing the size of the mirror and the PZT, an extended frequency range can be achieved. However, the dynamic range of the PZT is given by its length, and therefore a compromize must be made between these two parameters. One solution is to optimize the characteristics of one transducer for high frequencies, resulting in a first mechanical resonance of several hundred kHz but a dynamic range of the order of 0.1μ and to optimize a second transducer for a large dynamic range of several μm (and a maximum usable frequency of several kHz). Again, the power handling capability is limited by the mirrors used.

Acousto-optic (AO) modulators use the Bragg effect to create a frequency shift in the first-order diffracted light from an acoustic 'grating'. A voltage controlled oscillator (VCO) is used to set up the standing wave pattern that forms the grating, and changes in the VCO frequency (for which the center frequency is on the order of 75 MHz) change the frequency of the diffracted beam. This transducer is typically used outside of a resonator cavity. The frequency response per se of the transducer is typically limited by mechanical resonances in the modulator crystal to several hundred kHz. The most important limiting factor, when this transducer is used in a servo-loop, is the time delay between a change in the VCO command voltage and a change in the light frequency due to the propagation time of the (75 MHz) sound waves in the modulator crystal. Materials showing high diffraction efficiencies and good output beam shapes have typical delays of the order of 1 μs, which imply servo unity-gain-bandwidths not exceeding several hundred kHz. The diffraction angle is, with the frequency shift, a linear function of the VCO frequency; this change in output beam position is undesirable in a frequency transducer, and puts the upper limit on the usable dynamic range to several MHz. The crystals used can withstand powers on the order of tens of watts.

Electro-optic (EO) modulators utilize the Pockels effect. They exhibit a change in optical path length as a linear function of the applied electric field. They are used as phase modulators, either to impress a high fixed-frequency modulation for a detection scheme or to apply a phase correction. The change in the path length due to the Pockels effect is instantaneous with the establishment of the electric field, and the usable bandwidth is several tens of MHz (limited by the driving electronics). The sensitivity is most conveniently given as the phase change available; this is a function of the crystal used and the geometry of the modulator, but is typically $\phi_{max}=\pi/1000$ radians per Volt. Due to practical limitations in the electronics, the order of magnitude of the available dynamic range is about π radians. This phase modulation corresponds to a frequency modulation of $f= \phi_{max}.\Omega$ Hz, where Ω is the frequency at which the modulation takes place; this indicates that a maximum frequency modulation of the order of 1 Hz is possible at $\Omega= 1$ Hz, or 1 kHz at $\Omega=1$kHz, and so forth. This limits the usefulness of this transducer to high frequencies, where it is irreplaceable. Several practical problems should be mentioned : every crystal that exhibits the Pockels effect also exhibits the piezoelectric effect. This is bothersome because it allows mechanical resonances in the crystal to be excited and to influence the transfer function, and care in mounting the crystal is needed to damp these resonances. More important is the fact that there is some absorption in the crystal, and the consequent heating of the crystal causes deformation and depolarization of the laser beam (due to changes in the crystal optical index through heat-induced stress). Present modulators are useful at levels of several tens of watts.

This overview of transducers shows that there are methods which, when combined, allow the control over frequency fluctuations from very low to very high frequencies and at power levels such as will be found in the VIRGO interferometer and its laser. The next section will describe the topology and transfer functions of servo-loops that are designed to take advantage of the transducers available.

3.3.1.3.2) TRANSFER FUNCTIONS

To reach the goal of shot-noise limited frequency stability, the gain in the servo loop must be sufficient at all frequencies of interest to reduce the initial laser frequency noise to the measurement noise. If, for instance, the laser frequency noise at 1 kHz is 10^4 Hz/$\sqrt{\text{Hz}}$ and the shot noise limited frequency detection noise is 10^{-6} Hz/$\sqrt{\text{Hz}}$, a gain of $\geq 10^{10}$ at 1 kHz will be needed. Techniques for maximizing the gain given the transducers available, and topologies for the use of multiple transducers, will be shown, using a stabilized diode-pumped Nd:YAG laser (Shoemaker et al [1989], and Appendix 3.3) as an example. It is shown schematically in Fig. 3.3.2

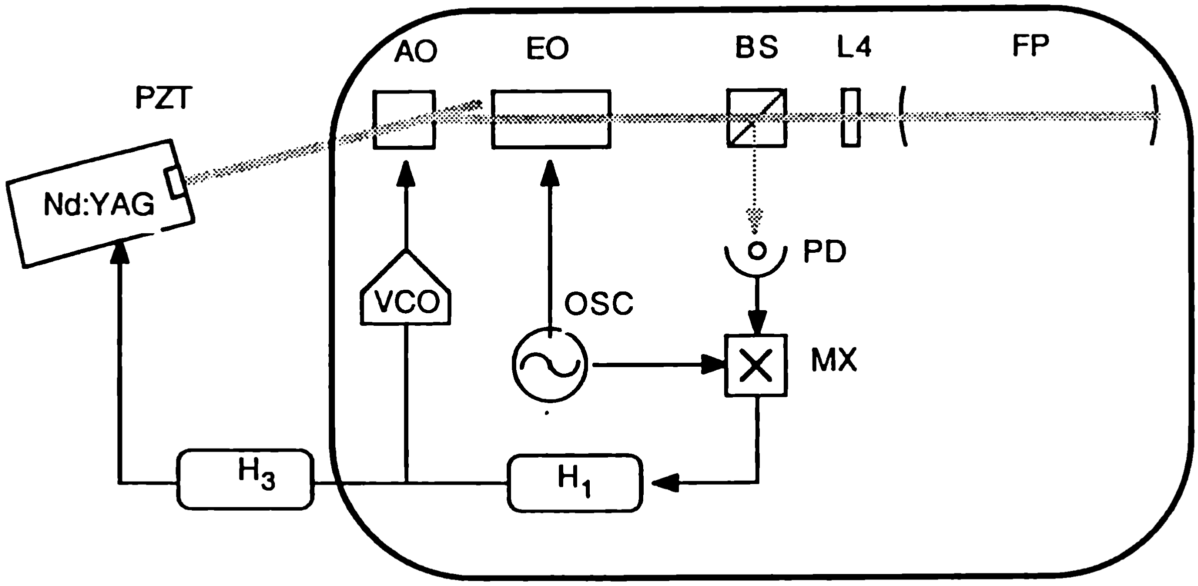

Fig. 3.3.2: Example of frequency stabilization

For a servo loop to be stable, the slope of the amplitude transfer function (TF) must be less than 12 dB/oct at the frequency where the gain is 1 (the unity-gain frequency or f_{UG}). Equivalently, on a Nyquist plot (where the two axis are the real (x) and imaginary (y) parts of the transfer function) the curve as a function of frequency must not encircle the point (-1 real , 0 imaginary). In a practical system, a slope of 9 dB/oct in the octave around the unity gain frequency f_{UG} gives a reasonable margin of stability (for fluctuations in gain) and a reasonable settling time. If the transfer function falls faster than 12

db/oct for lower frequencies than the f_{UG}, which allows higher gains at lower frequencies for a given f_{UG}, the loop is said to be 'conditionally stable' because it would oscillate if the gain were to be lowered. This is clearly not a desirable attribute, but is unavoidable: with the transducers available, and the needed frequency stabilization, conditionally stable loops offer the only possibility to reach the design goals.
The procedure for the design of a frequency stabilization servo-loop starts with the characteristics of the widest bandwidth transducer available, the shot-noise limited frequency detection noise, and a measurement of the frequency noise of the laser system to be stabilized. A unity-gain frequency f_{UG} is chosen, based on the highest frequency for which the transducer (or the amplifier or oscillator that drives it) has a usable response. This could be due to mechanical resonances in a PZT, a time delay in an AO, or a current limitation in the amplifier driving an EO. It could also be due to a limited usable bandwidth in the reference cavity, as will be the case for the full VIRGO arm-length cavity. The open loop transfer function is set at 6 to 9 dB/oct in this frequency range, including the reference cavity transfer function (which has a 6 dB/oct rolloff above $\Delta\nu_c$). At roughly one-half the f_{UG}, the loop transfer function can take on a much steeper characteristic, which can continue to very low frequencies. The fast actuator in the frequency stabilized diode pumped Nd:YAG laser is an acousto-optic modulator (AO in the Fig. 3.3.2) with a time delay of 1.2 µs, which corresponds to a 90° phase shift at 200 kHz; the corner frequency of the cavity $\Delta\nu_c$ is 1 MHz and thus does not limit the loop performance. We choose a unity-gain frequency of f_{UG}=120 kHz. The transfer function, implemented by the filter H_1, is roughly 6 dB/oct for frequencies higher than 60 kHz, 18 dB/oct between 6 and 60 kHz, and 30 dB/oct for lower frequencies. There is some subtlety in choosing the transfer function to take the maximum advantage of the gain-bandwidth available; the complete schematic of this filter is shown in Fig. 3.3.3

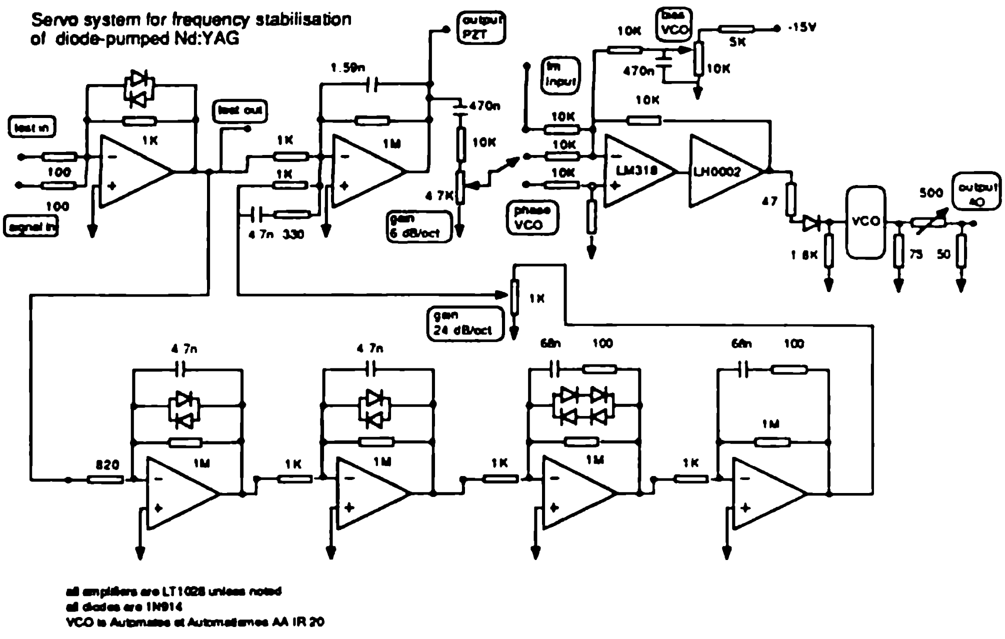

Fig. 3.3.3: The circuit diagram for the transfer function H_1

Now this loop can be reduced to a single element by characterizing it by the closed loop transfer function H_2, taken from the servo summing point (effectively the output of the mixer in the Pound-Drever detection scheme) to the control signal to the fast transducer. The loop for the next transducer, in the hierarchy of descending speed and ascending dynamic range, can now be designed using the modified transfer function H_2. The lower limit to the frequency range to be handled by this fastest transducer will be determined by the dynamic range of the transducer; the measured frequency noise of the laser can be integrated over the frequency range included to find the minimum desirable frequency f_{xo} to be handled by this 'fast loop'. This cross-over frequency f_{xo} must be lower than the maximum usable frequency for the transducer in the second 'slow loop'. The gain of the 'slow' loop can be chosen so that is takes over from the 'fast loop' at the frequency f_{xo} determined above. In the case of the frequency stabilized YAG, the second (and last) loop transducer is a slow piezoelectric device PZT with a lowest mechanical resonance at 3.3 kHz. The AO can successfully deal with signals down to several hundred Hz; thus a straightforward transfer function of 9 dB/oct for filter H_3 for the 'slow loop' is chosen, which allows a cross-over frequency from the 'fast loop' at $f_{XO} \approx 300$ Hz. A higher frequency would be possible with a faster rolloff for H_3 close to the resonance at 3.3 kHz.

The transfer function for the completed system is shown in Fig. 3.3.4. as a Bode diagram (amplitude and phase). A change in gain around the chosen operating point causes the phase to become oscillatory, or in the Nyquist diagram, the curve to cross the point (-1,0). The measured servo system characteristics agree well with the calculated parameters.

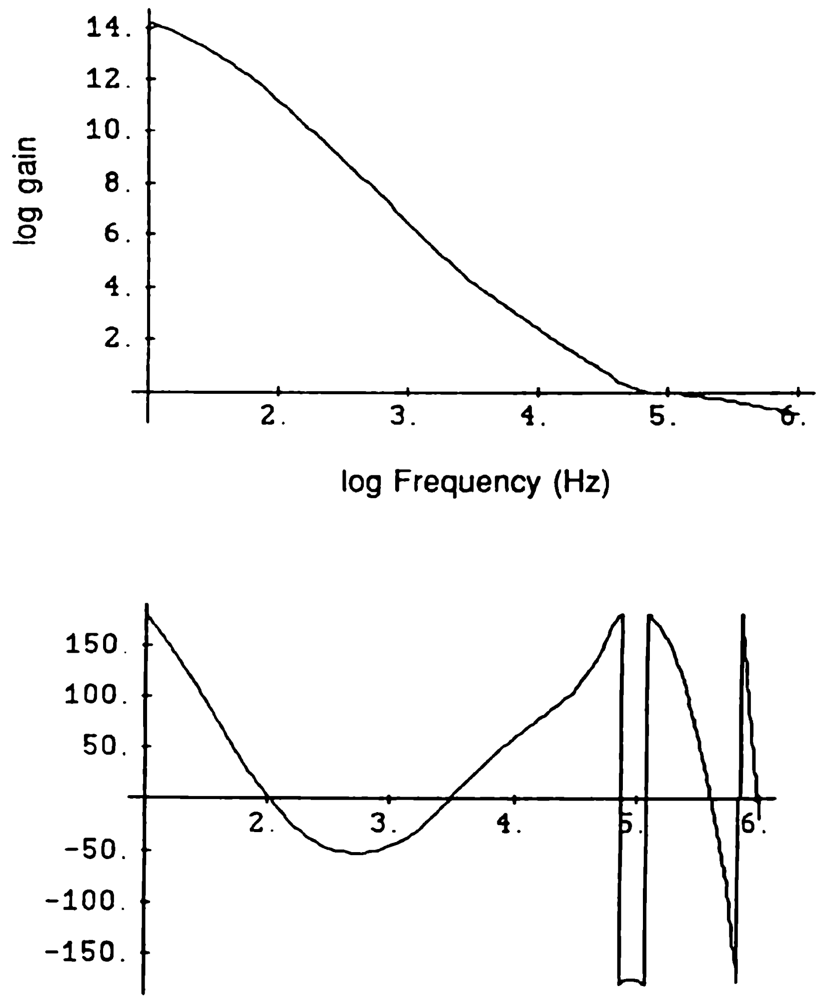

Fig. 3.3.4: Frequency stabilization transfer function

3.3.1.3.3) RESULTS FOR THE FREQUENCY STABILIZED DIODE-PUMPED ND:YAG

Fig. 3.3.5 shows the frequency noise of the Nd:YAG system measured at the summing point of the servo system. The top curve is the unstabilized noise; for these measurements, the shot noise limited noise floor of $12.5.10^{-3}$ Hz/$\sqrt{\text{Hz}}$ is indicated. This measured value is in agreement with the value calculated using the formula for the sensitivity of the Pound-Drever scheme given above and the experimental parameters. Local mechanical and acoustic disturbances are responsible for the steep rise for frequencies less than ≈10 kHz in the unstabilized laser frequency noise.

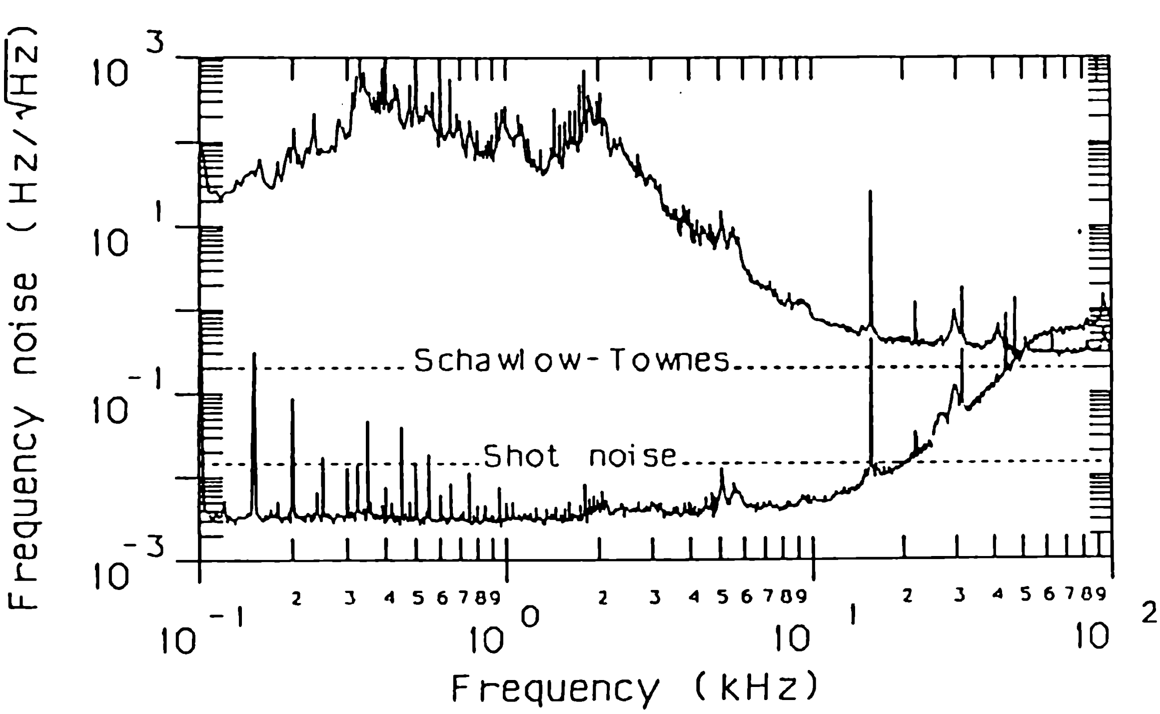

Fig. 3.3.5 : The frequency noise of the stabilized Nd:YAG laser

The bottom curve is the summing point signal for the stabilized laser. This curve shows the suppression available with the servo-system. For all frequencies less than ≈20 kHz, the design goal for this system is reached: the servo error is less than the shot noise of the detection scheme. In fact, there is a considerable excess in gain available, and increases in the detection system sensitivity would directly result in reductions in the frequency noise after stabilization, without other changes in the servo system. (it is interesting to note that the frequency noise of this stabilized laser is much lower than its "Schawlow-Townes" limit, which represents the natural quantum fluctuations of the same laser)

3.3.1.3.4) EXTRAPOLATION

The laser which will be used for the VIRGO interferometer (see section 3.2) will be a Nd:YAG laser with unstabilized noise characteristics which resemble those of the diode pumped Nd:YAG laser described above, and the transducers used (slow PZT and AO) will also be appropriate. Thus we can extrapolate from the results of the frequency stabilization performed on the frequency stabilized YAG to a full scale system for the VIRGO interferometer. The most notable change will be in the reference cavity used and the light power used for the frequency noise detection system, which will give a shot-noise limited frequency detection noise of 1.10^{-5} Hz/ $\sqrt{Hz}$ instead of the $\approx 10^{-2}$ Hz/ $\sqrt{Hz}$ found for the frequency stabilized YAG. With the present electrical gain and transfer function, the frequency stabilization system would be shot noise limited for frequencies less than about 1 kHz. With the addition of an EO modulator as a fast control element, the system could deliver 1.10^{-5} Hz/ $\sqrt{Hz}$ up to 10 kHz, which would be perfectly satisfactory for the prestabilization for the VIRGO interferometer. The design procedure for the added EO loop could follow the 'recipe' above, where first the EO loop would be designed, then the AO loop using the collapsed closed-loop transfer function for the EO loop, and finally the PZT loop using the collapsed closed-loop transfer function of the combined EO and AO loops. Additional refinements (Hall et al [1984]) can reduce the demands placed on the EO driving electronics.

3.3.1.4) CASCADED LOOPS

The second, and final step in the frequency stabilization uses the full VIRGO arm length as the detection cavity. As mentioned above, the shot noise limited frequency noise for this detection will be of the order of

2.10^{-7} Hz/$\sqrt{\text{Hz}}$. Given the prestabilization described in the previous section, a servo-loop using this detection cavity with a gain greater than 20 at all frequencies of interest will be sufficient to bring the stabilized frequency noise down to this level. The maximum unity-gain frequency f_{UG} permissible in this loop is of the order of 25 kHz, due to the very long round trip time in the reference cavity. Using the techniques described earlier, a servo system transfer function with 6 dB/oct in the region of the f_{UG} and with a characteristic of 30 dB/oct for frequencies lower than 15 kHz is chosen. This will allow the goal of shot-noise limited performance to be reached for all frequencies lower than 10 kHz.

There are several topologies possible for this 'second loop'. The most evident calls for a second set of transducers, which would receive the signal exclusively from the VIRGO cavity. It is also possible, however, to add the correction signals from the VIRGO cavity servo to the correction signals derived from the rigid cavity, and to apply this combined signal to the transducers. Each of the servo-loops retains its individual characteristics, and the transducer design and implementation is simplified (Schilling [1984])

There is one more complication to mention: The VIRGO test masses, which carry the mirrors for the 3 km cavity, are suspended as pendulums. At frequencies high compared to the resonant frequency ω_p of the pendulums, the cavity is extremely stable. However, at the resonant frequency ω_p, the motions of the mirrors can be quite large, and the short rigid cavity is a much better reference length. Thus another servo-loop is needed to control the VIRGO test mass mirrors in the frequency range around ω_p, effectively holding the VIRGO cavity 'on resonance' for the prestabilized laser frequency. A very low frequency servo-system, with a unity gain frequency in the range of several Hz, will take as its input the error signal from the VIRGO cavity The transducer for the servo-loop will be electromagnetic transducers mounted on the test-masses which will also be used as alignment transducers

In Fig.3.1.18 a schematic diagram of the complete frequency stabilization scheme for the VIRGO interferometer is shown. This system will allow the design sensitivity of the complete VIRGO gravitational wave detector to be met.

3.3.2) LASER POWER STABILIZATION

3.3.2.1) REQUIREMENTS AND LASER NOISE

As in the case of frequency fluctuations, the requirements on power stability result from the residual asymmetry of the interferometer arms. There are requirements of different origins in two distinct frequency ranges :

- in the low frequency range of astrophysical interest, power fluctuations of the laser can generate noise through the recoil of the masses under the effect of a fluctuating radiation pressure. At these frequencies, the mirrors can be considered as free masses to a good approximation, and their movement will be given by the relation :

$$\tilde{h} = \frac{\delta x}{L} = \frac{\alpha\, \delta P_s(\omega)}{L\, M.c.\omega^2}$$

Where $\delta P_S(\omega)$ is the spectral density of power fluctuations of the average energy stored in the arms at the frequency $f = \omega/2.\pi$, and α represents a measure of the asymmetry of the two arms. For a mass of 100 kg and an estimation of $\alpha \approx 10^{-2}$, one gets the condition $\delta P_S << 100$ mW for f=10 Hz, and $\delta P_S << 10$W for f=1 kHz, given the sensitivity goals in h:

$$\tilde{h} = 3.10^{-21}\, Hz^{-1/2} \text{ at 10 Hz, and}$$

$$\tilde{h} = 3.10^{-23}\, Hz^{-1/2} \text{ at 1 kHz}$$

Given that P_S is of the order of a 100 kilowatts inside the arms, the spectral density of the relative power fluctuations of the laser should be much less than 10^{-6} $Hz^{-1/2}$ at 10 Hz, and than 10^{-4} $Hz^{-1/2}$ at 1 kHz. This requires an active control, because most lasers are usually noisier than these figures by a few orders of magnitude (note that a similar effect could be produced by the frequency fluctuations of the laser, since the energy stored in the cavities is frequency dependent, but the constraints it puts on frequency stability are not as stringent as the other constraints we have already discussed).

The main causes for power noise at low frequencies are vibrations of the laser cavity structure, excited acoustically or mechanically through its support. In a high power laser, most of the noise at very low frequencies comes from thermal effects in the laser material, and most of the noise at acoustic frequencies is generated by the water circulation which cools the amplifier. The power noise of the Nd:YAG laser for VIRGO is not known yet, but it should be lower than 10^{-3} $Hz^{-1/2}$ in the interesting frequency range. One can expect a much lower value for the future diode-pumped laser.

• in the demodulation frequency range, i.e. around 10 MHz, one should ensure that the relative power fluctuations are not larger than the shot-noise corresponding to the total power received by the signal detector. The physical effects susceptible to produce excess noise at these high frequencies are hopefully not many; the main noise source in this range comes from the apparition of transverse modes of the laser, beating with the TEM_{00} mode, but this is not very dangerous because the beat frequency is well defined for a given laser and can be avoided by changing the frequency modulation. Typically, with an output mode-cleaner, the detected power will be of the order of a 0.1 Watt, which requires:

$$\frac{\delta Ps}{Ps} << \sqrt{\frac{2\,e}{Ps}} \approx 2.10^{-9}\,\mathrm{Hz}^{-1/2}$$

This is only one order of magnitude above the laser shot-noise, and difficult to check, but the measurements effected on the Garching and Orsay prototypes show that this is approximately verified. Furthermore, the input mode-cleaner removes efficiently the high-frequency amplitude modulation sidebands.

3.3.2.2) SERVO-LOOP DESIGN AND PERFORMANCE

3.3.2.2.1) POWER MEASUREMENT

The power stabilization studies which have been realized in Orsay and in Glasgow show that the measurement itself is noisy, if it is not effected in very well controlled conditions. In a typical scheme, a fraction of the laser power is deflected to a photodetector and the output current of the detector is compared with a reference current generated by an electronic current source in a differential amplifier. A servo-loop reacting on a power modulator maintains the equality of the photocurrent and the reference current. The laser beam is usually utilized in another place, and there are many reasons why it should not be as well stabilized there as it seems to be on the first detector:

• index fluctuations, or dust particles which scatter the beam, can add some extra noise, which is different on the two places

• spurious interference fringes may be produced by scattered light, or by the light reflected by the detector, for instance, and this will give power noise if either the laser frequency or the mechanical arrangement is not stable enough.

• geometry fluctuations of the laser beam, i.e. position jitter or sporadic apparition of transverse modes will result in extra noise if the photodetector response is not uniform, or if there is any diffracting object on the beam path

• polarization effects may also induce different changes in two different places.

• long term stabilization requires that the efficiency of the detector is constant, in spite of temperature changes.

For all these reasons, the reference detector for power stabilization of the Virgo laser must be placed as close as possible from the interferometer input,in the vacuum, and after the beam has been sufficiently well frequency stabilized and filtered by the optical fiber and the mode cleaner. Extrapolating from measurements made in a standard room environment, it should not be difficult to reach a stability level $\delta P_S/P_S << 10^{-8}$ Hz$^{-1/2}$.

3.3.2.2.2) TRANSDUCERS

There are three main possible ways of controlling the laser power :

• controlling the gain of the laser amplifier. The output power of the laser is often a monotonous function of the power delivered by its power supply. In that case, it is possible either to control directly the output current (or voltage) of the supply, or to place in parallel (in series) with it a supplementary circuit able to add or to remove some power. The first solution is not easy with a high power laser, because it is difficult to modulate very rapidly very high powers.We have tried the second solution with Argon lasers. The feedback loop had a dynamic range of ± 5% on the laser output power, and a unity gain bandpass of the order of 100 kHz. This was sufficient to achieve $\delta P_S/P_S \approx 10^{-7}\ Hz^{-1/2}$ around 1 kHz. This technique is not universal because some lasers are optimized for a given input power, where the output power goes through a maximum. This is the case for the present Nd:YAG laser.

• Acousto-optic modulators (AOM), such as described above, can also be used as power modulators, simultaneously with their use as frequency shifters, because the power diffracted in the first order is approximately a sinc function of the RF power delivered to the AOM. In order not to loose too much power, they will be operated slightly below the maximum. The offset from the maximum has to be adapted to the free-running laser fluctuations, and the power loss is necessary larger than half the peak to peak laser fluctuation. All the performances of the device are the same as those concerning its use as a frequency transducer.

• Electro-optic power modulators are another possibility. An electro-optic crystal, cut differently as for its use as a phase modulator, is placed between polarizers. The application of a voltage generates birefringence, and a power change in the light transmitted by the polarizer. A 100% power modulation requires a voltage of the order of 1000 V. The other characteristics (response time, power handling capability,...) have been described above. We have a ten years old experience in the realization of such servo-loops.

<u>3.3.2.2.3) LOOP PERFORMANCE</u>

Power stabilization loops are very similar to frequency stabilization loops, and they have the same performances as concerns gain and bandwidth. These performances are more than sufficient for our application.

3.3.3) BEAM GEOMETRY FILTERING AND STABILIZATION

3.3.3.1) MONOMODE FIBER

The best way to clean the geometry of a low power laser beam and to suppress its position and angle fluctuations is to pass it through a monomode fiber. This solution is used currently in Orsay and Pisa to couple the beam from the lasers to the interferometers, and is completely satisfactory. All the geometrical fluctuations are transformed in (second order) fluctuations of the power coupled in the fiber, and we found that the geometrical fluctuations of the output beam were not measurable. The parameters to be improved are the coupling efficiency and the power handling capability.

The fact that the core of a monomode fiber necessarily has a small radius (of the order of a few wavelengths) is responsible for these difficulties. Coupling the beam into a very small diameter requires short focal length, high aperture, aberration free lenses. This is currently done with microscope objectives, which are lossy because of their many components. The maximum efficiency we have observed with Argon lasers is only 60%. We are investigating different ways of increasing it to at least 80%, which would be a tolerable loss, given the many other advantages of this solution. The other difficulty is that the intensity inside the core rapidly gets very high, typically 10^7 W/cm^2 for one watt of power, and this generates nonlinear effects. We have nevertheless succeeded in transmitting up to 1W at 515 nm through 5m of a 2µm core radius fiber, without observing nonlinearities.

The solution to both problems is in using fibers with a larger core; this can be realized if the manufacturer is able to control very precisely the index of the fiber. A longer wavelength, such as 1.06 µm also helps in this direction. We should be able to get fibers for the YAG wavelength having a core radius of about 10 µm and the ability to transport a few tens of Watts.

3.3.3.2) MODE-CLEANER

3.3.3.2.1) GEOMETRICAL PROPERTIES

The other device used in VIRGO to define the beam geometry is what we call a "mode-cleaner" (Rüdiger et al., [1981]) : the geometry of the laser beam can be considerably stabilized by passing it through an optical

resonator. The geometric beam fluctuations can be described in terms of excitations of eigenmodes of the resonator.
The simplest mode cleaner (MC) consists of two mirrors of radius of curvature R_{c1} and R_{c2}, separated by a distance L. Let T_1 and T_2 be their respective transmission in intensity, R_1 and R_2 their reflectivities and p the mirrors' total losses. Let β_k be the coupling coefficient of the incident beam to the TEM_k mode of the cavity. When the TEM_{00} mode of the cavity is on resonance with the incident beam frequency, the fraction of the incident power transmitted by this MC on the k^{th} order mode is expressed by:

$$T_k = \beta_k \frac{T_1 T_2}{\left(1-\sqrt{R_1 R_2}\right)^2} \frac{1}{1+\left(\frac{2\sqrt{R_1 R_2}}{1-R_1 R_2}\sin(k\psi)\right)^2}$$

the phase angle ψ is the one way phase propagation term between the two mirrors:

$$\psi = \mathrm{Arc}\cos\sqrt{\cos\left(1-\frac{L}{R_{c1}}\right)\cos\left(1-\frac{L}{R_{c2}}\right)}$$

The first part of T_k is the transmission of the fundamental mode T_0. It can also be expressed in terms of the losses as :

$$T_0 = \frac{4T_1T_2}{\left(T_1+T_2+p\right)^2}$$

To ensure a high throughput for this mode, the losses have to be small compared to the mirror transmittances T_1 T_2 , which itself is a small quantity. The transmission is maximum when $T_1 = T_2$, but this condition is rather soft.
The relative suppression of the high order modes is determined by the second term in T_k. For a given pair of mirrors, the resonator geometry must avoid the peculiar configurations like the confocal one, the concentric and other degenerate cases, where some high order modes are coincident with the fundamental mode. The term:

$$\left(\frac{2\sqrt{R_1R_2}}{1-R_1R_2}\sin(k\psi)\right)$$

should be as high as possible for all the low order modes. The global cleaning efficiency of a cavity can be expressed by the merit factor M defined in 3.1.1.
In the case of a perfect matching of the incident beam, one can reach a transmission as high as 98%, for $T_1 = T_2 = 0.99$ and $p=10^{-4}$.

The other criteria which defines a cavity configuration is the power density on the optical surfaces. If P is the laser power we want to transmit, and w is the beam radius on the mirrors, the power density is:

$$I = \frac{F.P}{\pi\omega^2}$$

To avoid optical damage to the multilayer coatings of the mirrors, we have to keep the spot area πw^2 above:

$$\pi w_{min}^2 = \frac{P}{I_{max}}$$

where I_{max} is the limit power density of the coatings (around 10 kW/cm^2). In practice, this means that a mode cleaner cavity for a high power laser must have reasonably large dimensions.

3.3.3.2.2) FREQUENCY FILTERING PROPERTIES

When used in transmission, the Fabry-Perot has another beautiful property, which becomes usable with supermirrors and/or long cavities : it is an efficient low pass filter. All the laser fluctuations (amplitude and frequency) can be seen as a generation of sidebands. If the carrier is resonant with the cavity, the Fabry-Perot filters reflects (and does not transmit) all the sidebands corresponding to modulation frequencies higher than its linewidth, i.e. higher than : $\Delta\nu = \frac{c}{2LF}$., where F is the finesse of the cavity and L its length.

the transfer function of the cavity for the fluctuations of frequency f is:

$$H(f) = \frac{T_{00}}{1+\left(\frac{2f}{\Delta\nu}\right)^2}$$

This is a second order low pass filter, whose efficiency becomes interesting when both L and F are large (the cutoff frequency is of the order of 15 kHz for L= 10m and F= 1000).

Mode-cleaners will be used in VIRGO : at the input of the interferometer, a 6 to 15m long cavity, with a finesse of the order of 100 will serve both as a mode-cleaner and as a low-pass filter. The output beam of the interferometer will be passed through a second, shorter, mode-cleaner cavity in order to improve the detection noise and to reduce the optimum value of the modulation index.

3.4) Seismic isolation and thermal noise

3.4.1) SEISMIC ATTENUATION, SOME RESULTS

A full scale suspension system for the VIRGO project has been built and tested at the INFN PISA Laboratory. This system is called a Super Attenuator (SA).
The SA system consists of a cascade of 7 vertical gas springs, each weighing 100 Kg, interconnected by vertical wires $\cong .7$ m long as shown in Fig.3.4.1.
The SA can levitate heavy 400 Kg mirrors that can be useful for reducing the thermal noise.
The necessity to create a seismic isolation scheme allowing the suspension of mirrors weighing up to 400 Kg and giving 3 dimensional attenuation of 10^{-9} at 10 Hz has led (A. Giazotto [1987], R. Del Fabbro et al. [1987]) to design a vertical oscillator element (gas-spring) (R. Del Fabbro et al. [1988, a]).
Fig.3.4.2a shows a simple gas spring example: a vessel enclosed with a small bellows holding a mass M; Fig.3.4.2b,c,d shows schematic diagrams of a practical realization of the spring. The gas spring is composed of two major parts, a cylindrical vessel enclosed by two or four bellows, supporting a maximum of three atm, and a rigid part, called the cross, touching the bellow's flanges on the top and traversing the vessel along the axis. The two parts are constrained to move only vertically with respect to each other by means of centering wires 1 mm thick. The wire (3.5 mm diameter) from the previous stage is connected to the vessel, along the axis; while the cross is connected to the next stage. For example the mass attached to the last gas spring is the test mass plus the cross weight.
In Fig. 3.4.3 shows the SA transfer function (TF) that has been measured (R. Del Fabbro et al. [1988, b]) in the frequency interval $10 < \nu < 68$ Hz by the DCA accelerometer shown in Fig. 3.4.1; this measurement has to be considered an upper limit because it is limited by the DCA noise. Since the TF was measured by shaking the point below the first gas spring, not the suspension point, in reality we expect higher attenuation factors: the actual numbers at 10 Hz are 2.10^{-8} for the Vertical to Horizontal (VH) TF and 5.19^{-9} for the Horizontal to Horizontal (HH) TF. Correcting for the fact that the shaking point is not the suspension point gives an upper limit (VH) = 2.10^{-9} at 10 Hz. Since we have measured a seismic noise at 10 Hz of 2.3 10^{-9} $m/\sqrt{Hz}$ this gives $\tilde{h} \equiv 1.5\ 10^{-21}$

$1/\sqrt{Hz}$ at 10 Hz, comparable with the expected thermal noise level at 10 Hz. The normal modes behaviour has been extensively studied using an accelerometer mounted on one of the test masses. In Fig.3.4.4 the SA absolute displacement between 0 and 10 Hz excited by the seismic noise is shown (R. Del Fabbro et al. [1988, b]); the noise for ν>6 Hz is expected to be given by the accelerometer thermal noise. Fig.3.4.5 shows the ratio of the accelerometer displacement to the exciting seismic noise; the data, demonstrates the necessity to have a vertical isolation system having nearly the same attenuation as the horizontal does, showing a good agreement with the fitting model which gives the TF = HH + 10^{-2} VH.

From Fig.3.4.4 it follows that the largest mass displacement happens to be at 0.24 Hz (the fundamental pendulum frequency) with an amplitude of $\cong$ 14 μm ; this value, which can easily go up to 30 μm, is too large to allow locking to a fringe when the system will be mounted in the interferometer. The low frequency displacement must be less than few light wavelengths in order to lock the interferometer on a fringe. The usual way to do this is by electronic damping of the suspension resonances; it has already been shown that good results can be achieved on small test masses in three degrees of freedom (see for example D.H. Shoemaker, thesis [1988]). The improvement with respect to the original damping scheme is to apply the damping force to a point along the SA chain, instead of applying it directly to the suspended mass and to apply electronic cooling on all the six degree of freedom (C. Bradaschia et al. [1989, a]). In this way the sensitivity to noise introduced by the electronic cooling is very much reduced.

Fig.3.4.6 shows the lay out of one element of the electronic damping: a LED / photodiode system (shadow-meter) measures the relative displacement X_i-X_s of the i-th SA mass with respect to the ground, then the derivative is formed and the amplified signal is applied to a force transducer acting on the mass itself. The force transducer is composed of a permanent magnet attached to the mass M and a coil connected to the ground: a current $I=A(\dot{X}_i-\dot{X}_s)$ flows in the coil and produces a damping force $F_d = K \cdot I$ between the ground and the mass M_i, where K is a factor depending on the permanent magnet strength, the coil geometry, and the distance between the coil and the magnet; in our case K is, to first order, insensitive to the relative displacement of coil and magnet. Six independent feed back systems have been applied to the third from the top gas spring or second suspended mass.

Since the SA chain is itself an excellent seismic noise filter above 10 Hz, it is only necessary to apply electronic damping below 10 Hz. This will be achieved by an appropriate low pass filter.

In Fig.3.4.7 the damped displacement spectrum shows that the maximum displacement at 0.24 Hz is now ≅ 3.4 μm, hence very acceptable for allowing the locking of the interferometer to a fringe. ?

3.4.2) FRINGE LOCKING SYSTEM.

A fringe locking system is necessary for two reasons. First of all Virgo needs a system able to apply to the mirrors a displacement of the order of the light wavelength to find the position of the dark fringe; the force necessary to balance the gravity and to apply 1μm displacements to the SA suspended mass is of the order of 10^{-3} N.

Secondly the remnant seismic displacement below Hz, which is about 3 μm at the fundamental pendulum frequency, has to be compensated.

It is not difficult to apply forces of the order 10^{-3} N to a suspended mass with small magnets attached to the mass and coils connected to the ground, as it is shown in fig. 3.4.8, the current flowing in the coil gives a restoring force. The necessity for not reintroducing the seism above 10 Hz has led us to design a special configuration of coils for the Virgo locking system.

For simplicity let us consider two equal mirrors freely suspended with two simple pendulums, with ω_0 proper circular frequency and τ relaxation time. If x_1 and x_2 and $\bar{x}_1$ and $\bar{x}_2$ are the mirrors and suspension point seismic noise displacements respectively the equations of motions are

$$x_i = \frac{\omega_0^2 \bar{x}_i}{-\Omega^2 + i\frac{\Omega}{\tau} + \omega_0^2} \qquad i = 1,2 \qquad (3.4.1)$$

Let us suppose that mass 2 is locked to mass 1 by means of magnets and coils in such a way to have the force F on mass 2:

$$F = K\, I$$

$$I = \alpha\,(x_2 - x_1) \qquad (3.4.2)$$

where α is the feedback gain, I is the current flowing in the coils and K depends on the magnet and coils geometry.

Eq. (3.4.1) becomes

$$x_1 = \frac{\omega_0^2 \bar{x}_1}{-\Omega^2 + \omega_0^2 + i\frac{\Omega}{\tau}}$$

$$x_2 = \frac{\omega_0^2 \bar{x}_2 + \frac{K}{M}\alpha\left(x_2 - x_1\right)}{-\Omega^2 + \omega_0^2 + i\frac{\Omega}{\tau}} \qquad (3.4.3)$$

Where M is the test mass. Hence

$$x_2 - x_1 = \frac{\omega_0^2\left(\bar{x}_2 - \bar{x}_1\right)}{-\Omega^2 + i\frac{\Omega}{\tau} + \omega_0^2 - \frac{K}{M}\alpha} \qquad (3.4.4)$$

which in the limit $\alpha \to \infty$ gives the current

$$I = \frac{M\omega_0^2\left(\bar{x}_2 - \bar{x}_1\right)}{K} \qquad (3.4.5)$$

the current is independent upon the pendulum resonance function and in the multi-pendulum case we get a similar result because the maximum displacement is at 0.24 Hz the frequency associated with the total pendulum length (5 m).
Hence the magnetic force should be

$$K\,I = M\omega_0^2\left(\bar{x}_2 - \bar{x}_1\right) \qquad (3.4.6)$$

From measurements of the seismic noise power spectrum (R. Del Fabbro et al. [1988, c]) we have

$$\bar{x}_1 \equiv \frac{3\;10^{-7}}{\nu^2} \qquad \left(\bar{x}_2 \equiv \bar{x}_1\right) \qquad (3.4.7)$$

Assuming no correlation in eq. (3.4.6) between $\bar{x}_2$ and $\bar{x}_1$ above the cut-off frequency ν_c, the force integrated value is

$$\overline{KI} = M\omega_0^2\, 3\; 10^{-7}\left[\int_{\nu_c}^{\infty}\frac{d\nu}{\nu^4}\right]^{1/2} = \frac{M\omega_0^2\,10^{-6}}{\sqrt{3}}\;\frac{1}{\nu_c^{3/2}} \qquad (3.4.8)$$

where $\nu_c \cong 1$ Hz (considering 3700 m/s the sound speed in the ground), 300 Kg < M< 1000 Kg is the mass associated with the frequency ν_0 = 0.24 Hz of the SA and $\omega_0 = 2\pi\nu_0$; it follows that the average force we need in the locking system is

$$\overline{KI} \cong 2.10^{-3} \text{ N} \qquad (3.4.9)$$

Some independent measurements in our laboratory, giving a seismic acceleration R.M.S. of 9.10^{-6} m/s^2 for the SA suspended mass, have confirmed this extimation for $\overline{KI}$.

The seismic noise is reintroduced by a term proportional to $\frac{\partial K}{\partial x}$ thus the Riemann force gives the following constraint on $\frac{\partial K}{\partial x}\frac{1}{K}$

$$\frac{1}{K}\frac{\partial K}{\partial x}\,\bar{x}_1\,\overline{I.K} < M\Omega^2\,\tilde{h}\,L \qquad (3.4.10)$$

From eq.(3.4.9) and (3.4.7) it follows

$$\frac{1}{K}\frac{\partial K}{\partial x} < 0.6 \quad m^{-1} \qquad (3.4.11)$$

which is feasible as we will explain later.

Another source of noise is due to the noise current I_n in the circuits. In the fringe locking system we have designed $K \sim 2.10^{-2}$ N/A, the force produced by the noise current has to be less than the Riemann force

$$KI_n < M\,\Omega^2\,\tilde{h}\,L \qquad (3.4.12)$$

$$I_n < 2.2.10^{-10}\ A/\sqrt{Hz}$$

a value which is attainable with commercially available components.

<u>3.4.3) A COIL SYSTEM FEATURING A UNIFORM FIELD GRADIENT (STEERING COILS)</u>

The special requirement of the steering coils is that they must provide a force without introducing seismic noise into the system, as it is shown in eq.(3.4.11). The force on a small permanent magnet is proportional to the total magnetic moment of the magnet times the gradient of the magnet field. Seismic noise can be introduced into the system if derivatives of the magnetic field higher than the first are present. The axial field gradient due to a single coil has a maximum at $z = R/2$ where R is the radius of the coil and z is the axial distance from the coil. Therefore the second derivative vanishes at that point, which is where the permanent magnet is placed. Two additional coils with radii R/2 and R/4 are placed, respectively, at distances R/4 and R/8 from the permanent magnet in such a way as the second derivates of the fields also vanish. The currents in these two secondary coils are then adjusted so as to cause the third and fourth derivatives of the magnetic field to vanish. Fig.3.4.9b shows the derivation from a uniform gradient for the resulting configuration for a system with R = 0.1 m. For comparison the deviation for a single coil is also shown. It is seen that the requirement that $(\partial K/\partial x) / K < 0.6\ m^{-1}$ is satisfied for a interval of more than 10 mm. Derivations from uniformity in the transverse direction are correspondingly small.

3.4.4) AUTOMATIC ALIGNMENT SYSTEM

A problem, rising from the mechanical suspension of the mirrors, is the lack of perfect alignment of the mirror both in horizontal and vertical directions, due to imperfect mounting, balancing etc... .

In order to perfectly align the mirrors it is necessary to apply constant torques to the mirror's suspensions to create tilts in the horizontal and vertical directions. This can be done in principle by giving appropriate D.C. currents to the coil system shown in Fig.3.4.9a but this would give D.C. biases in eq. (3.4.10). To overcome this difficulty we have envisaged an intermediate stage suspension system which can provide the mirror tiltings without ground couplings as shown in Fig.3.4.10. The method consists in creating forces acting between the 7-th gas spring and an intermediate 60 Kg mass and in suspending the mirror with a two-wire sling suspension allowing tilting in both the vertical and horizontal direction. This tilting adjustment system can be driven by a quasi-DC feedback.

The interferometric mirrors and beam splitter have to be kept aligned; the standard technique to lock anything to an extremum is to create an error signal to be used to lock the mass to the appropriate position. The position of each mirror is vibrated at frequencies of the order of a few K Hz, in translation along the direction of the beam and in rotation around two axis which are orthogonal to the beam. For all these three degrees of freedom there is a maximum in power reflected by the interferometer rear mirror. The modulation at different frequencies allows the separation of the error signal for each degree of freedom. In the following we will show that it is possible to excite the longitudinal and rotational degrees of freedom by means of steering coils attached to the ground.

Let us suppose there is an error θ on the angular positioning of the mirror; the interferometer output power P will be affected in the following way

$$P = P_I\left(1 - \left(\frac{\theta L}{W_0}\right)^2\right) \qquad (3.4.13)$$

where L is the arm length, W_0 the waist of the mode and P_I is the incident power.

If the mirror's angle is modulated at circular frequency Ω_M we have

$$\theta_M = \theta + m \cos \Omega_M t \qquad (3.4.14)$$

where m is the modulation amplitude.

The output voltage of the lock-in detector is

$$V = P_1 \overline{\left(\frac{2\,m\,L^2 \cos \Omega_M t \cdot \theta}{W_0^2}\right) \cos \Omega_M t} \simeq \tag{3.4.15}$$

$$\simeq P_1 \left(\frac{L^2}{W_0^2}\right) 2\,m\,\theta \left(1 \;/\; \left(1 + \frac{\Omega_M}{2\pi\Delta\nu}^2\right)\right)$$

where $\Delta\nu = \frac{1}{2\pi} \sqrt{\frac{3\pi}{4}} \frac{c}{LF}$

where F is the cavity finesse.

In our case F = 30 L = 3 10^3m

$$\Delta\nu = \frac{2}{6} \frac{\cancel{3}.10^8}{\cancel{3}.10^3\;3.10^1} = \frac{1}{9}\,10^4 \cong 1\ \text{KHz}$$

assuming $\nu_M \cong 2$ KHz it follows

$$V \cong P_1 \frac{L^2}{W_0^2}\, 2\,m\,\theta \left(\frac{\Delta\nu}{\nu_M}\right)^2 \tag{3.4.16}$$

the photon shot noise $\sqrt{n}$ gives at $\nu = \nu_M$ a noise spectral density dV

$$dV = \frac{\Delta P}{P} = \frac{P_1}{\sqrt{n}} = \frac{P_1}{\sqrt{\frac{P_1 t}{2h\nu}}} = \sqrt{\frac{2h\nu\,P_1}{t}} \tag{3.4.17}$$

in order to have a clear signal we need

$$P_1 \frac{L^2}{W_0^2}\; 2\,m \left(\frac{\Delta\nu}{\nu_M}\right)^2 \theta > \sqrt{\frac{2h\nu\,P_1}{t}} \tag{3.4.18}$$

the modulation m has to be

$$m > \frac{1}{\theta\,P_1 \frac{L^2}{W_0^2}\, 2} \; \frac{\sqrt{\frac{2h\nu\,P_1}{t}}}{\left(\frac{\Delta\nu}{\nu_M}\right)^2} \tag{3.4.19}$$

Assuming that the system should be aligned in t = 10 s and as a "good" $\theta \cong 10^{-7}$ rad gives

$$m = \frac{1.6\ 10^{-13}}{3}\left(\frac{\nu_M}{\Delta\nu}\right)^2 \text{ rad.} \tag{3.4.20}$$

since $\Delta\nu = 10^3$ Hz $\quad \nu_M \cong 2.10^3$ Hz $\quad m \cong 2.10^{-13}$ rad.

The force F for moving the mirror of an angle $\theta \cos \Omega_M t$ is

$$F = M R \ddot{\theta} = M R m\ \Omega_M^2 \tag{3.4.21}$$

since M = 400 Kg and the mirror's radius R = 0.3 m

$$F = 3.8\ 10^{-4}\ \text{N} \tag{3.4.22}$$

This force can be easily obtained since the steering coils current driver system can supply 5A and, being $K \cong 2.10^{-2}$ N/A , the maximum force is about 0.1 N.

3.4.5) SA SUSPENSION NEEDED

All the interferometer parts, four mirrors and a beam splitter will be separately suspended by SA chains. An extra chain is needed before the beam splitter to support an optical table holding a mode cleaner and all the optical components in vacuum before the beam splitter as is shown in Fig.3.1.17. All these components have to be suspended separately from the beam splitter for several reasons. It is important to differentiate the vacuum with respect to the interferometer and to reduce the scattered light entering the interferometer, in fact a small pipe will put in communication with the beam splitter area and a valve will allow work on the optical table without breaking the vacuum in the interferometer. In Fig.3.1.17 are sketched these details together with the photodiode and a mode cleaner necessary to reduce the noise coming from the light scattered from the pipe walls going directly to the photodiode.

3.4.6) THERMAL NOISE OF THE SUSPENSION

In chapter 2 the thermal noise has been discussed, in the following we will show some measurements and possible solution to increase the quality factor Q of the suspension.
The major limiting noise at low frequency is expected to come from the contribution to the thermal noise from the suspension itself; i.e. losses taking place along the wires and on the suspension points. Our target, with masses of the order 300 ÷ 400 Kg is $Q \cong 10^6$; a figure like this has been obtained in vacuum with smaller mirrors.
In the SA the biggest contribution comes from the last stage, because noise from higher stage arrives filtered to the mirror. In the present design the mirrors will be suspended by two wire loops, for tilting purpose, and it will be tested in the near future using aluminium instead of silica, because their densities are close. A possible alternative solution is to make a single wire loop around the mirror, and splitting the wire in two separate ones when it is going to leave the mirror surface.
The measurement persued until now on the SA can, rather pessimistically, give a lower limit for the suspensions Q of about 10^4 , in a vacuum of 10^{-3} mbar. It is interesting to remember that the one loop wire suspension of the 2 ton cryogenic aluminium bar of the Rome Group has a mechanical Q factor higher than 10^7.

3.4.7) SEISMIC NOISE ATTENUATORS AND VACUUM CHAMBERS

As we have explained in section 3.4.5 Virgo needs six SA chains, four of them will be located in the central building and the other two in the two terminal areas. Each chain will be located inside a stainless steel vacuum chamber 7.5 m tall and with 2 m diam.
Fig. 3.7.6 shows a top view of the four vacuum chambers containing a SA chain each and located in the central area; details of the lateral reinforces used to reduce the vibration of the SA suspension points are also shown.
Fig. 3.4.11 shows a terminal unit vacuum chamber with some technical details. Each vacuum chamber has two removable pieces bolted together.
Fig. 3.4.12 shows a section of a vacuum chamber with inside an SA chain.

As it is shown in Fig. 3.4.12 the top gas spring of the chain is solidal to the vacuum chamber; it is mounted on a xy table having ±10 cm displacement range on the horizontal plate in order to compensate the horizontal displacements of the suspension point larger than those corrected by the steering system. The chamber is divided in two sections having differentiated vacuum, as it will be explained on the vacuum section, where the vacuum system is described in details. The lowest contains the test masses with 10^{-7} mbar vacuum.

3.5 Alignment control and data acquisition

3.5.1) FRINGE LOCKING SYSTEM : SOME RESULTS

The experiments for implementing a computer aided system for the automatic alignment (Barone et.al.[1988] ; Barone et.al.[1989] ; Solimeno et. al.[1989]) of the VIRGO antenna started with the testing of the fringe locking system (hereinafter FLS) in 1988. Taking into account that the useful band for gravitational waves detection of the VIRGO antenna is in the range 10Hz to 3 kHz, it is clear that the control system must achieve the following goals :

a) to control the whole interferometer in the range DC up to 10 Hz in order to avoid residual noises.

b) to fringe lock the interferometer in the useful band, 10Hz up to 3 kHz, so that a proper analysis of the control signal will give us, in the final realization of the VIRGO antenna, exactly what we want to detect, i.e. the GW signal. These goals can be achieved by implementing either an analog or a digital control system. We think that for our purposes the digital system of control is the best one, even if we are presently testing both systems, to check the validity of our concern. Until now , as far as we know, in all the implementations of GW test interferometers only analog schemes have been realized. We postpone the discussion on the advantages of the choice of a digital system of control to the next section.

We have performed some preliminary control tests by FLS, implementing a Michelson interferometer in air with two equal arms 0.15 m long, whose end mirrors were fixed to a vertically damped table. We referred one mirror to the one controlled via piezoelectric transducers. The control of this interferometer, sketched in Fig.3.5.1, was completely analog.

The technique we used in this case was a monodimensional FLS. We modulated the mirror position applying a sinusoidal signal with known amplitude and frequency to three piezoelectric transducers (PZT).

The output of the interferometer was sent via a photodiode to a lock-in amplifier for synchronous detection of the error signal that is proportional to the low frequency optical path length variations.

The control signal is generated by a proportional derivative control (PD) and is sent to the PZT via an HV amplifier. The control was performed with two correction bands, i.e. 0 to 100 Hz and 0 to 1 kHz to fully analyze the

different performance of the system. We tested also the performance of the same analog system using a plane Fabry-Perot cavity 0.15m long.
The experimental results are shown in Fig.3.5.2.
We see that the locking accuracy is rather good : with a modulation frequency of 2 kHz we obtained relative displacements between the mirrors of $5\ 10^{-10}$ m/√Hz and $5\ 10^{-12}$ m/√Hz for the Michelson and Fabry-Perot interferometers respectively. The peaks in the power spectra are mainly due to harmonics of the main.

3.5.2) GENERAL CONCEPTS OF THE DIGITAL CONTROL

We propose a digital control of the electronics involved in the apparatus. We emphasize that the control should always be digital, not the electronics itself. In fact efficiency and speed considerations may often suggest and impose the choice of analog components and circuits for the electronics. The advantage of a digital control is that a single system (duplicated for backup) may maintain the control of the whole experiment by coordinating the activities of several subsystems, each with its own CPU. The main system should be a workstation, whose windowing capabilities allow monitoring of each subsystem in separated windows as well as providing tools for data collection on high capacity devices (e.g. helical scan tapes).
Each subsystem performs monitoring and regulation of selected parts by means of computer-interfaced instruments via industry standard interfaces.
Briefly we may summarize the advantage of the choice of a digital system of control as follows:

a) Great flexibility using the right interface modules (in terms of speed and precision) the only things we have to study are the improvements or the modifications of the response of the controller, by changing a software program. This can be done more quickly way than in an analog scheme of control, and even with a higher precision.
Moreover it is possible to build an adaptive control filter, assigning a criteria for the best performance of the system, in which the software itself will choose the best parameters for the controller during the alignment phase. In this scheme, the first level control can be reduced to

compute discrete convolution between the impulse response of a suitable numerical filter (FIR, IIR,...) and the discrete error signal.

b) Implementation of a master module to control all the subsystems of the VIRGO antenna.

Because of the complexity of the control system for the whole interferometer,the problem of control is divided into a certain number of subproblems, each one on a dedicated CPU. The master module, however maintains knowledge of what is happening in every part of the antenna, and coordinates the actions of the subcontrollers. In this hierarchical two-level structure (more levels can be added, if needed) the master module may compensate for interaction errors among the subprocesses : coupling effects can in fact lead to small selfoscillations of the system, not only in the 0 ÷ 10 Hz band, but also in the 10 ÷ 3000 Hz band.

c) Digitization and acquisition of the GW signal is in fact part of the control system, since the error signal in the range 10 ÷ 1000 Hz is the GW signal itself. One needs only to store the data after using it to control the feedback system.

3.5.3) DIGITAL CONTROL SCHEME APPLIED TO FLS

Fig.3.5.3 shows a simplified digital scheme of control to be applied to the VIRGO antenna. The general scheme of the whole interferometer, showing the locking servoloops and the modulation frequencies, is sketched in Fig.3.1.17. In the global digital control system we must take care also of the slow servoloops for the mirrors alignment

These alignments can be performed by mechanical modulation technique and synchronous detection at low frequencies. At least 11 degrees of freedom must be controlled by slow servoloops; the choice of the modulation frequencies is not critical because the frequency band of tilts is very narrow. The only things we must take into account is to avoid overlapping of zones in which the second harmonics of the modulation frequencies are present, owing to the adopted coherent detection scheme (lock-in amplifiers) and, of course, to avoid mechanical resonances of the mirrors .

An experimental model of this control is now being implemented in Napoli, and will be operative at the end of Sept. 1989. The master computer is a Mac II, with a 68020 CPU and standard peripheral devices (disks,printers) with a large memory capacity (8Mb). This computer is connected via a bus adapter to a standard VME bus, where another 68020 CPU takes control of various interfaces on the VME bus. The subsystem controls a mirror degree of freedom by acting on actuators with a correction signal generated via software from an error signal coming from a lock-in amplifier whose input is the signal detected from a photodiode centered on an interference bright fringe in transmission from one cavity. The set up and control of the lock-in amplifier and of the spectrum analyzer is done by an IEE488 interface adapter on the VME bus. The signal for the actuators is generated by a DAC converter board on the same bus, and is amplified before being applied. An ADC converter reads the error signal from the lock-in amplifier whose reference signal is also generated by an interface on the VME bus (actually, another DAC board).

A digital signal processing board is used to implement an hardware FIR and by software we generate then an adaptive optimized PID (Proportional-Integral-Derivative) correction.

A 4 Mb memory board on the VME bus is used for program storage and as data buffer, in such a way that longer time intervals may be analyzed off-line, for example to study long-term instabilities. These data can then be transferred to the master computer,in our case a Mac II, and there dumped to a disk file with a time stamp. The Mac II needs a software to talk with the VME bus and the slave CPU. We have, for the time being, selected the RTF-68K, a code used at CERN. The Mac II is connected via Ethernet to the VAX 6320 computer of I.N.F.N., thus allowing easy and fast file transfer for subsequent post-processing. The protocol used is DECnet, but is going to migrate to TCP/IP when we will move to the OS9 operating system. We propose to implement similar modules to control the VIRGO antenna.

It is likely that the fast evolution of micro-controllers and DSP's will soon allow us to design much simpler and cheaper digital control loops.

3.5.4) REQUIREMENTS FOR DATA ACQUISITION

The characteristic signal of gravitational waves, which we propose to study can be divided, as presently known, into two groups. The first group consists of signals coming from star collapse, coalescent binary stars, etc. which are characterized by a short life span and have a band widths which are few KHz. The second group consists of periodic signals coming from pulsars which have a small band widths. This means that for periodic signals it is possible to employ a rather long integration time, improving in this way the sensitivity of our apparatus. But this also means, as it will be

seen later, that it will also be necessary to have a very long dynamic acquisition signal range.
Let us assume an integration time of one year, which would yield a sensitivity to h less than 10^{-25}. We would then obtain a frequency resolution of 3.10^{-8} Hz.
With the purpose to evaluate the dynamical range necessary for storing the signals we have to know the interferometer signal amplitude from 10 Hz up to 1 KHz.
From the data shown in Fig. 3.4.4 we can infer that a dynamic of about 10^3 is enough; this can easily be seen considering that at 10 Hz we expect 10^{-16} $\frac{m}{\sqrt{Hz}}$ while at KHz we expect (see eq.(1.6)) 3.10^{-23} x $L = 10^{-19}$ $\frac{m}{\sqrt{Hz}}$. A 16 bit (~90 dB) is then sufficient to the purpose.
With a frequency sample of 10 KHz and with two bytes per point we obtain a data rate of 20 KByte/sec equal to about 1.7 GByte/day. To be able to maintain a frequency resolution of 3.10^{-8} Hz at 1 KHz, it is necessary to use a sampling frequency with a long term stability of at least 3.10^{-11}. This will allow us to correct the Doppler effect due to the rotation and translation motion of the earth; it will then be necessary to know with a rather good precision the relative phase of the acquired signals every 6 months. The acquisition system clock must therefore be given by a cesium atomic clock which has a long term stability of about 10^{-12}. The use of a cesium clock will also allow us to know the exact instant at which will arrive a gravitational pulse signal with a precision better than 1 ms. That will allow us to know the direction of the signal using the information from other interferometers.

3.5.5) COMMUNICATION AND NETWORKING

There are two basic communication needs for the VIRGO antenna: a local Area Network to connect the various CPUs of the experiment, and a link between the instruments used in the arms of the antenna.
The network needs do not pose significant problems, since the data transfer rate from the data acquisition system is about 160 Kbit/sec and can be accomodated by existing network solutions. In particular, Ethernet (IEEE 802.3 standard) gives a bandwidth of 10 Mbit/sec at reasonably cheap prices. Because of the length of the arms of the antenna (3 Km) fiber optic cables must be used. This option has also been selected for the Gran Sasso experiments, therefore hands-on experience exists within INFN.

The recommended optical fiber for such application has a 62.5 micron core and a 125 micron cladding, dual window, graded-index profile, multimode glass-on-glass construction. This is an ANSI and EIA standard, and is manufactured by several companies (i.e. Pirelli in Italy).
Using a wavelength of 1300 nm, the attenuation is 0.8 ÷ 1.5 dB/Km, and the bandwidth is 500 MHz · Km; at 850 nm, the attenuation is still 2.8 ÷ 3.5 dB/Km, and the bandwidth 160MHz.In both cases, the bandwidth allows usage not only of the Ethernet protocol (10 Mbit/sec) but also of point-to-point communication between instruments at the extrema of the arms of the VIRGO antenna.

3.5.6) DATA STORAGE

A sampling rate of 10 KHz corresponds to about 1.7 Gbyte of data per day of operation.
These figures do not give problems of network speed, but problems of data storage, transport and data integrity. In our proposed implementation of the digital control, data are moved from memory buffers to dumping disks (local), both used as a circular buffer, and then via the network to the central system, where they must be written into a storage unit (see fig.3.5.4).
With a dumping disk of 600 Mbyte which is a standard 5,25 drive, about 8 hours of data acquisition can be stored locally. This is the time that the network can go down without any data loss. More than one local disk can be used if necessary, but since communication is crucial to the whole system, a 8 hour interruption should never occur. For the data storage on the central system, larger disks, in a "Shadow mode", and with 2.5 Gbyte capacity capacity sould be used. Since at present (mid 1989) disks with a 5,25 in form factor may have 600 Mbyte of user data and with 8 in form fatcor the capacity is already 1.2 Gbyte, it is safe to assume that 2.5 Gbyte disks shall be on the market at competitive prices in the early 90's.
The shadow set of disks will assure integrity of each bit of information, as data are automatically written to both disks, maintaining the system operational also in case of a disk crash. We note that this feature could be used also for the local dumping disk, but it seems to add unnecessary load on the data acquisition CPU: in case of a disk crash, the CPU can easily transfer data directly from the memory buffer to the central system via the network: in other words, the local dumping disk is already a safety mechanism to avoid data loss.

From the "Shadow" set the data have to be copied to a different device, for data storage and transport. We propose to use the new DAT tape device, an emerging standard, which uses pocket-size cassette with a capacity of 1.2 Gbyte. The main feature of such devices, apart from the compactness, is in the recording technology, in which data are written using an helical scan mechanism. This results in lower rotational speed, and therefore less friction, higher accuracy and lower error rate: with standard ECC algorithm, the bit error rate is less tha 1 in 10^{16}. The ECC is also able to recover data loss up to 500 bits. Data loss in fact occurs after the data have been written, and is generally due to dust or other micron-size contaminant parts.

The first European manufacturer of DAT tapes, originally introduced by Japanese companies (SONY) is a West Germany company. The end user price of such device is such that a redundant (up to four devices) implementation can be reccommended. An alternative, but which still uses helical scan technology, is the 8 mm video-standard.

Because of the non-availability, in early 1989, of DAT tape devices in Italy, the Napoli group has experimented with the EXABYTE device. The main difference is the media used, standard cassette for video cameras, which has the advantage of a higher capacity (2.3 Gigabyte respect to 1.2 of the DAT) but the disadvantage of a nominal error rate worst by a factor 10^2.

The tests performed were of two types. An accelerated lifetime test was done, writing the contents of 4 magnetic disks of 450 Mbyte each to a single cassette, twice a day, for a period of a month. Each complete copy operation required 8 hour of elapsed time, including verification. No error was found, including recoverable errors (A similar test conducted on 'old fashioned' 1/2 inch magnetic tapes started showing errors, recovered however by longitudinal CRC, after an 8 hour copy operation).

The DAT (or the 8mm video) cassette tape solves the problem of data transport and storage, but a more permanent archival medium is also necessary, as off-line post processing will occur after about 1 year. For this purpose, the optical disk technology gives us an off-the-shelf solution.

A great deal of experience has been achieved in Napoli on WORM type optical disks, in particular on 5,25 inch form factors. (We used the Maxtor RXT800S device, a SCSI-interfaced device whose media are double faced, 400 Mbyte per side. A write with verify test performed on two disks showed several errors (20), but all were corrected with a block re-allocation mechanism). Similar tests conducted on different devices (in particular, LMSI disks and Alcatel Thomson disks) at ESO in Garching by one of us (Russo G. et al.[1986a], [1987a], [1988]) showed a similar error rate, which therefore seems inherent of this kind of WORM device. The reason is that the non-eraseability does not allow error recovery by a simple block re-writing, and moreover the errors may not show up if a verification with a copy on a different media is not done. The conclusion is that WORM optical disk may be used for long term ($\sim$ 15 years) data archival only after a copy to the rewritable device (DAT tape) has been made. The copy from dat to WORM may be performed off-line from the experiment, on a daily routine basis, e.g. in the Pisa INFN section. Eraseable optical disks, using magneto-optical devices, have already been tested, but are only now (early 1989) appearing on the market (the FIJI and TAHITI models by Maxtor) and no operating experience exists.

We plan to test one of these devices in late 1989. The final choice of the technology to use will depend on later studies made on the function reliability and most of all on the data integrity once stored.

We plan to test one of these devices in late 1989. The final choice of the technology to use will depend on later studies made on the functions reliability and most of all on the data integrity once stored. It will be decided in collaboration with the other groups.

3.6 Vacuum system

3.6.1.) INTRODUCTION

The vacuum system is the most visible and the most costly part of the project. It basically consists of 2 tubes, each 3 km long, joined in the shape of an L and 6 tanks, one at each end of the tube and the others 4 at the corner of the L (fig. 3.7.5). All the tubes and the tanks are evacuated.

Due to the extreme performances required, this vacuum system is not an ordinary pipe line but a high technology product. It requires a very special raw material with very low outgassing rate and new manufacturing methods due to specifications of dimensions and precision.

The evacuation of the tubes is required in order to suppress many noise sources, each of them being strong enough at atmospheric pressure to prevent the observation of gravitational waves (see section 2.9). The main ones are:

-the random fluctuations of the optical index: fluctuations of the number of molecules inside the volume of the light beam produce variations of the optical index and, consequently, phase variations of the light. This kind of fluctuations may be produced either by statistical variations of the distribution of molecules or by sudden bursts of molecules, emitted mainly by the pumps (and possibly by the tube walls, due to thermal or mechanical shocks). In both cases, the effect is proportional to the polarizability of the molecules. Fortunately, we expect the dominant residual gas to be hydrogen, which has a low polarizability. The stochastic fluctuations require an average pressure lower than 10^{-5} Pa ($\approx 10^{-7}$ Torr). The bursts are to be avoided and/or monitored: their rate and amplitude should be minimized by the choice of the pumps and the thermal shielding of the tube.

-the scattering of light by the residual gas molecules: in order to achieve an intensity of light lower than that scattered by the mirror coatings, the pressure must be lower than 10 Pa. This effect is obviously not the most dangerous one.

-the transmission of acoustic noise: the experimental results obtained on various prototypes show that this is not a critical issue: a pressure of 10^{-3} Pa ($\approx 10^{-5}$ Torr) should be sufficiently low to avoid any problem.

-the brownian movement of the mirrors: in order to reduce it below 10^{-20} $mHz^{-1/2}$, it is necessary to reduce the pressure in the tanks below a value which

depends on the mass of the mirror. In our case, this value, approximately 10^{-4} torr for a 40 kg mirror, is not the critical one.
-the damping of the suspension by the residual gas, and the corresponding increase of its thermal noise: the viscosity of the residual gas surrounding the mirrors may damp the suspension pendulums. Since the thermal noise is inversely proportional to the square root of the Q of the suspension, this could increase the thermal noise. Below 10^{-3} Pa ($\approx 10^{-5}$ Torr), this effect should not be the limiting damping factor.

3.6.2.) SPECIFICATIONS

3.6.2.1.) OUTGASSING RATE

In order to obtain high vacuum, the most crucial parameter is the outgassing rate. Ultimate pressure, pump speed and spacing, pump down times and cost of the system are all directly related to the outgassing rate. For a given material, this rate depends on the processing of the material, like cleaning, annealing and baking. But the figures published in the scientific literature or indicated by manufacturers reveal quite a large spread (sometimes more than 4 orders of magnitude).
In order to get some confidence on an actual figure for the outgassing rate of 304 stainless steel, we have built in Pisa two prototype tubes, 12 m long and 1 m in diameter. One tube was degreased, cleaned and baked under vacuum for 24 hours at a temperature of 120°C. We measured an outgassing rate of $2\ 10^{-8}$ $Pa.m.s^{-1}$ ($\approx 2.10^{-11}$ Torr. l. $s^{-1}cm^{-2}$) or better. All the derivations for the vacuum system are based on this figure, which is low enough to allow the design of a reasonable vacuum system. *But such a low rate involves specifications on raw materials, manufacturing, treatment and conditioning of the element tubes, welding, assembling and baking of the whole tube.*

3.6.2.2.) LEAK RATE

In order to obtain the same magnitude on optical index fluctuations, the partial pressure of nitrogen, the major component of a gas leak flow, must be 20 times as big as the partial pressure of hydrogen, the major component of outgassing load. A safety factor of 5 being taken, thus the gas flow rate originating from leaks could be around 4 times the outgassing rate. But in order to keep the

pumping system as small it is necessary for the outgassing flow of the walls, the total leak rate will be required to be less than 1/100 of the outgassing flow.
It is said that the leak free specifications for the whole vacuum system would be accepted by contractors for a factor 2 increase in price. It seems more reasonable that this risk would have to be supported by the Project if leak free specifications on each element tube and welding are checked.

3.6.3.) THE TUBE

3.6.3.1.) RAW MATERIAL

In a vacuum system, the most crucial choice, because it is very quickly irreversible, is the choice of raw material. In fact, there are only two possible materials, aluminium and stainless steel, for the construction of a tube pumped at a pressure lower than 10^{-5} Pa ($\approx 10^{-7}$ Torr). Stainless steel would render manufacture (tooling, welding) easy and presents a better resistance to corrosion. For example the 316 L stainless steel presents the highest resistance to corrosion by chlorine compounds, thus we could choose 316 L stainless steel (Z2 CND 17/13 AFNOR standard). This quality could be particularly required if the interferometer is being built in a corrosive atmosphere (within 10 km of a sea, or in a polluted area). According to some tests made for the LIGO project, it is possible to ask for a special annealing of the steel, in order to reduce the hydrogen outgassing rate. This operation is cheap; it reduces the rate by a factor 10 at least, and may even suppress the need for baking. The manufacturer will be asked to produce a gas analysis for the delivered material in addition to the standard wet chemical analysis.

3.6.3.2.) LAY OUT

Each arm of the L, 3 km long, will be made up of 19 sections and 2 half-sections and will be terminated at both ends by a large valve. Each section (fig. 3.6.1), 150 m long, will be made of 2 sub-structures :
- a welded tube, 145 m long, ended by flanges ,
- an instrumentation sleeve, having a bellow and a flange at each end. The use of this sleeve is for pumping, measurements and monitoring (fig 3.6.2).

Tubes and sleeves will be jointed by stainless steel gaskets.

The sleeve and the middle of the tube will be clamped to the ground. The other parts of the section will be supported on sliding pads every 12 m to accommodate the thermal expansion that will be compensated by the elasticity of the bellows.
The tube will be 1000 mm in inner diameter, 5 mm in thickness and will be stiffened by hoops (10 x 50 mm) every 2 m. The structure will fulfil the appropriate standards. It would also be possible to use a much thinner corrugated tube, or at the contrary, a straight thick tube (10 mm), without the stiffening rings. The first possibility was rejected for reasons of safety and for the difficulty of cleaning it. The last one was rejected for its cost and its weight, which makes difficult to move large sections.

3.6.3.3.) MANUFACTURING

The tube will be manufactured from rolled sheet-metal, welded along a generative line of the cylinder, and welded together to form an element tube 12 m long. Stiffening hoops will be welded around the tube which will be cleaned, annealed at high temperature and packed in the manufacturer shop. Each tube will be cleaned and leak tested before being packed and sent to the site. After the installation of temporary hinges, the tube will be pumped down to 10^{-3} Pa ($\approx$ 10^{-5} Torr) and tested with an helium controller. If the leak rate is smaller than **4.10^{-10} Pa.m^3.s^{-1}** ,($\approx$ 4.10^{-11} torr.l.s^{-1}) the tube is accepted. The processes of cleaning, annealing and conditioning have to ensure an outgassing rate lower than 2.10^{-8} Pa.m.s^{-1} ($\approx$ 2.10^{-11} Torr. l. s^{-1}cm^{-2}), value defined at § 3.6.2.1.
On the site, a special machine will weld element tubes into 145 m long sections (plasma or TIG welding). The welding process will be defined in order to require no further cleaning action. As work proceeds, the section will be pulled off the welding machine. The finished section will be propelled on his permanent place.
Two welding machines, one for each arm, will be needed to mount the whole tube in one year (1 day per welding, 15 days per sections, 300 days per arm).
Each section will be checked for leak free specification. First each welding will be tested with helium controller. After installation of temporary hinges and thermal insulation, the entire section will be pumped down, baked up to 100° C during 96 hours, then cooled during 48 hours. A quantitative residual gas analysis (measurement of nitrogen to oxygen ratio) will check the leak free specification. After this test, the section will be filled with nitrogen up to a

pressure of 100 Pa, then filled with dry air up to atmospheric pressure, a filling with pure nitrogen being dangerous for workers safety.

3.6.3.4.) BAKING

If the conditioning and welding specifications are strictly observed and if careful attention is taken for handling, no cleaning operations will be needed, but a baking at 100° C of the whole tube could be fruitful. Thermal screens and insulation are required. Thus radiative and convective losses may be decreased by a factor 2 or 3. In spite of these insulations, the power required to achieve a temperature of 100° C is estimated to 3 MW . This power is only temporarily needed and may be supplied by rent generating sets.

3.6.4.) THE TANKS

The tanks are conceived to keep under vacuum the pendulum chains and the optical parts of the interferometer. The tanks have a cylindrical form, 7 m high, with a 2 m inner diameter; such a huge dimension is necessary to have a free cross-section of 1 m^2 for the installation of the chains, inside their support legs (Figs. 3.4.11, 12). The choice of the material for the tanks is stainless steel, as for the pipe, based on the same arguments. Each cylinder is subdivided in three parts: the central one, perfectly cylindrical, and an upper and a lower closing cup. The walls are 6 mm thick with one reinforcing ring in the middle of the central part and thick flanges serving as connection means as well as reinforcement rings.

The lower cup, containing the mirrors, has four 1 m circular apertures with standard flanges, serving as access ports for installation of the optical parts and to connect one tank with another or with the arms of the interferometer. The conjunction pipes have elastic bellows not to transmit mechanical forces due to unbalanced atmospheric pressure; for the same aim a few of the curved plates closing the apertures are strongly fastened to ground.

Due to the limited space available inside the tanks, the mechanical structures supporting the chains develop only in the vertical direction and have a limited cross-section. To increase the stability of the suspension point and the stiffness of the structures, they are rigidly connected to the cylindrical part of the tanks; the tanks are in turn stiffened by inclined steel pillars strongly clamped to

ground trough big concrete blocks (Figs. 3.4.11, 3.7.9). Also the inner supports of the pendula are well founded on the floor of the buildings by four legs passing through the bottom of the tanks.
The bottom part of each tank will be separated from the rest by an horizontal plate having only a small hole to leave a free passage for the suspension wire of the mirror. This plate is necessary to keep separate the two zones from the point of view of the vacuum. In fact it is expected that in the upper part of the tank it will not be possible to have a vacuum better of 10^{-5} torr, due to the large number of mechanical pieces, insulated electric cables and electronic components. Such a dynamic vacuum could not be tolerated in the interferometer.

3.6.5.) PUMPING

There are two distinct phases in the pumping procedure:

3.6.5.1.) PUMPDOWN

This phase consists in evacuating the tube from the atmospheric pressure (AP) down to 10^{-3} or 10^{-4} Pa ($\approx$ 10^{-5} or 10^{-6} Torr), where it becomes possible to start the high vacuum pumps without saturating them.
This sequence will happen very seldom (hopefully only once), so it is not necessary that it be very fast; the most important factor is "cleanliness", that is the absence of oil pollution of the tube.
A very slow pump down will guarantee the absence of turbulence in the gas flow, avoiding therefore the deposit on the optical parts of dust particles accumulated somewhere else.
Two steps seem to be necessary :

1. a rough pumping down to 1 Pa (10^{-2} torr)

2. an intermediate pumping down to 10^{-4} Pa (10^{-6} torr)

During the first step, mechanical pumps are used. For this stage, a pumping group is made of one Root pump 1000 m^3/h and two rotary pumps, 250 m^3/h each. The ancillary equipment (valves, oil traps, ...) is also included in the group.

It is proposed to have three such pumping groups, one at the end of the tubes, near the end tanks, and one at the corner of the L, near the central tank. A pumping group will be used either to pump down a tank or a tube. To pump down a tube, of course two such groups will be used. For a tube, the required time to pump down from the atmospheric pressure to 1 Pa (10^{-2} torr) is evaluated to about 20 hours.
For the second step (from 1 Pa to 10^{-4} Pa, or from 10^{-2} to 10^{-6} torr) turbomolecular pumps are used. If it is needed, the tube will be baked during this stage. After this process, the expected value for the outgassing rate is supposed to be achieved.
From technical and economical points of view, the optimal disposal seems to be three turbomolecular pumps, 1000 l/s each per tube and two such pumps per tank. In fact, during the pumping down of the tube, five pumps will be used, three proper of the tube plus one at each end, normally used for a tank.
Of course, a rough pump and a valve are needed for each turbomolecular pump.

3.6.5.2.) HIGH VACUUM REGIME

3.6.5.2.1.) PRESSURE SPECIFICATIONS

The permanent high vacuum pumping system must obtain the following specifications:

- average pressure $P_{ave} < 10^{-5}$ Pa ($\approx 10^{-7}$ Torr)
- fluctuations $\Delta P_{ave} < 10^{-10}$ Pa ($\approx 10^{-13}$ Torr) on a 1ms timescale
- partial pressures
  - hydrogen $< 10^{-5}$ Pa ($\approx 10^{-7}$ Torr)
  - water $< 10^{-6}$ Pa ($\approx 10^{-8}$ Torr)
  - nitrogen $< 10^{-6}$ Pa ($\approx 10^{-8}$ Torr)

Furthermore, the residual gas must be free of hydrocarbon, in order to keep the optical surfaces clean. A partial pressure of less than 10^{-10} Pa ($\approx 10^{-13}$ Torr) is required if one wants to avoid the cumulative deposition of a single layer of hydrocarbons on the optics in 4 years.

3.6.5.2.2.) VACUUM PUMP SELECTION

- Oil diffusion pumps must be eliminated because the oil partial pressure remains too high, in spite of some recent improvements
- Turbomolecular pumps require some maintenance, and their vibration level is too high, but their main drawback is that they do not produce a stable pressure (DANZINGER. Jnl. Vac. Sc. Tec. 21 p.893). They must also be discarded.
- Cryogenic pumps are very attractive because of their high pumping speed and their cleanliness, but these pumps produce vibrations and may not be able to function in the wide temperature range which is required. Also, when the external temperature rises, the semi-cold surfaces between the pump and the tube will release bursts of molecules. It could be possible to minimize this effect by adding a thermal control of the intermediate temperature area.
- Getter pumps would be the ideal solution if their capacity were a little bit higher (or if the outgassing rate could be made much smaller than 2.10^{-8} Pa.m.s^{-1} ($\approx$ 2.10^{-11} Torr.l.s^{-1}cm^{-2}). They do not pump noble gases, but they could be assisted by small turbomolecular or ion pumps.
At the present time, a getter pump is under test in Pisa, in order to evaluate its actual capacity, thus its lifetime. This component pumps down a prototype tube 12 m long, the outgassing of which being well known. The evolution of the pressure reveals the evolution of the pumping speed and thus the capacity of the getter pump.
- Ion pumps are probably the best suited devices for our application. Among them, the diode variety is to be preferred because it has a better capacity for hydrogen. There remain some questions concerning the production of occasional bursts by ion pumps, which we are trying to elucidate in cooperation with the German team.

3.6.5.2.3) PUMPING THE TUBE

The pump design in based on an outgassing rate of.2.10^{-11} torr.l.s^{-1}.cm^{-2}. For the tube (10^8 cm^2), the gas flow is then 2 10^{-3} torr l s^{-1}. In order to obtain an average pressure of about 10^{-7} torr, we propose fourty ion pumps of 500 l/s each. A couple of such pumps is fixed on each instrumentation sleeve. The need of valves is not obvious. Thus a minimal pressure of 10^{-7} torr, at the pumps, and a maximum pressure of 1.2 10^{-7} torr are obtained.

3.6.5.2.4.) PUMPING THE TANKS

There will be a differential pumping system for the tanks. A plate with a small aperture divides the tank into two parts : an upper compartment with a medium vacuum (10^{-5} torr), and a lower compartment with a high vacuum (10^{-7} torr). The conductance of the aperture is evaluated to few 10 l/s. Then, for each bottom compartment (high vacuum) a 1000 l/s ion pump group is required. The top compartment (medium vacuum) is continuously pumped down by a turbomolecular pump used also in the previous stage.

3.7 Site and buildings

The installation of the VIRGO interferometer has to satisfy the following requirements:

-keep the performances of the detector at the limits of present tecnologies

-build the apparatus on a flat, controlled area, as far as possible away from mechanical vibration sources, as hiways, trains, etc., within a reasonable distance from one of the collaborating laboratories

-keep the expenses for the acquisition of the land much lower than the cost of the apparatus itself

-give a minimum perturbation to the geological and biological equilibrium of the surrounding region.

A committee formed by members of the Pisa University, of the local administration and of INFN performed a very accurate search in a 100 km radius region around Pisa. A larger distance would result in untolerable logistic problems. All morphological, technical and administrative aspects have been investigated, including detailed seismic noise measurements. Two candidate sites, equivalent from a seismic noise point of view, have been selected as very suitable for the installation, and priority has been given to a private owned land, in the "comune" di Cascina (Fig.3.7.1). If the project will be approved, the Mayor of Cascina assures full collaboration to solve all the legal difficulties in the expropriation procedure. The second priority site is of public property, inside the natural park of Tombolo, and will be taken into account in case of an impossibility to stay in Cascina. The choice has been done to preserve the park from the ecological impact of the interferometer, even though it is extremely small.

Before to report on the seismic noise measurements on the sites, we like to remind that the "goodness" of the suspensions consists due to the fact that they transfer to the test masses the displacements of the suspension point reduced by a factor 10^9 at a frequency of 10 Hz; the reduction factor is 10^{13} at 20 Hz and 1 or less below 6 Hz (see section 2.14).

In figures 3.7.2 and 3.7.3 are shown two noise spectra taken in Cascina and Tombolo respectively, where an average acceleration noise level of 10^{-5} m/s^2 can be seen. As an example we report on figure 3.7.4 a measurement taken during the passage of an airplane; the broad noise bump will be easily cut by the suspension, being confined above 50 Hz. We believe that these noise figures allow good performances of the interferometer.

From the point of view of civil engineering, the apparatus consists of a Michelson interferometer with two 3 km arms, nominally orthogonal (angles in the range 60^o - 120^o can be accepted), operating inside a 1 m diameter vacuum pipe (Fig.3.7.5). At the crossing point a 20x20 m^2 building contains, under vacuum, four pendulum chains supporting the stabilizing optical parts, the beam splitter and the semitransparent mirrors of the two arms. At the other ends of the pipes, inside two 15x15 m^2 buildings, the chains supporting the other two mirrors of the interferometer are installed . The buildings will be 15 m high to allow to lift up the upper part of the vacuum tanks and make accessible the pendulum chains (Figs. 3.7.6, 7, 8, 9).

All the buildings are equipped with electricity, water, compressed air, and cranes. In the central building (Fig.3.7.6), inside appropriate rooms, are installed the lasers and part of the acquisition and control electronics. The central and terminal buildings will be temperature controlled to a few degree centigrade, kept under overpressure with respect to the outside and supplied only with filtered air, in order to perform as a clean room of low quality. A fraction of the volume of the buildings, surrounding the lower part of the vacuum tanks containing the mirrors, will be separated from the rest and kept clean at a higher level (class 10000) , since all the optical parts will be exposed during installation, tuning and maintenance (Fig.3.7.7). In the vertical direction the separation will be done at the same level where, in the vacuum tanks, a baffle is put to separate the upper from the lower part. As described in the vacuum section, above the baffle there will be the whole pendulum chain and therefore a rather dirty dynamical vacuum; below the baffle only the mirror, inside the clean vacuum ($< 10^{-7}$ Torr) of the interferometer. In this way, also when the vacuum tanks will be opened, the optical parts will be confined in a cleaner zone. The floor separating the two parts of the buildings will contain in its thickness air-ducts and filters to supply them with a clean laminar air flow to the room below it. The laser will be installed inside this cleaner area. Along two sides of the central and terminal buildings there will be rooms for mechanical and electronic laboratories and an assembly area.

To avoid mechanical vibrations all equipment containing motors or moving parts (air conditioning, laser power supplies and cooling, etc.) will be isolated and confined well outside the buildings. For the same reason the control room of the whole interferometer will be located in a separate building, 50 m apart from the central one, connected by a bunch of cables to the apparatus. This building, one floor high, with a surface of 10 x 20 m^2, will contain besides the computer and the data acquisition system, the remote controls of the servo-loops and of the

vacuum system. In this way, during data taking, nobody is expected to stay close to the test masses, with the risk of noise generation.
The 1 m diametre vacuum pipes, containing the arms of the interferometer, will be installed inside a channel of prestressed concrete, industrially produced. This channel (Fig.3.7.10) will have a rectangular cross-section, possibly with an inner height of 2 m, to allow the passage of a man for survey and maintenance. The channel and its cover will be shaped in order to prevent the entry of rain and animals; sump-pumps will be located at every pumping station, together with the vacuum pumps, to evacuate the water coming from condensation or any other source. In correspondence to all the pumping stations the cross-section of the channel will be enlarged (Fig.3.7.11, 12) to allow the installation of the pumps themselves, the vacuum control instruments and the bellows for thermal expansion compensation.
The channel will rest on a basement having a strength to guarantee the alignment of the vacuum pipe to a 1 cm precision (peak to peak). Along the pipes a service road, 5 m wide, will run from one building to the other. Due to the flatness of the choosen site, the installation of the vacuum pipe is forseen over the ground level, even taking into account the earth curvature, which gives a sagitta of 37 cm over a length of 3 km. Only a small amount of excavation will be necessary in particular locations and a few small bridges will be built to cross irrigation streams.

3.8. Data analysis

3.8.1) INTRODUCTION

As a preliminary remark, let us emphasize that the search for gravitational wave detection by Virgo is not an isolated activity. If a signal is suspected to have a gravitational origin, the level of confidence can be increased dramatically with coinciding observations with neutrino detectors, traditional observatories and other gravitational wave detectors including mechanical ones.

A common opinion in the groups involved in the detection of gravitational waves by interferometric means is that any group should have in the future an easy access to the data from any other groups. It appears as a physical necessity when the goal is the observation of short pulses in the kHz frequencies range; it is also the best way to reach the scientific final goal most effectively.

As a consequence of the international meeting held in Paris in February 89 working groups have been constituted with the participation of Virgo, Germany, United Kingdom and U.S.A. The first goal is to define the common requirements to be achieved, concerning especially data acquisition, data processing (on line and delayed), algorithm, etc..

The problems involved are important but are well known from other fields in physics and astronomy. The kind of gravitational signals which we are concerned with have already been considered by the groups working on mechanical detectors of gravitational waves, in the range of the kHz, as well as in the range of a few tenths of Hertz. No specific difficulties are expected, the solutions have only to be adapted. For these reasons, we will not develop here these technical questions but we will rather consider the more specific aspects in the present context. We will describe what kind of specific work is under development, what kind of work has been done and what are their consequences on the estimation of the feasibility, on the freedom of the implementation of the antennas.

A gravitational wave observatory cannot be compared to an astronomical observatory (as they exist today) because each gravitational wave detector will observe signals from every direction of the sky all the time.

It is the responsibility of data analysis to extract from the records the informations concerning a given direction or a given type of astrophysical events. It is thus very important that the data from every detector be available to every one who wants to work on the subject and to be prepared to extract physical informations from the observed signals.
It would be important to have a direct observational proof of the existence of gravitational waves as soon as possible.
Although it is not the most important physical goal, the *first detection* will have such a considerable impact that a competition between the groups involved will probably take place.
If a competition is to appear for the first detection, it should not involve any information retention but rather a global strategy which will have to be defined locally by every group as a complement to the international common agreements.
Starting from an origin which is the end of the construction, let us assume that the sensitivity of the various detectors will follow the same dependence on time in every group and that the algorithms used (if different) will have comparable performances. Then the crucial points are the answers which will be given to questions such as:
- What and in which direction to observe ?
- What is the lower level of confidence which will be convincing ?
- How must be the time shared between observation and development ?

It is clear that the answers depend on the performances of the antennas thus they will change with time and to start the first is an important advantage. In any case, Virgo is well positioned if it starts rapidly because of its specific ability to observe low frequencies (periodic) signals by its own.

3.8.2) THE INVERSE PROBLEM IN GENERAL RELATIVITY

The response of an interferometer is a function of time which depends on the history of the motion of the mirrors. From this signal we can calculate a linear combination of the two components of the gravitational wave field.
This linear combination depends on the direction of the gravitational wave source and on the location and the orientation of the antenna.

3.8.2.1) THE PHYSICS OF THE EXPERIMENT

In order to obtain this linear combination from the signal, one has to know precisely what is the dynamical behavior of the device. This is well known for frequencies of order of 1 kHz. At low frequency (a few tens of Hertz) a new phenomenon related to nonlinear retarded effects might give strong prescriptions on the way the apparatus must be operated, and a lowest boundary might appear in the observable frequency spectrum. This does not make the "low frequency strategy" questionable, however this is a strong motivation to the studies concerning the physics of the experiment. This aspect of the data analysis has been currently studied from the beginning by the Paris group in collaboration with Bilbao's university and is being considered now by the British group as well. (See appendix).

3.8.2.2.THE INVERSE PROBLEM

Once the linear combination of the gravitational polarization is known for each antenna, one has to solve the inverse problem i.e. to determine the direction of the source (2 angles) and the two gravitational wave polarizations (2 functions of time). This problem is almost trivial and the solutions are known. The main results are that

- 3 antennas would allow for solving completely the inverse problem if the signal to noise ratio is high enough;
- 1 antenna would allow a detection of a gravitational short pulse if no local perturbation is present.

However we expect random local perturbations not to be excluded for sure, then 2 antennas are necessary to achieve a high level of confidence by means of the observation of coincidences. Moreover, the signal to noise ratio will not be very high from the beginning.

The possibility of observing short pulses depends on the number of networked antennas. The results .are summarized in the EUROGRAV document (see appendix). This document puts forward the *basic physical reasons* why one can be confident in the future exchange of data between the various groups operating a detector in the kHz region.

The specificity of Virgo is the "low frequency strategy" which means that, due to the motion of the Earth, Virgo will detect periodic signals in various positions. This is approximately equivalent to the detection of one signal by several antennas. Thus Virgo will have the possibility to detect periodic gravitational waves and to solve the inverse problem by its own.

3.8.2.3) SPECTRAL AND DIRECTIONAL DISCRIMINATION OF PERIODIC GRAVITATIONAL WAVE SOURCES

The unique capability of VIRGO to detect periodic gravitational wave signals (PSR generated) in the range 10 to 1000 Hz can possibly be exploited for discriminating gravitational wave sources in frequency and/or direction of arrival. The following topics are being currently investigated in Napoli and in Salerno:

1) The design of efficient algorithms to implement "optimum" detection of gravitational wave signals modelled according to Livas (AM-FM type with unknown but constant phase). The feasibility of real-time algorithms using current hardware with 10^{-7} Hz frequency resolution over the whole range of frequencies and direction of arrival has been demonstrated.

2) The modelisation of the gravitational wave signals accounting for possible random time varying phase. For example under reasonable assumptions, gravitational wave signals are shown to possess cyclostationary property. Correspondingly, detection algorithms may be suggested which improve on the classical radiometer while preserving the computational and resolution features as in 1).

3.8.3.) THE FIRST DETECTION

The first detection is important for physical reasons and also because it will be the first milestone on the way towards the birth of gravitational wave astronomy which is the final goal. Everyone would like to shorten the delay until the first direct gravitational wave signal is observed. The search for the first detection will involve a situation where the noise will still remain important compared to the signal.

3.8.3.1.) THE NUMBER OF EVENTS PER YEAR

The Paris group has developed a sophisticated method which allows for calculating a factor of merit of a given network at a given sensitivity and for estimating the number of short pulses which could be observed per year by a given array of interferometric detectors:

- With the first goal (sensitivity $\approx 3\ 10^{-23}/\sqrt{\mathrm{Hz}}$), the evaluations obtained from astrophysical data put forward the order of magnitude of a few signals per year, with an important uncertainty ; this is consistent with other estimations. On the other hand estimations concerning pseudo-periodic signals from coalescing binaries are much more optimistic. From these orders of magnitude we conclude that the *feasibility is reasonably proved from an astrophysical point of view at this level of sensitivity.*
- The factor of merit of a given array does not depend very strongly on the orientation and on the location of the antennas (within the framework of reasonable assumptions concerning the participating countries): a factor

between 1 and 2 in term of sensitivity and likely near of one for the reasonable arrays which can be conjectured.
Considering the difficulties of finding suitable lands in Europe it has generally been considered that *the acquisition of the land can be disconnected from astronomical considerations and could be treated locally and independently by the different groups* without important consequences on the performances of the final array.
These results are summarized in the appendix. They prove that pulses might be observed very soon after the level of sensitivity of $3.10^{-23}/\sqrt{Hz}$ has been achieved. It is important not to be the third to achieve such a sensitivity if we want Virgo to be surely present in the first detection. Thus it is important not to delay the construction more than the inverse of the number of expected signals per year (which is of order a few months). However, if Virgo and the American Ligo (two antennas in U.S.A.) achieve the same sensitivity at the same time, it still remains a probability of order .5 to be involved in the first detection of the pulses, but, according to preliminary calculations, the probability is much lower for coalescing binaries.

3.8.3.2.) THE SHAPE OF THE SIGNALS

The situation is somewhat different for pseudo-periodic and periodic signals or short pulses in which a temporal structure can be found. It is well known that the optimal filter for a given signal is deduced from the shape of the signal itself. Thus the detection is possible even with a low signal to noise ratio when the shape of the signal is known or depends on a small number of parameters. The work which has been developed in Meudon will give the shape of realistic signals from astrophysical phenomena. The numerical codes are already available and the first results are expected in a near future. This point is crucial for a first detection, but the main interest is that *it is the tool for future astrophysics.*

3.8.4.) CONCLUSION

Signal analysis, in the sense of extracting the signal from the noise, is not a new problem and has been already solved in similar contexts; thus this question is not presently a first priority. However, Virgo participates to the international working groups on the question because the solutions have to be coherently chosen for all the groups involved and because if not urging, this question must not be neglected.

More important is the extraction of physical informations from the output signal: Virgo is best positioned from this point of view.
Another important point is the common agreements with the other groups and the relationship with the other fields which will have to be effective as soon as the first runs will take place. The Virgo participants are very attentive to this point.

Figure Captions, chapter 3

Fig. 3.4.1 Schematic diagrams of the experimental apparatus.
The two SA chains are suspended in the two vertical vacuum chambers. The two 400 Kg brass test masses, contained in the horizontal vacuum chamber, are also shown. The deep coil accelerometer (DCA) and a calibrating piezo (PZT) are shown attached to the right test mass.

Fig. 3.4.2 Schematic diagrams of the gas spring and its practical realization.

a) Simple example of a gas spring supporting the mass M. The bellow is used for gas containment

b) top view of the vessel and cross structure, showing the four bellows position and the wires concerning the two spring parts

c) vertical section, with details of the suspension wires: along the SA the vessel is connected to the previous stage and the cross to the next. The distance d between the two wires changes accordingly with the spring elongation

d) gas-spring bottom view showing centering wires.

Fig. 3.4.3 The measured SA vertical to horizontal (V-H) and horizontal to horizontal (H-H) transfer functions between $10 < \nu < 68$ Hz are shown by ● and Δ symbols respectively, while the total extrapolated transfer function are shown by O and ♦ respectively. The measurement has been done point by point excitating at fixed frequency the SA chain in the middle of the first suspension wire, after the first gas spring, it is limited by the DCA accelerometer noise and has to be considered as upper limit.

Fig. 3.4.4 Average power spectrum of the remnant seismic displacement of the SA suspended test mass, for $0 < \nu < 10$ Hz expressed in $m/\sqrt{Hz}$ and with bin width of 18.7 m Hz. The lower resonance peaks are mostly coming from the horizontal oscillators, while the other are mostly from the vertical oscillators. Above 6 Hz the measurement is limited by the DCA accelerometer noise.

Fig. 3.4.5 The continuous line is the SA seismic transfer function: the ratio between Fig. 3.4.4 power spectrum and the seismic noise measured with the DCA accelerometer. The dotted line is the theoretical transfer function computed as the sum of the horizontal transfer function plus one percent of the vertical one.

Fig. 3.4.6 Lay-out of one out of six damping systems. The magnet M is connected to the 2-nd suspended mass of the SA, the coil C is current driven by the derivative of the light signal in the photodiode PD modulated by the movement of the mass, then creating a damping force.

Fig. 3.4.7 Measured average power spectrum of the SA 400 Kg test mass while the damping system is working; being 18.7 mHz the bin width of the spectrum the remnant displacement at 0.25 Hz is 3.4 μm.

Fig. 3.4.8 Details of the steering system to keep the dark fringe locked.

Fig. 3.4.9 a)Coils and magnet design for the steering system.

b) Expected $\frac{1}{K} \frac{\partial K}{\partial x K}$ behaviour as function of the coils-magnet distance along the axis.

Fig. 3.4.10 Front and side view of the intermediate stage between last gas spring and the test mass. The intermediate stage has been designed to make DC torque to the test mass; it is composed of two pieces: the top one is rigidly connected to the last gas spring, the other is suspended by the SA wire and suspends the test mass by two wire loops. The two parts have cross shape, the higher has coils at each end of the cross and the lower magnets in order to create forces one respect to the other.

a) front view, the two coils for the horizontal tilting are shown; one of the other system coil and magnet is also shown in the center

b) side view, all the coils and three out out of the four magnets are shown; the SA wire supporting last intermediate stage and the two wire loops are also visible steering. On the right it is possible to see the coils system.

Fig. 3.7.4 Seismic noise spectrum in Tombolo, taken in coincidence with an airplane.

Fig. 3.7.5 General lay-out of the interferometer.

Fig. 3.7.6 Central building (plan) showing the four vacuum tanks, the assembly laboratories, the clean area (white room).

Fig. 3.7.7 Central building, side view (section).

Fig. 3.7.8 Terminal building (plan).

Fig. 3.7.9 Terminal building, side view (section).

Fig. 3.7.10 The prestressed concrete channel containing the vacuum pipe and the service road.

Fig. 3.7.11 The channel at a pumping station (cross-section).

Fig. 3.7.12 The channel at a pumping station (plan).

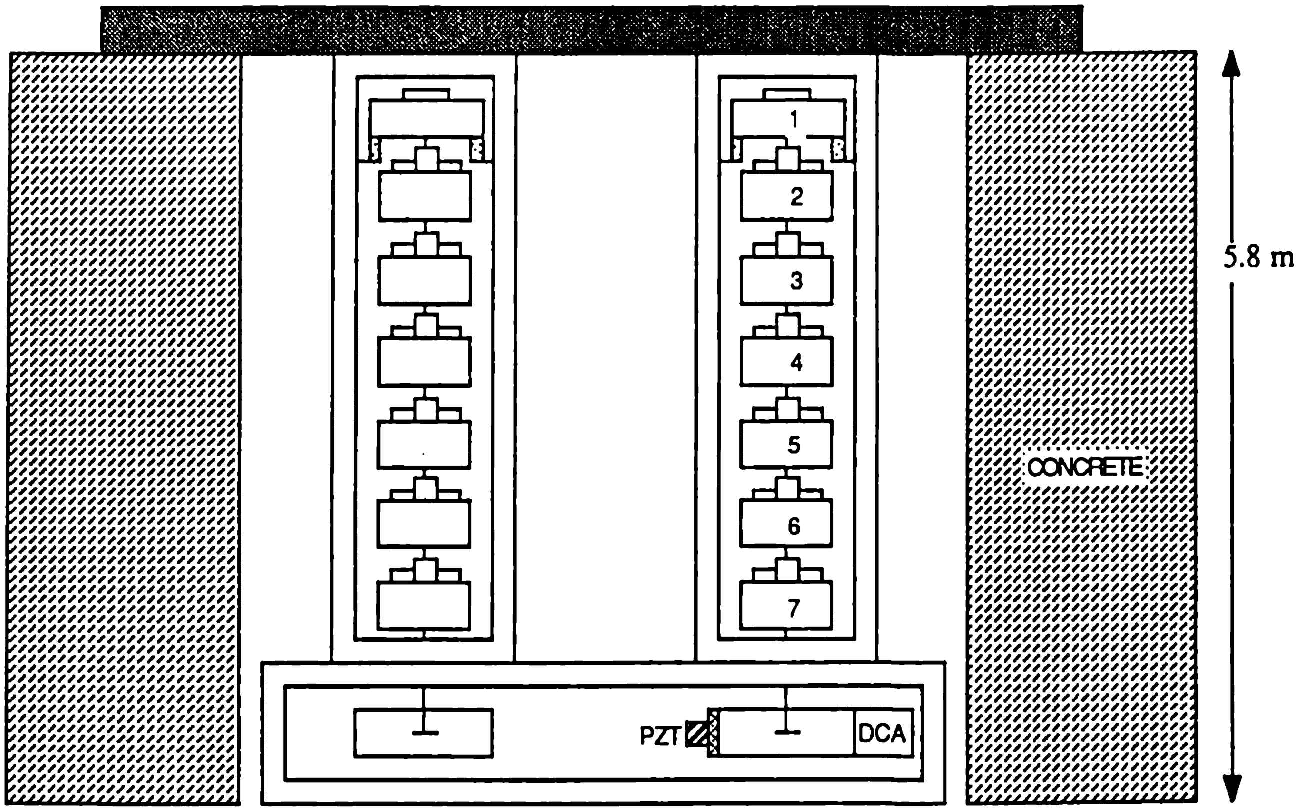

Fig. 3.4.1

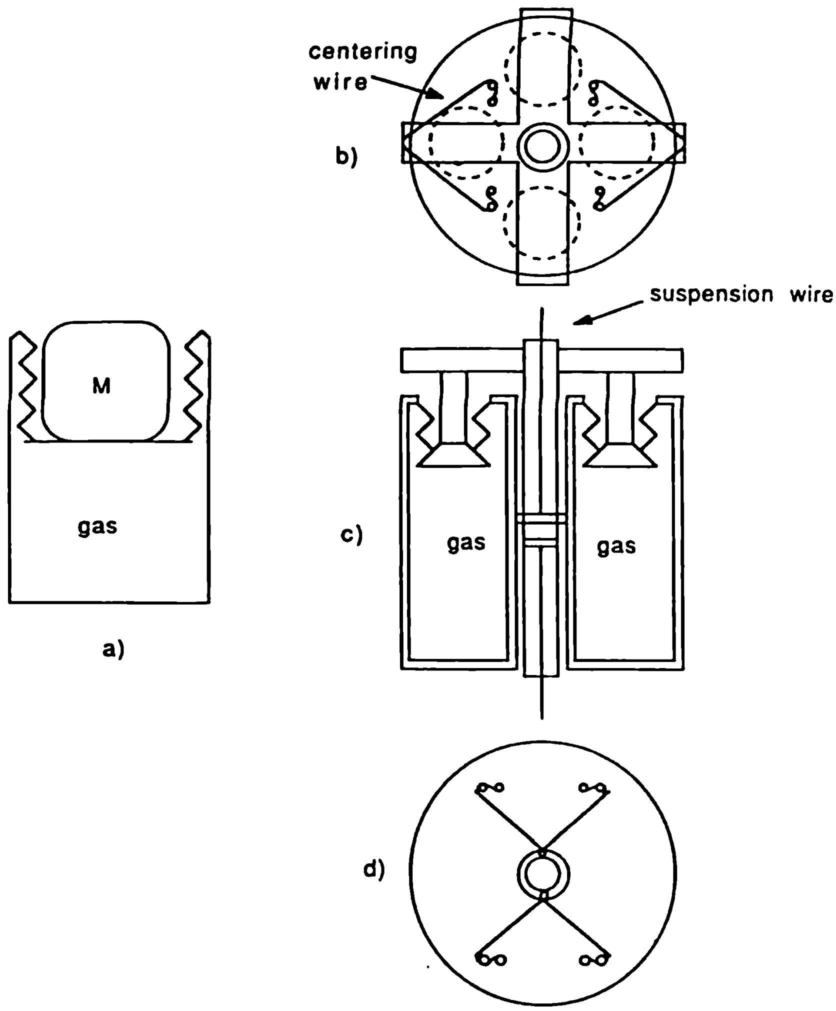

Fig. 3.4.2

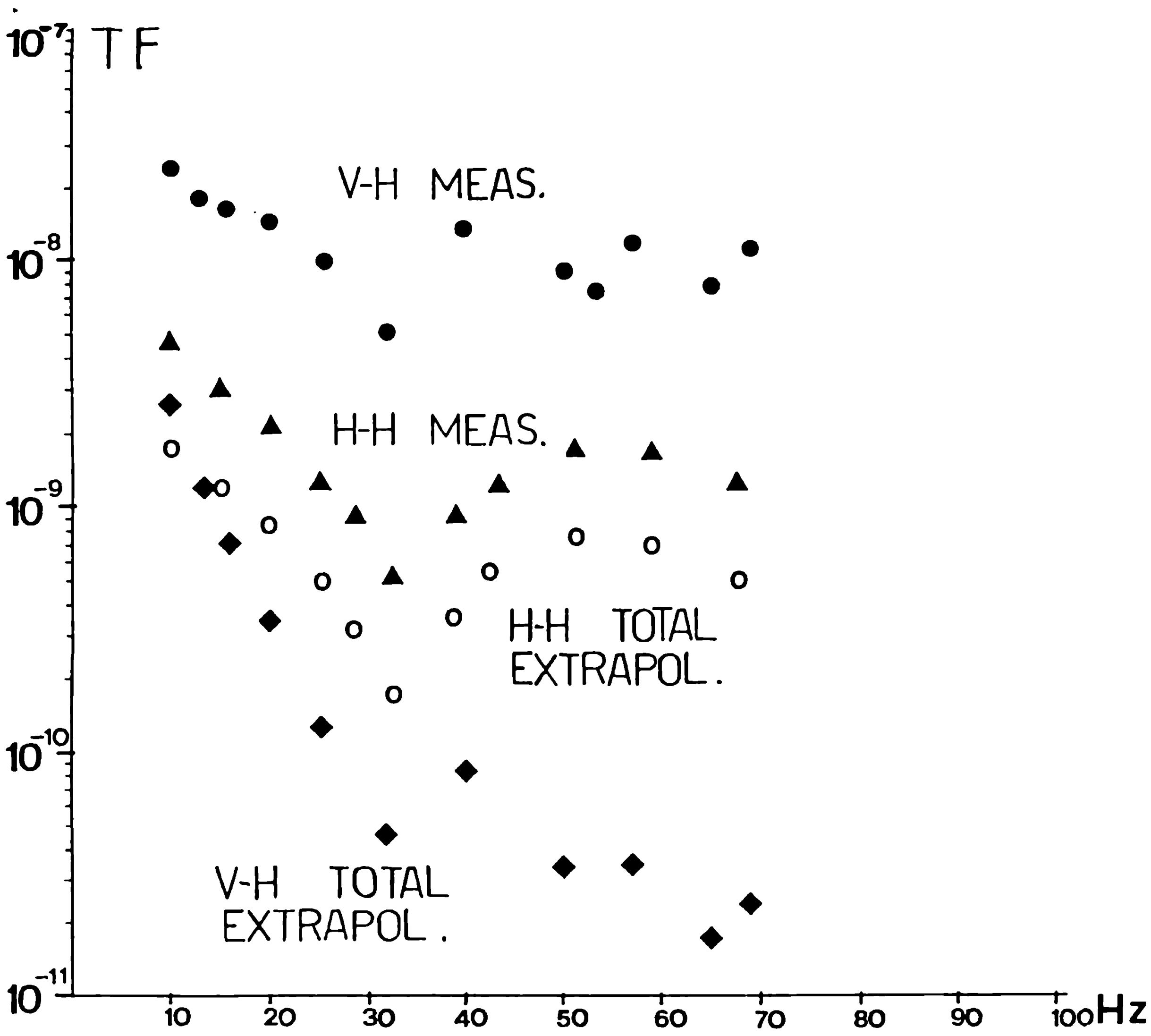
TF
10^{-7}
10^{-8}
10^{-9}
10^{-10}
10^{-11}
V-H MEAS.
H-H MEAS.
H-H TOTAL
EXTRAPOL.
V-H TOTAL
EXTRAPOL.
10
20
30
40
50
60
70
80
90
100 Hz

Fig. 3.4.3

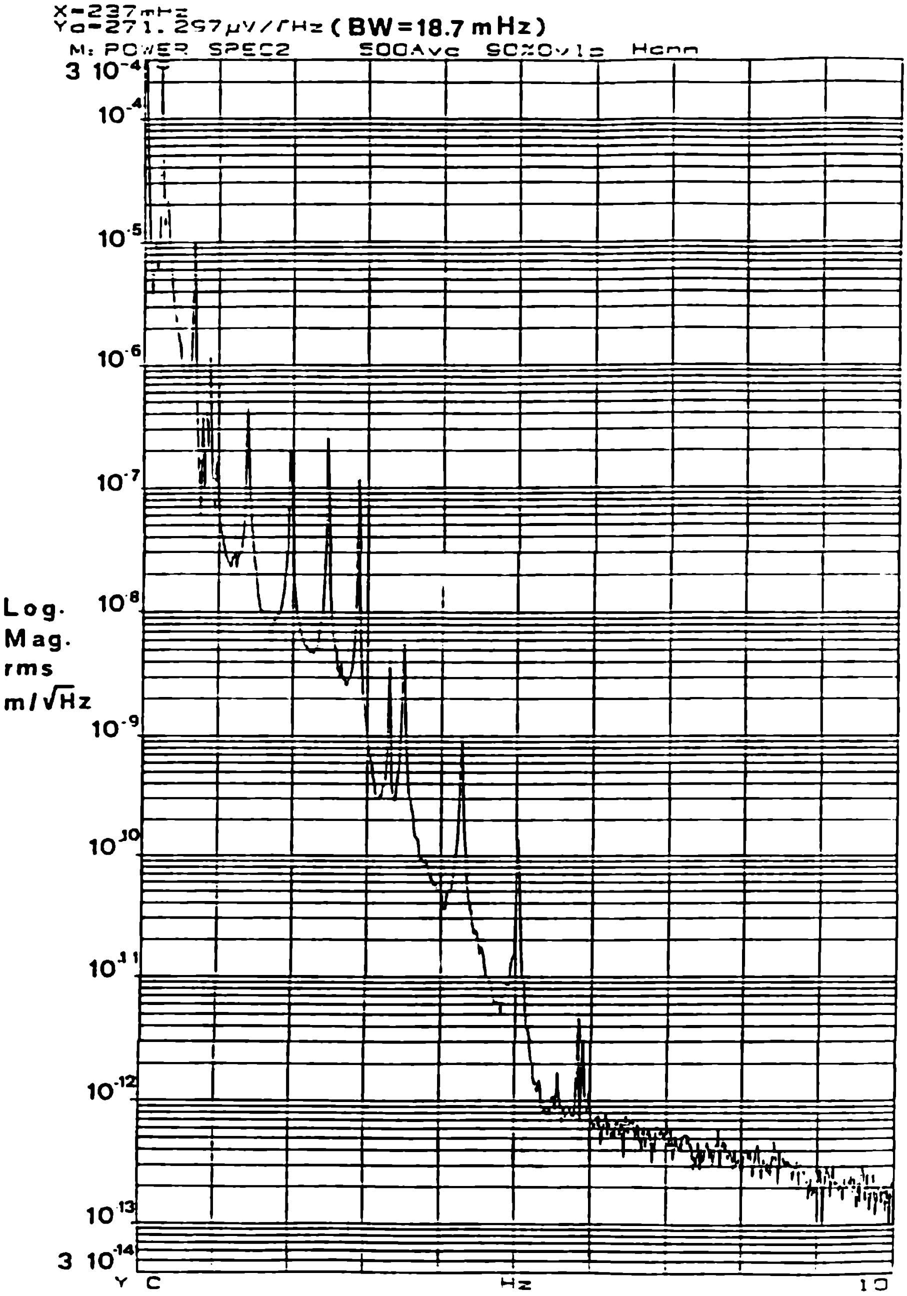
X=237mHz
Yo=271. 297µV/√Hz (BW=18.7 mHz)
M: POWER SPEC2 500Avg 50%Ovlp Hann
3 10^-4
10^-4
10^-5
10^-6
10^-7
10^-8
10^-9
10^-10
10^-11
10^-12
10^-13
3 10^-14
Log. Mag. rms m/√Hz
Y C
Hz
10

Fig. 3.4.4

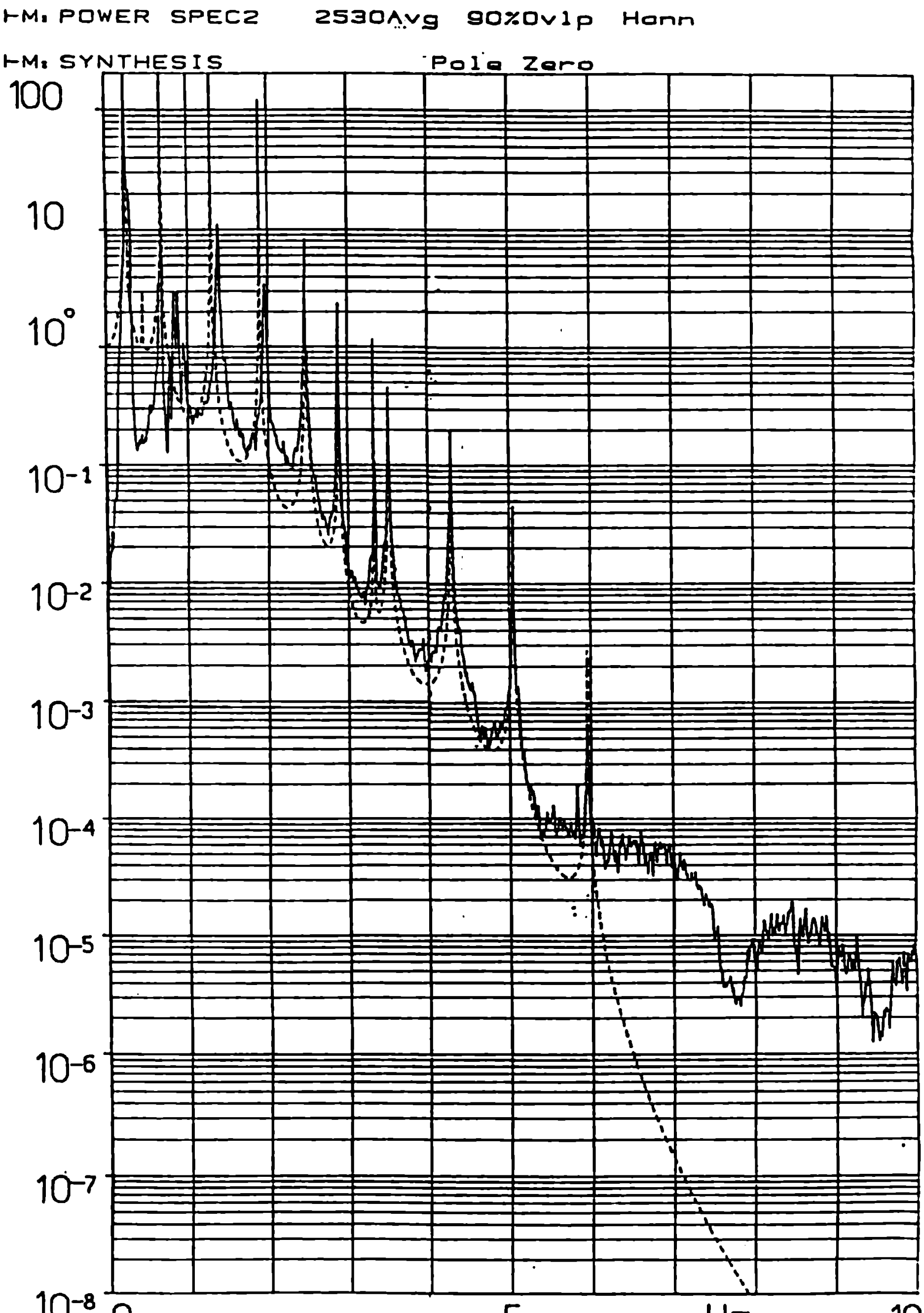

⊢M: POWER SPEC2 2530Avg 90%Ovlp Hann
⊢M: SYNTHESIS Pole Zero
100
10
10°
10-1
10-2
10-3
10-4
10-5
10-6
10-7
10-8
0
5
Hz
10

Fig. 3.4.5

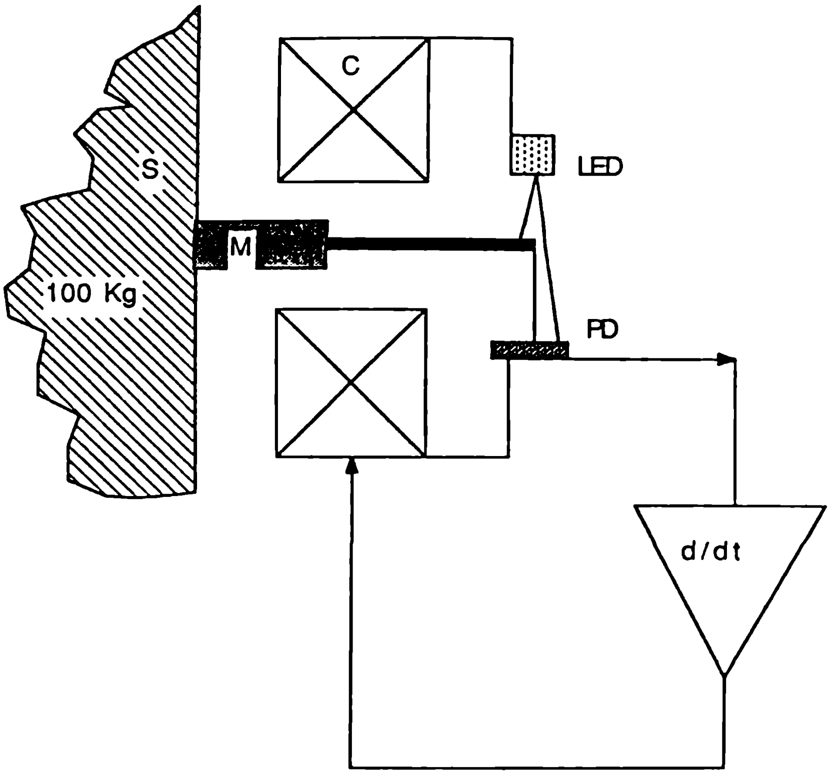

Fig. 3.4.6

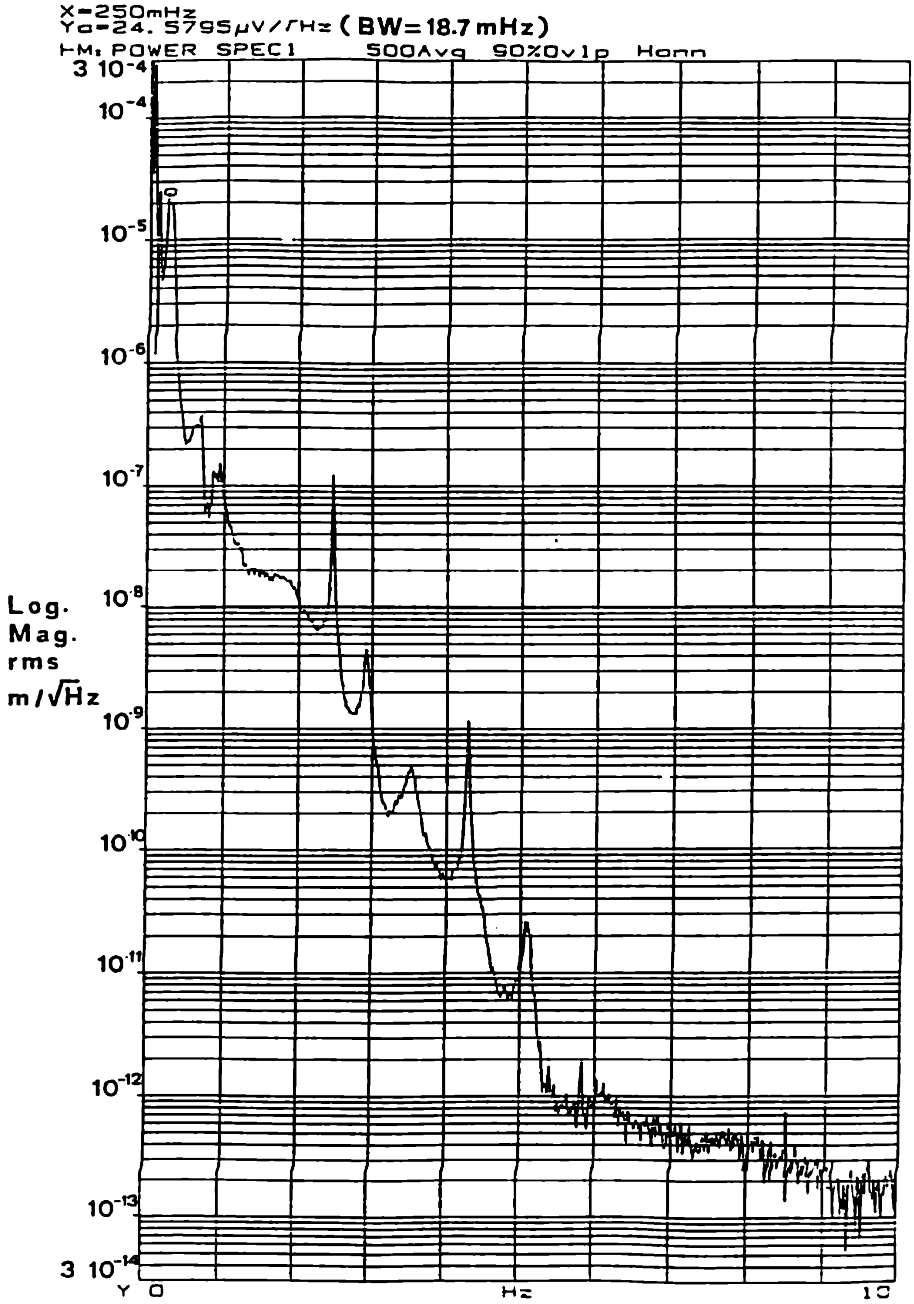
X=250mHz
Yo=24. 5795μV/√Hz (BW=18.7 mHz)
FM, POWER SPEC1 500Avg 50%Ovlp Honn
3 10^-4
10^-4
10^-5
10^-6
10^-7
10^-8
10^-9
10^-10
10^-11
10^-12
10^-13
3 10^-14
Log. Mag. rms m/√Hz
Y 0
Hz
10

Fig. 3.4.7

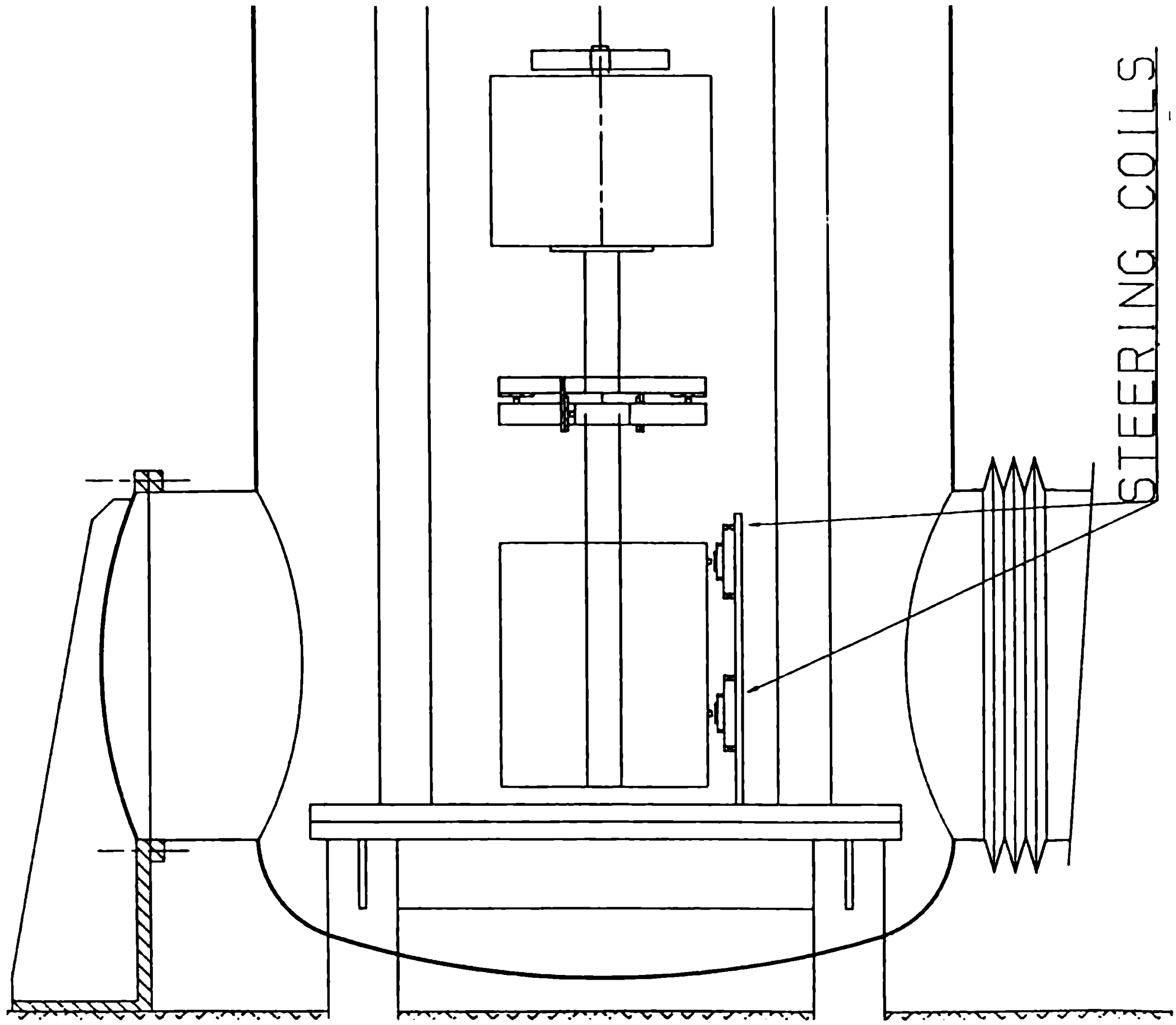

Fig. 3.4.8

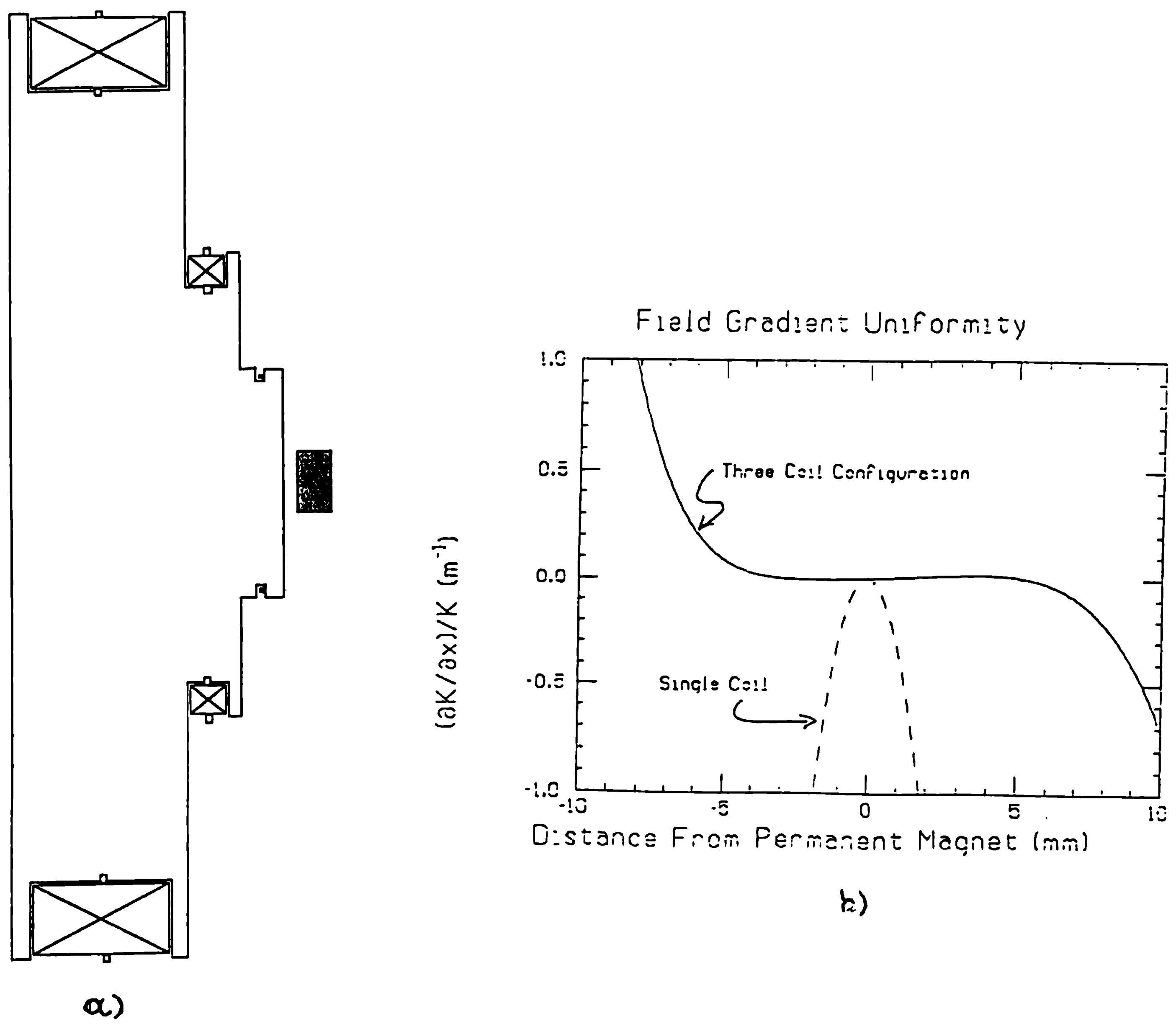
a)
Field Gradient Uniformity
Three Coil Configuration
Single Coil
(∂K/∂x)/K (m^-1)
1.0
0.5
0.0
-0.5
-1.0
-10
-5
0
5
10
Distance From Permanent Magnet (mm)
b)

Fig. 3.4.9

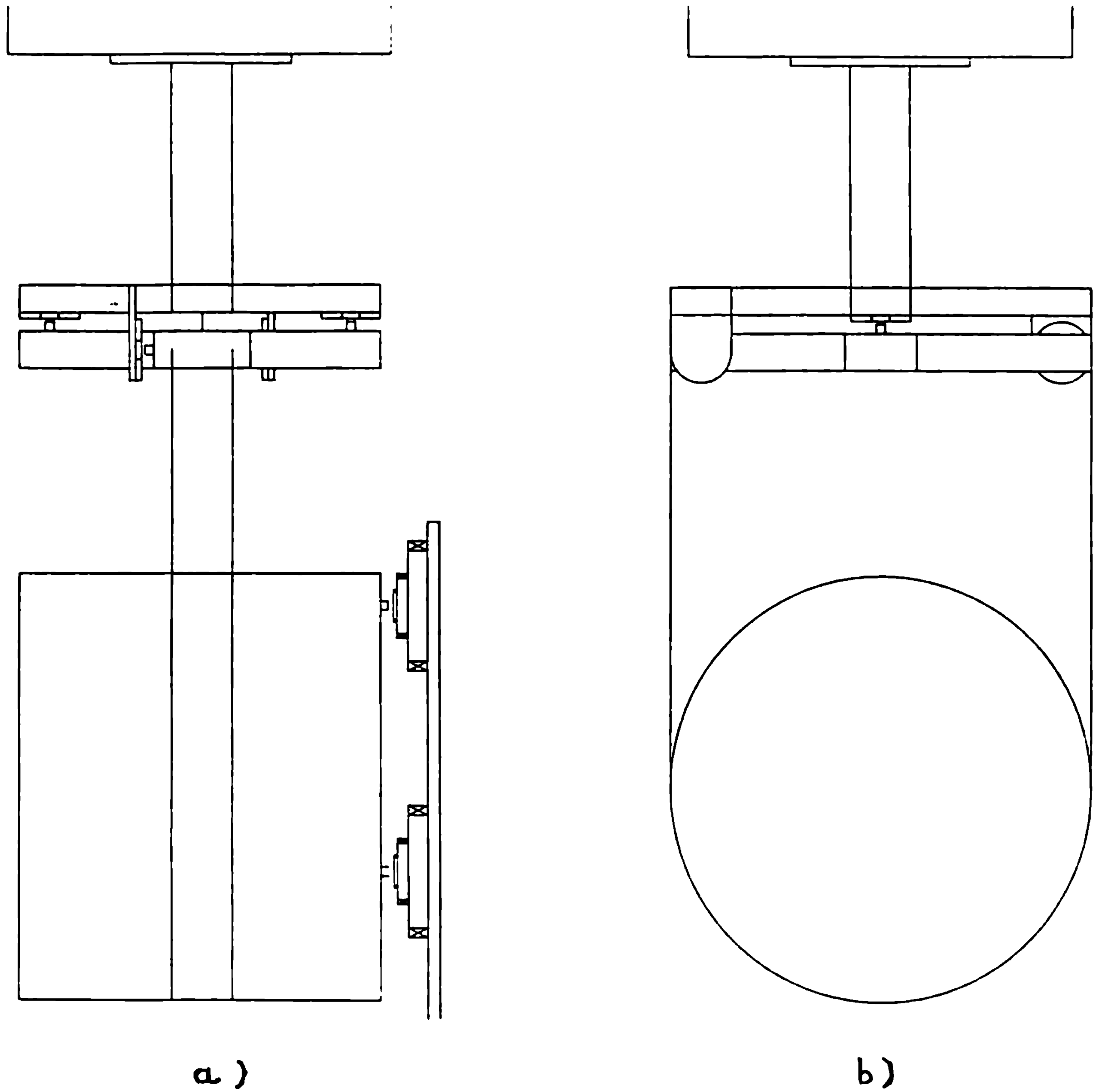

Fig. 3.4.10

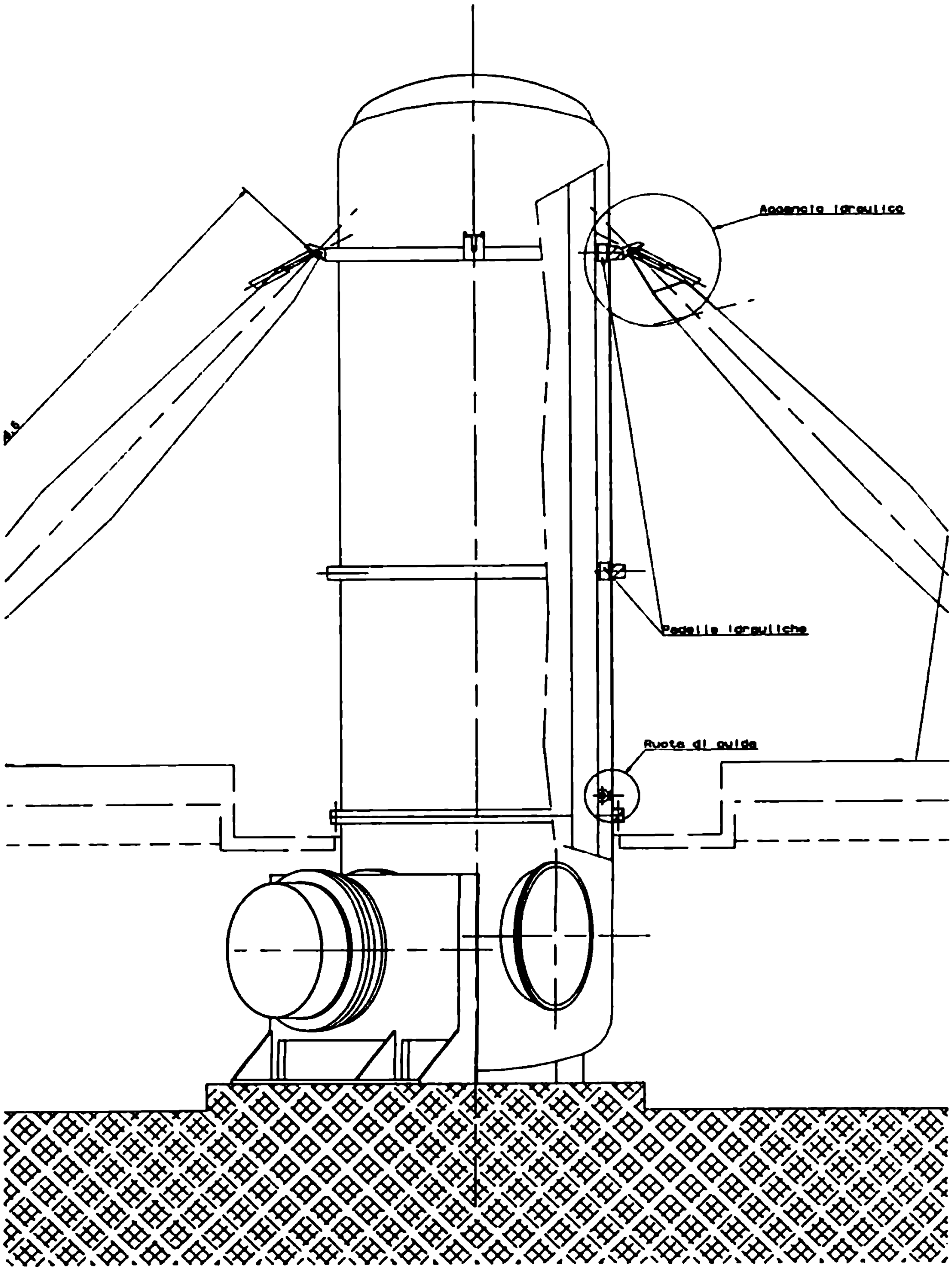

Fig. 3.4.11

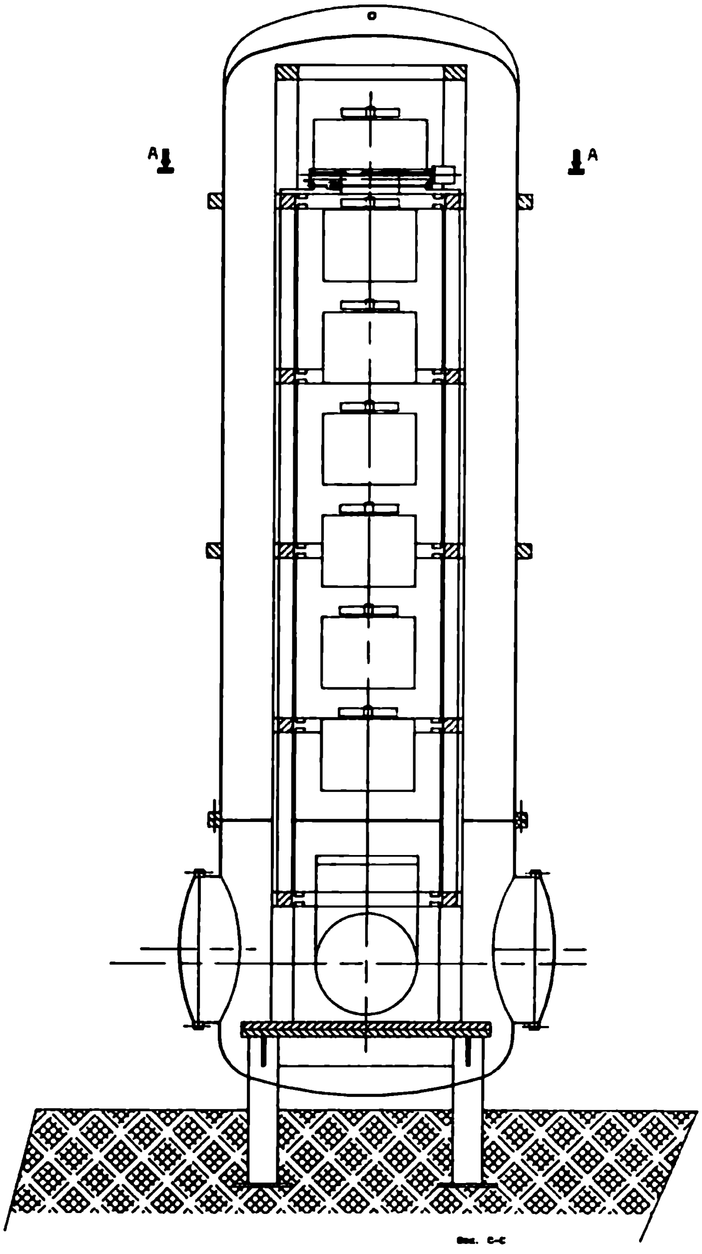

Fig. 3.4.12

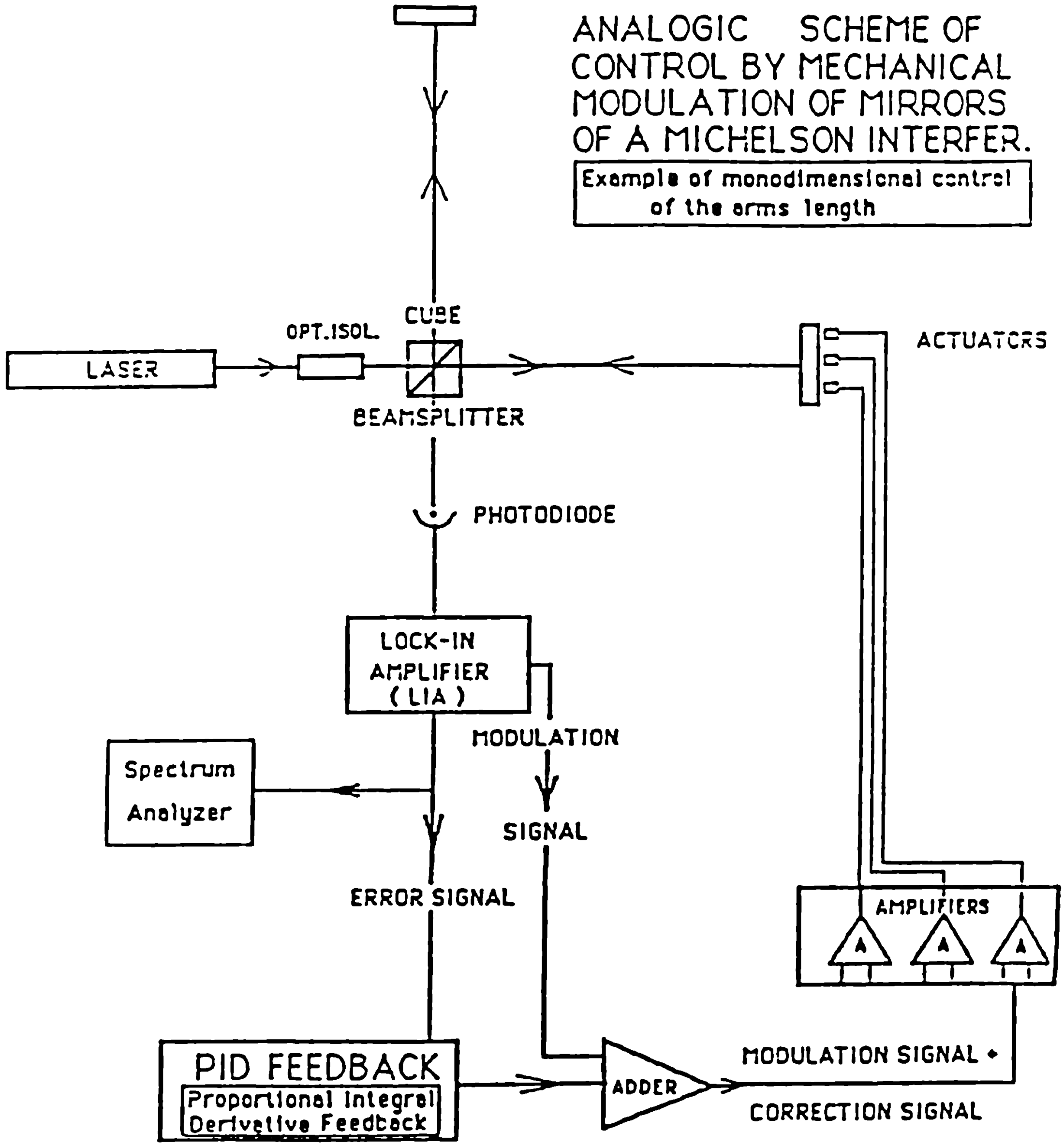
ANALOGIC SCHEME OF CONTROL BY MECHANICAL MODULATION OF MIRRORS OF A MICHELSON INTERFER.
Example of monodimensional control of the arms length
OPT.ISOL.
CUBE
LASER
BEAMSPLITTER
ACTUATORS
PHOTODIODE
LOCK-IN AMPLIFIER (LIA)
MODULATION
SIGNAL
Spectrum Analyzer
ERROR SIGNAL
AMPLIFIERS
A
A
A
PID FEEDBACK
Proportional Integral Derivative Feedback
ADDER
MODULATION SIGNAL +
CORRECTION SIGNAL

Fig. 3.5.1

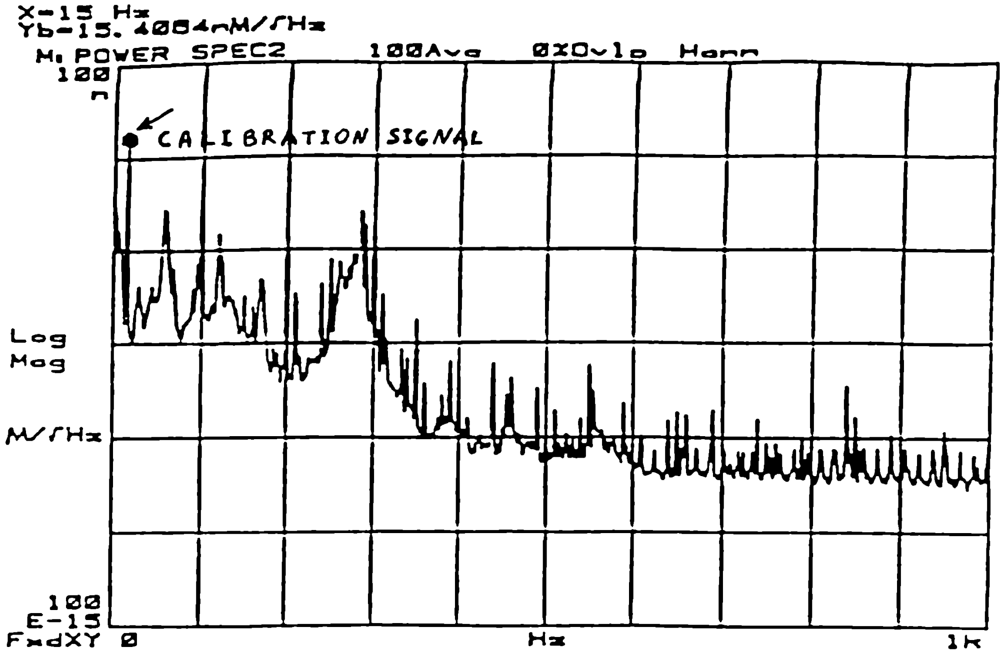

Fig. 3.5.2 a

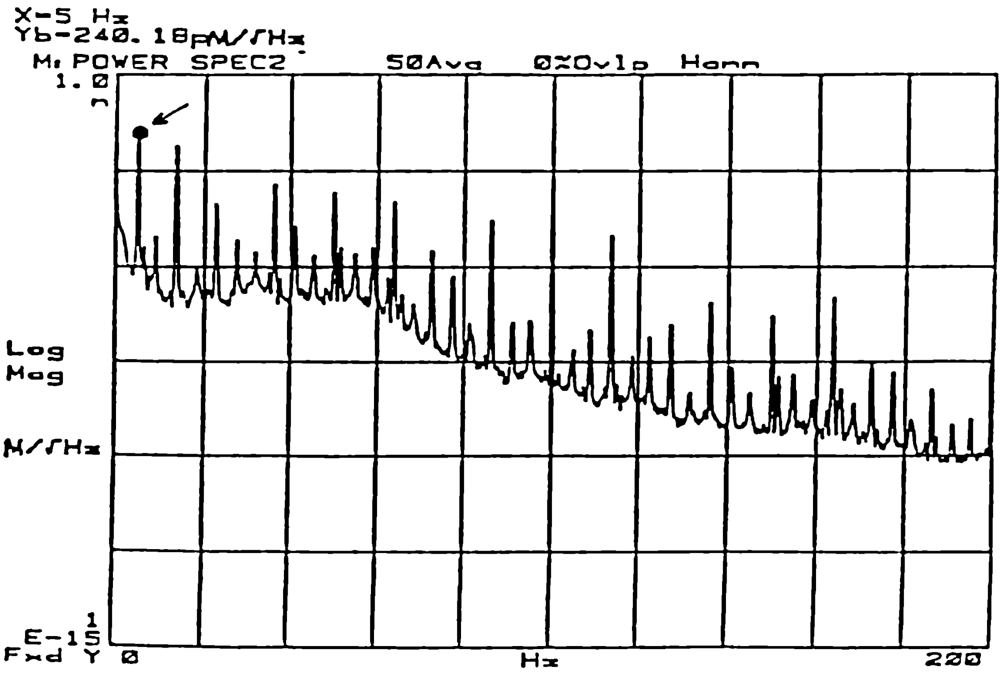

Fig. 3.5.2 b

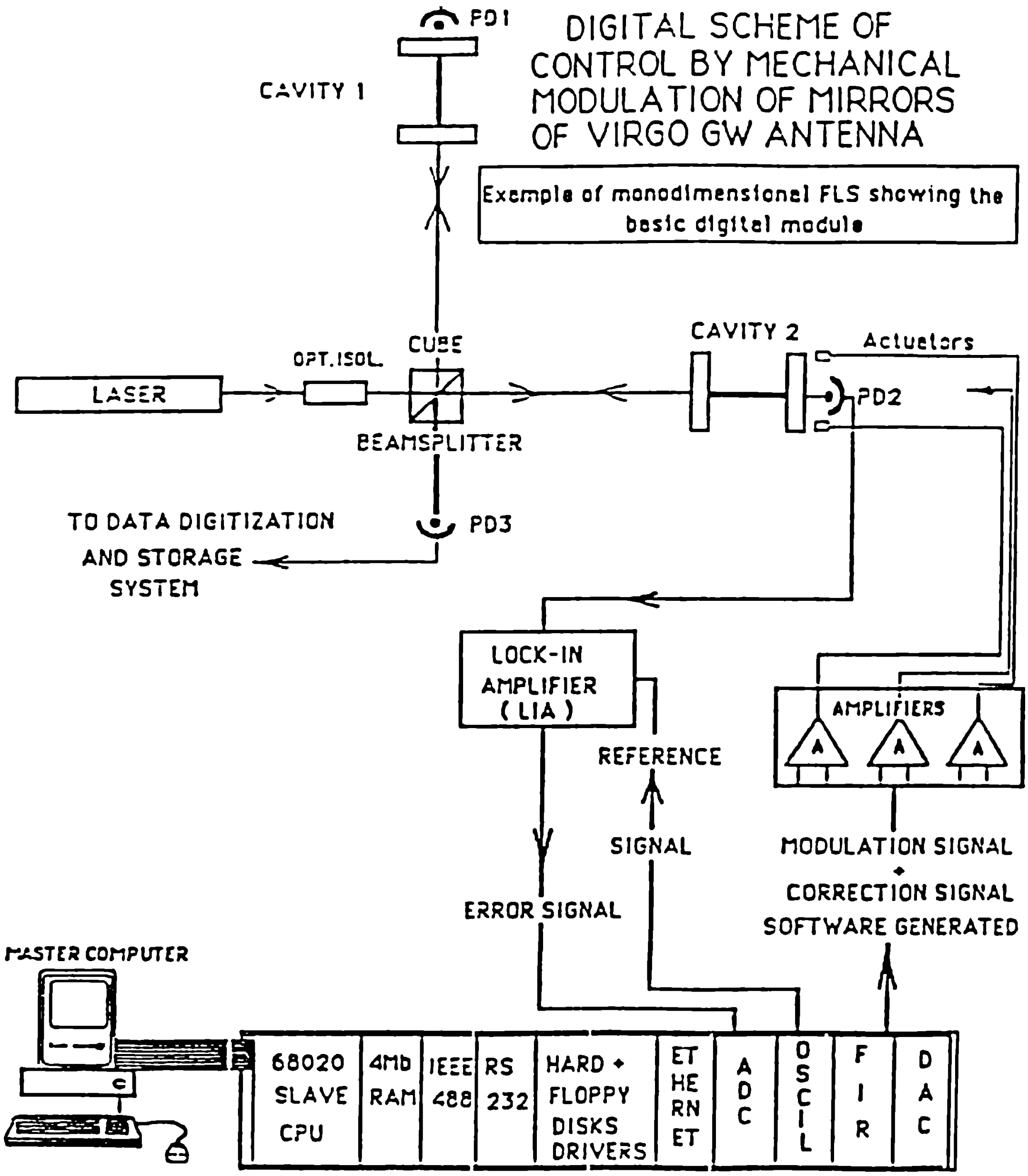

DIGITAL SCHEME OF CONTROL BY MECHANICAL MODULATION OF MIRRORS OF VIRGO GW ANTENNA
Exemple of monodimensional FLS showing the basic digital module
PD1
CAVITY 1
CAVITY 2
Actuators
LASER
OPT. ISOL.
CUBE
BEAMSPLITTER
PD2
PD3
TO DATA DIGITIZATION AND STORAGE SYSTEM
LOCK-IN AMPLIFIER (LIA)
REFERENCE
SIGNAL
ERROR SIGNAL
AMPLIFIERS
A
MODULATION SIGNAL + CORRECTION SIGNAL SOFTWARE GENERATED
MASTER COMPUTER
68020 SLAVE CPU
4Mb RAM
IEEE 488
RS 232
HARD + FLOPPY DISKS DRIVERS
ETHERNET
ADC
OSCIL
FIR
DAC

Fig. 3.5.3

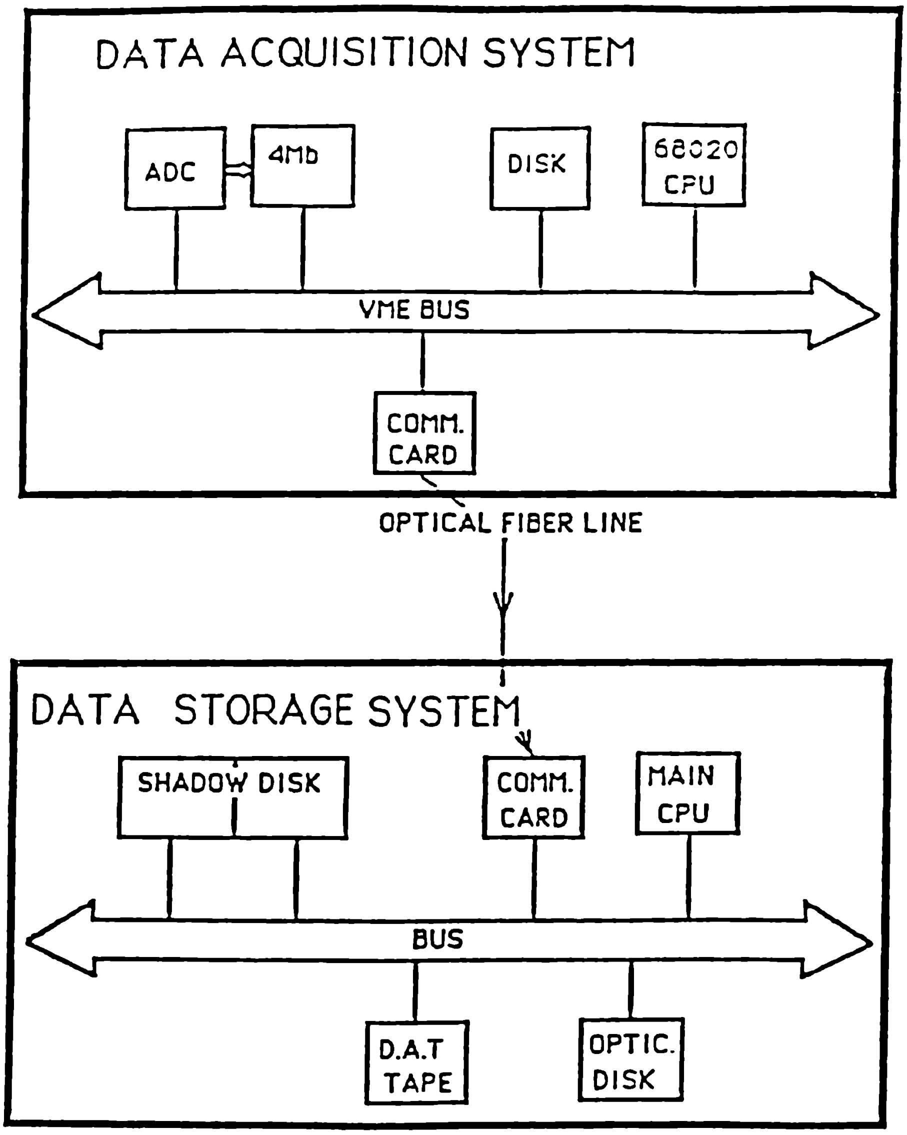
DATA ACQUISITION SYSTEM
ADC
4Mb
DISK
68020
CPU
VME BUS
COMM.
CARD
OPTICAL FIBER LINE
DATA STORAGE SYSTEM
SHADOW DISK
COMM.
CARD
MAIN
CPU
BUS
D.A.T
TAPE
OPTIC.
DISK

Fig. 3.5.4

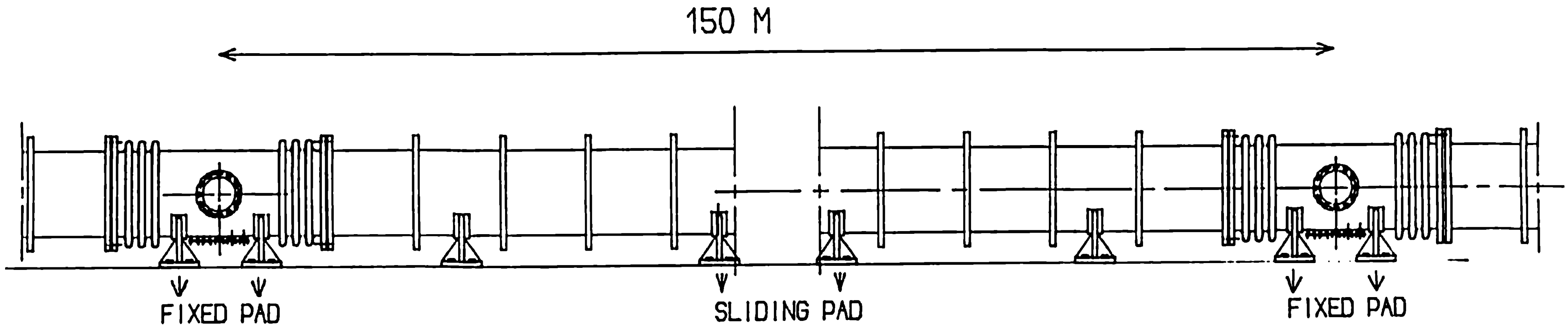

Fig. 3.6.1

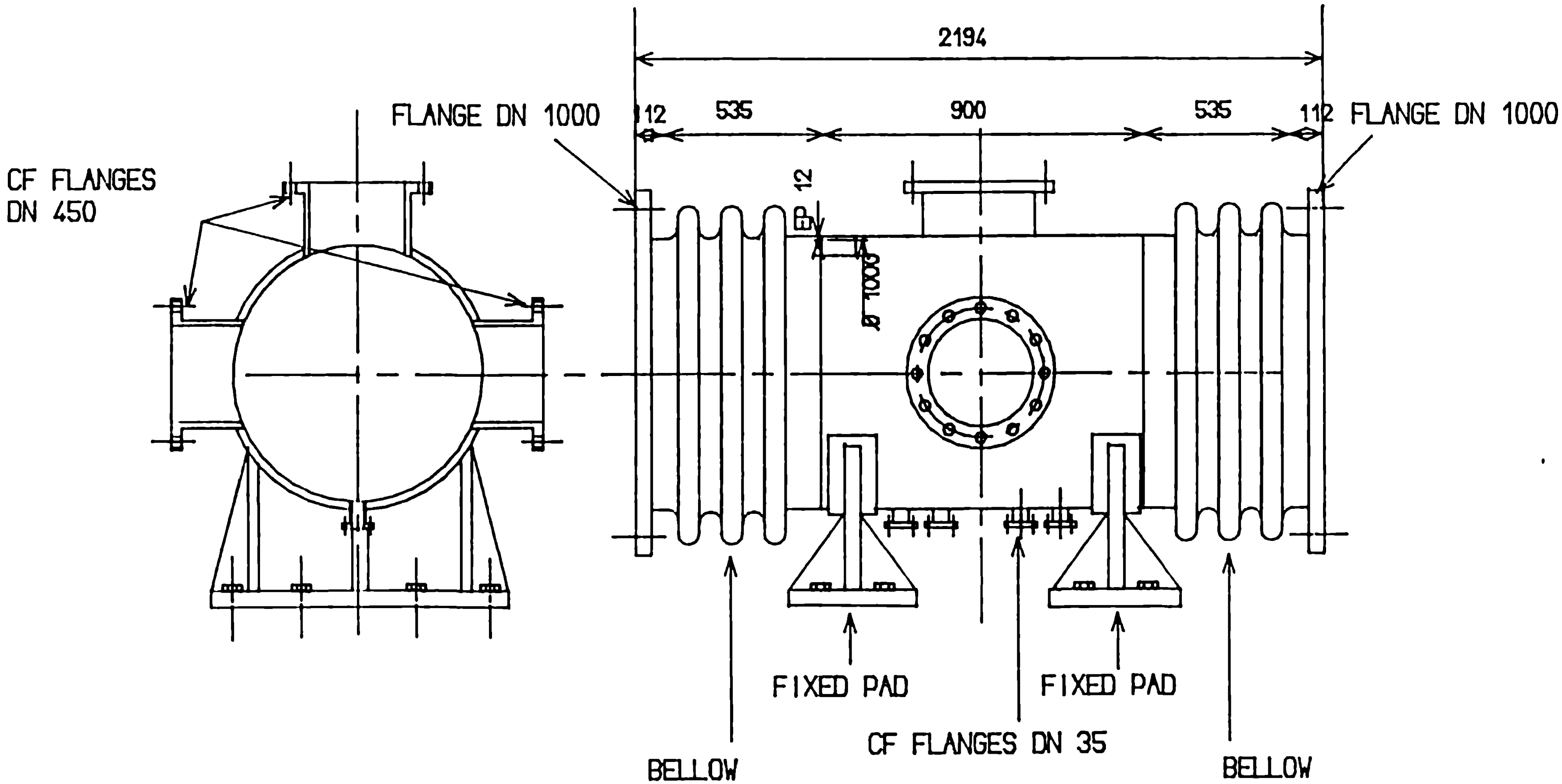

CF FLANGES
DN 450
FLANGE DN 1000
2194
12
535
900
535
112
FLANGE DN 1000
EP 12
Ø 1000
FIXED PAD
FIXED PAD
CF FLANGES DN 35
BELLOW
BELLOW

Fig. 3.6.2

Fig. 3.7.1

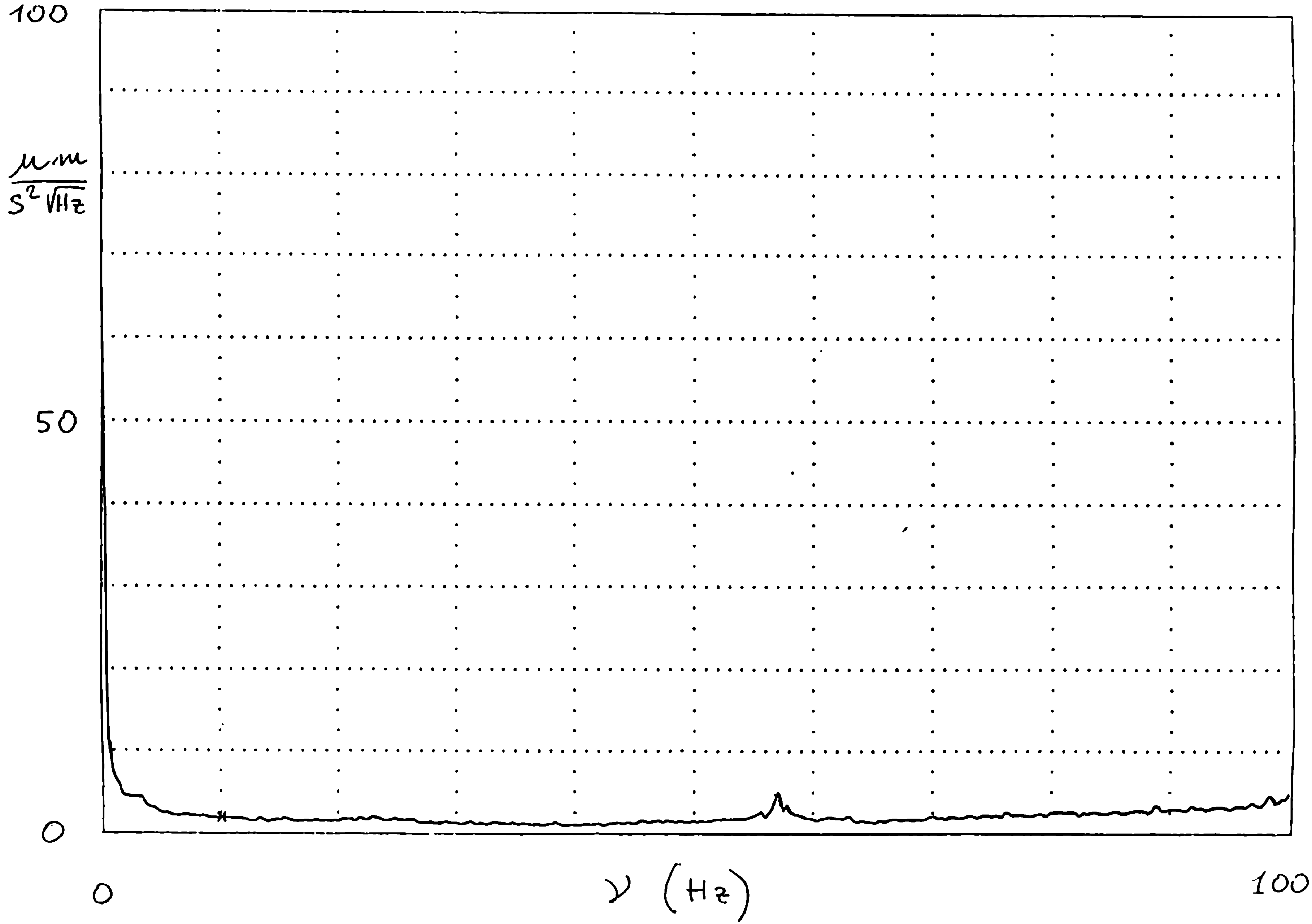

Fig. 3.7.2

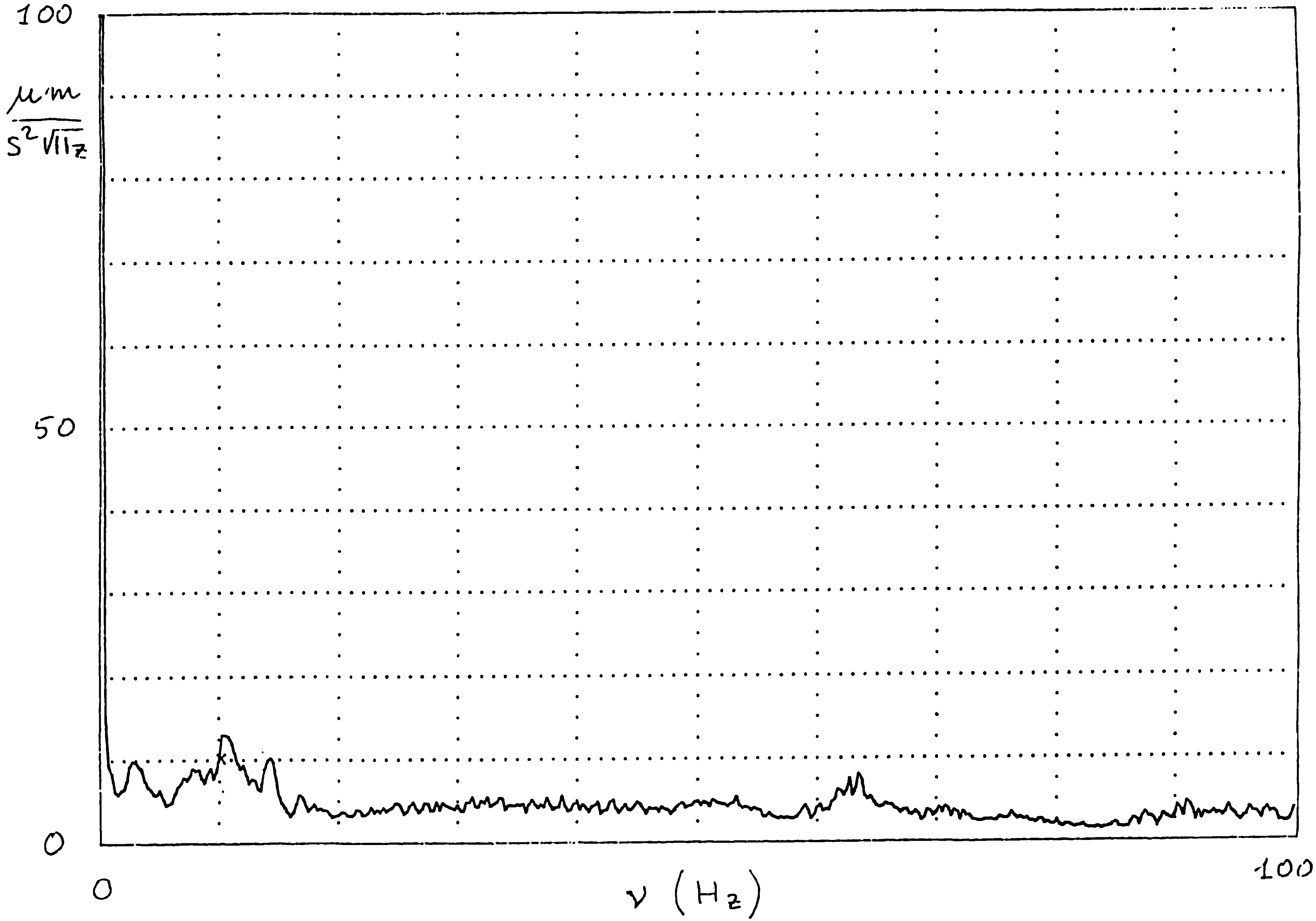

Fig. 3.7.3

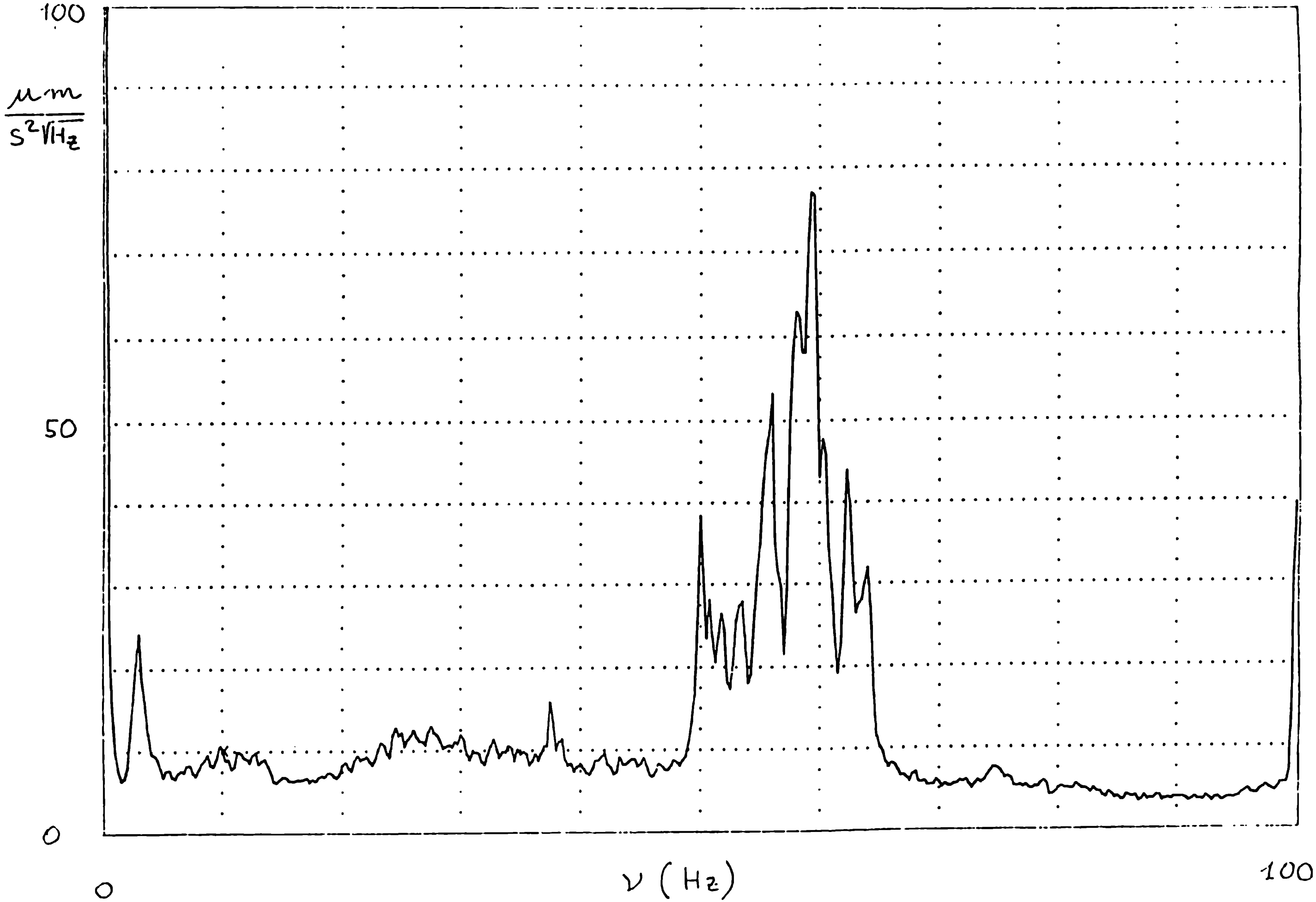

Fig. 3.7.4

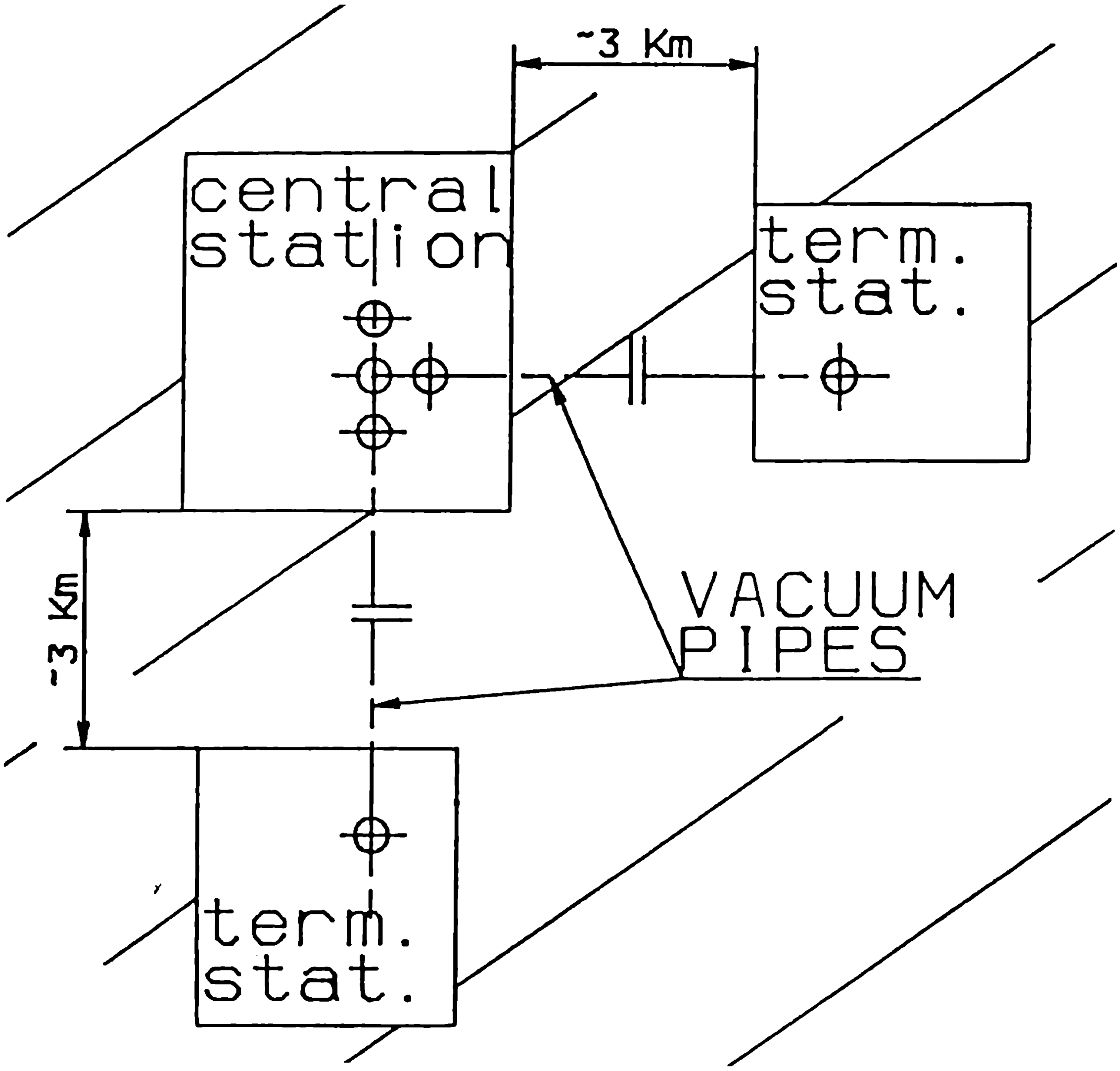

Fig. 3.7.5

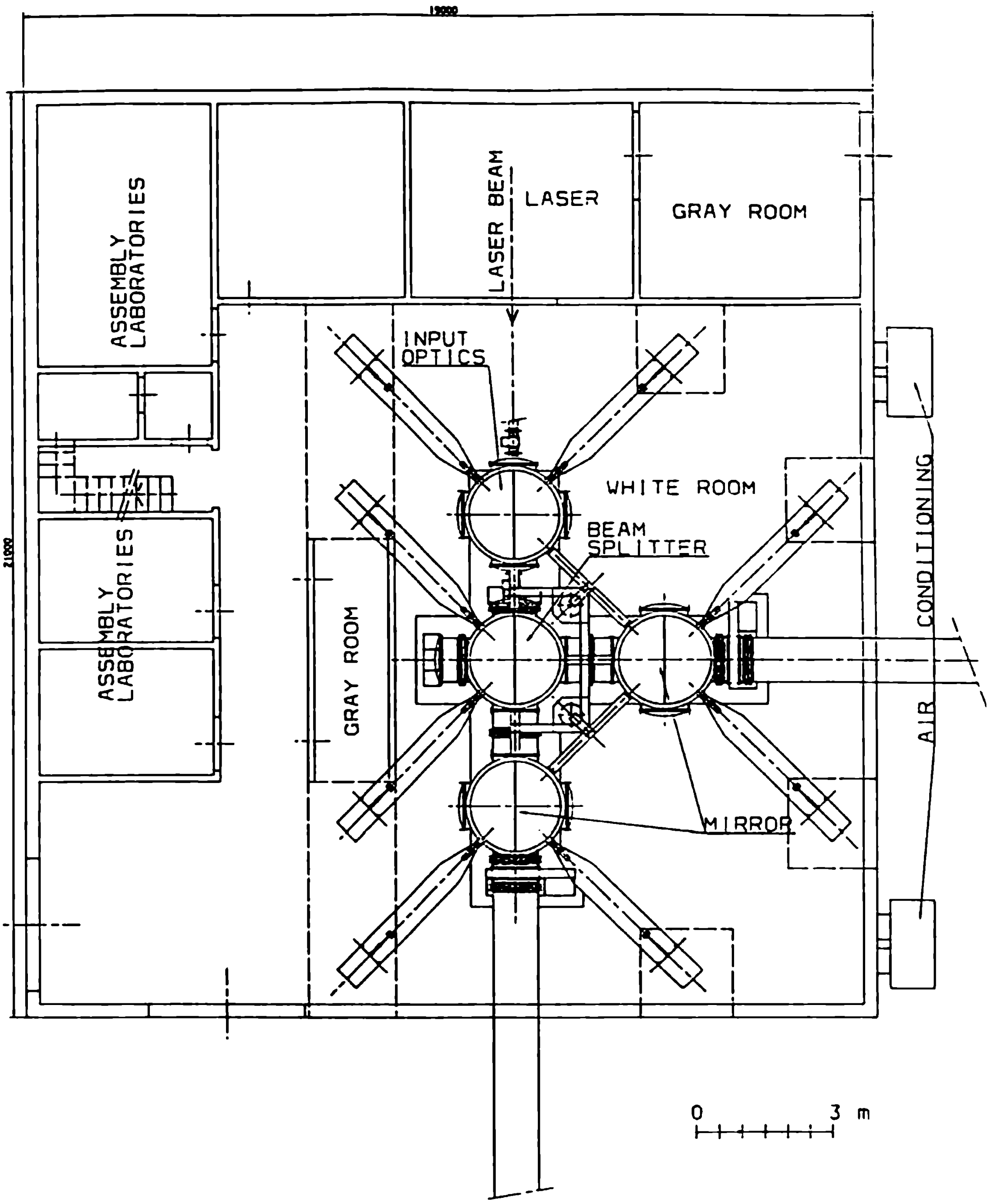
19000
21000
ASSEMBLY LABORATORIES
LASER BEAM
LASER
GRAY ROOM
INPUT OPTICS
WHITE ROOM
BEAM SPLITTER
ASSEMBLY LABORATORIES
GRAY ROOM
AIR CONDITIONING
MIRROR
0
3 m

Fig. 3.7.6

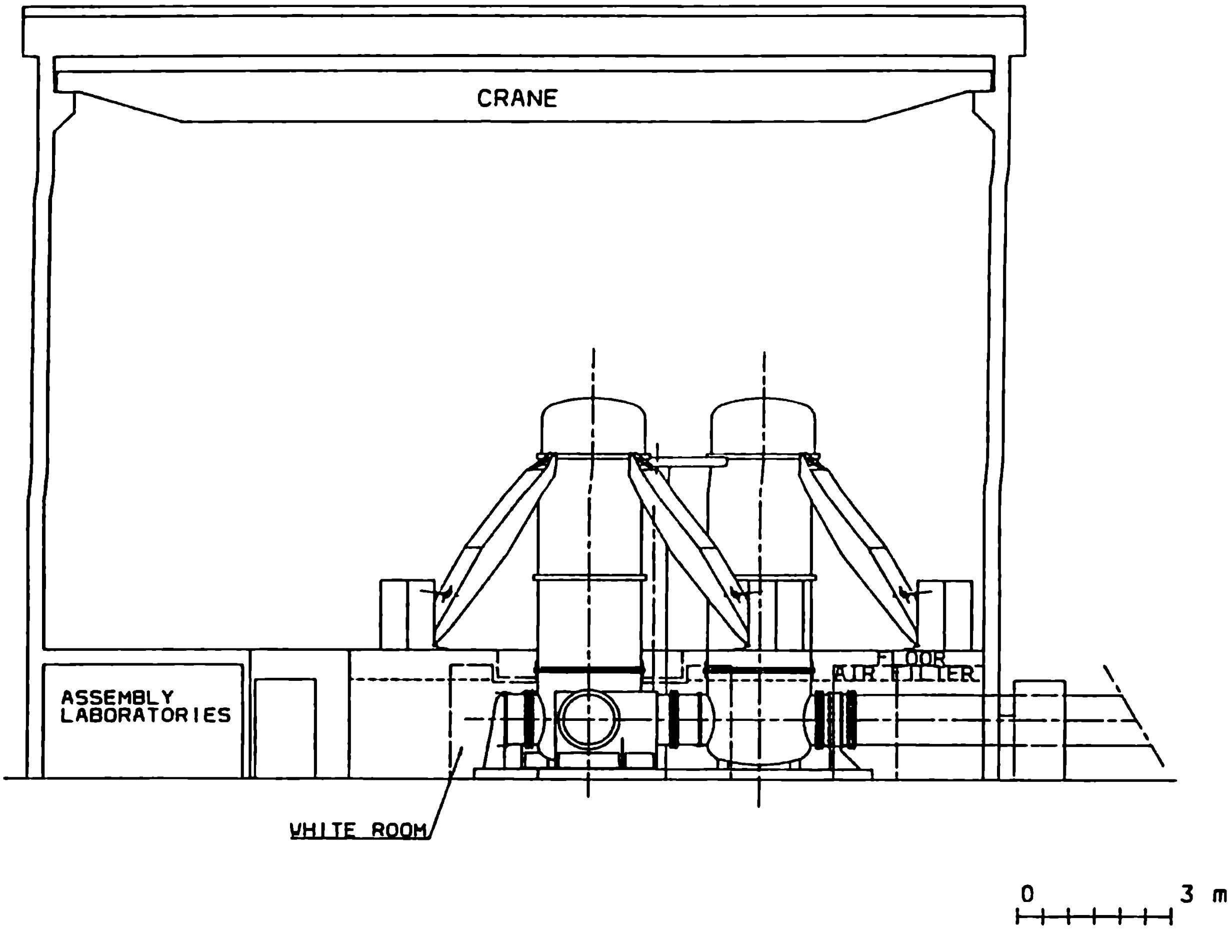
CRANE
ASSEMBLY
LABORATORIES
WHITE ROOM
FLOOR
AIR FILTER
0
3 m

Fig. 3.7.7

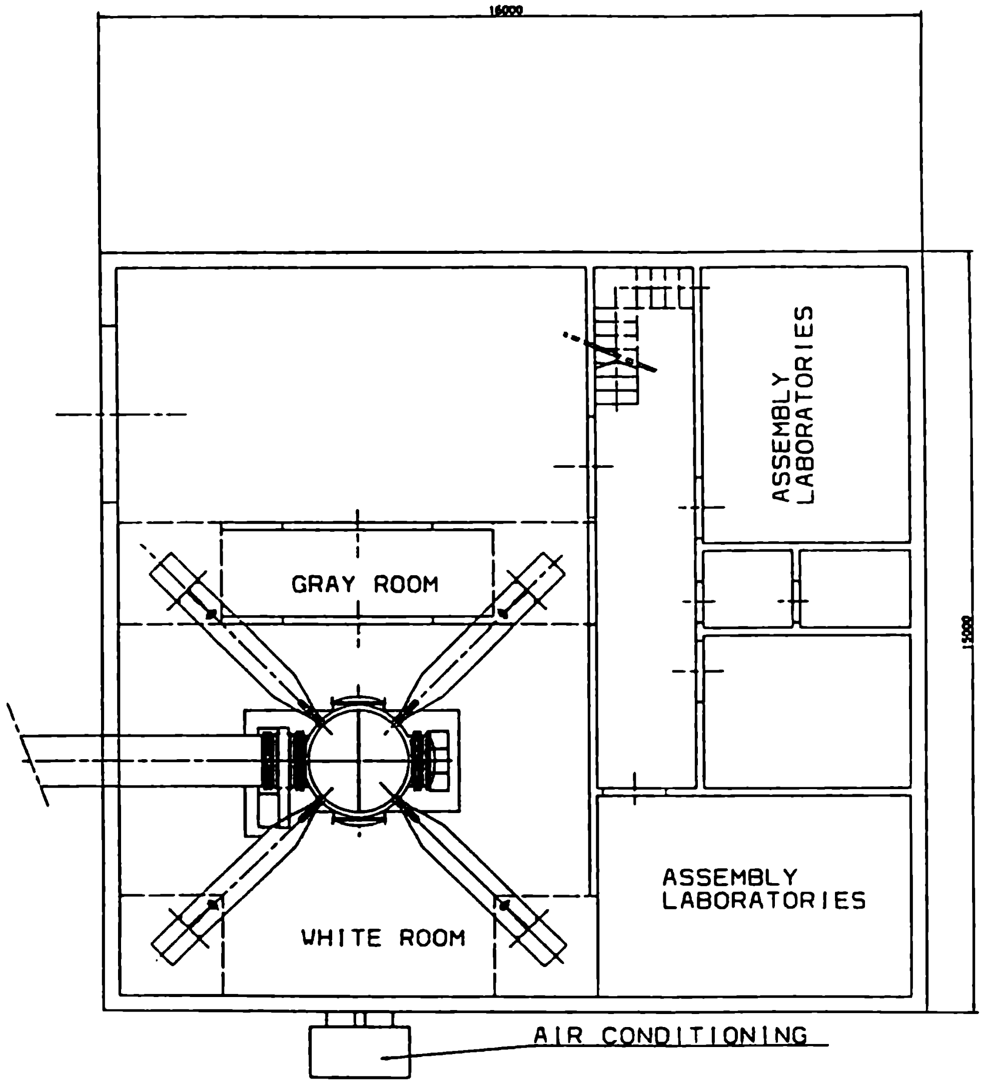
16000
15000
GRAY ROOM
WHITE ROOM
ASSEMBLY LABORATORIES
ASSEMBLY LABORATORIES
AIR CONDITIONING

Fig. 3.7.8

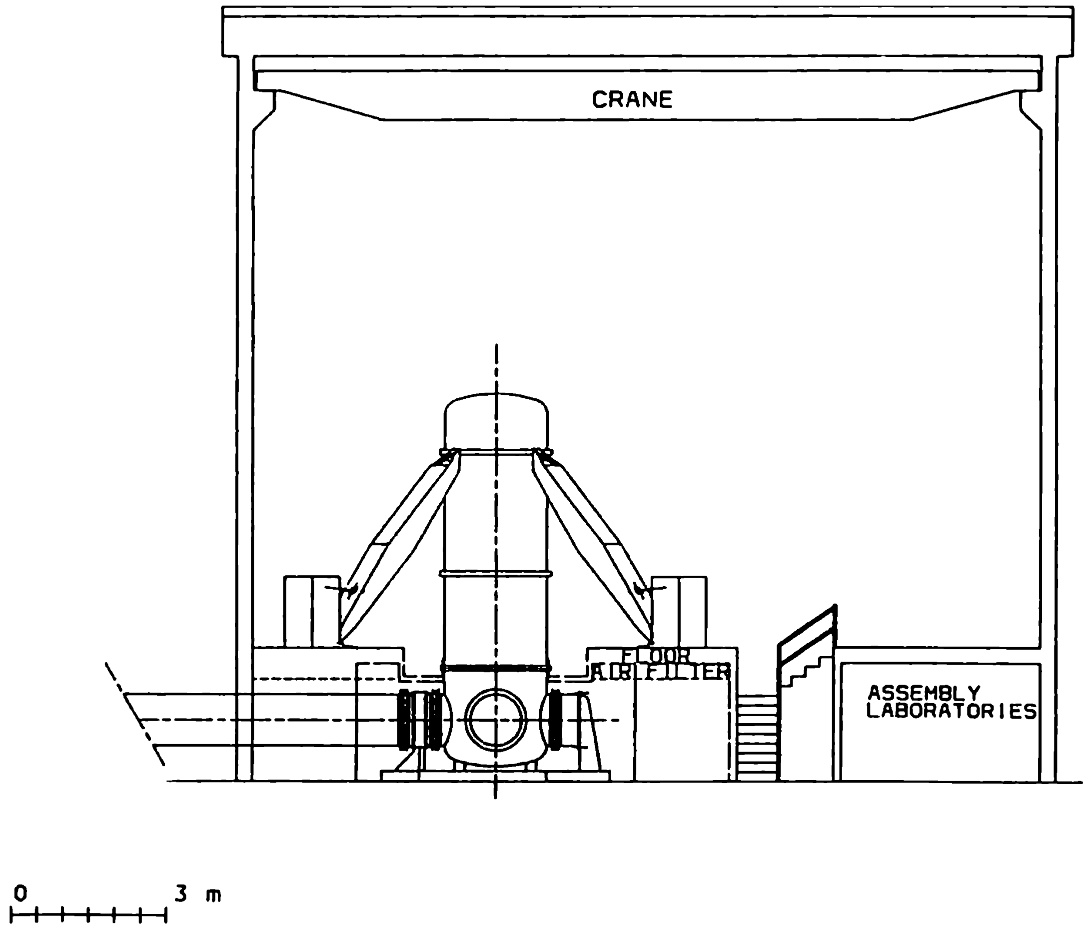

Fig. 3.7.9

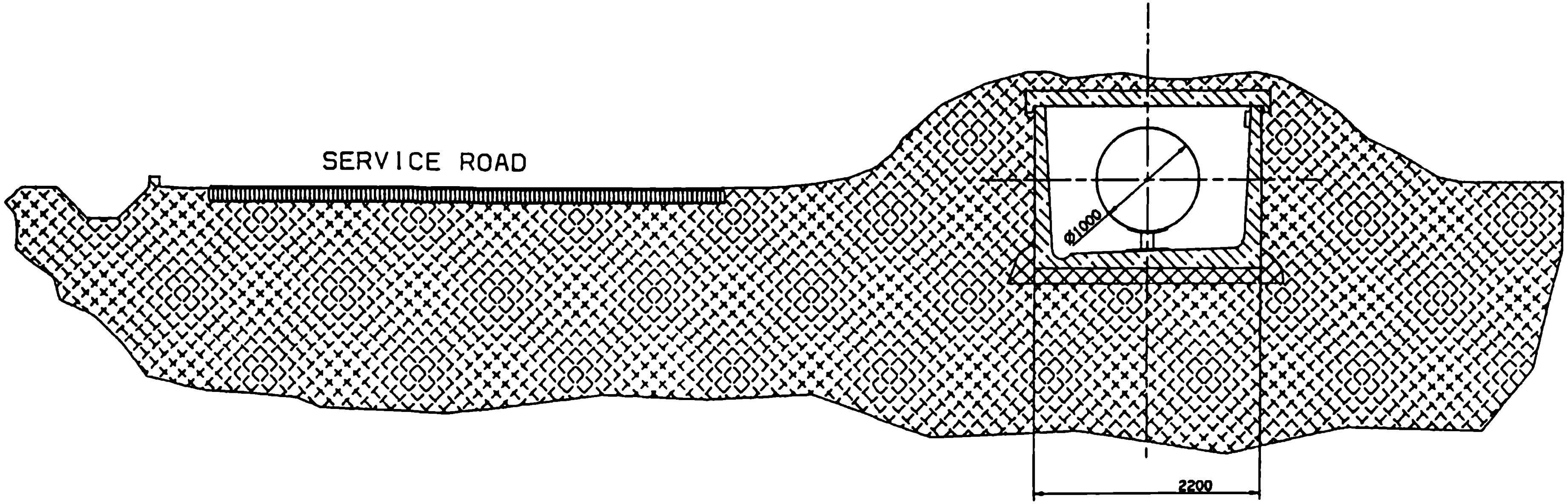

Fig. 3.7.10

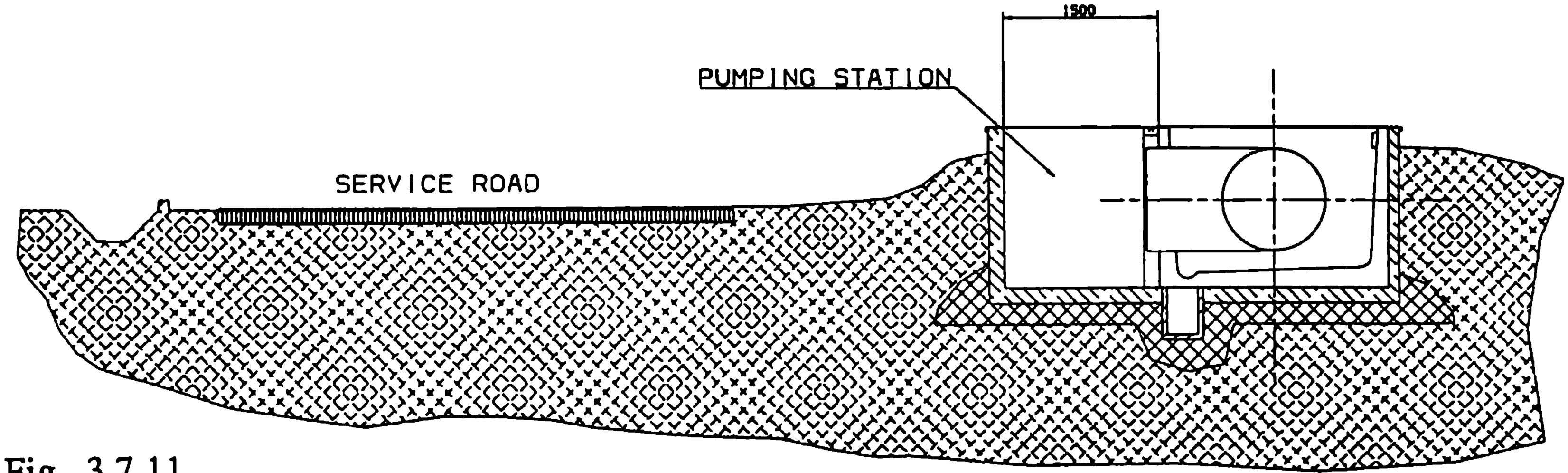

Fig. 3.7.11

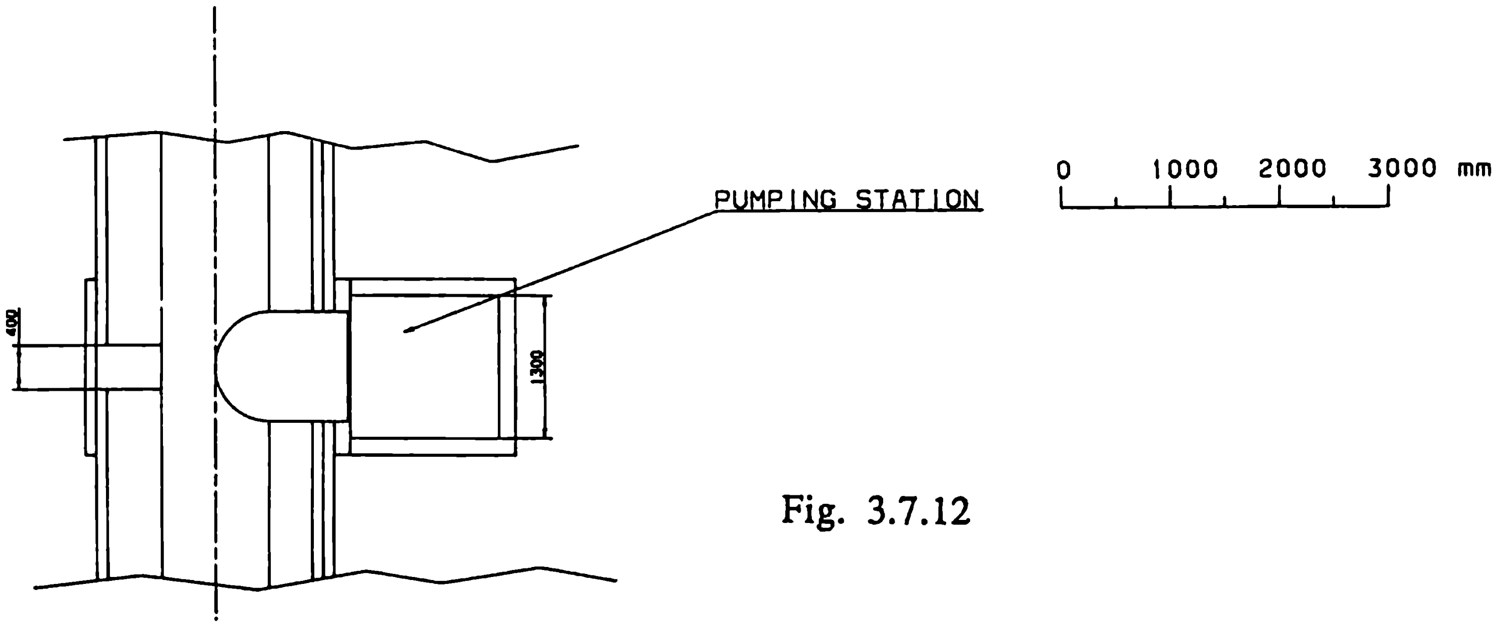

Fig. 3.7.12

Chapter 4

Description of VIRGO

4.1) The VIRGO collaboration

4.1.1) THE PRESENT COLLABORATION

The first step of the collaboration which has led to the VIRGO project was taken in fall 1986, when the GROG in Orsay and the IRAS group in Pisa, which were the two experimental groups most recently involved in the domain of Gravitational Waves Detection, realized their complementarity and decided to work together. In May 1987, they presented to INFN the first declaration of intention concerning the construction of a large interferometer, together with physicists and engineers from Frascati, Napoli, Paris and Salerno.
From the beginning, the roles in the collaboration are well defined as concerns the experimentalists:

- INFN-Pisa is responsible for the seismic isolation system, the data acquisition, the vacuum system and the site selection
- GROG-Orsay is responsible for the optics, the interferometry, the laser source and the vacuum system
- INFN-Napoli is responsible for the automatic alignment and control system.

As concerns the theoretical aspects:

- sources are studied in GROG-Meudon (binaries and supernovae) and in Napoli-Salerno (pulsars)
- the "physics of the experiment" are studied in the GROG-Paris and also in Salerno
- modelisation studies are done mainly inside the GROG-Palaiseau, but complementary work is done in Pisa and Napoli
- data analysis is being studied complementarily in INFN-Pisa, in GROG-Paris, in Meudon, in Naples and Salerno.

A complete list of institutions and individuals involved (as of May 1989) is given in the Appendix. The members of VIRGO have met altogether in two specific meetings, in Pisa (fall 1987) and in Sorrento (fall 1988), and individually in many occasions.
The approval of the project implies the attribution of about 10 new technicians, engineers, and physicists working full time for VIRGO.

4.1.2) EXTERNAL COLLABORATIONS

A European collaboration was initiated by the Paris group as soon as 1984, concerning the feasibility studies of the large interferometers. This collaboration, which involves Germany, Britain, Italy, and France was supported by two successive "twinning" grants from the EEC Stimulation program. It has allowed some collaborative work (and common publications), and the organization of three European Workshops (1985, at Schloss-Rindberg, 1986 in Chantilly, 1988 in Sorrento). It has also led to the redaction of a common document, Eurograv, published in March 1988, which is the basis for a European collaboration concerning the large interferometers. Eurograv justifies the construction of at least two detectors in Europe, and creates European Working Groups to work on the engineering problems of these large detectors. In February 1989, there was a meeting in Paris, involving the group leaders of the European and American projects, plus representatives of the funding bodies, including the directors of Nuclear Physics and of Gravitation from the NSF. It was decided there to enlarge the collaboration to the Americans, with the goals of avoiding unnecessary multiplication of the research efforts and of the engineering studies, and of ensuring the compatibility of the data acquisition systems of all the future detectors. The Working Groups were reconducted with slight modifications, each of them having a Principal Investigator in charge of coordinating the efforts in his field. The common agreement is detailed in Appendix 4.2

Let us make it clear that this agreement does not call for any unification of the projects nor does it suppress all competition between the groups, but it does ensure that every country which builds an interferometer will finally find its place in a future detector array, by establishing an organized information exchange and a standardization of the data acquisition and analysis and that technological improvments will be exchanged.

VIRGO is open to collaborations with all Italian, French or foreign institutions which intend to participate in it. VIRGO was recently joined by Relativistic Astrophysicists from Meudon Observatory. There are presently preliminary discussions with a Brasilian and with an Indian team who have expressed the wish of collaborating with VIRGO.

4.1.3) PROPOSED AGREEMENTS

The goal of the VIRGO project is three-fold :
- to construct a large interferometric antenna with the required sensitivity of 3.10^{-23} $Hz^{-1/2}$.
- to continue the research in order to increase the sensitivity and to widen the observation frequency range as much as possible.
- to prepare the exploitation of data for the astrophysicists.

4.1.3.1) INTERNAL ORGANIZATION

4.1.3.1.1) LEADERSHIP

From the beginning, VIRGO has two complementary, equally responsible, co-leaders :

A. Brillet and A. Giazotto

They will act together both as Project manager and also as Project scientist.

4.1.3.1.2) PROPOSED AGREEMENTS

The organization of the VIRGO group has been very light up to now: each subgroup was able to choose its own way, we noticed no sign of competition or of unnecessary redundancy within the group, and all the studies have progressed satisfactorily. Even if this loose organization has been well adapted for the phase of preliminary studies, it can obviously not be maintained anylonger as soon as the approval of the project by the funding bodies generates deadlines and milestones.
In France and in Italy, several groups are already involved in the project, and it becomes necessary to strengthen the links betwen them in order to ensure the maximum efficiency for the construction phase.
We have identified eight distinct domains of activity which require each a responsible and a few co-workers. These groups are listed below, with possible names for their principal investigators:

1) Passive seismic isolation	A. DI VIRGILIO	(2->4)
2) Active seismic isolation	L. HOLLOWAY	(2->4)
3) Optics, Laser and Detection	C. N. MAN	(5->6)

4) Numerical simulations of the experiment	J. Y. VINET	(2->4)
5) Mirror alignment system	L. MILANO	(2->4)
6) Data acquisition	D. PASSUELLO	(0.5->2)
7) Vacuum	A. MARRAUD and H. KAUTZKY	(1.5->3)
8) Buildings and infrastructure	C. BRADASCHIA	(0.5->2)

The number between parenthesis at the end of each line gives an estimate of the present and the required researchers for each group, in units of one full-time physicist or engineer. This evaluation may be modulated according to the amount of effective collaboration with the other groups, and the fraction of the tasks which may be committed to external firms or laboratories. Not all the tasks are permanent neither simultaneous, thus some of the "holes" can be filled by moving existing collaborators from one subject to another; the total number of required new collaborators is about 10. This should not be difficult to find once the project is approved

The organization could have the following structure:

A Project Committee would be responsible for the technical aspects of the project. It will be composed by the principal investigators, and co-chaired by the group leaders. It should meet about once per month until the final design is completed, and 4 to 6 times per year subsequently.

The Management Committee will serve to control the funding and to coordinate the funding bodies. It will be composed by a representative of each funding body. It will meet at intervals of 3-4 months. The project leaders will report to this committee.

4.1.3.2) THE LONG TERM RESEARCH

In order to prepare the future generations of interferometers, long range academic researches are necessary. One must distinguish clearly :

- the construction, where the goal is to achieve a sensitivity of 3 10^{-23} $Hz^{-1/2}$ using 'known' technologies
- the research activity, which involves the study of new ideas and technologies.

The groups directly involved in the construction and in the long range researches are :

- INFN-Pisa
- INFN and Dept. of Physical Sciences-Napoli

- GROG-Orsay and Palaiseau

In addition to the groups which are directly involved in the construction of VIRGO, other groups are involved in the development of long term researches to increase the performances of the interferometer in the future and to prepare the exploitation of the observations for the astrophysicists. They are:

- The Laboratoire de Gravitation et Cosmologie Relativistes (Ph.Tourrenc et al.)
- The Dept. of Electronic Engineering at Universita di Salerno (I.Pinto et al.)
- The Dept. of Electronic Engineering at Universita di Napoli (M.Longo et al.)
- The Groupe d'Astrophysique Relativiste (T.Damour et al.)

They have participated in the definition of the project and are active in all the international collaborations.

The subjects studied by these groups are the physics of the experiment, the data analysis and the modelisation of astrophysical sources. All these groups will need to be reinforced by one or two physicists or engineers.

The Laboratoire d'Optique Appliquee may decide to create a more important group around J.Y.Vinet, and the improvment of gravitational wave detectors is one of the justifications and long term goals of the development of the "squeezing techniques" at the Laboratoire de Spectroscopie Hertzienne de l'ENS in Paris.

4.1.3.3) PROPOSED GLOBAL ORGANIZATION

The INFN effectively initiated the VIRGO project, and it seems logical that INFN keeps the leadership among the agencies participating in VIRGO. Its principal partner will be the CNRS-INSU, and they must agree together on what should be the relative participations of Italy and France in the project.

Given that the scientific contribution to the project is approximatively equally shared between the two countries, but that the instrument will very likely be built in Toscana, we suggest that *the relative participation of France should range between one third and one half of the total cost of the project.* This situation should be maintained after the end of the construction, for the French astrophysicists to have access to the data and for the continuity of the collaboration towards the future generations of detectors.

The agreement between INFN and CNRS-INSU should ensure the balance between the contributions of each country and the scientific and technological fallouts they may expect.

The main other partners, up to now, have been the Universities of Naples, Pisa, Paris, Salerno, and the Observatory of Paris. Their contributions have been far from negligible, and they should be invited to take a participation in VIRGO.

4.2) COSTS AND MANPOWER

This section gives estimated costs, in FF and IL, at Spring 1989 prices. They are based on estimates from possible suppliers. The total cost of the study and construction of VIRGO is estimated to about 170 MF, or 35 Gigalire (GIL), excluding taxes.
The running cost, after the end of the construction, will be of the order of 6.5 MF, or 1.3 GIL per year, for one interferometer.
These costs do not include the long term research which must be pursued in view of future generations of antennas.

4.3.1) ENGINEERING STUDIES

This first subsection represents the cost of the engineering studies which must be realized before the final design is completed. The corresponding amount should be granted as soon as the project is approved in principle, in order to allow for the beginning of the construction in 1991.

Optical simulations	1.	MF	0.200	GIL
Mechanical C.A.D	0.6	"	0.120	"
Mirror substrates	0.6	"	0.120	"
Mirror coatings	0.7	"	0.140	"
Lasers and detectors	1.	"	0.200	"
Total	3.9	MF	0.78	GIL

4.3.2) INFRASTRUCTURE

Site acquisition	5.		1.	
Roads	1.		0.2	
Pipe concrete bed	6.5		1.3	
Pipe iron cover	11.5		2.3	
Buildings and air conditioning	11.5		2.3	
Clean room class 10000	2.7		0.54	
Total	38.2	MF	7.64	GIL

4.3.3) VACUUM SYSTEM

Pipe 6 km and diaphragms	48.5		9.7	
6 vacuum tanks with attenuators	4.7		0.94	
Electrical network & transformers	9		1.8	
Mounting	11.5		2.3	
Vacuum pumps	12.5		2.5	
4 gate valves	1.8		0.36	
Total	88	MF	17.6	GIL

4.3.4) INTERFEROMETER

This represents the cost of manufacturing and setting up the first interferometer.

Mirrors	25		5	
Optics	3		0.60	
Lasers	3		0.60	
Control electronics and data acquisition	6		1.20	
Total	37	MF	7.4	GIL

4.3.5) RUNNING COSTS

These costs will begin when the interferometer starts test runs. Development costs concern small improvements of the apparatus. They will decrease rapidly once the data acquisition starts.

Electrical power	0.8		0.12	
Water, Telephone, Services..	0.5		0.10	
Maintenance	1.2		0.24	
Development	1.5		0.30	
Travel expenses	1.0		0.20	
Data storage supports	1.5		0.30	
Total	6.5	MF	1.3	GIL

It is possible that new technological developments lead to a decrease of some of the costs, such as the low outgassing rate steel, which would suppress the need for baking the pipe and require a lower pumping speed, or developments in the optical technologies, which could make the mirrors cheaper. It is also possible that some of the technological studies may be done in common with the other groups with an external funding. Except for that, the costs look rather uncompressible. *Any modification of the project which could compromise the final sensitivity must be rejected*, because it would reduce the chances of success, and because it would destroy the basis of the collaboration with the other groups in view of future astrophysical observations, which is that all the detectors must have ultimately the same sensitivity.

4.3.6) MANPOWER

The total VIRGO manpower is presently the researchers, and six technicians. The design and the construction phase will require about 10 new positions for about 5 years as it is shown in Table 4.0. We already have evidence that once the project is approved, it will become very attractive for a few scientists and engineers who are already working with CNRS or INFN laboratories. It will be the responsibility of CNRS and INFN to create these internal changes.

ITALY				FRANCE		
Situation	Present	Final	Difference	Present	Final	Difference
Vacuum and Mechanics (technicians)	2	5	+3	1	2	+1
Electronics (engineers or technicians)	1	3	+2	1	2	+1
Optics engineer				0	1	+1
Laser engineer				0	1	+1
Mechanical project experts	1	2	+1			
Financial admin.	0	1	+1			
low level service personal.	0	2	+2			
Total	4	13	+9	2	6	+4

Table 4.0 : Technical support

4.4 TIMETABLE

As it has been noticed earlier, the time schedule of the project is directly related to its scientific content : the ambition of VIRGO to participate in the first detection of gravitational waves implies a fast decision process and a tight schedule. If the project was delayed by more than one or two years relative to the timescale proposed below, that would decrease very much the chances of participating to the first detection. The long term astrophysical goal and the technological fallouts would remain, but the scientific results would be much less spectacular and gratifying.

The first year after approval will be critical : the final design can be completed within a year, if some engineering studies can be committed to external partners and if the groups size can be slightly increased. (Without any extension of the present staff and funding level, this would rather require two years).

Infrastructure and buildings are not a difficult part of the project. They will easily be completed in two years, after the site acquisition. Manufacture, and on-site welding and testing of the vacuum pipe will require two years. They can be started simultaneously with the infrastructure works, if sufficient funding is available at that time. The instrumentation chambers could be mounted and tested within a year after the completion of the buildings. A safe total of three years is then needed before the optical instrumentation can start being integrated.

The manufacture of the optical components, and especially of the large mirrors, is where most of the high technology is involved.The only companies which are readily able to produce these components are American. Some European ones certainly have the technical ability, but would need to acquire some new equipment. We believe that this would be a useful investment, although it requires some preliminary studies, and the development of new machines, so that both the cost and the delays will be slightly larger. This will take two years if there is no unexpected difficulty.We consider a total of three years for the whole operation.

The development of a high power diode pumped Nd:YAG laser is already being projected by different European firms, because it represents a potentially important market for the future, when the cost of high power diodes (presently developed by Siemens and by Thomson, in particular) will become very low. There is no doubt that such a laser will be ready when needed.

The development of the control and monitoring system will take place mainly inside the VIRGO group.: its duration depends mainly on the available staff, but this point is not susceptible to delay the realization of VIRGO.

The data acquisition and analysis equipment is not critical either in this experiment. Appropriate hardware solutions already exist, their choice will be mainly a matter of standardization between the different groups. Software solutions to similar problems have already been studied for other experiments in astrophysics, radar technology, etc. This problem will be solved in time.

In optimum conditions, the whole instrument could start operating in the first half of 1995 and reach the expected sensitivity in 1996.

Table 4.1 shows the details of the proposed timetable. The bars are colored light for operations involving mainly the VIRGO staff, and dark for the work to be realized by private firms. Their thickness is an indication of the intensity of the required effort, in manpower or in cost, respectively

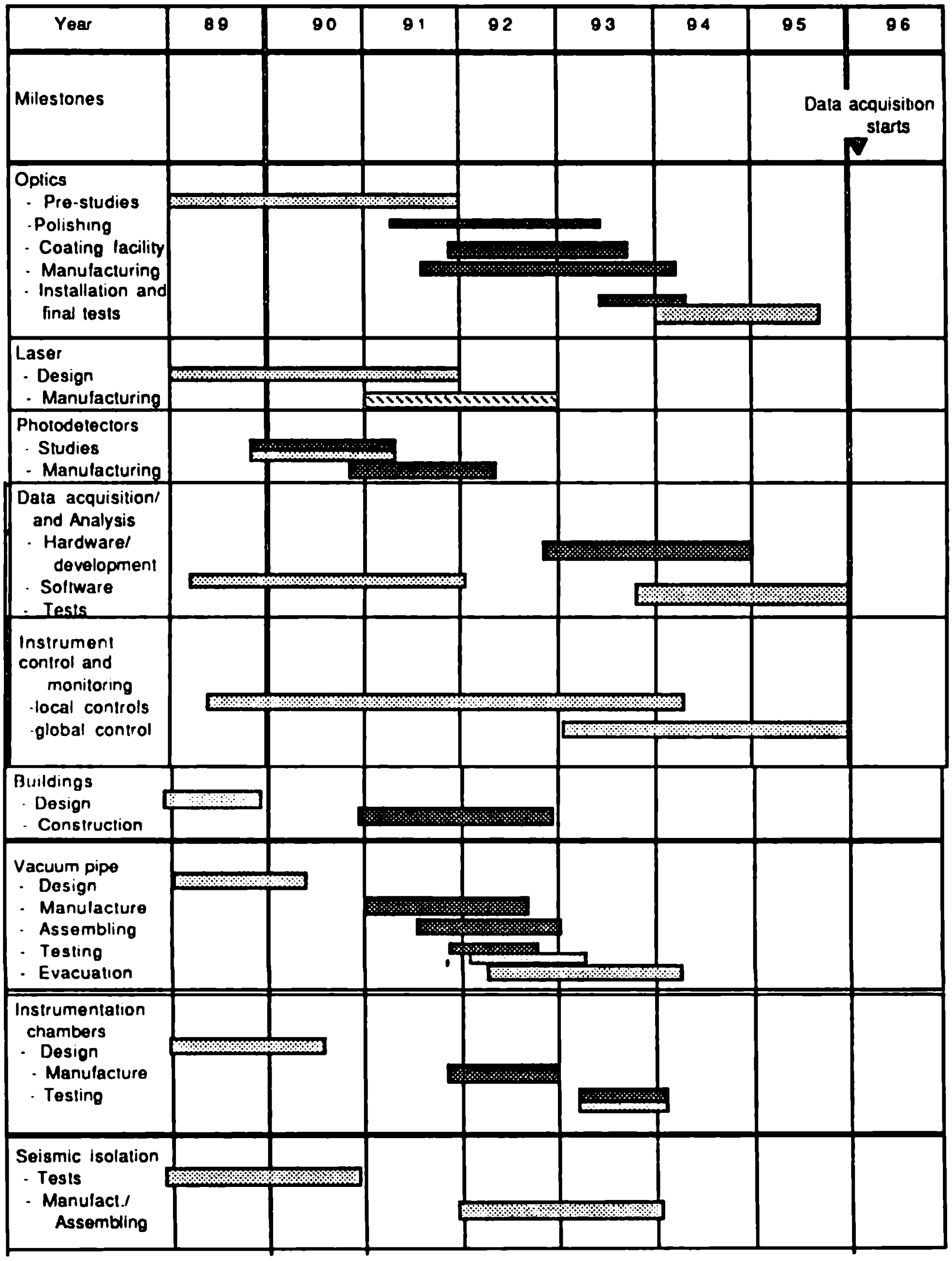

Table 4.1 Proposed timetable

4.5 PROPOSED SPENDING SCHEDULE

To match the optimum timetable described above, the spending curve should have the following shape, described on Fig.4.2. The dark areas represent the cost of the experiment itself, while the lighter areas represent the infrastructure, the buildings and the vacuum system. The fact that the spending curve is sharply concentrated over three years is difficult to avoid,

unless it is deliberately decided to slow down the construction : it reflects the fact that a large fraction of the cost goes into the huge vacuum system and its infrastructure, which can be manufactured and assembled rapidly.
The timetable and spending curve can certainly be reoptimized as a function of the financial constraints of the funding agencies, but one must try to avoid delaying the end of the realization.

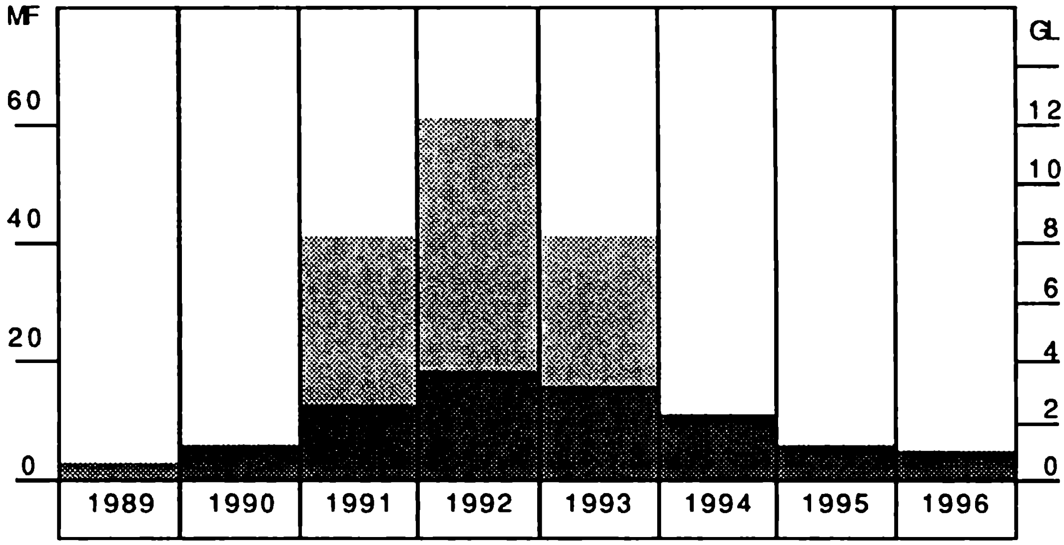

Table 4.2 : The spending curve corresponding to the proposed timetable

REFERENCES

Abderrazik -Annales des Télécommunications- t.22,n°1-2,p.41, (1967)

Aguirregabiria J.M., Bel L.; Phys.Rev. A 36, 3768 (1987)

Allega A.M., Cabibbo N.; Lett. Nuovo Cimento 38, 263 (1983)

Amaldi E., Pizzella G.; Il Nuovo Cimento 9C, N.2, 612 (1986)

Barone F., di Fiore L., Milano L., Restaino S.; -A computer aided system for the automatic alignment of a Michelson interferometer for detecting gravitational waves-, comunicazione all'VIII Convegno Nazionale di Relatività Generale e Fisica della Gravitazione, Cavalese (Trento) 30 agosto-3 settembre 1988

Barone F., di Fiore L., Milano L.; -Alignment of Michelson interferometer and Fabry-Perot interferometer- to be published (1989

Bayer-Helms ; PTB Bericht-Me-43, (1983)

Bel L., Boulanger J-L., Deruelle N.; Phys. Rev. A 37, 1210 (1988)

Beron B.L., Hofstadter R.; Phys.Rev.Lett. 23, 184 (1969)

Bernard C., De Rùjula A., Lautrup B.; Nucl.Phys.B 242, 93 (1984)

Billing H., Maischberger K., Rüdiger A., Schilling R., Schnupp L., Winkler W.; J.Phys. E:Sci Instrum. 12 (1979)

Billing H., Winkler W., Rüdiger A., Schilling R., Maischberger K., Schnupp L.; -The Munich gravitational wave detector using laser interferometry- from: Quantum Optic, Experimental Gravity and measurement Theory, ed. P.Meyestre and M.O.Scully (Plenum Publ. Cort. (1983))

Blair D., 1983, in Gravitational Radiation, eds N. Deruelle and T. Piran, North-Holland, Amsterdam, p. 339.

Born M., Wolf E., -Principles of Optics-, Pergamon Press, Oxford (1964)

References

Brillet A.; -The interferometric detection of gravitational waves- Lecture notes in Phys. 212, Gravitation, Geometry and Relativistic Physics, Proc.Aussois, France (1984)

Brillet A.; Ann.Phys.Fr. 10, 219-226 (1985)

Bradaschia C., Del Fabbro R.,Di Fiore L., Di Virgilio A.,Giazotto A., Kautzky H.,Montelatici V.,Passuello D.; -First results on the electronic cooling of the Pisa seismic noise super-attenuator for Gravitional Wave detection- In print on Phys. Lett.A (1989) (see appendix 4.3)

Caves C.M.; Phys.Rev.Lett. 45 N2, 75 (1980)

Damour T, 1987, in Gravitation in Astrophysics, eds B. Carter and J.B. Hartle, Plenum Press, New York, p. 3.

Damour T and Deruelle N., 1986, Ann. Inst. H. Poincaré (Phys. Théor.), 44, 263.

Del Fabbro R., Di Virgilio A., Giazotto A., Kautzky H., Montelatici V., Passuello D.; Phys.Lett. A, 124, 253 (1987) (see appendix 4.3)

Del Fabbro R., Di Virgilio A., Giazotto A., Kautzky H., Montelatici V., Passuello D.; Rev.Sci.Instrum. 59, 292 (1988a) (see appendix 4.3)

Del Fabbro R., Di Virgilio A., Giazotto A., Kautzky H., Montelatici V., Passuello D.; Phys.Lett.A 132, 237 (1988b) (see appendix 4.3)

Del Fabbro R., Di Virgilio A., Giazotto A., Kautzky H., Montelatici V., Passuello D.; Phys.Lett.A 133, 471 (1988c) (see appendix 4.3)

Drever R.W.P.; Ford G.M., Hough J., Kerr I.M., Munley A.J., Pugh J.R., Robertson N.A., Ward H.; Proc. of the Ninth International conference on General Relativity and Gravitation, Jena, (1980) -ed. E. Schmutzer- Deutscher Verlag der Wissenschften, Berlin

Drever R.W.P.; -Gravitational Radiation- N.Deruelle, T.Piran ed., (North Holland), p.321(1981)

Drever R.W.P., Hough J., Munley A.J., Lee S.A., Spero R., Whitcomb S.E., Ward H., Ford G.M., Hereld M., Robertson N.A., Kerr I., Pugh J.R., Newton G.P., Meers B., Brooks III E.D., Gursel Y.; -Optical cavity laser interferometers for gravitational wave detection- In Laser Spectroscopy V. Ed. A.R.W. McKellar, T.Oka, B.P.Stoicheff (Springer, Berlin, Heidelberg, New York 1981)

Drever R.W.P.; -Gravitational wave detectors using laser interferometers and optical cavities-I Ideas, principles and prospects- Invited lecture given at Nato Advanced Study Institute on Quantum Optics and General Relativity,Bad Windsheim,Germany, August 1981

Drever R.W.P.; -Interferometric detectors for gravitational radiation- for "Gravitational Radiation" ed. by T.Piran and N.Deruelle, Proceedings of the Les Houches Summer Institute, June 1982

Drever R.W.P., Hall J.L., Kowalski F.V., Hough J., Ford G.M., Munley A.J., Ward H.; Appl.Phys.B 31, 97-105 (1983)

Edelstein W.A., Hough J., Pugh J.R., Martin W., J.Phys.E: Sci.Instrum. Vol.11, 710 (1978)

Einstein A.; Preuss. Akad. Wiss. Berlin, Sitzungberichte der Physikalisch Matematischen Klasse, p.688 (1916)

Fattaccioli D., Boulharts A., Brillet A., Man C.N.; J.Optics (Paris) 17 N°3 (1986)

Forward R.L.; Phys.Rev.D, 17, 379 (1978)

Gea-Banacloche J., Leuchs G.; Journal of Modern Optics, 34 N°6/7, 793 (1987)

Gertsenshtein M.E., Pustovoit V.I.; Sov. Phys. JETP, 16 N°2, 433 (1963)

Giazotto A., Campani E., Passuello D., Stefanini A.; -Performance of an active pendulum with interferometric sensing- Proceedings of the fourth Marcel Grossman Meeting on general relativity, Rome,June 1985, Elsevier Science Publishers (1986a)

Giazotto A.; -The seismic noise challenge to the detection of low frequency gravitational waves- "7th congresso di relatività generale e fisica della gravitazione"-Rapallo,Italy, Sept. 1986. General relativity and gravitational physics- World Scientific Pub. (449) (1987)

Giazotto A.; Phys.Lett.A 128, 241 (1988b) (see appendix 4.3)

Goorvitch D.; Appl.Optics 14 (1975)

Grassi Strini A.M., Strini G., Tagliaferri G.; J. Appl. Phys. 51, 849 (1980)

Hall et al., (1984)

Hernandez G., -Fabry Perot Interferometer- Cambridge University Press, Cambridge (1986)

Herriott D., Kogelnik H., Kompfner R.; Appl.Optics 3 (1964)

Hough J., Meers B.J., Newton G.P., Robertson N.A., Ward H., Schutz B.F., Drever R.W.P., Mason R., Pollard C., Tolcher R., Bellenger D.W., Bernnett J.R.J., Corbett I.F., Percival M.D.; -A British long baseline gravitational wave observatory- GWD/RAL/86-001 (1986)

Hough J.; -Report on Round Table Discussion-Gravitational wave detectors- To be published in Proceedings of NATO Advanced Research Workshop on Gravitational Wave Data Analysis, Cardiff, July 1987

Hough J., Meers B.J., Newton G.P., Robertson N.A., Ward H., Schutz B.F., Corbett I.F., Drever R.W.P; Vistas in Astronomy Vol.30 pp.109-134 (1987a)

King A.R., 1988, Q. Jl. Roy. Astr. Soc., 29, 1.

Kuroda K., Tsubono K., Hirakawa H.; Phys.Lett 92A, 131 (1982)

Landau L., Lifshitz E.; -The classical theory of fields- Pergamon (1951)

Man C.N., Brillet A., Shoemaker D.S.; -Gravitational wave data analysis- Nato Workshop, Cardiff, June 1987

Man C.N.; G.W. Data Analysis Poceedings, Cardiff, July 1987

References

Man C.N. -External modulation and recyclings- European Collaboration Meeting on Interferometric Detection of GW, Sorrento 30/9/1988

Man et al.: European Meeting on Interferometric Detection of G.W, Sorrento Sept. 1988

Meers B.J.: Optics Com. 47, 237(1983)

Meers B.J.; Phys. Rev. D 38, 2317, (1988)

Pizzella G.: Rivista del Nuovo Cimento Vol. 5, N.3 (1975)

Ricci F. -Nuclear Instruments and Methods in Physics Research- A260, 491-500 (1987)

Rüdiger et al.: Optica Acta,vol.28, n°5,p.641, (1981)

Rüdiger A., Schilling R., Schnupp L., Winkler W., Billing H., Maischberger K.: Optica Acta, 28, 641-658 (1981)

Rüdiger A., Schilling R., Schnupp L., Winkler W., Billing H., Maischberger K.: J.Phys.42, C8-451 (1981)

Rüdiger A., Schilling R., Schnupp L., Shoemaker D., Winkler W., Leuchs G., Maischberger K.: -The garching 30-meter prototype and plans for a large gravitational wave detector- Proc.18th Texas Symposium on Relativistic Astrophysics, Chicago 1986, Ed.Melville P.Ulmer, World Scientific (1987)

Rüdiger A.; private communication (1988)

Ruggiero F.; -Alcuni problemi relativi alla rivelazione delle onde gravitazionali- Unpublished Thesis, Pisa University (1979)

Russo G., Albrecht R., Ochsenbein F.: -Optical mass storage for a 10 Terabyte archive: system integration problems and user interface- in SPIE Vol.695 Optical Mass Data Storage II, p.366 (1986)

Russo G., Richmond A., Ochsenbein F., McGlynn T.: -Optical storage for archiving astronomical data- Proc. of Optica '87, 331, (1987)

References

Russo G., Ochsenbein F.; -Optical disk trials at the ST-ECF- , ST-ECF Newsletter 9, 5, 1988

Schilling R., Schnupp L., Winkler W., Billing H., Maischberger K., Rüdiger A.; J.Phys. E: Sci.Instrum.14, 65(1981)

Schilling R.; (1984)

Schnupp L., Winkler W., Maischberger K., Rüdiger A., Schilling R.; J. Phys. E. Sci.Instrum. 18, 482 (1985)

Schnupp L.; Cardiff,id (1987)

Schnupp L.; Workshop on G.W. Detectors, Munich, Mai.1988

Shoemaker D., Winkler W., Maischberger K., Rüdiger A., Schilling R., Schnupp L.; -Progress with Garching 30-meter prototype for a gravitational wave detector- MPQ 100 (1985)

Shoemaker D., Schilling R., Schnupp L., Winkler W., Maischberger K., Rüdiger A.; -Noise behavior of the garching 30 meter prototype gravitational wave detector- MPQ 130 (1987a)

Shoemaker D., Brillet A., Man C.N.; -Wide bandwidth frequency and power stabilization of a laser-diode-pumped Nd : YAG laser- Proc. of the Conference on Lasers and Electro-Optics, Vol.14, Optical Society of America (1987b)

Shoemaker D.; -Contributions à l'etude de la detection interferometrique des ondes de gravitation- Thesis de l'Université Paris XI (1987)

Shoemaker D., Brillet A., Man C.N., Crégut O., Kerr G.; -A frequency-stabilized laser-diode pumped Nd : YAG laser- Submitted to Optics Letters (1989)

Shoemaker et al., to be published in Optics Letters, June 1989

Schutz B.F., 1986, in Gravitational Collapse and Relativity, eds H. Sato and T. Nakamura, World Scientific, Singapore, p. 350.

Schutz B.F., 1989a, in Gravitational Wave Data Analysis, ed. B.F. Schutz, Kluwer, Dordrecht.

References

Schutz B.F., 1989b, in Gravitational Radiation, ed. D. Blair, Cambridge University Press, Cambridge, in press.

Spero R.; -The CALTECH laser-interferometric gravitational wave detector- Proceedings at the fourth Marcel Grossmann Meeting on the Recent Developments of General Relativity, R.Ruffini (ed.) Elsevier Sci.Publ. B.V.(1986)

Stark R.F. and Piran T., 1989, in Proceedings of the 4th Marcel Grossmann Meeting, ed. R. Ruffini, Elsevier, Amsterdam, p. 327.

Sziklas E.A and Siegman A.E, Applied Optics vol 14, n°8, 1874 (1975)

Taylor J.H., 1987, in General Relativity and Gravitation, ed. M.A.H. Mac Callum, Cambridge University Press, Cambridge, p. 209.

Taylor J.H. and Weisberg J.M., 1989, Astrophys. J., in press.

Thorne K.S., 1983, in Gravitational Radiation, eds N. Deruelle and T. Piran, North-Holland, Amsterdam, p. 1.

Thorne K.S., 1987, in 300 Years of Gravitation, eds S.W. Hawking and W. Istrael, Cambridge University Press, Cambridge, p. 330.

Thorne K.S.; scattering [to be published]

Tourrenc P., Deruelle N.; Ann.Phys.Fr. 10, 241-252 (1985)

Vinet J-Y.; J.Phys. 47, 639-643 (1986)

Vinet J-Y., Meers B., Man C.N., Brillet A.; Phys.Rev.D 38 (1988)

VIRGO project: Pisa, Napoli, Frascati, Orsay, Paris collaboration - INFN PI/AE 87/1, Pisa 12 May 1987.,

VIRGO project: a progress report - Paris, Orsay, Pisa, Napoli, Frascati collaboration - Presented to the Fifth Marcel Grossmann Meeting, Perth, Australia 8-13 August 1988, INFN PI/AE 88/10

Wagoner R.V., 1984, Astrophys. J., 278, 345.

Ward H., Hough J., Kerr G.A., Mackenzie N.L., Mangan J.B., Meers B.J., Newton G.P., Robertson D.I., Robertson N.A.; -The Glasgow

References

gravitational wave detector-Present progress and future plans- Proceedings of the International Symposium on Experimental Gravitational Physics, Guangzhou, China,August 1987

Weiss R.; Quarterly Progress Report of the Research Laboratory of Electronics of the MIT 105, 54 (1972)

Winkler W.; -Experimental gravitation- Atti dei Convegni Lincei (1977)

Zel'dovich Ya.B. and Novikov I.D., 1983, Relativistic Astrophysics, vol.2, University of Chicago Press, Chicago.

APPENDICES

SUMMARY OF VIRGO DESIGN PARAMETERS

CONCEPT

3 km armlength Michelson interferometer

Fabry-Perot type gravito-optic transducers

SENSITIVITY GOALS

$\tilde{h} < 3\ 10^{-23}\ \mathrm{Hz}^{-1/2}$ at 1 kHz

$\tilde{h} < 10^{-25}$ at 10 Hz (for one year integration time)

OPTICAL DESIGN

Standard recycling, for 500 W noise equivalent power

Low finesse Fabry-Perot cavities (finesse= 40), to avoid instabilities

Input and output mode cleaners

Light injection through monomode fiber

ALIGNEMENT CONTROL

CCD cameras for visual control

Low frequency modulation of each degree of freedom, feedback through low gradient coil and magnet system

SEISMIC ISOLATION

6 multidimensional Superattenuators for the critical optical components

Active damping with coils and magnets

Puppet type wire suspensions

LASER SOURCE

1.06 μm Nd:YAG lasers, >15 W ouput power

Low and medium power stages: diode pumping

High power stage: krypton lamp or diode pumping

Multistage frequency stabilization

BUILDINGS AND INFRASTRUCTURE

3x3 km L-shaped instrument

3 laboratory buildings, with clean rooms, 15 m high, 10x20m for the end buildings, and 20x20m for the central one.

1m diameter vacuum tube, at ground level, enclosed in a concrete channel, with parallel service road

Control room (10x20 m)

VACUUM

Oversized, to allow for light baffling, future modifications and improvments

Instrumentation chambers

2 m diameter diameter, 7 m high, for each attenuator

required vacuum: 10^{-8} in mirror area, "differential pumping"

Turbo pumps, and ion pumps in the mirror area

Tubes

length: 3 km, diameter 1 m, thickness 5 mm with reinforcing rings,

316L Stainless steel annealed for low outgassing rate,

required vacuum: 10^{-7} torr

designed for low maintenance over >10 years, evacuated "only once"

turbo plus ion or getter pumps

ON LINE DATA ACQUISITION AND ANALYSIS

Acquisition

signal, 10 kHz sampling rate, 16-bit

monitoring of Tp, pressure, seismic, magnetic, lock contrrols, laser frequency and power...

Storage

optical disks, or digital tapes

Analysis

on site: prefiltering of pulse data and low pass filtering for pulsar data storage, sets of matched filters (DSP's)

off line: validated pulse data for coincidences

"Fourier" transforms for pulsar search

APPENDIX 3.1

THEORY OF RECYCLING INTERFEROMETERS

(reprinted from Physical review D, with the permission of the American Physical Society)

Appendix 3.1

Optimization of long-baseline optical interferometers for gravitational-wave detection

Jean-Yves Vinet
*Groupe de Recherche sur les Ondes de Gravitation (G.R.O.G.), Bâtiment 104, Université Paris-Sud, 91405 Orsay, France
and Laboratoire d'Optique Appliquée, Ecole Polytechnique–Ecole Nationale Supérieure
de Techniques Avancées, 91120 Palaiseau, France*

Brian Meers
Department of Physics and Astronomy, The University, Glasgow, G12 8QQ Scotland

Catherine Nary Man and Alain Brillet
Groupe de Recherche sur les Ondes de Gravitation, Bâtiment 104, Université Paris-Sud, 91405 Orsay, France
(Received 22 February 1988)

The goal of this paper is to analyze and to evaluate the different configurations currently considered for the interferometric detectors of gravitational waves. We first study the properties of elementary gravito-optic transducers (i.e., delay lines or Fabry-Perot resonators) using an original formalism which allows one to understand and to compare easily the properties of complex interferometers involving these elements, such as recycling or synchronous recycling interferometers. We also describe the new idea of using detuned Fabry-Perot resonators, and we show that, in some cases, it may represent the best compromise between bandwidth and peak sensitivity.

I. INTRODUCTION

Long-baseline interferometers for the detection of gravitational radiation are presently being studied in a few countries (France, Italy, Germany, U.K., and U.S.A.).[1] All these projects are based on the construction of a large, Michelson-type interferometer with an arm length of 1–3 km, containing some kind of gravito-optic transducer in each arm. In order to decrease the shot-noise level, all these interferometers will use high-power lasers, in conjunction with light recycling techniques. The basic idea of recycling was proposed by Drever:[2] it consists in building a resonant optical cavity which contains the interferometer, so that, if the losses are low and if the cavity is kept on resonance with the incoming monochromatic light, there is a power build-up which results in a reduction of the shot noise. This can be realized in different ways, depending on the geometry of the gravito-optic transducer [delay line or Fabry-Perot (FP) resonator]. While the validity of this idea has recently been demonstrated experimentally,[3] its theory remained to be published.

The aim of the present study is to establish several simple models and associated formulas giving the ultimate photon-noise-limited sensitivities of both the current interferometric configurations and their planned extensions. In order to carry out this program some special tools are useful. A common formalism will be developed which allows a straightforward derivation of the properties of arbitrary optical configurations. Comparison of different detector configurations is facilitated by the use of a set of standard parameters.

The cases of nonrecycling delay-line and Fabry-Perot Michelson interferometers will first be treated in order to develop the formalism. Then we will apply these results to various recycling configurations and discuss the relative merits of each configuration according to the frequency range, to the bandwidth of the signal and to the value and the localization of the optical losses which limit the power build-up.

II. OPTICS IN A WEAKLY MODULATING MEDIUM

A. General principles

Consider a plane, transverse, traceless, monochromatic gravitational wave of frequency ν_g, which propagates perpendicularly to the interferometer plane ($z=0$), and is linearly polarized along the directions of the (orthogonal) interferometer arms ($x=0$ and $y=0$, respectively):

$$[h_{ij}(x,y,z,t)]_{z=0}=h_{ij}\cos(\Omega t+\Phi) ,$$

with

$$h_{ij}=\mathrm{diag}(h,-h,0),\quad \Omega=2\pi\nu_g .$$

At every point of the optical path, the light frequency spectrum will resolve in a carrier frequency

$$\nu_{opt}$$

and two sidebands

$$\nu_{opt}\mp\nu_g$$

The enormous ratio between optical and gravitational frequencies allows us to neglect the polarization effects and we shall use a scalar representation of the optical amplitudes. Only first-order effects in h will be considered. The optical amplitudes at an arbitrary point of the interferometer are therefore of the form

$$A(t)=(A_0-\tfrac{1}{2}hA_1e^{i(\Omega t+\Phi)}-\tfrac{1}{2}hA_2e^{-i(\Omega t+\Phi)})e^{-i\omega t},$$

$$\omega=2\pi\nu_{opt}.$$

We will represent the action of gravitational transducers upon already modulated light by linear operators S acting upon generalized amplitudes

$$\mathbf{A}=(A_0,A_1,A_2)$$

as

$$\mathbf{A}'=\mathbf{S}\cdot\mathbf{A}.$$

According to the formalism developed in a previous paper,[4] these operators have the general form

$$\mathbf{S}=\begin{vmatrix} S_{00} & 0 & 0\\ S_{10} & S_{11} & 0\\ S_{20} & 0 & S_{22}\end{vmatrix}$$

In this formalism, the diagonal elements S_{ii} represent the ordinary reflectance (or transmittance) of the transducer for each frequency (carrier and sidebands) whereas S_{10} and S_{20} characterize the power transfer from the carrier to the sidebands, i.e., the sensitivity to the gravitational wave. Optical elements with dispersion and no gravitational sensitivity will be represented by diagonal matrices, elements without dispersion nor G sensitivity by scalar matrices (mirrors, splitters, etc.). Owing to the $\pi/2$ phase lag between the reflected and the transmitted waves at a mirror, we shall represent the action of a mirror upon the complex amplitude of an optical wave by $i\sqrt{R}$ for a reflection, and by $\sqrt{T}$ for a transmission.

The whole interferometer is itself a gravitational transducer and has therefore an associated global operator S. In the following we will encounter three different cases: when S_{10} and S_{20} are of equal moduli, the phase relationships between both and S_{00} will denote either pure phase modulation or pure amplitude modulation, and when S_{10} and S_{20} are not equal, one of them is much larger than the other. Therefore, if the limiting noise reduces to the shot noise, we have, for the signal-to-noise ratio (SNR),

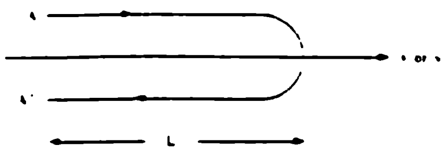

FIG. 1. Round trip in the vacuum (notation).

$$\mathrm{SNR}=h\left|\frac{\eta P\tau_i}{\hbar\omega_{opt}}\right|^{1/2}S,\quad S=|S_{10}|+|S_{20}|,$$

where τ_i and η are, respectively, the integration time and quantum efficiency of the photodetector, and P the power of the source. In other words, the minimum, photon-noise-limited, detectable h is

$$h_{PN}=\left|\frac{\hbar\omega_{opt}}{\eta P}\right|^{1/2}\frac{1}{S}\sqrt{\delta\nu},$$

where $\delta\nu$ is the bandwidth of the detector. In what follows we shall consider the quantity S, that we shall call normalized signal to noise ratio (NSNR), as the quantity to be optimized.

B. Standard gravito-optic transducers

Gravito-optic transducers are optical devices in which the gravitational wave (GW) is supposed to have a detectable perturbing effect. Current examples are the delay lines and the Fabry-Perot cavities. Both have associated operators D and F which can be related to the elementary propagation operator X corresponding to a round trip in the perturbed vacuum[4] (see Fig. 1). We have $\mathbf{A}'=\mathbf{X}\cdot\mathbf{A}$ with

$$\mathbf{X}=\begin{vmatrix} e^{2i\omega L/c} & 0 & 0\\ i\epsilon\dfrac{\omega L}{c}\dfrac{\sin(\Omega L/c)}{\Omega L/c}e^{i(2\omega-\Omega)L/c} & e^{2i(\omega-\Omega)L/c} & 0\\ i\epsilon\dfrac{\omega L}{c}\dfrac{\sin(\Omega L/c)}{\Omega L/c}e^{i(2\omega+\Omega)L/c} & 0 & e^{2i(\omega+\Omega)L/c}\end{vmatrix}. \tag{1}$$

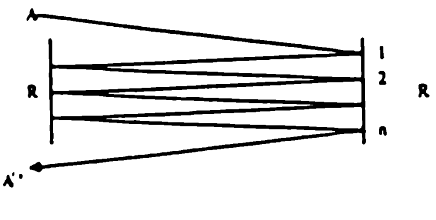

FIG. 2. n-fold delay line (notation).

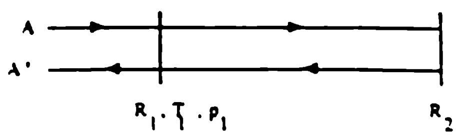

FIG. 3. Reflecting Fabry-Perot cavity (notation).

Appendix 3.1

The value of ϵ is -1 for a round trip along the x axis, and -1 along the y axis. Consider now an n-fold delay line with two mirrors of intensity reflection coefficients R (see Fig. 2). It consists in n iterations of the X operator and $2n-1$ iterations of the operator $i\sqrt{R}$. Its associated operator is thus $i\mathrm{D}$ where

$$\mathrm{D}=(-1)^{n-1}\sqrt{R}^{\,2n-1}\mathrm{X}^n$$

Consider a Fabry-Perot cavity (see Fig. 3) with a front mirror of intensity reflection and transmission coefficients R_1, T_1, with losses p_1, and with a rear mirror of intensity reflection coefficient R_2. The associated operator $i\mathrm{F}$ looks like the ordinary reflectance of a Fabry-Perot cavity but with the ordinary phase factor replaced by X:

$$\mathrm{F}=[\sqrt{R_1}+(1-p_1)\sqrt{R_2}\mathrm{X}](1-\sqrt{R_1R_2}\mathrm{X})^{-1} .$$

1. Response of delay-line-type detectors

In more detail, the delay-line operator involves the three following elements:

$$D_{00}=(-1)^n\sqrt{R}^{\,2n-1}e^{4in\pi\nu_{\rm opt}L/c} ,$$

$$D_{10}=(-1)^n\sqrt{R}^{\,2n-1}i\epsilon\frac{\nu_{\rm opt}}{\nu_g}\sin\left[\frac{2n\pi\nu_gL}{c}\right]e^{2i\pi(2\nu_{\rm opt}-\nu_g)nL/c} ,$$

$$D_{10}=(-1)^n\sqrt{R}^{\,2n-1}i\epsilon\frac{\nu_{\rm opt}}{\nu_g}\sin\left[\frac{2n\pi\nu_gL}{c}\right]e^{2i\pi(2\nu_{\rm opt}-\nu_g)nL/c} .$$

The action of this operator on an unmodulated wave is therefore a pure phase modulation. It is convenient to introduce some parameters which have their counterparts in the case of cavities.

By introducing the storage time

$$\tau_s=\frac{2nL}{c} ,$$

the time constant

$$\tau''=\frac{2L}{cR^*},\quad R^*=1-R ,$$

and the normalized storage time $t=\tau_s/\tau''$ which has the minimum value $t_m=R^*$, we get

$$R^{n-1/2}=e^{-(t-t_m/2)}$$

In what follows we shall consider kilometric interferometers ($L\simeq3$ km) so that the minimum value of τ_s, i.e., $2L/c$ is about 2×10^{-5} s, and high reflectivity coatings ($R^*\simeq10^{-4}$) so that τ'' is about 0.2 s. This set of parameters will be referred to as the reference antenna. As will be shown later, the best τ_s for a given gravitational frequency $\nu_g^{(0)}$ is of order $1/2\nu_g^{(0)}$. So far as we consider gravitational frequencies smaller than a few kilohertz we can assume $t\gg t_m$. Two more parameters are useful—the normalized gravitational frequency $f=2\pi\nu_g\tau''$ and the maximum quality factor $Q=2\pi\nu_{\rm opt}\tau''$. (In the reference antenna, when visible light is used, the quality factor Q is about 7.5×10^{14} and $f\simeq1.26\nu_g/\mathrm{Hz}$.)

The approximate form of the operator D simplifies now to

$$|D_{00}|=e^{-t} ,$$

$$|D_{10}|=|D_{20}|=\frac{Q}{f}e^{-t}\left|\sin\left[\frac{ft}{2}\right]\right| . \qquad (2)$$

If the detection system involves two delay lines, it has a NSNR

$$S(f)=\frac{2Q}{f}e^{-t}\left|\sin\left[\frac{ft}{2}\right]\right| . \qquad (3)$$

For a given gravitational frequency corresponding to f_0, there exists an optimal normalized storage time:

$$t_0=\frac{2}{f_0}\arctan\left[\frac{f_0}{2}\right] .$$

Note that $f_0\to0$ yields $\tau_S^{(0)}\to\tau''$, and thus τ'' may be interpreted as the maximum value of the optimal storage time.

The optimized NSNR is then

$$S(f)=\frac{2Q}{f}\left|\sin\left[\frac{f}{f_0}\arctan\left[\frac{f_0}{2}\right]\right]\right| \times\exp\left[-\frac{2}{f_0}\arctan\left[\frac{f_0}{2}\right]\right] . \qquad (4)$$

We have, at $f=f_0$,

$$S(f)=\frac{2Q}{\sqrt{f_0^2-4}}\exp\left[-\frac{2}{f_0}\arctan\left[\frac{f_0}{2}\right]\right] .$$

Therefore, we can give the limiting value of S when $f_0\to0$:

$$S(0)=Q/e .$$

For $f_0 >> 1$, a good approximation of the optimal storage time is given by $t_0 = \pi / f_0$: i.e.,

$$\tau_S^{(01)} = \frac{1}{2\nu_g^{(01)}}$$

and the NSNR becomes simply

$$S(f) = \frac{2Q}{f} \left| \sin \left[\frac{\pi}{2} \frac{f}{f_0} \right] \right| ;$$

i.e.,

$$S(\nu_g) = \frac{2\nu_{\rm opt}}{\nu_g} \left| \sin \left[\frac{\pi \nu_g}{2\nu_g^{(01)}} \right] \right| .$$

2. Response of Fabry-Perot-type detectors

For the Fabry-Perot cavity operator, the relevant elements are

$$F_{00} = \frac{(1-p_1)\sqrt{R_2}e^{2i\omega L/c} + \sqrt{R_1}}{1+\sqrt{R_1 R_2}e^{2i\omega L/c}} ,$$

$$F_{10} = i\epsilon T_1 \sqrt{R_2} \frac{\nu_{\rm opt}}{\nu_g} \sin \left[\frac{\Omega L}{c} \right] \frac{e^{i(2\omega-\Omega)L/c}}{(1+\sqrt{R_1R_2}e^{2i\omega L/c})(1+\sqrt{R_1R_2}e^{2i(\omega-\Omega)L/c})} ,$$

$$F_{20} = i\epsilon T_1 \sqrt{R_2} \frac{\nu_{\rm opt}}{\nu_g} \sin \left[\frac{\Omega L}{c} \right] \frac{e^{i(2\omega+\Omega)L/c}}{(1+\sqrt{R_1R_2}e^{2i\omega L/c})(1+\sqrt{R_1R_2}e^{2i(\omega-\Omega)L/c})} .$$

The eigenfrequencies of the cavity are determined by the condition $\exp(-2i\omega_0 L/c) = -1$ and consequently, when the optical source is resonant, the preceding operator denotes pure phase modulation. We need now some dimensionless parameters analogous to the delay line's. We may define the time constant of the cavity by

$$\tau_S = \frac{2L}{c(1-\sqrt{R_1R_2})} .$$

Owing to the constraint $0 < R_1 < 1 - p_1$, we have

$$\frac{2L}{c} < \tau_S < \tau'' \equiv \frac{2L}{c[1-\sqrt{(1-p_1)R_2}]} .$$

The ratio of the time constant to its maximum value will be named normalized time constant t; it obeys

$$t_m < t < 1 \quad \text{with } t_m \equiv 1 - \sqrt{(1-p_1)R_2} .$$

In the general case, the source is eventually detuned from $\Delta\nu_{\rm opt}$ from a resonance ν_0 which leads us to introduce the normalized detuning defined by $\Delta f = 2\pi\Delta\nu_{\rm opt}\tau''$. With these notations, the ordinary reflectance of the cavity has the exact expression

$$|F_{00}|^2 = \frac{1}{R_2} \frac{(1-2t+tt_m)^2 + (1-t_m)^2(1-t_m/t)\Delta f^2 t^2 \operatorname{sinc}^2(\Delta f t_m/2)}{1+\Delta f^2 t^2 (1-t_m/t)\operatorname{sinc}^2(\Delta f t_m /2)} ,$$

where the notation $\operatorname{sinc}(x)$ denotes the function $\sin(x)/x$. Fortunately a simple approximate form can be given when Δf is much smaller than the free spectral range and when $t_m << 1$ which is satisfied when gravitational frequencies are restricted to a range of values less than a few kilohertz:

$$|F_{00}| = \left[1 - \frac{4t(1-t)}{1+\Delta f^2 t^2} \right]^{1/2}$$

The minimum value of $|F_{00}|$ is reached at resonance where

$$|F_{00}|_{\rm res} = |1-2t| .$$

Within the same approximation, we have

$$\operatorname{Arg} F_{00} = \pi + \arctan \left[\frac{2\Delta f t(1-t)}{1-2t-\Delta f^2 t^2} \right] .$$

We have further

$$|F_{10}| = \frac{Qt(1-t)}{\sqrt{1+\Delta f^2 t^2}\sqrt{1+(\Delta f - f)^2 t^2}} ,$$

$$|F_{20}| = \frac{Qt(1-t)}{\sqrt{1+\Delta f^2 t^2}\sqrt{1+(\Delta f + f)^2 t^2}} .$$

In particular when the source is resonant ($\Delta f = 0$), we have the special case

$$|F_{00}| = |1-2t| ,$$

$$|F_{10}| = |F_{20}| = \frac{Qt(1-t)}{\sqrt{1+f^2t^2}} .$$

We have consequently, for the NSNR,

$$S(f) = \frac{2Qt(1-t)}{\sqrt{1+f^2t^2}} . \qquad (5)$$

When the normalized gravitational frequency $f_0 = 2\pi\nu_g^{(0)}\tau''$ tends to zero, the optimal value of τ_S' has the limiting value $\tau''/2$ and the limiting value of the SNR turns out to be $Q/2$. When $f_0 >> 1$, the function $S(t)$ begins to saturate as soon as

$$t_0 = \frac{2}{f_0}, \quad \text{i.e.,} \quad \tau_S'^{(0)} = \frac{1}{\pi\nu_g^{(0)}} .$$

This value will be taken as a reasonable choice, for the true optimal value is much higher but irrelevant, giving only a slightly better value of S. In this case, we have, for the NSNR,

$$S(f) = \frac{\sim 4Q}{(f_0^2 + 4f^2)^{1/2}} ;$$

in particular, (6)

$$S(f_0) = 1.78\frac{Q}{f_0} .$$

In dimensional expression, this is

$$S(\nu_g) = (4\nu_{opt}/\nu_g)[1 + (2\nu_g/\nu_g^{(0)})^2]^{-1/2}$$

and

$$S(\nu_g^{(0)}) = 1.78\nu_{opt}/\nu_g^{(0)} .$$

Let us point out an important feature—with Fabry-Perot cavities, it is possible to use a detuned source with respect to the cavity eigenfrequency of an amount $\Delta f = f_0$ so that the sideband generated by the gravitational wave is resonant

$$\nu_{opt} = \nu_0 + \nu_g^{(0)} ,$$

leading to

$$|F_{00}| = \left| 1 - \frac{4t(1-t)}{1 + f_0^2 t^2} \right|^{1/2}$$

and

$$|F_{10}| = \frac{Qt(1-t)}{(1 + f_0^2 t^2)^{1/2}[1 + (f - f_0)^2 t^2]^{1/2}} .$$

When $f_0 >> 1$, a reasonable choice of τ_S' is again

$$\tau_S' = \frac{1}{\pi\nu_g^{(0)}}$$

and with only one resonant sideband, the optimized NSNR becomes

$$S(f) = 0.89\frac{Q}{f_0}\frac{1}{[1 + 4(1 - f/f_0)^2]^{1/2}} \quad (7)$$

or

$$S(\nu_g) = (0.89\nu_{opt}/\nu_g^{(0)}) \times [1 + 4(1 - \nu_g/\nu_g^{(0)})^2]^{-1/2} .$$

Figure 4 gives a comparison of the sensitivities versus ν_g for a delay line, for a Fabry-Perot both at resonance and with detuning, in the conditions we have described above.

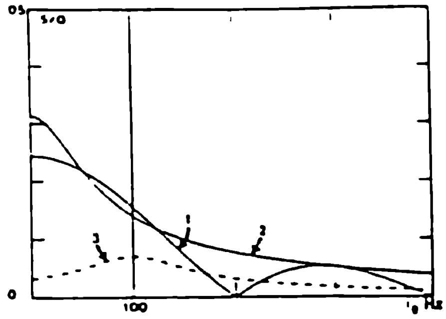

FIG. 4. Transfer function of a Michelson interferometer with multipass arms (optimized at 100 Hz): (1) delay lines; (2) resonant FP cavities; (3) detuned FP cavities.

The detuned Fabry-Perot is less sensitive than the other configurations, but the fact that it brings a higher reflectance makes it interesting when recycling is applied, as we will see in the next part.

III. STANDARD RECYCLING

A. Principles of standard recycling

A classical Michelson interferometer tuned at a dark fringe behaves just like a mirror—most of the power incoming from the source is reflected back. We can use it as the second mirror of a cavity, the front mirror of it is called the recycling mirror. It will be shown that this configuration increases the SNR by allowing more efficient use of the available power. Figure 5 shows the principle of operation. Let R_r, T_r, p_r be the parameters (reflectivity and transmittivity coefficients, losses) of the recycling mirror and R_S, T_S, p_S those of the splitter. It is easy to show that at a dark fringe we have an operator S for the whole system:

$$A' = S \cdot A ,$$

where the relevant coefficients of S are

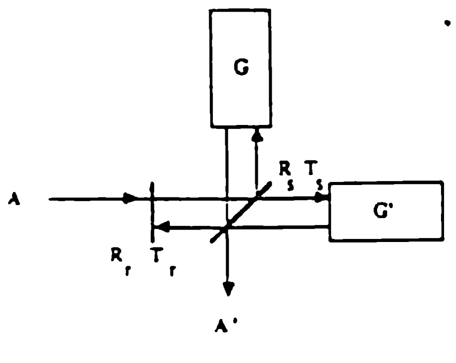

FIG. 5. Sketch of the standard recycling setup.

$$|S_{10}| = (1-p_S)\sqrt{T_r}\frac{|G_{10}|}{1-(1-p_S)\sqrt{R_r}|G_{00}|},$$

$$|S_{20}| = (1-p_S)\sqrt{T_r}\frac{|G_{20}|}{1-(1-p_S)\sqrt{R_r}|G_{00}|}$$

G is the operator associated with a gravito-optic transducer, either a delay line or a Fabry-Perot cavity, directed along the y axis, and G' the operator associated with the same transducer, directed along the x axis; both have the same coefficients G_{ii} but opposite coefficients G_{01} and G_{02}. One sees already that the recycling rate can be optimized for given losses and G, we find

$$(\sqrt{R_r})_{opt} = (1-p_r)(1-p_S)|G_{00}| .$$

So that it is possible to give optimized values of the components of the NSNR:

$$|S_{10}| = |G_{10}|\left|\frac{(1-p_r)(1-p_S)^2}{1-(1-p_r)(1-p_S)^2|G_{00}|^2}\right|^{1/2},$$

$$|S_{20}| = |G_{20}|\left|\frac{(1-p_r)(1-p_S)^2}{1-(1-p_r)(1-p_S)^2|G_{00}|^2}\right|^{1/2}$$

By assuming low extra cavity losses $p = p_r + 2p_S$ we may write simply

$$|S_{10}| = \frac{|G_{10}|}{\sqrt{1-(1-p)|G_{00}|^2}},$$

$$|S_{20}| = \frac{|G_{20}|}{\sqrt{1-(1-p)|G_{00}|^2}}. \quad (8)$$

In the reference antenna we shall take $p_r = 10^{-4}$ and $p_S = 10^{-3}$. The problem to be discussed below is the optimization of either the storage time for delay lines, or the decay time for cavities, when recycling is applied. In the general situation, the optimal value of that time constant will depend on the gravitational frequency f_0 at which one wants to optimize, and on the recycling losses denoted by p. Two frequency ranges will appear: the low-frequency range and the high-frequency range. In the low-frequency range, long storage times are required, the recycling losses are therefore dominated by the reflectivity losses in the arms, and the optimal storage time is almost independent of p. In the high-frequency range, the required storage times are relatively short, so that the losses in the arms may happen to be comparable with the recycling losses p, and the optimal storage time will depend on both p and f_0. The effective value of p will be determined not only by the losses of the recycling mirror and of the beam splitter, but also by the fact that the interference on the beam splitter may be affected by small misalignments or by a slight asymmetry between the two arms of the Michelson interferometer.

B. Standard recycling with delay lines

In the case when G represents a delay line, as shown earlier, we have

$$|G_{00}| = e^{-t},$$

$$|G_{10}| = |G_{20}| = \frac{Q}{f}\left|\sin\left(\frac{ft}{2}\right)\right|e^{-t}.$$

So that, assuming low losses, the phase relations denote pure amplitude modulation, and the NSNR of the global system is given (for extracavity losses $p = p_r + 2p_S$) by

$$S(f) = \frac{2Q}{f}\frac{\left|\sin\left(\frac{ft}{2}\right)\right|}{\sqrt{1-(1-p)e^{-2t}}}e^{-t}. \quad (9)$$

For a given gravitational frequency denoted by f_0, the corresponding optimal normalized storage time is given by the implicit equation

$$t_0 = \frac{2}{f_0}\arctan\left|\frac{f_0}{2}[1-(1-p)e^{-2t_0}]\right|$$

which is easily solved by iterations. For values of f_0 small compared to $1/p$ (say $\nu_g^{(0)} < 50$ Hz in the reference interferometer), t_0 is seen to be almost independent of p and takes a value near 0.8 for zero frequency. The corresponding limit for the NSNR is $0.4Q$. A convenient interpolation formula valid within this range is

$$t_0 = (1.56 + 0.18f_0^2)^{-1/2} .$$

Now, in the case when the normalized gravitational frequency is large enough (say $n_g^{(0)} > 50$ Hz in the reference interferometer), we can put $t = x/f_0 \ll 1$ and write

$$S(f_0) = Q\left|\frac{2}{f_0}\right|^{1/2}\frac{|\sin(x/2)|}{\sqrt{x + pf_0/2}} .$$

The optimal value of x is solution of

$$x + \frac{pf_0}{2} = \tan\left|\frac{x}{2}\right| .$$

The solution x_0 takes values in the range $[2.33, \pi]$ for values of $pf_0/2$ in the range $[0, \infty]$. A good interpolation formula valid except for low frequencies is

$$x_0 = 2.33 + \frac{0.81pf_0}{4.25 + pf_0} \quad \text{then } \tau_S = \frac{x_0}{2\pi\nu_g^{(0)}} .$$

The optimized frequency response of the recycling setup is now

$$S(f) = \frac{Q}{f}\left|\frac{2f_0}{x_0}\right|^{1/2}\left|\sin\left(\frac{x_0 f}{2f_0}\right)\right| . \quad (10)$$

In particular, if the frequency f_0 is within the especially interesting band $1 \ll f_0 \ll 1/p$ say 50 Hz to 500 Hz in the reference antenna, we can write

$$S(f) = 0.92\frac{Q}{f}\sqrt{f_0}\left|\sin\left(\frac{1.17f}{f_0}\right)\right| ,$$

in particular $S(f_0) = 0.85(Q/\sqrt{f_0})$ or, in ordinary notation,

$$S(\nu_g) = 0.92\,\frac{\nu_{opt}}{\nu_g}\,(2\pi\nu_g^{(0)}\tau)^{1/2}\,|\sin(1.17\nu_g/\nu_g^{(0)})|$$

Such an optimized transfer function (for 100 Hz) is plotted in Fig. 6.

C. Case of resonant Fabry-Perot cavities

The relevant operator G is now F:

$$|F_{00}| = |1-2t| \;,$$

$$|F_{10}| = |F_{20}| = Qt(1-t)/\sqrt{1+f^2t^2}\;.$$

The phases are such that the NSNR with the optimal recycling rate takes the form

$$S(f) = \frac{2Qt(1-t)}{\sqrt{1+f^2t^2}\sqrt{1-(1-p)(1-2t)^2}}\;. \qquad (11)$$

In the low-frequency domain, when the extra cavity losses are small compared to the reflectivity losses of the cavities, i.e., $p \ll t$, which corresponds typically to the frequency range 0—50 Hz for the reference antenna, $S(f)$ becomes independent of p:

$$S(f) = Q\left|\frac{t(1-t)}{1-f^2t^2}\right|^{1/2}$$

The optimal value of t at $f = f_0$ is then

$$t_0 = \frac{1}{1-(1-f_0^2)^{1/2}}\;.$$

The corresponding optimized transfer function is

$$S(f) = \frac{Q}{\sqrt{2}}\,\frac{1}{\left|1+\sqrt{1-f_0^2}-\dfrac{f^2-f_0^2}{2\sqrt{1+f_0^2}}\right|^{1/2}}\;.$$

If now f is large enough (> 50 Hz in the reference antenna), we can set $t = x/f_0 \ll 1$ so that the NSNR becomes

$$S(f_0) = \frac{Q}{\sqrt{f_0}}\,\frac{x}{\sqrt{1-x^2}\left|x-\dfrac{pf_0}{4}\right|^{1/2}}$$

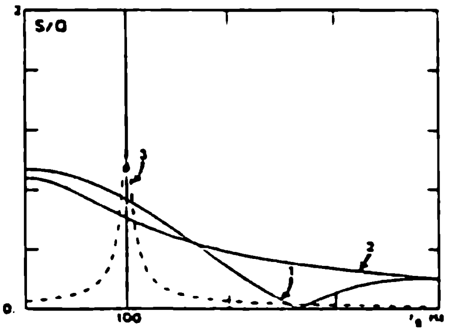

FIG. 6. Transfer function of a Michelson interferometer with multipass arms and standard recycling (optimized at 100 Hz): (1) delay lines; (2) resonant FP cavities; (3) detuned FP cavities.

The value of x which makes S optimal is solution of

$$x^2 - x - \frac{pf_0}{2} = 0$$

The exact solution is somewhat cumbersome but the following interpolation formula is quite sufficient for our purposes:

$$t_0 = \frac{1}{f_0}\left|1-\frac{pf_0}{2}\right|^{-1/3}$$

In fact, if f_0 is not too high (within the band 50—500 Hz in the reference antenna), the solution differs little from $x_0 = 1$, so that we can take $t_0 = 1/f_0$; i.e.,

$$\tau_s^{(0)} = \frac{1}{2\pi\nu_g^{(0)}}$$

The optimized frequency response of the recycling setup is now

$$S(f) = Q\left|\frac{f_0}{f^2-f_0^2}\right|^{1/2}$$

in particular $\qquad (12)$

$$S(f_0) = \frac{Q}{\sqrt{2f_0}}$$

In ordinary notation we have

$$S(\nu_g) = \nu_{opt}\left|\frac{2\pi\tau}{\nu_g^{(0)}}\right|^{1/2}\frac{1}{[1-(\nu_g/\nu_g^{(0)})]^{1/2}}$$

An optimized transfer function (for 100 Hz) is represented on Fig. 6 so as to be compared with the case of delay lines.

D. Case of detuned Fabry-Perot cavities

As already noted, Fabry-Perot cavities can be driven out of resonance, leading to a different response to gravitational frequencies, to a slightly worse signal amplitude, but a higher reflectivity. This mode of operation is expected to give interesting results in a recycling configuration. Let us discuss this idea.

Assume the optical frequency to be detuned with respect to an eigenfrequency of the cavity by an amount equal to the gravitational frequency to be detected:

$$\nu_{opt} = \nu_0 + \nu_g^{(0)}\;.$$

The detuned cavity operator, as shown earlier, contains the following elements:

$$|F_{00}|^2 = 1 - \frac{4t(1-t)}{1+\Delta f^2t^2}\;,$$

$$|F_{10}| = \frac{Qt(1-t)}{\sqrt{1+\Delta f^2t^2}\sqrt{1+(\Delta f-f)^2t^2}}\;.$$

With an optimal recycling rate for $\nu_g = \nu_g^{(0)}$ and with

$\Delta f = f_0$, we find the NSNR as

$$S(f)=\frac{S(f_0)}{[1-(f-f_0)^2t^2]^{1/2}}$$

The peak value, $S(f_0)$ is

$$S(f_0)=\frac{Qt(1-t)}{[p(1+f_0^2t^2)+4t(1-t)(1-pt)]^{1/2}} . \qquad (13)$$

We shall consider that $p << t$, for it will be seen that this approximation holds even for relatively high frequencies (up to the kilohertz in the reference antenna) due to the fact that high values of the optimal time constant τ_S' are required in the detuned system. The resulting expression for the peak value of the NSNR is

$$S(f_0)=Q\left|\frac{t(1-t)^2}{(pf_0^2-4)t+4}\right|^{1/2}$$

The optimal value of t is

$$t_0=\frac{2}{3+(1+2pf_0^2)^{1/2}}$$

$$\to S(f_0)=Q\left|\frac{2(1-\sqrt{1+2pf_0^2})}{(3+\sqrt{1+2pf_0^2})^3}\right|^{1/2} \qquad (14)$$

The NSNR has a narrow-band-type behavior characterized by a bandwidth of

$$\delta f=[3+(1+2pf_0^2)^{1/2}]\sqrt{3} .$$

The transfer functions of delay line and resonant FP interferometers are not essentially changed by standard recycling apart from a gain factor, but the transfer function of the detuned FP interferometer becomes resonant, due to the long time constant required. It is easily seen that, in the limit $pf_0\to 0$, $S(f_0)\to Q/4$, and $\delta f\to 4\sqrt{3}$. It is more interesting to compare these characteristics to those of the following section concerning synchronous recycling. With a choice of x_0 two or three times less than the optimal value, the linewidth is seen to be increased while the peak value is only slightly decreased, giving interesting transfer functions, with a finite-band response localized in the gravitational spectrum. Examples of transfer functions corresponding to that mode of operation are plotted in Fig. 7. Figure 8 summarizes the discussion of standard recycling systems by a plot of the optimal NSNR value for the different systems.

IV. SYNCHRONOUS RECYCLING

A. General principles of synchronous recycling

The basis of synchronous recycling is to include two mutually orthogonal gravito-optic transducers in a ring cavity of high finesse. If the effective storage time in each arm is equal to half the gravitational period, the phase lag between the perturbed and nonperturbed light waves, or better, between two counterpropagating waves, is expected to increase with time up to a limiting value imposed by the finite losses of the recycling cavity. We consider a ring cavity (see Fig. 9) with a recycling mirror of parameters R_r, T_r, p_r as in the previous section, and a transfer mirror of parameter R_t. In this ring cavity, two orthogonal gravito-optic transducers, G and G' are included. Let G and G' be the two corresponding operators—both have the same G_{ii} coefficients, but opposite G_{01}, G_{02} coefficients. The global operator associated with the ring cavity included in the recycling setup is S with

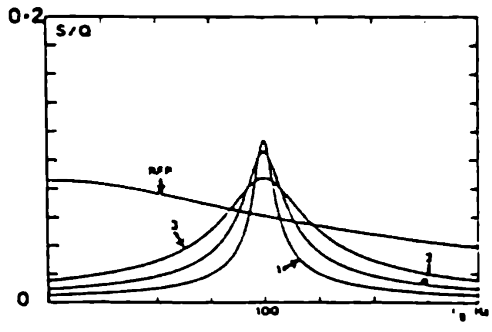

FIG. 7. Transfer function for standard recycling with detuned FP cavities and nonoptimal time constant. (1) $t = t_{opt}$; (2) $t = t_{opt}/2$; (3) $t = t_{opt}/4$. RFP: standard recycling interferometer with resonant FP cavities (for comparison).

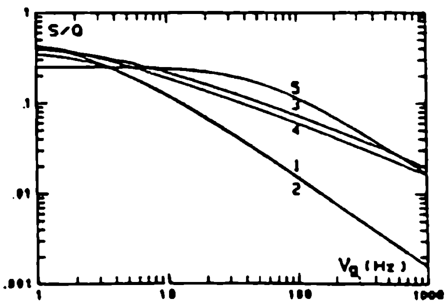

FIG. 8. Optimal values of the NSNR versus gravitational frequency for standard recycling systems: (1) delay lines—no recycling (for comparison); (2) resonant FP—no recycling (for comparison); (3) delay lines—standard recycling; (4) resonant FP—standard recycling; (5) detuned FP—standard recycling (peak value).

$$S=[\sqrt{R_r}-(1-p_r)\sqrt{R_r}e^{2i\omega a/c}G'\cdot G](1-\sqrt{R_rR_r}e^{2i\omega a/c}G'\cdot G)^{-1}\,,$$

where $2a$ is the total length of the transfer paths. A direct computation of the coefficients of S gives

$$S_{0i}=\frac{-T_r\sqrt{R_r}e^{2i\omega a/c}G_{0i}(G_{ii}-G_{00})}{(1-\sqrt{R_rR_r}e^{2i\omega a/c}G_{00}^2)(1-\sqrt{R_rR_r}e^{2i\omega a/c}G_{ii}^2)}\quad (i=1,2)\,.$$

B. Synchronous recycling with delay lines

In the case of delay lines, the preceding setup may be regarded as a very long ring cavity of length of $4nL+2a$. It follows that the free spectral range between two eigenfrequencies is $c/4nL$ (a being very small compared to L) and that a gravitational wave of frequency $c/4nL$ will be able to transfer light power from a carrier at resonance to two resonant sidebands. Let us develop this idea.

By replacing G by the delay line operator in the recycling formula, we obtain, assuming $n \gg 1$,

$$S_{10}=\frac{-2T_r\sqrt{R_r}e^{iz}R^{2n}e^{4in\omega L/c}e^{-2in\Omega L/c}\frac{\nu_{opt}}{\nu_g}\sin\left|\frac{n\Omega L}{c}\right|^2}{(1-\sqrt{R_rR_r}e^{iz}R^{2n}e^{4in\omega L/c})(1-\sqrt{R_rR_r}e^{iz}R^{2n}e^{4in\omega L/c}e^{-4in\Omega L/c})}\,,$$

where $z=2\omega a/c$. S_{20} has a similar expression with Ω replaced by $-\Omega$. It is always possible to choose z in such a way that the carrier frequency is a resonance of the global ring cavity:

$$e^{iz}e^{4in\omega L/c}=1\,.$$

Then,

$$S(f)=\frac{4T_r\sqrt{R_r}e^{-2i}\frac{Q}{f}\sin^2\left|\frac{ft}{2}\right|}{(1-\sqrt{R_rR_r}e^{-2t})|1-\sqrt{R_rR_r}e^{-2t}e^{-2ft}|} \tag{15}$$

We intend to optimize the maximum of this function of Ω which is reached for $f_0t=\pi$, i.e., $\nu_g^{(0)}=1/2\tau_r$. This means that for that particular gravitational frequency, the optical carrier and its two sidebands are resonant in the ring cavity:

$$\nu_{opt}-\nu_g^{(0)},\ \nu_{opt},\ \nu_{opt}+\nu_g^{(0)}$$

are successive eigenfrequencies. At

$$\nu_g=\nu_g^{(0)}$$

we have

$$S(f_0)=\frac{4T_r\sqrt{R_r}e^{-2\pi/f_0}\frac{Q}{f_0}}{(1-\sqrt{R_rR_r}e^{-2\pi/f_0})^2}\,.$$

The optimal value of the recycling rate is therefore

$$\sqrt{R_r}=(1-p_r)\sqrt{R_r}e^{-2\pi/f_0}$$

yielding an optimal peak value ($R_r=1$):

$$S(f_0)=\frac{4Q}{f_0}\frac{e^{-2\pi/f_0}}{1-(1-p)e^{-4\pi/f_0}}$$

with (16)

$$p=1-(1-p_r)R_r\,.$$

A plot of $S(\nu_g)$ is given in Fig. 14. The limiting value for very low frequencies is therefore $S(0)=0$; for f_0 not too low we have

$$S(f_0)=\frac{Q}{\pi+pf_0/4}\,.$$

When extra cavity losses p are weak (in the reference antenna, p has been given the same value as in the case of standard recycling, namely, $p=2.1\times10^{-3}$), we have a flat maximum of the function $S(f_0)$: within the region $1\ll f_0\ll 4/p$, $S(f_0)\approx Q/\pi$. In the general case, the transfer function can be expressed as

$$S(f)=S(f_0)\times\left|1+\left|\frac{2(\pi/f_0)(1-p)e^{-4\pi/f_0}}{1-(1-p)e^{-4\pi/f_0}}(f-f_0)\right|^2\right|^{-1/2} \tag{17}$$

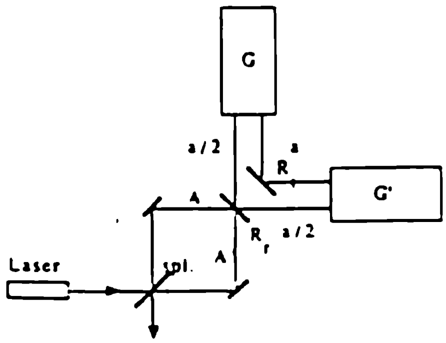

FIG. 9. Sketch of the whole synchronous recycling setup.

This is a resonant type response characterized by a bandwidth [full width at half maximum (FWHM)] of

$$\delta f = \frac{\sqrt{3}[1-(1-p)e^{-4\pi/f_0}]}{f_0(1-p)e^{-4\pi/f_0}}$$

for the central band $1 \ll f_0 \ll 4\pi/p$, we have the very simple result:

$$S(f) = \frac{Q}{\pi}\frac{1}{[1+\frac{1}{4}(f-f_0)^2]^{1/2}}, \quad \delta f = 4\sqrt{3}\ . \tag{18}$$

C. Synchronous recycling with Fabry-Perot cavities

1. *Classical properties of coupled cavities*

When the gravito-optic transducers are Fabry-Perot cavities, the recycling setup may be viewed as a system of three cavities: two long cavities of length L coupled by means of a third short one of length a (see Fig. 10). If we ignore losses and external coupling, we can see that such an optical device has a system of eigenfrequencies obtained by duplication from the spectrum of a single isolated cavity—each eigenfrequency ν_0 of the isolated FP cavity is split into two new eigenfrequencies: ν_A, ν_S corresponding to symmetric and antisymmetric eigenmodes. The values of ν_A, ν_S depend on the tuning of the coupling short cavity. When the coupling cavity is at a maximum of transmission, the coupling is strong and the difference

$$|\nu_A - \nu_S|$$

is of the same order of magnitude as the free spectral range. On the contrary, if the coupling cavity is at a maximum of reflection, the coupling is weak, and the frequency gap becomes small. Assuming extremely high reflectivities of the rear mirrors and finite reflectivities of the front mirrors, it can be shown that

$$2\pi(\nu_A - \nu_0)L/c = \arctan\left[\frac{1-\sqrt{R_1}}{1+\sqrt{R_1}}\cot(z/4)\right],$$

$$2\pi(\nu_s - \nu_0)L/c = -\arctan\left[\frac{1-\sqrt{R_1}}{1+\sqrt{R_1}}\tan(z/4)\right],$$

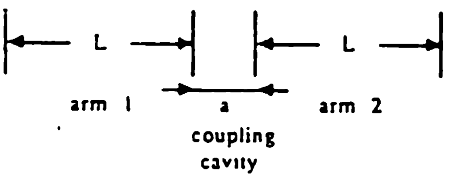

FIG. 10. Coupled cavities.

where z is the propagation phase over the length $2a$, i.e., the tuning of the short cavity (see Fig. 11). We have, furthermore,

$$\nu_A - \nu_S = \frac{c}{2\pi L}\arctan\left[\frac{1-R_1}{2\sqrt{R_1}\sin(z/2)}\right] \tag{19}$$

For z near 0 or 2π, that is, for a high transmission coefficient of the coupling cavity, we have

$$|\nu_A - \nu_S| = \frac{c}{4L}\ ,$$

which is the free spectral range of a ring cavity of length $4L$. Because of the strong coupling, the front mirrors are ignored.

For $z=\pi$, at the maximum of reflectivity of the coupling cavity, we have

$$|\nu_S - \nu_A| = \frac{cR_1^*}{4\pi L} = \frac{1}{\pi\tau_S'}, \quad R_1^* = 1 - R_1 \ll 1\ ,$$

where τ_S' is the common time constant of both long cavities. For high values of τ_S', values of $|\nu_A - \nu_S|$ comparable with gravitational frequencies can be attained, and power can be transferred from the carrier to one sideband provided that their frequencies coincide with ν_A and ν_S, respectively. We are going to discuss this idea below.

2. *Synchronous recycling with FP cavities*

Figure 12 summarizes the notation involved. The optical paths were separated for more clarity. We have assumed a separation between the two counterpropagating waves so that we can apply the preceding formula for synchronous recycling which is valid for a ring cavity. This can be practically done by suitable elements which are not taken into account here, for their losses can be included in the transfer losses. By using the matrix algebra presented in Secs. II A and II B, it can be shown that the operator associated with the whole system is such that

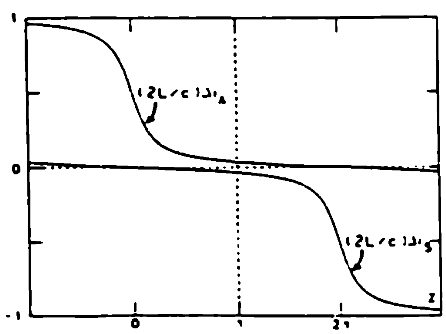

FIG. 11. Eigenfrequencies of a system of coupled cavities.

$$|S_{10}| = \frac{2T_r\sqrt{R_r}T_1^2R_2\frac{\nu_{opt}}{\nu_g}\sin\left|\frac{\Omega L}{c}\right|^2}{|1+Re^{2i\omega L/c}|^2|1+Re^{2i(\omega-\Omega)L/c}|^2|1-\sqrt{R_rR_r}e^{iz}F^2||1-\sqrt{R_rR_r}e^{iz}F_-^2|} .$$

We have used the following notation:

$$z=\frac{2\omega a}{c},\quad R=\sqrt{R_1R_2},\quad F=\frac{(1-p_1)\sqrt{R_2}e^{2i\omega L/c}+\sqrt{R_1}}{1+Re^{2i\omega L/c}},\quad F_-=\frac{(1-p_1)\sqrt{R_2}e^{2i(\omega-\Omega)L/c}+\sqrt{R_1}}{1+Re^{2i(\omega-\Omega)L/c}} .$$

Only one sideband can be made resonant at time. We shall confine our attention on S_{10}. The discussion for S_{20} is quite analogous. The NSNR is therefore $S(f)=|S_{10}|$.

Let Δf be the normalized detuning of the source with respect to an eigenfrequency of an isolated cavity: $\Delta f\equiv 2\pi(\tilde{\nu}_{opt}-\nu_0)\tau''$, and let f be the normalized gravitational frequency: $f\equiv 2\pi\nu_g\tau''$. With this notation we obtain

$$S(f)=\frac{2T_r\sqrt{R_r}T_1^2R_2\frac{Q}{f}\sin^2\left|\frac{ft_m}{2}\right|}{|1-\sqrt{R_1R_2}e^{ift_m}|^2|1-\sqrt{R_1R_2}e^{i(\Delta f-f)t_m}|^2AB} \tag{20}$$

with

$$A=|1-\sqrt{R_rR_r}e^{iz}F^2|,\quad B=|1-\sqrt{R_rR_r}e^{iz}F_-^2|$$

We assume the frequency of the source (carrier) to coincide with the antisymmetric eigenfrequency of the system:

$$\frac{z}{2}+\mathrm{Arg}F\equiv\pi \pmod{2\pi} .$$

In order to find the peak value of $S(f)$ we assume further the lower sideband frequency to coincide with that of the symmetric eigenmode:

$$\frac{z}{2}+\mathrm{Arg}F_-\equiv 0 \pmod{2\pi} .$$

Let us see at which value of f the preceding coincidence takes place. We must have

$$\tan(\mathrm{Arg}F)=\tan(\mathrm{Arg}F_-)=-\tan(z/2) .$$

A general form of the phase of a detuned cavity was given in Sec. II B 2 yielding

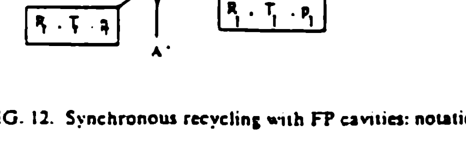

FIG. 12. Synchronous recycling with FP cavities: notation.

$$\mathrm{Arg}F=\pi+\arctan\left|\frac{2\Delta ft(1-t)}{1-2t-\Delta f^2t^2}\right| ,$$

$$\mathrm{Arg}F_-=\pi+\arctan\left|\frac{2(\Delta f-f)t(1-t)}{1-2t-(\Delta f-f)^2t^2}\right| .$$

By solving in f the preceding equations we obtain the gravitational resonant frequency as a function of the carrier detuning:

$$f_0t=\frac{1-2t+\Delta f^2t^2}{\Delta ft} . \tag{21}$$

The requirement that Δf makes the carrier to coincide with the antisymmetric eigenmode is now

$$\frac{2\Delta ft(1-t)}{1-2t-\Delta f^2t^2}=-\tan\left|\frac{z}{2}\right|$$

the solution of which relates the antisymmetric detuning Δf_A to the tuning of the coupling cavity:

$$\Delta f_At=(1-t)\cot\left|\frac{z}{2}\right|+\left|(1-t)^2\cot^2\left|\frac{z}{2}\right|+1-2t\right|^{1/2} . \tag{22}$$

The same equation would give the symmetric detuning:

$$\Delta f_St=(1-t)\cot\left|\frac{z}{2}\right|-\left|(1-t)^2\cot^2\left|\frac{z}{2}\right|+1-2t\right|^{1/2} \tag{23}$$

The resonant gravitational frequency can be related to z by

$$f_0t=(\Delta f_A-\Delta f_S)t$$
$$=2\left|(1-t)^2\cot^2\left|\frac{z}{2}\right|+1-2t\right|^{1/2}$$

The laser source can be properly tuned to coincide with the antisymmetric eigenfrequency, by locking it on the minimum of reflection of the ring cavity corresponding to the antisymmetric resonance. We intend now to optimize $S(f_0)$ when f_0 has its minimum value, namely, when $z \equiv \pi$; then

$$\Delta f_A t = \sqrt{1-2t} \ ,$$
$$\Delta f_S t = -\sqrt{1-2t} \ ,$$
$$f_0 t = 2\sqrt{1-2t}$$

In this same special case, the reflectivities of the cavities are the same for the carrier and the sideband and we have

$$|F_-^2| = |F^2| = 1-2t \ .$$

If $f_0 >> 1$, we have $t \simeq 2/f_0$ and consequently $\tau_S' = 1/\pi \nu_g^{(0)}$ as found in Sec. IV C 1.

Taking into account that $\Delta f_A, \Delta f_S, f_0$ are small compared with the free spectral interval of the cavities, we find an approximate form for the peak value of the NSNR:

$$S(f_0) = \frac{1}{4} Q f_0 t^2 \frac{T_r}{[1-\sqrt{R_r R_r}(1-2t)]^2} \ .$$

The optimal value of R_r is $\sqrt{R_r} = (1-p_r)\sqrt{R_r}(1-2t)$, so that the optimal peak value is finally

$$S(f_0) = \frac{1}{4} Q f_0 t^2 \frac{1}{1-(1-p_r)R_r(1-2t)^2} \tag{24}$$

(see Fig. 14). The relation giving $f_0 t$ as a function of t can be inverted giving

$$t = \frac{4}{f_0^2}(\sqrt{1+f_0^2/4}-1) \tag{25}$$

so that, if $f_0 >> 1$, the approximation $t \simeq 2/f_0$ holds. Then

$$S(f_0) = \frac{Q}{4} \frac{1}{1+pf_0/8} \ ,$$

where p has the same definition and value as in Sec. IV B. If further f_0 is not too high ($f_0 << 8/p$) we have an estimation of the optimal value of $S(f_0)$: $S_{max} \simeq Q/4$. In fact, $S(f_0)$ has a flat maximum of about that value in the range $1 << f_0 << 8/p$ (50 Hz to 500 Hz in the reference antenna, and falls to zero when f_0 becomes either very small or very large.

Let us return now to the general case, when z denotes an arbitrary tuning of the coupling cavity, not near $z \equiv 0$ (mod 2π) however, and let us study the transfer function $S(f)$. It is possible to give a very simple approximate form of $S(f)$ when f is near f_0 and f_0 in the optimal range defined above: $1 << f_0 << 8/p$. Let us set

$$\kappa = \frac{f-f_0}{f_0} << 1$$

neglecting second-order terms in t or κ, only the phase term in the quantity named B will change and with

$$e^{i(2\mathrm{Arg}F_- - z)} = e^{-4i\kappa\tan(z/4)}$$

we obtain

$$S \simeq \frac{1}{4} Q f_0 t \frac{\sin^2(z/2)}{[1+2\sin^2(z/4)][1+2\cos^2(z/4)]} \times \frac{1}{\left|1+\dfrac{2i\kappa\cot(z/4)}{2t[1+2\sin^2(z/4)}\right|}$$

which yields, owing to the relation $f_0 t = 2/\sin(z/2)$,

$$S(f) = \frac{Q|\sin(z/2)|}{3+\sin^2(z/2)} \left[1+\frac{4(f-f_0)^2\cos^4(z/4)}{[1+2\sin^2(z/4)]^2}\right]^{-1/2} \tag{26}$$

The gravitational bandwidth is, therefore,

$$\delta f = \sqrt{3}\frac{1+2\sin^2(z/4)}{\cos^2(z/4)} \quad \text{(FWHM)} \ .$$

In the special case $z \equiv \pi$ we have simply

$$S(f) = \frac{Q}{4}\frac{1}{[1+(f-f_0)^2/4]^{1/2}}, \quad \delta f = 4\sqrt{3} \ . \tag{27}$$

The preceding form is quite similar to that found for delay lines. The synchronous recycling system using Perot-Fabry cavities is however continuously tunable in gravitational frequency by adjusting the optical path in the coupling cavity and the corresponding reflectance phase of the cavities (see Fig. 13) by tuning the frequency of the laser, instead of discretely (by changing n) in the case of delay lines. Figure 14 summarizes the results obtained for the sensitivities of the two types of synchronous recycling systems.

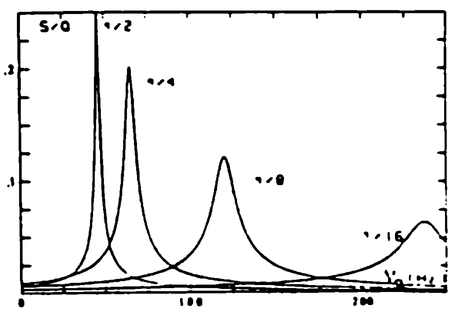

FIG. 13. Transfer functions of a synchronous recycling interferometer with FP cavities at various reflectivity phase ($\mathrm{Arg}F = \pi/2, \pi/4, \pi/8, \pi/16$): tunability.

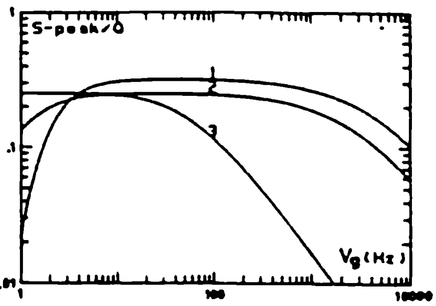

FIG. 14. Synchronous recycling interferometers: peak value of the NSNR: (1) case of delay line; (2) case of FP cavities; (3) standard recycling with detuned FP and optimal time constant (for comparison).

V. WIDEBAND AND NARROW-BAND ANTENNAS

The discussion of the different recycling schemes has shown that the gravitational frequency response of the corresponding interferometers can be deeply different from that of the initial nonrecycled transducers. As a first approximation we can distinguish between the cases of wideband responses, and the cases of resonant, or narrow-band responses. In all the following cases we will give numerical estimations of the shot-noise limited sensitivity based on the reference antenna and on an effective laser power ηP of 10 W at a wavelength of 0.5 μm, which yields

$$\left|\frac{\hbar\omega_{\rm opt}}{\eta P}\right|^{1/2}=2\times10^{-10}\ {\rm Hz}^{-1/2}$$

A. Wideband antennas

Apart from the ordinary nonrecycling interferometers involving delay lines or FP cavities, the standard recycling scheme provides us three new wideband systems that are to be compared. Recall the essential features of each.

1. Michelson interferometer with delay lines and no recycling

Zero-frequency limit of the NSNR amplitude:

$$S(0)=Q/e\ .$$

Optimal storage time for $f_0>>1$, corresponding optimal response and minimum detectable, photon noise limited h:

$$t_0=\frac{\pi}{f_0},\quad S(f)=\frac{2Q}{f}\left|\sin\left|\frac{\pi}{2}\frac{f}{f_0}\right|\right|,\quad S(f_0)=\frac{2Q}{f_0}\ .$$

at $\nu_g^{(0)}=100$ Hz, we have $h_{PN}=1.7\times10^{-23}\ {\rm Hz}^{-1/2}$.

2. Michelson with FP cavities and no recycling

Zero-frequency limit of the NSNR amplitude: $S(0)=Q/2$.

Optimal time constant and optimized response:

$$t_0=\frac{2}{f_0}\ ,$$

$$S(f)=\frac{4Q}{f_0}\frac{1}{(1+4f^2/f_0^2)^{1/2}}\ ,$$

$$S(f_0)=\frac{4}{\sqrt{5}}\frac{Q}{f_0}\ ,$$

for $\nu_g^{(0)}=100$ Hz we obtain $h_{PN}=1.9\times10^{-23}\ {\rm Hz}^{-1/2}$.

3. Michelson with delay line and standard recycling

Zero-frequency limit of the NSNR amplitude: $S(0)=0.4Q$.

Near-optimal time constant, optimized response in the band $1<<f_0,\ pf_0<<1$,

$$t_0=\frac{2.3}{f_0}\ ,$$

$$S(f)=0.92\frac{Q}{f}\sqrt{f_0}\left|\sin\left|\frac{1.17f}{f_0}\right|\right|\ ,$$

$$S(f_0)=0.85\frac{Q}{\sqrt{f_0}}$$

for $\nu_g^{(0)}=100$ Hz, we have $h_{PN}=3.5\times10^{-24}\ {\rm Hz}^{-1/2}$

4. Michelson with resonant FP cavities and standard recycling

Zero-frequency limit of the NSNR: $S(0)=Q/2$.

Optimal time constant, optimized response in the band $f_0>>1,pf_0<<1$:

$$t_0=\frac{1}{f_0}\ ,$$

$$S(f)=\frac{Q}{\sqrt{f_0}}\frac{1}{(1+f^2/f_0^2)^{1/2}}\ ,$$

$$S(f_0)=\frac{Q}{\sqrt{2f_0}}\ ,$$

for $\nu_g^{(0)}=100$ Hz, we have $h_{PN}=4.2\times10^{-24}\ {\rm Hz}^{-1/2}$.

We can conclude that delay lines and Fabry-Perot systems are almost equivalent from this theoretical point of view, either in conventional or recycling antennas. Furthermore we note that standard recycling provides a gain of $0.4\sqrt{f_0}$ within the preceding range. When no recycling is applied, the optimal NSNR is proportional (for $f_0>>1$) to Q/f_0, i.e., to $\nu_{\rm opt}/\nu_g^{(0)}$ and thus, is independent of the interferometer arm length, provided that the suitable time constant is achieved: Whether it has been obtained by many reflections over a short distance or by few reflections over a long distance does not matter. On the other hand, when recycling is applied, we see that the NSNR becomes proportional to $Q/\sqrt{f_0}$ and that the interferometer size is now important. A larger size allows fewer reflections in achieving the optimal time constant thus lowers the reflectivity losses of the arms, which permits a higher power buildup in the system and finally a better SNR. If we now examine the very-low-frequency limit, all systems are limited by their upper bound on the possible storage times: this is why the zero-frequency limits for all wideband systems is a fraction of Q. In that very-low-frequency part of the gravitational spectrum, the photon noise limited sensitivity will improve linearly with the length of the detector.

B. Narrow-band antennas

Let us recall briefly the essential features of the three types of narrow-band receivers for GW that we have encountered up to now.

1. The standard recycling setup with detuned FP cavities

Zero-frequency limit of the peak value of the SNR: $S(0)=Q/4$.

Optimal time constant, optimized response in the band $1 \ll f_0$, $pf_0 < 1$:

$$t_0=\frac{2}{3-(1+2pf_0^2)^{1/2}} ,$$

$$S(f_0)=Q\left|\frac{2(1+\sqrt{1+2pf_0^2})}{(3+\sqrt{1+2pf_0^2})^3}\right|^{1/2}$$

$$S(f)=\frac{S(f_0)}{[1-(f-f_0)^2t_0^2]^{1/2}} .$$

Bandwidth: $\delta f=[3+(1+2pf_0^2)^{1/2}]\sqrt{3}$; for the reference antenna at $\nu_g^{(0)}=100$ Hz, we get $h_{PN}=2.3\times10^{-24}$ $\mathrm{Hz}^{-1/2}$, $\delta\nu_g=15.4$ Hz.

The features of this kind of recycling become identical to that of synchronous recycling when p tends to zero.

2. The synchronous recycling setup with delay lines

Zero-frequency limit of the peak value of the NSNR: $S(0)=0$.

Optimal storage time, optimized response in the band $f_0 \gg 1$, $pf_0 \ll 1$:

$$t_0=\frac{\pi}{f_0},\quad S(f)=\frac{Q}{\pi}\frac{1}{[1+\frac{1}{4}(f-f_0)^2]^{1/2}} .$$

Bandwidth: $\delta f=4\sqrt{3}$; for the reference antenna we have at $\nu_g^{(0)}=100$ Hz, we get $h_{PN}=8.3\times10^{-25}$ $\mathrm{Hz}^{-1/2}$, $\delta\nu_g=5.5$ Hz.

3. The synchronous recycling setup with FP cavities

Zero-frequency limit of the peak value of the NSNR: $S(0)=0$.

Optimal time constant, optimized response in the range $f_0 \gg 1$, $pf_0 \ll 1$ assuming an antiresonant coupling cavity ($z \equiv \pi$)

$$t_0=\frac{2}{f_0},\quad S(f)=\frac{Q}{4}\frac{1}{[1+\frac{1}{4}(f-f_0)^2]^{1/2}} .$$

Bandwidth: $\delta f=4\sqrt{3}$; for the reference antenna: at $\nu_g^{(0)}=100$ Hz, we get $h_{PN}=10^{-24}$ $\mathrm{Hz}^{-1/2}$, $\delta\nu_g=5.5$ Hz.

Delay lines or Fabry-Perot cavities in synchronous recycling systems are thus almost equivalent. We can say that the gain obtained at the peak value of the NSNR by synchronous recycling is roughly a factor of $0.15f_0$ with respect to no recycling, and a factor of $0.4\sqrt{f_0}$ with respect to standard recycling, when the optimal decay time is achieved, we also note that standard recycling with detuned Fabry-Perot cavities is characterized in the realistic part of the gravitational frequency spectrum by the same characteristics as the synchronous recycling. For shorter values of the decay time, a smaller peak value of the NSNR, but a larger bandwidth are obtained. Moreover, the product (peak value)×(bandwidth) is larger in the standard recycling system with detuned cavities, which means that it should be especially interesting in the case of not purely monochromatic sources.

The scaling factor Q shows the importance of the interferometer arm length. The synchronous recycling system is very sensitive to intracavity losses: an increase of the apparatus size results in fewer reflections to reach the suitable time constant, therefore, in a higher finesse of the ring cavity, which increases the SNR.

VI. CONCLUSION AND PERSPECTIVE

We have presented here a unified formalism for the study of all the kinds of passive interferometers which have been proposed so far for the detection of gravitational waves. This allowed us to compare directly the relative shot-noise limited sensitivities of these interferometers. The important results are the following.

(i) The sensitivity gain brought by the use of recycling techniques varies with the gravitational frequency. for the reference antenna, in the frequency range between 50 and 500 Hz, it is roughly equal to the square root of this frequency (expressed in Hz) in the case of a wideband antenna (standard recycling), and to the frequency in the case of a narrow-band antenna (synchronous recycling). It lies between these two values in the intermediate case of detuned recycling.

(ii) The use of a recycling technique calls for very long arm lengths: the sensitivity is proportional to the length in the case of a narrow-band recycling system, and to the square root of the length, in the case of standard recycling.

(iii) Delay-line or Fabry-Perot gravito-optic transducers show essentially the same sensitivity in all cases, but the Fabry-Perot systems are much more versatile: while any modification of the transfer function of a delay-line system requires a major change of the apparatus (moving or changing mirrors), the response of a Fabry-Perot system can be adapted rapidly with just a slight change of the laser frequency or a micrometric movement of one mirror.

(iv) The new technique of standard recycling with detuned cavities gives the possibility of finding a compromise between bandwidth and peak sensitivity, which should prove to be very useful, specially at the time of the detection of the first signals, when the sensitivity of wideband systems will still be marginal.

(v) The smallest detectable gravitational-wave amplitude $h_{3\sigma}$ obtainable with a realistic laser ($\eta P = 10$ W) and the use of recycling techniques should guarantee the observation of a few events per year, since the present theoretical estimations for strong extragalactic sources in the local cluster give amplitudes h around 3×10^{-23}.

ACKNOWLEDGMENT

The G.R.O.G. is part of the Laboratoire de Cosmologie et Gravitation Relativiste (Université Pierre et Marie Curie and CNRS) and of the Laboratoire de l'Horloge Atomique (CNRS).

University of Glasgow and Rutherford Appleton Laboratory (U.K.), Design study report, 1988 (unpublished); Max Planck Institut (F.R.G.), Report No. MPQ 129, 1987 (unpublished); VIRGO group (France and Italy): Report No. Istituto Nazionale Di Fisica Nucleare PI/AE 87/1, 1987 (unpublished); M.I.T., California Institute of Technology (U.S.A.): NSF Grant (PHY-8109581) report, 1983 (unpublished).

[2]R. W. P. Drever, in *Gravitational Radiation*, edited by N. Deruelle and T. Piran (North-Holland, Amsterdam, 1983), p. 321.

[3]C. N. Man, D. Shoemaker, and A. Brillet (unpublished).

[4]J-Y. Vinet, J. Phys. (Paris) 47, 639 (1986).

APPENDIX 3.2

FREQUENCY STABILIZATION OF A YAG LASER

(to be published in Optics Letters)

A frequency-stabilized laser-diode pumped Nd:YAG laser

David Shoemaker, Alain Brillet, C. Nary Man, Olivier Crégut

Groupe de Recherches sur les Ondes de Gravitation

Bâtiment 104, CNRS, 91405 Orsay France

Graham Kerr

Department of Physics and Astronomy

University of Glasgow, Glasgow G12 8QQ Scotland

Abstract: We describe a frequency stabilized diode pumped Nd:YAG laser, which is actively frequency stabilized relative to a reference Fabry-Perot cavity using the Pound-Drever technique. We describe the servo-loop and the measurement of its noise and gain performance, and demonstrate its ability to reduce the laser frequency noise close to the shot noise limit of 12.5 $\mathrm{mHz}/\sqrt{\mathrm{Hz}}$. This corresponds to a linewidth of ≈ 1 mHz, well below the Schawlow-Townes 'limit' of 0.13 Hz which applies for a free-running laser.

Appendix 3.2

Laser sources exhibiting very good short-term frequency stability are necessary in most schemes for the interferometric detection of gravitational radiation [1,2] and in other precision metrology and spectroscopy experiments. The technique of stabilization to a reference Fabry-Perot cavity, either in transmission [3] or in reflection [4,5] is well established, and has been applied to various lasers (Argon [2], HeNe [6], Dye [7]). Nd:YAG lasers showing very good long-term passive stability have been demonstrated [8]. We report here on the application of the Pound-Drever technique to Nd:YAG lasers, and present a comparison between calculated and measured signal to noise ratios for our system.

The laser consists of a linear cavity of 7.5 cm which contains the Nd:YAG crystal, an étalon to select a single longitudinal mode, a Brewster plate to select a linear polarization, and the output coupler. One end of the Nd:YAG crystal, which is pumped longitudinally with a laser diode (*SDL 2420*), is coated for maximum reflection at 1.06 μm and $> 90\%$ transmission at 807 nm (the pump wavelength); the other end is anti-reflection coated for 1.06 μm. The output coupler is mounted on a piezoelectric transducer to allow slow changes in the length of the cavity to be corrected. The laser threshold is at 80 mW of pump power, and the maximum single-frequency power at 1.06 μm is 20 mW.

The fundamental source of laser frequency noise is spontaneous emission, which contributes a small but random phase jitter to the stimulated emission [9]. An estimate for the linear spectral density $\tilde{\nu}$ measured in $\mathrm{Hz}/\sqrt{\mathrm{Hz}}$ of this white noise source is given by [10] $\tilde{\nu} = \Delta\nu_c\sqrt{2h\nu_\ell/P}$, where $\Delta\nu_c$ is the FWHM linewidth of the laser cavity, h is Planck's constant, ν_ℓ is the laser frequency, and P the total power lost from the cavity (output power plus losses). This is the Schawlow-Townes limit for the frequency noise of a free running laser. For the measurements presented here, one has $\tilde{\nu} \approx 0.2\ \mathrm{Hz}/\sqrt{\mathrm{Hz}}$. For our work, the linear spectral density of frequency fluctuations is the relevant measure of this noise source, and is also the quantity most directly measured; however, to aid in comparison with other lasers, one can calculate the laser linewidth $\Delta\nu_\ell$ due to a white frequency noise; it is given by [11] $\Delta\nu_\ell = \pi\tilde{\nu}^2$. Thus, the laser frequency noise due to spontaneous emission can be expressed as a total linewidth of the laser $\Delta\nu_\ell \approx 0.13$ Hz.

The optical path for the frequency stabilization is indicated in Fig. 1. A Faraday isolator F is followed by an acousto-optic modulator AO, which serves as a fast frequency control element. An electro-optic modulator EO impresses a 10 MHz phase modulation on the beam for the system of synchronous detection. A Fabry-Perot cavity FP is used as the frequency reference. The incoming laser beam is closely matched to the TEM_{00} mode of the reference cavity with the lens L_3. To reduce the coupling from transverse motions of the beam into apparent frequency fluctuations, the cavity is kept far from the degenerate case; thus, excitation of higher-order modes in the cavity will not result in a change of the shape of the resonance curve (which would be possible if the cavity were very close to, but not exactly, degenerate). The light reflected from the cavity is separated from the incoming beam with polarization optics Pol and $\lambda/4$, and falls on the photodetector PD.

The calculated and measured signal voltage of the output of the mixer as a function of the difference in frequency between the cavity resonance and the incident laser light is shown in Fig. 2. The analytical form follows from a consideration of the interference between the light directly reflected from the entrance mirror and the light stored in the optical cavity [4,12]. In normal operation, the Fabry-Perot cavity is used in the immediate neighborhood of resonance. In this regime, we can derive the signal voltage at the output of the mixer:

$$v_s = \Delta\nu \frac{16l}{\pi c} \frac{\mathcal{F}^2 T_1}{r_1 r_2} M \; J_0(\delta) J_1(\delta) \; G_1 I_{max} \left[1 + \left(\frac{2\nu_F}{\Delta\nu_c}\right)^2\right]^{-\frac{1}{2}}$$

where $\Delta\nu$ is the difference between the cavity resonant frequency and the incident light frequency. The Fabry-Perot cavity is of length l and finesse $\mathcal{F} = \pi r_1 r_2/(1 - r_1 r_2)$; the two mirrors have amplitude reflectivities of r_1 and r_2; the entrance mirror has a power transmission of T_1. A fraction M of the incident light is matched to the TEM_{00} mode of the cavity. The Bessel functions $J_0(\delta)$ and $J_1(\delta)$ have as their argument the phase modulation strength δ impressed by the Pockels cell. The photocurrent off resonance is I_{max} and G_1 is the net gain, in V/A, of the photodiode amplifier and the mixer. The Fourier frequency of the laser frequency fluctuations is ν_F. Here we have assumed that the frequency of phase modulation is much greater than the cavity linewidth $\Delta\nu_c = c/2l\mathcal{F}$, that the deviation from resonance $\Delta\nu$ is much smaller than $\Delta\nu_c$, and that higher order terms in the Bessel function expansion are negligeable.

This sensitivity is to be compared with the noise voltage $\tilde{v}_n$ resulting from the quadratic sum of the photodiode amplifier noise and the shot noise of the photocurrent

$$\tilde{v}_n = G_1\sqrt{2}\sqrt{2e(I_{mod} + I_{amp})} \ ,$$

where I_{amp} is the amplifier noise expressed as an equivalent photocurrent, and I_{mod} is the photocurrent on resonance and with the 10 MHz modulation. The additional factor of $\sqrt{2}$ comes from the fact that the noise in the upper and lower sidebands are both mixed down to the same (positive) frequency, and add incoherently.

Fits to the experimental curves, for both the demodulated signal of Fig. 2 and the transmitted light intensity, allow an accurate determination of the experimental parameters r_1r_2 and δ. To determine M, the transmitted light intensity for the TEM$_{00}$ mode I_{00} is measured, as well as the sum all of the peaks $\sum I_{nm}$ of the unwanted higher order modes which are excited when the laser frequency is scanned over one free spectral range of the reference cavity. Then $M = I_{00}/(I_{00} + \sum I_{mn})$, where typically 20 higher order modes make a measurable contribution. The photodiode amplifier noise I_{amp} is determined by finding the zero-intercept of the linear relationship between the measured noise power (in V^2/Hz) and the photocurrent for a shot-noise limited light source; the expected linear behavior is observed, assuring that shot noise is correctly measured.

For a typical measurement, we have l=0.18 m, M=0.91,
$\mathcal{F}$=813 and $\Delta\nu_c$=1.1 MHz, δ=0.36, I_{max} = 0.614 mA, I_{mod} = 0.279 mA, and I_{amp} =

0.063 mA. Using the calculated values for the signal and noise, one expects a unity signal-to-noise ratio for 12.5 mHz/$\sqrt{\text{Hz}}$.

The sensitivity and noise can also be measured. A calibrated frequency modulation at $\tilde{f}_{cal}$=50 kHz is added to the VCO (see below), with the servo-loops closed but with a unity-gain frequency less than f_{cal}. This gives the sensitivity in V/Hz. To determine the noise, light directly from the laser is put on the photodiode; the noise is measured at the mixer output for a photocurrent equal to I_{mod}. (An incandescent light source drawing the same photocurrent $\tilde{P}_{mod}$ gives the same noise as the laser, indicating that the laser is shot-noise limited at 10 MHz.) This independent determination of the unity signal-to-noise ratio yields a value of 14.3 mHz/$\sqrt{\text{Hz}}$ for the measurement above. Extensive experiments in which the finesse, modulation, matching, and power were varied verify that the formulæ for the signal and noise above describe well the measurement system. Special care has to be taken to ensure the linearity at every step of the detection system in order to reach the close agreement observed ($\approx$ 1.2 dB) between the calculated and measured signal-to-noise ratios.

The signal path for the servo system is indicated by the solid lines in Fig. 2. Two loops are nested to obtain a combination of wide bandwidth and large dynamic range. The inner loop, consisting of the photodiode PD, mixer M, amplifier G_1, filter H_1, and the voltage controlled oscillator VCO, uses the acousto-optic modulator AO as the control element; the principal limitation in the gain-bandwidth of the servo-system is given by the delay τ = 1.2 μs in this modulator. The outer loop takes its input from filter H_1. It consists of filter H_2 and high-voltage amplifier G_2, and utilizes the piezo-electric transducer of the laser output coupling mirror as the control element. The laser frequency can be controlled over about one-half free spectral range, or 500 MHz. Here the first mechanical resonance of $\approx$3.3 kHz in the transducer limits the gain-bandwidth possible. The unity-gain frequency of the inner loop is typically 120 kHz and the crossover frequency to the outer loop typically 300 Hz. To take advantage of the limited bandwidths available, the slope of the feedback network H_1 is 30 dB/octave at up to $\approx$ 1 kHz, and then 18 dB/octave until the region of the unity-gain frequency, where it becomes 6 dB/octave; and for H_2 it is maintained at 9 dB/octave. The gain of the combined loops at, for instance, 1 kHz is of the order of 10^6 (or 120 dB), and exceeds 10^9 at 10 Hz. The calculated and measured closed-loop transfer-functions for frequency fluctuations agree well.

Fig. 3 shows the frequency noise of the Nd:YAG laser as measured at the error point of the servo-system. The top curve is the unstabilized noise; for these measurements, the shot noise limited noise floor of 12.5 $\mathrm{mHz}/\sqrt{\mathrm{Hz}}$ is indicated. Local mechanical and acoustic disturbances are responsible for the steep rise for frequencies less than $\approx$10 kHz. The relaxation oscillation results in a peak at $\approx$ 90 kHz. In the region between 10 kHz and 70 kHz, the spontaneous-emission induced laser frequency noise of 0.2 $\mathrm{Hz}/\sqrt{\mathrm{Hz}}$ dominates.

The bottom curve is the error point signal for the stabilized laser. While it is not an independent measure of the frequency fluctuations, this curve shows the suppression available with the servo-system, which agrees well with the predictions of the loop performance. The servo-loop performance is limited at frequencies above $\approx$ 10 kHz by the gain in the servo-loop, and at lower frequencies by the noise of the amplifier which forms the summing junction for the servo-loop. This floor of 3 $\mathrm{mHz}/\sqrt{\mathrm{Hz}}$ is lower than the the actual frequency noise of the stabilized laser, which, for all frequencies lower than $\approx$40 kHz, cannot be less than the detection noise of 14.3 $\mathrm{mHz}/\sqrt{\mathrm{Hz}}$; however, the reduction of the noise below the Schawlow-Townes 'limit' of $\approx$ 200 $\mathrm{mHz}/\sqrt{\mathrm{Hz}}$ is perfectly feasible. If the frequency noise is limited by the detection noise, the resulting total laser linewidth is of the order of $\Delta\nu_\ell = 1$ mHz.

The first steps toward a high-power short-term frequency stable Nd:YAG laser have been made. A practical system for a low-power reference oscillator has been demonstrated, which will be used to injection-lock [13] a high-power Nd:YAG laser. The excellent agreement between the measured and calculated signal-to-noise ratios for the detection system is reassuring for the plans for laser-based gravitational wave detectors and other critical applications of short-term stabilized lasers. Higher powers and narrower reference cavity linewidths will allow substantially better shot-noise limited performance if the gain-bandwidth of the servo system is also increased; possible solutions are the use of the electro-optic modulator for fast phase corrections [14] or the implementation of two cascaded reference cavities [2].

We wish to thank R. Schilling of the Max-Planck Institut für Quantenoptik for his helpful comments concerning the calculation of signal and noise. This work has been partially sponsored by EEC stimulation grant #ST2J-0093-2F.

References

[1]:R. Weiss, Quarterly Progress Report, Research Laboratory of Electronics, MIT 105 (1972) 54

[2]:D. Shoemaker, R. Schilling, L. Schnupp, W. Winkler, K. Maischberger, A. Rüdiger, Phys. Rev. D, 38 (1987) 423

[3]:D. Hils, J. Hall, Rev. Sci. Inst. 58 (1988) 1406

[4]:A. Schenzle, R. DeVoe, G. Brewer, Phys. Rev. A 25 (1982) 2606

[5]:R. Drever, J. Hall, F. Kowalski, J. Hough, G. Ford, A. Munley, H. Ward, Appl. Phys. B 31 (1983) 97

[6]:Ch. Salomon, D. Hils, J. Hall, J. Opt. Soc. Am. B 5 (1988) 1576

[7]:J. Helmcke, S. Lee, J. Hall, Appl. Opt. 21 (1982) 1686

[8]:T. Kane, A. Nilsson, R. Byer, Opt. Lett. 12 175

[9]:A. Schawlow, C. Townes, Phys. Rev. 112 (1958) 1940

[10]:A. Yariv, W. Caton, IEEE JQE QE-10 (1974) 509

[11]:F. Hartmann, F. Stoeckel, J. de Physique 39 (1978) C1-32

[12]:M. Houssin, M. Jardino, B. Gely, M. Desaintfuscien, Opt. Lett. 13 (1988) 823

[13]:C.N. Man, A. Brillet Opt. Lett. 9 (1984) 333

[14]:J. Hall, T. Hänsch, Opt. Lett. 9 (1984) 502

Figure Captions

Fig. 1: The actively stabilized laser. Optical components: YAG, Nd:YAG laser (with PZT length control); L_1, L_2, L_3, collimating and matching lenses; F, Faraday isolator; AO, acousto-optic modulator; EO, electro-optic modulator; Pol. polarizing beamsplitter; $\lambda/4$, $\lambda/4$ plate; FP, Fabry-Perot cavity. Electronic components: PD, photodiode; OSC, 10 MHz oscillator; MIX, mixer; G_1, H_1, amplifier and filter for the acousto-optic 'fast' loop; VCO, voltage-controlled oscillator; G_2, H_2, amplifier and filter for the PZT 'slow' loop.

Fig. 2: The error signal as a function of the laser frequency. The solid line is the superposition of the measured curve and the fitted analytical curve; the two are effectively indistinguishable. Also shown is a $\times 100$ horizontal expansion of the central part of the curve; the dotted line is the fitted analytical curve, with the measured data points indicated.

Fig. 3: Top curve: the frequency noise, expressed as a linear spectral density, of the unstabilized laser. For frequencies greater than 10 kHz, the noise is dominated by the Schawlow-Townes limit of 0.2 $Hz/\sqrt{Hz}$. Bottom curve: the stabilized laser, measured at the error point of the servo-system.

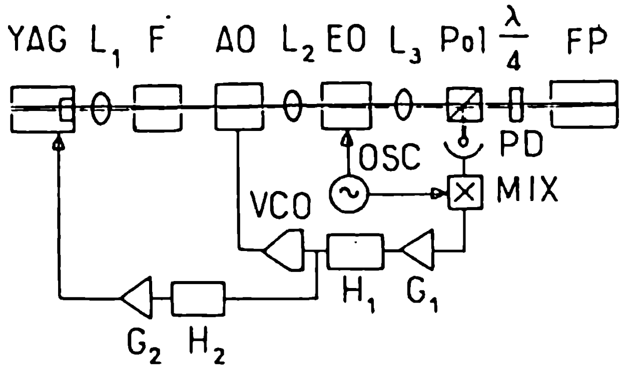
YAG
L1
F
AO
L2
EO
L3
Pol
λ/4
FP
OSC
PD
MIX
VCO
H1
G1
G2
H2

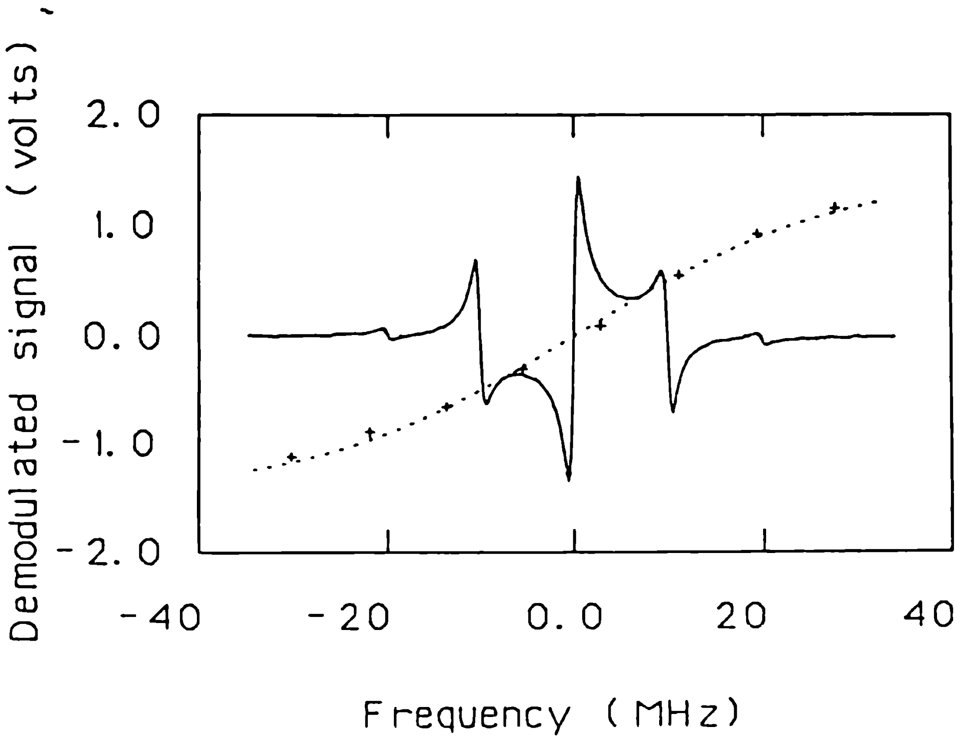
Demodulated signal (volts)
2.0
1.0
0.0
-1.0
-2.0
-40
-20
0.0
20
40
Frequency (MHz)

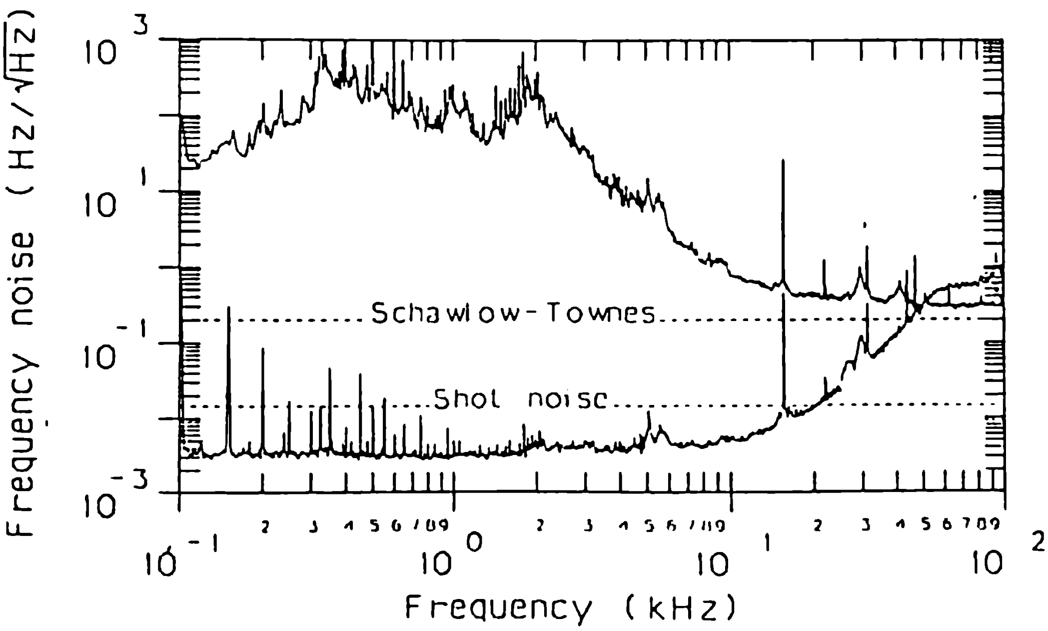
Frequency noise (Hz/√Hz)
10^3
10^1
10^-1
10^-3
Schawlow-Townes
Shot noise
10^-1
10^0
10^1
10^2
Frequency (kHz)

Appendix 3.3

Noise caused by gravitational attraction

The force due to gravitational attraction between massive objects in movement and the Virgo test masses has to be less than the Riemann force. Let us consider in a plane xy, a mass M moving along x with velocity v and the closer antenna test mass m having coordinates x = 0 , y = -D ; the gravitational force is:

$$F_x(t) = \frac{m\ M\ G\ D}{(D^2 + x^2(t))^{3/2}}$$

$$F_y(t) = \frac{m\ M\ G\ x(t)}{(D^2 + x^2(t))^{3/2}} \qquad 3.3.1$$

where G is the Universal gravitational constant. The computation of $\widetilde{F}_x$ and $\widetilde{F}_y$ compared to the Riemann force gives the following limits for h

$$\tilde{h}_x > \frac{M\sqrt{n}\ G}{\omega\ L\sqrt{\pi}\ v^2}\ \Gamma\left(\tfrac{3}{2}\right) K_0\left(\frac{\omega D}{v}\right)$$

$$\tilde{h}_y > \frac{M\sqrt{n}\ G}{\omega\ L\sqrt{\pi}\ v^2}\ \Gamma\left(-\tfrac{1}{2}\right) K_1\left(\frac{\omega D}{v}\right) \qquad 3.3.2$$

where Γ is the gamma function, K_0 and K_1 are Bessel functions of imaginary argument, $\omega = 2\pi\nu$, ν is the frequency, L is the interferometer arm length and n is the number per second of massive objects. The behaviour of the h_x and h_y depends on the K functions, in fact these functions are deeply falling increasing the argument $\frac{\omega D}{v}$.

In Fig. 3.3.1 is shown $h = \sqrt{h_x^2 + h_y^2}$ integrated in a year and D = 25 m. The continuous line refers to n = 1. s^{-1} , v = 130 K/h and M = 1 Ton; the dotted line refers to n = 0.1 $sec.^{-1}$, v = 90 Km/h and M = 100 Ton. We have chosen for Virgo 50 m of respect area around the SA chains.

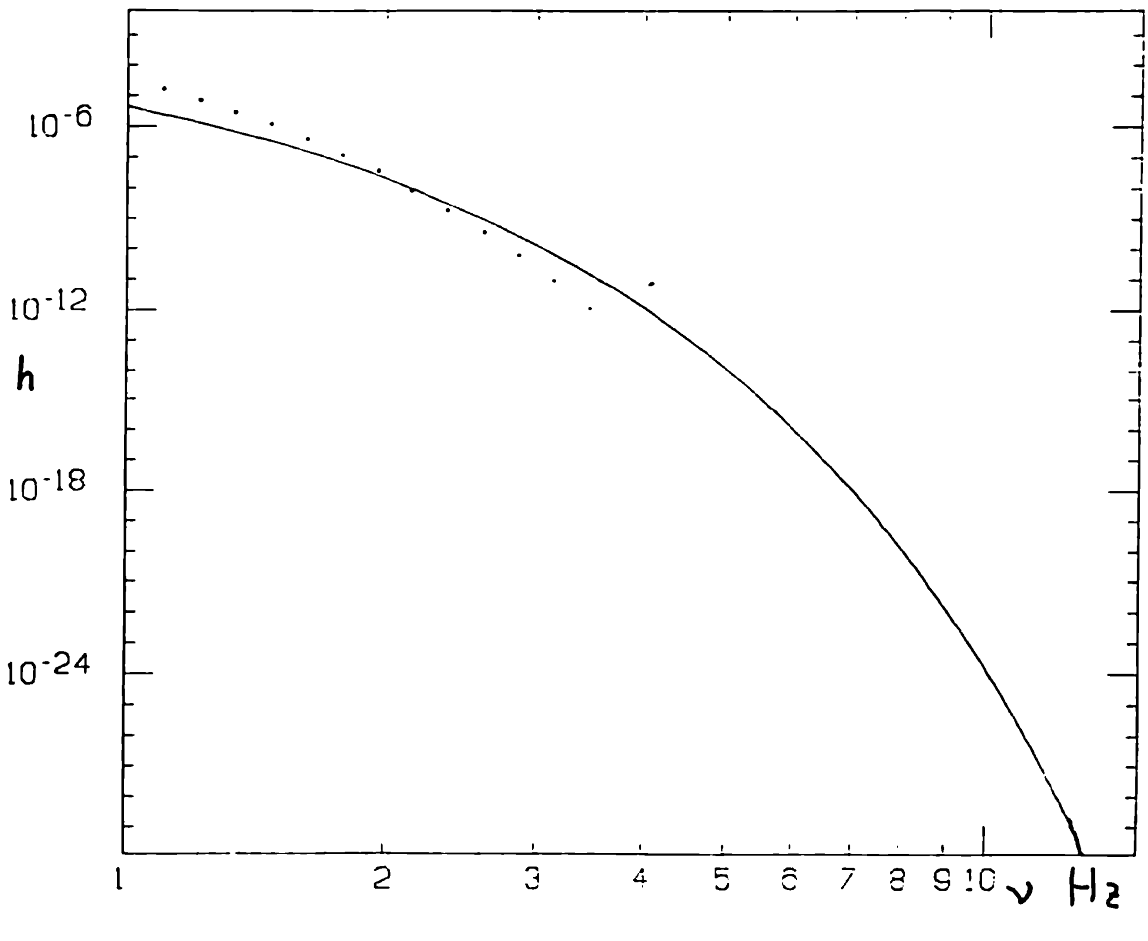

Fig. 3.3.1 Noise due to gravitational attraction. The computation is done for massive object M, passing with rate n and travelling along a line with constant speed, with minimum distance D = 25 m from a Virgo test mass. The continuous line refers to objects travelling at 130 Km/H with a mass m = 1 Ton and with a rate of 1 per second. The dotted line refers to objects travelling at 90 Km/H, with m = 100 Ton and a rate of 0.1 per second.

REPORT OF AN AD-HOC WORKING GROUP ON THE FUTURE OF INTERFEROMETRIC GRAVITATIONAL WAVE ANTENNAS IN EUROPE.

MARCH 1988

Membership of Working Group:

A.Brillet CNRS - Univ. Pierre et Marie Curie, Paris
I.F.Corbett Rutherford Appleton Laboratory
A.Giazotto INFN sezione di Pisa e Univ. di Pisa
J.Hough University of Glasgow
G.Leuchs Max-Planck-Institut fur Quantenoptik, Garching
B.F.Schutz University College, Cardiff
Ph.Tourrenc CNRS - Univ. Pierre et Marie Curie, Paris
W.Winkler Max-Planck-Institut fur Quantenoptik, Garching

1.SUMMARY

This report examines the scientific case for constructing interferometric gravitational wave antennas, and argues that a network of detectors is required if complete astrophysical observations are to be possible. For Europe this need is best satisfied by the construction of three independent, but networked, interferometers. For each instrument, the limiting background signal spectral density should be significantly better than 3.10-23/Hz (corresponding to a strain sensitivity of better than 10-21 for a 1 kHz bandwidth), over a frequency range extending from a few kilohertz down to tens of hertz, if possible. Such a sensitivity over a wide bandwidth could result in the annual observation of several hundred events of various origins.

Although the detailed scientific priorities and strategies that have been selected are different, the proposals presented to their respective funding bodies by UK, German and Italian-French groups already incorporate these goals, and the working group has

established a framework for active collaboration between these groups. This is now operational, and five specialist groups have been formed to work on different aspects of the design of long-baseline interferometers. The aim is to find cost-effective solutions to the many common design problems whilst retaining the independence and flexibility necessary to respond to different funding scenarios.

Collaboration in the construction of detectors would probably best be done through conventional bi-lateral agreements.

2.BACKGROUND

All the European groups working on the interferometric detection of gravitational radiation have been collaborating successfully for several years. Early in 1987 it became clear that the rate of progress and the performance levels actually achieved were such that the groups should put forward a coherent plan for the joint development and realisation of a network of interferometric antennas. As a result, a representative ad hoc group met on three occasions to discuss and formulate the objectives and working principles of a European collaboration, now christened EUROGRAV, to design, build and operate such a network. This report is a summary of the conclusions of that group : it is directed to the concerned scientific community and especially to the funding bodies whose support is required if this ambitious but timely project is to be realised.

3.PRESENT EXPERIMENTAL SITUATION

There are three European groups (the Max-Planck-Institut fur Quantenoptik, Garching, the University of Glasgow, Glasgow, and the Italo-French group, named VIRGO: Istituto Nazionale di Fisica Nucleare and Universite Pierre et Marie Curie) and three other groups (MIT and Caltech in the USA and the ISAS group in Japan) developing interferometric detectors.

The Garching group has a 30m delay line interferometer, with which they achieved a limiting strain sensitivity spectral density of the order of 10-19/Hz in 1986.

The Glasgow group has a 10m Fabry-Perot interferometer and has recently achieved a displacement sensitivity of 1.2 10-18m/Hz at about 1kHz, which also corresponds to a strain sensitivity spectral density of the order of 10-19/Hz.

The VIRGO prototype is smaller (O.5m, with the possibility of extension to 5m): it is used to test new ideas and techniques rather than to achieve a high strain sensitivity, and has reached the shot noise limited sensitivity for O.3W of light power.

In parallel with the development of interferometric detectors, groups in Maryland, Stanford, Louisiana State, Rome, Perth (West Australia), and China operate bar detectors.

The interferometric prototypes in Garching and Glasgow have reached a sensitivity comparable to that of the best bar detectors, namely strains of the order of a few x10-18. However, it is generally accepted that the interferometers have important potential advantages over the bars : the quantum limit to their sensitivity is a few orders of magnitude better, and they are likely to be more able to operate in a wideband and frequency tunable mode, thus providing much more information once a signal is detected. It is believed that the next major step will be the construction of large interferometers : the straightforward extension of the arm length of the well understood Garching prototype to 3 km, for instance, should result in an immediate gain in sensitivity of nearly two orders of magnitude for signals around 1 KHz. Moreover, several techniques to reduce the noise are now being developed that should lead to a sensitivity considerably better than the first goal of 3.10-23/Hz (or 10-21 in strain), which is achievable within the limits of present proven technology. Thus, for the purposes of assessing event detection rates, a strain sensitivity of 10-22 can reasonably be assumed.

The current position of world leadership in the development of interferometric detectors enjoyed by the European groups is due, at least in part, to the excellent level of cooperation achieved over the past few years (assisted by a European Commission "Twinning" award) and to the fact that their interests are (given the diversity of their approaches) to a certain extent complementary. Thus the Garching group is at the forefront of development of the delay line technique and the Glasgow group is in the same position with the Fabry-Perot system, while the VIRGO group is advanced in low frequency seismic isolation, interferometric techniques, and laser technology. Both the Garching and the VIRGO groups have successfully demonstrated light recycling (which gives increased light power in the interferometer and hence an improved sensitivity).

This broad-based range of skills is enhanced by various collaborations with interested European companies which have initiated their own development programmes, with matching technological goals. This should help to ensure that a collaborative European project will remain at the forefront of the development of the field, and will continue to make innovative contributions. The considerable advantages accrued through this fruitful collaborative diversity can be best maintained through the "simultaneous" construction of the three proposed detectors, as will be discussed below.

4.THE CURRENT PROPOSALS, AND RELATED ACTIVITIES

The scientific motivation for, and the historical development of, gravitational wave detection is sufficiently well known for its repetition to be unnecessary, while the case for building a network of detectors will be given in detail in the next section.

The three European groups have presented three separate proposals for the construction of long baseline interferometric detectors to their respective funding authorities. Similar proposals have been made jointly to NSF by MIT and Caltech.

The instruments in these proposals are logical evolutions of the present prototypes, incorporating ideas which are now, or soon will be, under test in one or more of the laboratories involved. It should be noted that within a few years the present prototypes will have reached the limits of their practical development, from the point of view of ultimate sensitivity, although they will still be invaluable as developmental test-beds for equipment for the long-baseline instruments.

All these proposals have the strong support of their respective institutions, and have received positive endorsement for their outstanding scientific value, but actual funding is not yet assured.

The Glasgow group first presented their ideas in 1984 and a detailed Design Study was prepared with the help of the Rutherford Appleton Laboratory and University College, Cardiff, and was presented to the SERC early in 1986. This group has very strong support from the University of Glasgow, which has now secured planning permission for a 3 km detector at either of two sites in central Scotland and has an option to build at one of them.

The group from MPQ, Garching, has been active in the planning of a large antenna for about the same length of time as Glasgow. They first presented a proposal for a long-baseline detector to the Max-Planck Society in early 1985. Since then they have continued to develop their ideas and presented an updated version of the proposal to the Bundesministerium fur Forschung und Technologie in early 1987.

The VIRGO project has been considered, and has been supported since June 1987, by the Commission II of INFN, which recommends that funding for the project should start in 1991; as a consequence of this recommendation the VIRGO project has been officially included in the 1989/93 INFN scientific plan approved by the INFN Directive Board. The project is also supported by the Universite Pierre et Marie Curie, Paris, and by the region of Toscana, which has offered two possible sites.

It must be stressed that expertise, interest and active collaboration in Europe is not confined to the experimentalists: theoretical subgroups are included in the VIRGO group together with experimental ones (Relativistic Gravitation, Optics, Astrophysics) and the Relativistic Astrophysics group at University College, Cardiff is also involved in the overall project (sources, data analysis, numerical relativity). Theorists provide the input concerning various expected gravitational events, the evaluation of the different possible networks, the underlying fundamental physics of the final devices, and future data analysis.

The work of several other groups is strongly associated with the needs of the EUROGRAV project. Quantum optics groups at MPQ in Garching, at the Ecole Normale Superieure in Paris and at Strathclyde University, Glasgow, are interested in contributing to the development of the sophisticated laser technology required, and in particular to the development of "squeezed states". In the Observatoire de Paris the full importance of the studies on numerical General Relativity, wave emission and wave propagation are being examined in anticipation of the birth of gravitational astronomy: this sharpens the existing interests of their Department of Relativistic Astrophysics and Cosmology.

There are two groups in the USA : MIT and Caltech. The MIT has a long history of activity in gravitational radiation research, while the Caltech group is somewhat more recent. They have combined to produce a joint proposal for two long baseline antennas in the USA : the LIGO project. Although this project has in the past suffered various delays, it was strongly recommended by an NSF panel in late 1986. The collaboration has recently been reconstituted, and will be seeking funds from NSF during 1988: their schedule suggests construction is unlikely to begin before mid-1990.

The MIT group is currently re- activating their experimental programme after a major reconstruction of their delay-line prototype, while the Caltech group is continuing work with their 40m Fabry-Perot prototype. Quite recently, the sensitivity achieved at Caltech has come close to that of the Garching and Glasgow prototypes, also yielding a strain sensitivity of about 10-19/Hz .

In summary, the European groups are well advanced in their plans for long baseline detectors, they continue to maintain a high rate of progress with their prototypes, and have established leadership in the field. The availability of the prototypes during the detailed design and construction phases of new long baseline detectors means that new ideas and techniques can be efficiently evaluated without compromising the main projects. The existence of these well understood prototypes also completely removes any need to build a "demonstrator" long baseline detector.

5.CASE FOR A EUROPEAN NETWORK OF LARGE INTERFEROMETRIC DETECTORS

The fundamental reason for building an array of large interferometers is to give birth to gravitational wave astronomy. This is an attainable and timely goal: the probability of success with today's proposals is high, and there is no reason to expect it to increase significantly if the project is delayed.

While an array of detectors is essential, there are two important thresholds for doing good science with a worldwide network of detectors: three detectors and five detectors. The significance of these thresholds is described below, but first a brief explanation of the scientific objectives in observing gravitational waves might be helpful.

The observation of gravitational radiation is important because:

The astrophysical information obtained by a network is likely to make major contributions to the study of cosmology, stellar evolution, and nuclear astrophysics.

For instance, one can expect the most convincing evidence for the existence of black holes to be given by gravitational astronomy.

Observations of supernovae and of other gravitational collapses would illuminate and perhaps even finally settle old questions like the rates at which collapses occur and pulsars and black holes are formed, the stiffness of matter at high densities, and the role of neutrinos in the explosion.

Observations of the spiralling together of two compact astrophysical objects in a binary system (called a coalescing binary) are likely to be even more frequent than supernova detections, and will be one of the richest source of physical information as well. They are among the best "standard candles" in astronomy, and as such can provide the distance scale and age of the universe (Hubble's constant), surveys of the mass distribution of the universe out to redshifts of order 1 with no absorbtion or obscuration in any direction (on account of the weakness of the gravitational interaction), and the study of many more important astrophysical questions (e.g., the equation of state of matter at high densities, the maximum mass of neutron stars, the fraction of stars that become black holes, their mass distribution, the evolution of the star formation rate out to redshifts of order 1, the nature of the "missing mass" in clusters of galaxies, the existence of an early generation of star formation).

Observations of a stochastic background of gravitational waves could confirm or falsify current theories whereby cosmic strings act as the seeds for galaxy formation.

As one of the four fundamental forces of nature, the direct detection and study of the free dynamical gravitational field is of great importance to physics. There is little doubt that "gravitons" exist: any relativistic theory of gravity predicts them; Einstein's general relativity theory is well tested in many aspects and makes specific predictions about their properties; and indirect evidence from the "binary pulsar" system PSR 1913+16 fully supports the predictions of general relativity. But fundamental theories of physics must be tested as directly as possible, and observations of gravitational waves with a network will allow a more or less complete study of the property of the graviton (mass, spin), depending on the number of antennas in the array.

The immense densities of matter in sources that give rise to detectable gravitational waves make such sources attractive "laboratories" in which we can study fundamental nuclear physics beyond the limitations of present and foreseeable particle accelerators. Gravitational radiation is our only direct probe of these laboratories. Gravitational wave observations could play a role in nuclear physics similar to that played today in high-energy physics by cosmological observations.

Recent estimates of the number of events per year that one could expect a network to observe have been made by the European theoretical groups on the basis of the physics of the sources and the expected sensitivity of arrays of detectors. Assuming a broadband strain sensitivity equivalent to 10-22 in a one kiloHertz bandwidth, even the most pessimistic assumptions lead to event rates of a few per year for the primary sources mentioned above, and optimistic rates reach several million per year for coalescing binary systems.

Recent studies by the same theory groups have shown how significantly a coordinated network improves the sensitivity and the event rate, and thus the scientific return of the detectors over earlier estimates based on their operation in a simple two-detector coincidence mode. The efficiency of an array (the fraction of all events it can capture) increases dramatically with the number of interferometers. The volume which can be observed increases by a factor 1.7 from two to three antennas and by a factor 3 from three European antennas to five U.S.-Europe antennas. Several other examples could be put forward but of course the efficiency is not the only point to be considered; given finite resources, a considered balance has to be made in choosing between more detectors and better thresholds in each.

In order to be able to use detected gravitational radiation signals to make the observations described above, it is necessary to be able to extract the following information:

the position of the source in the sky;
the amplitude of the signal as a function of time;
the polarisation of the signal as a function of time.

Determining this information is conventionally referred to as solving the inverse problem.

If general relativity is assumed as a model, then three broadband antennas (of comparable sensitivity, so that all detect the radiation with equal efficiency) are absolutely necessary, and even then there is a two-fold ambiguity in the solution. This ambiguity is easy to understand. The time delay between the arrivals of the signal at any two detectors determines a circle on the sky (in a plane perpendicular to the line joining the detectors), on which the source must lie. Among three detectors there are two independent time delays, giving two circles on the sky, which will intersect in general at two different points. Thus, four detectors are the minimum needed to give a unique solution to the inverse problem. However, practical considerations plus the gain in sensitivity and therefore in the volume of the universe observable to the network, point strongly to a requirement for five detectors worldwide.

A comparison of the performance of different sized networks of detectors shows why this is so. The assumptions made in this comparison are that the countries involved are the European ones and the U.S.A., that the interferometers are built on reasonable sites with reasonable relative orientations, and that they operate with a broadband sensitivity equivalent to 10-22 over a one kHz bandwidth.

FIVE LARGE INTERFEROMETERS.

Scientifically, the major benefits of having five detectors are the increased accuracy with which the inverse problem can be solved and the greater size of the observable volume of space: roughly 3 times as large as for three detectors. (This is because the limitation to the sensitivity of the detectors is their internal noise, which is independent from one detector to another, so that a five-detector network can operate at a lower threshold than a four-detector network can, for a given "false-alarm" rate.) The great range of the network means that it could detect coalescing binary events out to a distance of 2.3 Gpc, or 7 x 10 9 light years: these events occurred nearly half the age of the universe ago. The expected event rate would be many per day. Finally, the redundancy of information from five detectors would be invaluable in analysing and interpreting the gravitational waves from unanticipated sources: the new discoveries that gravitational wave detectors will almost surely make, which present-day theorists were not clever enough to predict.

Five networked detectors would also allow a study of the tensorial nature of the graviton. They would provide a complete set of differential measurement for the polarisations of metric theories. Theories with massive gravitons, extra gravitational fields, or "fifth-force"-type couplings might be distinguishable from general relativity in an analysis of the data from such a network.

An extremely important practical advantage of five detectors is the redundancy within the network. No detector will be able to operate 100% of the time: there will be interruptions or reductions in sensitivity for servicing and improvements, as well as for mechanical failures (vacuum pumps, lasers, etc.). With five detectors it would be possible to schedule at least the interruptions for servicing sensibly so as to ensure that the minimum requirement of four operational detectors was always satisfied.

We believe that a network of five detectors worldwide should provide such a rich source of data that it will revolutionise astronomy and rapidly establish a role for itself as one of the major astronomical observing instruments for the next 25 years.

Appendix 4.1

FOUR LARGE INTERFEROMETERS.

Four detectors is the minimum number required to give a unique solution to the inverse problem. In principle the information provided by four detectors contains enough redundancy to start a test of general relativity's predictions with bursts. The directional error box is smaller than for three detectors, and is some five times smaller for a joint US-European network of four than for a purely European three-detector network. The volume observable by a four-detector network is only 60% of the volume observable by five detectors, but is 70% larger than that accessible to a three-detector network, giving corresponding changes in the event rate.

THREE LARGE INTERFEROMETERS.

This is the threshold, or minimum requirement, for observations that can give birth to the new science of gravitational wave astronomy. As explained above, the inverse problem for bursts -- determining the direction, amplitude, and polarisation of the waves -- has a nearly unique solution, provided that one assumes general relativity as a model for the waves. Observations by three detectors give directional error boxes of the order of a few degrees for a European network, depending on the strength of the waves, the nature of the source and the correlation times of the detectors. In going from two to three antennas, the fraction of events missed because they occur in only one antenna drops from 60% to 10%, and the volume which can be observed increases by a factor 1.7.

If three independent detectors are placed near to one another, they lose directional resolution but gain effective observable volume, because they have a high probability of coincidences for supernova-type bursts from all over the sky. The coincidence probability is typically bigger by 60% for a pure European array of three interferometers than for an array of two interferometers in USA and one in Europe. In the case of a three interferometer network, Europe has the ideal size for significant directional resolution without any significant decrease of the effective observable volume. A European array would also give good spacings for the observation of the stochastic background, in the sense that the distance between any two interferometers would not greatly exceed the wave length of the observed radiations.

A network of three antennas has such a large advantage over only two antennas that it must be a reasonable European goal to build three detectors, which should define as large a triangle as possible (for the best directional resolution). Such a network would be capable of providing extremely useful scientific information on its own, regardless of what happens elsewhere in the world.

TWO LARGE INTERFEROMETERS.

Two gravitational wave detectors is the minimum number needed for a positive detection of bursts of gravitational waves; if only a single detector were operating one could never be certain that a possible gravitational wave burst event was not generated by some poorly understood local noise source. Unless bar detectors reach a sensitivity better than 10-21, two interferometers will be required in order to give a reasonable chance of detecting gravitational waves. Two is also the minimum number needed for the detection of a stochastic background of gravitational waves.

Apart from this particular case, however, the astronomical return from two detectors is limited because the most interesting sources for astrophysics will be those giving off short bursts of radiation (supernovae and coalescing binary systems, for example). Even with two interferometers, these can only be detected, not measured: because of the almost omni-directional antenna pattern of each detector, two detectors cannot provide enough information to determine the amplitude, polarisation, and direction of the waves. This also means that it would not be possible to test whether the waves obey Einstein's polarisation predictions.

ONE LARGE INTERFEROMETER.

One large interferometer alone could be used for the detection of the periodic radiation from nearby pulsars, if its useful frequency range extended to low enough frequencies. If bar detectors are able to reach a sensitivity of better than 10-21, a single interferometer could also be used to search for events in coincidence with them.

Such a big laboratory might be useful in the initial stages of a network project; it would allow flexible scheduling of the construction programme and would serve as a common research and development base for all the groups of the collaboration. It must, however, be stressed that there is no scientific argument for delaying the decision to construct an array of detectors until such a single detector laboratory is operational, both because the existing prototypes are available for the development work that would be carried out, and because the time delay implicit in this course of action serves no purpose other than to increase the final cost of the network that is essential if astronomically useful observations are to be made. Thus as many antennas as can be funded should be constructed on essentially the same timescale.

6.THE COLLABORATION - EUROGRAV

The European groups currently involved in the development of interferometric gravitational radiation detectors have agreed to form a collaboration, EUROGRAV. All members of the collaboration will work towards establishing the best possible European network compatible with funding and other restrictions, with the aim of establishing a gravitational astronomy.

Membership is not exclusive, and it is to be hoped that any other groups interested in the field will participate in the collaborative programme. EUROGRAV extends to all aspects of the development of long baseline interferometric detectors, and is a logical extension of the existing EC supported programme of research and development.

The collaboration functions through a Coordination Committee, which is representative of all the interests involved in the observation of gravitational radiation by interferometric means. This Committee meets at least three times per year to coordinate and review

(a) the EC funded collaborative programme,
(b) the various working parties (see below),
(c) interactions with external bodies on behalf of the collaboration.

The Committee chooses a "spokesman" who will act as the interface between the collaboration as a whole and the outside world, and who could, for example, be expected to speak for the collaboration at conferences etc.

Through the Committee, five specialist working groups to study five immediately important topics (vacuum systems, seismic isolation, optics, experimental facilities and data acquisition, and data analysis) have already been formed and coordinators chosen from among the Committee members. These working groups will study common design requirements and problems, and will aim at evolving uniformly acceptable cost effective technical solutions. The starting point, in all cases, will be the existing proposals, for which a great deal of preliminary conceptual design work has been completed.

It must be stressed that the aim is not to arrive at a single design for three absolutely identical antennas, but rather to ensure the adoption of optimised solutions where there is scientific and technical evidence for the existence of such solutions. In addition, of course, duplication of effort will be avoided, so that there should be very significant savings of both direct and indirect costs.

There are certain areas, for example in the choice of Fabry- Perot or delay line optical systems, where the superiority of one approach over another has not yet been demonstrated. In some cases, of which the above is an example, it may not be possible to establish that superiority, if any, without constructing a full, long-baseline, interferometer. It is important, and has been accepted by all the working groups, that a flexible approach to these problems is adopted from the outset. The final designs that evolve will be capable of easy modification, so that even quite major technological changes can be incorporated at a later stage.

Within this collaborative framework the different groups will retain their independence, scientific and financial, and this will be maintained when the construction and operation of antennas is under way. It is envisaged that, in general terms, the finances would be handled by a series of bi-lateral agreements between the various funding bodies involved in the construction of an antenna. It is appreciated that many practical details would remain to be settled before collaborative construction of a network of detectors could begin, but it is felt that the outline framework agreed is sufficiently simple and flexible to allow a solution acceptable to all parties.

CONCLUSION

The scientific case for proceeding rapidly towards the "simultaneous" construction of three detectors in Europe is an extremely strong one.There is no scientific reason to delay the construction and there are several good reasons not to do so, e.g.the high probability of success, the human and material costs of any delay in the present situation, and the timescale necessary for the construction and commissioning of each individual detector.

An array of three detectors in Europe would give the European groups the minimum scientific independence necessary to enable Europe to maintain its leading position in the field. Technically and scientifically the European groups have the capability to construct and operate a network that could make the first detection of gravitational waves and that could reach the critical number of three antennas that would see the birth of gravitational wave astronomy.A decision to build only, say, one European detector in the hope that the U.S.would build two would have serious disadvantages and long term consequences: the three detectors would not be able to pinpoint sources on the sky, they could not test general relativity, and the sensitivity of the network would be only marginally adequate if the most pessimistic estimates of event rates turn out to be correct.On the other hand, three European detectors operating with an American array, built either simultaneously or subsequently, would become one of the most important astronomical instruments of the modern age.

The European funding bodies involved in the proposals presented to date are invited to endorse the formation of a collaborative European programme directed towards the construction of a network of detectors, and to discuss how best the objectives of that programme can be realised in order that European science can capitalise on its past investment and present scientific and technological lead.

Appendix 4.2

GRAVITATIONAL WAVE RADIATION DETECTION

COLLABORATION AGREEMENT BETWEEN US GROUP AND EUROPEAN GROUPS

A meeting was held in Paris on February 14 1989. It was attended by representatives of the BMFT, CNRS, NSK, SERC and of the British, French, German, Italian and US Groups, and was able to agree on the following points :

•That the time was now appropriate for the existing informal cooperation arrangements between US and Europe to be formalised into a collaboration which would cover all aspects of the design, construction, development and operation of independent long baseline interferometric gravitational radiation detectors. Subject only to the normal constraints of commercial confidentiality, this collaboration must be free and open in the exchange of ideas and information.

• These detectors would be separately built and maintained by collaborations formed specifically for this purpose, but would be operated as a single network. Thus all detectors should have closely similar sensitivities which must be such as to allow astrophysically interesting observations to be made. The technology proposed in the current projects (USA, French/Italian, and British/German) is compatible with the aim of a strain sensitivity of 10-22 at 1kHz, and with the dual longer-term goals of enhanced sensitivity at higher frequencies and increased bandwidth by improving the low frequency (<100HZ) sensitivity.

• Several topics, which will be detailed later, were provisionally selected as being of immediate interest.

• In each of the selected topic areas, a 'lead' group would undertake to provide the driving force to ensure that the collaborating partners did actually work together in a mutually acceptable way on an agreed programme.

• Each of the lead groups would nominate an individual to act as coordinator for that specific activity.

• It is not necessary for all groups to contribute to every activity.

• The existence of these collaborative activities does not remove or diminish the freedom each group has to adopt its own solutions to common problems.

• The agreed topics, lead groups and nominated coordinators are given below :

.Lasers	France	Brillet
Mirrors, beam splitters etc	Germany	Leuchs
Isolation systems	Italy	Giazotto
Data Acquisition	UK	Ward
Data Analysis	UK	Schutz
Control Systems	USA	Spero
Vacuum	USA	Weiss
Detector Simulation	France	Vinet
Astrophysics (Signals, sources etc)	USA	Thorne

.

• In addition, the MPQ group has undertaken the responsibility of coordinating work funded by the European Commission from 1989: the coordinator is A Ruediger

• It was further agreed that it was essential that the Data Acquisition and Data Analysis groups should include both hardware and software in their brief and would aim at establishing long term agreed international standards.

ACTIONS:

The nominated coordinators, including the two from the US group yet to be named, would solicit information on activities in their specific topic areas from other groups by Easter (March 24).

This information would be collated by the coordinator, distributed :hp1.to all groups:ehp1. with an outline programme/plan of action for the collaboration to consider.

Rapid feedback, which means total commitment from all participants, is essential if this process is to converge on an agreed programme and way of working.

A meeting of all coordinators plus group leaders would be held in July, most probably to coincide with GR-12 (Boulder, 3-8 July). This meeting would review and evaluate progress and future plans.

Appendix 3.3

Appendix 4.3

Articles on seismic isolation and others (Pisa Group)

THREE-DIMENSIONAL SEISMIC SUPER-ATTENUATOR FOR LOW FREQUENCY GRAVITATIONAL WAVE DETECTION

R. DEL FABBRO, A. DI VIRGILIO, A. GIAZOTTO, H. KAUTZKY [1], V. MONTELATICI [2] and D. PASSUELLO
INFN Sezione di Pisa and Dipartimento di Fisica, Università di Pisa, Pisa, Italy

Received 26 June 1987; accepted for publication 27 July 1987
Communicated by J.P. Vigier

We present the study of a passive n-fold pendulum to be used as a three-dimensional seismic noise attenuator. A 7-fold pendulum, under construction at the INFN laboratory in Pisa, is expected to provide a horizontal and vertical attenuation factor of 10^{-11} and 10^{-9} respectively at 10 Hz and is capable to sustain a 400 kg test mass used in a large base interferometric gravitational wave antenna.

1. The seismic noise reduction is a crucial problem in the task of setting up a gravitational wave antenna sensitive in the low frequency range, where one hopes to detect waves emitted by rotating massive stellar objects like pulsars as well as signals due to coalescing neutron stars and collapsing bodies.

In this paper we present the results we have obtained in calculating the attenuation functions of a passive n-fold pendulum. Such a pendulum is capable of seismic noise reduction both in horizontal and vertical direction. These seismic attenuators are designed in such a way as to be capable to sustain heavy test masses for a large base interferometric gravitational wave antenna and to reach a horizontal and vertical attenuation factor of the order of 10^{-11} and 10^{-9} at 10 Hz respectively.

One-dimensional active seismic attenuation systems have been realized [1-3] reaching a horizontal attenuation value of about 10^{-6} at 10 Hz. These systems are rather difficult to operate at a high amplification level, due to the presence of feedback instabilities, and furthermore it is rather inconceivable to design a multi-stage three-dimensional (3D) system capable of sustaining such heavy test masses. For these reasons we were led to study a passive three-dimensional attenuator. In particular the attenuation in the vertical direction is exploited by gas springs, which have the advantage of not having hysteresis and low frequency normal modes as mechanical springs have. Furthermore a gas spring can lift very heavy loads and still have a very low stiffness.

2. First we present a study devoted to solving the problem of obtaining a relevant suppression of the horizontal component of the seismic noise in a frequency range as low as possible. Let us consider a system composed by a cascade of n masses connected by wires and suspended at a fixed frame. We call this system an n-fold passive pendulum.

In the small angle approximation the equations of the horizontal motion can be decoupled, therefore we limit ourselves to study the system in one dimension. In our scheme we suppose the wires to be unstretchable and the pendulum masses concentrated in their own CMS. In the study of the n-fold pendulum we have assumed the following conditions:

(a) the total length L of the pendulum is a fixed input parameter;

(b) the pendulum masses have an equal value of m, with the exception of the test mass, which has mass fm, where f is an input parameter;

(c) the distance between the contiguous masses is L/n;

[1] Fermilab, Batavia, USA.
[2] Laboratorio ENEA, Frascati, Italy.

(d) the relaxation time coefficient τ is equal for all pendulum stages, τ is a fixed input parameter.

For each pendulum mass one can write the equation of the motion, therefore for an n-fold pendulum one obtains

$$[Z/\Omega_0^2+2(n+f-k)-3]X_{k+1}=(n+f-k-1)X_k$$
$$+(n+f-k-2)X_{k+2} \quad (k=0,n-2),$$
$$(Z/\Omega_0^2+1)X_n=X_{n-1}, \tag{1}$$

where the last equation cannot be represented in the sequential form, since it refers to the last mass, and the other $n-1$ are labelled by the index k, where the value $k=0$ refers to the suspension point. The quantity X_k represents the horizontal displacement of the kth mass. The complex quantity Z and the real one Ω_0^2 are defined as follows:

$$Z=-\Omega^2+\mathrm{i}\Omega/\tau, \quad \Omega_0^2=gn/L,$$

where Ω is the circular frequency and g is the gravity acceleration constant. If we define a set of n quantities A_k:

$$A_{k+1}=A_0+2(n+f-k)-3 \quad (k=0,n-2),$$
$$A_n=A_0+1, \tag{2}$$

where A_0 is defined as Z/Ω_0^2, then the system of equations (1) can be written in the form

$$A_{k+1}X_{k+1}=(n+f-k-1)X_k$$
$$+(n+f-k-2)X_{k+2} \quad (k=0,n-2),$$
$$A_nX_n=X_{n-1}. \tag{3}$$

The system of equations (3) can be put in the following way:

$$X_k=B_{k+1}X_n \quad (k=0,n-2),$$
$$X_{n-1}=B_nX_n, \tag{4}$$

where the $n+1$ quantities B_k are defined as follows:

$$B_{n+1}=1, \quad B_n=A_n=A_0+1,$$
$$B_{k+1}=\frac{A_{k+1}B_{k+2}-(n+f-k-2)B_{k+3}}{(n+f-k-1)}$$
$$(k=0,n-2). \tag{5}$$

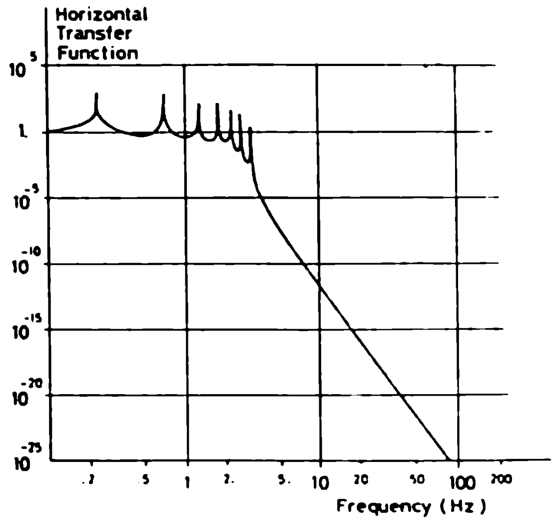

Fig. 1. Horizontal attenuation function ($n=7$) versus frequency.

From the set (4) we can take the equation for $k=0$:

$$X_n/X_0=1/B_1, \tag{6}$$

which gives the ratio of the amplitudes of the last mass over the amplitude of the pendulum suspension point. Hence the complex function $1/B_1$ expresses the horizontal transfer function of the n-fold pendulum. The study of the absolute value of the transfer function (6) shows three well separated regions in the frequency parameter:

(a) a flat region at the lowest frequencies, where the attenuation is 1;

(b) a region where n resonance peaks rise over an almost flat base, the peak widths depend on the parameter τ;

(c) a region where the attenuation function decreases with the law of ν^{-2n}.

The third region is suitable in suppressing seismic noise. Pushing this region toward the low frequencies implies keeping the pendulum resonances as low as possible. In fig. 1 a typical horizontal transfer function in the case of $n=7$ and $f=4$ is shown. The flat region ranges from 0 to about 0.1 Hz; from 0.1 Hz to about 4 Hz there is the peaks region and above 4 Hz the attenuation function begins to decrease. The last region from 4 Hz to infinity shows an exponential falling with a power -14. The noise suppression

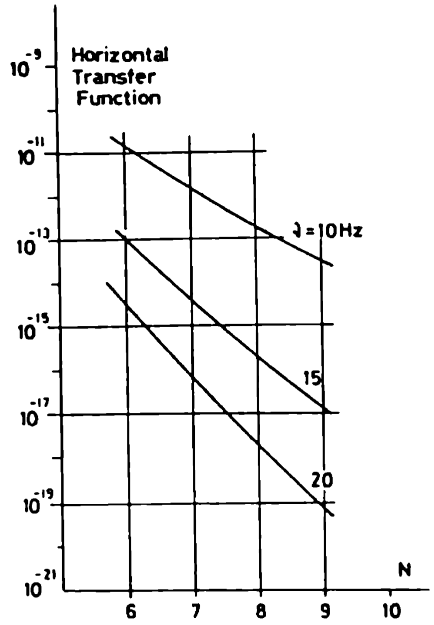

Fig. 2. Horizontal attenuation versus n.

factor is rather impressive: at 10 Hz the transfer function reaches the value of 1.45×10^{-12}. In fig. 2 is shown the attenuation function of a multiple pendulum versus the number of stages ($n=6, 7, 8, 9$) at three fixed frequencies: 10, 15 and 20 Hz.

3. Let us present now the study of an n-fold pendulum having a gas spring at each stage in the vertical direction only. It is easy to verify that a vertical cascade of n springs and n masses is capable to suppress the vertical component of the seismic noise. The choice of gas springs instead of mechanical ones is due to some merits of the former:

(a) the capability of bearing heavy masses with a rather low stiffness;

(b) the lack of hysteresis effects;

(c) the ease of operation in adjusting the spring length.

This last point is rather important if one has to arrange a long chain of gas springs. The performance of a gas spring is described elsewhere [4], in this section we discuss the attenuation factor of a vertical n-fold harmonic oscillator. The stiffness K_i of each spring is given by (see ref. [3])

$$K_i=\gamma(P_0+Mg/S_0)S_0^2/V+K_m, \tag{7}$$

where V is the cylinder volume, S_0 the piston area, P_0 the external pressure, γ the adiabatic constant and Mg the total weight supported by the jth stage and K_m the total stiffness of mechanical origin (bellows etc.).

The n equations of the n-fold harmonic oscillators are

$$ZY_j=\Omega_j^2(Y_{j-1}-Y_j)+\Omega_{j+1}^2(Y_{j+1}-Y_j)$$

$$(j=1, n-1),$$

$$ZY_n=\Omega_n^2(Y_{n-1}-Y_n)m/M_t, \tag{8}$$

where $\Omega_i^2=K_i/m$ and $Z=-\Omega^2+i\Omega/\tau$ and Y_j is the vertical displacement of the jth mass. Ω is the circular frequency and τ the relaxation time, supposed to be equal for all springs. M_t is the lowest mass i.e. the test mass of the antenna. In expression (8) the vertical displacement Y_{j-1} for $j=1$ represents the displacement of the suspension point. Let us define the $n+1$ quantities A_j,

$$A_n=1,\quad A_{n-1}=(M_t/m)(Z/\Omega_n^2)+1,$$

$$A_{n-1-j}=[(Z+\Omega_{n-j}^2+\Omega_{n+1-j}^2)A_{n-j}$$

$$-\Omega_{n+1-j}^2A_{n+1-j}]/\Omega_{n-j}^2,\quad (j=1, n-1). \tag{9}$$

Substituting eqs. (9) into eqs. (8) we obtain

$$Y_{j-1}=A_{j-1}Y_n\quad (j=1, n). \tag{10}$$

From the first equation of the system (10) ($j=1$), we get the relation between the displacement of the suspension point and the test mass:

$$Y_n/Y_0=1/A_0. \tag{11}$$

The complex function $1/A_0$ is called the vertical transfer function and its absolute value is plotted in fig. 3 versus the frequency for $n=7$. The stiffness values K_j have been deduced by fitting the experimental data (see fig. 6 of ref. [3]) and extrapolating to higher masses. The vertical attenuation function looks very similar to the horizontal one, and in complete analogy three different regions can be distinguished with the same characteristics. The vertical attenuation function is 2.38×10^{-9} at 10 Hz. In fig. 4 the attenuation function is shown at 10, 15 and 20

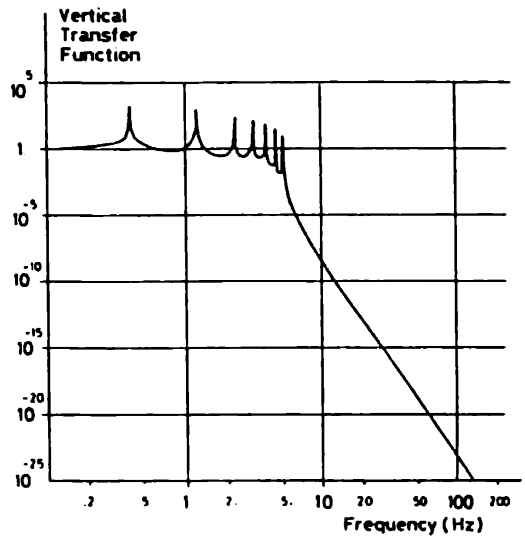

Fig. 3. Vertical attenuation function ($n=7$) versus frequency.

Hz as a function of n ($n=6, 7, 8, 9$). A criterium to equalize the horizontal and vertical attenuation, leads to the choice of $n=7$, assuming the vertical to horizontal coupling of the motion to be of the order of 10^{-2}.

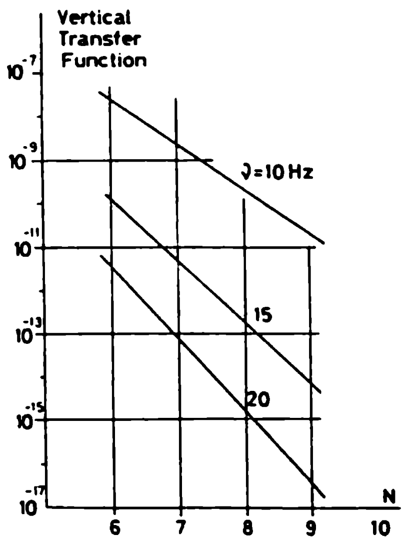

Fig. 4. Vertical attenuation versus n.

4. Let us evaluate the oscillator resonances coming from the described attenuator. Both the horizontal and vertical transfer functions (eqs. (6) and (11)), can be represented as a complex polynomial expression of the order $2n$ in the following way:

$$\mathrm{TF}=1/F,$$

$$F=\sum a_j(\mathrm{i}\Omega)^j \quad (j=0,2n). \tag{12}$$

Since the a_j are real it follows that the roots of F are conjugate. If we indicate with $\mathrm{i}\Omega=\mathrm{i}\omega_j-1/2\tau_j$ the roots of F, the TF can be written

$$\mathrm{TF}=\prod\frac{\omega_j^2}{\omega_j^2-\Omega^2+\mathrm{i}\Omega/\tau_j} \quad (j=1,n). \tag{13}$$

The TF absolute value which results is:

$$|\mathrm{TF}|=\prod\frac{\omega_j^2}{[(\omega_j^2-\Omega^2)^2+(\Omega/\tau_j)^2]^{1/2}} \quad (j=1,n). \tag{14}$$

From expression (14) it appeares that the TF behaviour in the different frequency regions is:

$$\mathrm{Re}\,\Omega\ll\omega_j,\quad \mathrm{Re}\,\Omega\sim\omega_j,\quad \mathrm{Re}\,\Omega\gg\omega_j,$$

as discussed above and grafically shown in figs. 1 and 3.

The resonance frequency $\nu_j=\omega_j/2\pi$ has been calculated both in the horizontal and vertical case for $L=5$ m, $\tau_j=10^3$ s and K_j taken by the experimental data of ref. [3] and extrapolated up to $M=10^3$ kg. The values obtained are listed in table 1.

Table 1

j	ν_j (Hz) horizontal	ν_j (Hz) vertical
1	0.24401	0.39565
2	0.75831	1.22524
3	1.35458	2.26042
4	1.90512	3.12087
5	2.37280	3.84846
6	2.78994	4.61551
7	3.25575	5.17409

5. The 3D 7-fold pendulum discussed in this paper seems to meet the attenuation factors as required by a low frequency interferometric gravitational wave antenna [5] working down to 10 Hz. The construction of such a seismic attenuator is under way at the INFN Laboratory in Pisa.

The authors are grateful to Professor A. Stefanini for valuable suggestions and useful discussions.

References

[1] A. Giazotto, D. Passuello and A. Stefanini, Rev. Sci. Instrum. 57 (1986) 1145.

[2] N.A. Robertson, R.W.P. Drever, L Kerr and J. Hough, J. Phys. E 15 (1982) 1101.

[3] P.R. Saulson, Rev. Sci. Instrum. 55 (1984) 1315.

[4] R. Del Fabbro, A. Di Virgilio, A. Giazotto, H. Kautzky, V. Montelatici and D. Passuello, Performance of a gas spring harmonic oscillator, to be published.

[5] A. Giazotto et al., Proposal for "Antenna interferometrica a grande base per la ricerca di onde gravitazionali", May 1987, INFN PI/AE 87/1.

Performance of a gas spring harmonic oscillator

R. Del Fabbro, A. Di Virgilio, A. Giazotto, H. Kautzky,[a] V. Montelatici,[b] and D. Passuello

I.N.F.N. Sezione di Pisa and Dipartimento di Fisica, Università di Pisa, Pisa, Italy

(Received 25 June 1987; accepted for publication 28 September 1987)

The characteristics and the performances of a gas spring, to be used in the future in a three-dimensional multiple attenuation system, designed to support the heavy test masses for a low-frequency gravitational wave interferometric antenna, are presented. This multiple system is expected to attenuate 10^{-9} (10^{-11}) at 10 Hz in the vertical (horizontal) direction. This experiment, in which masses up to 430 kg have been levitated, has shown that the height of the resonance peaks in the gas spring vertical and horizontal transfer functions should not prevent us from obtaining the required high attenuation factors. A gas temperature feedback system, for the gas volume control, has given satisfactory results.

INTRODUCTION

The interaction of gravitational waves (GW) with the test masses of conceivable detectors is expected to produce a very small signal; consequently keeping the test masses clear from noise contamination is a relevant problem.

In particular the seism introduces a noise through the suspension point of the test masses; the seismic noise becomes more and more dangerous at low frequency where its amplitude spectrum increases according with the approximate locality-dependent law:

$$X_s = 10^{-6}/\nu^2 \ \mathrm{m}/\sqrt{\mathrm{Hz}}, \tag{1}$$

where ν is the frequency.

Active systems have been proposed [1-3] as attenuators of seismic noise both in the vertical and horizontal direction; however, since the suspension point suffers of noise displacements in every direction, it is important to conceive an attenuator acting in three dimensions (3D).

In fact, even if the optical phase measured in an interferometric antenna for GW detection is moderately insensitive to the vertical displacements of the mirrors, vertical motion can show up in the horizontal direction because of nonlinearities and inhomogeneities in the wire attachments points. The vertical to horizontal displacement conversion factor ϵ is dependent upon the very particular experimental setup, but it is generally assumed to be $\leqslant 10^{-2}$; we shall give the following experimental evidence for it.

We plan to build a large interferometric antenna[4] (arm length $A = 3$ km) for GW detection, intended to have high sensitivity down to 10 Hz (GW amplitude $h = 10^{-25}$ for 1 year data taken at 10 Hz). Given this sensitivity, it follows from Eq. (1) that the horizontal seismic attenuation factor H has to be $< 10^{-11}$ at 10 Hz: this value takes into account a factor of 10 fluctuation of the noise around the average value of Eq. (1). We have calculated[5] that this attenuation factor can be obtained using a multiple pendulum composed by seven masses suspended in a cascade, having a 70-cm separation between their contiguous centers of masses. The weight of the test mass (the lowest one) is dictated by the maximum allowed thermal noise; assuming a mechanical quality factor $Q \sim 10^6$ it follows that the test mass should weigh > 400 kg to fulfill the previous sensitivity limits at 10 Hz. The upper six masses have been chosen to weigh 100 kg each, the total weight of the multiple pendulum being 10^3 kg; with this choice of the parameters the calculated horizontal attenuation is $H = 1.4 \times 10^{-12}$ at 10 Hz and the seven eigenfrequencies of the pendulum[5] are < 3.25 Hz. It follows from the previous arguments that the vertical attenuation factor V should be $\sim 10^{-9}$ at 10 Hz. This cannot be obtained by making use of the suspension wire longitudinal compliance, since, due to the wire cross section ($\simeq 10$ mm^2), the vertical normal mode frequencies reach 50 Hz. Springs 100 times more compliant are needed to obtain $V \sim 10^{-9}$; since the steel wires have a stiffness of $\sim 3 \times 10^6$ N/m, we must insert springs having stiffness $K < 3 \times 10^4$ N/m, giving normal modes with frequencies < 5 Hz.

A mechanical spring bearing $M = 10^3$ kg and having such a stiffness will elongate by the amount $d = 0.3$ m. As an example, a common helical steel spring[6] having $K = 3 \times 10^4$ N/m and a length of 20 cm when unloaded, has a diameter of 15 cm, 1.7-cm wire diameter, 12 turns, and a mass $M_h \sim 10$ kg. The longitudinal normal modes frequencies ν_n are approximately given by the formula $\nu_n \sim n/2\pi\sqrt{4K/M_h} = n \times 18$ Hz$(n = 1, 2, \ldots)$. Since these modes are falling right into the frequency interval of interest ($\nu > 10$ Hz), damping has to be applied; this is not an easy task because, the relaxation time being proportional to M_h, exceedingly large damping forces are needed. Furthermore, care has to be taken to decrease the spring rocking frequency, which, due to the large d value and to the large tension ($\sim 10^4$ N), can be close to 10 Hz; this implies that a device has to be inserted in the spring termination with the purpose of reducing the effective d. The previous difficulties, the hysteresis, and the lack of an easy adaptability to different loads have led us to look for an alternate solution.

A gas spring (GS) is a possible choice; in this device, gas containment is performed by means of thin wall bellows. Due to the low M_b value (0.4 kg), damping of the bellow normal modes can be achieved, for example, by wetting the convolutions with oil. The gas normal modes have frequency $\nu > 300$ Hz and they should be, due to the low gas mass, hardly visible at all in the measured transfer functions. A remarkable property of the GS is that d can be kept small and constant, even with different loads. These characteristics allow us to use the same modular GS elements in a very different configuration of the multiple pendulum, i.e., different number of stages and different weight of the masses.

A relevant point to examine is how the thermal noise, produced by the multiple pendulum elements, reaches the test mass. For frequencies above the fundamental modes ($\nu > 5$ Hz), the rms displacements $\delta_{n,i}$ of the nth mass due to thermal noise is

$$\delta_{n,i} = \left[\sqrt{4K_b T/(\tau_{n,i} M_n)}\,\right]/\Omega^2 \ \mathrm{m}/\sqrt{\mathrm{Hz}} \quad i = 1,\ 2, \tag{2}$$

where $i = 1, 2$ defines the vertical and horizontal direction, respectively, $\tau_{n,1}$ and $\tau_{n,2}$ are the relaxation times for the mass vertical and horizontal motion, respectively, K_b is the Boltzmann's constant, T is the absolute temperature, M_n is the mass of the nth element, and $\Omega = 2\pi\nu$ the observed circular frequency. If $V_{n,7}(\Omega)$ and $H_{n,7}(\Omega)$ are the vertical and horizontal displacement transfer functions from the nth element ($n = 0$ is the suspension point) to the test mass ($n = 7$), the total displacement of the test mass, in the horizontal direction (the relevant one) due to the thermal noise of the chain, is

$$\delta_{7,2} = \sqrt{4K_b T}/\Omega^2 \left[\Sigma H^2_{n,7}/(\tau_{n,2} M_n) + \epsilon^2 \Sigma V^2_{n,7}/(\tau_{n,1} M_n)\right]^{1/2} \ \mathrm{m}/\sqrt{\mathrm{Hz}}, \tag{3}$$

where ϵ is the vertical to horizontal displacement conversion factor. Since[5] $H_{n,7} \sim V_{n,7} \sim O\,[1/\Omega^{2(7-n)}] \ll 1$ and $H_{7,7} = V_{7,7} = 1$, it follows

$$\delta_{7,2} = \sqrt{4K_b T}/\Omega^2 \left[1/(\tau_{7,2} M_7) + \epsilon^2/(\tau_{7,1} M_7)\right]^{1/2} \ \mathrm{m}/\sqrt{\mathrm{Hz}}. \tag{4}$$

Equation (4) shows that the relevant contribution to the thermal noise of the test mass is only given by the lowest gas spring. The first term is the contribution of the energy losses in the horizontal direction of the test mass; these are minimized taking care that the wire attachment points in the GS do not relatively displace in the horizontal direction. This is achieved by allowing the GS piston to move only along the vertical axis by means of centering wires. The second term, due to the vertical to horizontal conversion of the vertical motion, despite the smallness of the $\tau_{7,1}$, is strongly reduced by the presence of ϵ^2; hence, care has to be taken to keep ϵ to a minimum.

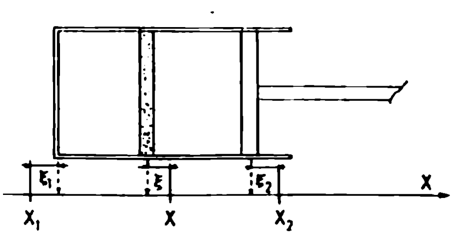

FIG. 1. Schematic diagram of a gas spring including the coordinate system used in the text.

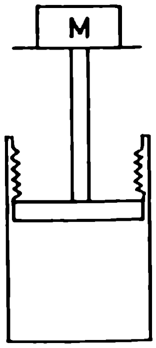

FIG. 2. Schematic example of a gas spring supporting the mass M. The bellow is used for gas containment.

We can evaluate a lower limit for $\tau_{7,1}$ from Eq. (4) assuming $\epsilon \sim 10^{-2}$, $M_7 \sim 4\times 10^2$ kg, $\nu = 10$ Hz, $T = 3\times 10^2$ K, the bandwidth $\Delta\nu = 1$/year, the GW amplitude $h \sim 10^{-25}$, and the interferometer arm length $A = 3$ km:

$$\tau_{7,1} > \epsilon^2 4K_b T\Delta\nu/(\Omega^2 M_7 h^2 A^2) \approx 10^2 \ \mathrm{s}. \tag{5}$$

In the following we show that this value is achievable.

In Sec. I we briefly present the theory of the GS and in Sec. II we give the experimental results of the prototype.

I. TRANSFER FUNCTION (TF) AND RESONANCES OF THE GAS SPRING

A GS can be represented as a gas-filled cylinder with a frictionless piston (see Fig. 1). At the time $t = 0$, the coordinates of the cylinder end and of the piston are X_1 and X_2, respectively, while at $t > 0$ they become $X_j + \xi_j(t)$ ($j = 1, 2$).

Let us consider an infinitesimal gas volume having coordinate X at $t = 0$ as shown in Fig. 1; if $\xi(t, X)$ is its displacement from the initial coordinate X, the equation of motion of this volume according to the D'Alambert equation is

$$\frac{\partial^2 \xi}{\partial t^2} = v^2 \frac{\partial^2 \xi}{\partial X^2}, \tag{6}$$

where v is the sound speed in the gas. The force F acting on the piston is

$$F = (P_e S_0 + Mg)\gamma\left(\frac{\partial \xi}{\partial X}\right)_{X=X_2} + K_m(\xi_1 - \xi_2), \tag{7}$$

where P_e is the external pressure, S_0 the piston area, M the mass (see Fig. 2), g is the acceleration of gravity, γ the adiabatic gas constant, and K_m is the sum of the bellows stiffness K_b and of all other stiffnesses of mechanical origin. The solution is

$$\begin{aligned}
\xi_2(\Omega) &= \xi_1(\Omega)H/Q,\\
H &= \gamma\left(g + \frac{P_e S_0}{M}\right)\left(\frac{i\Omega}{v}\right) \times 2e^{i\Omega L/v}(e^{2i\Omega L/v} - 1)^{-1} + \frac{K_m}{M},\\
Q &= -\Omega^2 + \frac{i\Omega}{\tau} + \gamma\left(g + \frac{P_e S_0}{M}\right)\left(\frac{i\Omega}{v}\right) \times (e^{2i\Omega L/v} + 1)(e^{2i\Omega L/v} - 1)^{-1} + \frac{K_m}{M},
\end{aligned} \tag{8}$$

where τ is the piston relaxation time and $L = X_2 - X_1$.

In the limit $\Omega L/v \ll 1$, Eqs. (8) become

$$H = \gamma(g + P_e S_0/M)/L + K_m/M,$$

$$Q = -\Omega^2 + \frac{i\Omega}{\tau} + \gamma\left(g + \frac{P_e S_0}{M}\right)\Big/L + \frac{K_m}{M}. \quad (9)$$

Equations (9) show that a GS behaves like a spring having stiffness coefficient $K_{gas} = \gamma(P_e S_0 + Mg)/L$; this expression coincides with that deduced from the state equation of the adiabatic gas compression.

Since in the real case the piston and the cylinder end areas are different, K_{gas} beomes

$$K_{gas} = \gamma(P_e + Mg/S_0)S_0^2/V, \quad (10)$$

where V is the vessel volume.

In the general case, the function H/Q has poles for

$$\Omega = \Omega_n + K_{gas}/(M\Omega_n) + O(\Omega_n^{-2}),$$
$$\Omega_n = nv\pi/L, \quad (11)$$
$$n = 1, 2, 3, \ldots .$$

In our case, since $L = 0.5$ m and $K_{gas} \ll nM\Omega_n^2$, the resonant modes have frequencies $\nu_n \sim n \times 360$ Hz$(n = 1, 2, \ldots)$.

The temperature variation of the environment surrounding the apparatus creates a piston vertical displacement $\Delta Y = (\Delta T/T)(V/S_0)$, where T and ΔT are the gas temperature and its variation, respectively; in our case $\Delta Y/\Delta T$ is 5.4 mm/°C and 10.8 mm/°C for the four and two bellows condition, respectively.

As previously mentioned, we have envisaged the necessity to mount centering wires (see Fig. 3) to force the piston motion to be parallel to the cylinder axis. We can evaluate the centering wires section S as a function of the piston mass M_p, of the transverse oscillation frequency ν_t of the piston, of the Young modulus E and the length b of the wires:

$$S = 2\pi^2 \nu_t^2 M_p b/E. \quad (12)$$

The violin mode frequencies ν_w of the wires are

$$\nu_w = n[T_0/(\rho S)]^{1/2}(2b)^{-1}, \quad (13)$$
$$n = 1, 2, 3, \ldots,$$

where T_0 and ρ are the wires tension and density, respectively. Since we need the frequency interval 10–100 Hz to be as free as possible from high-intensity mechanical resonances, we require both frequencies ν_t and ν_w to be larger than 100 Hz; from this condition we obtain $S = 10^{-6}$ m^2 and $T_0 = 13$ N. Due to the wires small mass we do not expect a relevant contribution to the overall *TF*.

The resonance peak of the bellows at 50 Hz is very high and reaches about -10 dB in the *TF*, but since the bellow mass is small it can be damped. For this purpose we have tested the following solutions:

(a) Filling the bellows vacuumside with vacuum oil. This solution, which requires a very soft gasket (with a separate vacuum circuit) to avoid oil vapors from diffusing into the vacuum, completely damps the peak, but makes the piston heavier.

(b) Wetting the bellows pressureside with high viscosity oil; the oil does not flow away, due to its surface tension. This solution seems to be good enough, even if it does not completely cancel the resonance peak.

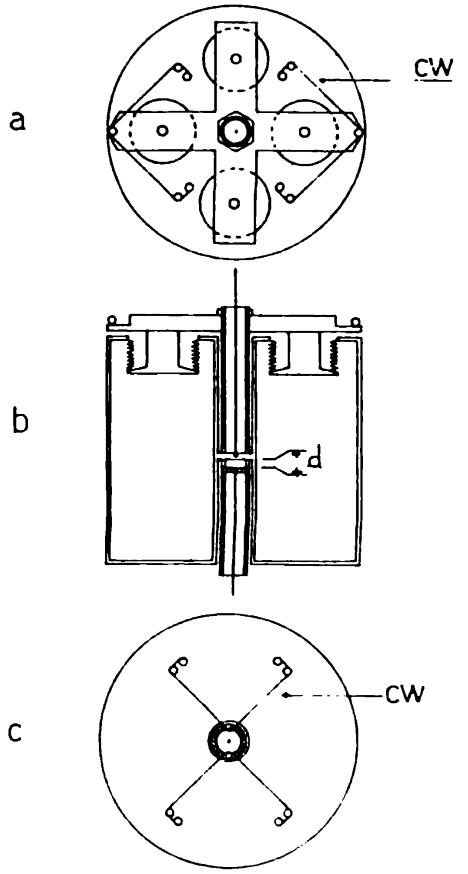

FIG. 3. Schematic diagram of the gas spring vessel: (a) vessel top end view showing the four bellows position and the centering wires (CW); (b) vessel side view; (c) vessel bottom view showing CW.

(c) Using a soft solid-state damper such as rubber or rubber sponge touching the bellow convolutions. Care has to be taken to avoid an increase in the overall stiffness.

Since the measurement frequency range of the antenna has to be kept free from any type of resonance, it is important that the rocking frequency of the gas spring be sufficiently low. The rocking frequency can be written

$$\nu = (dMg/I)^{1/2}/2\pi, \quad (14)$$

where d is the spring length (see Fig. 3) and I the cylinder momentum of inertia with respect to the spring center. The frequency of about 1 Hz is reached for $d \approx 10^{-2}$ m.

A resonance peak is produced at the normal longitudinal mode frequency of the wire suspending mass M:

$$\nu_{wire} = [ES(M + M_p)/(L_w M M_p)]^{+1/2}/2\pi, \quad (15)$$

where M_p is the piston mass, S the wire section, and L_w its length. For a steel wire having $S = 10^{-5}$ m^2, $L_w = 0.7$ m, and $M_p = 6$ kg, we obtain $\nu_{wire} = 100$ Hz. This resonance can be damped by means of the bellows damping system if M_p is sufficiently low.

II. EXPERIMENTAL APPARATUS AND RESULTS

A stainless-steel cylindrical vessel, of 50 cm length and 48 cm diameter, is equipped with two or four bellows symmetrically located at one end (see Fig. 3).

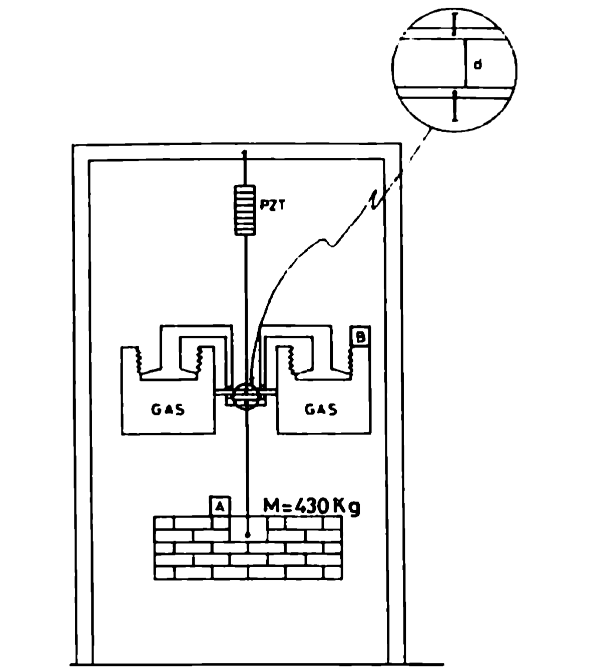

FIG. 4. Layout of the experimental setup: the piezoelectric transducer (PZT) produces vibration along the vertical direction (the PZT producing horizontal vibration is not shown). The gas spring supports the test mass M (the composite one is shown). The two accelerometers A and B measure the vibration amplitudes of the mass M and of the gas spring, respectively

These bellows, covering a total mean effective area of 280 or 560 cm^2, respectively, make up the cylinder piston. The cylinder has mass $M_c = 60$ kg and can sustain a maximum weight of 1.3×10^3 kg. The junction points of the upper and lower wires of the cylinder are arranged to be as close as possible. In our prototype this distance ranges from 0 to 1 cm. Two test weights are used: the first one, having $M < 430$ kg, is a variable mass made of lead bricks; the second one, a monolithic 200-kg mass, is used to avoid the complex resonances of the first one. We have limited the maximum weight to 430 kg, so as not to stress the wire terminations too much,

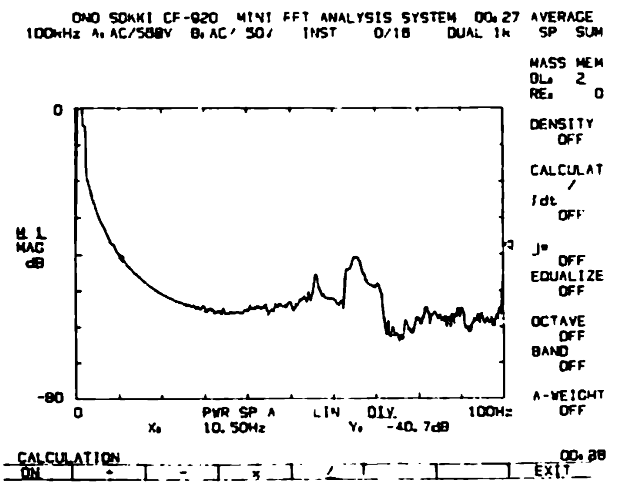

FIG. 5. Vertical TF measurement of the gas spring in the frequency range 0–100 Hz, $M = 430$ kg and two bellows. The bellows resonance peak has been damped filling the bellows with oil.

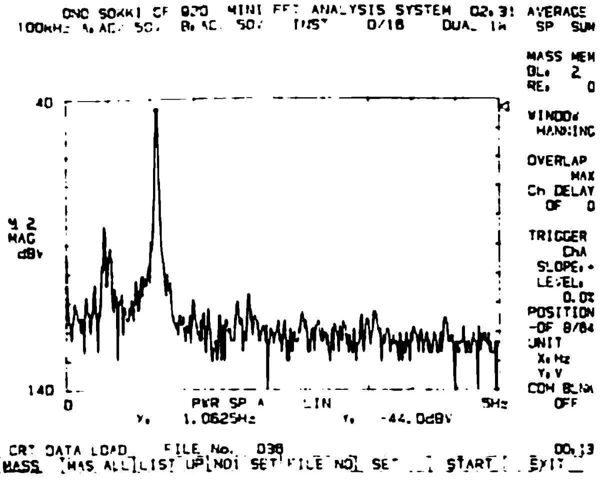

FIG. 6. The resonance peak at 1.06 Hz of the gas spring in the same condition as in Fig. 5

but a termination reaching 1.3 tons is now under test. The experimental apparatus is shown in Fig. 4.

Since our aim is to measure the vertical and horizontal TF, we inject vibrations at the suspension point of the pendulum by means of a piezoelectric transducer. We can measure the TF computing the ratio of the output of two accelerometers (Bruel Kjear 8306) located on the cylinder top end and on the mass, respectively. Figure 5 shows the TF in the frequency range 0–100 Hz, when the excitation and the accelerometers are vertical for a loading mass of 430 kg and with two bellows; Fig. 6 shows the resonance peak at 1.06 Hz.

Up to 30 Hz, the TF behavior follows the theoretical prediction

$$TF(\Omega) = (K_{tot}/M)(-\Omega^2 + i\Omega/\tau + K_{tot}/M)^{-1}, \tag{16}$$

where $K_{tot} = K_{gas} + K_m$. At higher frequency the resonances of the lead bricks composite mass make worse the precise measurement of the TF. The bellow resonance peak at ~ 50 Hz has been damped, filling the bellows with oil.

In Fig. 7 the vertical oscillation amplitude is shown as a

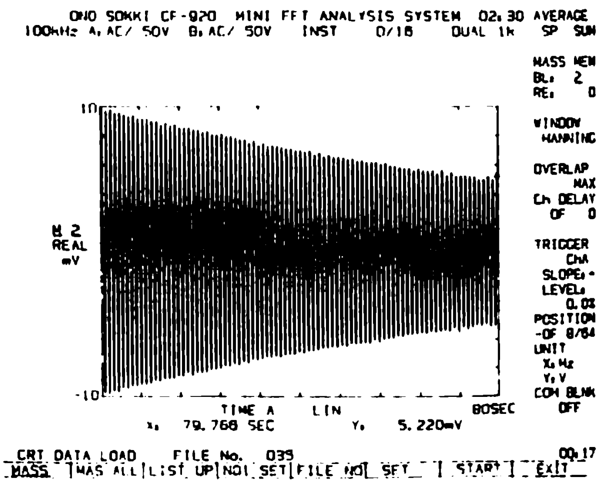

FIG. 7. Plot showing the amplitude decay time of the gas spring in the same condition as Fig. 5

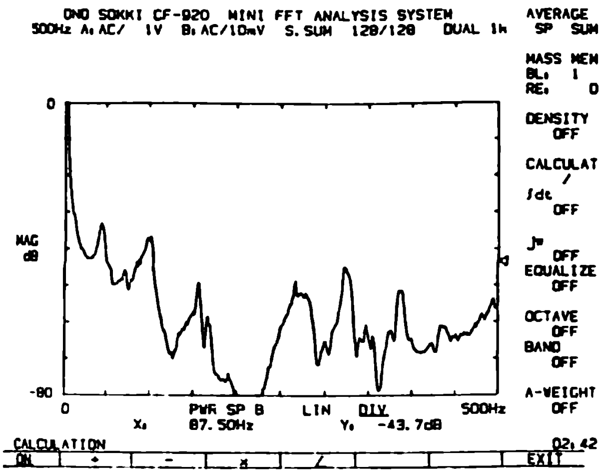

FIG. 8. The vertical *TF* (0–500 Hz) for $M = 200$ kg and four bellows; the excitation and the accelerometers are vertical.

function of time. An evaluation of the relaxation time gives $\tau = 160$ s, in fairly good agreement with the computed relaxation time due to the friction of the lead bricks mass with the air; this value satisfies the limit given by Eq. (5). A more precise measurement of this parameter can only be done in vacuum.

Figure 8 shows the vertical *TF* in the frequency range 0–500 Hz, with four bellows, with the monolithic loading mass and damping obtained by wetting the bellow convolutions with oil (this experimental condition will be the same for all the subsequent measurements); the 50-Hz bellow resonance peak (-33 dB) and the wire longitudinal mode at 100 Hz (-35 dB) are very visible. Even if the two resonance peaks are not completely damped, we believe that in the total *TF* of the multiple pendulum, it will appear the product of their height ($\simeq 10^{-11}$). In Fig. 9 the vertical to horizontal *TF*, in the frequency range 0–500 Hz, is shown; in this measurement the excitation and the upper accelerometer are vertical, while the accelerometer on the 200-kg mass is horizontal. The *TF* is $\simeq -40$ dB in the frequency interval $10 < \nu < 350$ Hz.

Figure 10 shows the *TF* measured in the same condition

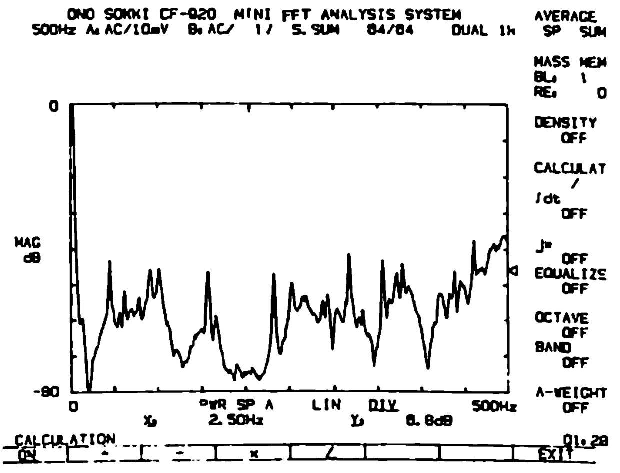

FIG. 9. The vertical to horizontal *TF* (0–500 Hz): the excitation and the top accelerometer are vertical, while the accelerometer on the 200-kg mass is horizontal, four bellows are mounted.

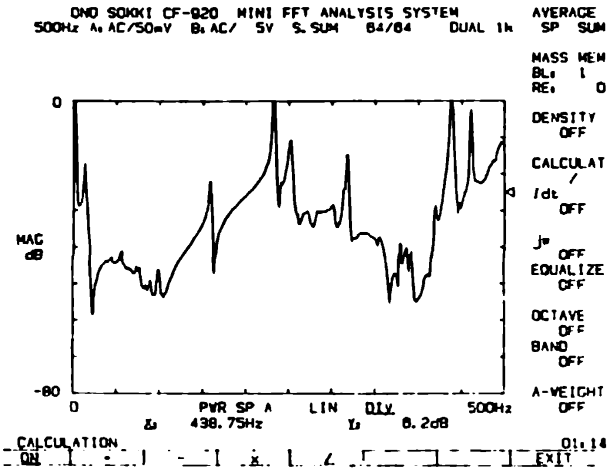

FIG. 10. The vertical to horizontal *TF* as in Fig. 9, but without gas in the gas spring ($d = 0$), showing the vertical to horizontal displacement coupling.

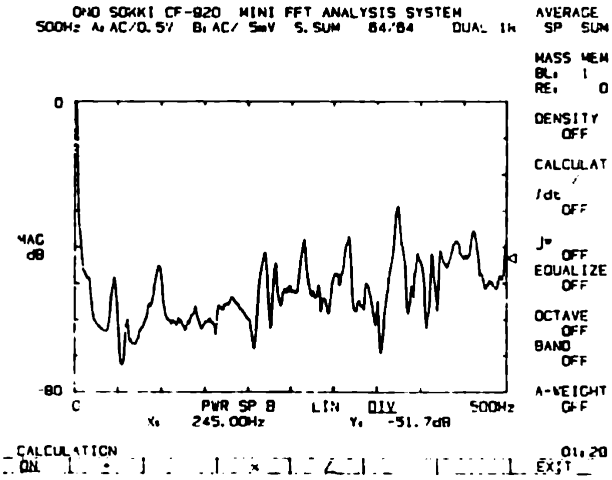

FIG. 11. The horizontal *TF* (0–500 Hz) for $M = 200$ kg and four bellows. In this measurement the excitation and the two accelerometers are horizontal.

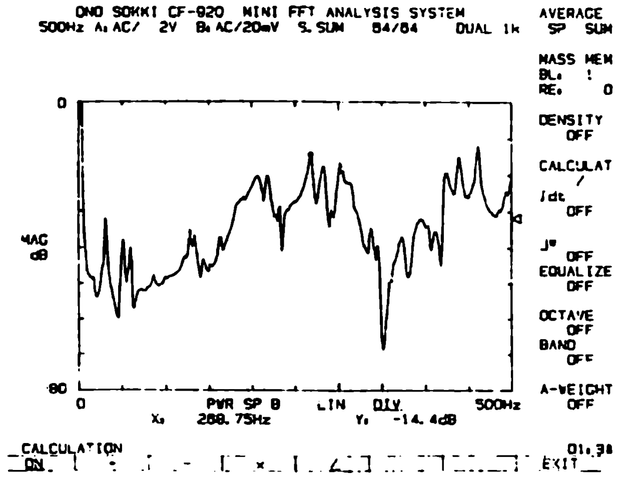

FIG. 12. The horizontal *TF* as in Fig. 11, but without gas in the gas spring ($d = 0$).

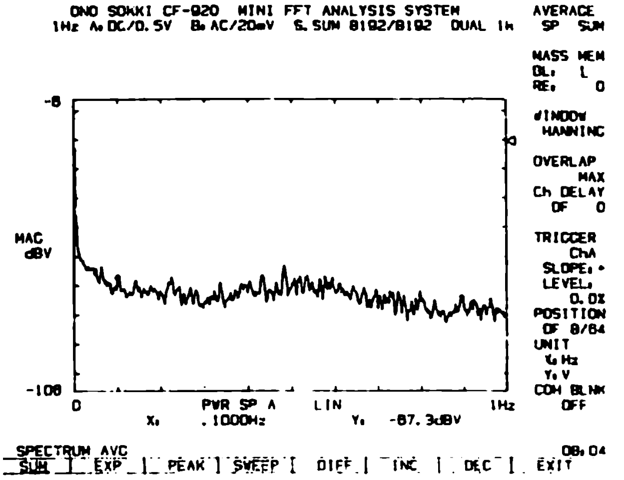

FIG. 13. The noise spectrum of the piston position-sensitive circuit (diode + electronic) in the 0–1-Hz frequency interval (bandwidth 5×10^{-3} Hz). The sensitivity of the system is 6×10^{4} V/m with a displacement noise of 10^{-7} m/$\sqrt{\mathrm{Hz}}$.

as in Fig. 9, but without gas (i.e., $d=0$); this measurement, which takes into account the vertical–horizontal response of the accelerometer (3%), shows the importance of having vertical isolation even if the direction of interest is the horizontal one.

In Fig. 11 the horizontal *TF* in the 0–500 Hz is shown; in this measurement the excitation and the accelerometers are horizontal. Even if the bellows and the wire resonance peaks at 50 and 100 Hz, respectively, are quite visible (-43 dB), their contribution to the total horizontal *TF* of the multiple pendulum seems to be negligible.

Figure 12 shows the same measurement as in Fig. 11, but without gas; as in Fig. 10 this histogram shows the effect of the isolation produced by the vertical spring.

The relative position of the piston with respect to the vessel is measured by means of a position-sensitive diode (UDT LSC/5D). The sensitivity is typically 6×10^{4} V/m with a noise spectrum of 10^{-7} m/$\sqrt{\mathrm{Hz}}$; Fig. 13 shows this spectrum between 0–1 Hz (bandwidth 5×10^{-3} Hz). When the gas spring will be mounted in vacuum the thermal coupling with the outside world will be mainly radiative; hence, we can use the diode signal to feed back (FB) the temperature of the vacuum tank. Since we do not have a vacuum tank, we have tested the temperature FB of our prototype in air using two 25-W reflector bulbs, heating the GS vessel, powered by a controlled power amplifier (ELIND 30 HL 20). Despite abrupt temperature variations in our laboratory, the FB system controls the piston height with the precision of $\pm20\times10^{-6}$ m for a 5 °C variation.

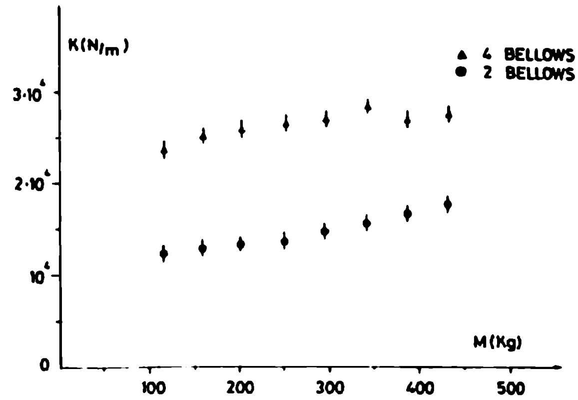

FIG. 14. Measurements of the total stiffness coefficient vs the load mass for the two and four bellows conditions.

In Fig. 14, the measured stiffness coefficient K_{tot} as a function of the loading mass M, in the interval 0–430 kg, is shown for two and four bellows, respectively. The agreement with the theoretical prediction is good within 15% for the four bellows setup and within 20% for the two bellows setup, probably due to strong pressure effects in the bellow convolutions. Theoretical evaluation of these complex phenomena is beyond the purpose of this paper.

ACKNOWLEDGMENT

The authors are grateful to Professor A. Stefanini for valuable suggestions and useful discussions.

[a] Present address: Fermilab, Batavia, IL.
[b] Present address: Laboratorio E.N.E.A., Frascati, Italy.
[1] A. Giazotto, D. Passuello, and A. Stefanini, Rev. Sci. Instrum. 57, 1145 (1986).
[2] N. A. Robertson, R. W. P. Drever, I. Kerr, and J. Hough, J. Phys. E 15, 1101 (1982).
[3] P. R. Saulson, Rev. Sci. Instrum. 55, 1315 (1984).
[4] A. Giazotto *et al.*, proposal for Antenna interferometrica a grande base per la ricerca di Onde Gravitazionali, May 1987, INFN PI/AE 87/1.
[5] R. Del Fabbro, A. Di Virgilio, A. Giazotto, H. Kautzky, V. Montelatici, and D. Passuello, Phys. Lett. A. 124, 253 (1987).
[6] A. E. H. Love, *A Treatise on the Mathematical Theory of Elasticity*, 2nd ed. (Cambridge University, Cambridge, 1906).

FIRST RESULTS FROM THE PISA SEISMIC NOISE SUPER-ATTENUATOR FOR LOW FREQUENCY GRAVITATIONAL WAVE DETECTION

R. DEL FABBRO, A. DI VIRGILIO, A. GIAZOTTO, H. KAUTZKY, V. MONTELATICI and D. PASSUELLO

INFN, Sezione di Pisa and Dipartimento di Fisica, Università di Pisa, Pisa, Italy

Received 29 July 1988; accepted for publication 1 August 1988
Communicated by J.P. Vigier

The detection of gravitational wave (GW) signals requires the test masses of an interferometric antenna to be carefully made free from seismic noise coming from the suspension point. In this paper we report the first results coming from the Pisa super-attenuator. We have measured both the test mass absolute noise upper limit to be $\leqslant 10^{-11}/\nu$ m/$\sqrt{\mathrm{Hz}}$ for $10<\nu<200$ Hz and the transfer functions (TF). These TF applied to the measured seismic noise spectral displacement should allow in a 3 km long interferometric antenna a maximum spectral strain sensitivity $\tilde{h}<1.9\times10^{-20}\ \mathrm{Hz}^{-1/2}$ at 10 Hz and $\tilde{h}<7.5\times10^{-19}/\nu^2\ \mathrm{Hz}^{-1/2}$ for $\nu\geqslant 20$ Hz; this gives at the Vela (Crab) pulsar frequency the limit $h<3\times10^{-25}$ ($h<4\times10^{-26}$), for 1 year integration time.

In this paper we present the first generation results of the seismic noise super attenuator [1,2] constructed at the INFN Laboratory in Pisa. The system has been originally conceived [1] with the purpose of giving three dimensional seismic noise attenuation to a 400 kg suspended mass, at a level of $<10^{-10}$ at 10 H. We have measured in our laboratory the seismic spectral noise displacement (see fig. 1); the

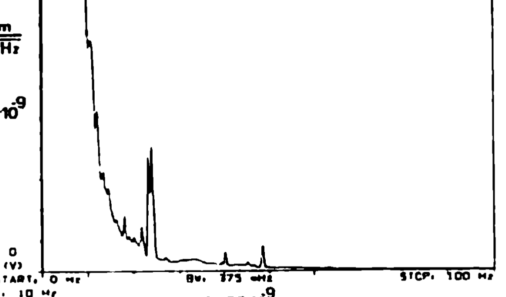

Fig. 1. The rms spectral seismic noise displacement as measured in our laboratory. The monocromatic peaks are due to running electric motors.

noise can be well approximated, above 20 Hz, with the function $\Delta x\sim1.5\times10^{-7}/\nu^2$ m/$\sqrt{\mathrm{Hz}}$, where ν is the frequency in Hz. Hence a 3 km arm length interferometric antenna, to be built in our laboratory [3], should have a limiting sensitivity, due to the seismic noise, $\tilde{h}\leqslant5\times10^{-21}/\nu^2\ \mathrm{Hz}^{-1/2}$. The presence of the thermal noise in the mirrors, of the laser shot noise and of the less known low frequency laser noise, can make this limit a worst case at low frequency. The attenuator consists of a seven-fold pendulum for the attenuation in the horizontal plane, and seven gas springs [4] for the attenuation in the vertical direction. The seven masses attenuator, six weighing 100 kg each plus a 400 kg test mass, are common to both the vertical and horizontal oscillators; in fig. 2 the schematic diagram of the experimental apparatus is shown, together with the vacuum chamber surrounding it. The gas springs are air inflated by means of 2.4 mm diameter copper tubing; the free play (8 mm) of every gas spring is measured by means of a position sensitive diode. The gas pipes and the electrical wires are connected to the outer world at the top position of the gas spring, with the purpose of avoiding direct seismic noise transmission to the test mass.

For the purpose of measuring the remnant noise

0375-9601/88/$ 03.50

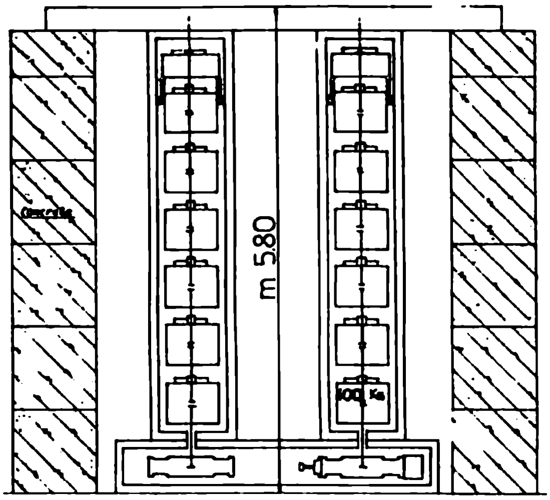

Fig. 2. Schematic diagram of the experimental apparatus. The two attenuators, composed of a seven-fold three-dimensional pendulum, are suspended in the two vertical vacuum chambers. The 400 kg brass masses, contained in the horizontal vacuum chamber, are also shown.

of the test masses, in the first generation experiment, a dip-coil accelerometer (home built) is being used; subsequently, an interferometric sensor will be adopted to achieve a higher sensitivity (10^{-16} m/$\sqrt{\text{Hz}}$). The configuration test mass–accelerometer is shown in fig. 3. If x and x_c are the coordinates of the 400 kg test mass and of the 0.5 kg coil accelerometer mass respectively, then

$$x_c = \frac{\omega_0^2 + i\Omega/\tau}{-\Omega^2 + i\Omega/\tau + \omega_0^2}\, x\,, \tag{1}$$

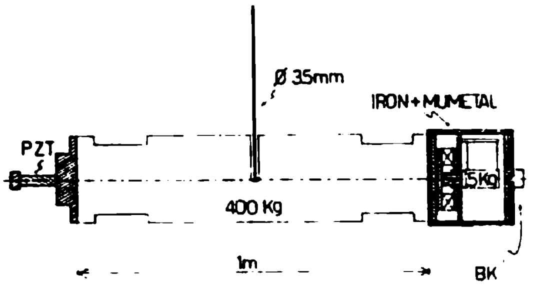

Fig. 3. Schematic diagram of the 400 kg brass test mass; the dip-coil accelerometer is shielded by iron + mumetal layers. The calibration excitation is produced by the piezoelectric transducer PZT and measured by the accelerometer BK.

where $\nu_0 = \omega_0/2\pi = 3.1$ Hz and $\tau \approx 0.1$ s are the coil suspension frequency and the relaxation time respectively and $\Omega = 2\pi\nu$. Eq. (1) has been evaluated neglecting the accelerometer mass with respect to the test mass. From eq. (1) we obtain the coil voltage output:

$$V = K(\Omega)(x - x_c)i\Omega$$

$$= -K(\Omega)\frac{i\Omega^3 x}{-\Omega^2 + i\Omega/\tau + \omega_0^2}\,, \tag{2}$$

where $K(\Omega)$ is an unknown function of the magnetic field, coil geometry, and of the overall electronic readout. The spectral voltage noise of the electronics when the input is loaded by a 170 Ω resistor (the same as the coil resistance) is shown in the frequency interval 0–100 Hz in fig. 4. The noise is the sum of the operational amplifier LT1028 input noise and of the 170 Ω resistor Johnson noise, times the amplification factor 100. A three pole Butterworth high pass filter (8 Hz cut off) prevents the Spectrum Analyzer to be saturated by th attenuator normal modes. By longitudinally exciting the test mass by means of the piezoelectric exciter PZT (see fig. 3), we have measured $K(\Omega)$ using a Bruel Kjear accelerometer 4370 (BK) time integrated output to give the test mass speed. The experimental value has been measured to be ~6000 for $\nu > 20$ Hz and 4500–6000 in the interval $10 < \nu < 20$ Hz. When the input is loaded by the dip-coil accelerometer, the only new feature in the spectral voltage noise is due to the presence of

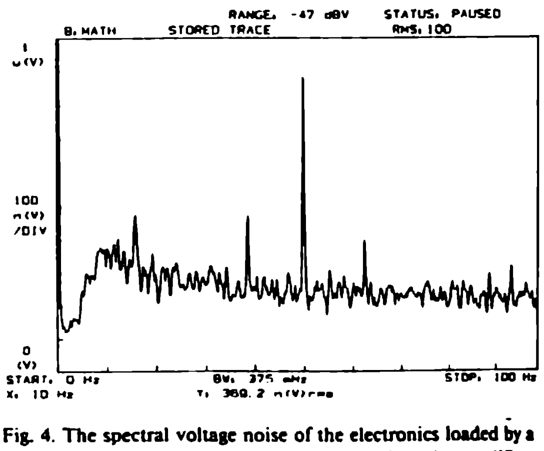

Fig. 4. The spectral voltage noise of the electronics loaded by a 170 Ω resistor, measured at $0 < \nu < 100$ Hz; since the amplification is ~100, the input noise is ~3 nV/$\sqrt{\text{Hz}}$.

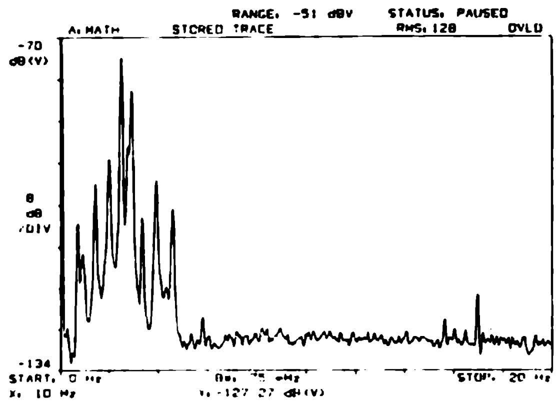

Fig. 5. The dip-coil amplified accelerometer signal, measured at $0<\nu<20$ Hz clearly shows the attenuator normal modes at frequencies <5 Hz.

the attenuator normal modes at frequencies $\nu<5$ Hz, which are clearly visible in the spectrum of fig. 5 in the frequency interval 0–20 Hz obtained in vacuum. The spectrum of the accelerometer noise in vacuum in the frequency interval 0–100 Hz, shown in fig. 6, does not show for $\nu>10$ Hz, any difference with respect to the one shown in fig. 4 apart from few fix frequency peaks also visible in fig. 4, presumably due to external e.m. induction. In the interval $100<\nu<200$ Hz the noise ($\sim 250\ \mathrm{nV}/\sqrt{\mathrm{Hz}}$) is also purely of electronic origin. Figs. 4 and 6 show that our sensitivity is limited by the dip-coil and electronic noise; since for $\nu>10$ Hz the average voltage noise is $\sim 300\ \mathrm{nV}/\sqrt{\mathrm{Hz}}$, from eq. (2) it follows that the upper limit on the test mass displacement is

$$|x| \sim \frac{3\times10^{-7}}{\Omega\times6000} = \frac{8\times10^{-12}}{\nu}\frac{\mathrm{m}}{\sqrt{\mathrm{Hz}}}. \tag{3}$$

At 10 Hz this is presumably the quietest, with respect to the fixed stars, suspended mass on earth. It is relevant to note that the previous data have been obtained without any electronic damping of the attenuator. The damping system and the interferometric sensor are now under construction in Pisa.

With the purpose of measuring in the first generation experiment the vertical to horizontal (V–H) and horizontal to horizontal (H–H) transfer functions (TF), we have applied vertical and horizontal excitation by means of two excentered dc motors (DCM). The excitation force was applied between the first and the second filter out of a total of seven filters, as shown in fig. 7. The excitation was measured by means of the two accelerometers BK. Since $M=100$ kg is the mass of each filter and $K_1=36000$ N/m is the vertical rigidity of the first filter, then the

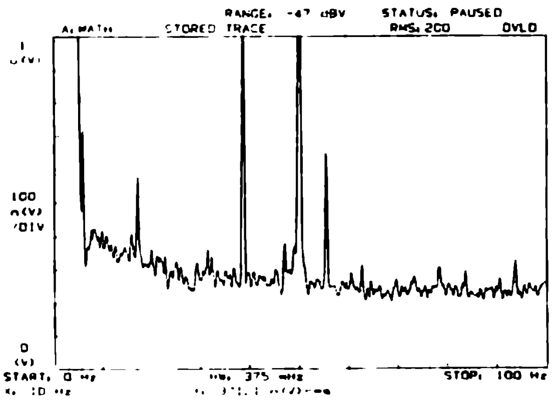

Fig. 6. The spectral voltage noise of the accelerometer dip-coil amplified signal measured at $0<\nu<100$ Hz. Above 10 Hz the noise is the same as that of fig. 4. The attenuator normal modes are visible at $\nu<5$ Hz

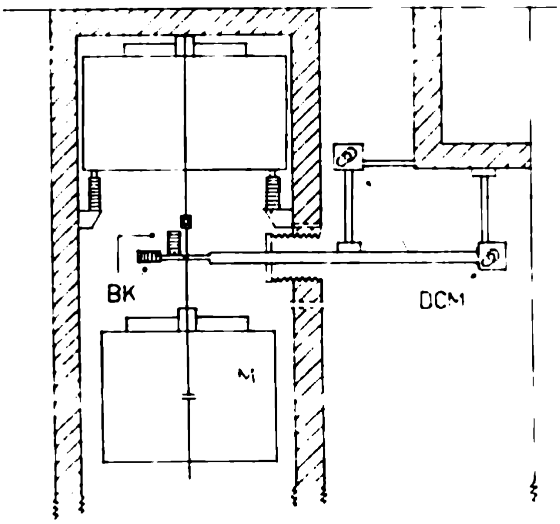

Fig. 7. Schematic diagram of the mechanical excitation device. Two dc motors (DCM) give vertical and horizontal displacement to the suspension wire; the excitation is measured by means of two accelerometers (BK).

total vertical TF is obtained by correcting the measured TF by a factor $A \approx K_1/\Omega^2 M$ when $\nu > 10$ Hz. Similarly the total horizontal TF is obtained by correcting the measured one by a factor $B \approx 0.41$ when $\nu > 10$ Hz. These corrections take into account the fact that the excitation point is not the suspension point. The vertical and horizontal TF are shown in fig. 8 in the frequency interval 10–68 Hz. No remnant peak was seen in the dip-coil spectrum when the excitation was horizontal, but in some measurements having very high excitation the DCM brushes where creating an excessive noise. A remnant peak was present in some of the vertical excitation measurements; this happened only when the excitation was very high. This could be explained considering that in the latter condition the whole attenuator vacuum chamber (made of carbon steel) was vibrating heavily. This phenomenon in presence of the dip-coil-magnet fringe field is inducing in the dip-coil a signal at the same frequency. This vibration was clearly observed by means of an extra accelerometer.

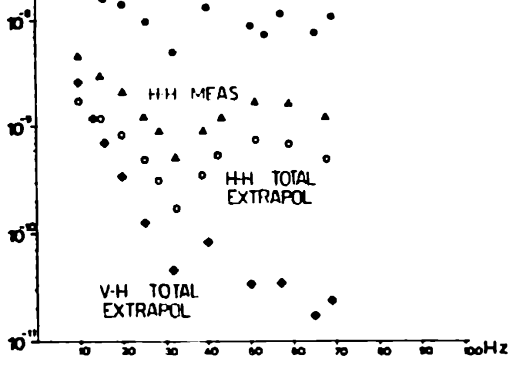

Fig. 8. The measured (V–H) TF and (H–H) TF in the frequency interval $10 < \nu < 68$ Hz. The total extrapolated TF are (V–H)·A and (H–H)·B respectively.

For the reasons mentioned above we consider the measured TF values to be upper limits. The change of the excenters, clearly visible at ~33 Hz, shows that the TF could be improved by increasing the excitation. In the second generation experiment we will measure the remnant signal of the test masses by interferometric techniques not sensitive to the vacuum chamber vibrations. Multiplying the (V–H) TF by the measured seismic noise spectrum of fig. 1 we obtain, in the worst case, for a 3 km long interferometer, a limit on the GW spectral amplitude $\tilde{h} < 1.9 \times 10^{-20}$ Hz$^{-1/2}$ at 10 Hz and $\tilde{h} < 7.5 \times 10^{-19}/\nu^2$ Hz$^{-1/2}$ for $\nu > 20$ Hz. At the frequency of the Vela (22 Hz) and Crab (60 Hz) pulsars, this gives, in 1 year integration time, the limit $h < 3 \times 10^{-25}$ and $h < 4 \times 10^{-26}$ respectively.

We wish to thank our technicians G. Ciampi, R. Cosci, E. Fagioli, R. Lagnoni and C. Magazzu; their dedicated support to the experiment was precious. We are also very grateful to G. Mazzacurati of the loudspeaker factory RCF for having supplied the dip-coils and the magnet.

References

[1] A. Giazotto, The seismic noise challenge to the detection of low frequency gravitational waves, invited talk to the "7mo congresso di relatività generale e fisica della gravitazione", Rapallo, Italy, September 1986, General relativity and gravitational physics World Scientific Pub. 449 (1987).

[2] R. Del Fabbro, A. Di Virgillio, A. Giazotto, H. Kautzky, V. Montelatici and D. Passuello, Phys. Lett. A 124 (1987) 253.

[3] Parigi collaboration (Pisa, Napoli, Frascati, Orsay), Proposta di antenna interferometrica a grande base per la ricerca di onde gravitazionali, INFN PI/AE 87/1 (Pisa, 1987).

[4] R. Del Fabbro, A. Di Virgilio, A. Giazotto, H. Kautzky, V. Montelatici and D. Passuello, Rev. Sci. Instrum. 59 (1988) 292.

LOW FREQUENCY BEHAVIOUR OF THE PISA SEISMIC NOISE SUPER-ATTENUATOR FOR GRAVITATIONAL WAVE DETECTION

R. DEL FABBRO, A. DI VIRGILIO, A. GIAZOTTO, H. KAUTZKY [1],
V. MONTELATICI [2] and D. PASSUELLO
INFN Sezione di Pisa and Dipartimento di Fisica, Università di Pisa, Pisa, Italy

Received 5 September 1988; accepted for publication 15 September 1988
Communicated by J.P. Vigier

The absolute displacements, for frequencies below 20 Hz, of the 400 kg test mass seismically isolated by the Pisa super-attenuator, to be used in long base interferometer for gravitational wave research, are presented. In the region below 6 Hz, the maximum displacement is about 14 μm. The displacements, at 10 and 20 Hz, are $\leqslant 1.5\times10^{-13}$ and $\leqslant 4\times10^{-14}$ m/$\sqrt{\text{Hz}}$ respectively and represent presumably the lowest ever reached by a suspended mass on earth. The super-attenuator transfer function, which has been measured using the seism as an exciter for $0<\nu<6$ Hz, shows a remarkable agreement with the theoretical one and demonstrates the necessity of having an attenuating system working in three dimensions.

The three dimensional super-attenuator (SA) [1-3] is now operating at the INFN laboratory in Pisa and its transfer function above 10 Hz has been already shown [4] to be adequate to reduce the seismic noise at least by a factor 2×10^{-8}.

Our seismic isolator acts above 10 Hz, but at lower frequency the test mass displacement is larger than the seismic displacement itself due to the presence of suspension normal modes [2]. We plan to use the SA for suspending the mirrors of a large interferometric antenna for gravitational wave (GW) dectection [5], but it is unlikely to lock the interferometer to a fringe if the mirrors have large displacement. With the purpose of projecting an effective damping system it is necessary to study the normal mode behaviour of the SA.

In fig. 1 the layout of the experimental apparatus is shown [5], together with the vacuum chamber surrounding it; at the end of the chain the 400 kg brass test mass is shown together with the box containing the accelerometric transducer and the piezoelectric transducer used for calibration purposes. The transducer is a dip coil accelerometer (DCA)

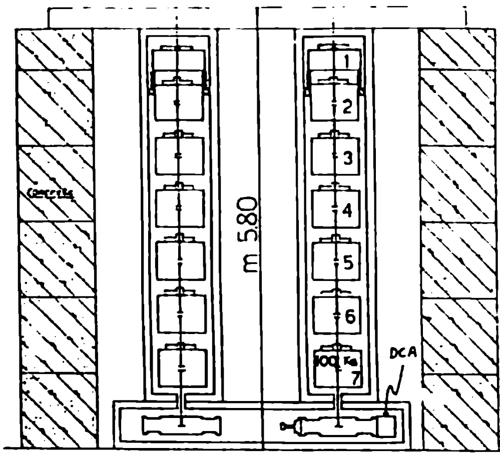

Fig. 1. Layout of the experimental apparatus. The two attenuators, composed of a seven fold three dimensional pendulum, are suspended in the two vertical vacuum chambers. The filters are numbered from 1 to 7. The 400 kg brass masses, contained in the horizontal vacuum chamber, are also shown together with the dip coil accelerometer DCA.

[6]; we have measured the transducer self-frequency and relaxation time to be $\nu_0=3$ Hz and $\tau=0.24$ s respectively. The analysis of the SA signal has been done using an HP 3562 two channel spectrum ana-

[1] Present address: Fermilab, Batavia, IL, USA.
[2] Present address: Laboratorio ENEA, Frascati, Italy.

lyzer, having an 80 dB dynamical range. Due to this reduced dynamical range, we had to use a two channel simultaneous data acquisition: in channel one we have analyzed the amplified DCA signal, in channel two the same amplified signal filtered by a nine pole high pass Butterworth filter (BF), having 7 Hz as cut frequency. In this way we have a good dynamics in both the low and high frequency region of the spectrum between 0 and 10 Hz. If X is the displacement of the test mass, the accelerometer voltage V_i ($i=1$, 2 depending on the channel) is

$$V_i = K_i(\omega)\left|\frac{\mathrm{i}\omega^3}{-\omega^2+\mathrm{i}\omega/\tau+\omega_0^2}\right| X + V_{n,i},$$

$$i=1,2, \tag{1}$$

where $\omega/2\pi$ is the frequency and $\omega_0=2\pi\nu_0$; $K_1(\omega)=5400$ V s/m is a factor depending on the magnetic field, the coil geometry and the overall electronic read-out and $K_2(\omega)=K_1(\omega)\times\mathrm{FTF}(\omega)$, where $\mathrm{FTF}(\omega)$ is the BF transfer function. $V_{n,i}$ is the sum of the elctronic noise and the coil Johnson noise; we have measured $V_{n,i}$ loading the electronic chain

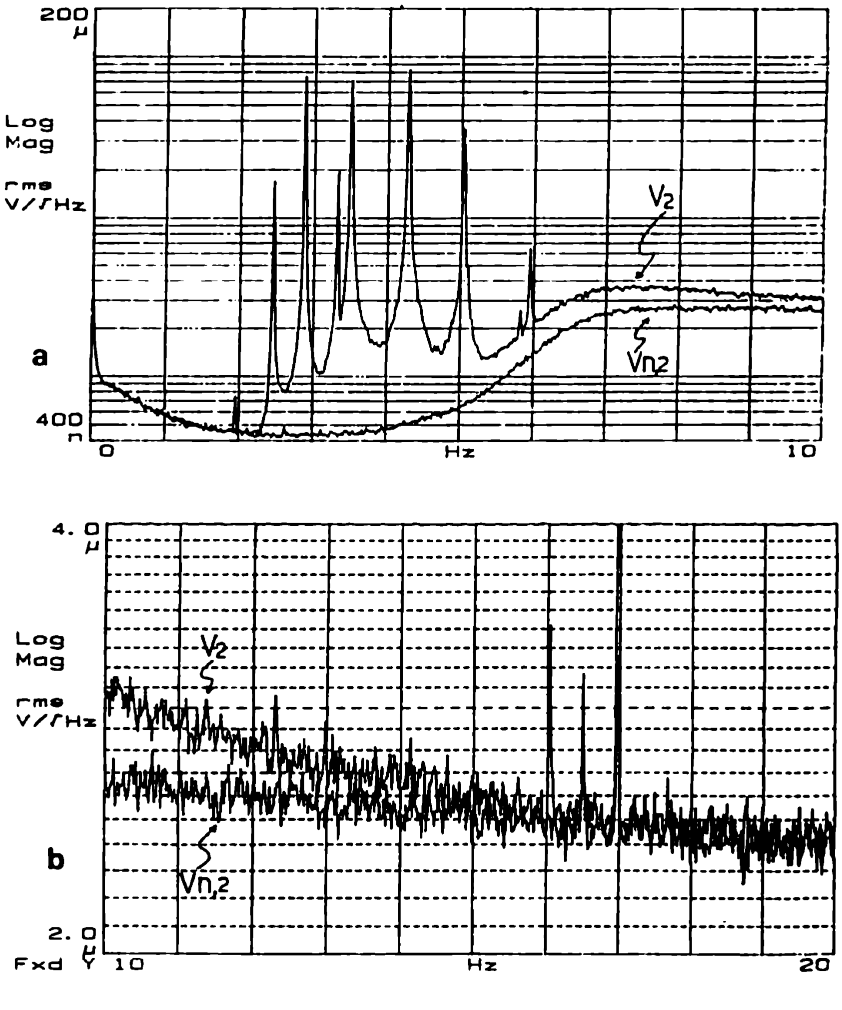

Fig. 2. (a) The spectra of the signals V_2 and of the noise $V_{n,2}$ for $0<\nu<10$ Hz. (b) The spectrum of the signals V_2 and of the noise $V_{n,2}$ for $10<\nu<20$ Hz.

with a shielded coil, equal to the one used in the DCA. The noise measurement has been done in vacuum in order to have the amplifier working at the same temperature. Figs. 2a and 2b show V_2 and $V_{n,2}$ superimposed for $0<\nu<10$ Hz and $10<\nu<20$ Hz respectively: the electronic noise subtraction is important above 5 Hz, where the real displacement of the test mass gives a signal smaller than the transducer voltage noise. From our measurement we are able to compute X:

$$X_i = \frac{V_i - V_{n,i}}{K_i(\omega)} \left| \frac{-\omega^2 + i\omega/\tau + \omega_0^2}{i\omega^3} \right| . \qquad (2)$$

Fig. 3 shows the composition of the two spectra X_1 ($0 \leqslant \nu \leqslant 5$ Hz) and X_2 ($\nu > 5$ Hz); no discrepancy was found between the two spectra in the overlapping region. For $\nu < 6$ Hz it shows clearly that this spectrum is the sum of the horizontal plus some of the vertical SA normal modes. In the frequency region around 0.25 Hz, we observe that the shaking is larger than the seism itself, due to the high Q of the suspension (we have measured a lower limit of Q to be 10^4); the maximum displacement is about ~ 14 μm at 0.25 Hz (bin width 18.7 mHz) and the remnant displacement at 10 Hz is less than 1.5×10^{-13} m/$\sqrt{\text{Hz}}$. These results are the best ever obtained in this frequency interval. A better measurement will be obtained by using the interferometric sensor which is under construction in our laboratory.

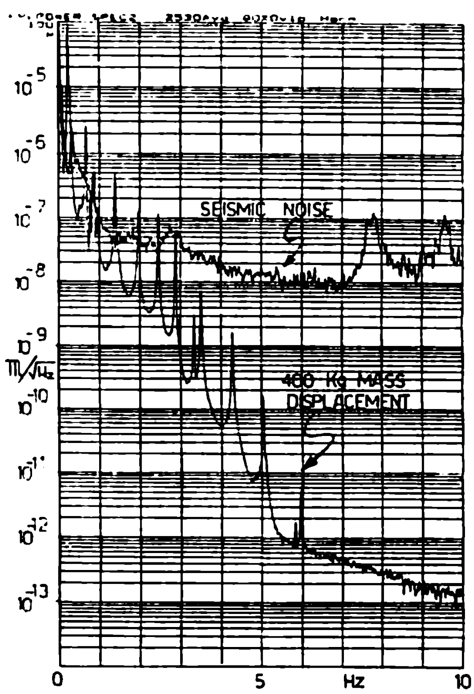

Fig. 3. Spectrum of the test mass displacement for $0<\nu<10$ Hz, expressed in m/$\sqrt{\text{Hz}}$ and bin width 18.7 mHz. The seismic displacement spectrum measured by locking the 400 kg test mass to the ground is also shown.

Table 1
Gas spring frequency and rigidity.

Filter	ν (mHz)	K (N/m)
1	975	37530
2	975	33780
3	1050	34820
4	1125	34980
5	975	22520
6	1025	20738
7	1109	19108

Using the gas spring [3] length monitoring photodiodes we have measured the self-frequencies ν_i ($i=1-7$) and the rigidity K_i of each vertical gas spring of the SA by making the gas springs work one at a time in vacuum; the measured values of the rigidities are shown in table 1.

With the same photodiodes and with the SA on, we have been able to distinguish the vertical normal from the horizontal ones: table 2 shows the measured and computed resonance frequency for the horizontal and vertical normal modes.

The theoretical values of table 2 have been evaluated introducing the SA measured parameters in the formulas of ref. [2].

Table 2
Measured and computed resonance frequency (in mHz) for the horizontal and vertical mode.

Horizontal		Vertical	
$\nu_{\text{meas.}}$	$\nu_{\text{theor.}}$	$\nu_{\text{meas.}}$	$\nu_{\text{theor.}}$
240	240	450	420
680	740	1350	1350
1390	1340	2500	2470
1960	1920	3510	3410
2460	2430	4290	4240
2890	2880	5050	5000
3320	3320	5960	5840

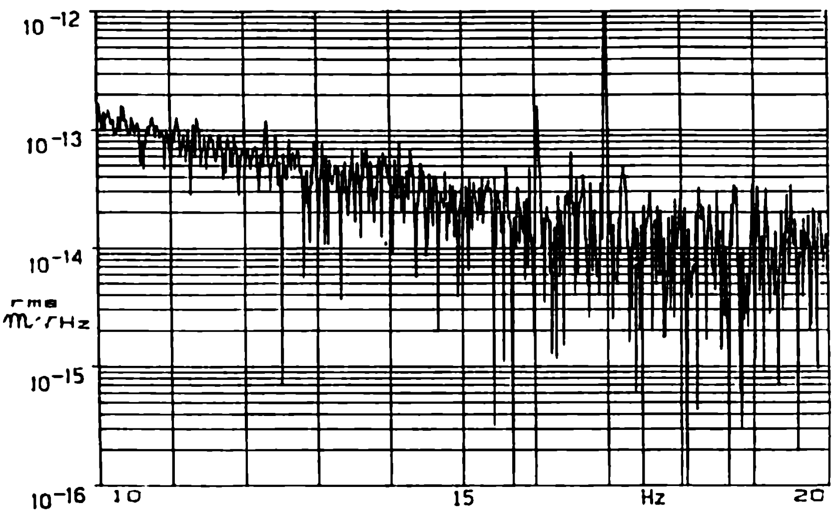

Fig. 4. Spectrum of the test mass displacement for $10<\nu<20$ Hz, expressed in $m/\sqrt{Hz}$ and bin width 18.7 mHz.

Fig. 4 shows the displacement of the test mass between 10 and 20 Hz; no mechanical structures are evident and the two small and thin resonances around 16 and 17 Hz are more likely to be electronic peak up, in fact they are present in the relative V_n spectrum too. The remnant displacement at 20 Hz is $\leqslant 4\times 10^{-14}$ $m/\sqrt{Hz}$.

In fig. 5 the DCA voltage output between 0 and 10 Hz is shown when the 400 kg mass is lying on the ground and the DCA is excited by the seismic noise; this spectrum clearly shows the accelerometer resonance peak at 3 Hz. The remnant displacement for $6<\nu<10$ Hz could be explained considering the DCA displacement X_t due to thermal noise:

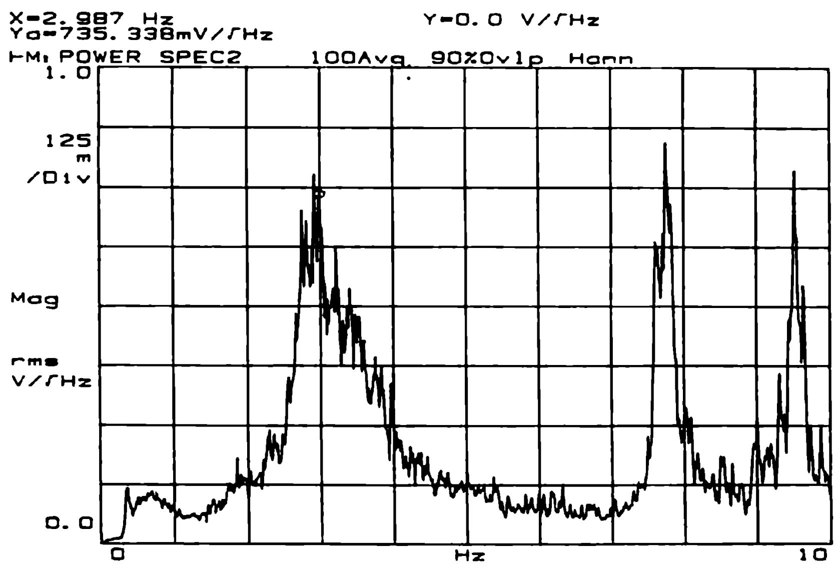

Fig. 5. Spectrum of the DCA signal measuring the seismic displacement; the 3 Hz DCA resonance is clearly visible.

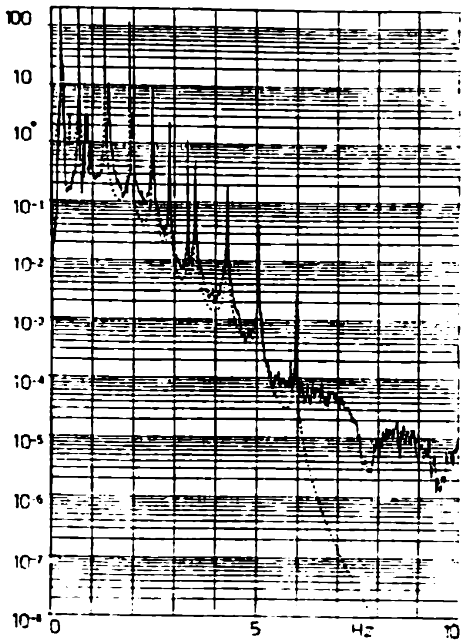

Fig. 6. The continuous line is the super-attenuator TF, the ratio of the two spectra shown in fig. 3. The dotted line is the theoretical transfer function sum of the horizontal TF plus the vertical one divided by 100.

$$X_t = \sqrt{\frac{4kT}{m\tau}} \frac{1}{-\omega^2 + i\omega/\tau + \omega_0^2} \text{ m}/\sqrt{\text{Hz}}, \qquad (3)$$

where $m = 270$ g is the DCA mass, k the Boltzmann constant and T the absolute temperature. At 10 Hz eq. (3) gives $X_t \sim 1.5 \times 10^{-13}$ m/$\sqrt{\text{Hz}}$.

We have also evaluated the SA transfer function (TF) between 0 and 10 Hz by using the seism measurement shown in fig. 3. In fig. 6 the continuous line shows the measured TF and the dotted line the computed one which is the sum of the horizontal TF plus the vertical divided by 100. Above 6 Hz the measured TF is limited by both the DCA sensitivity and the smallness of the seismic excitation. The results of a measurement up to ~60 Hz are presented in ref. [4]. The overall agreement between the two curves is very good, showing that the theoretical model presented in ref. [2] well describes the system. The 1% mixing factor between the horizontal and the vertical TF clearly shows the importance of having filters working simultaneusly in all three degrees of freedom.

References

[1] A. Giazotto, The seismic noise challenge to the detection of low frequency gravitational waves, invited talk to the 7mo congresso di relatività generale e fisica gravitazione, Rapallo, Italy, September 1987, General relativity and gravitational physics, World Scientific Pub. 449 (1987).

[2] R. Del Fabbro, A. Di Virgilio, A. Giazotto, H. Kautzky, V. Montelatici and D. Passuello, Phys. Lett. A 124 (1987) 253.

[3] R. Del Fabbro, A. Di Virgilio, A. Giazotto, H. Kautzky, V. Montelatici and D. Passuello, Rev. Sci. Instrum. 59 (1988) 292.

[4] R. Del Fabbro, A. Di Virgilio, A. Giazotto, H. Kautzky, V. Montelatici and D. Passuello, Phys. Lett. A 132 (1988) 237.

[5] Parigi collaboration (Pisa, Napoli, Frascati, Orsay), Proposta di antenna interferometrica a grande base per la ricerca di onde gravitazionali, INFN PI/AE 87/1 (Pisa, 1987).

[6] R. Del Fabbro, A. Di Virgilio, A. Giazotto, H. Kautzky, V. Montelatici and D. Passuello, A low noise, dip coil accelerometer transducer, to be published.

April 10, 1989
INFN PI/AE 89/3

First Results on the Electronic Cooling for the Pisa Seismic Noise Super-Attenuator for Gravitational Wave detection

C.Bradaschia, R.Del Fabbro, L.Di Fiore[a], A.Di Virgilio, A.Giazotto, H.Kautzky[b], V.Montelatici[c], D.Passuello

I.N.F.N. Sezione di Pisa
and
Dipartimento di Fisica
Università di Pisa, Pisa, Italy

Accepted by Phys. Lett. A

UNIVERSITÀ DEGLI STUDI DI PISA
DIPARTIMENTO DI FISICA

Istituto Nazionale di Fisica Nucleare
Sezione di Pisa

First results on the electronic cooling of the Pisa seismic noise super-attenuator for Gravitational Wave detection

C. Bradaschia, R. Del Fabbro, L. Di Fiore[a], A. Di Virgilio, A. Giazotto, H. Kautzky[b], V. Montelatici[c], D. Passuello

I.N.F.N. Sezione di Pisa and Dipartimento di Fisica, Universita' di Pisa, Pisa, Italy

The seismic noise excitation of the normal modes in the three dimensional Pisa Super Attenuator, to be used in a long base interferometric gravitational antenna, produces large movements of the 400 Kg test mass. In this paper it is shown, for the first time, that it is possible to damp, in a stable way, these normal modes using a six dimensional damping system acting on the second suspended mass instead of the test mass itself, with the purpose to do not reintroduce seismic noise. In this way the large displacement normal modes, including the verticals and the rotations, have been damped and the pendulum maximum displacement, originally varying from 15 to 30 μm according to the seismic noise intensity, has been reduced to less than 3.4 μm allowing locking to a fringe of the interferometer.

A three dimensional Super Attenuator (SA), designed to make free from seismic noise the mirrors of a long baseline interferometer at frequencies above 10 Hz [1,2,3], has been built at the INFN laboratory in Pisa. At the lower SA normal modes (.24 Hz) the test mass displacement varies from 15 to 30 μm[6], according to the seismic noise intensity.

Since the test mass will be the mirror of a suspended Michelson interferometer, the low frequency displacement must be less than few light wavelengths in order to lock the interferometer on a fringe [1]. The usual way to do this is by electronic damping of the suspension resonances; it has already been shown that good results can be achieved on small test masses in three degrees of freedom [7,8,9]. We report now the first successful attempt to damp in all the six degrees of freedom the displacements of a heavy mass (400 Kg), similar to those foreseen for the Virgo interferometer [1]. The improvement with respect to the original damping scheme [10] is to apply the damping force to a point along the SA chain, instead of applying it directly to the suspended mass. In this way the damping force does not couple the suspended mass directly to the ground seismic displacements.

In fact in a simple pendulum the damping force (viscous) is:

$$F = K\,(\dot{X}-\dot{X}_s) \qquad (1)$$

where X and X_s are the displacements of the mass and of the ground respectively. This gives for the displacement X

$$X = \frac{\omega_0^2 X_t + i\omega K X_s}{-\omega^2 + i\omega(K + 1/\tau) + \omega_0^2} \qquad (2)$$

where X_t is the suspension point displacement, ω is the circular frequency, τ the relaxation time and ω_0 the resonance circular frequency. The electronic cooling introduces a noise displacement given by $X_n = {}^{KX_s}\!/_{\omega}$ at frequencies well above ω_0. To have a pendulum recovering its equilibrium position without oscillating around it (critical damping), the K factor in the viscous force is given by $K + {}^{1}\!/_{\tau} = 2\omega_0$, neglecting ${}^{1}\!/_{\tau}$ (typically $\tau > 10^3$ s in vacuum) $K = 2\omega_0 = 3\ s^{-1}$ at the lowest normal mode (0.24 Hz). The corresponding noise displacement at 10 Hz is $X_n = {}^{KX_s}\!/_{\omega} = 5.10^{-10}\ {}^{m}\!/\!\sqrt{Hz}$ with the usual assumption ($X_s = {}^{10^{-6}}\!/_{\nu^2}\ {}^{m}\!/\!\sqrt{Hz}$) for the spectral seismic noise.

This figure, seven orders of magnitude larger than the design sensitivity of the Virgo interferometer, is by far unacceptable.

In principle this problem could be solved achieving a K factor strongly decreasing with the frequency, using a very steep low-pass filter. This method has been carefully analysed, but it has been abandoned due to the very strong instability of the system.

A practical solution has been found investigating the possibility of applying the viscous force to an intermediate point of the chain, between the suspension point and the final mass. In this way the sensitivity to the noise introduced by the electronic cooling (X_n) is very much reduced and the needed filter is much weaker.

All these theoretical studies have been performed by a computer program flexible enough to make possible the study of the transfer functions in different conditions, including the feed-back acting along the chain in different points with different filters.

Fig. 1 shows the lay out of the electronic damping: a LED / photodiode system (shadow-meter) measures the relative displacement $X_i - X_s$ of the i-th SA mass with respect to the ground, then the derivative is formed and the amplified signal is applied to a force transducer acting on the mass itself. The force transducer is composed of a permanent magnet attached to the mass M and a coil connected to the ground: a current $I=A(\dot{X}_i-\dot{X}_s)$ flows in the coil and produces a damping force $F_d= K\cdot I$ between the ground and the mass M_i, where K is a factor depending on the permanent magnet strength, the coil geometry, and the distance between the coil and the magnet; in our case [8] K is, to first order, insensitive to the relative displacement of coil and magnet.

In a previous paper [2] we have computed the transfer function (TF) of a passive 3-dimensional SA. Here we generalize the computation to the case of a SA with an active damping servo system. The computation as been done for a general one dimensional N-fold pendulum (small oscillations approximation), considering pointlike masses and massless, unstretchable wires. The equations of motion are:

$$-\Omega^2 m_j X_j = D_j(X_{j-1}-X_j)+D_{j+1}(X_{j+1}-X_j)-i\Omega\frac{m_j}{\tau_j}X_j-\frac{F_j}{B_j}(X_j-X_s) \qquad j=1,N-1$$

$$-\Omega^2 m_N X_N = D_N(X_{N-1}-X_N)-i\Omega\frac{m_N}{\tau_N}X_N-\frac{F_N}{B_N}(X_N-X_{sN}) \tag{3}$$

with:

$$D_j=M_j\frac{g}{L_j}+i\Omega\frac{m_j}{\tau_{j,j-1}} \qquad \text{for the horizontal direction motion equations}$$

$$D_j=K_j+i\Omega\frac{m_j}{\tau_{j,j-1}} \qquad \text{for the vertical direction motion equations}$$

where X_j is the displacement of the j-th mass, X_0 the suspension point displacement, L_j and m_j are respectively the length and mass of the j-th stage of the pendulum, K_j the stiffness of the j-th spring; τ_j and $\tau_{j,j-1}$ are relaxation times on the j-th mass due respectively to the medium surrounding the pendulum and to the friction in the connection between the j-th and the (j-1)th masses, g is the acceleration of gravity, $M_j=\sum_{i=j}^{N} m_i$ and $\omega=2\pi\nu$, where ν is the frequency. The last term in eq. (3) is the external force applied by the damping feed-back system; F and B are real polynomials in $s = i\Omega$ and X_{sj} is the seismic displacement of the reference point for the measure of X_j. The presence of the term $-{}^{F}\!/_{B}X_{sj}$ in the equation of motion takes into account the seismic noise reintroduced in the test mass by the servo system. In this calculation F is introduced in a general way and it represents, for example, an elastic force (zero order polynomial) or a purely viscous one (first order term only). The dimensionless polynomial B is a low pass filter. It is important to have a lowpass filter, with cutoff frequency less than 10 Hz, in order to preserve the suspension performances above 10 Hz; but care has to be taken because the presence of phase shifts near the cutoff frequency induces instabilities. The system (3) can be solved with standard methods giving

$$X_j = \frac{\left(Q_0(s)X_0 + \sum_{i=1}^{N} Q_i(s)X_{si}\right)}{Q(s)} \qquad (4)$$

where the Q(s) are real polynomials in s. The study of the complex zeros of Q, allows one to determine wether the feedback system is stable or not. For a N-fold pendulum without damping Q is a 2N-order polynomial; if we introduce an active damping with a M-poles lowpass filter, Q becomes a 2N+M-order polynomial.

From previous measurements we know that in the frequency range below 10 Hz the mechanical structure doesn't show resonances, we can therefore assume that all the seismic noise sources X_{sj} in different points along the chain are approximately equal in phase and amplitude:

$$X_{0}\sim X_{sj}\sim X_{s} \qquad (5)$$

X_s has been measured [6] to be $\sim 10^{-6}\mathrm{m}/\sqrt{\mathrm{Hz}}$. From (4) and (5) we get for the TF:

$$\frac{\langle X_7\rangle}{\langle X_s\rangle}=\frac{\left|\sum_{i=0}^{N}Q_i\right|}{|Q|} \qquad (6)$$

In our SA we have chosen to apply a 6-dimensional damping to the second suspended mass; in fig. 2 the quantity HTF+.02 VTF [6] is plotted, where HTF is the horizontal TF and VTF is the vertical one calculated for three F values (100, 500, 2500 Kg/s). In fig. 3 the remnant seismic displacement of the SA is shown in the frequency interval 0-10 Hz; the 0.24 Hz peak is clearly visible togeter with other horizontal and vertical normal modes [6]. The maximum displacement is ~ 30 μm. When the damping is applied the general displacement amplitude is strongly reduced, many normal modes disappear and the amplitude of the peak at 0.24 Hz decreases to ~ 3.4 μm, as shown in fig. 4.

With the purpose of evaluating the damping coefficient F we have measured the total TF using the seismic noise as an exciter; in fig. 5 this TF is shown together with the theoretical one corresponding to HTF + .02 VTF evaluated for F=500 Kg/s; the vertical to horizontal coupling coefficient is higher (0.02 instead of 0.01) than the one of the passive SA due probably to the damping system itself; the noise for $\nu > 5$ Hz is due to the accelerometer sensitivity limit ($10^{-13} \mathrm{m}/\sqrt{\mathrm{Hz}}$) and at this level of sensitivity we were not able to detect any reintroduction of seismic noise due to the damping system. A Michelson interferometer supposed to have a sensitivity of $10^{-16} \mathrm{m}/\sqrt{\mathrm{Hz}}$ at 10 Hz is being built in Pisa, with the purpose of measuring the remnant test mass displacement with higher sensitivity.

We are also performing experimental tests to improve the damping without reintroducing the seism by substituting the shadow meters with very sensitive accelerometers.

We wish to thank our technicians G.Ciampi and R.Lagnoni who carefully prepared the mechanical parts and C.Magazzu' and F.Morganti for the electronic set-up of this experiment.

a) Present address: I.N.F.N. Sezione di Napoli, Napoli, Italy

b) Present address: Fermilab, Batavia, Il.

c) Present address: Laboratorio E.N.E.A, Frascati, Italy.

References

[1] Pisa, Napoli, Frascati, Salerno, Parigi, Orsay Collaboration: "Antenna interferometrica a grande base per la ricerca di Onde Gravitazionali"; INFN PI/AE 87/1,Pisa 12 May 1987.

[2] R. Del Fabbro, A. Di Virgilio, A. Giazotto, H. Kautzky, V. Montelatici, D. Passuello; Phys. Lett. A, 124 (1987) 253.

[3] R. Del Fabbro, A. Di Virgilio, A. Giazotto, H. Kautzky, V. Montelatici, D. Passuello; Rev. Sci. Ins., 59; 292 (1988) 292.

[4] R. Del Fabbro, A. Di Virgilio, A. Giazotto, H. Kautzky, V. Montelatici, D. Passuello; Phys . Lett A., 132(1988) 237.

[5] R. Del Fabbro, A. Di Virgilio, A. Giazotto, H. Kautzky, V. Montelatici, D. Passuello: "A low noise, dip coil accelerometer transducer", to be published.

[6] R. Del Fabbro, A. Di Virgilio, A. Giazotto, H. Kautzky, V. Montelatici, D. Passuello; Phys. Lett. A, 133(1988) 471.

[7] G.Leuchs et. al." Vorschlag zum Bau grossen Laser Interferometers zur Messung von Gravitationswellen"; M P Q 129, june 1987, Munchen.

[8] D.H. Shoemaker: "Contributions a l'etude de la detection interferometrique des ondes de gravitation"; Unpublished Thesis, Universite de Paris-Sud, Paris.

[9] J. Hough et. al.: "A British long baseline Gravitational Wave Observatory"; GWD/RAL/86-001,Glasgow.

[10] R.L. Forward; J. Appl. Phys. 50(1979)1.

Figure captions

Figure 1: Lay out of one out of six damping systems. The magnet M is connected to the 2-nd suspended mass of the SA, the coil C is current driven by the derivative of the light signal in the photodiode PD modulated by the movement of the mass, then creating a damping force.

Figure 2: HTF+.01VTF of the SA with damping on the 2-nd suspended mass for three values of F; (a) F= 100 Kg/s, (b) F=500 Kg/s, (c) F=2500 Kg/s.

Figure 3: Spectrum of the SA test mass displacement without damping, expressed in $m/\sqrt{Hz}$ for $0.<\nu<10.$ Hz and bin width 18.7 mHz.

Figure 4: Spectrum of the SA test mass displacement with damping, expressed in $m/\sqrt{Hz}$ for $0.<\nu<10.$ Hz and bin width 18.7 mHz.

Figure 5: TF of the Pisa SA, measured using the seism as an exciter,compared with the theoretical curve HTF+ 0.02·VTF, computed for a damping coefficient F=500 Kg/s.

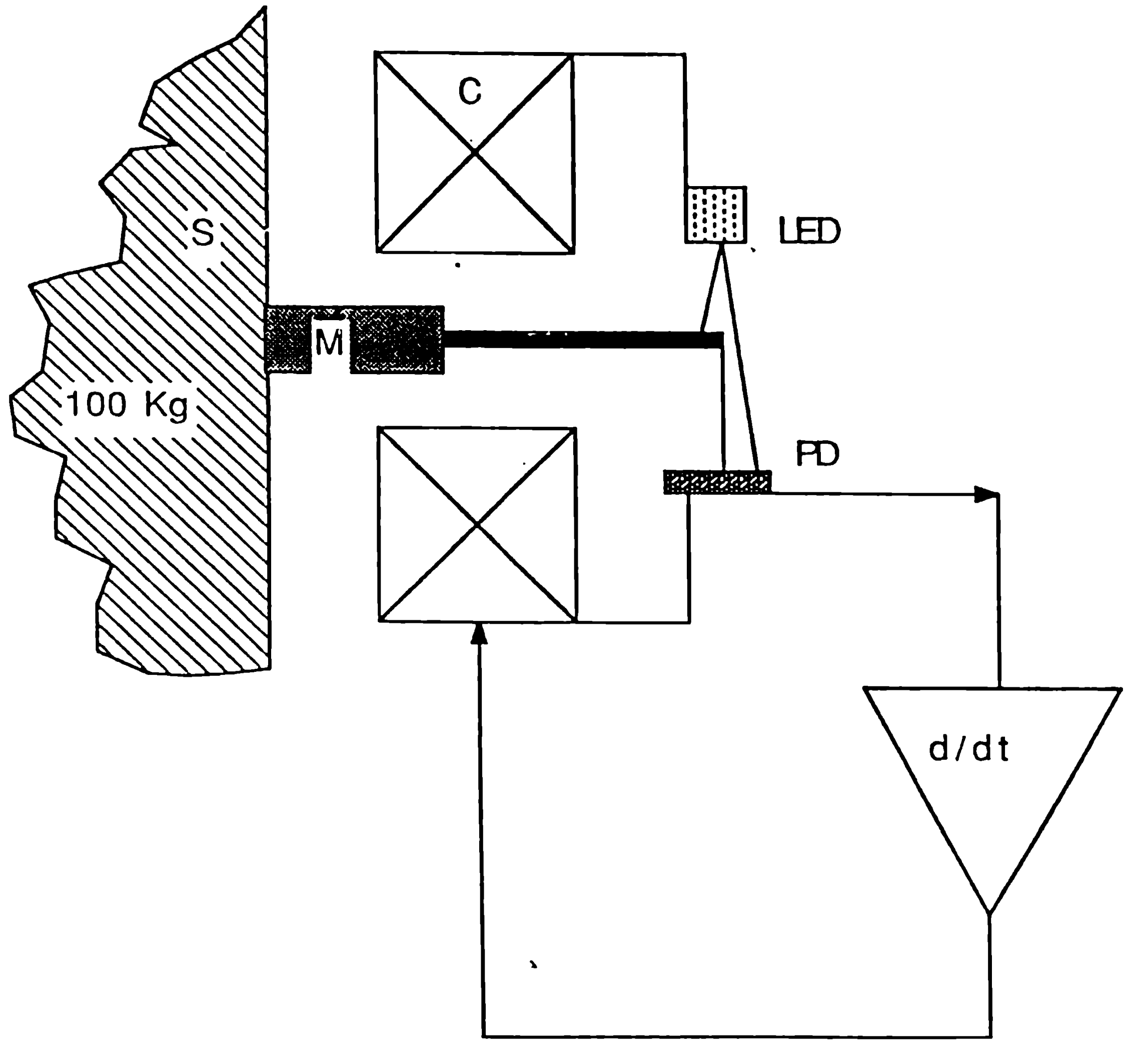

Fig. 1

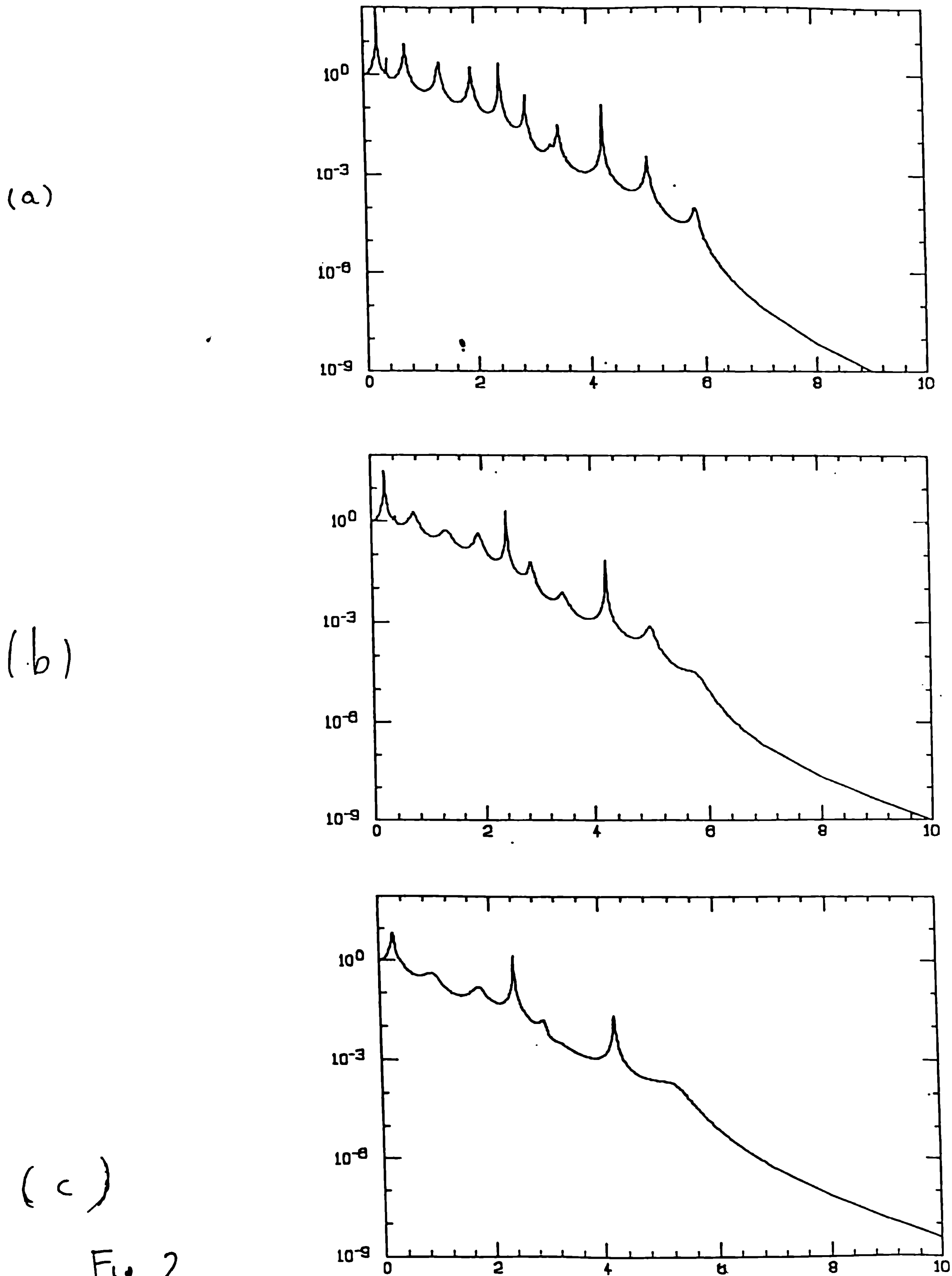

Fig 2

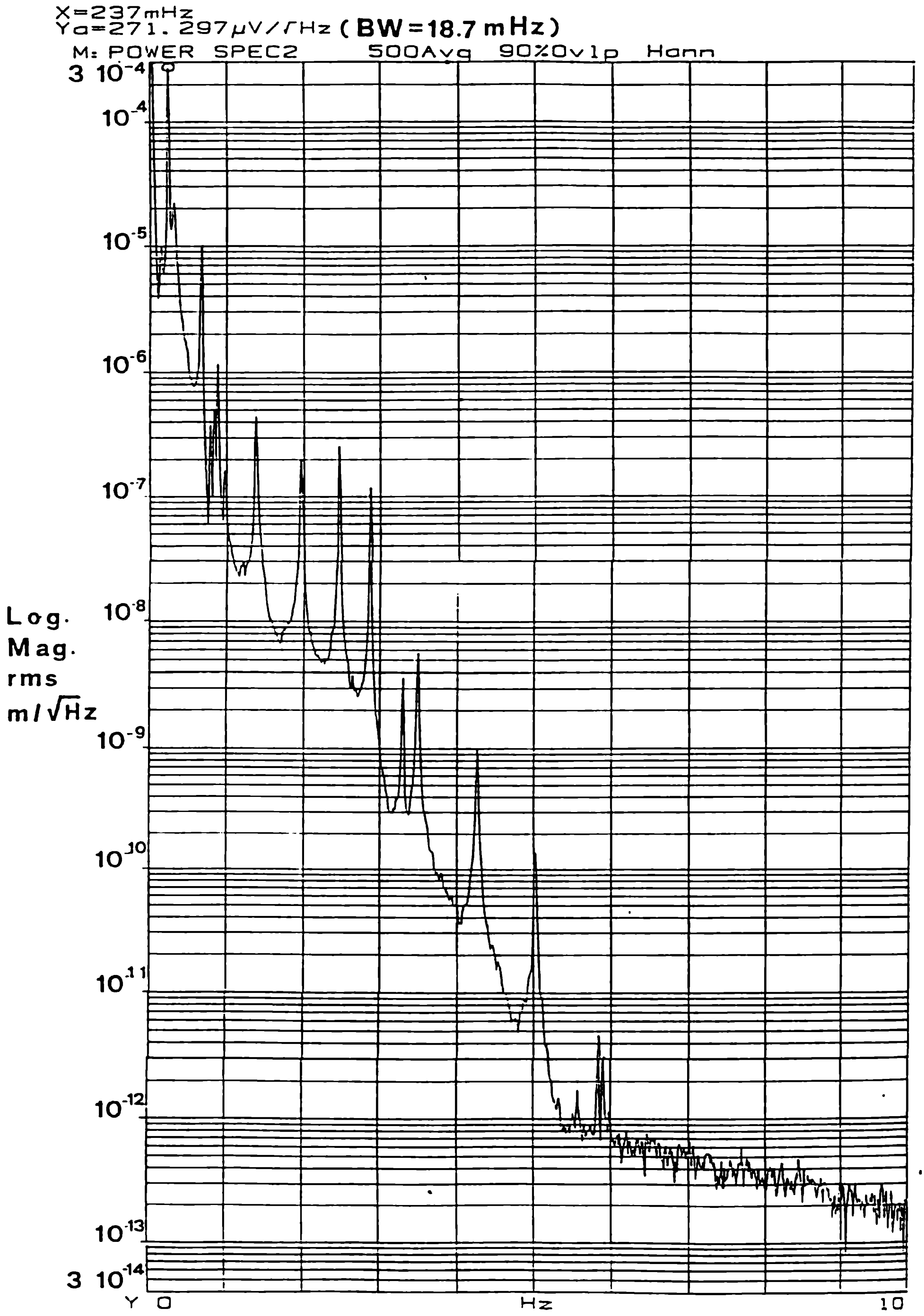
X=237mHz
Ya=271.297μV/√Hz (BW=18.7 mHz)
M: POWER SPEC2 500Avg 90%Ovlp Hann
3 10-4
10-4
10-5
10-6
10-7
10-8
10-9
10-10
10-11
10-12
10-13
3 10-14
Log. Mag. rms m/√Hz
Y 0
Hz
10

Fig 3

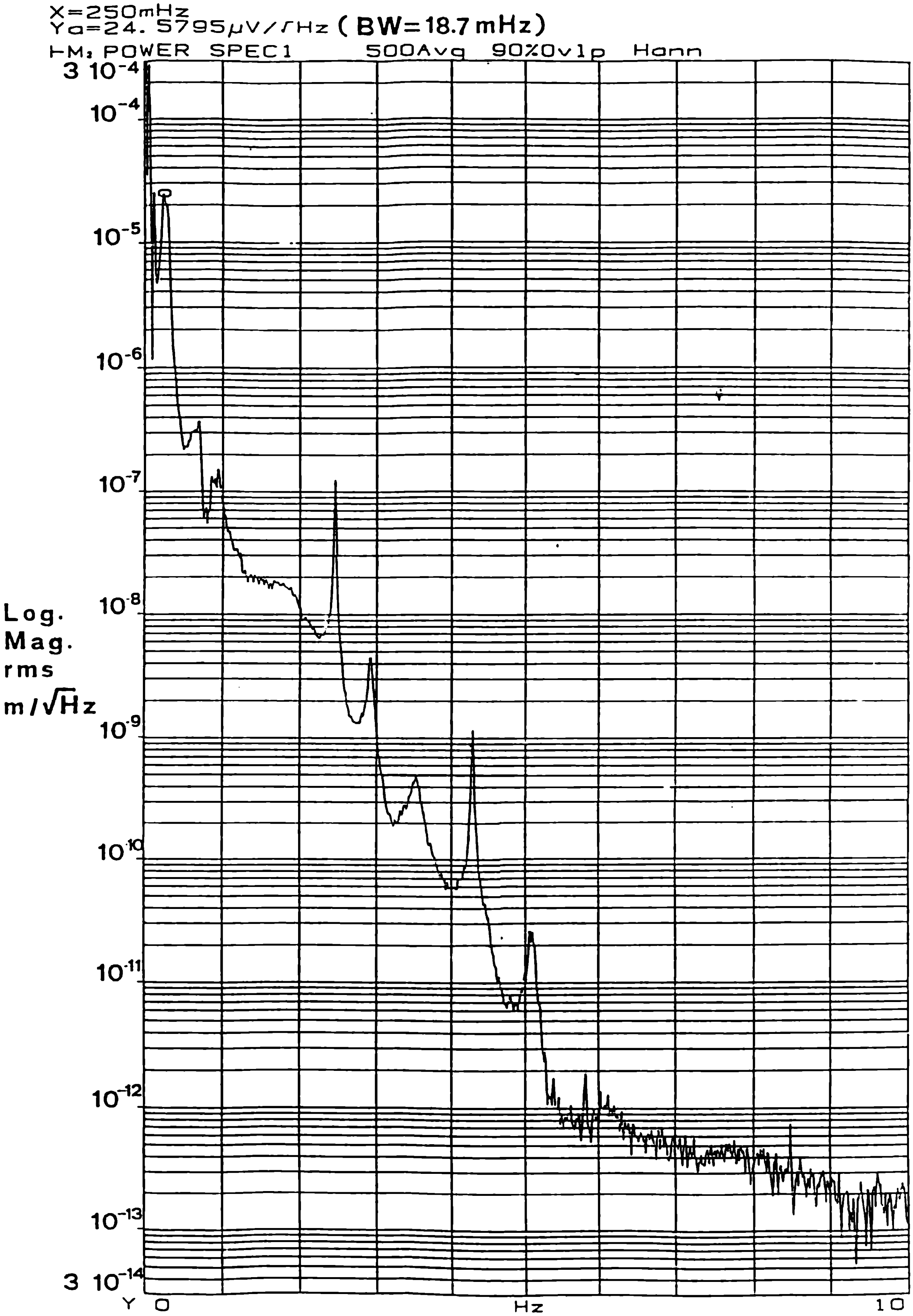

X=250mHz
Ya=24.5795µV/√Hz (BW=18.7 mHz)
FM: POWER SPEC1 500Avg 90%Ovlp Hann
3 10^-4
10^-4
10^-5
10^-6
10^-7
10^-8
10^-9
10^-10
10^-11
10^-12
10^-13
3 10^-14
Log. Mag. rms m/√Hz
Y 0
Hz
10

Fig 4

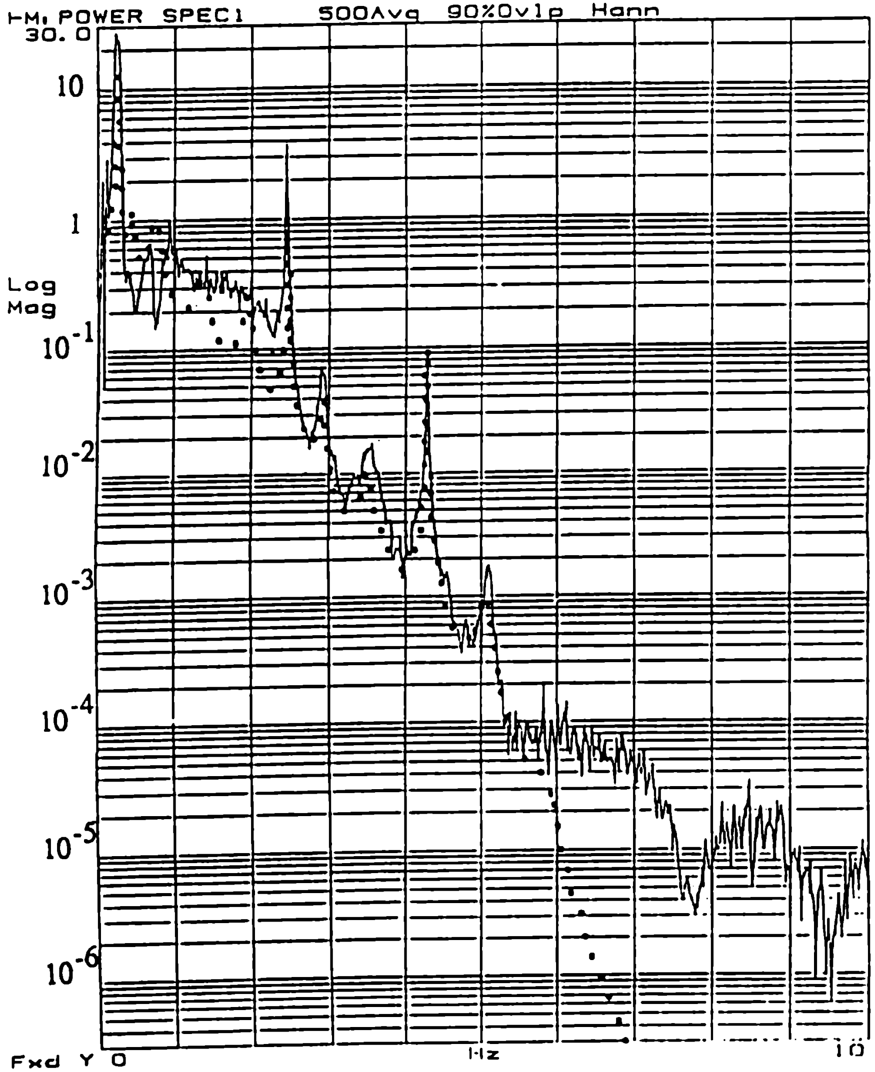

HM: POWER SPEC1
500Avg 90%Ovlp Hann
30.0
10
1
Log
Mag
10^{-1}
10^{-2}
10^{-3}
10^{-4}
10^{-5}
10^{-6}
Fxd Y 0
Hz
10

Fig 5

INTERFEROMETRIC DETECTION OF GRAVITATIONAL WAVES

Adalberto GIAZOTTO

Istituto Nazionale di Fisica Nucleare, Sezione di Pisa, Via Vecchia Livornese 582/a, 56010 S. Piero a Grado, Pisa, Italy

NORTH-HOLLAND - AMSTERDAM

PHYSICS REPORTS (Review Section of Physics Letters) 182, No. 6 (1989) 365–424. North-Holland, Amsterdam

INTERFEROMETRIC DETECTION OF GRAVITATIONAL WAVES

Adalberto GIAZOTTO

Istituto Nazionale di Fisica Nucleare, Sezione di Pisa, Via Vecchia Livornese 582/a, 56010 S. Piero a Grado, Pisa, Italy

Received May 1989

Contents

Abstract

The theoretical and experimental methods involved in the interferometric detection of gravitational waves are reviewed and an attempt of historical analysis is given. The delay line and Fabry–Pérot techniques for storing light in the interferometer are analyzed together with the types of noise competing with the gravitational wave signal.

Single orders for this issue

PHYSICS REPORTS (Review Section of Physics Letters) 182, No. 6 (1989) 365–425.

Copies of this issue may be obtained at the price given below. All orders should be sent directly to the Publisher. Orders must be accompanied by check.

Single issue price Dfl. 45.00, postage included.

Introduction

This Report has not been conceived for specialist readers but for those who are interested in the techniques and the calculation methods involved in the project of interferometric antennas for gravitational wave (GW) detection. I think that my contribution to this didactical approach is more useful than to make a repetition of the already excellent review articles on the field of GW generation and detection [Braginskii and Rudenko 1978, Douglass and Braginskii 1979, Weiss 1979, Thorne 1980, 1987, Hough et al. 1987]. On the other hand, daily contact with the problems arising from the technical solutions necessary to plan the very large interferometer VIRGO gave me the push to write this Report; I realize that regretfully many authors will not be quoted in the text, as will be some experimental results. I apologize for such omissions.

The generation of laboratory GWs with the purpose of detecting them in a "Hertz experiment" [Misner, Thorne and Wheeler 1973 (MTW), Braginskii and Manoukine 1974, Douglass and Braginskii 1979] is unfortunately an almost hopeless enterprise. Extremely high-energy particles accelerated in the next generation accelerators have been considered as potential candidates for the "laboratory" generation of GWs [Braginskii et al. 1977, Vinet 1981, Diambrini, Palazzi and Fargion 1987], but even in this case many more years will be needed to succeed. Astrophysical sources seem to be nowadays the only possible emitters of detectable gravitational radiation; in the following I will mention briefly the best candidate sources likely to be detected in the coming years.

The amplitude of the GWs emitted will be denoted by means of the dimensionless quantity (see section 1)

$$h_{\alpha\beta}^{\mathrm{TT}} \simeq \frac{2G}{c^4 R_0} \frac{\mathrm{d}^2}{\mathrm{d}t^2} \int \rho(3x^\alpha x^\beta - \delta_{\alpha\beta} x^2)\,\mathrm{d}v\,, \tag{I.1}$$

where G is the Newton constant, c the light speed, R_0 the distance from the source, ρ the source mass distribution and the integral is calculated over the source volume. The effect it produces on the separation L of two freely falling masses (see section 2) is a variation $\Delta L_\alpha \sim \frac{1}{2} L^\beta h_{\alpha\beta}^{\mathrm{TT}}$, which is a measurable quantity. Hence I will denote by $h = h_{\alpha\beta}^{\mathrm{TT}}$ the strength of the sources.

Historically the most discussed and most likely producer of detectable GWs has been the collapse of a star. In this process the matter explosion, due to eq. (I.1), must not be of spherical shape for the emission of GW; an approximate formula is

$$h \simeq 5\times 10^{-21}\left(\frac{\eta}{10^{-2}}\right)^{1/2}\left(\frac{15\,\mathrm{Mpc}}{R_0}\right)\left(\frac{1\,\mathrm{kHz}}{\nu}\right)\left(\frac{10^{-3}\,\mathrm{s}}{\tau}\right)^{1/2}, \tag{I.2}$$

where $\eta = \Delta E/M_0 c^2$ is the fraction of energy emitted in GWs, R_0 the distance, ν the observation frequency and $\tau \simeq d_s/c$ the time it takes the collapse shock to traverse the source dimension d_s. The quantity η is the fraction of total energy converted in GW, supposed to be <0.2. The explosion rate is expected to be 1 in 40 years in the galaxy and a few per year in the Virgo cluster. The pulse duration τ is usually considered to be $\simeq 1$ ms, hence detectors are tuned accordingly.

Other classes of events, of far less certain predictability, are those involving black holes. The infall of a particle strongly produces GWs; moreover, if the particle spirals into the black hole, the radiation is 100 times more intense than for radial infall [Kojima and Nakamusa 1984].

A mechanism surely emitting high-intensity GWs is the rotation of compact binary objects such as neutron stars; since the star diameter can be $\simeq 10$ km, the mutual distance can be so small that before coalescence very intense radiation is produced. The signal amplitude is

$$h \simeq 10^{-23}\left(\frac{100\ \mathrm{Mpc}}{R_0}\right)\left(\frac{M}{M_0}\right)^{2/3}\left(\frac{\mu}{M_0}\right)\left(\frac{\nu}{100\ \mathrm{Hz}}\right)^{2/3}, \tag{1.3}$$

where M and μ are the total and reduced mass, respectively, and M_0 the solar mass. The time elapsed around the frequency ν is

$$t \simeq 7.8\left(\frac{100}{\nu}\right)^{8/3}\left(\frac{M_0}{M}\right)^{2/3}\left(\frac{M_0}{\mu}\right)\mathrm{s}. \tag{1.4}$$

Since the detector S/N ratio is proportional to $t^{1/2}$, it follows from (1.4) and (1.3) that the S/N ratio increases as $\nu^{-2/3}$, i.e., detectors having an extended bandwidth at low frequency are more likely to detect these sources. An estimate of Clark et al. [1979] gives $\simeq 3$ events per year in a sphere of 100 Mpc radius.

Pulsars have been interpreted as rotating neutron stars having an off-axis magnetic dipole field [Pacini 1968, Gold 1968], and are considered to be the best candidates as continuous GW emitters. A surface protuberance or aspherical shape with an ellipticity ε could give an amplitude [Zimmermann and Szedenits 1979, Zimmermann 1980]

$$h \simeq 10^{-23}\varepsilon\left(\frac{\nu}{10\ \mathrm{Hz}}\right)^{2}\left(\frac{10\ \mathrm{kpc}}{R_0}\right), \tag{1.5}$$

where ν is the GW frequency, twice the rotation frequency because of eq. (1.1). Upper limits to the GW emission from the Vela and Crab pulsars have been estimated by Zimmermann [1978] to be $h \simeq 3\times 10^{-24}$ and 2×10^{-26} (standard Crab model), respectively, but according to the model of Pandharipande et al. [1976], the Crab pulsar may have an amplitude upper limit of $h \simeq 10^{-25}$.

Since the total number of pulsars in the Galaxy has been estimated to be $\sim 10^5$ [Taylor and Manchester 1977, Lyne et al. 1985] and the fraction of pulsars with GW frequency >10 Hz is about 5% [Manchester and Taylor 1981, Rawley et al. 1986, Barone et al. 1988] we can expect several thousand pulsars having GW frequency $\nu > 10$ Hz and in the frequency range of the kilometric interferometric detectors.

The Heisenberg uncertainty principle sets a fundamental limit to the strain sensitivity measured by means of two freely falling masses M separated by a distance L, in a time $\bar{T}$,

$$h \simeq \frac{1}{\Omega L}\sqrt{\frac{2\hbar}{M\bar{T}}} \simeq 1.5\times 10^{-25}\left(\frac{10^3\ \mathrm{m}}{L}\right)\left(\frac{1\ \mathrm{Hz}}{\nu}\right)\left(\frac{10^7\ \mathrm{s}}{\bar{T}}\right)^{1/2}\left(\frac{10^2\ \mathrm{kg}}{M}\right)^{1/2}, \tag{1.6}$$

where $\Omega = 2\pi\nu$ and $\hbar$ is the reduced Planck constant. With $M = 300$ kg, $\bar{T} = 3\times 10^7$ s, $L = 3\times 10^3$ m, at the Crab frequency ($\nu = 60$ Hz) eq. (1.6) gives $h > 1.5\times 10^{-28}$.

If a pulsar and a star form a binary system there may be a drainage of star matter from the pulsar's surface due to the high gravitational field. This matter is accreting around the neutron star, which is then spun up; the accretion may then reach the Chandrasekhar [1970]–Friedman–Schutz [1978] instability point and strongly emit GWs with an expected amplitude [Wagoner 1984]

$$h \simeq 2 \times 10^{-28}\left(\frac{300\ \mathrm{Hz}}{\nu}\right)\left(\frac{F_x}{10^{-17}\ \mathrm{J/cm^2\,s}}\right)^{1/2}, \tag{1.7}$$

where F_x is the flux of the emitted X-rays.

The stochastic background of GWs produced by all sources has an expected amplitude (for a review see Hough et al. [1986], Thorne [1987])

$$h \simeq 6 \times 10^{-26}\left(\frac{\Omega_{GW}}{10^{-10}}\right)^{1/2}\left(\frac{100\ \mathrm{Hz}}{\nu}\right), \tag{1.8}$$

where Ω_{GW} is the ratio of the source energy density in a bandwidth ν to that necessary to close the universe ($10^{-15}\ \mathrm{J/cm^3}$).

The basic and, to my opinion, the first idea of the interferometric detection of GWs is, clearly stated, contained in a paper of Gertsenshtein and Pustovoit [1963]; their idea is that ". . . . it should be possible to detect gravitational waves by the shift of the bands in an optical interferometer". The first complete work on the noise competing with the GW signal in an interferometric antenna is due to Weiss [1972]; it is also his merit to have advanced the idea of using a "stable" cavity such as the Herriot [1964] delay line, and fast light phase modulation to get rid of the laser's amplitude fluctuations. But the very first experimental attempt, giving high sensitivity in the measurement of the test mass displacement is due to Forward [1978]. Forward used retroflectors to reflect the beam back to a beam splitter and used active controls to lock the interferometer to a fringe; he obtained a spectral strain sensitivity of $\tilde{h} > 2 \times 10^{-16}\ \mathrm{Hz}^{-1/2}$ for $\nu > 2\ \mathrm{kHz}$. The Max Planck at Munich group [Billing et al. 1979], following Weiss' delay lines idea, carried out the construction of a 30 m interferometer having a sensitivity $\tilde{h} \simeq 8 \times 10^{-20}\ \mathrm{Hz}^{-1/2}$.

The alternative to using delay lines is using Fabry–Pérot cavities; this scheme, which was pursued by Drever [Drever et al. 1980, 1981], is very elegant even though it requires more sophisticated optical and feed back design than in the delay line case. Two Fabry–Pérot interferometers are now working in Glasgow and Caltech with a sensitivity $\tilde{h} \simeq 1.2 \times 10^{-19}\ \mathrm{Hz}^{-1/2}$ [Ward et al. 1987] and $\tilde{h} \simeq 5 \times 10^{-19}\ \mathrm{Hz}^{-1/2}$ [Spero 1986], respectively.

Several optical schemes have been invented for increasing the interferometer's sensitivity: light power recycling [Drever 1982] allows the reuse of the unused light from the interferometer; the synchronous recycling scheme [Ruggiero 1979, Drever 1981] allows an increase in the interferometer's sensitivity to periodic signals as do the methods of detuned recycling [Vinet et al. 1988] and dual recycling [Meers 1988]. Of all these schemes only that of power recycling has been tested experimentally [Rüdiger et al. 1987, Man et al. 1987] with success. All the signal recycling schemes will be tested, perhaps painfully, in the future kilometric interferometers.

Another approach to increasing the sensitivity has been given by Caves [1980], who was the first to realize that photon number fluctuations in the interferometer's arms could be produced by vacuum fluctuations of the light field at the unused port of the beam splitter; the idea was to inject into this port a squeezed photon state, i.e. a state having phase fluctuations smaller than Poissonian but with larger amplitude fluctuations. The existence of these states has been demonstrated experimentally and this has led the Munich group [Gea-Banacloche and Leuchs 1987] to experimentally explore the sqeezing route.

At this very moment (February 1989) it seems that there is a likely chance that the construction of four large interferometers will be approved: the German–Scottish one, the French–Italian one and the two American ones. Japan and Australia are likely to join this group. The need of several large interferometers is also dictated by the necessity of making coincidence detection of GW signals.

There is also a finite chance that GWs will be discovered meanwhile by the bar detectors and this will finally convince physicists from other fields to join what I consider the most exciting and, at the same time, frustrating experience a physicist can have.

This Report has been subdivided into 14 sections: in section 1 the generation mechanism of GWs and in section 2 the interaction of GWs with matter are described. Delay lines and Fabry–Pérot optical interferometers are described in sections 3 and 4, respectively. The recycling schemes are described in section 5, the laser intensity noise in section 6 and the noise due to the laser linewidth in section 7. The laser lateral beam jitter noise is described in section 8 and the noise due to gas pressure fluctuations in section 9. The thermal noise is described in section 10, the seismic noise in section 11, the radiation pressure effects in section 12, the cosmic ray background in section 13 and finally, a pictorial description of source intensities and relevant noises is presented in section 14.

1. The generation of gravitational waves and the transverse traceless gauge

In Einstein's Theory of General Relativity (TGR) [Einstein 1916] Gravitational Waves (GWs) are shown to be ripples in the space–time curvature propagating with the speed of light. Under the hypothesis of weak fields a perturbation $h_{\mu\nu}$ to the flat metric tensor

$$\eta_{\mu\nu} = \begin{pmatrix} 1 & 0 & 0 & 0 \\ 0 & -1 & 0 & 0 \\ 0 & 0 & -1 & 0 \\ 0 & 0 & 0 & 1 \end{pmatrix} \tag{1.1}$$

is created by the energy-momentum tensor τ_{ik} according to the equation (see MTW)

$$\square \Psi_{ik} = (8\pi G c^{-4})\tau_{ik} , \tag{1.2}$$

where $\Psi_{ik} = h_{ik} - \frac{1}{2}\delta_{ik} h^{\mu}_{\mu}$, G is the Newton constant and c the speed of light. From momentum–energy conservation,

$$\partial_{\mu} \tau_{\mu\nu} = 0 , \tag{1.3}$$

and considering that $\tau_{00} = \rho c^2$, where ρ is the matter density, it follows that [Landau and Lifshitz 1951]

$$\Psi_{\alpha\beta} = -\frac{2G}{c^4 R_0}\left(\frac{\partial^2}{\partial t^2}\int \rho x^{\alpha} x^{\beta}\, \mathrm{d}v\right)_{t-R_0/c} , \tag{1.4}$$

where R_0 is the distance from the source; eq. (1.4) is valid when the matter speed is far less than c and when the GW wavelength is much larger than the source dimensions. From eq. (1.4) it follows that the GW field is produced by the second moment of the mass distribution.

Since $\Psi_{\mu\nu}$ is a symmetric tensor it has 10 independent elements, which are reduced to 6 since eq. (1.3) gives

$$\partial_{\mu} \Psi_{\mu\nu} = 0 \tag{1.5}$$

The number of independent elements of $\Psi_{\mu\nu}$ can be further reduced by applying the coordinate transformation

$$x'_\mu = x_\mu + \varepsilon_\mu , \tag{1.6}$$

where ε_μ are infinitesimal functions which must leave unchanged the line element

$$ds^2 = g_{\mu\nu}\, dx^\mu\, dx^\nu . \tag{1.7}$$

Equation (1.7) imposes

$$\Box \varepsilon_\mu = 0 , \tag{1.8}$$

$$h'_{\mu\nu} = h_{\mu\nu} - \partial\varepsilon_\mu/\partial x_\nu - \partial\varepsilon_\nu/\partial x_\mu . \tag{1.9}$$

Hence writing Ψ_{ik} as a plane wave propagating in the k direction at speed c,

$$\Psi_{ik} = A_{ik}\, e^{ik_r x^r} , \qquad k^r k_r = 0 , \tag{1.10}$$

and putting [see eq. (1.9)]

$$\varepsilon_\mu = C_\mu\, e^{ik_r x^r} , \tag{1.11}$$

we can define a four-velocity V^k and choose C_μ such as to give

$$A_{ik} V^k = 0 . \tag{1.12}$$

But these four equations are not independent since $k^i A_{ik} V^k = 0$ for any given k; hence a further condition can be applied and we impose

$$A^\mu_\mu = 0 . \tag{1.13}$$

This condition gives $h^\mu_\mu = 0$ and

$$\Psi_{\mu\nu} = h_{\mu\nu} . \tag{1.14}$$

Equations (1.5), (1.12) and (1.13) define the Transverse Traceless (TT) gauge (see MTW); by choosing $V^0 = 1$, $V = 0$ we obtain

$$\begin{aligned} &h^{TT}_{\mu 0} = 0 , && \text{i.e. only spatial components} \neq 0 , \\ &h^{TT}_{KJ,J} = 0 , && \text{i.e. divergence-free spatial components} , \\ &h^{TT}_{KK} = 0 , && \text{traceless} . \end{aligned} \tag{1.15}$$

Let us assume the wave propagates along the x_3 axis; then

$$k = (k, 0, 0, k)\,, \tag{1.16}$$

and from eq. (1.15) it follows that

$$h^{TT}_{3k} = 0\,, \qquad h^{TT}_{11} = -h^{TT}_{22} \neq 0\,, \qquad h^{TT}_{12} = h^{TT}_{21}\,. \tag{1.17}$$

In matrix form

$$h^{TT}_{ik} = \begin{pmatrix} 0 & 0 & 0 & 0 \\ 0 & h^{TT}_{11} & h^{TT}_{12} & 0 \\ 0 & h^{TT}_{12} & -h^{TT}_{11} & 0 \\ 0 & 0 & 0 & 0 \end{pmatrix} = h^{TT}_{11}\begin{pmatrix} 0 & 0 & 0 & 0 \\ 0 & 1 & 0 & 0 \\ 0 & 0 & -1 & 0 \\ 0 & 0 & 0 & 0 \end{pmatrix} + h^{TT}_{12}\begin{pmatrix} 0 & 0 & 0 & 0 \\ 0 & 0 & 1 & 0 \\ 0 & 1 & 0 & 0 \\ 0 & 0 & 0 & 0 \end{pmatrix} = A_+ e^{+}_{ik} + A_\times e^{\times}_{ik}\,. \tag{1.18}$$

The two polarizations e^{+}_{ik} and $e^{\times}_{ik}$ are exchanged by a rotation R of $\pi/4$ around the x_3 axis, i.e.,

$$R(\pi/4) = \frac{1}{\sqrt{2}}\begin{pmatrix} 0 & 0 & 0 & 0 \\ 0 & 1 & 1 & 0 \\ 0 & -1 & 1 & 0 \\ 0 & 0 & 0 & 0 \end{pmatrix}\,,$$

$$R(\pi/4)e^{+}R^{-1}(\pi/4) = -e^{\times}\,, \qquad R(\pi/4)e^{\times}R^{-1}(\pi/4) = e^{+}\,. \tag{1.19}$$

This behaviour under rotation is proper to a spin-2 field.

The Riemann tensor

$$R_{iklm} = \frac{1}{2}\left(\frac{\partial^2 h_{im}}{\partial x^k\,\partial x^l} + \frac{\partial^2 h_{kl}}{\partial x^i\,\partial x^m} - \frac{\partial^2 h_{km}}{\partial x^i\,\partial x^l} - \frac{\partial h^2_{il}}{\partial x^k\,\partial x^m}\right) \tag{1.20}$$

with the conditions of eq. (1.11) becomes simply

$$R_{iklm} \Rightarrow R_{0\alpha 0\beta} = -\tfrac{1}{2}\ddot{h}^{TT}_{\alpha\beta}\,. \tag{1.21}$$

The TT part of eq. (1.4) can be evaluated by applying to $\Psi_{\alpha\beta}$ the TT projection operator (see MTW)

$$P_{jk} = \delta_{jk} - n_j n_k\,, \tag{1.22}$$

where $\boldsymbol{n}$ is the unit vector in the direction in which we want to evaluate the TT part of the GW amplitude; hence

$$\Psi^{TT}_{\alpha\beta} = P_{\alpha l}\Psi_{lj}P_{j\beta} - \tfrac{1}{2}P_{\alpha\beta}\Psi_{lm}P_{lm}\,. \tag{1.23}$$

It is easy to verify that from eqs. (1.23), (1.4) and (1.15) it follows that $\Psi^{TT}_{\alpha\beta}n_\beta = 0$, $\Psi^{TT}_{\alpha\alpha} = 0$, and

$$h^{TT}_{\alpha\beta} = -\frac{2G}{c^4 R_0}\left(\frac{\partial^2}{\partial t^2}\int \rho(P_{\alpha l}x^l x^j P_{j\beta} - \tfrac{1}{2}P_{\alpha\beta}x^l x^m P_{lm})\,\mathrm{d}v\right) = -\frac{2G}{c^4 R_0}\ddot{D}^{TT}_{\alpha\beta}\,, \tag{1.24}$$

where $D_{\alpha\beta}$ is the reduced quadrupole momentum of the GW emitting mass system.

2. The detection of gravitational waves

A particle moving freely under the action of a gravitational force has its coordinates x^μ satisfying the geodesic equation

$$\frac{d^2x^\mu}{d\tau^2} + \Gamma^\mu_{\nu\lambda}\frac{dk^\nu}{d\tau}\frac{dx^\lambda}{d\tau} = 0\,, \tag{2.1}$$

where τ is proportional to the particle's proper time and

$$\Gamma^\mu_{\nu\lambda} = \tfrac{1}{2}g^{\mu m}\left(\frac{\partial g_{m\nu}}{\partial x^\lambda} + \frac{\partial g_{m\lambda}}{\partial x^\nu} - \frac{\partial g_{\nu\lambda}}{\partial x^m}\right) \tag{2.2}$$

are the Christoffel symbols. It is always possible to find a space–time trajectory in which $\Gamma^\mu_{\nu\lambda} = 0$ at any time; along this trajectory the particle is freely falling. It is easy to show that the separation ξ^α between two particles A and B satisfies the geodesic deviation equation

$$\frac{D^2\xi^\alpha}{d\tau^2} + R^\alpha_{\beta\gamma\delta}\xi^\gamma\frac{dx^\beta}{d\tau}\frac{dx^\delta}{d\tau} = 0\,, \tag{2.3}$$

where D^2 is the second covariant derivative,

$$\frac{D^2\xi^\alpha}{d\tau^2} = \frac{d^2\xi^\alpha}{d\tau^2} + \frac{d\Gamma^\alpha_{\beta\mu}}{d\tau}\xi^\beta\frac{dx^\mu}{d\tau} + \Gamma^\alpha_{\beta\mu}\frac{d}{d\tau}\left(\xi^\beta\frac{dx^\mu}{d\tau}\right) + \Gamma^\alpha_{\beta\mu}\left(\frac{d\xi^\beta}{d\tau} + \Gamma^\alpha_{\beta\mu}\xi^\beta\frac{dx^\mu}{d\tau}\right)\frac{dx^\mu}{d\tau}\,. \tag{2.4}$$

With the purpose of evaluating ξ^α let us put $x = 0$ in the center of mass system (CMS) of particle A (see MTW), the time x_0 equal to the proper time τ and the coordinate axis connected to gyroscopes carried by A. At $x = 0$, since A is freely falling along the geodesic line, we obtain

$$(\Gamma^\alpha_{\beta\gamma})_{x=0} = (d\Gamma^\alpha_{\beta\gamma}/d\tau)_{x=0} = 0\,, \tag{2.5}$$

and eq. (2.2) becomes

$$D^2\xi^\alpha/d\tau^2 = d^2\xi^\alpha/d\tau^2\,. \tag{2.6}$$

Introducing eqs. (1.21) and (2.6) into eq. (2.3) and considering that, to first order in $h^{TT}_{\mu\nu}$, $t \cong \tau$, where t is the observation time, we obtain

$$d^2\xi^\alpha/dt^2 = -R_{\alpha0\beta0}\xi^\beta = \tfrac{1}{2}(d^2/dt^2)h^{TT}_{\alpha\beta}\xi^\beta\,. \tag{2.7}$$

From eq. (2.7) we can see the effects of GW polarization on the detector; if the GW is propagating along the z axis and the masses A and B are located as in fig. 2.1, then

$$\xi^\alpha = (x_A - x_B)^\alpha\,. \tag{2.8}$$

Putting

$$F_\alpha = M\,d^2\xi^\alpha/dt^2 = \tfrac{1}{2}M\,(d^2/dt^2)h^{TT}_{\alpha\beta}\xi^\beta\,, \tag{2.9}$$

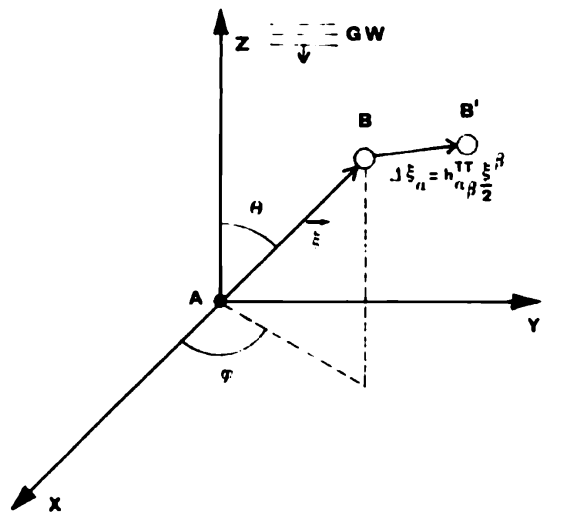

Fig. 2.1. In an inertial system having the origin in the center of mass of mass A the effect of a GW traveling along the z axis is to displace the mass B from the equilibrium position by an amount $\Delta\xi^\alpha = \frac{1}{2}h^{TT}_{\alpha\beta}\xi^\beta$ [see eq. (2.7)]

and considering that the only independent components of $h^{TT}_{\alpha\beta}$ are h^{TT}_{11} and h^{TT}_{12}, we can write the projection F of F_α along the line connecting A to B,

$$F(\theta, \varphi) = F_\alpha \xi^\alpha/|\xi| = \tfrac{1}{2}|\xi| M(\ddot{h}^{TT}_{11} \sin^2\theta \cos 2\varphi + \ddot{h}^{TT}_{12} \sin^2\theta \sin 2\varphi) . \tag{2.10}$$

In eq. (2.10) the tidal character of the force produced by a GW is clearly shown by the term $|\xi|$. It is also evident from eq. (2.10) that $F = 0$ if the mass separation ξ^α is in the GW propagation direction.

In the interferometric antenna the mirrors are attached to masses suspended with wires like pendula. With reference to fig. 2.2, the beam splitter in the origin has mass m_1 and the other two mirrors have mass m_2 and m_3, respectively, and are placed at a distance L from the origin; ξ_i are the coordinates of the masses m_i in the CMS. The CMS coordinates are

$$x_{cms} = Lm_3/(m_1 + m_2 + m_3) , \qquad y_{cms} = Lm_2/(m_1 + m_2 + m_3) . \tag{2.11}$$

For the sake of simplicity we assume that the GW is propagating along the z axis; under this condition, using eq. (2.7), the acceleration of the mirrors produced by the GW interaction becomes

$$\begin{aligned} (\ddot{x}_1)_{GW} &= -\tfrac{1}{2}(\ddot{h}^{TT}_{11} x_{cms} + \ddot{h}^{TT}_{12} y_{cms}) , & (\ddot{x}_3)_{GW} &= -\tfrac{1}{2}[\ddot{h}^{TT}_{11}(L - x_{cms}) - \ddot{h}^{TT}_{12} y_{cms}] , \\ (\ddot{y}_1)_{GW} &= -\tfrac{1}{2}(\ddot{h}^{TT}_{21} x_{cms} + \ddot{h}^{TT}_{22} y_{cms}) , & (\ddot{y}_2)_{GW} &= \tfrac{1}{2}[-h_{21} x_{cms} + h^{TT}_{22}(L - y_{cms})] . \end{aligned} \tag{2.12}$$

The equations of motion of the mirrors read

$$\begin{aligned} &\ddot{x}_1 + \tau_1^{-1}(\dot{x}_1 - \dot{\bar{x}}_1) + (g/l_1)(x_1 - \bar{x}_1) = (\ddot{x}_1)_{GW} , & &\ddot{x}_3 + \tau_3^{-1}(\dot{x}_3 - \dot{\bar{x}}_3) + (g/l_3)(x_3 - \bar{x}_3) = (\ddot{x}_3)_{GW} , \\ &\ddot{y}_1 + \tau_1^{-1}(\dot{y}_1 - \dot{\bar{y}}_1) + (g/l_1)(y_1 - \bar{y}_1) = (\ddot{y}_1)_{GW} , & &\ddot{y}_2 + \tau_2^{-1}(\dot{y}_2 - \dot{\bar{y}}_2) + (g/l_2)(y_2 - \bar{y}_2) = (\ddot{y}_2)_{GW} , \end{aligned} \tag{2.13}$$

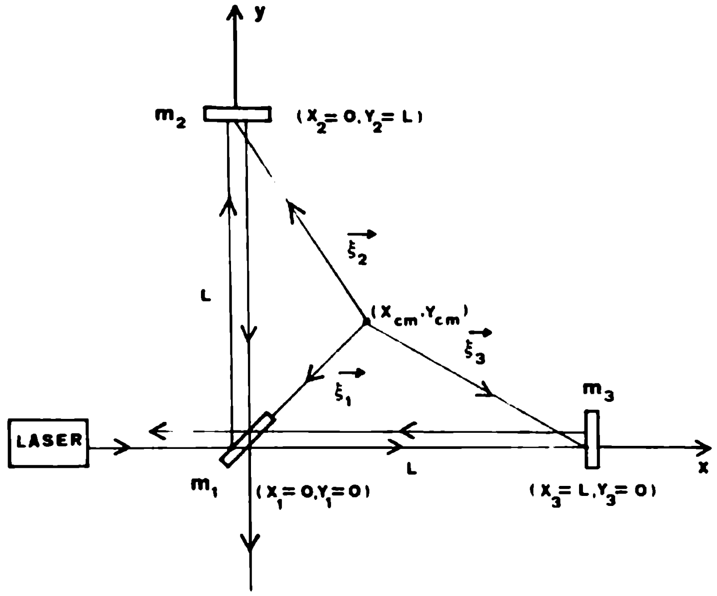

Fig. 2.2. The interferometer's mirrors, having mass m_1, m_2 and m_3, are located at (x, y) positions $(0, 0)$, $(0, L)$ and $(L, 0)$, respectively. The acceleration of the mirrors produced by a GW traveling along the z axis is calculated introducing their coordinates in the CMS, ξ_i, into eq. (2.9). The inertial reference system has the origin in the center of mass of the mirror system.

where τ_i and l_i are, respectively, the relaxation time and the length of the ith pendulum and $\bar{x}_i$, $\bar{y}_i$ are the pendulum suspension point displacements due to seismic noise. Equations (2.13) can be solved exactly, but for the sake of simplicity we assume $\tau_i = \tau_j$ and $l_i = l_j$; then we can subtract the first equation from the second and the third from the fourth, obtaining

$$\Delta\ddot{x} + \tau^{-1}(\Delta\dot{x} - \Delta\dot{\bar{x}}) + (\Delta x - \Delta\bar{x})\omega_0^2 = -\tfrac{1}{2}\ddot{h}_{11}^{TT} L\,, \quad \Delta\ddot{y} + \tau^{-1}(\Delta\dot{y} - \Delta\dot{\bar{y}}) + (\Delta y - \Delta\bar{y})\omega_0^2 = -\tfrac{1}{2}\ddot{h}_{22}^{TT} L\,, \tag{2.14}$$

where $\Delta x = x_1 - x_3$, $\Delta y = y_1 - y_2$, $\Delta\bar{x} = \bar{x}_1 - \bar{x}_3$ and $\Delta\bar{y} = \bar{y}_1 - \bar{y}_2$, $\omega_0^2 = g/l$ and $\tau = \tau_i$.

In a single-pass interferometer the phase change is

$$\Delta\varphi = 4\pi(\Delta x - \Delta y)/\lambda\,, \tag{2.15}$$

where λ is the light wave length; hence, considering that, when the GW is propagating along the z axis, $h_{11}^{TT} = -h_{22}^{TT}$ and putting $\Delta\bar{\varphi} = 4\pi(\Delta\bar{x} - \Delta\bar{y})/\lambda$, we obtain

$$\Delta\ddot{\varphi} + \tau^{-1}(\Delta\dot{\varphi} - \Delta\dot{\bar{\varphi}}) + \omega_0^2(\Delta\varphi - \Delta\bar{\varphi}) = \frac{4\pi}{\lambda}\ddot{h}_{11}L\,. \tag{2.16}$$

This equation can be easily integrated giving [Pizzella 1975]

$$\Delta\varphi(t) = \frac{4\pi L}{\lambda\tilde{\omega}_0}\int_0^t \sin\tilde{\omega}_0(t-\eta)\,e^{-(t-\eta)/2\tau}[\ddot{h}_{11}^{TT}(\eta) + \tau^{-1}\Delta\dot{\bar{\varphi}}(\eta) + \omega_0^2\,\Delta\bar{\varphi}(\eta)]\,d\eta\,,$$
$$\tilde{\omega}_0 = \sqrt{\omega_0^2 - 1/(4\tau^2)}\,. \tag{2.17}$$

To understand the effect of the GW on $\Delta\varphi$ we can neglect the seismic noise contribution and study the behaviour of eq. (2.17) assuming two simple functional forms for $h(t) = h_{11}^{TT}(t)$. In the first case we assume $h(t)$ to be a pulse of duration $\Delta t \ll 1/\omega_0$ and amplitude h_0,

$$h(\eta) = h_0[\theta(\eta) - \theta(\eta - \Delta t)] . \tag{2.18}$$

Inserting eq. (2.18) in eq. (2.17) and assuming the mechanical quality factor of the pendula $Q = \omega_0\tau \gg 1$ we obtain

$$\Delta\varphi(t) = \frac{4\pi L}{\lambda}\, h(t) + \frac{4\pi L}{\lambda}\, h_0[\omega_0\, \Delta t \sin(\omega_0 t)\, e^{-t/\tau} + O((\omega_0\, \Delta t)^2) + O(1/Q^2)] . \tag{2.19}$$

Equation (2.19) shows that in the interferometric detector the measurement of $\Delta\varphi$ gives a precise measure of $h(t)$; the term in h_0, which represents the "memory" that the pendula have of the GW for $t > \Delta t$, can be neglected since it is multiplied by $\omega_0\, \Delta t \ll 1$.

In the second case we consider a periodic GW with amplitude

$$h(t) = h_0\, e^{i\Omega_g t} . \tag{2.20}$$

Inserting $h(t)$ in eq. (2.17) we obtain for $t \gg \tau$

$$\Delta\varphi = -\frac{4\pi L}{\lambda}\, \frac{\Omega_g^2\, e^{i\Omega_g t} h_0}{\omega_0^2 - \Omega_g^2 + i\Omega_g/\tau} . \tag{2.21}$$

For $\Omega_g > \omega_0$ and $Q \gg 1$, eq. (2.20) becomes

$$\Delta\varphi = (4\pi L/\lambda)/h_0\, e^{i\Omega_g t} . \tag{2.22}$$

Equation (2.22) shows that with an interferometric detector it is possible to measure distortionless $h(t)$ even for a periodic GW; hence the very peculiarity of this detector is due to the low value of the pendulum resonance frequency ν_0, which can be made as low as a few Hz, giving the possibility, in principle, to detect low-frequency GWs. Furthermore the possibility of making L very large (some km), in virtue of eq. (2.9), would allow the operation of the antenna at room temperature while maintaining high sensitivity even in the presence of noise, such as thermal noise, which is dominant at low frequency.

For the evaluation of the phase shift due to the GW interaction of a photon beam bouncing between two mirrors, it is opportune to choose a coordinate system in which the mirrors are at rest; in this system the only GW interaction with the photon beam is due to the change of the metric coefficients. In fact if the mirrors are freely falling (i.e. with suspensions having no rigidity), then in the TT system they are at rest; this is easily shown considering that to first order in $h_{\alpha\beta}^{TT}$ from eqs. (2.2) and (2.4) it follows that

$$\Gamma^{\alpha}_{\beta\mu} \;\rightarrow\; \Gamma^{\alpha}_{\beta 0} = -\tfrac{1}{2}\dot{h}^{TT}_{\alpha\beta} , \qquad \frac{D^2\xi^{\alpha}}{d\tau^2} = \frac{d^2\xi^{\alpha}}{dt^2} - \tfrac{1}{2}\ddot{h}^{TT}_{\alpha\beta}\,\xi^{\beta} = -R^{\alpha}_{0\gamma 0}\xi^{\gamma} = -\tfrac{1}{2}\ddot{h}^{TT}_{\alpha\beta}\,\xi^{\beta} . \tag{2.23}$$

and hence $(\ddot{\xi}^{\alpha})_{TT} = 0$.

A matrix approach, used extensively for the evaluation of the phase shift due to the GW interaction with a photon bouncing between freely falling mirrors, is due to Vinet [1986]. The method is based on the consideration that due to eq. (2.23) the only effect of the GW on a photon is contained in the perturbed ds^2,

$$ds^2 = c^2\,dt^2 - [1 + h(t)]\,dx^2 - [1 - h(t)]\,dy^2 , \tag{2.24}$$

where $h(t) = h\cos\phi$, with $\phi = \Omega_g t + \varphi$ and the photon is supposed to travel along the x or y axis.

If the photon is scattered back by a mirror at distance $x = L$, then from eq. (2.24) it follows that the round trip retarded time is

$$t_r = t - \frac{2L}{c} - \varepsilon h\,\frac{L}{c}\,\frac{\sin\eta}{\eta}\cos(\phi - \eta) , \tag{2.25}$$

where $\eta = \Omega_g L/c$ and $\varepsilon = \pm 1$ if the photon is traveling along x or y, respectively.

If the time dependent part of the EM fields along the trajectory is taken to be

$$A(t) = (A_0 + \tfrac{1}{2}h\,e^{i\phi}A_1 + \tfrac{1}{2}h\,e^{-i\phi}A_2)\,e^{-i\omega t} , \tag{2.26}$$

where $\omega = 2\pi\nu_0$ (ν_0 is the laser frequency) then substitution of eq. (2.25) in eq. (2.26) gives (to first order in h)

$$\begin{aligned} A(t) = e^{i\omega(2L/c - t)}\Big[& A_0 + \tfrac{1}{2}h\,e^{i\phi}\Big(A_1\,e^{-2i\Omega_g L/c} + i\omega\varepsilon\,\frac{L}{c}\,\frac{\sin\eta}{\eta}\,e^{-i\eta}A_0\Big) \\ & + \tfrac{1}{2}h\,e^{-i\phi}\Big(A_2\,e^{2i\Omega_g L/c} + i\omega\varepsilon\,\frac{L}{c}\,\frac{\sin\eta}{\eta}\,e^{i\eta}A_0\Big)\Big] . \end{aligned} \tag{2.27}$$

This can be put in matrix form,

$$\begin{pmatrix} A_0 \\ A_1 \\ A_2 \end{pmatrix}' = D\begin{pmatrix} A_0 \\ A_1 \\ A_2 \end{pmatrix} , \tag{2.28}$$

$$D = x\begin{pmatrix} 1 & 0 & 0 \\ i\varepsilon\xi\,\dfrac{\sin\eta}{\eta}\,e^{-i\eta} & \bar{y} & 0 \\ i\varepsilon\xi\,\dfrac{\sin\eta}{\eta}\,e^{i\eta} & 0 & y \end{pmatrix} , \tag{2.29}$$

$\xi = \omega L/c$, $x = e^{2i\xi}$, $y = e^{2i\eta}$.

This approach can be applied to interferometric GW detectors because in this kind of antenna the observation frequency is always above the mirror suspension mode frequencies, hence the mirrors can be considered as being freely falling.

The case of mirrors elastically bound with self-frequency $\nu_m = \Omega_m/2\pi$ has been treated by Pegoraro et al. [1978]; they found a gauge transformation

$$\varepsilon^{0} = \frac{1}{2c}\,\lambda\dot{h}^{\mathrm{TT}}_{\alpha\beta}x^{\alpha}x^{\beta}\,, \qquad \varepsilon^{3} = \frac{1}{2c}\,\lambda\dot{h}^{\mathrm{TT}}_{\alpha\beta}x^{\alpha}x^{\beta}\,,$$

$$\varepsilon^{\alpha} = \lambda h^{\mathrm{TT}}_{\alpha\beta}x^{\beta}\,, \quad \beta, \alpha = 1, 2\,, \tag{2.30}$$

$$\lambda = \tfrac{1}{2}\Omega^2_{\mathrm{m}}/(\Omega^2_{\mathrm{m}} - \Omega^2)\,, \quad \Omega \neq \Omega_{\mathrm{m}}\,, \tag{2.31}$$

giving a $h_{\mu\nu}$, evaluated by means of eq. (1.9), which leaves at rest a mirror initially at rest.

An eikonal equation expansion to first order in $h_{\mu\nu}$ has been studied by Linet and Tourrenc [1976]; they found that the photon phase shift can be put in the form

$$\varphi = \frac{c^2}{hE}\int_{t_0}^{t_1} h_{\mu\nu}p^{\mu}p^{\nu}\,\mathrm{d}t\,. \tag{2.32}$$

where p^{μ} is the photon four-momentum, and showed that in the resonance arising from the GW and photon interaction [Braginskii and Menskii 1971, Braginskii et al. 1974] the photon phase shift increases linearly with time and is proportional to the ratio $\omega/\Omega_{\mathrm{g}}$.

3. Delay line interferometers

The need to increase the interferometer phase shift due to a GW signal is dictated by the existence of noise which affects only the phase of the optical rays without creating real displacements of the mirrors. To overcome the effects due to this noise, which will be called "phase noise" in contrast to "displacement noise", it is very important to find an optical scheme allowing the beams to bounce back and forth in the optical cavities.

Actually the ultimate phase noise is the photon counting noise $\Delta\phi_{\mathrm{pc}}(t)$ due to the anticorrelated fluctuations Δn of the photon number n in the interferometer arms according to the uncertainty relation

$$\langle \Delta\phi_{\mathrm{pc}}(t)^2\rangle^{1/2} = \Delta\phi_{\mathrm{pc}} \geq 1/\Delta n\,. \tag{3.1}$$

For a photon coherent state $\Delta n = \sqrt{n}$, hence

$$\Delta\phi_{\mathrm{pc}} \geq 1/\sqrt{n} = \sqrt{h\nu_0/W_{\mathrm{eff}}t}\,. \tag{3.2}$$

where h is Planck's constant, ν_0 the laser frequency, W_{eff} the light power in the interferometer arms and t the measurement time. If the light makes $2N$ reflections (see fig. 3.1), the phase shift due to a mirror displacement $\Delta x_{1,2} = \pm\frac{1}{2}h(t)L$ is

$$\varphi_{1,2} = \frac{4N\pi}{\lambda}\,\Delta x + \bar{\varphi}_{1,2} = \varphi_{\mathrm{s}}/2 + \bar{\varphi}_{1,2}\,, \tag{3.3}$$

where $\bar{\varphi}_{1,2}$ are given fixed phase shifts in the two arms and Δx has been evaluated in the limit $\Omega_{\mathrm{g}}L/c \ll 1$.

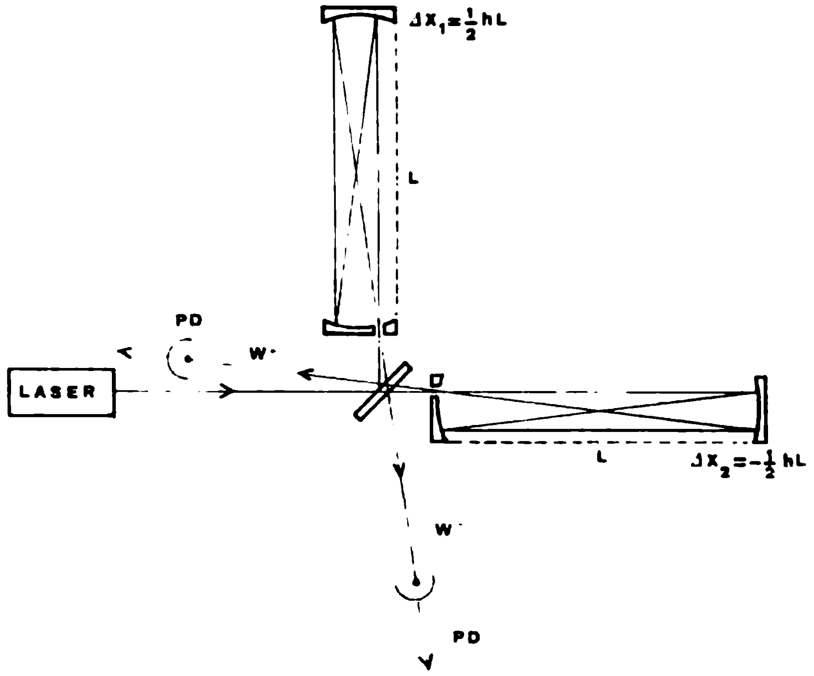

Fig. 3.1. In the delay line scheme, the laser beam enters the two optical cavities and bounces 2N times between the mirrors with the purpose to increase the S/N ratio of the GW signal to the photon counting noise.

With reference to fig. 3.1 the power of the recombined beams is

$$W_{\pm} = R^{4N}(W/2)[1 \pm \cos(\varphi_{s} + \varphi_{0} + \Delta\phi_{PC})] . \tag{3.4}$$

where R^2 is the intensity reflectivity of the mirrors, $\varphi_0 = \bar{\varphi}_1 - \bar{\varphi}_2$ and $\Delta\phi_{PC}$ has been evaluated for $W_{eff} = WR^{4N}$. Putting $\varphi_0 = \pi/2$, measuring $W_{\pm}$ with photodiodes PD having efficiency η and forming the current difference, we obtain

$$\Delta I^2 \cong I_0^2\{[(4N\pi/\lambda)h(t)L]^2 + \Delta\phi_{PC}^2\} + \Delta I_{SN}^2 , \tag{3.5}$$

where

$$I_0 = (We/h\nu_0)\eta R^{4N} \quad \text{and} \quad \Delta I_{SN} = e\sqrt{(WR^{4N}/th\nu_0)\eta(1-\eta)}$$

are the photodiode mean current and current fluctuation, respectively; e is the electric charge. The GW detection condition, introducing eq. (3.2) in eq. (3.5) and using eq. (3.3), reads

$$h(t) > \frac{\lambda}{4N\pi L}\sqrt{\frac{h\nu_0}{Wt\eta R^{4N}}} . \tag{3.6}$$

where the assumption $2\Omega_g NL/c \ll 1$ has been made. Equation (3.6) shows that $2N$ reflections increase accordingly the S/N ratio for the photon counting noise.

The delay line (DL) scheme was first studied by Herriot et al. [1964]: the laser beam enters the cavity through a hole in the near mirror with coordinate (x_0, y_0) and slope (x'_0, y'_0) (see fig. 3.2) and is reflected back and forth between the mirrors having distance L and focal length f, respectively. Defining

$$\cos\theta = 1 - L/2f, \tag{3.7}$$

where θ is the rotation angle of the beam spot on the mirrors (see fig. 3.3), the coordinates of the nth spot are

$$\begin{aligned} x_n &= x_0 \cos n\theta + \sqrt{\frac{L}{4f - L}}\,(x_0 + 2fx'_0)\sin n\theta, \\ y_n &= y_0 \cos n\theta + \sqrt{\frac{L}{4f - L}}\,(y_0 + 2fy'_0)\sin n\theta, \quad 4f - L > 0. \end{aligned} \tag{3.8}$$

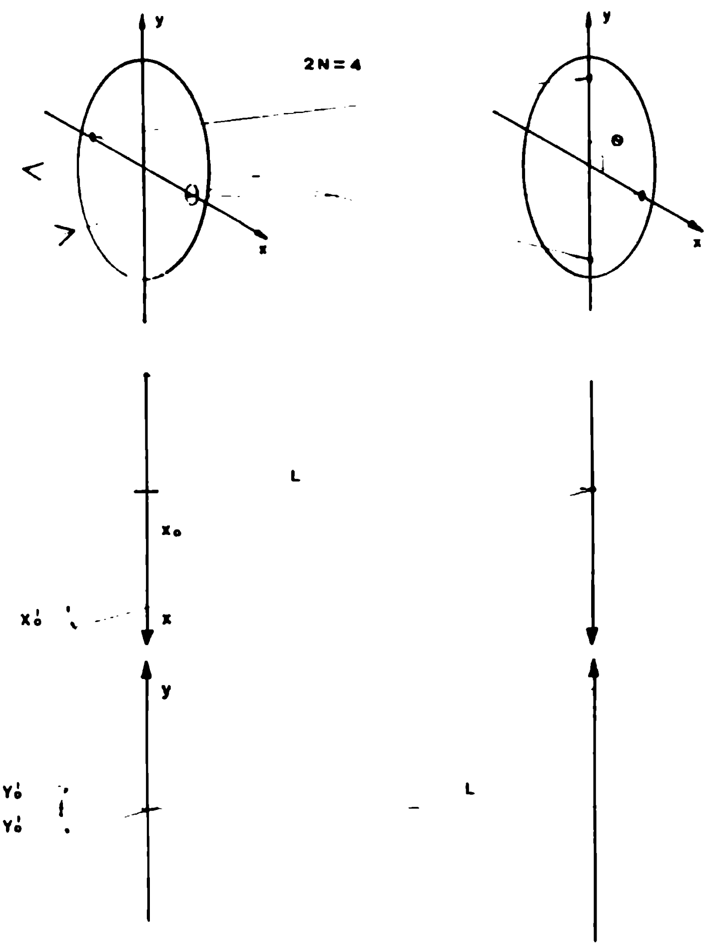

Fig. 3.2 The laser beam enters the DL at position (x_0, y_0) and angle (x'_0, y'_0), then bounces $2N$ times and leaves the cavity through the entrance hole.

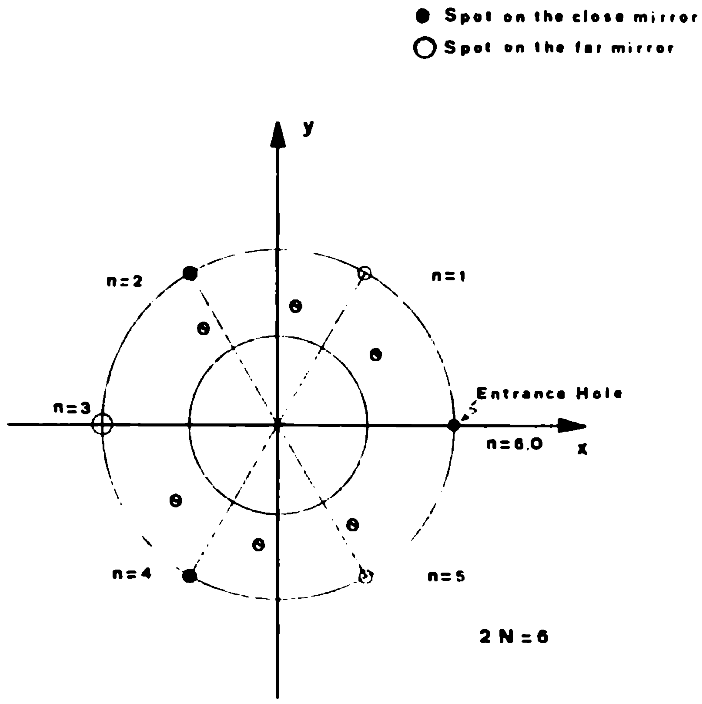

Fig. 3.3. The beam enters the DL at position $n = 0$, is reflected from the far mirror at positions $n = 1, 3, 5$ and from the close one at positions $n = 2, 4$. $2N\theta$ can be larger than 2π.

which can be put in the form

$$x_n = A \sin(n\theta + \alpha)\,, \qquad y_n = B \sin(n\theta + \beta)\,, \tag{3.9}$$

where

$$A^2 = \frac{4f}{4f - L}\,[x_0^2 + L x_0(x_0') + Lf(x_0')^2]\,, \qquad \operatorname{tg}\alpha = \sqrt{\frac{4f}{L} - 1}\;\frac{1}{1 + 2f x_0'/x_0}\,. \tag{3.10}$$

and similarly for B and β. If $A = B$ the spots lie on a circle; the beam reentrance condition is fulfilled when

$$2k\theta = 2J\pi\,, \quad J, k \text{ integers}, \; J \neq k\,, \tag{3.11}$$

k being the number of spots on a single mirror.

The DL is a very flexible method to cope with misalignments due to mirror movements [Goorvitch 1975, Billing et al. 1979]. Fattaccioli et al. [1986] have shown that the total optical phase shift is independent of tilting ($\Delta\vartheta$) and transverse mutual mirror translations (Δx) up to second order in $\Delta x/R$ and $\Delta\vartheta$, respectively, R being the radius of the spot circle on the mirrors, if the DL is perfectly reentrant and aligned.

With the purpose of reducing the light scattering from the entrance hole in the mirrors close to the beam splitter [Schilling et al. 1981], the size of the input beam should be sufficiently reduced increasing the beam angular spread $\Delta x'_0$ and $\Delta y'_0$. The spot diameters due to this spread,

$$\Delta x_n = \sqrt{\frac{L}{4f-L}}\, 2f \sin n\theta\, \Delta x'_0 , \qquad \Delta y_n = \sqrt{\frac{L}{4f-L}}\, 2f \sin n\theta\, \Delta y'_0 , \tag{3.12}$$

do not increase indefinitely with N but vary cyclically with n; this focusing characteristic is very relevant for avoiding beam size divergence when N is large, and a careful evaluation of the beam entrance parameters is needed to avoid geometrical overlapping of the spots. Actually two contiguous spots on a mirror are associated with different delays; if they do overlap the light diffused by the mirror coatings is sent in the wrong beam, causing noise due to the finite size of the laser line width.

The light phase shift due to GW interaction in a DL without the constraint $2\Omega_g NL/c \ll 1$ has been calculated by Vinet [1986] and Vinet et al. [1988].

Let us consider a DL of length L in which the beam is reflected $2N$ times and which has mirrors with amplitude reflectivity iR_1 and iR_2. By repeated application of the operator D [see eq. (2.29)] we obtain the $2N$ reflection operator,

$$iM = (iR_1)^{N-1}(iR_2)^N D^N = (-)^{N-1} R_1^{N-1} R_2^N x^N \begin{pmatrix} 1 & 0 & 0 \\ i\varepsilon\xi \dfrac{\sin \eta N}{\eta}\, e^{-i\eta N} & y^{-N} & 0 \\ i\varepsilon\xi \dfrac{\sin \eta N}{\eta}\, e^{i\eta N} & 0 & y^{N} \end{pmatrix} , \tag{3.13}$$

where the signal is contained in the two matrix elements M_{12} and M_{13}; putting

$$\tau_s = 2NL/c , \tag{3.14}$$

we see that M_{12} and M_{13} are maximum when

$$\eta N = \tfrac{1}{2}\Omega_g \tau_s = \pi/2 , \tag{3.15a}$$

while the signal is zero when

$$\tfrac{1}{2}\tau_s \Omega_g = n\pi \quad (n = 1, 2, \ldots) . \tag{3.15b}$$

From eqs. (2.27) and (3.7) it follows that the maximum phase shift $\Delta\phi_{\rm DL}$ of the light wave due to GW interaction in two DLs (see fig. 3.1) is

$$\Delta\phi_{\rm DL} = 2h\omega \frac{L}{c} \frac{\sin \Omega_g (L/c) N}{\Omega_g L/c} . \tag{3.16}$$

Typical DL schemes are those adopted by Forward [1978] at Malibu with $2N = 4$, MIT with $2N = 56$ and Max-Planck-Institut in Munich with $2N \cong 90$.

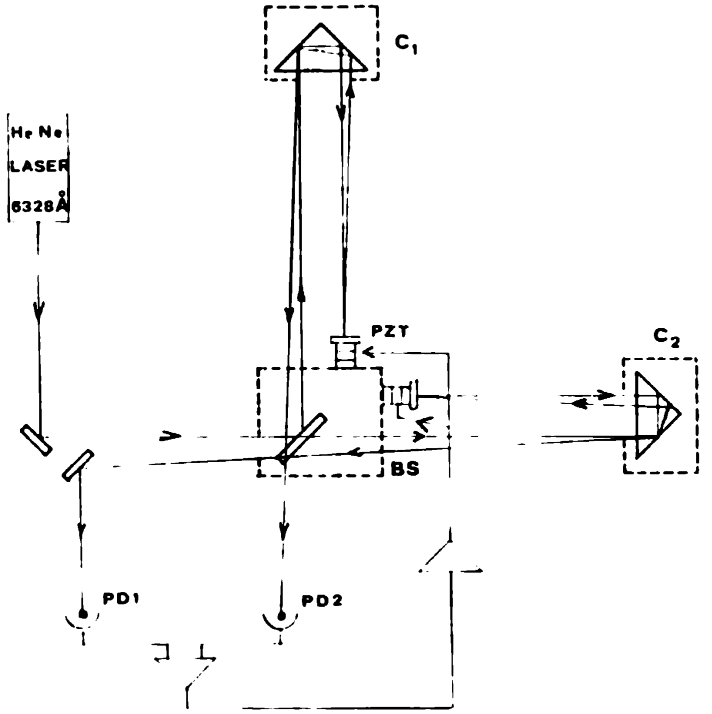

Fig. 3.4. The optical layout of the Malibu interferometer. The beam splitter BS is mounted on the central mass where the piezoelectric transducers PZT, driven by the filtered difference signal of the photodetectors PD1 and PD2, keep the interferometer output locked to null. The retroreflectors C1 and C2 are mounted on the far masses, which are ~2 m away from BS. The detector is lit by a 30–50 mW HeNe laser.

In the Malibu interferometer, the world's first working prototype, the optical system (see fig. 3.4) is composed of a beam splitter and two retroreflectors mounted on the far masses. The optical path is ~8 m and the strain sensitivity is $\tilde{h} \gtrsim 10^{-16}\ \mathrm{Hz}^{-1/2}$ for $\nu \gtrsim 2\ \mathrm{kHz}$.

The MIT interferometer, shown in fig. 3.5, is a system with $2N = 56$ and a mirror separation of 1.46 m. The mass supporting the beam splitter also supports two Pockels cells used both for keeping the interferometer locked to a fringe and for giving phase modulation with the purpose of reducing the laser amplitude noise. The noise due to the laser lateral beam jitter is reduced by transporting the laser light through an optical fiber. The mirror's pendulum oscillations are damped by means of electrostatic dampers [Linsay and Shoemaker 1982]. The strain sensitivity obtained [Livas et al. 1986] is $\tilde{h} \simeq 3 \times 10^{-17}\ \mathrm{Hz}^{-1/2}$.

In the Munich interferometer (see fig. 3.6) the mirror distance can be adjusted between 29 m and 32 m with the purpose of obtaining different numbers of beams. Locking to a fringe is obtained both by using Pockels cells inserted in the DL and a magnet and coil [Billing et al. 1979] damping system on the mirrors; more details about the use of these systems will be given in subsequent sections. The laser is a 5 W argon ion laser stabilized by means of an external reference cavity and by the interferometer itself used as a reference cavity. The laser light is fed to the interferometer by means of an optical fiber. The maximum sensitivity achieved [Shoemaker et al. 1987a] with $2N = 90$ is $\tilde{h} \simeq 8 \times 10^{-20}\ \mathrm{Hz}^{-1/2}$.

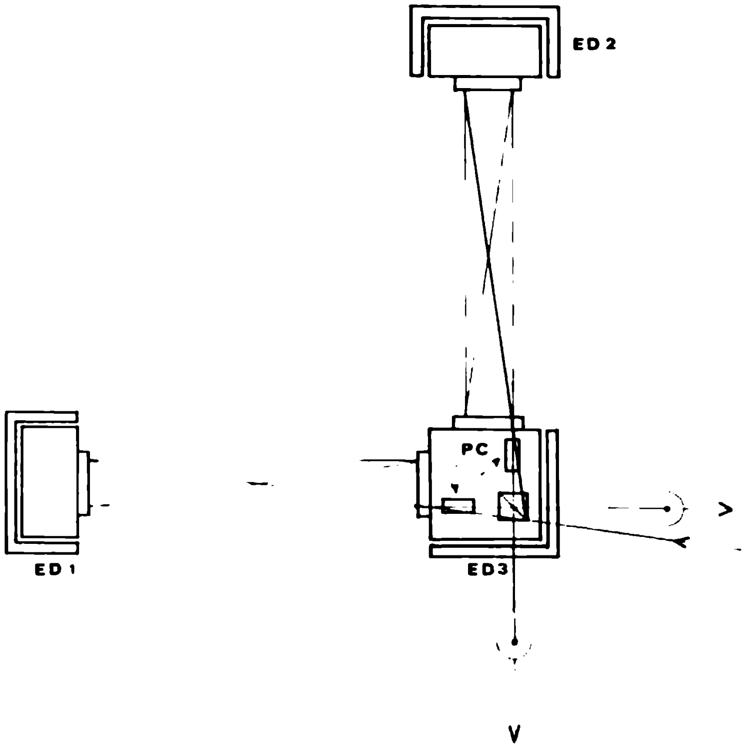

Fig. 3.5. The MIT interferometer, a DL system with 2N = 56 and 1.46 m long arms. The optical phase is locked by means of Pockels cells PC mounted on the beam splitter. An optical fiber is used to feed the laser light and to reduce the laser lateral beam jitter. The pendulum motions of the masses are damped by means of the electrostatic dampers ED.

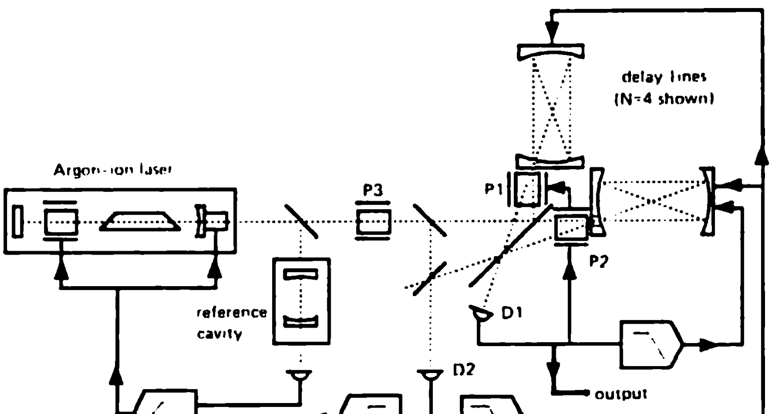

Fig. 3.6. Layout of the Munich interferometer (from Shoemaker et al. [1987a]) showing the laser stabilization scheme. The laser is locked both to the reference cavity and the interferometer itself used as a frequency reference. Locking of the interferometer to a fringe and phase modulation are performed by the Pockels cells P1 and P2. Magnets and coils are used to damp the pendulum oscillations of the mirrors.

4. Fabry–Pérot interferometers

Fabry–Pérot (FP) theory is largely described in many books (see, for example, Born and Wolf [1964], Hernandez [1986]); with reference to fig. 4.1, M_1 and M_2 are two mirrors located at positions x_1 and x_2, respectively ($x_2 - x_1 = L$); the amplitude reflectance iR_i, the transmittance T_i and the loss B_i of the mirrors satisfy the relation

$$T_i^2 + R_i^2 + B_i^2 = 1\,, \quad i = 1, 2\,. \tag{4.1}$$

A light beam of frequency $\nu_0 = \omega_0/2\pi$ entering the cavity with amplitude A_0 is partially transmitted with amplitude A_t and partially reflected with amplitude A_r.

If A_2 and A_3 are the transmitted and reflected amplitudes inside the cavity, then

$$A_r = iR_1A_0 + T_1A_3\,, \qquad A_2 = T_1A_0 + iR_1A_3\,, \qquad A_3 = iR_2DA_2\,, \tag{4.2}$$

where D is defined in eq. (2.29). The solution is

$$A_r = i[R_1 + (R_1^2 + T_1^2)R_2D](1 + R_1R_2D)^{-1}A_0 = iFA_0\,. \tag{4.3}$$

An evaluation of F gives the relevant matrix elements [Vinet 1986],

$$\begin{aligned}
F_{11} &= i\,\frac{R_1 + (R_1^2 + T_1^2)R_2x}{1 - R_1R_2x}\,, \\
F_{21} &= \frac{\varepsilon T_1^2R_2\xi\sin(\eta)/\eta}{1 - R_1R_2x}\,\frac{e^{-i\eta}x}{1 - R_1R_2xy}\,, \\
F_{31} &= \frac{\varepsilon T_1^2R_2\xi\sin(\eta)/\eta}{1 - R_1R_2x}\,\frac{e^{i\eta}x}{1 - R_1R_2xy}\,,
\end{aligned} \tag{4.4}$$

where x and y have been defined in eq. (2.29).

From eqs. (2.27) and (4.4) it is possible to evaluate the maximum phase shift $\Delta\phi_{FP}$ for a cavity configuration similar to the one shown in fig. 3.1 under the condition $x = +1$ (optical resonance condition).

$$\Delta\phi_{FP} = 2\,\frac{T_1^2R_2h\omega L/c}{(1 - R_1R_2)^2}\,\frac{1}{\sqrt{1 + F'\sin^2\Omega_g L/c}}\,. \tag{4.5}$$

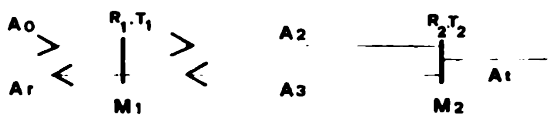

Fig. 4.1. Schematic diagram of the light field amplitudes inside a cavity, composed of the mirrors M_1 and M_2 having reflectivity iR_1 and iR_2 and transmittance T_1 and T_2, respectively. The amplitude A_3 is connected to A_2 through the operator defined in eq. (2.29) containing the effect due to the GW interaction.

where $F' = 4R_1R_2/(1-R_1R_2)^2$, $T_2 \ll T_1$ and the realistic condition $\Omega_g L/c \ll 1$ has been assumed. In analogy to eq. (3.8), defining the cavity storage time

$$\tau_s = 2\frac{L}{c}\frac{\sqrt{R_1R_2}}{1-R_1R_2}, \tag{4.6}$$

making the approximation $R_i \simeq 1-\frac{1}{2}(T_i^2+B_i^2)$ and putting $B_i \ll T_i$ we finally obtain

$$|\Delta\phi_{FP}| \simeq \omega h \tau_s \frac{2T_1^2}{T_1^2+T_2^2}\sqrt{\frac{R_2}{R_1}}\frac{1}{\sqrt{1+\Omega_g^2\tau_s^2}}. \tag{4.7}$$

The comparison between $|\Delta\phi_{DL}|$ and $|\Delta\phi_{FP}|$ is shown in fig. 4.2; $|\Delta\phi_{FP}|$ is plotted for $T_2 \ll T_1$: this experimental condition is particularly useful in interferometers using light recycling because very little power flows out of the far mirror.

Effects due to misalignment of the FP cavity have been evaluated by Fattaccioli et al. [1986].

Typical FP prototype interferometers are in Glasgow and at CALTECH. The Glasgow interferometer [Ward et al. 1987] (see fig. 4.3) is composed of two 10 m long cavities. The laser is frequency locked to one of the cavities; this is achieved by adjusting the laser frequency by means of a piezoelectrically driven mirror and an intracavity Pockels cell. The length of the second cavity is then adjusted by means of forces produced by magnets connected to the mirrors pushed by electrical coils, and maintained in resonance with the first one by means of a servo loop. The GW signal is obtained from the electronically recombined arm beams. With 30 mW light power the strain sensitivity [Ward et al. 1987] was $1.2\times10^{-19}\ \mathrm{Hz}^{-1/2}$ for frequencies greater than 1500 Hz.

The CALTECH interferometer [Spero 1986] has two 40 m long cavities; one of them is used to frequency stabilize the laser by means of an intracavity Pockels cell and the other cavity is kept in

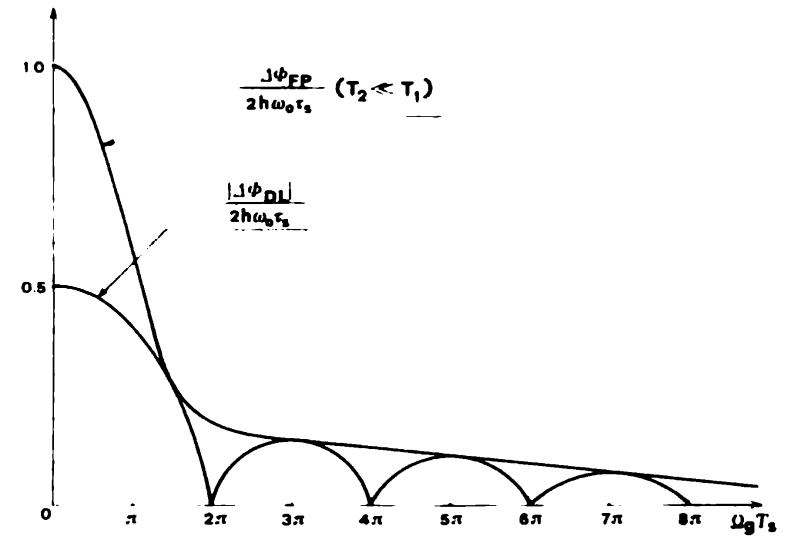

Fig. 4.2. Comparison between the phase shift due to the GW amplitude h of a FP ($T_2 \ll T_1$) and a DL interferometer having the same storage time τ_s. When $\Omega_g\tau_s \gg 1$ the phase shifts are comparable, as is shown by eqs. (4.7) and (3.16).

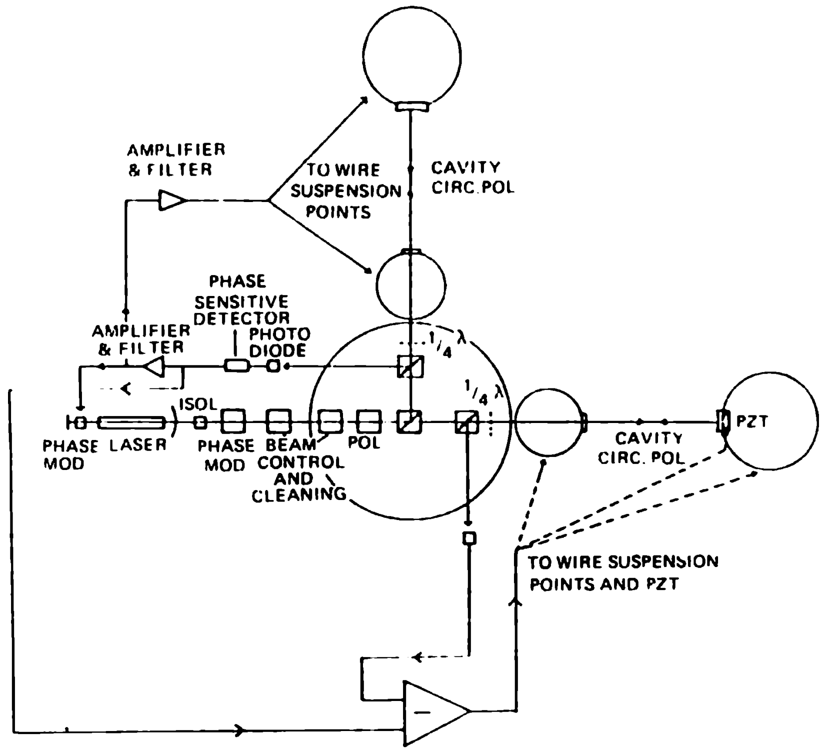

Fig. 4.3. The Glasgow interferometer (from Newton et al. [1986]). One of the two 10 m FP cavities is used for stabilizing the laser; the other is, via a feedback system, kept in resonance with the laser frequency. The GW signal is contained in the feedback signal.

resonance with the first one by means of forces applied to the mirrors. The strain sensitivity with a light power of 2 mW was $\tilde{h} \cong 5 \times 10^{-19}\ \mathrm{Hz}^{-1/2}$ [Spero 1986].

Optical recombination of the two beams has been achieved in Orsay by Man et al. [1986] with a phase sensitivity of $1.5 \times 10^{-8}\ \mathrm{rad\ Hz}^{-1/2}$.

5. The noise due to photon counting errors and recycling

In section 3 we have shown how the phase fluctuations in the two interferometer arms produce noise: in particular the fluctuations of the photodiode currents [see eq. (3.5)] ΔI_{SN} have been considered as a source of photon counting errors. But also if $\Delta I_{SN} = 0$ ($\eta = 1$) the interferometer's output current still fluctuates. To explain this fact it was necessary to make an accurate analysis of the photon beam–beam splitter interaction.

Two approaches lead to the same result: in the first [Edelstein et al. 1978] the beam splitter is shown to create two anticorrelated photon beams having n_1 and n_2 photons each, in such a way that the difference of the photon number fluctuations Δn_1 and Δn_2 in the two beams does not cancel even when $\bar{n}_1 = \bar{n}_2$. In the second approach [Caves 1980] the zero point vacuum fluctuations of the photon field entering from the open beam splitter port (see fig. 5.1) produce anticorrelated photon number fluctuations in the interferometer arms.

The rms fluctuations $\Delta n_i^2 = n_i$ produce both phase noise $\Delta\phi_{PC} \simeq 1/\sqrt{n}$, where $n = n_1 + n_2$, and a

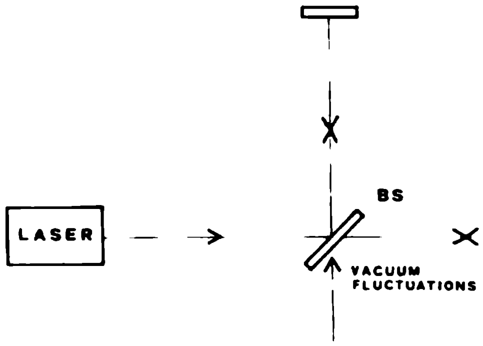

Fig. 5.1. The light field vacuum fluctuations entering the unused port of the beam splitter BS produce the anticorrelated intensity fluctuations in the interferometer arms.

fluctuation in the differential radiation pressure on the interferometer's mirrors, which produces the differential momentum $\Delta P = \sqrt{\bar{n}}\,(h\nu_0/c)\,2N$.

The equivalent displacement noise producing the phase shift $\Delta\phi_{pc}$ is $\Delta x_{pc} = (\Delta\phi_{pc}/2N)\lambda/4\pi$; hence in the measurement time t the total displacement $\sqrt{\Delta x_{pc}^2 + (\Delta P\, t/2M)^2}$ is minimum when

$$W = (4N^2)^{-1} Mc^2/\omega t^2 \tag{5.1}$$

The existence of this optimal laser power relies on the fact that the photon number fluctuations are anticorrelated in the two interferometer arms. The minimum displacement is

$$\Delta x_{\min} = \sqrt{\hbar\, 4\pi t/M}\,. \tag{5.2}$$

which is very close to the standard quantum limit for the accuracy with which the displacement of a mass M can be measured in a time t.

As we have seen in section 3, in a multireflection interferometer the h sensitivity, with respect to the photon counting error, increases with the number of reflections, with the arm length and with the effective detected power. Using eqs. (3.2) and (3.16) we see that the best sensitivity in h for a DL system is obtained when $\tau_s = \frac{1}{2}T_g$.

$$h_{\min} = \frac{1}{2\nu_0 T_g}\sqrt{\frac{h\nu_0}{\eta W T_g R^{1/2}}}\,. \tag{5.3}$$

where T_g is the GW pulse length.

If the GW is periodic the sensitivity increases with the square root of the number of cycles observed. If $\frac{1}{2}\Omega_g \tau_s \ll 1$, eq. (5.3) becomes

$$h_{\min} > \frac{1}{\omega\tau_s}\sqrt{\frac{h\nu_0}{\eta W t R^{1/2}}}\,. \tag{5.4}$$

Analogously for a FP system, from eqs. (3.2) and (4.7) we obtain

$$h_{\mathrm{FP}} > \frac{1}{\omega} \frac{T_1^2 + T_2^2}{2T_1^2} \sqrt{\frac{R_1}{R_2}} \frac{\sqrt{1 + \Omega_g^2 \tau_s^2}}{\tau_s} \sqrt{\frac{h\nu_0}{\eta W t}} .$$

For $T_2 \ll T_1$, $(R_1/R_2)^{1/2} \cong 1$, and $\Omega_g \tau_s > 1$, eq. (5.5) becomes

$$h_{\mathrm{FP}} > \frac{1}{2\nu_0 T_g} \sqrt{\frac{h\nu_0}{\eta W T_g}} \cong h_{\mathrm{DL}} . \tag{5.6}$$

The difference between eqs. (5.3) and (5.6) lies in the fact that for the FP case, unlike the DL case, the maximum sensitivity is obtained for any $\tau_s > 1/\Omega_g$. If $\Omega_g \tau_s < 1$, eq. (5.5) becomes

$$h_{\mathrm{FP}} > \frac{1}{2\omega\tau_s} \sqrt{\frac{h\nu_0}{\eta W T}} \cong \tfrac{1}{2} h_{\mathrm{DL}} . \tag{5.7}$$

It has also been shown [Edelstein et al. 1978] that maximum sensitivity occurs when the signal is taken from one of the photodiodes with the illuminating beam brought to extinction. The argument runs as follows. Equation (3.4) gives the current

$$I = \tfrac{1}{2} I_0 [1 - \cos(\varphi_0 + \varphi_s)] , \tag{5.8}$$

the current ΔI_s due to the signal being

$$\Delta I_s \cong \tfrac{1}{2} I_0 (\sin \varphi_0) \varphi_s .$$

The current fluctuations are the sum of the Poissonian beam fluctuations and the statistical fluctuations due to the diode detection inefficiency $1 - \eta$ [see eq. (3.5)], i.e.,

$$\Delta I^2 = e[\eta I_0 (1 - \cos\varphi_0)/2t + (1 - \eta) I_0 (1 - \cos\varphi_0)/2t] = e \frac{I_0(1 - \cos\varphi_0)}{2t} , \tag{5.9}$$

where t is the measurement time. The measurability condition for φ_s reads $\Delta I_s^2 \geq \Delta I^2$, hence

$$h > \frac{\lambda}{4N\pi L} \sqrt{\frac{h\nu_0}{\cos^2(\frac{1}{2}\varphi_0) W R^{4N} \eta t}} , \tag{5.10}$$

which is minimum for $\varphi_0 = 0$ [see eq. (3.6)], i.e. when the beam is extinguished.

From this condition, using eq. (3.4), putting $\bar{\varphi}_1 - \bar{\varphi}_2 = \varphi_0 \ll 1$ and with $\varphi_s = (4N\pi/\lambda) h(t) L \ll 1$, it follows that the two light beams have the intensities

$$W_{\pm} \cong \tfrac{1}{2} R^{4N} W [1 \pm (\cos\varphi_0 - \varphi_s \sin\varphi_0)] , \tag{5.11}$$

where we have chosen the relative fixed phase in such a way as to have $W_+ = R^{4N} W$ going toward the laser. This light can be recycled [Drever 1982] according to the scheme of fig. 5.2. In this arrangement the beam W_+ is recycled by means of the mirrors BSR and MR. The position of the latter, and hence the phase shift, is changed by the transducer PZT driven by the PD2 signal.

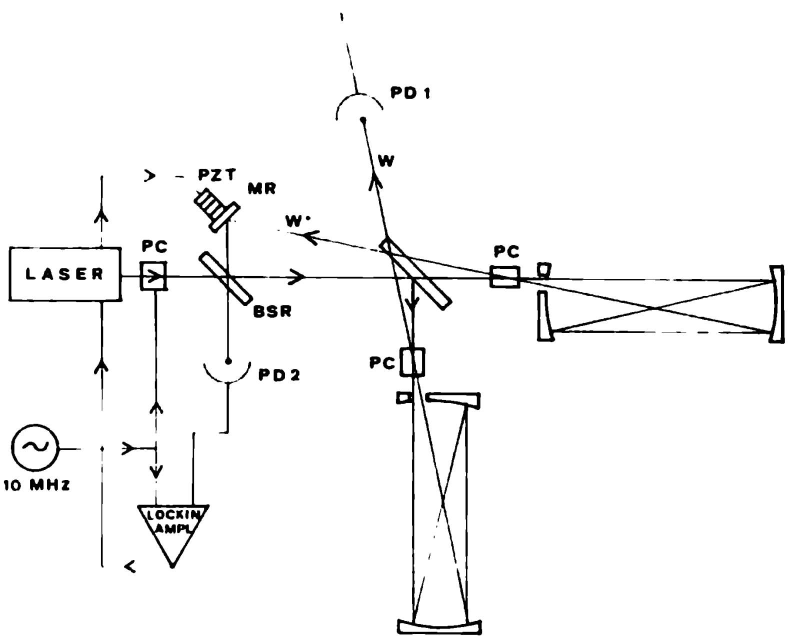

Fig. 5.2. The beam W* can be brought to extinction by means of the Pockels cells PC; then W is maximum and can be reused when MR gives the right phase shift. This is obtained by displacing MR by means of the piezoelectric transducer PZT driven by the signal of PD2.

To evaluate the power increase due to recycling in a DL, let us consider that the typical energy loss per cycle is

$$\Delta W = (1 - R^{4N})W . \tag{5.12}$$

The maximum sensitivity in a DL system occurs for $\tau_s = 1/(2\nu_g)$ and since

$$R^{4N} \cong 1 - 2(\pi c/L\Omega_g)(1 - R^2)/2 , \tag{5.13}$$

it follows that

$$W_R = WL\Omega_g/\pi c(1 - R^2) . \tag{5.14}$$

Hence, from eq. (5.13) it follows that the overall power gain is a function of Ω_g and the sensitivity in h [see eq. (5.3)] becomes

$$(h_{\min})_R = \sqrt{\frac{(1 - R^2)\pi c}{L\Omega_g}}\, h_{\min} = \frac{1}{2}\sqrt{\frac{h\lambda\pi(1 - R^2)\nu_g}{R^{4N}\eta WL4\pi T_g}} . \tag{5.15}$$

Let us now evaluate the analog of eq. (5.14) in case of a FP system. The schematic diagram of fig. 5.3 shows that in the FP recycling scheme the recycling mirror MR is positioned directly in the laser beam. The correct phase, obtained by driving the PZT with the signal of the photodiode PD2, gives a minimum signal in PD2. In analogy with the DL system we evaluate the light power lost in the mirror

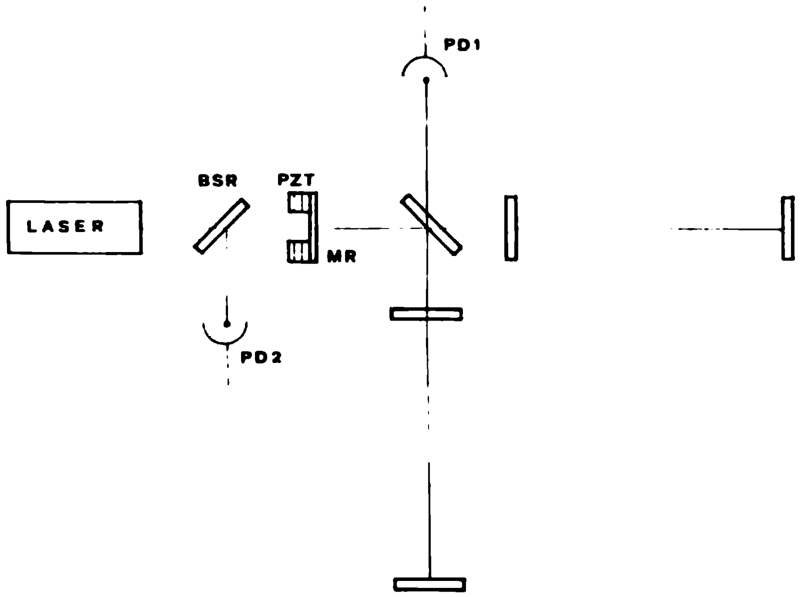

Fig. 5.3. The power recycling scheme for a FP interferometer. In analogy to the scheme of fig. 5.2 the signal of the photodiode PD2 is used to displace the mirror MR in such a way as to have minimum illumination of PD2.

collision; let us suppose that $T_2 \ll T_1$; in this case the reflected amplitude is, at optical resonance,

$$A_r \cong \frac{-R_1 + R_1^2 + T_1^2}{1 - R_1} A_0 \mathrm{i} . \tag{5.16}$$

Using the equation $R_1^2 + T_1^2 + B_1^2 = 1$, it follows that

$$A_r = A_0[1 - B_1^2/(1 - R_1)]\mathrm{i} . \tag{5.17}$$

In a single mirror hit the power loss is

$$\Delta W \cong -W \cdot 2B_1^2/(1 - R_1) . \tag{5.18}$$

Hence, if we attribute the whole loss to the near mirror, the power enhancement due to recycling should be

$$W_R \cong W(1 - R_1)/2B_1^2 . \tag{5.19}$$

Since the storage time in the cavities should be comparable to the recycling time and because it is convenient to have $\Omega_g \tau_s = 1$, it follows that

$$\tau_s = \frac{2L}{c} \frac{\sqrt{R_2 R_1}}{1 - R_1 R_2} = \frac{1}{\Omega_g} . \tag{5.20}$$

Since, for the sake of simplicity, we have put $R_2 = 1$, then

$$1 - R_1 \cong 2L\Omega_g/c . \tag{5.21}$$

This gives

$$W_R = WL\Omega_g/cB_1^2 , \qquad (h_{1p})_R \cong h_{1p}(B_1^2 c/L\Omega_g)^{1/2} . \tag{5.22}$$

Experimental results on power recycling have been obtained by Rüdiger et al. [1987] using a simple 0.3 m arm DL interferometer having $2N = 2$. A recycling factor of up to 15 was obtained with a total power of 2 W.

Similar results were obtained in Orsay (Man et al. [1987]). It was shown that the recycling factor was limited by the loss in the Pockels cells situated in the arms of the interferometer. Better results were obtained later using the external modulation technique (see below).

It has been pointed out [Ruggiero 1979, Drever 1981] that it is possible to increase the signal phase shift by allowing the photons to go synchronously with a periodical GW from one cavity to the other, when the cavities have $\tau_s = \pi(2n + 1)/\Omega_g$ (n integer). This method is called synchronous recycling (SR). The laser beam (see fig. 5.4) is split by the mirror M_0 and the light enters the two DLs from M_1; in M_2

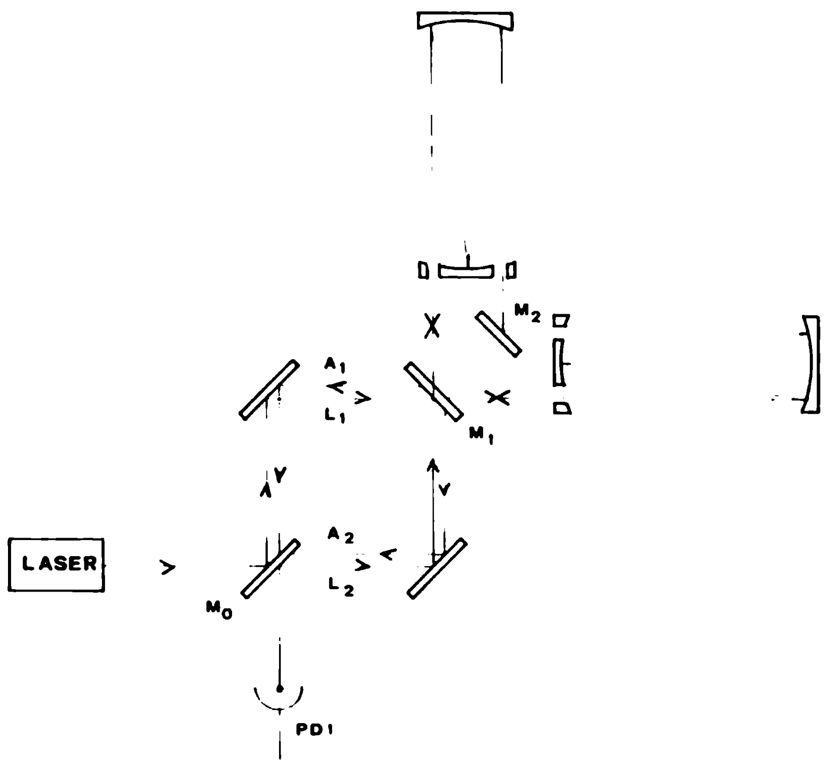

Fig. 5.4. Scheme of synchronous recycling for a DL interferometer. The laser beam enters the beam splitter M_0 and is switched, synchronously with the GW period, from one DL to the other. The photons can increase the phase shift due to the GW according to the number of switchings depending on the optical losses.

the light is switched from one DL to the other; M_2 is connected to M_1. The two beams entering the DL experience opposite phase shifts due to the GW; they then come out after having interfered on M_0 (beams A_1 and A_2) and are finally recombined by M_1 and observed by the photodiode PD1.

The reflected amplitude is easily evaluated considering the ensemble of the two cavities and of the mirrors M_0, M_3 as a generalized reflector [Vinet 1986, Vinet et al. 1988]. If the two cavities have transfer matrices G and G', then the equations for the reflected amplitude, according to fig. 5.5, are

$$A_r = ir_1 A_0 + t_1 A_2 , \qquad A_1 = t_1 A_0 + ir_1 A_2 , \qquad A_2 = iZr_2 GG'A_1 , \tag{5.23}$$

where $Z = \exp(i\omega_0 \sum_{i=1}^{4} l_i/c)$, G, G' are the DL matrices of eq. (3.13) and iR_i and t_i ($i = 1,2$) are the reflectivity and transmittance of mirrors M_1 and M_2.

From eq. (5.23) we can obtain the generalized reflectance,

$$S = (r_1 + \sigma_1 r_2 GG'Z)(1 + r_1 r_2 GG'Z)^{-1} , \quad \sigma_i = r_i^2 + t_i^2 . \tag{5.24}$$

The relevant matrix elements are S_{11},S_{21}, S_{31}, but to evaluate the effect of the resonance we can consider S_{21},

$$S_{21} = -2t_1^2 r_2 Z\xi \frac{\sin^2(N\eta)}{\eta} \overline{y^N} b^2 (1 - r_1 r_2 Z b^2)^{-1} (1 - r_1 r_2 Z b^2 \overline{y^{2N}})^{-1} , \tag{5.25}$$

where $b = (-r)^{N-1} \rho^N x^N$, $y = \exp(i\Omega_g L/c)$. r and ρ are the reflectivities of the near and far DL mirrors, respectively.

Making $Z = +1$ and $x^N = 1$ we meet the resonant condition for the ring cavity; from eq. (5.25) it is evident that due to the synchronous recycling, the amplitude goes to zero when $\Omega_g \to 0$. A resonance occurs when $\bar{y}^{2N} = 1$, i.e., $\nu_g = \bar{\nu}_g = c/LN$. Putting $\nu_g = \bar{\nu}_g + \Delta\nu_g$, eq. (5.25) becomes

$$S_{21} \cong (-1)^{n-1} \frac{t_1^2 \omega \tau^{+}}{1 - r_1 r_2 b^2} \frac{1}{\pi r_1} \frac{1}{(1 + i\,\Delta\nu_g \tau^* 2\pi)} . \tag{5.26}$$

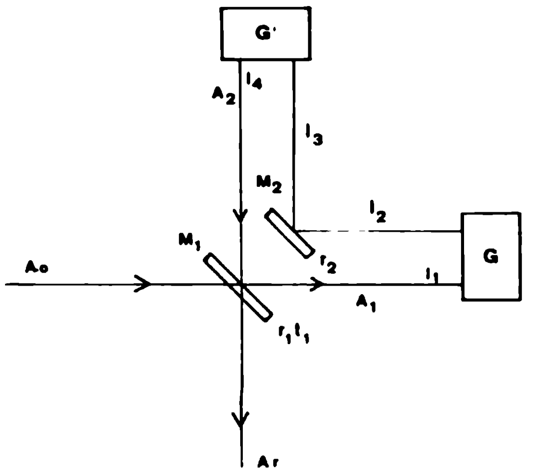

Fig. 5.5. The synchronous recycling scheme considered as a generalized reflector. A_0 and A_r are the incident and the reflected fields, respectively.

where $\tau^* = \tau_s r_1 r_2 b^2/(1 - r_1 r_2 b^2)$ is the recycling storage time. Since the resonance condition is satisfied for $\nu_g = c/4LN = \Delta\nu_0$, where $\Delta\nu_0$ is the cavity free spectral range, S_{21} is at resonance too.

As an example we may evaluate the difference between a normal DL and a SR DL, both fulfilling the condition $\nu_g = 1/(2\tau_s)$ as a function of $\Delta\nu_g/\nu_g$. From eq. (3.7) the matrix element D_{21} in the limit $\Omega_g L/c \ll 1$ becomes

$$|D_{21}| \simeq \omega/\Omega_g \tag{5.27}$$

Similarly we obtain for S_{21}

$$|S_{21}| = \frac{\omega}{\Omega_g}\,\frac{t_1^2 B}{\pi r_1(1-B)^2}\left|1 + \left(\frac{\Delta\nu_g}{\nu_g}\,\frac{2\pi B}{1-B}\right)^2\right|^{-1/2}, \quad B = r_1 r_2 b^2 . \tag{5.28}$$

Equation (5.28) is valid under the condition $|\Delta\nu_g| < 1/(4\pi\tau_s)$ or $|\Delta\nu_g/\nu_g| < 1/(2\pi)$.

In fig. 5.6 $|D_{21}|\Omega_g/\omega$ and $|S_{21}|\Omega_g/\omega$ are plotted as functions of $\Delta\nu_g/\nu_g$ for $t_1^2 = 10^{-2}$ and $B = 0.99$. The maximum of $|S_{21}|\Omega_g/\omega$, having the value $t_1^2 B/[\pi r_1(1-B)^2] = 30$, has to be compared with $|D_{21}|\Omega_g/\omega = 1$: at this gain increase one has the reduced band width (HWHM)

$$\Delta\nu_g \simeq 2\nu_g\sqrt{3}\,\frac{1-B}{2\pi B} \simeq 5\times 10^{-3}\,\nu_g .$$

The SR for the FP case can be evaluated from eq. (5.23) and eq. (4.3) by putting $G = F$, $r_1 = r_2$, $t_1 = t_2$, $l_1 = l$, and $l_3 = l_1$. The layout, shown in fig. 5.7, corresponds to a system of three coupled FP cavities. If the gravitational frequency is equal to the difference of the symmetric, ν_S, and antisymmetric, ν_A, mode frequencies, when the middle cavity is antiresonant ($Z = -1$), then the GW will be able

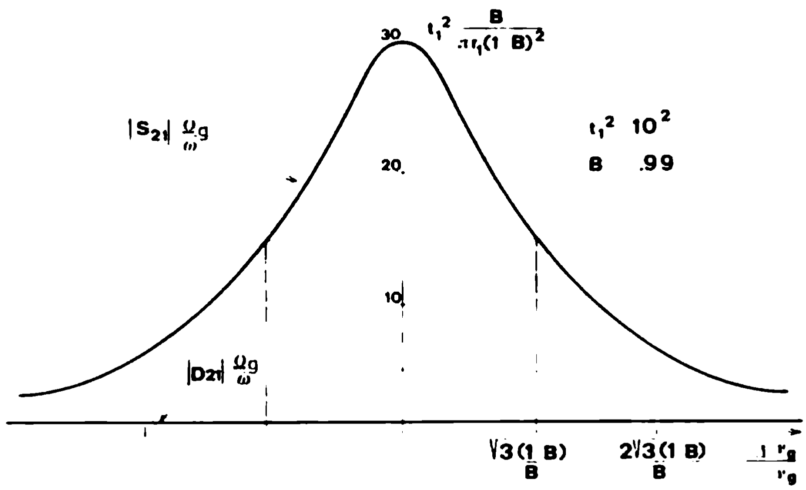

Fig. 5.6. Comparison of the side band amplitude D_{21} of a normal DL interferometer to that of a synchronous recycling DL interferometer, S_{21}. If the intensity transmittance $t_1^2 = 10^{-2}$ and the overall reflectance $B = 0.99$, then at resonance the sensitivity gain with respect to a normal DL is $\simeq 30$.

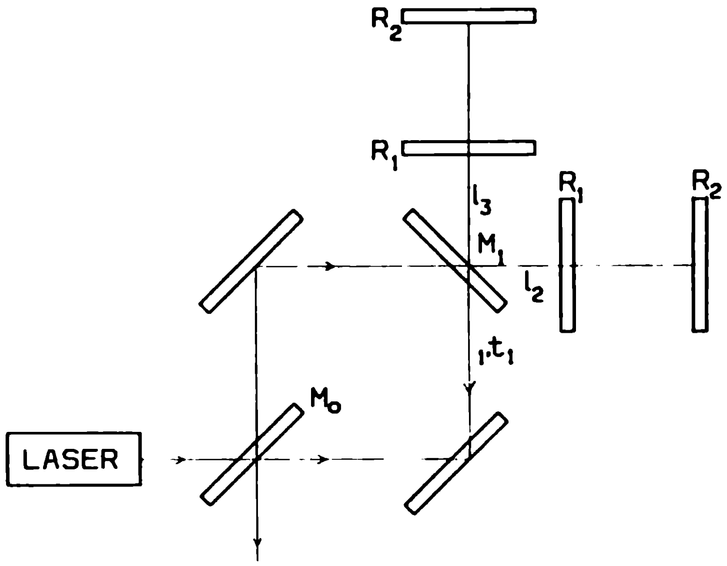

Fig. 5.7. The synchronous recycling scheme for a FP interferometer. If the GW frequency ν_g is equal to the difference of the symmetric and antisymmetric mode frequencies when the middle cavity is antiresonant, then the GW may transfer energy from one mode to the other if $\nu_g = 1/(\pi\tau_s)$.

to transfer energy from one mode to the other if $\nu_g = 1/(\pi\tau_s)$, i.e.,

$$\nu_A - \nu_S = \nu_g = 1/(\pi\tau_s) ,$$

where τ_s is defined in eq. (4.6).

The matrix element S_{31} [see eqs. (5.24), (4.4) and (2.29)] is

$$S_{31} = -2t_1^2 r_1 T_1^2 R_2^2 \xi \,\frac{\sin^2(\Omega_g L/c)}{\Omega_g L/c}\, \frac{x^2 y Z}{P(\omega)P(\omega + \Omega_g)} . \tag{5.29}$$

$$P(\omega) = (1 + R_1 R_2 e^{2i\omega L/c})^2 + r_1^2 Z[R_1 + (R_1^2 + T_1^2) R_2 e^{2i\omega L/c}]^2 . \tag{5.30}$$

Let us assume an antiresonant ($Z = -1$) middle cavity; if $T_1^2 \ll R_1^2$ a maximum of $|S_{31}|$ is obtained when

$$\omega = \frac{c}{L}\,(2n + 1)\,\frac{\pi}{2} - \frac{\Omega_g}{2} \quad n \text{ integer}, \qquad \Omega_g = \frac{c}{L}\,\frac{1 - R_1 R_2}{\sqrt{R_1 R_2}} = \frac{2}{\tau_s} . \tag{5.31}$$

Due to eq. (5.29) only one of the two sidebands S_{31} and S_{21} can be made to resonate [S_{21} would require $\omega = (2n + 1)\frac{1}{2}\pi c/L + \Omega_g/2$] and this gives a S/N ratio $\sqrt{2}$ worse than in the SR for the DL case. In an analogous way to eq. (5.26) we obtain

$$S_{31} \cong \frac{t_1^2 \omega \tilde{\tau}}{1 + r_1^2 a_0}\,\frac{1}{2r_1}\,\frac{1}{1 + 2i\pi(\Delta\nu_g)\tilde{\tau}} , \tag{5.32}$$

where

$$\Delta\nu_g = \nu_g - 1/(\pi\tau_s)\,, \qquad a_0 = [R_1 - (R_1^2 + T_1^2)R_2]/(1 - R_1R_2) \simeq -1\,,$$

$$\tilde{\tau} = 2r_1^2|a_0|\tau_s/(1 + r_1r_2a_0)$$

is the recycling time. A comparison of $|S_{31}|\Omega_g/\omega$ and $|F_{31}|\Omega_g/\omega$ [see eq. (4.4)] as a function of $\Delta\nu_g/\nu_g$ under the conditions $T_1 \gg T_2$ and $\Omega_g = 2/\tau_s$ assuming $t_1^2 = 10^{-2}$ and $r_1^2a_0 = -0.99$, is shown in fig. 5.8.

Non-resonant recycling can be also performed with a detuned FP cavity [Vinet et al. 1988] with the purpose of increasing the cavity reflectivity. If an FP cavity is pumped with the laser frequency equal to the tuned optical frequency plus ν_g, the S/N is slightly worse than in the tuned case but the reflected intensity is closer to the incident one. This allows a larger power recycling rate and a S/N ratio closer to the SR case.

Finally in the dual recycling scheme [Meers 1988] (see fig. 5.9), a simple interferometer composed of a beamsplitter BS and far mirrors M_1, M_2 is brought to both signal and intensity resonance by means of the mirrors M_3 and M_0, respectively. The sensitivity gain is similar to that of SR but the advantage is that, unlike SR, the interferometer arms do not need to be in resonance with the GW before recycling. The tuning of the sideband to the GW frequency is done by moving the mirror M_3; this operation does not change the power stored because the beam on M_3 is at the extinction point but allows the sideband amplitude to build up.

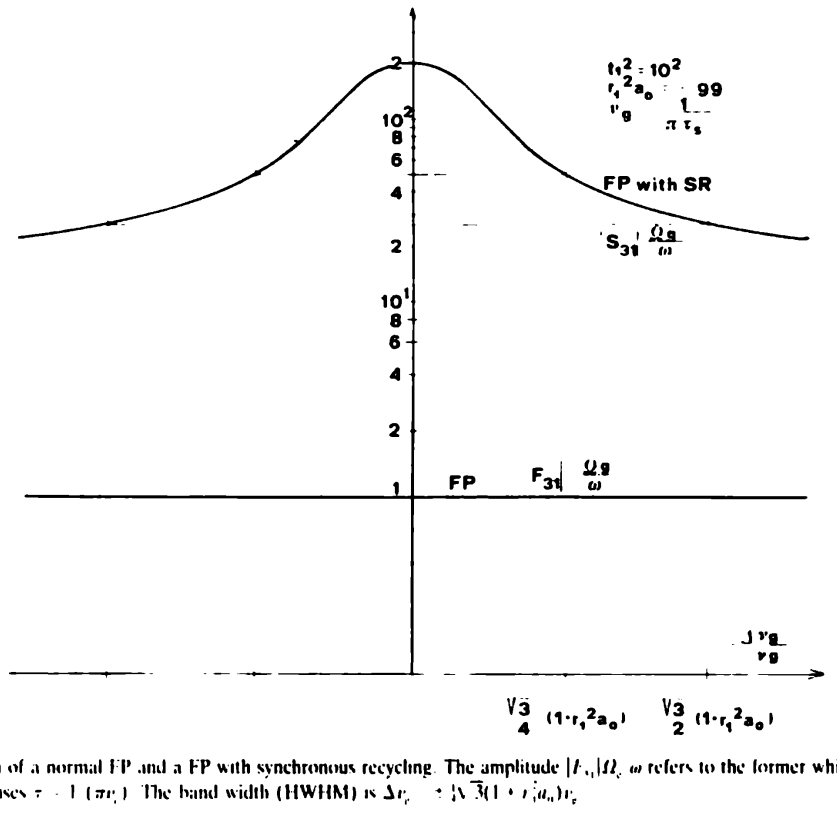

Fig. 5.8. Comparison of a normal FP and a FP with synchronous recycling. The amplitude $|F_{31}|\Omega_g/\omega$ refers to the former while $|S_{31}|\Omega_g/\omega$ refers to the latter. In both cases $\tau = 1/(\pi\nu_g)$. The band width (HWHM) is $\Delta\nu_g = \pm\frac{1}{2}\sqrt{3}(1 + r_1^2a_0)\nu_g$.

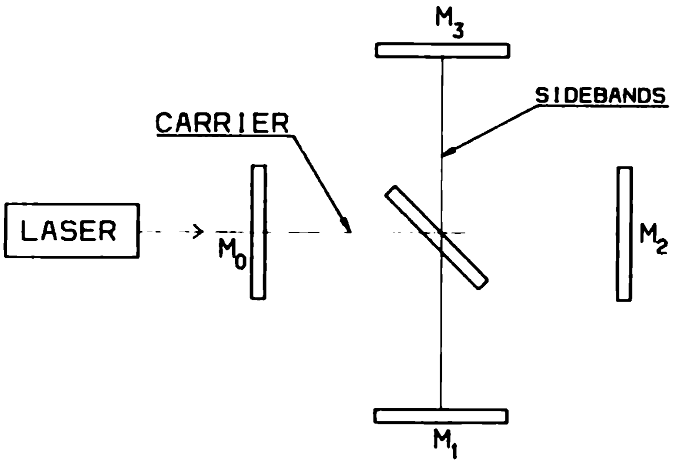

Fig. 5.9. In the dual recycling scheme both carrier and sideband are brought to resonance by moving the mirrors M_0 and M_2, respectively. The S/N ratio is similar to that obtained with synchronous recycling with the advantage that the interferometer storage time before recycling does not need to be comparable with the GW period.

6. Laser intensity noise

The laser power can be represented as

$$W(t) = W_0 + \delta W(t)\,, \tag{6.1}$$

where W_0 is the mean power and $\delta W(t)$ is the instantaneous power fluctuation. The current I_- of eq. (5.8) refers to an ideal case where the optical elements have no losses; in a realistic case we have

$$I_- = e\,\frac{W(t)}{h\nu}\,[A - B\cos(\varphi_0 + \varphi_s)]\,, \qquad I_+ = e\,\frac{W(t)}{h\nu}\,[C + D\cos(\varphi_0 + \varphi_s)]\,, \tag{6.2}$$

where $A \geq B \geq 0$ and $C \geq D \geq 0$ are coefficients close to the detection efficiency η and in general unequal, $\varphi_s = 4N\pi hL/\lambda$ and φ_0 is a given phase.

It is then evident that, since $A \neq B$, then $I_- \neq 0$ when $\varphi_0 = 0$ and this produces the noise

$$\Delta I_- = \delta W(t)\,(A - B)e/h\nu\,.$$

The power spectral noise $\delta W(\omega)/W_0$ typically reaches the shot noise limit $\sqrt{h\nu/W}$ for frequencies larger than $\sim 10^7$ and $\sim 10^5$ Hz for A_r [Winkler 1977, Rüdiger et al. 1981a, b] and Nd:YAG lasers, respectively.

Hence it is possible to modulate at high frequency the relative phase of the interferometer arms [Weiss 1972] by means of Pockels cells, as shown in figs. 3.5 and 3.6, and then synchronously detect the signal. This phase can be represented as

$$\varphi_M = \epsilon_M \sin \omega_M t + \bar{\varphi}_0(t)\,, \tag{6.3}$$

where ε_M and ω_M are the amplitude and frequency of the modulation and $\bar{\varphi}_0(t)$ is a slowly varying phase, with respect to ω_M, determined by the feedback (FB) loop in such a way as to minimize I. Introducing eq. (6.3) in eq. (6.2) and retaining terms up to $\sin(\omega_M t)$ we obtain

$$I = \frac{eW(t)}{h\nu}\left[A - B\cos(\varphi_S + \varphi_0 + \bar{\varphi}_0)\, J_0(\varepsilon_M) - 2B\sin(\varphi_S + \varphi_0 + \bar{\varphi}_0)\, J_1(\varepsilon_M)\sin(\omega_M t)\right]. \tag{6.4}$$

where J_0 and J_1 are Bessel functions. The synchronous detection gives

$$U = \frac{1}{T}\int_t^{t+T} I(t)\sin(\omega_M t)\,\mathrm{d}t$$

$$= \frac{eW_0}{h\nu}\left\{\left[A - B\cos(\varphi_S + \varphi_0 + \bar{\varphi}_0)\, J_0(\varepsilon_M)\right]\frac{\delta W(\omega_M)}{W_0} - B\sin(\varphi_S + \varphi_0 + \bar{\varphi}_0)\, J_1(\varepsilon_M)\right\}. \tag{6.5}$$

where $\delta W(\omega_M)$ is the spectral density of the laser power noise evaluated at the frequency $\omega_M/2\pi$ and the integration time satisfies the inequality $2\pi/\omega_M \ll T \ll 1/\nu_g$.

It is possible to drive the Pockels cells with the low pass filtered signal U with the purpose of keeping

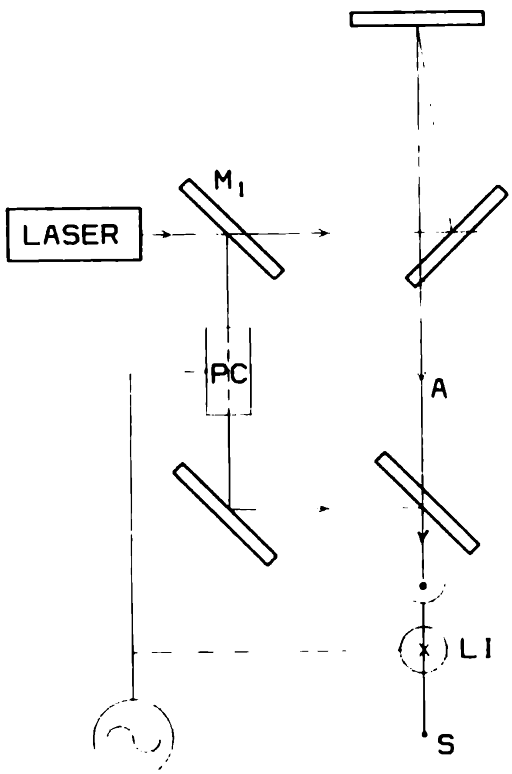

Fig. 6.1. The external modulation scheme: a small fraction of the incident power is sent through the Pockels cell PC to interfere with the outgoing amplitude A containing the GW signal. The PC is modulated at a frequency where the laser amplitude noise reaches the shot noise. Synchronous detection gives the signal S.

I close to extinction, hence minimizing the photon counting noise; in the limit of very large loop gain this gives $\bar{\varphi}_0 = -\varphi_0$. From this condition and from eqs. (6.4) and (6.5) it follows that the currents due to the signal (U_S) and to the noise (U_N) are

$$
\begin{aligned}
U_S &\cong \frac{eW_0}{h\nu} B\varphi_S J_1(\varepsilon_M)\,, \\
U_N &= \left| \left(\frac{eW_0}{h\nu} |A - BJ_0(\varepsilon_M)| \frac{\delta W(\omega_M)}{W_0} \right)^2 + \frac{e^2 W_0}{h\nu} |A - BJ_0(\varepsilon_M)| \right|^{1/2}
\end{aligned}
\tag{6.6}
$$

The last term on the r.h.s. of U_N is due to the photon counting noise. The best value of ε_M maximizes the S/N ratio, or equivalently the quantity $J_1(\varepsilon_M)/U_N$ [Shoemaker et al. 1987a].

It should be emphasized that in FP interferometers laser frequency fluctuations with respect to the cavity resonance frequency induce intensity fluctuations due to the narrow resonance width, and hence low frequency noise in the mirrors. To overcome this effect a precise locking of the interferometer to the laser frequency is needed.

In a large kilometric interferometer the beam size will be of the order of 10^{-1} m with the purpose of minimizing the size on the far mirror; this implies the use of Pockels cells having large aperture, impractical for being carried by the test masses. This requirement can be circumvented using an external modulation scheme, shown in fig. 6.1, in which a small fraction of the incident light is sent through a Pockels cell to interfere with the beam containing the GW signal. The Pockels cell is modulated at a frequency where the laser amplitude noise has reached the shot noise; the signal is obtained by making synchronous detection with the modulation signal. In this scheme the noise is $\simeq\sqrt{2}$ times higher [Man 1988, Paris, Orsay, Pisa, Napoli, Frascati Collab. 1988] than in the internal modulation one, but the external modulation has the advantage of bringing a net sensitivity improvement because it enhances the recycling factor.

7. The noise due to the laser linewidth

Laser frequency fluctuations produce phase noise in an interferometer with arms having unequal length. If ν_0 and $\Delta\nu$ are the laser mean frequency and the r.m.s. frequency fluctuation, respectively, then the r.m.s. phase fluctuation due to the difference in arm length ΔL is

$$\Delta\varphi \cong 2\pi\, \Delta\nu\, \Delta L/c\,. \tag{7.1}$$

It is then very important to avoid that rays having large ΔL interfere.

In a multipass DL interferometer the light hitting the mirrors is scattered by the reflecting coating and enters the optical path of one of the other DL beams. This phenomenon, even if the scattered beam intensity is of the order of $\varepsilon \cong 10^{-4}$–$10^{-5}$ of the incident one, may create a large background because the interference of the scattered beam with the main one has an amplitude proportional to $\sqrt{\varepsilon}$.

Different methods have been adopted to get rid of this phenomenon [Schilling et al. 1981, Schnupp et al. 1985]; one method [Rüdiger et al. 1981a, b] consists in "whitening" the laser light spectrum in such a way that rays having a different path length create a phase shift having an r.m.s. value equal to zero.

A more precise evaluation of this noise can be made supposing that the laser frequency fluctuations can be taken into account by means of a random phase $\phi_R(t)$ introduced into the wave function representing a monochromatic wave, i.e.,

$$\psi = A_0 \exp[i\omega t + i\phi_R(t)] , \tag{7.2}$$

where ϕ_R satisfies the correlation relation

$$\langle \dot{\phi}_R(t)\dot{\phi}_R(t')\rangle = (2\pi)^2 \Delta\nu^2 g(t-t') , \tag{7.3}$$

and $g(0) = 1$.

If the wave ψ is split by the beam splitter and then brought to interference after reflection on the far mirrors (at a distance L and $L + \Delta L$, respectively), the intensity of the interference will be

$$I \propto \sin^2[\phi_R(t - L/c) - \phi_R(t - (L + \Delta L)/c) + 2\phi_g(t)] , \quad \phi_g(t) = h\omega \frac{L}{c} \frac{\sin \Omega_g(L/c)N}{\Omega_g L/c} e^{i\Omega_g t} , \tag{7.4}$$

where ϕ_g [see eq. (3.10)] is the phase shift produced in the DL interferometer by the GW assumed to be periodical. Since $\Delta L/c \ll 1/\Delta\nu$ it follows that we can expand ϕ_R in a Taylor series, obtaining

$$I \propto \sin^2[\dot{\phi}_R(t)\,\Delta L/c + 2\phi_g(t)] . \tag{7.5}$$

We can now evaluate the noise Fourier spectrum,

$$|\phi_N(\Omega)|^2 = \left|\frac{\Delta L}{c}\int_0^T \dot{\phi}_R(t)\, e^{i\Omega t}\, dt\right|^2 , \tag{7.6}$$

and compare it with the signal,

$$|\phi_s(\Omega)|^2 = \left|\int_0^T \phi_g(t)\, e^{i\Omega t}\, dt\right|^2 , \tag{7.7}$$

where T is the measurement time. From eqs. (7.3) and (7.6) it follows that

$$|\phi_N(\Omega)|^2 = (\Delta L/c)^2 (2\pi)^2 \Delta\nu^2 \int_0^T\int_0^T g(t-t')\, e^{i\Omega(t-t')}\, dt\, dt' , \tag{7.8}$$

where the measurement time $T \gg 1/\Omega$. Putting $g(z) = \int_{-\infty}^{\infty} Q(\omega)\, e^{-i\omega z}\, d\omega$, eq. (7.8) becomes

$$|\phi_N(\Omega)|^2 = (\Delta L/c)^2 (2\pi)^2 \Delta\nu^2 \int_{-\infty}^{\infty} Q(\omega)\, \frac{4\sin^2(\Omega - \omega)T/2}{(\Omega - \omega)^2}\, d\omega . \tag{7.9}$$

Since the function $\sin^2(xT/2)/x^2$ can be approximated with $\frac{1}{2}T\pi\delta(x)$, we obtain

$$|\phi_N(\Omega)|^2 \cong (\Delta L/c)^2 (2\pi)^2 \Delta\nu^2 \tfrac{1}{2}\pi T Q(\Omega) . \tag{7.10}$$

The quantity $S = 2\pi\sqrt{\tfrac{1}{2}\pi}\, \Delta\nu\, Q^{1/2}$ is measured in $\mathrm{Hz}/\sqrt{\mathrm{Hz}}$ and gives the linear spectral density of the laser frequency fluctuations.

Comparing eq. (7.10) with eq. (7.7) we obtain the measurability condition for h when the DL storage time is optimal [see eq. (3.9)],

$$h(\Omega_g) > \frac{\Delta L\, \Delta\nu}{\omega c}\, \Omega_g \sqrt{\tfrac{1}{2}\pi^3 Q(\Omega_g)/T} . \tag{7.11}$$

Equation (7.10) shows that $S(\Omega)$ can be measured by means of an imbalance of the arm length, ΔL.

The line width can be reduced by means of active systems; one method consists in operating a reference FP cavity [Drever et al. 1983, Hough et al. 1987, Shoemaker et al. 1987a] fed with a small fraction of the laser light phase modulated at the frequency ν_M by means of a Pockels cell (see fig. 3.6). If the laser frequency is tuned to one of the FP resonances the reflected light has the two sidebands at frequency $\pm\nu_M$ having amplitudes of opposite sign, giving zero output in a photodiode. If the laser frequency fluctuates the two sideband amplitudes will not cancel anymore and give a signal in the photodiode, which can be detected synchronously. The signal is proportional to the laser frequency displacement $\Delta\nu$ with respect to the FP resonance frequency. It can be fed to a laser intracavity Pockels cell (for high-frequency FB) and to a PZT (for low-frequency FB), which moves one of the laser mirrors for stabilizing the frequency. The limiting noise is the shot noise; taking it into account for a cavity having no losses, the line width becomes

$$\Delta\nu > \frac{1}{2\pi\tau_s} \sqrt{\frac{h\nu}{w_s t}} , \tag{7.12}$$

where τ_s is the reference cavity storage time, w_s is the power used in the stabilization circuit and t is the observation time.

With the purpose of further reducing the laser linewidth, the Munich group [Billing et al. 1983, Shoemaker et al. 1985] let the beam W_r interfere (see fig. 3.7) with a small fraction of the laser beam, obtaining an output from the photodiode PD2 proportional to $\Delta\nu\, L$, where L is the total optical path length in the DL. This signal and that from the reference FP were added for improving the stabilization; in fig. 7.1 [Shoemaker et al. 1985] the upper curve represents the unstabilized laser line spectral density, the middle curve the line spectral density reduced by means of the reference FP cavity while the lower curve is the line spectral density when both reference cavity and the whole interferometer are used. The final integrated line width was $\simeq 3$ Hz, a reduction of $\simeq 10^6$ with respect to the unstabilized one.

A frequency noise level of $12.5\ \mathrm{mHz}/\sqrt{\mathrm{Hz}}$ was obtained with a diode pumped Nd:YAG laser, actively frequency stabilized with respect to a reference FP cavity [Shoemaker et al. 1989].

The effects due to the laser linewidth in FP interferometers involve a more complex mechanism than in a DL interferometer: from eqs. (7.2) and (4.2) we can evaluate the reflected amplitude,

$$A_r(t) = \mathrm{i}R_1\psi(t) + \mathrm{i}R_1 T_1^2 \sum_{n=0}^{\infty} (-R_1R_2)^n \psi(t - 2(n+1)L/c) ; \tag{7.13}$$

putting

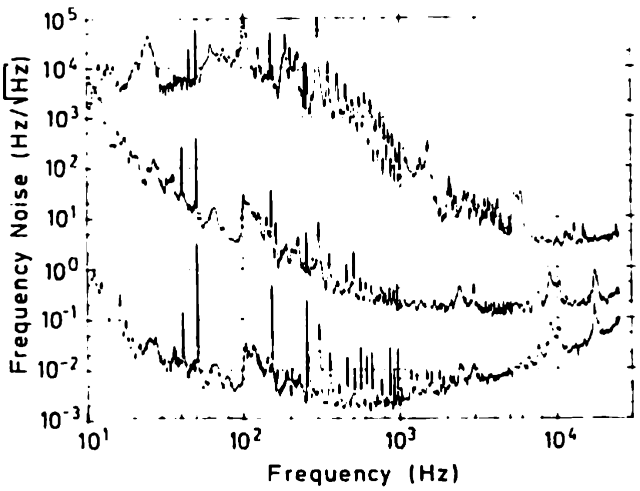

Fig. 7.1. The laser spectral line density before stabilization (from Shoemaker et al. [1985]) is shown in the upper curve; in the middle one the spectral line density after stabilization with a reference FP cavity is shown while in the lower one the spectral line density is shown after combined stabilization with the reference FP cavity and the total DL optical path.

$$\psi(t) = \int_{-\infty}^{\infty} \psi(\omega)\, \mathrm{e}^{\mathrm{i}\omega t}\, \mathrm{d}\omega$$

we obtain

$$A_i(t) = \mathrm{i} \int_{-\infty}^{\infty} \mathrm{d}\omega\, \psi(\omega) \left(R_1\, \mathrm{e}^{\mathrm{i}\omega t} + R_2 T_1^2 \frac{\mathrm{e}^{\mathrm{i}\omega(t-2L/c)}}{1 + R_1 R_2\, \mathrm{e}^{-2\mathrm{i}\omega L/c}} \right). \tag{7.14}$$

In an analogous way to eq. (7.4), combining the A_i from the two arms onto the beam splitter, the intensity on the photodiode is

$$I \propto \left| \int_{-\infty}^{\infty} \left[\left(R_1\, \mathrm{e}^{\mathrm{i}\omega t} + R_2 T_1^2 \frac{\mathrm{e}^{\mathrm{i}\omega(t-2L/c)}}{1 + R_1 R_2\, \mathrm{e}^{-2\mathrm{i}\omega L/c}} \right)_{\mathrm{arm}\,1} \right.\right.$$
$$\left.\left. + \mathrm{e}^{\mathrm{i}\varphi} \left(R_1\, \mathrm{e}^{\mathrm{i}\omega t} + R_2 T_1^2 \frac{\mathrm{e}^{\mathrm{i}\omega(t-2L/c)}}{1 + R_1 R_2\, \mathrm{e}^{-2\mathrm{i}\omega L/c}} \right)_{\mathrm{arm}\,2} \right] \psi(\omega)\, \mathrm{d}\omega \right|^2 . \tag{7.15}$$

where φ is a given phase shift. It is evident from eq. (7.15) that unlike in the DL case, even when $(L)_{\mathrm{arm}\,1} = (L)_{\mathrm{arm}\,2}$, there is incomplete cancelation of the laser line width noise unless the mirror transmittance and losses in the two arms are equal.

In the Glasgow [Newton et al. 1986] and the Caltech [Spero 1986] FP interferometers the laser line width is stabilized by using the cavity of one of the interferometer arms as a reference (see fig. 4.3). In this case, since the stabilizing cavity is very long, the sensitivity to laser frequency changes is much higher than that of a shorter reference cavity having the same finesse.

The presence of the laser intracavity Pockels cell gives non-negligible power losses; stabilization using extracavity phase acousto-optic modulators has been performed by Hall et al. [1977] and Camy et al. [1982]. In an experiment [Kerr et al. 1985] the use of an extracavity electro-optic modulator yielded a typical laser frequency fluctuation of $\simeq 0.01\ \mathrm{Hz}/\sqrt{\mathrm{Hz}}$ at 1 kHz.

8. The noise produced by the lateral beam jitter

If the beam splitter is not symmetrical between the two interferometer arms, but deviates by an angle $\delta\alpha$, then a lateral beam jitter δx will produce the phase shift [Billing et al. 1979]

$$\Delta\phi \cong 2\,\delta\alpha\,\delta x\,4\pi/\lambda\,. \tag{8.1}$$

Two methods have been adopted for reducing this type of noise: the first uses a mode cleaner [Rüdiger et al. 1981a, b, Meers 1983], while the second, a simpler one even though 30–50% of the laser power is lost, is the use of a monomode optical fiber coupler as suggested by R. Weiss of MIT. The experimental set up, shown in fig. 8.1, consists of a monomode fiber lit by a microscope objective; a $\lambda/2$ plate placed before the fiber and a linear polarizer placed behind it keep the right polarization. In fig. 8.2 [Shoemaker et al. 1985] the residual lateral beam jitter is shown as measured by a position sensitive diode: the top curve represents the laser beam jitter, the middle one the beam jitter after a mode

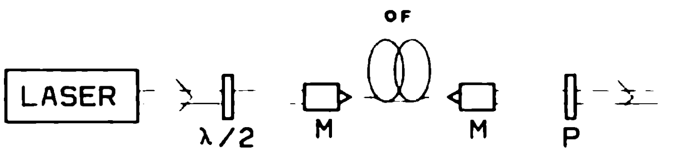

Fig. 8.1. The laser beam jitter is strongly reduced by injecting the beam in the monomode optical fiber OF. The injection is performed by means of the microscope objective M; the $\lambda/2$ plate and the polarizer P restore the plane polarization.

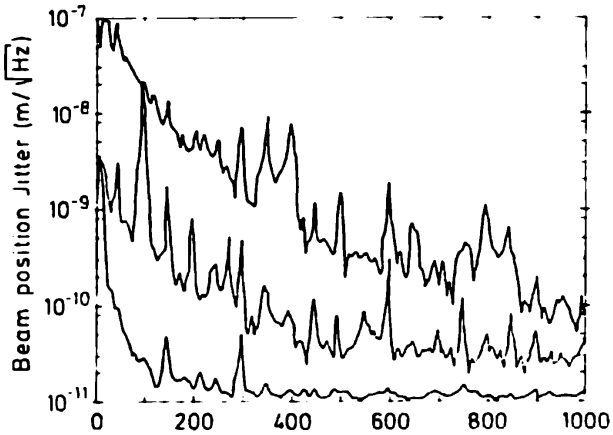

Fig. 8.2. The lateral beam jitter (from Shoemaker et al. [1985]) as measured with a position sensitive diode; the upper curve is the unfiltered laser beam, the middle one represents the beam jitter after a mode cleaner and the lower represents the jitter after a monomode optical fiber.

cleaner and the lower one the beam after the monomode fiber; a displacement of $\simeq 10^{-11}$ m/$\sqrt{\mathrm{Hz}}$ for $\nu > 100$ Hz was obtained.

A recycling cavity would filter out the fast laser frequency and amplitude fluctuations, as well as most of the beam geometry jitter.

9. The noise due to the gas pressure fluctuations

This type of phase noise originates from the fluctuations of the refractive index in the interferometer's vacuum pipes. The laser light bounces between the mirrors of either the FP or the DL system; the number of gas molecules contained in the light pipe then fluctuates almost in a Poissonian way (there may be convective motion also), hence varying the refraction index [Brillet 1984, 1985, Hough et al. 1986].

This can be shown as follows: if V is the average light pipe volume (not the vacuum pipe diameter), the total number of gas atoms in this volume is

$$n(t) = V \sum_i \frac{\rho_i(t)}{m_i} = V \sum_i n_i(t) , \tag{9.1}$$

where ρ and m_i are the density and the mass of the ith gas component and $n_i(t)$ the instantaneous number of molecules of the ith gas component. The number fluctuations $\delta n_i(t)$ of the ith component satisfy the correlation relation

$$\overline{\delta n_i(t)\, \delta n_i(t')} = \bar{n}_i g_i(t - t') , \tag{9.2}$$

where $\bar{n}_i$ and g_i are the average number and the correlation function of the ith gas component, respectively, with the condition $g_i(0) = 1$.

The function g_i is a complex function of the light beam geometry; let us for the sake of simplicity, approximate the light pipe volume by a cylinder having length L and diameter D. Under this condition the correlation time is D/V_i, where V_i is the speed of the molecules of the ith gas component. The light phase shift due to the gas refraction index ε_i is (we are considering a DL)

$$\phi_G(t) = \frac{4\pi NL}{\lambda} \sum [\varepsilon_i(t) - 1] . \tag{9.3}$$

The phase fluctuation $\delta\phi_G$ is

$$\delta\phi_G(t) = \frac{4\pi NL}{\lambda} \sum \frac{\delta n_i(t)}{\bar{n}_i} (\varepsilon_i - 1) . \tag{9.4}$$

In Ω space, using eq. (9.2), the noise is

$$|\delta\phi_G(\Omega)|^2_{\mathrm{tot}} = \left(\frac{4\pi NL}{\lambda}\right)^2 \sum_i \int_0^T e^{i\Omega(t-t')} \int_0^T \frac{(\varepsilon_i - 1)^2 g_i(t - t')}{\bar{n}_i} \,dt\, dt' . \tag{9.5}$$

where T is the measurement time.

Assuming the simple correlation function $g(t - t') = 1 - \theta(|t - t'| - D/V_i)$, $\bar{\varepsilon}_i - 1 = \alpha_i P_i / P_{0i}$, where P_i and P_{0i} are the pipe and atmospheric partial pressure, respectively, $\bar{n}_i = P_i \frac{1}{4}\pi D^2 L / K\tilde{T}$ ($\tilde{T}$ is the temperature), eq. (9.5) becomes

$$|\delta\phi_G(\Omega)|^2_{DL} = \left(\frac{4\pi NL}{\lambda}\right)^2 \sum_i \frac{2\sin(\Omega D/V_i)}{\Omega}\, T(\alpha_i P_i / P_{0i})^2 \frac{K\tilde{T}}{2NP_i \frac{1}{4}\pi D^2 L}\,. \tag{9.6}$$

The h measurability condition for a DL interferometer is [see eq. (7.6)]

$$\tilde{h}_{DL}(\Omega) > \left[16 \sum_i \frac{\sin \Omega D/V_i}{\Omega}\left(\frac{\alpha_i}{P_{0i}}\right)^2 \frac{K\tilde{T}P_i}{N\pi D^2 L}\right]^{1/2} \frac{NL\Omega}{c \sin \Omega NL/c}\,. \tag{9.7}$$

For a FP interferometer working at optical resonance we obtain the following result [for the definitions see eqs. (4.2) and (4.5)]:

$$|\delta\phi_G(\Omega)|^2_{FP} = \sum_i |\sqrt{8}\, T_1^2 R_2 \omega(L/c)(\bar{\varepsilon}_i - 1)|^2 \frac{T}{\bar{n}_i} \frac{\sin(\Omega D/V_i)}{\Omega} \frac{1}{(1 - R_1 R_2)^4} \frac{1}{1 + F' \sin^2 \Omega L/c}\,. \tag{9.8}$$

Comparing eq. (9.8) with the Fourier transform [see eq. (7.7)] of eq. (4.5) we obtain the measurability condition

$$\tilde{h}_{FP} \gtrsim \left(\sum_i 2 \frac{(\bar{\varepsilon}_i - 1)^2}{\bar{n}_i} \frac{\sin(\Omega D/V_i)}{\Omega}\right)^{1/2} \tag{9.9}$$

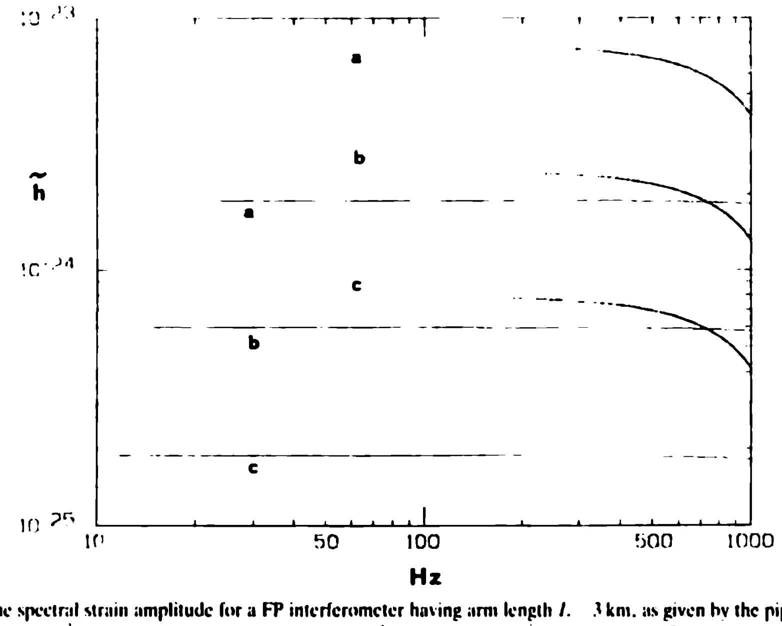

Fig. 9.1. The limits on the spectral strain amplitude for a FP interferometer having arm length $L = 3$ km, as given by the pipe vacuum fluctuations in the frequency interval $0 < \nu < 10^3$ Hz and for three pressures, a, $p = 10^{-6}$ mbar, b, $p = 10^{-7}$ mbar, c, $p = 10^{-8}$ mbar. The dotted lines are for N_2 and the solid lines are for H_2.

$\tilde{h}_{FP}$ is larger than $\tilde{h}_{DL}$ because the light pipe volume in the FP case is $2N$ times smaller than that of the DL.

In fig. 9.1, $\tilde{h}_{FP}$ is plotted as a function of the pressure for H_2 and N_2 in the frequency interval $0 < \nu < 10^4$ Hz.

A calculation taking into account a better approximation of the correlation function has been performed by Rüdiger [1988].

10. Thermal noise

The mass of the mirror is driven by the stochastic forces produced by thermal noise; we are considering here both the forces acting on the mirror suspensions and those producing an excitation of the mirror normal modes.

For the former case, if τ is the mirror suspension relaxation time, the r.m.s. stochastic spectral force is [Uhlenbeck and Ornstein 1930]

$$F = \sqrt{\frac{2K\tilde{T}M}{\tau}} \; \frac{\mathrm{N}}{\sqrt{\mathrm{Hz}}} \tag{10.1}$$

where M is the mirror mass, $\tilde{T}$ the temperature and K the Boltzmann constant. The thermal stochastic force $f(t)$ satisfies the correlation relation

$$\overline{f(t)f(t')} = F^2\delta(t - t') . \tag{10.2}$$

The mirror displacement $x(\Omega)$ in Ω space is evaluated using eqs. (2.17) and (10.2); in analogy with eq. (7.7) we obtain

$$|x_i(\Omega)|^2 \simeq T\,\frac{2K\tilde{T}}{M\tau}\,\frac{1}{(\Omega^2 - \omega_p^2)^2 + \Omega^2/\tau^2} . \tag{10.3}$$

where T is the measurement time and $\nu_p = \omega_p/2\pi$ the pendulum frequency. The pendulum thermal noise gives the following limit on the measurability of $\tilde{h}$:

$$\tilde{h} > \frac{1}{\Omega^2 L}\sqrt{\frac{2K\tilde{T}}{M}\sum\frac{1}{\tau}} \tag{10.4}$$

where the sum is over the mirrors.

With the purpose of evaluating the thermal noise produced by the mirror normal modes we can approximate the mirror by many harmonic oscillators each having frequency ν_i, relaxation time τ_i and equivalent mass M_i. In the proximity of the ith frequency the displacement in Ω space is sufficiently well described by eq. (10.3) replacing ω_p with $\omega_i = 2\pi\nu_i$. Since we consider the frequency region $\nu_p \ll \nu \ll \nu_i$ we can approximate eq. (10.3) in the following way:

$$|x_i(\Omega)|^2 \cong T\,\frac{2K\tilde{T}}{M_i\tau_i}\,\frac{1}{\omega_i^4} . \tag{10.5}$$

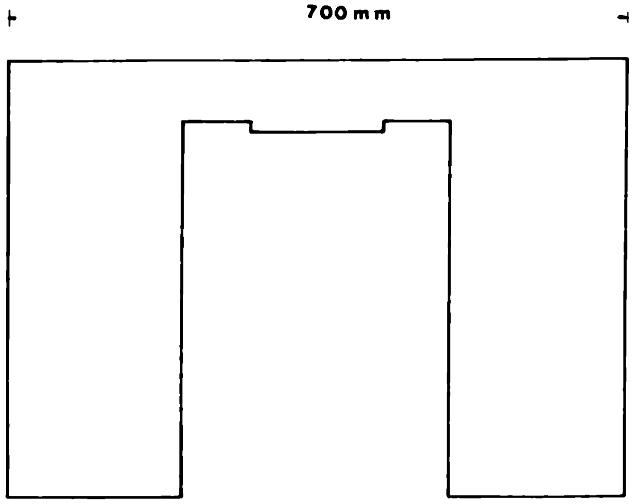

Fig. 10.1. A possible scheme of a 350 kg quartz mirror to be used in a 3 km FP interferometer for GW detection. A distortion $< \lambda/8$ is expected to be given by the 80 mm thick quartz window. The lowest-frequency mode (bell mode) at 1900 Hz it is not expected to give longitudinal mirror oscillations. The first longitudinal mode is at 2500 Hz

with $\omega_i \tau_i = Q_i$. The $\tilde{h}$ measurability condition is

$$\tilde{h} > \frac{1}{L} \sqrt{2K\tilde{T} \sum \frac{1}{M_i Q_i \omega_i^3}} . \tag{10.6}$$

where the sum is over the mirrors and over the longitudinal modes.

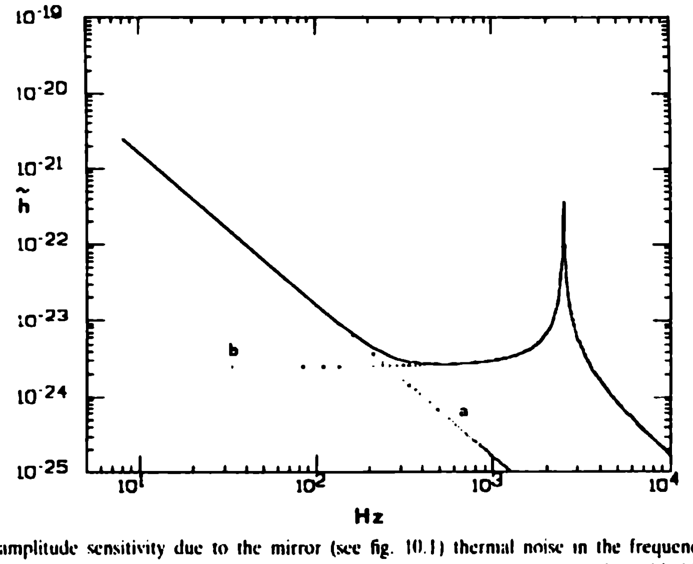

Fig. 10.2. The spectral strain amplitude sensitivity due to the mirror (see fig. 10.1) thermal noise in the frequency range $10 < \nu < 10^4$ Hz for interferometer arm length $L = 3$ km. Curve a represents the contribution from the mirror pendulum motion with $M = 300$ kg and $Q = 10^6$, while curve b represents the contribution to the thermal noise due to the mirror longitudinal normal modes. In b only the contribution from the first normal mode at 2500 Hz, having assumed an oscillator equivalent mass of $M_1 = 150$ kg and $Q_1 = 10^6$, is taken into account

Assuming Q_i to be invariant under a scale transformation changing the mirror dimensions, it follows that eq. (10.6) is invariant too. This is not true anymore for eq. (10.4), which shows that an increase in the mass M reduces the thermal noise. At low frequency it then seems convenient to use mirrors weighing several 100 kg if possible.

The scheme of a possible 350 kg quartz mirror to be used in the 3 km FP interferometer of the VIRGO project [Pisa, Napoli, Frascati, Orsay, Paris Collab. 1987, Paris, Orsay, Pisa, Napoli, Frascati Collab. 1988] is shown in fig. 10.1; the quartz window is expected to give $<\lambda/8$ error to the wave front. The lowest frequency mode at $\simeq 1990$ Hz (bell mode), due to the cylinder hole, does not give a longitudinal oscillation to the mirror; the first longitudinal mode is at 2500 Hz.

The values of $\tilde{h}$ given for this kind of mirror considering that four mirrors will be mounted in the interferometer and assuming $Q = \tilde{\omega}_p \tau = 10^{6}$ in eq. (10.5), $Q_i = 10^{6}$ in eq. (10.7), $L = 3$ km and $\tilde{T} = 300$ K, are shown in fig. 10.2 in the frequency interval $10 < \nu < 10^{4}$ Hz.

11. Seismic noise

Seismic noise is the dominant source of displacement of the mirror suspension points. The r.m.s. spectral displacement can be sufficiently well approximated by the formula

$$x_1 = a\,\nu \quad \mathrm{m}/\sqrt{\mathrm{Hz}}, \tag{11.1}$$

where $a \cong 10$ at a depth of $\sim 10^{3}$ m up to $a \cong 10$ at the Earth's surface in a relatively quiet place. Extensive measurements of the Earth's strain spectrum from 10 to 10 Hz using a laser interferometer have been performed by Berger and Levine [1974].

Experimental evidence of this type of noise [see eq. (2.13)] is clearly shown in fig. 11.1 [Shoemaker et al. 1985]; from these data the value $a \cong 10$ can be inferred. Active systems have been used to reduce seismic noise both in the vertical [Faller and Rinker 1979, Saulson 1984a, b] and horizontal directions [Robertson et al. 1982, Giazotto et al. 1986a, b]. Three-dimensional pneumatic active systems have been developed by Lorenzini [1972].

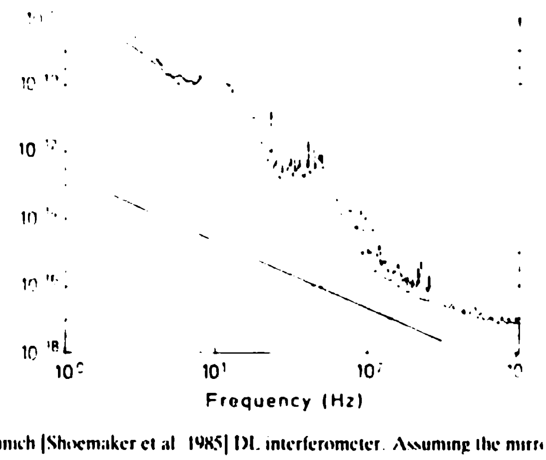

Fig. 11.1. Displacement noise of the Munich [Shoemaker et al. 1985] DL interferometer. Assuming the mirror to be suspended by a 1 m long wire, it follows that the suspension point is approximately shaken by a spectral seismic noise displacement $\Delta x = 10 \;\nu$ m/$\sqrt{\mathrm{Hz}}$.

The basic idea consists in using an accelerometer to sense the displacement of the suspended mass, then using the accelerometer signal to create a force on the mass in such a way that the signal becomes null. In the experiment of Faller and Rinker, a sensor measured the elongation Δy of a vertical spring with respect to a fixed reference point y_0. This signal was fed to a transducer displacing the suspension point y_1 by an amount $y_0 + \alpha\,\Delta y$, where α is the amplification. This gives the spring motion equation

$$y = \frac{y_0\omega_0^2(1-\alpha)}{-\Omega^2 + \mathrm{i}\Omega/\tau + \omega_0^2(1-\alpha)}\,, \tag{11.2}$$

where $\nu_0 = \omega_0/2\pi$ is the open loop resonance frequency. From eq. (11.2) it follows that the equivalent spring length increases by the factor $1/(1-\alpha)$; about 1 km was obtained.

In Saulson's experiment the acceleration of the end point of a horizontal beam was measured in the vertical direction by means of an accelerometer; the amplified signal was fed to a force transducer acting on the beam end point. In the limit of ideal accelerometer the effect of this loop was to increase the beam mass; the open loop 4.5 Hz resonance frequency was reduced, when the loop was closed, to 4×10^{-2} Hz.

The layout of the horizontal direction isolation experiment of Robertson et al. is shown in fig. 11.2. The relative displacement of the test mass with respect to the suspension point was measured by means of condensers connected to a reference arm correcting for the effects due to the ground rotations. Neglecting the ground rotations the equation of motion for the test mass in the horizontal x direction is

$$\ddot{x} + \dot{x}/\tau + (g/l)x = x_s g/l\,. \tag{11.3}$$

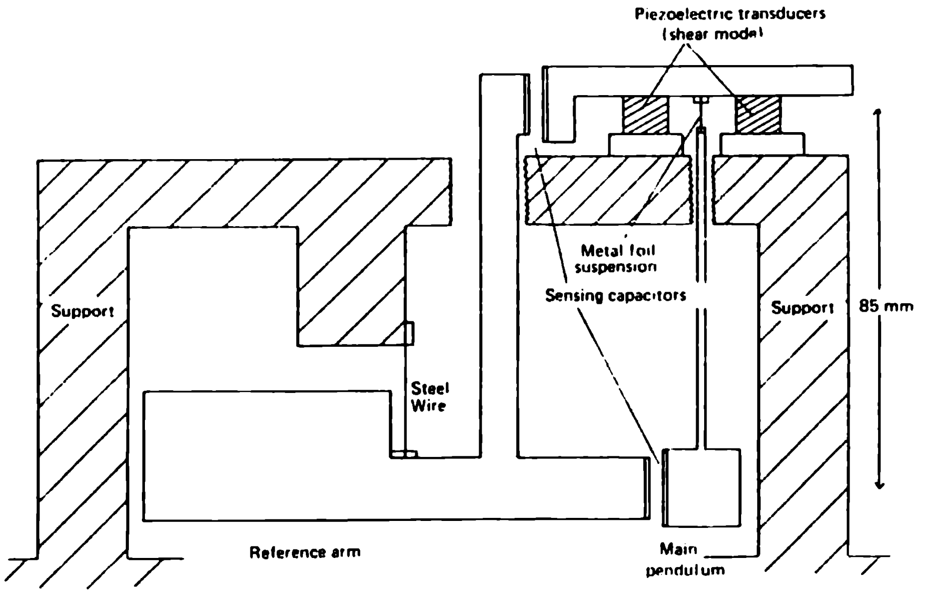

Fig. 11.2. The layout of an active horizontal direction seismic isolation experiment (from Robertson et al [1982]). The relative displacement of the test mass with respect to the suspension point was measured by means of a capacitive transducer and fed back to a PZT acting on the pendulum suspension point. A reference arm corrected for the effects due to ground rotations. With this experiment an amplification $A = 60$ was obtained and the pendulum length was increased up to ≈ 5 m

where τ is the relaxation time, x the mass coordinate, x_s is the horizontal displacement of the pendulum attachment point, g is the acceleration of gravity and l the pendulum length.

Since the capacitor c senses $x - x_s$, the PZT transducer displacement is

$$x_s = (\alpha + \beta \int \mathrm{d}t)(x - x_s) + x_1 \,. \tag{11.4}$$

where x_1 is the horizontal ground seismic noise [see eq. (11.1)] and the integral creates "cool" damping [Forward 1978].

From eqs. (11.3) and (11.4) it follows that

$$x = \left(\frac{g}{l}\,\frac{x_1}{1+\alpha}\right)\Big/\left[\Omega^2 + i\Omega\left(\frac{1}{\tau} + \frac{\beta}{1+\alpha}\right) - \left(\frac{\beta}{\tau}\quad\frac{g}{l}\right)\frac{1}{1+\alpha}\right]. \tag{11.5}$$

From eq. (11.5) it follows that the effect of α in the FB is to make the pendulum virtual length equal to $l(1+\alpha)$ and that of β is to introduce a new damping with relaxation time $(1+\alpha)/\beta$. With a 0.47 kg mass and $l = 85$ mm, $\alpha = 60$ on a band width of 30 Hz was obtained.

In the experiment of Giazotto et al., shown in fig. 11.3, in which a large mass (100 kg) and an interferometric sensor were used, a 1 m pendulum was brought to a virtual length of 1600 m at 10 Hz by

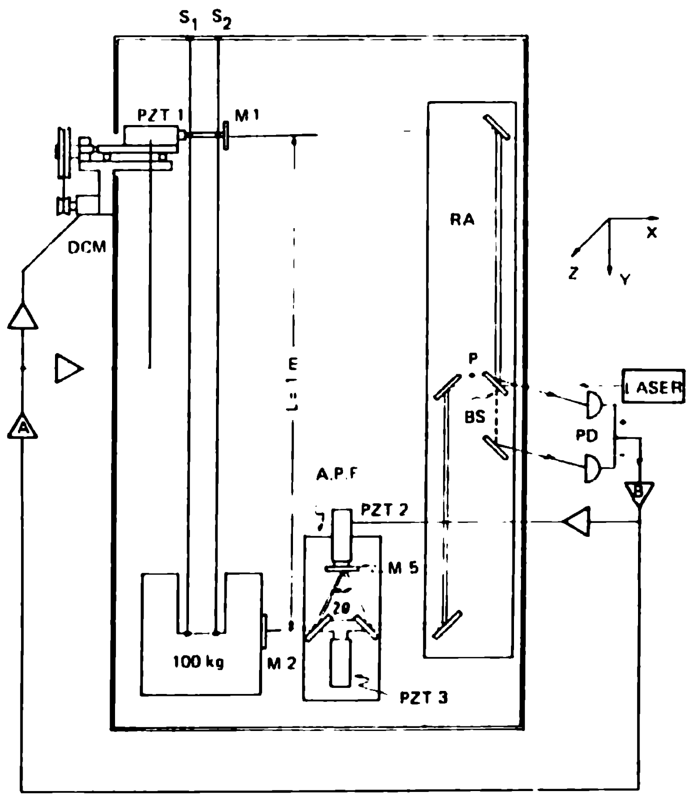

Fig. 11.3. Schematic diagram of the interferometric pendulum for seismic noise reduction (from Giazotto et al. [1986b]). The relative displacement of the 100 kg test mass with respect to the suspension point was measured interferometrically. The 1 m pendulum was brought to a length of 1600 m.

means of an analog phase follower [Campani et al. 1986], whose purpose was to transform in real time the interferometer output, proportional to $\sin \varphi$ (φ is the interferometer phase shift), to a signal proportional to φ suitable to be used as a FB signal. The pendulum suspension point was displaced by both a PZT and a DC motor; the use of the latter was crucial for obtaining high FB amplification.

A method for actively reducing the damping produced by the flexure of the pendulum suspension wire at its attachment point has been proposed and tested by Faller et al. [1987]; they obtained an increase of 5.6 in the damping time and a lowering of the pendulum resonance frequency.

The use of active seismic isolation schemes is strongly limited by the difficulty of making multiple three-dimensional (3D) systems; this necessity is dictated by the fact that a non-isolated degree of freedom reintroduces the seismic noise even if the other degrees of freedom are isolated. For this reason passive schemes have been adopted, able to isolate in the vertical direction as well [Giazotto 1987, Shoemaker et al. 1987a].

The basic idea is to use a multiple-stage pendulum with the masses supported by springs. It can be shown that the frictionless transfer functions for both the vertical and horizontal directions can be brought to the following canonical form:

$$F = \prod_{n=1}^{N} \omega_n^2/(-\Omega^2 + \omega_n^2) , \tag{11.6}$$

where F is the transfer function, $\nu_n = \omega_n/2\pi$ is the nth mode frequency and N is the number of masses. Above the resonances $F \propto \Omega^{-2N}$, but the presence of friction and nonlinearities can give a slower decrease with frequency as well as coordinate mixing.

In the interferometric antennas aiming to reach very low frequency ($\nu \geq 10$ Hz) seismic isolation requires a very careful design with the purpose of avoiding mechanical resonances falling into the interval $10 \leq \nu < 100$ Hz; these are produced mainly by the springs' rocking and normal modes.

To this end a 3D seven-stage seismic attenuator (see fig. 11.4) equipped with gas springs [Del Fabbro et al. 1988a] has been built by the Pisa group [Del Fabbro et al. 1987]; this attenuator is able to levitate a 400 kg test mass. The gas springs, shown in fig. 11.5, are able to levitate 10^3 kg with a rigidity of 3.4×10^4 N/m when used with four bellows and 5×10^2 kg with a rigidity of 2×10^4 N/m when used with two bellows; the normal modes of the bellows are damped by means of dry mechanical adsorbers. The rocking modes are kept at very low frequency (1 Hz) by making the wire attachment points very close to each other (5 mm).

The transfer functions for the vertical and horizontal directions [Del Fabbro et al. 1988b] in the frequency interval $10 \leq \nu \leq 68$ Hz are shown in fig. 11.6. The absolute test mass noise was measured with a dip-coil accelerometer having a sensitivity of 10^{-13} m/$\sqrt{\text{Hz}}$; fig. 11.7 shows the test mass displacement in the frequency interval $0 \leq \nu \leq 10$ Hz together with the exciting seismic noise. Taking the ratio between these two spectra, the transfer function measured for $0 \leq \nu \leq 10$ Hz shows that there is a $\sim 10^{-2}$ vertical to horizontal coupling [Del Fabbro et al. 1988c].

The general problem of cool damping [Forward 1978, Kuroda et al. 1982] of the pendulum normal modes has been solved by means of both electromagnetic or electrostatic force actuators. In the Munich, Glasgow and Caltech interferometers use was made of magnet and coils, while in the MIT interferometer electrostatic transducers were used.

The basic layout of an electromagnetic damping scheme [Shoemaker 1987] is shown in fig. 11.8. The mass position is read by means of a position sensitive diode PSD illuminated by a LED. After differentiating the signal with respect to time, which produces an effective viscous force, it is applied to coil C producing a force on magnet M connected to the test mass.

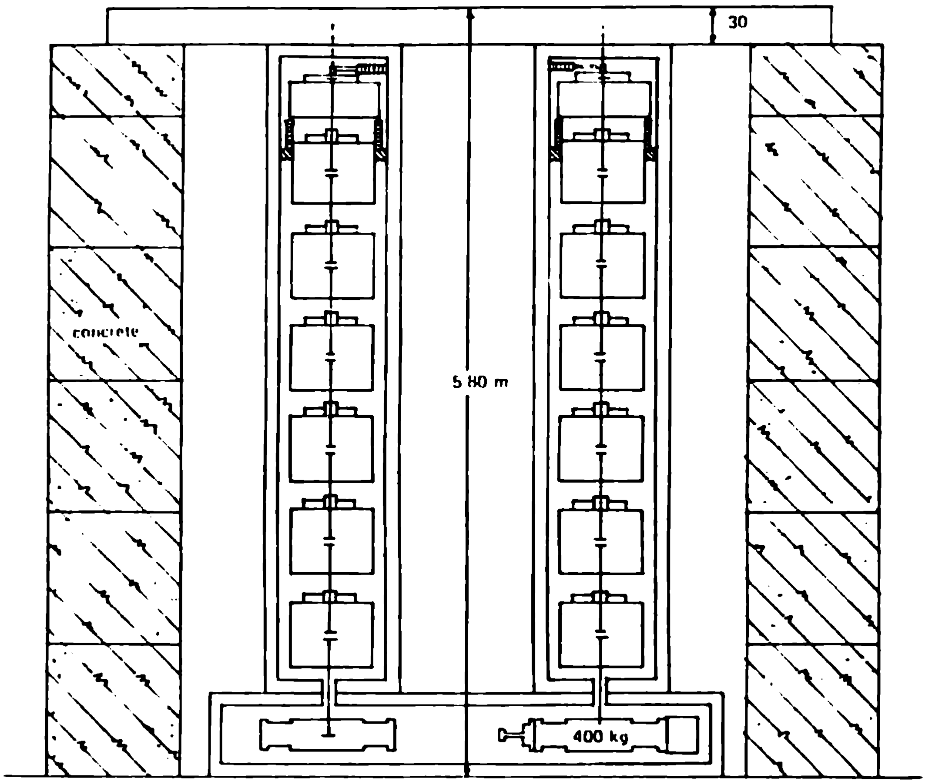

Fig. 11.4. Schematic diagram of the seismic noise attenuator (from Del Fabbro et al. [1988b]). The two attenuators, composed of a 7-fold three-dimensional harmonic oscillator, are able to give isolation in the vertical direction as well. The 400 kg test masses contained in the vacuum chamber are also shown. This device is able to attenuate the seismic noise in the vertical direction by a factor of $\sim 2 \times 10^{-[illegible]}$ at 10 Hz.

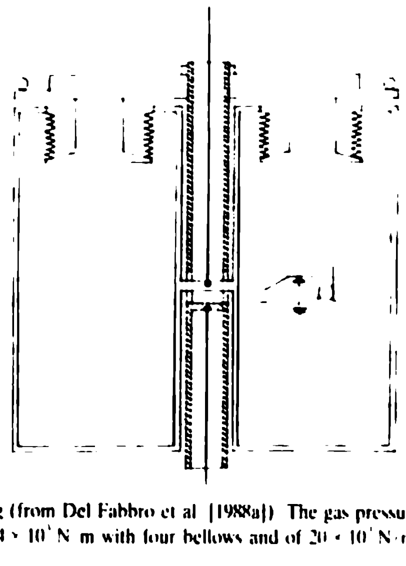

Fig. 11.5. The schematic diagram of a gas spring (from Del Fabbro et al. [1988a]). The gas pressure pushes the bellow piston, which levitates the load attached to the lower wire. A rigidity of 3.4×10^{3} N/m with four bellows and of 2.0×10^{3} N/m with two bellows was obtained.

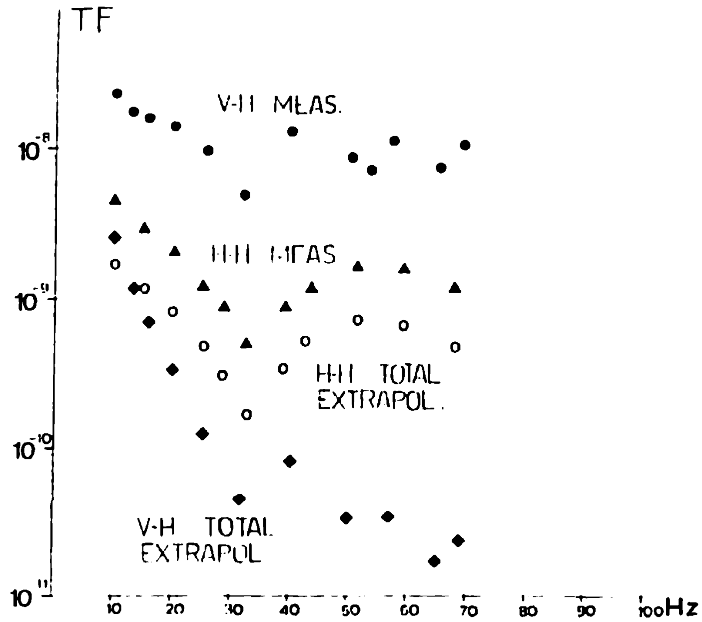

Fig. 11.6. The vertical and horizontal TF for the seismic noise attenuator of fig. 11.4 (from Del Fabbro et al. [1988b]) in the frequency interval $10 < \nu < 68$ Hz. The excitations were applied to the second stage in the chain: hence these plots give upper limits. At 10 Hz the vertical-horizontal (V-H) TF was $< 2.8 \times 10^{-8}$, while the horizontal-horizontal (H-H) TF was $< 5 \times 10^{-9}$. An extrapolation to the suspension point excitation gives at 10 Hz, V-H $\approx 3 \times 10^{-11}$ and H-H $\approx 2 \times 10^{-9}$.

A low-pass filter (LPF) prevents the damping system to reintroduce seismic noise. This problem, which is easily solved for interferometers designed to work at high frequency ($\nu \geq 200$ Hz), becomes crucial for those aimed to work at low frequency. In the Pisa attenuator, having normal modes for $\nu \leq 6$ Hz, it is necessary to have an LPF cutting the FB at 10 Hz not giving instabilities; this is a complex problem to be solved. A six-dimensional damping system using PSD has been built to reduce the amplitude of the 0.24 Hz pendulum mode of the Pisa attenuator; an absolute displacement of the test mass of $\simeq 3$ μm was obtained [Bradaschia et al. 1989]. The use of accelerometers instead of PSD could prevent the injection of seismic noise.

Seismic noise affects the interferometer phase also by means of the interaction of the mirror scattered light with the vacuum pipe walls [Billing et al. 1983]: the scattered light is reflected by the pipe walls and then reenters the main beam by means of a second scattering process. Since the pipe walls are vibrating, due to the seismic noise, they change the phase of the scattered beam; the interference of the scattered beam with the main one then reintroduces the seismic noise despite the seismic isolation of the mirrors. The use of diaphragms in the vacuum pipe could prevent the scattered light which hits the pipe walls to reenter the main optical path. A thorough evaluation of the effects of light scattering and a study of baffle configurations inside the vacuum pipe has been made by Thorne [1989]; the use of seismically isolated diaphragms for low-frequency GW detectors has been proposed by Giazotto [1988a].

The effects of the Newtonian forces produced by moving objects have been evaluated by Saulson [1984a, b] and found to be negligible with respect to other type of noise at the expected sensitivity of the new generation of antennas.

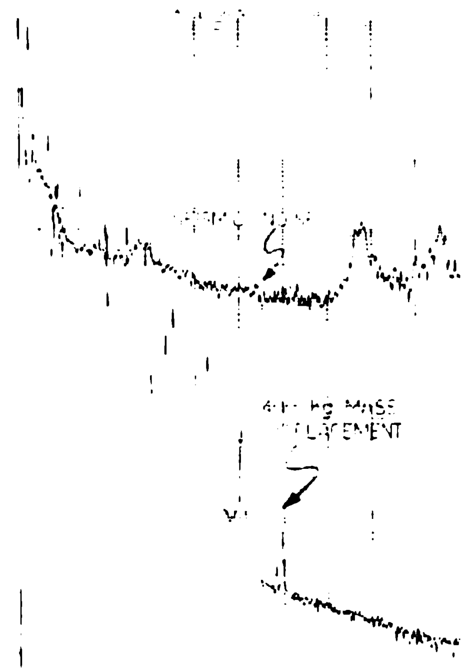

Fig. 11.7. The displacement spectrum of the 400 kg test mass of the apparatus shown in fig. 11.4 in the frequency interval $0 < \nu < 10$ Hz (from Del Fabbro et al. [1988c]). Despite the fact that the accelerometer sensitivity is maximal in the horizontal direction, many vertical normal mode peaks are visible; a 10 [illegible] mixing vertical–horizontal was measured, showing the necessity to have the vertical isolation as good as the horizontal one.

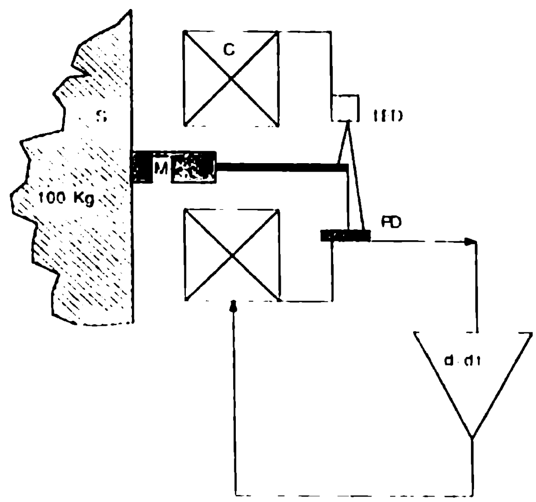

Fig. 11.8. Schematic diagram of a shadow meter damping system: the displacement of the mass S is measured by photodiode PD; the time differential of this signal is applied to coil C, which creates a viscous force on magnet M.

12. Effects due to the radiation pressure on the mirrors

As has been shown in section 5, radiation pressure creates a differential motion of the interferometer mirrors and this effect can be easily evaluated. Since $\sqrt{n} = \sqrt{Wt/h\nu}$ is the fluctuation of the number of photons impinging on the mirrors in a time t, the momentum fluctuation is $\Delta P = (h\nu/c)\sqrt{Wt/h\nu}$, from which it follows that the rms differential spectral force is given by $\Delta\tilde{F} = (h\nu/c)\sqrt{W/h\nu}$.

In a DL system having $2N$ beams, these force fluctuations are coherently added and the measurability condition for $\tilde{h}$ is [see eq. (2.9)]

$$\tilde{h}_{\mathrm{DL}} > \frac{1}{M\Omega^2 L}\,\frac{2N}{c}\,\sqrt{Wh\nu}\,, \tag{12.1}$$

where W is the incident power.

In a FP cavity whose input and far mirrors have amplitude transmittance T_0 and T_1, respectively, the intracavity power at optical resonance is

$$W_{\rm in} = WT_0^2F^2/\pi^2 . \tag{12.2}$$

where $F \cong \pi\sqrt{R_0R_1}/(1 - R_0R_1)$ is the cavity "finesse". If $T_0 \gg T_1$ eq. (12.2) becomes

$$W_{\rm in} \simeq W(2/\pi)F \tag{12.3}$$

The fluctuations of the incident power will be coherently transmitted to the mirror for frequencies smaller than $1/\tau_s$; in this case the measurability condition for $\tilde{h}$ is

$$\tilde{h}_{\rm rp} > \frac{1}{M\Omega^2 L}\,\frac{2F}{\pi c}\sqrt{Wh\nu} . \tag{12.4}$$

Assuming $\Omega = 60\,{\rm rad/s}$, $M = 4 \times 10^2\,{\rm kg}$, $L = 3 \times 10^3\,{\rm m}$, $h\nu \simeq 10^{-19}\,{\rm J}$, $(2/\pi)F \simeq 2N \simeq 30$ it follows from eqs. (12.1) and (12.4) that

$$\tilde{h}_{\rm ph} = \tilde{h}_{\rm rp} \simeq 2 \times 10^{-20}\sqrt{W}\,{\rm Hz}^{-1/2} . \tag{12.5}$$

Equation (12.5) shows that kilowatts of power can be used before reaching the photon counting limit of eq. (3.2).

In a FP interferometer the radiation pressure can create multistability; this phenomenon was experimentally observed in a cavity composed of a fixed mirror and a 60 mg moving suspended mirror [Dorsel et al. 1983]. When the intracavity power reached 100 mW a bistable response was obtained.

This effect has been theoretically investigated by Deruelle and Tourrenc [1984], Tourrenc and Deruelle [1985] and by Meystre et al. [1985]. Bistability in a three-mirror system was investigated by Meystre et al. [1985]. Following the approach of Aguirregabiria and Bel [1987] we consider a pendular cavity as shown in fig. 12.1. The reflection and transmittance coefficients of mirror M_1 are $R = (\cos\theta)\,e^{i\mu}$ and $T = i(\sin\theta)\,e^{i\mu}$, respectively; P is the incident light power, $D_s + x(t)$ the mirror separation and $\phi_\lambda = \sqrt{P}\exp[-i(2\pi/\lambda)(ct + \alpha)]$ the incident light field. The light field $\phi(t)$ on mirror M_2 is

$$\phi(t) = T\phi_\lambda\{t - [D_s + x(t)]/c\} - R\phi(\hat{t}) . \tag{12.6}$$

where the retarded time $\hat{t}$ is defined as

$$c(t - \hat{t}) = D_s + x(t) + x(\hat{t}) . \tag{12.7}$$

Neglecting the effects of the delay, the equation of motion of mirror M_2 is

$$\begin{aligned} \ddot{x} + (\Omega/Q)\dot{x} &= -\Omega^2 x + 2|\phi|^2/Mc \\ &= -\Omega^2 x + \frac{2P}{Mc}\,\frac{\sin^2\theta}{1 + \cos^2\theta + 2\cos\theta\,[(4\pi/\lambda)(D_s + x) - \mu]} . \end{aligned} \tag{12.8}$$

where M is the mass of mirror M_2, Ω the pendulum angular frequency and Q the mechanical quality

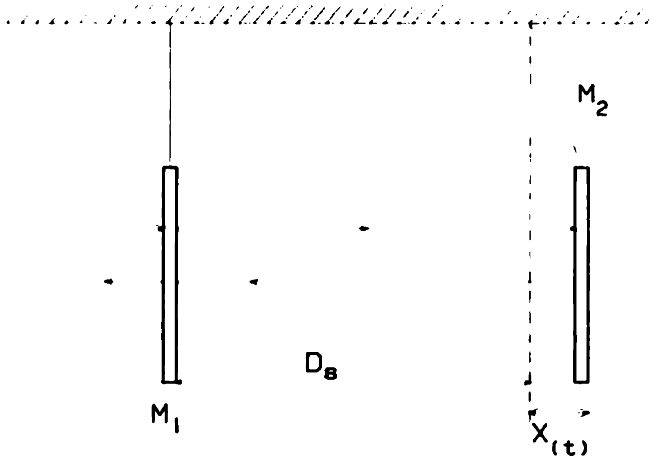

Fig. 12.1. Radiation pressure displaces mirror M from its equilibrium position. x(t) is then a multistable function of the radiation pressure

factor. The relative maxima of the r.h.s. of eq. (12.8), to a good approximation, occur when

$$x = (\lambda/4\pi)[(2n+1)\pi + \mu] - D_s = x_n \quad (n = 0, \pm 1, \pm 2, \ldots)\,,$$

as shown in fig. 12.2 The peak heights $J = (4P/Mc\Omega^2)(F/\pi)$, where F is the finesse, can be increased more and more in such a way that a new peak crosses the $y = 0$ axis and consequently a new stability point emerges ($\partial y/\partial x < 0$).

The delay can be taken into account writing eq. (12.6) in the following way [Aguirregabiria and Bel 1987]:

$$f(t) = 1 + (\cos\theta)\, e^{i\mu}\, e^{i[x(t-r_1)-x_s]} f(t - r_1)\,. \tag{12.9}$$

where r_1 is the time needed by the light to make a round trip in the cavity ending at time t, x_s is the equilibrium point and

$$f(t) = -\frac{i\phi(t)}{\sqrt{P}\sin\theta}\exp\{i[(2\pi/\lambda)(ct - D_s - x + \alpha) + \sigma]\} \tag{12.10}$$

Iteration of eq. (12.9) gives

$$f = 1 + \sum_{n=1}^{\infty} (\cos\theta\, e^{i\mu})^n \exp\left(i \sum_{J=1}^{n} (x_{(J)} - x_s)\right). \tag{12.11}$$

where $x_{(J)} \simeq x(t - Jr)$ and $r = 2D_s/c$.

The equation of motion of the pendulum becomes

$$\ddot{x} + (\Omega/Q)\dot{x} = -\Omega^2 x + (2P/Mc)\sin^2\theta\,|f|^2 \tag{12.12}$$

The dominant reduction of the hereditary equation of motion, evaluated up to second order in the

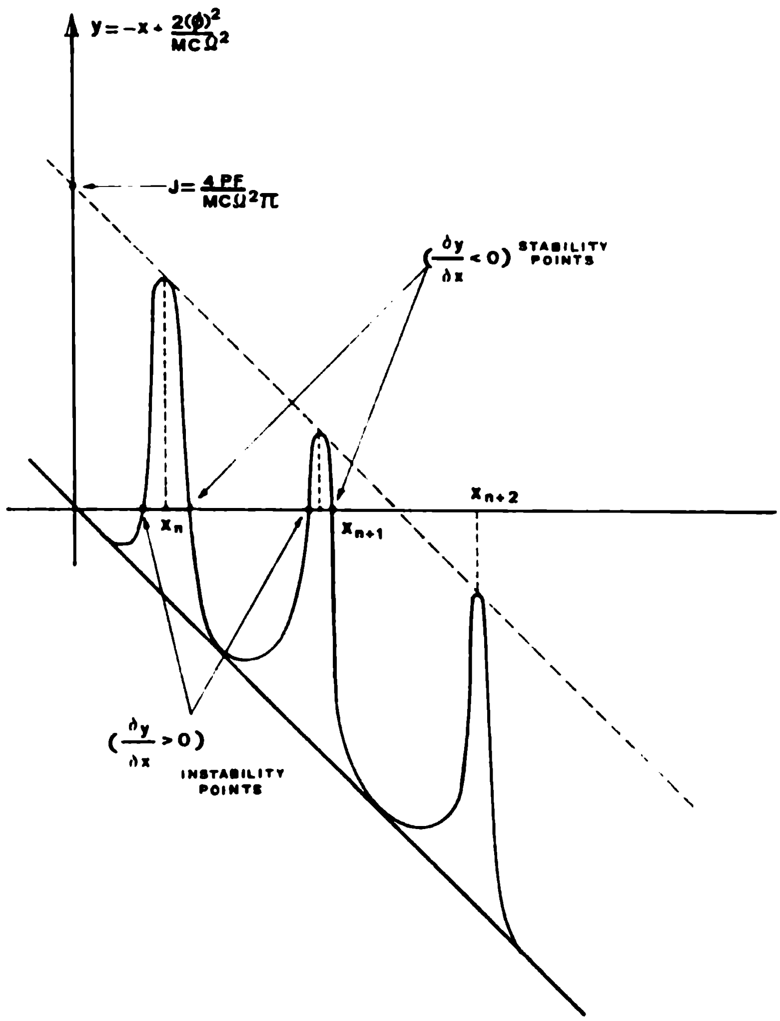

Fig. 12.2. Plot of the r.h.s. of eq. (12.8); if the laser power P increases, the peak at x_n may cross the $y = 0$ axis, thus creating a new stability point ($\partial y/\partial x < 0$).

displacement $x(t) - x_s$, can be put in the form [Bel et al. 1988]

$$\ddot{Y} + K\dot{Y} + \bar{\Omega}^2 x = 0 ,$$

$$K = \left[\left(\frac{1}{Q} - \frac{8ry_s}{\beta\theta^2(1+y_s^2)^3}\right) - \frac{8r(1-5y_s^2)}{\beta\theta^2(1+y_s^2)^4}\, y\right]\Omega , \tag{12.13}$$

$$\bar{\Omega}^2 = \left[\left(1 + \frac{2y_s}{\beta(1+y_s^2)^2}\right) + \frac{1-3y_s^2}{\beta(1+y_s^2)^3}\, y\right]\Omega^2 ,$$

where $y_s = 2x_s/\theta^2$, $\beta = \theta^4 MC/16P$ and $Y = 2[x(t) - x_s]/\theta^2$. The effect of the delay is then to add a new "friction" term [Deruelle and Tourenc 1984].

To demonstrate the presence of chaos we write eq. (12.12) putting $z = x(t) - x_s$,

$$\ddot{z} + (\Omega/Q)\dot{z} + z = (|g|^2 + 2\,\mathrm{Re}\,g)S\,, \tag{12.14}$$

where

$$\varepsilon = (4\pi/\lambda)(D_s + x_s) - \mu - (2n+1)\pi\,, \qquad S = \frac{2P}{Mc}\,\frac{\sin^2\theta}{1 + \cos^2\theta - 2\cos\theta\cos\varepsilon}\,,$$
$$g = f/f_0 - 1 = \cos\theta\, e^{i\varepsilon}\{e^{i[(4\pi/\lambda)z(t)]}[g(\hat{t}) + 1] - 1\}\,, \qquad c(t - \hat{t}) = 2(D_s + x_s) + z + z(\hat{t})\,. \tag{12.15}$$

Linearizing and then iterating eq. (12.15), eq. (12.14) becomes [Aguirregabiria and Bel 1987]

$$\ddot{z} + \frac{\Omega}{Q}\dot{z} + r^2 z = -\frac{8\pi}{\lambda} S \sum_{k=1}^{\infty} \mathrm{Im}(\cos\theta\, e^{i\varepsilon} z(\hat{t}_k))\,, \tag{12.16}$$

where $(\hat{t}_k)$ is the retarded time iterated k times. Putting

$$z = e^{\lambda t}\,, \tag{12.17}$$

we obtain the characteristic equation

$$\lambda^2 + \frac{\Omega}{Q}\lambda + r^2 = -\frac{8\pi}{\lambda} S\cos\theta\sin\varepsilon\,\frac{1}{R}\,\frac{1}{1 + R^{-1}[(e^{\lambda r} - 1) + (e^{-\lambda r} - 1)\cos^2\theta]}\,, \tag{12.18}$$

where $R = 1 + \cos^2\theta - 2\cos\theta\cos\varepsilon$ and $r = 2(D_s + x_s)/c$. Due to eq. (12.17) instability occurs when $\mathrm{Re}\,\lambda > 0$; hence the point $\mathrm{Re}\,\lambda = 0$ is the bifurcation point. The power P for any r, giving rise to instability, has also been evaluated.

In the VIRGO project [Pisa, Napoli, Frascati, Orsay, Paris Collab. 1987, Paris, Orsay, Pisa, Napoli, Frascati Collab. 1988] having arm length of 3 km, $\lambda = 1\ \mu$m, power 500 W, mirror mass 400 kg, finesse $F = 30$ and pendular mechanical quality factor $Q \simeq 10^6$, the retarded effects [Tourrenc, private communication] give the unstable equation of motion for the mirror

$$Y = A\exp(2\times 10^{-3}\,t)\sin(6t + \phi)\,. \tag{12.19}$$

This instability seems to be easily corrected for by means of active feedback of the mirror damping.

13. Cosmic ray background

The interaction of particles with matter excites oscillation modes which can be experimentally detected. In an experiment [Beron and Hofstadter 1969] the modes of a piezoelectric disc have been excited by an electron beam containing 10^4–10^6 particle per pulse of 1 μs duration.

In a subsequent experiment [Grassi Strini et al. 1980] the interaction of 30 MeV protons with an Al rod 0.2 m long and 3×10^{-2} m diameter was studied. The effect was the excitation of the rod's fundamental longitudinal mode with an amplitude

$$\xi = \frac{\alpha}{C_V} \frac{2WL}{\pi M} \cos \pi x / L \,, \tag{13.1}$$

where L is the rod length, W the energy lost by the hitting particles, α the rod thermal linear expansion coefficient, C_V the specific heat at constant volume, M the mass of the rod and x the distance from the center at which the particles cross the rod. Theoretical calculations [Allega and Cabibbo 1983, Bernard et al. 1984] have been performed giving good agreement with eq. (13.1).

The interferometer mirrors when hit by a cosmic ray undergo both excitation of the internal degree of freedom and of the suspension pendulum modes. The mirror's internal degrees of freedom are excited both by the heat produced with an amplitude given by eq. (13.1), and by the differential momentum released by the cosmic rays. The excitation of the mirror pendulum mode by cosmic muons has been evaluated by Weiss [1972] considering only ionization losses.

In a subsequent work of Amaldi and Pizzella [1986] the effect of production of knock-on electrons, bremsstrahlung, direct pair production and photonuclear interactions by muons was shown to be crucial for the evaluation of the cosmic muon noise in a bar antenna. A Monte Carlo simulation of the background due to high-energy cosmic muons in a bar antenna has been done by Ricci [1987].

A calculation taking into account both ionization losses and the four processes mentioned for an antenna having 3 km arm length and 400 kg quartz mirror mass, has been done by Giazotto [1988b]. The results show that muons of 10^3 GeV give 1 ms pulses having $h \simeq 10^{-23}$ with a frequency of 10^{-2} yr^{-1} and 10^4 GeV muons give $h \simeq 10^{-21}$ with a frequency of 10^{-6} yr^{-1}.

For periodic GW the calculation gives the following measurability condition for $\tilde{h}$:

$$\tilde{h} > 10^{-25}/\nu^2 \ \mathrm{Hz}^{-1/2} \,, \tag{13.2}$$

where the GW frequency ν has been assumed to be larger than the pendulum frequency and smaller than the frequency of the lowest mode of the mirror.

14. Conclusions

In this section the relevant types of noise described previously, limiting the interferometer's sensitivity, are evaluated as a function of the GW frequency and compared with the GW strain amplitude of some astrophysical sources. For the evaluation of these types of noise the following parameters characterizing the interferometer are assumed: arm length $L = 3$ km, FP finesse $F = 40$, suspension quality factor $Q = 10^6$, mirror quality factor $Q_1 = 10^5$, temperature $T = 300$ K, frequency and mass of the lowest longitudinal mode of the mirror $\nu_1 = 2500$ Hz and $M_1 = 150$ kg, respectively, mirror mass $M = 300$ kg, vacuum pipe pressure $P = 10^{-7}$ mb assuming the residual gas to be H_2, recirculated light power $W = 1$ kW and seismic noise spectral displacement $x_1 \cong 3 \times 10^{-7}/\nu^2$ m/$\sqrt{\mathrm{Hz}}$.

In fig. 14.1 the interferometer sensitivity is shown as a function of the characteristic frequency of the incident GW, which is assumed to be the inverse of the pulse duration of the GW, together with some relevant types of noise and astrophysical GW source amplitudes. Line a is the sensitivity limit due to seismic noise reaching the mirrors suspended as a simple 1 m pendulum, line b represents the limit due

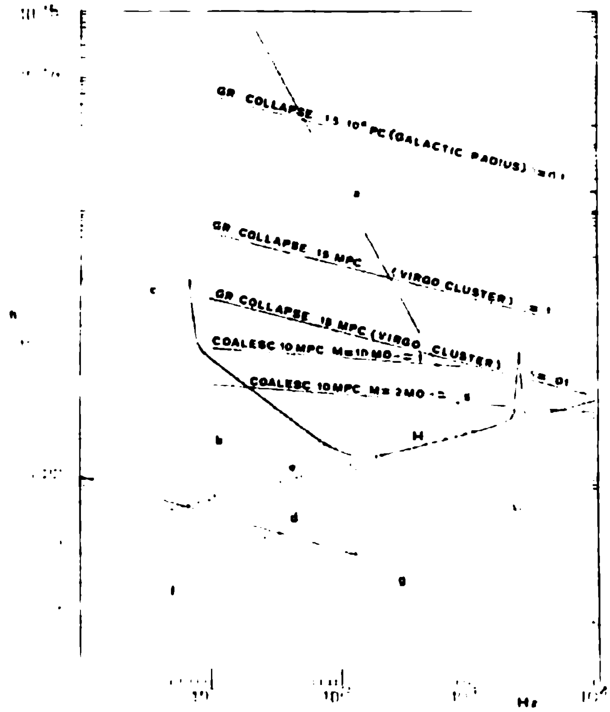

Fig. 14.1. The sensitivity to an incident GW of a 3 km arm length interferometer, whose physical parameters are defined in the text; the observation frequency is assumed to be the inverse of the GW pulse duration. The types of noise are: a, seismic noise (1 m simple pendulum), b, seismic noise [Del Fabbro et al. 1988b], c, mirror suspension thermal noise, d, mirror first longitudinal mode thermal noise, e, photon counting noise, f, pressure fluctuations in the vacuum pipe (FP), g, quantum limit. H is the resulting interferometer sensitivity assuming the seismic noise to be given by curve b. The expected amplitudes for gravitational collapse [see eq. (1.2)] in the Galaxy ($\eta = 0.1$) and in the Virgo cluster ($\eta = 0.1, 0.01$) are also shown; the amplitudes for coalescing binaries have been evaluated for ($M = 2 M_{\odot}$, $\mu = 0.5$) and ($M = 10 M_{\odot}$, $\mu = 0.1$), integrating over the time given by eq. (1.4).

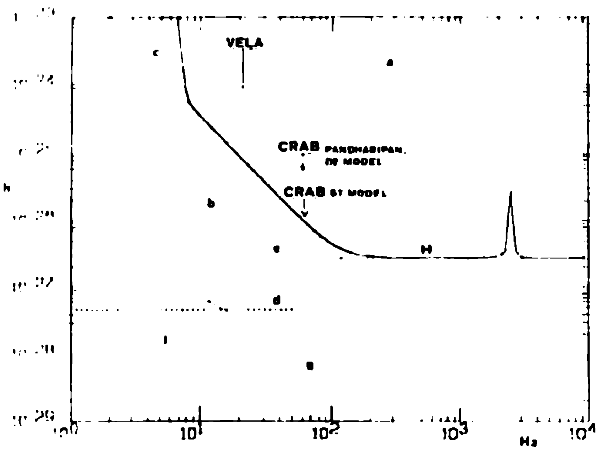

Fig. 14.2. The sensitivity of a 3 km arm length interferometer, whose physical parameters are defined in the text, to periodical GW, assuming a 1 yr integration time. The symbols are explained in the caption to fig. 14.1. The upper limits to the GW amplitudes of the Vela and Crab pulsars [Zimmermann 1978, Pandharipande et al. 1976] are expected to be in the sensitivity range of the interferometer (curve H) if seismic noise is assumed to be given by curve b.

to seismic noise filtered by the attenuator described by Del Fabbro et al. [1988b], line c represents the suspension thermal noise and line d the mirror's first longitudinal normal mode thermal noise, line e represents photon counting noise, line f represents the noise due to vacuum pipe gas fluctuations and line g the quantum limit.

The amplitudes of gravitational collapse have been evaluated using eq. (1.2) assuming the frequency to be the inverse of the collapse duration. The coalescence amplitudes have been evaluated using eq. (1.3) integrated over the time elapsed given by eq. (1.4). The total noise b + c + d + e + f + g is shown by the line H.

The interferometer sensitivity to periodic signals integrated over 1 year is shown in fig. 14.2; the noise symbols are the same as in fig. 14.1. The upper limits to the GW amplitudes emitted by the Vela and Crab pulsars are also shown.

Acknowledgements

I am deeply grateful to A. Brillet, L. Holloway and C. Bradaschia for their careful reading of the manuscript and for important suggestions. I wish to thank N. Galeotti for the accurate typing of the manuscript.

References

Aguirregabiria, J.M. and L. Bel, 1987, Phys. Rev. A 36 3768.
Allega, A.M. and N. Cabibbo, 1983, Lett. Nuovo Cimento 38, 263
Amaldi, E. and G. Pizzella, 1986, Nuovo Cimento 9C, 612.
Araki, H., J. Ehlers, K. Hepp, R. Kippenhahn, H.A. Weidenmüller and J. Zittartz, 1984, in: Gravitation, Geometry and Relativistic Physics, Proc (Aussois, France, 1984), Lecture Notes in Physics, Vol. 212 (Springer, Berlin).
Barone, F., L. Milano, I. Pinto and G. Russo, 1988, Astron. Astrophys. 203, 322.
Bel, L., J-L. Boulanger and N. Deruelle, 1988, Phys. Rev. A 37, 1210.
Berger, J. and J. Levine, 1974, J. Geophys. Res. 79, 8.
Bernard, C., A. De Rújula and B. Lautrup, 1984, Nucl. Phys. B 242, 93
Beron, B.L. and R. Hofstadter, 1969, Phys. Rev. Lett. 23, 184
Billing, H., K. Maischberger, A. Rudiger, R. Schilling, L. Schnupp and W. Winkler, 1979, J. Phys. E 12, 1043-1050.
Billing, H., W. Winkler, A. Rüdiger, R. Schilling, K. Maischberger and L. Schnupp, 1983, The Munich gravitational wave detector using laser interferometry, in: Quantum Optics, Experimental Gravity and Measurement Theory, eds P. Meyestre and M.O. Scully (Plenum, New York)
M. Born and E. Wolf, 1964 Principles of Optics (Pergamon, Oxford).
Bradaschia C., R. Del Fabbro, L. Di Fiore, A. Di Virgilio, A. Giazotto, H. Kautzky, V. Montelatici and D. Passuello, 1989, Phys. Lett. A 137, 329
Braginskii, V.B. and A. Manoukine, 1974, Mesure de Petites Forces dans les Experiences Physiques (Mir, Moscow).
Braginskii, V.B. and M. Menskii, 1971, JEPT Lett. 13, 417.
Braginskii, V.B. and V.N. Rudenko, 1978, Phys. Rep. 46, 165
Braginskii, B.V., L.P. Grishchuk, A.G. Doroshkevich Ya.B. Zel'Dovich, I.D. Novikov and M.V. Sazhin, 1974, Sov. Phys.-JETP 38, 865.
Braginskii, V.B., C.M. Caves and K.S. Thorne, 1977, Phys. Rev. D 15, 2047.
Brillet, A., 1984, The interferometric detection of gravitational waves, in: Gravitation, Geometry and Relativistic Physics, Proc (Aussois, France 1984), Lecture Notes in Physics, Vol 212 (Springer, Berlin)
Brillet, A., 1985, Ann. de Phys. 10, 219–226
Campani, E., A. Giazotto and D. Passuello, 1986, Rev. Sci. Instrum. 57, 79.
Camy, G., D. Pinayd, N. Courtier and Hu Chi Chuan, 1982, Rev. Phys. Appl. 17, 357-363
Caves, C.M., 1980, Phys. Rev. Lett. 45, 75.
Chandrasekhar, S., 1970, Phys. Rev. Lett. 24, 611.
Clark, J.P.A., E.P.J. van den Heuvel and W. Sutantyo, 1979, Astron. Astrophys. 72, 120.
Del Fabbro, R., A. Di Virgilio, A. Giazotto, H. Kautzky, V. Montelatici and D. Passuello, 1987, Phys. Lett. A 124, 253

Del Fabbro, R., A. Di Virgilio, A. Giazotto, H. Kautzky, V. Montelatici and D. Passuello, 1988a, Rev. Sci. Instrum. 59, 292.

Del Fabbro, R., A. Di Virgilio, A. Giazotto, H. Kautzky, V. Montelatici and D. Passuello, 1988b, Phys. Lett. A 132, 237.

Del Fabbro, R., A. Di Virgilio, A. Giazotto, H. Kautzky, V. Montelatici and D. Passuello, 1988c, Phys. Lett. A 133, 471.

Deruelle, N. and P. Tourrenc, 1984, in: Gravitation, Geometry and Relativistic Physics, Proc. (Aussois, France, 1984), Lecture Notes in Physics, Vol. 212 (Springer, Berlin).

Diambrini Palazzi, G. and D. Fargion, 1987, Phys. Lett. B 197, 302.

Dorsel, A., J.D. McCullen, P. Meystre, E. Vignes and H. Walther, 1983, Phys. Rev. Lett. 51, 1550.

Douglass, H.D. and V.B. Braginskii, 1979, in: General Relativity (Cambridge Univ. Press, Cambridge).

Drever, R.W.P., 1981, Gravitational wave detectors using laser interferometers and optical cavities, I. Ideas, principles and prospects, Invited lecture given at Nato Advanced Study Institute on Quantum Optics and General Relativity (Bad Windesheim, Germany).

Drever, R.W.P., 1982, Interferometric detectors for gravitational radiation, in: Gravitational Radiation, Proc. Les Houches Summer Institute, eds T. Piran and N. Deruelle.

Drever, R.W.P., G.M. Ford, J. Hough, I.M. Kerr, A.J. Munley, J.R. Pugh, N.A. Robertson and H. Ward, 1980, in: Proc. Ninth Intern. Conf. on General Relativity and Gravitation (Jena, 1980), ed. E. Schmutzer (Deutscher Verlag der Wissenschaften, Berlin).

Drever, R.W.P., J. Hough, A.J. Munley, S.A. Lee, R. Spero, S.E. Whitcomb, H. Ward, G.M. Ford, M. Hereld, N.A. Robertson, I. Kerr, J.R. Pugh, G.P. Newton, B. Meers, E.D. Brooks III and Y. Gursel, 1981, Optical cavity laser interferometers for gravitational wave detection, in: Laser Spectroscopy V, eds A.R.W. McKellar, T. Oka and B.P. Stoicheff (Springer, Berlin).

Drever, R.W.P., J.L. Hall, F.V. Kowalski, J. Hough, G.M. Ford, A.J. Munley and H. Ward, 1983, Appl. Phys. B 31, 97–105.

Edelstein, W.A., J. Hough, J.R. Pugh and W. Martin, 1978, J. Phys. E 11, 710.

Einstein, A., 1916, Preuss. Akad. Wiss. Berlin, Sitzungsber. Phys. Math. Kl., 688.

Faller, J.E. and R.L. Rinker, 1979, Super Spring, Dimensions, September, p. 25.

Faller, J.E., P.L. Bender and R.T. Stebbins, 1987, The development of very low frequency isolation systems for ground-based gravitational wave interferometers, NSF Grant No. Phy 87 12072.

Fattaccioli, D., A. Boulharts, A. Brillet and C.N. Man, 1986, J. Opt. (Paris) 17, No. 3, 115–128.

Forward, R.L., 1978, Phys. Rev. D 17, 379.

Forward, R.L., 1979, J. Appl. Phys. 50, No. 1, 1–6.

Friedman, J.L. and B.F. Schutz, 1978, Astrophys. J. 222, 345.

Gea-Banacloche, J. and G. Leuchs, 1987, J. Mod. Optics 34, 793.

Gersenshtein, M.E. and V.I. Pustovoit, 1963, Sov. Phys. – JETP 16, 433.

Giazotto, A., 1987, The seismic noise challenge to the detection of low frequency gravitational waves, in: 7th Congr. of General Relativity and Gravitational Physics (Rapallo, Italy, 1986) (World Scientific, Singapore) p. 449.

Giazotto, A., 1988a, The VIRGO project: a wide band antenna for gravitational wave detection, in: Proc. VIII Convegno Nazionale di Relatività Generale e Fisica della Gravitazione (Cavalese).

Giazotto, A., 1988b, Phys. Lett. A 128, 241.

Giazotto, A., E. Campani, D. Passuello and A. Stefanini, 1986a, Performance of an active pendulum with interferometric sensing, in: Proc. Fourth Marcel Grossman Meeting on the Recent Developments of General Relativity (Rome, 1985), ed. R. Ruffini (Elsevier Sci. Publ., Amsterdam).

Giazotto, A., D. Passuello and A. Stefanini, 1986b, Rev. Sci. Instrum. 57, 1145.

Gold, T., 1968, Nature 218, 731.

Goorvitch, D., 1975, Appl. Opt. 14, 1387–1390.

Grassi Strini, A.M., G. Strini and G. Tagliaferri, 1980, J. Appl. Phys. 51, 849.

Hall, J.L., H.P. Layer and R.D. Deslattes, 1977, IEEE J. Quantum Electron. QE-13, 45–46D.

Hernandez, G., 1986, Fabry Perot Interferometer (Cambridge Univ. Press, Cambridge).

Herriott, D., H. Kogelnik and R. Kompfner, 1964, Appl. Opt. 3, 523–526.

Hough, J., 1987, Report on round table discussion – gravitational wave detectors, in: Proc. NATO Advanced Research Workshop on Gravitational Wave Data Analysis (Cardiff, 1987).

Hough, J., R.W.P. Drever, A.J. Munley, S.-A. Lee, R. Spero, S.E. Whitcomb, H. Ward, G.M. Ford, M. Hereld, N.A. Robertson, I. Kerr, J.R. Pugh, G.P. Newton, B. Meers, E.D. Brooks III, Y. Gursel, 1983, Gravitational wave detectors using laser interferometers and optical cavities: some practical aspects and results, in: Quantum Optics, Experimental Gravity and Measurement Theory, eds P. Meyestre and M.O. Scully (Plenum, New York).

Hough, J., D. Hils, M.D. Rayman, L.-S. Ma, L. Hollberg and J.L. Hall, 1984, Appl. Phys. B 33, 179–185.

Hough, J., B.J. Meers, G.P. Newton, N.A. Robertson, H. Ward, B.F. Schutz, R.W.P. Drever, R. Mason, C. Pollard, R. Tolcher, D.W. Bellenger, J.R.J. Bennett, I.F. Corbett and M.D. Percival, 1986, A British long baseline gravitational wave observatory, GWD-RAL 86-001.

Hough, J., B.J. Meers, H.P. Newton, N.A. Robertson, H. Ward, B.F. Schutz, I.F. Corbett and R.W.P. Drever, 1987, Vistas Astron. 30, 109–134.

Kerr, G.A., N.A. Robertson, J. Hough and C.N. Man, 1985, Appl. Phys. B 37, 11–16.

Kojima, Y. and T. Nakamusa, 1984, Prosp. Theor. Phys. 71, 79.

Kuroda, K., K. Tsubono and H. Hirakawa, 1982, Phys. Lett. 92A, 131.

Landau, L. and E. Lifshitz, 1951, The Classical Theory of Fields (Pergamon, New York).

Leuchs, G., K. Maischberger, A. Rudiger, R. Schilling, L. Schnupp and W. Winkler, 1987, Proposal for the construction of a large laser interferometer for the measurement of gravitational waves, MPO 129 and MPO 131.

Linet, B. and P. Tourrenc, 1976, Can. J. Phys. 34, 1129–1133.
Linsay, P. and D. Shoemaker, 1982, Rev. Sci. Instrum. 53, 1014.
Livas, J., R. Benford, D. Dewey, A. Jeffries, P. Linsay, P. Saulson, D. Shoemaker and R. Weiss, 1986, The MIT prototype gravitational wave detector, in: Proc. Fourth Marcel Grossmann Meeting on the Recent Developments of General Relativity (Rome, 1985), ed. R. Ruffini (Elsevier Sci. Publ., Amsterdam).
Lorenzini, D.A., 1972, Active control of a pneumatic isolation system, in: Proc. AIAA Guidance and Control Conf. (Stanford, CA, 1972), Paper No. 72-843.
Lyne, A.G., R.N. Manchester and H.J. Taylor, 1985, Mon. Not. R. Astron. Soc. 213, 613.
Maischberger, K., A. Rüdiger, R. Schilling, L. Schnupp, W. Winkler and H. Billing, 1979, Noise investigation in a laser interferometer for the detection of gravitational radiation, presented by A. Rüdiger at Second Marcel Grossmann Meeting on the Recent Developments of General Relativity (Trieste, Italy, 1979).
Man, C.N., 1988, External modulation and recyclings, at: European Collaboration Meeting on Interferometric Detection of GW (Sorrento, 1988).
Man, C.N., A. Brillet and D.S. Shoemaker, 1986, at: European Collaboration Meeting on Large Interferometers (Chantilly, 1986).
Man, C.N., A. Brillet and D.S. Shoemaker, 1987, Gravitational wave data analysis, at: Nato Workshop (Cardiff, 1987).
Manchester, R.N. and J.H. Taylor, 1981, Astron. J. 86, 1953.
Meers, B.J., 1983, Opt. Commun. 47, 237.
Meers, B.J., 1988, Phys. Rev. D 38, 2317.
Meystre, P., E.M. Wright, J.D. McCullen and E. Vignes, 1985, J. Opt. Soc. Am. B 2, 1830.
Misner, C.W., K.S. Thorne and J. Wheeler, 1973, Gravitation (Freeman, San Francisco) (cited in the text as MTW).
Newton, G.P., J. Hough, G.A. Kerr, B.J. Meers, N.A. Robertson, H. Ward, J.B. Mangan, S. Hoggan and R.W.P. Drever, 1986, Some improvements to the Glasgow gravitational wave detector, in: Proc. Fourth Marcel Grossmann Meeting on the Recent Developments of General Relativity (Rome, 1985), ed. R. Ruffini (Elsevier Sci. Publ., Amsterdam).
Pacini, F., 1968, Nature 219, 145.
Pandharipande, V.R., D. Pines and R.A. Smith, 1976, Astrophys. J. 208, 550.
Paris, Orsay, Pisa, Napoli, Frascati Collab., 1988, VIRGO project: a progress report, presented to Fifth Marcel Grossmann Meeting (Perth, Australia, 1988), INFN PI/AE 88/10.
Pegoraro, F., E. Picasso and L.A. Radicati, 1978, J. Phys. A 11, 1949.
Pisa, Napoli, Frascati, Orsay, Paris Collab., 1987, VIRGO project, INFN PI/AE 87/1.
Pizzella, G., 1975, Riv. Nuovo Cimento 5, No. 3.
Rawley, L.A., J.H. Taylor and M.M. Davis, 1986, Nature 319, 383.
Ricci, F., 1987, Nucl. Instrum. Methods Phys. Res. A 260, 491–500.
Robertson, N.A., R.W.P. Drever, I. Kerr and J. Hough, 1982, J. Phys. E 15, 1101–1105.
Rudiger, A., 1988, private communication.
Rüdiger, A., R. Schilling, L. Schnupp, W. Winkler, H. Billing and K. Maischberger, 1981a, Opt. Acta 28, 641–658.
Rüdiger, A., R. Schilling, L. Schnupp, W. Winkler, H. Billing and K. Maischberger, 1981b, J. de Phys. 42, C8-451.
Rüdiger, A., R. Schilling, L. Schnupp, D. Shoemaker, W. Winkler, G. Leuchs and K. Maischberger, 1987, The Garching 30-meter prototype and plans for a large gravitational wave detector, in: Proc. 18th Texas Symp. on Relativistic Astrophysics (Chicago 1986), ed. M.P. Ulmer (World Scientific, Singapore).
Ruggiero, F., 1979, Alcuni problemi relativi alla rivelazione delle onde gravitazionali, Thesis, Pisa Univ., unpublished.
Saulson, P.R., 1984a, Phys. Rev. D 30, 732.
Saulson, P.R., 1984b, Rev. Sci. Instrum. 55, 1315.
Schilling, R., L. Schnupp, W. Winkler, H. Billing, K. Maischberger and A. Rüdiger, 1981, J. Phys. E 14, 65.
Schilling, R., L. Schnupp, D.H. Shoemaker, W. Winkler, H. Billing, K. Maischberger and A. Rüdiger, 1984, Improved sensitivities in laser interferometers for the detection of gravitational waves, in: Gravitation, Geometry and Relativistic Physics, Proc. (Aussois, France, 1984), Lecture Notes in Physics, Vol. 212 (Springer, Berlin).
Schnupp, L., W. Winkler, K. Maischberger, A. Rüdiger and R. Schilling, 1985, J. Phys. E 18, 482.
Shoemaker, D., 1987, Contributions à l'etude de la detection interferometrique des ondes de gravitation, Thesis, Univ. Paris XI.
Shoemaker, D., W. Winkler, K. Maischberger, A. Rüdiger, R. Schilling and L. Schnupp, 1985, Progress with the Garching 30-meter prototype for a gravitational wave detector, MPQ 100.
Shoemaker, D., R. Schilling, L. Schnupp, W. Winkler, K. Maischberger and A. Rüdiger, 1987a, Noise behavior of the Garching 30 meter prototype gravitational wave detector, MPQ 130.
Shoemaker, D.S., A. Brillet and C.N. Man, 1987b, Wide bandwidth frequency and power stabilization of a laser-diode-pumped Nd:YAG laser, in Proc. Conf. on Lasers and Electro-Optics, Vol. 14 (Opt. Soc. Am.).
Shoemaker, D.S., A. Brillet, C.N. Man, O. Crégut and G. Kerr, 1989, A frequency-stabilized laser-diode pumped Nd:YAG laser, Opt. Lett., in press.
Spero, R., 1986, The Caltech laser-interferometric gravitational wave detector, in: Proc. Fourth Marcel Grossmann Meeting on the Recent Developments of General Relativity (Rome, 1985), ed. R. Ruffini (Elsevier Sci. Publ., Amsterdam).
Taylor, J.H. and R.N. Manchester, 1977, Astrophys. J. 215, 885.
Thorne, K.S., 1980, Rev. Mod. Phys. 52, 285.

Thorne, K.S., 1987, in: Three Hundred Years of Gravitation (Cambridge Univ. Press, Cambridge).
Thorne, K.S., 1989, Light Scattering and Proposed Baffle Configuration for the LIGO-GRP 200 (Caltech).
Tourrenc, P. and N. Deruelle, 1985, Ann. de Phys. 10, 241–252.
Uhlenbeck, G.E. and L.S. Ornstein, 1930, Phys. Rev. 36, 823.
Vinet, J-Y., 1981, Nuovo Cimento 64A, 163.
Vinet, J-Y., 1986, J. de Phys. 47, 639–643.
Vinet, J-Y., B. Meers, C.N. Man and A. Brillet, 1988, Phys. Rev. D 38, 433–447.
Wagoner, R.V., 1984, Astrophys. J. 278, 345.
Ward, H., J. Hough, G.A. Kerr, N.L. Mackenzie, J.B. Mangan, B.J. Meers, G.P. Newton, D.I. Robertson and N.A. Robertson, 1987, The Glasgow gravitational wave detector – present progress and future plans, in: Proc. Intern. Symp. on Experimental Gravitational Physics (Guangzhou, China, 1987).
Weiss, R., 1972, Quart. Progr. Rep. Res. Lab. Electron. MIT 105, 54.
Weiss, R., 1979, in: Sources of Gravitational Radiation, ed. L.L. Smarr (Cambridge Univ. Press, Cambridge).
Winker, W., 1977, Experimental gravitation (Atti dei Convegni Lincei).
Zimmermann, M., 1978, Nature 271, 525.
Zimmermann, M., 1980, Phys. Rev. D 21, 891.
Zimmermann, M. and E. Szedenits Jr, 1979, Phys. Rev. D 20, 351.

ESTIMATE OF THE COSMIC RAY BACKGROUND IN AN INTERFEROMETRIC ANTENNA FOR GRAVITATIONAL WAVE DETECTION

Adalberto GIAZOTTO
INFN, Sez. di Pisa, Pisa, Italy

Received 5 October 1987; revised manuscript received 4 December 1987; accepted for publication 8 February 1988
Communicated by J.P. Vigier

The effect of the cosmic ray interaction in the test masses of an interferometric antenna for gravitational wave (GW) detection is evaluated. In a 3 km antenna this background, mainly due to muons gives a limit, for 1 ms GW pulses, of $h\sim 8.5\times 10^{-23}$ with a frequency of 2×10^{-1} events/year and 8.5×10^{-26} with 4.1×10^{6} events/year. For periodic GW having frequency > 10 Hz the sensitivity limit is $h\sim 1.7\times 10^{-31}$. This background seems to allow unshielded operation of the interferometer test masses.

It has been experimentally shown [1] that charged particles traversing an aluminum rod can create mechanical vibrations whose fundamental mode has amplitude

$$\xi(x)=\frac{\alpha}{C_v}\frac{EL}{M}\frac{2}{\pi}\cos(\pi x/L)\,, \tag{1}$$

where E is the energy lost by the particle in the bar, α the thermal linear expansion coefficient, C_v the specific heat at constant volume, L and M are the bar length and mass respectively and x ($|x|<L/2$) the distance of the particle hit point from the bar center. Amaldi and Pizzella [2] have shown that cosmic rays can create in a high sensitivity aluminum bar antenna for gravitational waves (GW) detection signals such as to require underground operation. It is then important to examine the effect of this background on the phase of a large base interferometric antenna [3]. Let us consider a cosmic ray hitting one of the interferometers mirrors at an angle θ (see fig. 1). From the energy–momentum conservation follows:

$$\boldsymbol{P}_M=\boldsymbol{P},\quad E_t\approx E\,, \tag{2}$$

where E, $\boldsymbol{P}$ are the cosmic ray energy momentum lost in the mirrors, $\boldsymbol{P}_M$ is the mirror CMS momentum in

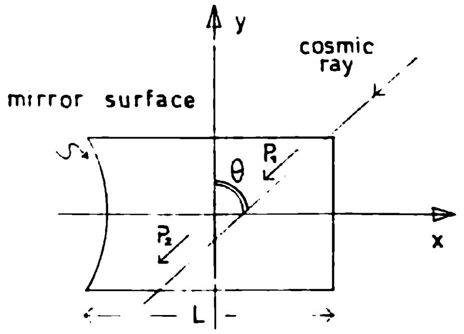

Fig. 1. The mirror section with a traversing cosmic ray losing the total momentum P_1+P_2. The momenta difference P_1-P_2 excites the mirror's resonance modes.

the laboratory system, M the mirror mass, E, the energy inelastically released to the mirror by the cosmic ray. In the second equation the rod CMS and vibrational kinetic energies have been neglected.

If P_1 and P_2 are the momenta lost in the mirror for $x>0$ and $x<0$ respectively, it follows that the mirror first longitudinal mode is excited by the momentum

$$\Delta P_x = \left(\frac{P_1 - P_2}{2}\right)_x . \tag{3}$$

For the sake of simplicity we can consider the mirror to be a simple harmonic oscillator, composed by a spring of stiffness $K/2$ and two masses $M/2$, having circular frequency $\omega_0 = \sqrt{K/M}$ and suspended in its CMS by means of a wire, whose pendular circular frequency is ω_p. The mirror surface displacement Δx due to the cosmic ray interaction is

$$\Delta x = \xi(x) \exp[-(t-t_n)/\tau_0] \sin[\omega_0(t-t_n)]\theta(t-t_n) + \frac{1}{M\omega_0}\int_0^t \exp[-(t-\eta)/\tau_0] \sin[\omega_0(t-\eta)]F_1(\eta)\, d\eta$$

$$+ \frac{1}{M\omega_p}\int_0^t \exp[-(t-\eta)/\tau_p] \sin[\omega_p(t-\eta)]F_2(\eta)\, d\eta , \tag{4}$$

where F_1 and F_2 are the impulsive forces

$$F_1 = \Delta P_x \delta(t-t_n), \quad F_2 = (P_M)_x \delta(t-t_n) . \tag{5}$$

and t_n is the cosmic ray arrival time.

We can maximize Δx putting $\Delta P_x \sim (P_M)_x \sim E/c$ (c is the speed of light) and $x=0$; with these conditions from eqs. (4) and (5) we obtain

$$\Delta x \leqslant \left[\left(\xi(0) + \frac{E}{Mc\omega_0}\right) \exp[-(t-t_n)/\tau_0] \sin[\omega_0(t-t_n)]\right.$$

$$\left. + \frac{E}{Mc\omega_p} \exp[-(t-t_n)/\tau_p] \sin[\omega_p(t-t_n)]\right][\theta(t-t_n)] . \tag{6}$$

The Δx Fourier transform, in the approximation $\omega_p\tau_p \gg 1$, and $\omega_0\tau_0 \gg 1$, is

$$\Delta x(\Omega, t_n) \leq E \exp(i\Omega t_n)\left[\left(\frac{2\alpha L\omega_0}{C_v M\pi} + \frac{1}{cM}\right)\frac{1}{-\Omega^2 + 2i\Omega/\tau_0 + \omega_0^2} + \frac{1}{cM}\,\frac{1}{-\Omega^2 + 2i\Omega/\tau_p + \omega_p^2}\right] . \tag{7}$$

For a quartz mirror having [3] $M=400$ kg, $L=0.6$ m, $\alpha/C_v = 7\times 10^{-10}$ kg °C/J, $\nu_0 = \omega_0/2\pi = 5\times 10^3$ Hz, $\nu_p = \omega_p/2\pi = 0.5$ Hz, eq. (6) gives

$$\Delta x(\Omega, t_n) = \exp(i\Omega t_n) E\left(\frac{3\times 10^{-8}}{-\Omega^2 + 2i\Omega/\tau_0 + \omega_0^2}\;\frac{8\times 10^{-12}}{-\Omega^2 + 2i\Omega/\tau_p + \omega_p^2}\right) . \tag{8}$$

Since eq. (8) has poles for $\Omega = \omega_0$ and $\Omega = \omega_p$ we limit the frequency interval to the region $\omega_p < \Omega < \omega_0$; however this is not a relevant limitation due to the high value of ν_0. Two experimental conditions are particularly important; the search for GW impulsive and periodical signals.

For the first case we can compared the Fourier transform $S(\Omega)$ of the mirror displacement produced by an impulsive GW signal having time length Δt, with $\Delta x(\Omega, t_n)$.

For $\Omega < 1/\Delta t$, $|S(\Omega)|$ becomes

$$|S(\Omega)| \approx h\frac{A}{2}\Delta t . \tag{9}$$

where A is the interferometer arm length and h the GW amplitude.

The measurability condition for h is

$$h > \frac{2E}{A\,\Delta t}\left(\frac{3\times10^{-8}}{\omega_0^2}+\frac{8\times10^{-12}}{\Omega^2}\right), \quad \omega_p < \Omega < \omega_0 . \tag{10}$$

We can choose a frequency, such that the GW impulse area is only slightly reduced, for example $\Omega = 1/10\Delta t$; with this value h becomes

$$h > 1.6\times10^{-9} E\,\frac{\Delta t}{A} . \tag{11}$$

Assuming $A = 3\times10^{3}$ m, $\Delta t = 10^{-3}$ s, we obtain

$$h > 8.5\times10^{-26} E_{\mathrm{GeV}} , \tag{12}$$

where E_{GeV} is E measured in GeV. Eq. (12) shows that a cosmic ray event giving in the antenna pulses comparable with those expected by the Virgo Cluster ($h \sim 10^{-21}$), should release 10^4 GeV. These events are mainly produced by muons [2] releasing into the mirrors almost entirely their incident energy by means of four processes: knock-on electrons [4], bremsstrahlung [5], direct pair production [4] and photo nuclear interaction [6].

The number N of events per second which deposit into the mirror an energy $> E$ is evaluated by means of the double integral:

$$N \approx \frac{\rho N_a S L}{\sum_i A_i} \sum_j \int_{\varepsilon}^{\infty} \mathrm{d}W \int_{E_j(W)}^{\infty} \frac{\mathrm{d}I(E_\mu)}{\mathrm{d}E_\mu}\,\frac{\mathrm{d}\sigma_j(Z_i, W, E_\mu)}{\mathrm{d}W}\,\mathrm{d}E_\mu . \tag{13}$$

where $\rho = 2.2\times10^{3}$ kg/m^3 is the mirror density, N_a the Avogadro number, $S \sim 3.6\times10^{-1}$ m^2 the mirror projected area, A_i and Z_i are the atomic weight and number of the ith atomic component of the mirror, σ_j is the cross section of the jth process. W and E_μ are the deposited and the incident muon energies respectively, $E_j(W)$ is the minimum muon energy necessary to release the energy W by means of the jth process and $\mathrm{d}I(E_\mu)/\mathrm{d}E_\mu$ is the muon differential intensity spectrum at sea level [7] integrated over the solid angle.

In table 1 the sensitivity limits on h for 1 ms pulses for a few relevant values of E_{GeV} together with N(ev/s) and N_y (ev/year) are given. For periodical GW of circular frequency $\Omega_g = 2\pi\nu_g$, $|S(\Omega)|$ becomes

$$|S(\Omega_g)| = h\,\frac{A}{2}\,T , \tag{14}$$

where T is the measurement time. Comparing eq. (13) with eq. (8) we obtain the measurability condition

$$h > \frac{2}{AT}\left(\frac{3\times10^{-8}}{\omega_0^2}+\frac{8\times10^{-12}}{\Omega_g^2}\right)\left|\sum_n \exp(\mathrm{i}\Omega t_n)\,W_n\right| , \quad \omega_p < \Omega_g < \omega_0 . \tag{15}$$

Table 1

E_{GeV}	h (1ms pulses)	N (ev/s)	N_y (ev/year)
1	8.5×10^{-26}	1.4×10^{-1}	4.1×10^{6}
10	8.5×10^{-25}	1.9×10^{-3}	5.7×10^{4}
10^{2}	8.5×10^{-24}	7.2×10^{-6}	2.3×10^{2}
10^{3}	8.5×10^{-23}	$7\ \times10^{-9}$	$2\ \times10^{-1}$
10^{4}	8.5×10^{-22}	$7\ \times10^{-14}$	$2\ \times10^{-6}$

where W_n is the energy of the nth cosmic ray and $\sum_n$ is extended to cosmic ray events having $0<t_n<T$. Since t_n is a random variable we obtain

$$U^2=\left|\sum_n \exp(\mathrm{i}\Omega t_n)\,W_n\right|^2=\sum_i W_i^2\Delta n_i\,, \tag{16}$$

where Δn_i is the number of cosmic ray events having energy between W_i and W_{i+1}. Substituting the sum with the integral we obtain

$$U^2=\int_{W_1}^{\infty} W^2\frac{\mathrm{d}n(W)}{\mathrm{d}W}\,\mathrm{d}W=\frac{\rho N_A SLT}{\sum_i A_i}\sum_i\int_{W_1}^{\infty}W^2\,\mathrm{d}W\int_{E_i(W)}^{\infty}\frac{\mathrm{d}J(E_\mu)}{\mathrm{d}E_\mu}\,\frac{\mathrm{d}\sigma_i(Z_i,W,E_\mu)}{\mathrm{d}W}\,\mathrm{d}E_\mu\,, \tag{17}$$

where W_1 is a low energy cut off that we have assumed to be equal to the total ionization energy loss in the mirror due to minimum ionizing particles i.e. $E_1\sim0.26$ GeV. This choice is justified by the fact that energy losses lower than W_1 are taken into account by the ionization losses.

A numerical computation of eq. (17) gives $U=1.3\times10^{-6}$ J for $T=3\times10^7$ s; with this value we obtain from eq. (15)

$$h>\frac{2}{AT}\left(\frac{3\times10^{-8}}{\omega_0^2}+\frac{8\times10^{-12}}{\Omega_g^2}\right)U=0.6\times10^{-31}\,. \tag{18}$$

where we have assumed $\nu_g=10$ Hz.

The ionization losses can be evaluated putting in eq. (16) $W_i=E_1$; since the charged cosmic ray flux at sea level is [8] $I_c=2.4\times10^2\ (\mathrm{m}^2\,\mathrm{s})^{-1}$ we obtain, assuming $T=3\times10^7$ s, $U=2.2\times10^{-6}$ J. With this value, eq. (15) evaluated at $\nu_g=10$ Hz, gives

$$h>1.1\times10^{-31}\,. \tag{19}$$

The sum of eqs. (18) and (19) gives, for periodic GW having $\nu_g>10$ Hz, the limit $h>1.7\times10^{-31}$, well below the sensitivity of the future interferometric antennas.

I am very grateful to G. Pizzella for having raised the problem, and to L. Bracci for illuminating discussions

References

[1] A.M. Grassi Strini, G. Strini and G. Tagliaferri, J. Appl. Phys. 51 (1980) 948.
[2] E. Amaldi and G. Pizzella, Nuovo Cimento 9 (1986) 612;
F. Ricci, Nucl. Instrum. Methods A 260 (1987) 491.
[3] Antenna Interferometrica a grande base per la rivelazione di onde gravitazionali, Italian–French Collaboration. INFN PI/AE 87/1, Pisa, 12 May 1987.
[4] B. Rossi, High energy particles (Prentice-Hall, Englewood Cliffs, 1952).
[5] A.A. Petrukhin and V.V. Shestakov, Can. J. Phys. 46 (1968) S377.
[6] L.B. Bezrukov and E. Bugaev, Sov. J. Nucl. Phys. 33 (1981) 635.
[7] O.C. Allkofer and P.K.F. Grieder, Physics data, Fachinformationszentrum Energie-Physik-Matematik GMBH Karlsruhe, ISSN 0344-8407, No. 25-1 (1984).
[8] Particle Data Group, M. Roos et al., Review of particle properties, Phys. Lett. B 111 (1982) 1.

socomin impianti s.r.l.
progettazione costruzione montaggio impianti industriali

Ceccano 17/05/89

Ns./rif. 133/OF/mf

Vs./rif.

Spett.le

I.N.F.N.
Istituto Nazionale di Fisica Nucleare

Sezione di PISA

All'attenzione del Dr. Prof. Adalberto GIAZZOTTO

Oggetto: - Progetto VIRGO

La presente quotazione è accompagnata da una sommaria descrione delle opere per quanto possibile quantizzate.

Le fasi di lavoro e le specifiche tecniche Vi verranno inviate tra qualche tempo dopo aver con Voi chiarito alcuni elementi che in linea di massima non dovrebbero alterare i costi di seguito indicati.

Dalla presente offerta, per mancanza di elementi di valutazione, sono state escluse alcune forniture e cioè:

- Tutte le pompe a vuoto
- Le valvole
- Gli specchi
- Gli apparecchi di esperimento (Laser ecc.)
- Il baking
- Le cabine di trasformazione elettriche (solo parte edile.
- Le camere sterili ubicate nei fabbricati Centrale e terminali al di sotto dei serbatoi a vuoto.

%

03023 CECCANO (FR)
Sede e Stabilimento
S.S. 156 Km. 6 - Loc. Colle S. Paolo
Telefoni 0775/641481 - 641482

Cap. soc. 90.000.000 int. vers.
P.I. e C.F. n. 01475120604
Trib. Frosinone 3859
C.C.I.A.A. Frosinone 82628

PROGETTO VIRGO

- Descrizione delle opere e valutazione economica aggiornata alla data del 16/05/1989.

A - OPERE EDILI

A1 - Strada - E' prevista una strada in terra battuta e massicciata in misto di cava, per una larghezza di mt. 3 e di una lunghezza pari alla lunghezza della tubazione Ø 1000, cioè in due tratte da mt. 3000 che collegano le palazzine terminali con quella centrale.

Ogni 144 mt., in corrispondenza con le cabine delle pompe a vuoto detta strada verrà allargata di ulteriori 3 mt. per una lunghezza di mt. 15, in modo da creare delle piazzole di lavoro e scorrimento.

Non è previsto in questa fase il manto di asfalto.

I lavori da eseguire sono:

Sbancamento del terreno per una profondità di mt. 0,50 per un totale di mc. 9000 circa, e spargimento del terreno tolto nell'area circostante.

Riempimento con breccia di cave per un'altezza di mt. 0,5 per un totale di mc. 9000 circa e successiva rullatura.

Importo £. 228.000.000=

A2 - Pavimento appoggio tubo Ø 1000 - E' prevista una pavimentazione continua (con giunti di dilatazione) in calcestruzzo della larghezza di mt. 2,5 di uno spessore di mt. 0,30, e una lunghezza pari alla lunghezza delle tubazioni Ø 1000 cioè in due tratte da mt. 3000 cadauna.

Il massetto di calcestruzzo è armato con doppia rete metallica di spessore adeguato.

%

I lavori da eseguire sono:

- Sbancamento del terreno per una profondità di mt. 0,50 per un totale di mc. 9000, e spargimento del terreno di risulta nell'area circostante.
- Riempimento con breccia di cava per un'altezza di mt. 0,5 per un totale di mc. 9000.
- Rilevato con stabilizzato per un'altezza di mt. 0,10 per un totale di mq. 18000 e rullatura.
- Pavimento in calcestruzzo per un'altezza di mt. 0,30 con interposte n° 2 reti metalliche con filo Ø mm. 2,5 per un totale di cemento di mc. 4500 ed un peso di rete di Kg. 73.000.

Importo £. 1.400.000.000=

A3 - Costruzioni - Fabbricato centrale - mt. 20x20x15 di altezza - N° 1
Fabbricato terminale- mt. 15x15x15 di altezza - N° 2
Cabine pompe vuoto - mt. 2x 2x 2 di altezza - N°44

I fabbricati sono previsti in cemento armato con pareti, pilastri e copertura in elementi prefabbricati.

I pannelli di tamponatura spessore 20 cm.

I solai di copertura sono c.a.p. estruso di spessore 15 cm.

Copertura coibentata con materassini di lana di roccia dello spessore di cm. 4 poste al di sotto del manto impermeabilizzante in lastre piane nervate di cemento - amianto.

Pilastri con mensole per carroponte.

Portoni, porte o finestre occorrenti, in metallo.

Pavimento del tipo industriale.

%

4 Rif. 133/OF/mf

Le cabine per pompe a vuoto sono previste con pareti in blocchi di cemento o prefabbricate, copertura in solaio prefabbricate, pavimento in cemento in proseguimento di quello di appoggio del tubo.

Porta di accesso metallica.

Nei fabbricati sono previsti:

n° 1 carroponte da 5 tonn. ogni fabbricato totale n° 3

Impianti di riscaldamento e condiz. " 3

Impianti idraulici e serv.sanitari " 3

E' prevista la sistemazione a breccia rullata del perimetro dei fabbricati per un'ampiezza media di mq. 3600 cad.

Importo £. 2.617.000.000=

A4 - Copertura tubo Ø 1000 - E' prevista la copertura con archi in lamiera di Fe ondulata dello spessore di mm. 3 (Vedi disegno), costituita da 3 - Sezioni ogni metro lineare da assemblare in opera a mezzo bullonatura.

Lunghezza totale da coprire mt. 6000, lunghezza totale della copertura comprese le sovrapposizioni mt. 7200.

La base dell'arco è di mt. 2,18, mentre l'altezza è di mt. 1,90.

Il peso totale stimato è di circa Kg. 1.100.000=

Importo £. 2.580.000.000=

B - OPERE MECCANICHE

B1 - Tubo Ø 1000 - Materiale AISI 304 L - Spessore mm. 3 - Ø nominale mm. 1000 Ø interno mm.
Lunghezza mt. 3000 + 3000 = totale 6000 mt.

stesso prezzo per rinforzi fatti con tubo a spirale per eventuale backing

Il tubo verrà costruito in officina in tratte da mt. 12, ogni 6 barre da 12 mt. ve ne saranno n° 2 flangiate.

All'esterno del tubo sono previsti anelli di irrigidimento in ferro piatto spessore mm. 10 per larghezza mm. 100, messi di taglio e saldati al tubo. Lunghezza della tratta tra gli estremi flangiati mt. 72.

Peso del tubo Kg. 456.000 circa.

Peso delle cerchiature esterne Kg. 153.000 circa.

il tubo include bocchelli per eventuali diaframmi asismicizzati

Gli staffaggi di appoggio sono previsti ogni mt. 6 per un totale di circa Kg. 172.000=

Lo scorrimento del tubo per effetto della dilatazione è assicurato da rulli in gomma o similari per un totale di n° 3000 circa.

Nel punto di contatto dei rulli con il tubo è previsto un irrigidimento esterno dello stesso con una fascia di lamiera in Fe saldata a tratti.

il prezzo include 88 diaframmi a doppio cono in inox lucidato a specchio

Ogni 144 metri sono previsti dei pezzi speciali a T flangiati per l'inserimento delle pompe a vuoto con stacchi Ø 450 ed alle estremità, saldati o flangiati, n° 2 giunti di dilatazione ad onde in AISI 304 L Ø 1000.

- Lo spessore dei pezzi speciali a T è di mm. 6+8
- Pezzi speciali a T n° 4 per Kg. 22000 circa
- Giunti di dilatazione n° 88
- Saldature sul posto Ø 1000 n° 420.

Importo £. 10.780.000.000=

%

B2 - Serbatoio a vuoto - Materiale AISI 304L - spess. mm. 6 Ø mm. 2000 - H mm. 7860

- Contenitore a vuoto per apparecchiature cilindrico verticale con fondi bombati, e fondo inferiore flangiato, bocchelli e passi d'uomo come da Vs/disegni.

Irrigidimenti esterni in Fe.

Puntoni in carpenteria in Fe - di sostegno n° 4 cadauno.

Pezzi n° 6

- Apparecchiatura interna in AISI 304L comprese carpenterie di sostegno.

Il tutto secondo Vs/indicazioni, disegni ed esemplari già esistenti. Esclusi soffietti ammortizzanti.

- Escluse camere sterili.

Il tutto quanto sopra in opera.

Importo £. 1.040.000.000=

B3 - Impianti elettrici - La valutazione è stata fatta senza reali dati pertanto è supposto quanto segue.

n° 1 Cabina di trasformazione - da alta a media tensione

n° 1 Cabina di trasformazione - da media a bassa tensione

n° 1 Quadro di Cabina

n° 1 Quadro per utenze a fabbricato centrale

n° 1 Quadro per utenze di 2 fabbricati estremi

n° 44 Quadri per pompe a vuoto

n° 3 Quadri per macchinari di condizionamento

n° 77 Alimentazioni delle pompe a vuoto

n° 3 Distribuzioni nei fabbricati per FM e illuminazioni

n° 3 Distribuzioni nei fabbricati per FM condizionamento

n° 2 Linee da mt. 3000 cad. per alimentazione pompe vuoto.

Linea messa a terra.

Linea interfonica tra i fabbricati.
Illuminazione esterna delle aree esterne dei fabbricati.

Allarmi e segnali di ritorno dalle cabine pompe.

Illuminazione delle 44 cabine pompe.

Importo stimato £. 1.950.000.000=

B4 - Montaggi - Montaggio tubo Ø 1000 - mt 6000 - kg. 600.000 circa
- " n° 77 pompe a vuoto
- " n° 1000staffaggi
- " n° 3000rulli di scorrimento
- " n° 44 pezzi speciali o T
- " n° 88 compensatori di dilatazione
- " n° 3 Impianti di condizionamento
- " n° 3 Impianti servizi generali
- Lavaggio decapaggio n° 84 tratte da 72 mt. cad.
- Prova di tenuta di n° 84 tratte da 72 mt. cad.

Importo £. 2.590.000.000=

8 Rif. 133/OF/mf

RIEPILOGO

A - OPERE EDILI

A1 -	Strade	228.000.000=	
A2 -	Pavimento tubo	1.400.000.000=	
A3 -	Fabbricati e piazzali	2.617.000.000=	
A4 -	Copertura tubo	2.580.000.000=	
	TOTALE VOCE A		6.825.000.000=

B - OPERE MECCANICHE

B1 -	Tubo	10.780.000.000=	
B2 -	Serbatoi a vuoto	1.040.000.000=	
B3 -	Imp. elettrici	1.950.000.000=	
B4 -	Montaggi	2.590.000.000=	
	TOTALE VOCE B		16.360.000.000=
	TOTALE GENERALE		23.185.000.000=

ESCLUSIONI

1) Pompe a vuoto
2) Valvole
3) Specchi
4) Coni antiviflesso
5) Ottica (Laser, strumenti, ecc.)
6) Baking
7) Fabbricati per Cabine elettriche e Centrali Servizi
8) Camere sterili al disotto dei serbatoi a vuoto.
9) Quanto altro non specificato in offerta.

SOCOMIN IMPIANTI S.r.l.
IL CONSIGLIERE DELEGATO
(Osvaldo Fiorani)

SOCOMIN IMPIANTI s.r.l.
progettazione costruzione montaggio impianti industriali

Ceccano 18/05/89

Ns./rif 135/OF/mf

Vs./rif.

Spett.le
I.N.F.N.
Istituto Nazionale di Fisica Nucleare
Sezione di Pisa

All'attenzione del Dr.Prof. Adalberto Giazotto

Oggetto: - Progetto VIRGO

In caso di appalto globale per le opere da noi quantizzate nella ns/offerta n° 133/OF/mf inviataVi a mezzo Fax riteniamo di poter aderire alla Vs/richiesta e, praticarVi una riduzione sul costo globale del 10%.

Pertanto il prezzo globale dell'opera alla data odierna passa da:

£. 23.185.000.000=

a £. 20.866.000.000=

Distinti saluti.

SOCOMIN IMPIANTI S.r.l.
IL CONSIGLIERE DELEGATO
(Osvaldo Fioroni)

03023 CECCANO (FR)
Sede e Stabilimento
S.S. 156 Km. 6 - Loc. Colle S. Paolo
Telefoni 0775/641481 - 641482

Cap. soc. 90.000.000 Int. vers.
P.I. e C.F. n. 01475120604
Trib. Frosinone 3859
C.C.I.A.A. Frosinone 82628

Tecnica del vuoto | Tecnica dei processi industriali del vuoto | Tecnica di misura e analisi

LEYBOLD S.p.A

Telefono (02) 28/1521
Telefax (02) 2871521
Telex 330348 Imm

Spett.le
I. N. F. N.
S. PIERO A GRADO
(Pisa)

Alla c.a. prof. Giazzotto-dr. Bradaschia

Data 11.5.1989
Ns. rif. RC/ggc
Vs. rif.

Oggetto **Ns. offerta n. WV/110/74/89/RC**

N. 3 gruppi di pompaggio di prevuoto completamente assemblati e ogni gruppo è costituito da:

N. Cat.		
11170	2	Pompe rotative a palette tipo D 250 F doppiostadio Portata effettiva 250 m^3/h. Vuoto parziale finale $2x10^{-4}$ mbar Alimentaz. 380 V trifase 50 Hz. Valvola di sicurezza e filtri lato scarico incorporati
SO	2	Filtri in acciaio inox con Al_2O_3 per olio delle rotative
11743	1	Pompa Roots tipo WSU 10001 Portata nominale 1000 m^3/h Motore direttamente flangiato S.V. Alimentazione 380 V trifase 50 Hz.
28826	1	Valvola di intercettazione elettro-pneumatica NW100 ISOK ad angolo in inox
28785	1	Indicatore di fine corsa
88766	1	Giunto elastico NW100ISOK inox
88716	1	Flangia saldabile in inox NW100 ISOK
88765	2	Giunti elastici NW63 ISOK inox

../..

LEYBOLD S.p.A.

89648	1	Pirani tipo PG3 con uscita standard RS232C Campo di misura $1000 \div 10^{-3}$ mbar Possibilità di collegare tre teste di misura con moduli aggiuntivi e tre consensi regolabili su tutta la scala Alimentazione 220 V 50 Hz.
89630	1	Testa di misura tipo TR 901
89678	1	Cavo l.= 3 m.

PREZZO CAD. L. 63.400.000=

PREZZO TOTALE L. 190.200.000=

N. 18 gruppi medio vuoto; ogni gruppo è costituito da:

85647	1	Pompa turbomolecolare tipo 1000 H Possibilità di posizionarla girata di 90° Portata 1100 l/sec. per N_2 Attacco NW200CF Attacco prevuoto NW40KF
85578	1	Alimentatore tipo Turbotronik 1000/1500 H
85544	1	Raffreddamento ad aria
85549	1	Valvola di ventilazione elettomagnetica 220 Volt
28698	1	Valvola elettropneumatica NW200 CF
89646	1	Misuratore combinato pirani-ionizzazione tipo IONI IG3 Campo di misura $1000 \div 10^{-10}$ mbar Possibilità di collegare due teste tipo Pirani e una testa ad ionizzazione Uscita standard RS 232 C Tre consensi regolabili su tutta la scala Alimentazione 220 V 50 Hz.

../..

LEYBOLD S.p.A.

89685	1	Testa tipo IGC con attacco NW35CF
89656	1	Modulo per pirani
89632	1	Testa tipo TR 905 con attacco NW16CF
89687	1	Cavo per IGC l.=3 m.
89678	1	Cavo per TR 905 l.=5 m.
11266	1	Pompa rotativa a palette tipo D16B - doppio stadio Portata nominale 18,9 m^3/h. Vuoto finale $<1x10^{-4}$ mbar Alimentazione 220/380 V 50 Hz. Valvola di sicurezza antiritorno olio incorporata
18911	1	Filtro lato scarico tipo AF 16-25
85415	1	Trappola inox per Al_2O_3
85410	1	Confezione di Al_2O_3
88516	1	Riduzione 40 KF-25KF inox
86803	1	Tubo flessibile in inox NW25KF l. = 1 m.
SO	1	Raccordo speciale 200 CF con un attacco NW35CF e un attacco NW16CF
SO	1	Flangia saldabile NW200CF

PREZZO CAD L. 38.600.000=
PREZZO TOTALE L. 694.800.000=

4 Valvole NW 1000 elettropneumatiche tipo Gate
Prezzo di massima L. 89.000.000=
(sarebbe opportuno contattare direttamente la ditta Vat per un prezzo definitivo)

../..

LEYBOLD

LEYBOLD S.p.A.

N. 52 gruppi di alto vuoto e ogni gruppo è costituito da:

SO	1	Pompa ionica IZ 1000 diodo Portata 1000 l/sec. per N_2 Attacco NW 200 CF
85167	1	Alimentatore tipo NIZ4S con lettura del vuoto incorporata
85170	1	Cavo per pompa ionica l.= 5 m.
85169	1	Modulo per alimentatore tipo NIZ4S

PREZZO TOTALE L. 1.580.000.000=

I prezzi sopra indicati sono stati calcolati con un rapporto £/D.M. = 733 e nella fornitura non è compreso il montaggio presso il Vs. Istituto dei vari gruppi di pompaggio.

Consegna: 8-10 mesi
Pagamento: 50% all'ordine
50% consegna materiale
Resa: f.co Vs. Istituto
Validità offerta: settembre 1990

Distinti saluti.

LEYBOLD Carlo Coselli

Sede Legale
20144 Milano - Corso Vercelli, 25
Uffici Amm. e Commerciali:
Via Brunelleschi, 44
20090 Trezzano s/N - (Milano) ITALIA
☎ (02) 4452141 r.a.
Telex 314478 THSTEM I
Telefax 02 - 4455487
Part. IVA e Cod. Fisc. N. 08948530152
Reg. Trib. MI 274612 - C.C.I.A.A. 1256867

Spettabile
ISTITUTO RICERCA
DI FISICA

Condizionamento dell'aria - Clean Rooms - Spegnincendio

ns. rif. GB/sb/80201

Trezzano s/N. 4 Maggio 1989

Alla cortese attenzione Egregio Prof. Bradaschaa

RingraziandoVi per la cortese richiesta, Vi inviamo il nostro preventivo con i prezzi di larga massima per impianti di condizionamento di n. 3 capannoni e di n. 3 camere bianche in classe 10.000.

THERMOSYSTEM S.p.A.

IMPIANTI DI CONDIZIONAMENTO CAPANNONI

- Temp. est. : 33°C con 50% U.R. estivo
- Temp. amb. : 27°C con 50% U.R. estivo
- Temp. est. : 2°C con 80% U.R. invernale
- Temp. amb. 20°C con 50% U.R. invernale
- Tolleranze sulle temperature : ± 1,5°C
- Tolleranze sulla umidità : ± 10%

CAPANNONE

- Dimensioni : 20 x 20 m x 15H
- Volume : 6.000 m3

n. 1 condizionatore portata 36.000 m3/h, potenzialità frigorifera installata 120.000 frig/h, potenza termica 100.000 kcal/h.

Prezzo orientativo : L. 350.000.000.=

N. 2 CAPANNONI UGUALI

- Dimensioni : 15 x 15 x 15H
- Volume : 3.375 m3

n. 1 condizionatore da 25.000 m3/h, potenzialità frigorifera 85.000 frig/h, potenza termica installata 75.000 kcal/h

Prezzo orientativo : L. 250.000.000.= CAD.

CAMERE BIANCHE CLASSE 10.000

- Temperatura ambiente
  (per tutte le stagioni) : 24°C con 50% U.R.

- Tolleranze sulla temperatura : ± 1°C

- Tolleranze sull'umidità : ± 5%

N.1 CAMERA

Dimensioni : 16 x 10 x 2H

n. 1 condizionatore da 20.000 m3/h con alimentazione fluidi caldi e freddi dalle centrali del capannone completa di pareti e controsoffitti

Prezzo orientativo : L. 300.000.000.-

N. 2 CAMERE

- Dimensioni : 7 x 7 x 2H
- Volume : 100 m3

n. 1 condizionatore da 6.000 m3/h con alimentazione fluidi caldi e freddi dalle centrali del capannone completa di pareti e controsoffitti

Prezzo orientativo : L. 120.000.000.- CAD.

ESCLUSIONI

- Opere murarie, linee e quadri elettrici

THERMOSYSTEM s.p.a.
Direttore Commerciale
ROBERTO STORTI

COPIA PER ESTRATTO

comune di cascina

deliberazione del consiglio comunale
n. 100 del 8 Maggio 1989

OGGETTO: **Antenna interferometrica a grande base per la ricerca di onde gravidazionali.**

L'anno millenovecentottanta **nove** , addì **otto** del mese di **Maggio** alle ore **21,00** nel palazzo Comunale, convocato nei modi di legge, si è riunito il Consiglio Comunale.

All'inizio della seduta risultano presenti i membri contrassegnati

Risultano quindi assenti N. **12** membri.

☒ 1 - VIEGI Franco	☐ 21 - PALAMÀ Antonio
☒ 2 - CACCIAMANO Carlo	☐ 22 - PUNTONI Paolo
☒ 3 - MARMUGI Franco	☒ 23 - PIERINI Luigi
☐ 4 - VIEGI Carlo	☐ 24 - RASETTI M. Stella
☒ 5 - BELLAGAMBA Flavio	☒ 25 - NANNIPIERI Piero
☒ 6 - LORENZETTI Sergio	☐ 26 - ANTONELLI Giuseppe
☒ 7 - BERTELLI Claudio	☐ 27 - CONFORTI Franco
☒ 8 - BETTI Grazia	☐ 28 - BELLINI Massimo
☒ 9 - BACCIARDI Giuseppe	☒ 29 - PATTARO Luciano
☒ 10 - MENICHETTI Franco	☒ 30 - MACCHIA Enzo
☒ 11 - BARSOTTI Maurizio	☒ 31 - ROSSI Renzo
☐ 12 - BANI Fabrizio	☒ 32 - MORETTI Elia
☒ 13 - FANALI Annibale	☒ 33 - BERNI Paolo
☐ 14 - SBRANA Giuliana	☐ 34 - BIZZARRI Dante
☒ 15 - PARRI Fernando	☒ 35 - RICOVERI Giordano
☒ 16 - CORSI Leila	☒ 36 - ROSSI Giuseppe
☐ 17 - TOMMASINI Massimiliano	☒ 37 - PUCCINI Luigi
☒ 18 - BERRUGI Paolo Egisto	☒ 38 - POLI Fabio
☒ 19 - BUCCHIONI Vally	☒ 39 - GOBBI Sergio
☒ 20 - DEL CESTA Angiolo	☐ 40 - MARCHESINI Luigi

Presiede la seduta il Sig. **VIEGI FRANCO**

nella sua qualità di **Sindaco**

Assiste alla seduta il Segretario Generale **Dott. Gabriele Orsini**

Il presidente, accertato che i presenti sono in numero legale, dichiara aperta la seduta.

IL CONSIGLIO COMUNALE

Premesso che l'Istituto Nazionale di Fisica Nucleare sezione di Pisa ha presentato un progetto di notevole interesse scientifico per la realizzazione di un'antenna interferometrica a grande base per la ricerca di onde gravitazionali da installare nel territorio del Comune di Cascina;

visto che a seguito degli incontri avuti col gruppo di ricercatori interessati, la scelta dell'area é caduta su una zona in località S.Stefano a Macerata;

che questa Amministrazione Comunale é interessata a che l'Istituto realizzi il progetto nel Comune di Cascina per la rilevanza scientifica dell'iniziativa;

dato atto che l'area interessata é prevista nel P.R.G. come zona agricola ai sensi art.81 D.P.R. N.616/1977;

a voti unanimi, resi palesemente dai n.28 Consiglieri presenti e votanti,

D E L I B E R A

- di esprimere parere favorevole di massima al progetto per la installazione dell'antenna interferometrica a grande base per la ricerca di onde gravitazionali, come da proposta dall'Istituto di Fisica Nucleare e dall'Università di Pisa qui allegata (N.1), da realizzare nell'are di cui alla planimetrica allegata (N.2);
- di dare atto che la presente deliberazione non é soggetta a controllo ai sensi dell'articolo unico L.R. n.44/84.

Il presente verbale è stato approvato e qui di seguito sottoscritto.

IL PRESIDENTE

f.to Viegi

IL CONSIGLIERE ANZIANO

f.to Cacciamano

IL SEGRETARIO GENERALE

f.to Orsini

Per copia conforme all'originale per uso amministrativo.

IL SINDACO

IL SEGRETARIO GENERALE

Cascina, li 2 6 MAG. 1989


COMUNE DI CASCINA
ufficio tecnico - settore urbanistica

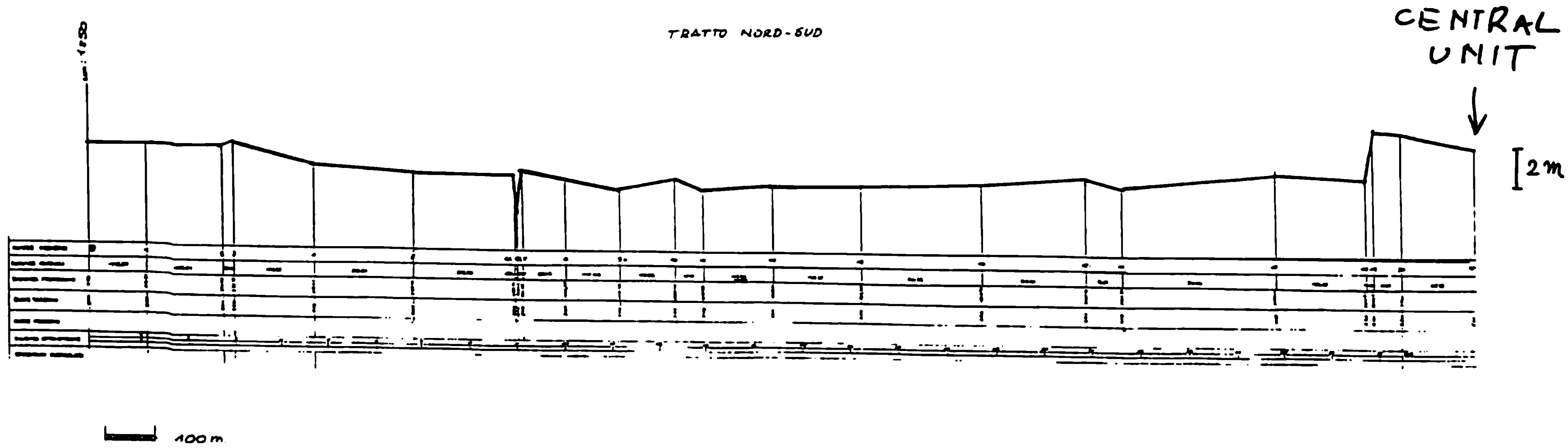
TRATTO NORD-SUD
CENTRAL UNIT
2 m
100 m